Author:
Rees, Kathryn Tara

Title:
Behavioural study of the deposition and removal of cross-linked PDMS droplets on macroscopic surfaces

BEHAVIOURAL STUDY OF THE DEPOSITION AND REMOVAL OF CROSS-LINKED PDMS DROPLETS ON MACROSCOPIC SURFACES

PhD Thesis

BRISTOL UNIVERSITY SPONSORED BY URPSL

Academic Supervisor: Prof. Brian Vincent

Industrial Supervisor: Dr. Neil Shaw

KATHRYN TARA REES

University of BRISTOL

Unilever

EPSRC
Engineering and Physical Sciences Research Council

Behavioural study of the deposition and removal of cross-linked PDMS droplets on macroscopic surfaces

by

Kathryn Tara Rees

A thesis submitted in fulfillment of the requirements for the degree of Doctor of Philosophy in the University of Bristol, UK.

December, 2005

The work described in this thesis was carried out in the Department of Physical Chemistry, University of Bristol, under the supervision of Professor B.Vincent during October 2001 to October 2004. The work is original except where acknowledged by reference in the text, and has not been submitted for a degree at any other University.

Acknowledgments

Primarily, I wish to thank my mother, Gill, and my partner, Ciarán, for their unwavering assistance, support and deep understanding, without which I would have been a much poorer person.

I am also extremely grateful to my academic supervisor Prof. Brian Vincent, University of Bristol, and industrial supervisor Dr. Neil Shaw, Unilever, Port Sunlight for their theoretical knowledge and interpretation. In addition I would like to express my gratitude to the many university students and staff who provided expert technical assistance. These include; Dr.S.Davies from the microscopy department of the University of Bristol who provided the detailed TEM images of the deformable PDMS droplets, Dr.K.MacNeil, Dr. M. Murray and Ms.R.Silvester from the mass spectrometry service and NMR service, University of Bristol respectively for the mass spectra and both invaluable expertise in H' NMR and Si^{29} NMR techniques. I was also fortunate to obtain the assistance of Prof.G.Allan from the Interface analysis center, University of Bristol. He introduced me to the fascinating XPS technique and provided an incredibly detailed understanding of the importance of the substrate surface composition on the deposition process. Dr A. Young from the Physics department, University of Bristol, was invaluable in adapting the tapping AFM technique for this project. I am extremely grateful to Noesis. S.A, France for their expertise and personal tuition through the minefield of imaging software. Finally, I wish to thank Dr. Theo. Van de Ven, the Godfather of Stagnation point flow cells, for his patience and the many invaluable communications I have had the pleasure of receiving during my studies.

Abstract

In this work the rate of deposition, spreading behaviour and removal of cross-linked PDMS droplets (0.8-2.5 μm diameter) onto model substrates, under a variety of conditions, has been monitored. The model substrates used were optically flat mica and chemically modified glass plates. The stagnation point flow geometry was arranged so that the droplets impinged, through a jet, onto the substrate. A stagnation point region near the substrate surface, vertically adjacent to the mouth of the jet, which ensures droplets reached the surface by a diffusion process, Brownian motion.. The deposition rate of the droplets was monitored visually using a microscope and a CCD camera linked to an image-analysis system. This allowed the partial radial distribution of droplets, droplet number per unit area and any droplet spreading to be quantitatively recorded.

Deposition rates and maximum coverage values were manipulated by altering the cross-linker volume fraction, the electrolyte concentration, NaCl , the presence of anionic surfactant, SDS, and finally by chemically modifying glass substrates. The deposition results obtained were modeled using standard theories for rigid, solid particle-surface and particle-particle interactions. Those systems containing >10 (v/v) MTMS, (Methyltrimethoxysilane), and high substrate surface asperity showed good agreement with theoretical predictions, while the addition of NaCl or SDS enhanced the deformability of the droplets and so induced significant deviations from classical DLVO predictions.

CONTENTS

	Page
CHAPTER 1: Introduction	1
1.2 Emulsion formation	2
1.3 PDMS emulsions	4
1.4 Emulsification by nucleation and growth	5
1.5 Apparent spontaneous emulsification	6
1.6 Application of emulsions	8
1.7 PDMS emulsion preparation	8
1.8 Chemical model of hair	9
1.8.1 Surface chemistry of hair	10
1.8.2 Surface roughness of hair	12
1.8.3 Surface charge of hair	13
1.9 PDMS deposition onto hair	14
1.10 Objectives	15
1.11 References	18
CHAPTER 2: O/W emulsions; Inter-droplet interaction	22
2.1 EDL interactions	22
2.2 London van der Waals interactions	26
2.3 Interaction energy, V_T	28
2.4 Steric interactions stabiisation effect on van der Waals and EDL	30
2.5 Thin film thinning; droplet coalescence	33
2.6 Thermodynamics of film thinning	35
2.7 Forces acting across a thin film; disjoining pressure	36
2.8 Hydrodynamics of film thinning	37
2.9 Film rupture	39
2.10 References	39
CHAPTER 3: Cross-linked PDMS emulsions	41
3.1 Introduction	41
3.2 Monodisperse emulsion systems	43
3.3Preparation of cross-linked PDMS emulsions	44

	Page
3.4 Proposed reaction scheme	45
3.5 References	48
CHAPTER 4: Experimental	49
4.1. Introduction	49
4.2 Materials	49
4.3 Emulsion characterisation	50
4.3.1 PCS (photon correlation spectroscopy)	50
4.3.2 Electrophoretic mobility and ζ-potential	51
4.4 Oil phase analysis	53
4.4.1 Viscosity and density	53
4.4.2 TEM (Transmission electron microscopy)	53
4.4.3 Mass spectroscopy (FAB)	54
4.4.4 Interfacial tension	54
4.4.5 High resolution.Si^{29} and H^{1} NMR	56
4.4.6 GPC (Gel permeation chromatography)	56
4.5 PDMS-substrate interaction characterisation	57
4.5.1 Three phase contact angle	57
4.5.2 Streaming potential	59
4.5.2.2 Influence of particle deposition on substrate surface potential	63
4.5.3 XPS (X-ray photo-electron spectroscopy)	64
4.5.4 AFM (Atomic force microscopy)	66
4.6 Colloidal deposition	67
4.6.1 Stagnation point flow cell design	67
4.6.2 Observation system	71
4.6.3 Imaging software	72
4.7 Colloidal detachment	74
4.7.1Horizotal flow cell design	75
4.7.2 Experimental set-up	79
4.8 References	80
CHAPTER 5: Cross-linked PDMS emulsion characterisation	83
5.1Introduction	83
5.2 Emulsion characterisation	83

Page

5.2.1 Emulsion turbidity 83
5.2.2 TEM 84
5.2.3 Influence of NH_3 concentration 87
5.2.4 PCS 88
5.2.5 Zeta-potential measurements 96
5.3 Characterisation of cross-linked PDMS oil 102
5.3.1 Isolation of oil phase 102
5.3.2 Determination of PDMS ϕ 103
5.3.3 Mass spectra 104
5.3.4 Elemental analysis 106
5.3.5 GPC 107
5.3.6 High resolution H^1 NMR and Si^{29} 110
5.3.7 Surface and interfacial tension 114
5.4 References 116

CHAPTER 6: Introduction of a fluorescent dye 118
6.1 Refractive index contrast 118
6.2 Fluorescence 118
6.3 Fluorescein 119
6.4 References 123

CHAPTER 7: Droplet deposition and removal 124
7.1Colloidal deposition 124
7.2.1 Interaction forces between approaching droplet and a flat plate 126
7.2.2 Interaction forces between approaching droplet and adsorbed species 129
7.2.3 Droplet bond number 131
7.2.4 Stagnation point deposition parameters 132
7.2.5 Deposition coverage 135
7.2.6 Tubular pinch effect 137
7.2.7 "Blocking" effects 138
7.2.8 Adhesion 141
7.2.9 Contact deformation 142
7.2.10 Film thinning and rupture 144

Page

7.2.11 Spreading dynamics on smooth & rough surfaces 146
7.3 Colloidal removal 148
7.4 Horizontal flow cell parameters 152
7.4.2 Removal data and analysis 155
7.5 References 156

CHAPTER 8: Substrate preparation and characterisation 160
8.1introduction 160
8.2Substrate surface modification 161
8.2.1 Preparation of acid cleaned glass slides 161
8.2.2 Adsorption of 3-Aminopropyltriethoxysilane onto glass slides 161
8.2.3 Adsorption of Repelcote modified glass slides 163
8.2.4 Mica substrates 164
8.2.5 L-Lysine modified glass 164
8.3 Substrate characterisation 165
8.3.1 Substrate surface topography (AFM) 165
8.3.2 Streaming potential characterisation of substrate surfaces 169
8.3.4 XPS spectra of substrate surfaces 176
8.3.5 Three phase contact angle characterisation 181
8.4 References 186

CHAPTER 9: Colloidal deposition results and discussion 189
9.1 Colloidal deposition in stagnation point flow cell 189
9.2.Colloidal deposition as a function of cross-linked PDMS 190
9.2.2Colloidal deposition as a function of electrolyte, NaCl 207
9.2.3Colloidal deposition as a function of surfactant, SDS 222
9.2.4 Colloidal deposition as a function of substrate surface properties 236
9.3 References 249

	Page
CHAPTER 10: Results and discussion: Horizontal flow cell	250
10.1Colloidal removal as a function of cross-linked PDMS	250
10.1.2Colloidal removal as a function of electrolyte, NaCl	254
10.1.3 Colloidal removal as a function of surfactant, SDS	257
10.1.4Colloidal removal as a function of substrate surface properties	260
10.2References	264
CHAPTER 11: Conclusions and further work	265
11.1 Conclusions	265
11.2 Suggestions for further work	270
11.3 References	271
APPENDICES : Additional work	285
A1.Droplet-droplet interaction profiles	286
A2. Phase stability study	289
A3. Influence of Fluorescein on O/W interfacial tension	291
A4. Substrate XPS spectra	292
A5. Deposition on uniform substrate surface heterogeneity	296
A6. Deposition on Human epidermis	299
A7. Stagnation point flow deposition rate profiles	301
A8. Study of deposition thickness (Reflectometry)	302
A9. Deposition under shear force (Diastrom)	303

LIST OF FIGURES

	Page
Figure 1.1 The layers of keratin on hair surface	11
Figure 1.2 Oil deposition onto hair shaft	14
Figure 2.1 Schematic representation of EDL structure	23
Figure 2.2 Schematic representation of the potential energy curves for two identical PDMS droplets	29
Figure 2.3 Schematic representation of interaction curve in presence of high neutral homopolymer coverage	32
Figure 2.4 Schematic representation of the thin film between two PDMS droplets	35
Figure 2.5 Schematic representation of the "dimple" between two PDMS droplets	38
Figure 3.1 General synthesis of silicons	41
Figure 3.2 The general structure of cyclic silicons	42
Figure 3.3 Proposed reaction scheme for cross-linked PDMS	46
Figure 3.4 Structure of PDMS as a function of cross-linker ϕ	47
Figure 4.1 Schematic representation of three phase contact angle cell	57
Figure 4.2 Schematic representation of streaming potential instrument	60
Figure 4.3 Schematic representation of streaming potential mechanisms	61
Figure 4.4 Application of streaming potential determination methods	62
Figure 4.5 Schematic representation of XPS instrument	66
Figure 4.6 Principles of AFM	67
Figure 4.7 Schematic representation of Stagnation point cell	69
Figure 4.8 Schematic representation of Stagnation point formation	70
Figure 4.9 Stagnation point flow cell set up	71
Figure 4.10 Schematic representation of observation	72
Figure 4.11 Droplet detection and analysis macro	74
Figure 4.12 Schematic representation of Horizontal flow cell	78

Page

Figure 5.1 Turbidity change of cross-linked PDMS emulsions 84

Figure 5.2 TEM images of cross-linked PDMS droplets as a function of NH_3 88

Figure 5.3 Influence of cross-linker ϕ on droplet hydrodynamic diameter 89

Figure 5.4 Droplet hydrodynamic diameter as a function of total monomer ϕ 91

Figure 5.5 Droplet hydrodynamic diameter as a function of time 93

Figure 5.6 Droplet hydrodynamic diameter as a function of electrolyte NaCl 95

Figure 5.7 Droplet hydrodynamic diameter as a function of adsorbed anionic surfactant SDS 96

Figure 5.8 Droplet surface ζ-potential as a function of total monomer ϕ 98

Figure 5.9 Droplet surface ζ-potential as a function of MTMS ϕ 100

Figure 5.10 Mass spectra of isolated cross-linked PDMS oil 105

Figure 5.11 GPC Molecular weight distribution of isolated cross-linked PDMS 109

Figure 5.12 H' NMR spectra of isolated cross-linked PDMS oil 111

Figure 5.13 Si^{29} NMR spectra of isolated cross-linked PDMS oil 113

Figure 5.14 DT network structural combinations 112

Figure 6.1 Structural configurations of Fluorescein in aqueous solutions 120

Figure 6.2 Absorption intensity of Fluorescein as a function of time 121

Figure 6.3 Influence of Fluorescein concentration on surface tension of water 122

Figure 7.1 Schematic representation of droplet-substrate interactions 125

Figure 7.2 Schematic side view of a droplet deposited under a substrate 132

Figure 7.3 Schematic representation of coating density 136

Figure 7.4 Spatial arrangement of adhering droplet 141

Figure 7.5 Droplet spreading mechanisms on a rough substrate 148

Figure 7.6 Hydrodynamic and frictional forces acting on a deformed particle 149

Figure 8.1 APTES conformations on glass substrate 162

Figure 8.2 Reaction of dichlorodimethylsilane with glass hydroxyl surface groups 163

Figure 8.3 Mica molecular structure 164

Page

Figure 8.4 L-Lysine molecular structure 165

Figure 8.5 Streaming potential of Mica and unmodified glass as a function of electroyte NaCl 172

Figure 8.6 Streaming potential of Mica substrate as a function of SDS 173

Figure 8.7 Streaming potential of mica surface adsorption as a function of electrolyte NaCl 176

Figure 8.8 XPS spectra of Mica 177

Figure 8.9 XPS spectra of acid cleaned glass 178

Figure 9.1 Detail of contact area between PDMS droplet and mica substrate 196

Figure 9.2 Deposition profiles as a function of cross-linker ϕ on mica 198

Figure 9.3 Droplet contact area as a function of time with varying MTMS ϕ 201

Figure 9.4 Comparison of radial distribution functions for varying MTMS ϕ 203

Figure 9.5 Evidence of aqueous film and droplet coalescence in presence of electrolyte NaCl 213

Figure 9.6 Evidence of direct contact between cross-linked PDMS droplets and mica 216

Figure 9.7 Deposition profiles as a function of electrolyte NaCl 215

Figure 9.8 Droplet-substrate contact area spread as a function of electrolyte NaCl 217

Figure 9.9 Radial distribution of cross-linked PDMS as a function of electrolyte concentration, NaCl 218

Figure 9.10 Surfactant packing arrangement on an hydrophobic surface 221

Figure 9.11 Evidence of direct contact between cross-linked PDMS droplets and mica surface 222

Figure 9.12 Aqueous film between cross-linked PDMS droplet-mica surface in presence of SDS 227

Figure 9.13 Deposition profiles as a function of time on Mica 229

Figure 9.14 Deposition contact area as a function of time on mica 230

	Page
Figure 9.15 Comparison of partial radial distribution function in presence of SDS	232
Figure 9.16 Deposition profiles as a function of time	240
Figure 9.17 Droplet area spread as a function of time	243
Figure 9.18 Deposition partial radial distribution as a function of substrate	244
Figure 10.1 Droplet removal profiles as a function of MTMS ϕ	254
Figure 10.2 Droplet removal profiles as a function of electrolyte	261
Figure 10.3 Droplet removal profiles as a function of anionic surfactant concentration, SDS	268
Figure 10.4 Droplet removal profiles as a function of substrate surface	274
Figure A1.1 Potential energy profiles as a function of droplet surface charge	286
Figure A1.2 Potential energy profile as a function of electrolyte concentration NaCl	287
Figure A1.3 Potential energy profile as a function of MTMS ϕ	287
Figure A1.4 Potential energy profile as a function of cross-linked PDMS droplet diameter	288
Figure A2.1T(t) profiles at fixed scan height as a function of electrolyte concentration NaCl	290
Figure A3.1 DSA image of Fluorescein / MTMS interface	291
Figure A4.1XPS spectra untreated glass surface	292
Figure A4.2 XPS spectra APTES modified glass substrate surface	293
Figure A4.3 XPS spectra of Repelcote modified glass substrate surface	294
Figure A4.4 XPS spectra of L-Lysine modified glass substrate surface	295
Figure A5.1 Schematic representation of (a) square grid, (b) hexagonal grid	296
Figure A5.2 Square grid 0.05(v/v)MTMS as a function of time	297
Figure A5.3 Hexagonal grid 0.05(v/v)MTMS as a function of time	298

	Page
Figure A6.1SEM image of human epidermis	299
Figure A6.2 Deposition images on human epidermis as a function of time	300
Figure A7.1 Deposition rate profiles as a function of time; varying MTMS ϕ, [NaCl], [SDS] and substrate surfaces	301
Figure A8.1 Deposition profiles as a function of time with varying MTMS ϕ	303
Figure A9.1 Deposition under shear force as a function of (a) [NaCl], (b) MTMS ϕ	304

LIST OF TABLES

	Page
Table 1.1 Amino acid composition of human hair	12
Table 3.1 Emulsion parameters	44
Table 5.1 Influence of MTMS ϕ on droplet hydrodynamic diameter	92
Table 5.2 Influence of MTMS ϕ on droplet surface potential	99
Table 5.3 Mobility and ζ-potential of cross-linked PDMS droplets as a function of electrolyte, NaCl	101
Table 5.4 Droplet surface ζ-potential as a function of anionic surfactant	101
Table 5.5 Calculated average molecular weight as a function of MTMS ϕ	104
Table 5.6 Elemental composition of cross-linked PDMS oil	107
Table 5.7 Determination of cross-linked PDMS oil molecular weight	108
Table 5.8 Characterisation of cross-linked PDMS oil as a function of MTMS ϕ	115
Table 6.1 Fluorescence quantum yields and lifetimes of fluorescein	122
Table 7.1 Substrate-PDMS-water Hamaker constant, A_{123}	155
Table 7.2 Parameters used for calculation of hydrodynamic force	156
Table 8.1 AFM substrate surface topography	167
Table 8.2 Streaming potential of surface substrates	170
Table 8.3 XPS chemical composition of modified glass substrates	179
Table 8.4 Three phase contact angle as a function of cross-linker ϕ	183
Table 8.5 Three phase contact angle as a function of substrate	185
Table 9.1 Cross-linked PDMS emulsion parameters	190
Table 9.2 Deposition parameters with varying MTMS ϕ	199
Table 9.3 Cross-linked PDMS emulsion parameters as a function of electrolyte, NaCl	211
Table 9.4 Comparison of deposition profile rates as a function of electrolyte NaCl	213

	Page
Table 9.5 Cross-linked PDMS emulsion parameters in the presence of SDS	219
Table 9.6 Comparison of deposition profiles as a function of SDS	228
Table 9.7 Substrate surface properties	234
Table 9.8 Comparison of rate values on different substrates	241
Table 10.1 F_{H50} removal data as a function of MTMS ϕ	247
Table 10.2 F_{H50} removal data as a function of electrolyte concentration Nacl	262
Table 10.3 F_{H50} removal data as a function of anionic surfactant concentration, SDS	267
Table 10.4 F_{H50} removal data as a function of substrate surface	276

List of plates

		Page
Plate I	TEM images of cross-linked PDMS droplets	86
Plate II	AFM images of substrate surfaces	168
Plate III	Inverted three phase contact angle as a function of MTMS ϕ	182
Plate IV	Inverted three phase contact angle as a function of substrate	184
Plate V	Deposition of 0.00(v/v) MTMS droplets on mica	191
Plate VI	Deposition of 0.005(v/v) MTMS droplets on mica	192
Plate VII	Deposition of 0.01(v/v) MTMS droplets on mica	193
Plate VIII	Deposition of 0.05(v/v) MTMS droplets on mica	194
Plate IX	Deposition 0.1(v/v) MTMS droplets on mica	195
Plate X	Deposition in the presence of 10^{-5} mol dm^{-3} NaCl	205
Plate XI	Deposition in the presence of 10^{-4} mol dm^{-3} NaCl	206
Plate XII	Deposition in the presence of 10^{-3} mol dm^{-3} NaCl	207
Plate XIII	Deposition in the presence of 10^{-2} mol dm^{-3} NaCl	208
Plate XIV	Deposition in the presence of 10^{-1} mol dm^{-3} NaCl	209
Plate XV	Deposition in the presence of $3x10^{-1}$ mol dm^{-3} NaCl	210
Plate XVI	Deposition in the presence of 0.08 mM SDS	223
Plate XVII	Deposition in the presence of 0.8 mM SDS	224
Plate XVIII	Deposition in the presence of 8.0 mM SDS	225
Plate XIX	Deposition on acid clean glass	235
Plate XX	Deposition on APTES modified glass	236
Plate XXI	Deposition on Repelcote modified glass	237
Plate XXII	Deposition on Lysine modified glass	238
Plate XXIII	Deposition on mica substrate	239
Plate XXIV	Removal of 0.00(v/v) MTMS droplets from mica	248
Plate XXV	Removal of 0.005(v/v) MTMS droplets from mica	249

		Page
Plate XXVI	Removal of 0.01(v/v) MTMS droplets from mica	250
Plate XXVII	Removal of 0.05(v/v) MTMS droplets from mica	251
Plate XXIX	Removal of 0.15(v/v) MTMS droplets from mica	252
Plate XXX	Removal of 0.20(v/v) MTMS droplets from mica	253
Plate XXXI	Removal in the presence of 10^{-5} mol dm^{-3} NaCl	258
Plate XXXII	Removal in the presence of 10^{-3} mol dm^{-3} NaCl	259
Plate XXXIII	Removal in the presence of $3x10^{-1}$ mol dm^{-3} NaCl	260
Plate XXXIV	Removal in the presence of 0.08mM SDS	264
Plate XXXV	Removal in the presence of 0.8mM SDS	265
Plate XXXVI	Removal in the presence of 8.0mM SDS	266
Plate XXXVII	Removal from an acid clean glass	270
Plate XXXVIII	Removal from an APTES modified glass	271
Plate XXXIX	Removal from a Repelcote modified glass	272
Plate XXXX	Removal from a L-Lysine modified glass	273

Abbreviations

AFM	Atomic force microscopy
APTES	Aminopropyltriethoxysilane
cmc	Critical micelle concentration
CCC	Critical electrolyte concentration
DMDES	Dimethyldiethoxysilane
DMT	Derjaguin, Muller, Toporov theory
DLVO	Derjaguin, Landau, Verwey and Overbeek theory of electrical double layer interactions between two colloidal particles
EDL	Electrical double layer
F_{ad}	Force of adhesion
F_{H50}	Hydrodynamic force required to detach 50% of deposited particles
HCP	Hexagonal close packing
JKR	Johnson, Kendall, Roberts theory
MTMS	Methyltrimethoxysilane
PCS	Photon Correlation Spectroscopy
PDMS	Polydimethylsiloxane
SDS	Sodium dodecylsulphate
TEM	Transmission Electron Microscopy
ϕ	volume fraction
θ	Deposition ratio
ζ-potential	Zeta potential

Chapter 1: Study introduction

1.1 Introduction

Deposition of colloidal particles onto solid surfaces is of great importance in a variety of processes[1]. It may be used to achieve selective or non-selective separation of particles from a host medium. This may be used either as a route to extract a valuable component, or as a means of purification by removing any unwanted particles. Particle deposition can also play an important part in manufacturing processes. These operations demand an understanding of the mechanisms for the deposition and the corresponding inter-particle forces that control the particle deposition.

Silicone oil is one of the most significant components within Unilever's shampoo and conditioner formulations. This project will focus on the fundamental parameters that control the deposition, spreading and removal of silicone oil droplets during the washing and rinsing of hair.

Monodisperse PDMS droplets will represent the silicone oil droplets and their behaviour studied as a function of shear force using macroscopic flat surfaces within flow cell systems. The PDMS emulsions used within this study are prepared without surfactant and due to their monodispersity are chosen to represent a system as close to an ideal Newtonian system as possible. The flat flow cell surfaces will be treated with a variety of substrates including a keratin substitute to gain a detailed insight into the droplets behaviour in different chemical environments. A stagnation flow cell will be used to investigate droplet deposition and spreading, while a horizontal flow cell will be used to study droplet removal.

Enhanced understanding of the mechanisms involved in droplet deposition and removal is of great significance to many industries including personal care products. The study of deposition and detachment mechanisms can provide valuable information into the adhesion properties of shampoos and their performance efficiency. These mechanisms are the main controlling factors in washing and rinsing processes and it is crucial to be able to observe them in real time experiments.

1.2 Emulsion formation

An emulsion is defined as " a dispersion of droplets of one liquid in an other one with which it is immiscible" [2]. Emulsions of droplets of an organic liquid (an oil) in an aqueous solution are known as oil/water emulsions (or O/W), and emulsions of aqueous droplets in an organic liquid are known as water/oil emulsions (or W/O). In general, the average droplet size in an emulsion tends to be greater than 100 nm in diameter. Emulsions generally have an appearance ranging from a milky-white opaqueness to a grey translucence depending on the droplet diameter.

The formation of an emulsion from two immiscible bulk liquids (α and β) is generally a non-spontaneous process. This may be understood in terms of the free energy change associated with the dispersion, in the form of droplets, of one of the liquids in the other, which (neglecting inter-particle interactions) can be considered to consist of two parts.

All emulsions require an input of energy in order to become dispersed[1]. This is normally provided either by an external source such as the mechanical energy in a

comminution mechanism or the energy is associated with a phase change. The free energy of emulsion formation is given by [1.1];

$$\Delta G = \Delta A\gamma^{\alpha\beta} - T\Delta S_{disp} \qquad [1.1]$$

where ΔA is the increase in the interfacial area, $\gamma^{\alpha\beta}$, the interfacial tension between the two immiscible liquids α and β and ΔS_{disp} is the entropy change associated with the dispersion of fine liquids droplets. In general, the first term on the right hand side of the equation [1] is the dominant term. ΔG is nearly always positive so emulsification is usually a non-spontaneous process.

Conditions can occur when ΔG is negative and emulsification is spontaneous. In order for this to happen the value of $T\Delta S_{disp}$ must exceed $\Delta A\gamma^{\alpha\beta}$. This occurs in the case of microemulsions [3-5], where equilibrium values of $\gamma^{\alpha\beta}$ are low enough for this to be the case. The important criterion with microemulsions is that the dynamic value of $\gamma^{\alpha\beta}$ decreases transiently to very small values.

Most emulsions are formed using dispersion methods[6,7]. This usually involves mechanical agitation (comminution) to disperse the oil in the aqueous phase or vice versa. It can be achieved by mechanical shearing of large droplets by equipment such as a colloid mill, an homogeniser, ultrasonic or just simple agitation of two phases together with an emulsifier.

Emulsions can also be prepared by utilising the chemical-physical properties of surfactants as emulsifiers, i.e., the phase inversion technique (PIT method)[8,9] or the surfactant-phase emulsification technique[10,11], etc.

The emulsions produced by these techniques tend to be polydisperse. This is because the emulsification conditions cannot be precisely controlled. A totally monodisperse emulsion is almost impossible. A more realistic "monodisperse" emulsion system will have a narrow droplet size distribution.

An alternative route to spontaneous emulsification is through controlled nucleation and growth of separating phases from an initial single-phase system. Such processes can be induced by the adjustment of a suitable thermodynamic parameter; for example by (i) temperature or concentration for a two-component system with an accessible consulate point such that a two-phase region is entered: (ii) or by the addition of a component which may give rise to chemical reaction and formation of a new phase.

1.3 PDMS emulsions

The last method[2] referred to, in the previous section, is commonly used in the production of solid / liquid dispersions but is rarely used to form liquid / liquid colloidal systems. Obey and Vincent[12] presented a route to spontaneous emulsion formation in which emulsions of relatively monodisperse poly(dimethylsiloxane) (PDMS) in water are prepared via the base catalysed hydrolysis and polymerisation of diethyldiethoxysilane (DMDES). The resultant emulsions are not thermodynamically stable, since they will eventually break down to give the thermodynamically stable state: the two separate bulk liquids. However, an energy barrier to coagulation can provide kinetic stability. The droplet size and electrophoretic mobility of the emulsions has been studied using dynamic light scattering and electrophoresis. The effect of the ammonia and monomer

concentration on the average droplet size was investigated. These PDMS / water emulsions can be prepared in sizes ranging from 0.5μm – 5.0μm and with a range of zeta potentials.

The preparation of a relatively monodisperse emulsions is an important, but only recently achieved, objective for understanding the fundamental principles governing emulsion behaviour. Emulsion preparative techniques include membrane emulsification[13-17], fractionated crystallisation[18-25] and aerosol sprays[27-32]. These techniques will not be discussed further in this work.

One possible method to form relatively monodisperse emulsions is via a nucleation and growth mechanism from an initially homogeneous phase. Nucleation describes the spontaneous appearance of a new phase from a meta-stable solution of the material in question. This will be discussed in section 1.4.

1.4 Emulsification by Nucleation and Growth

The PDMS emulsion used in this work was synthesised by a mechanism analogous to the base-catalysed hydrolysis and polymerisation of Tetra-ethoxysilane (TEOS) to form colloidal silica particles[33]. The method of formation of the PDMS emulsions is discussed later, (see section 1.7). It proceeds via a nucleation and growth mechanism without any added surfactant. This process also occurs in the preparation of emulsifier-free or emulsifier-starved polymerisation reactions[34-36]. Nucleation involves the initial formation of small nuclei from a homogeneous phase. When the monomer has a high degree of solubility in water, initiation of polymerisation occurs in the aqueous phase.

Intermediates, or radicals, generated in the aqueous phase add monomer units until they exceed their solubility and precipitate. The precipitated molecules form spherical droplets, which will absorb any emulsifier present, or surface-active oligomers can be formed in solution, and will act as an in-situ surfactant in the case of the PDMS droplets described in this thesis, and also monomer to form primary droplets. These primary droplets thus formed, particularly in the situation of an expanding interface, are not stable in the colloidal sense. Stability is obtained when enough charged groups have formed at the interface to give the droplet an adequate electrostatic surface potential. Thus, primary droplets may either persist or coagulate and coalesce with already existing droplets or other primary droplets. This will occur until the potential energy of electrostatic repulsion between the droplets is sufficient to ensure colloidal stability in the ionic environment in which the droplet is formed.

Droplet nucleation continues throughout polymerisation. The formation of new droplets is moderated by the capture and flocculation of precipitating oligomeric radicals and primary droplets by already existing mature droplets. A steady state is reached where the rate of nucleation of primary droplets and the rate of primary droplet capture is equal. Generally the quicker the polymerisation is to reach this steady state, the narrower the final size distribution will be. The longer the nucleation stage proceeds, the broader will be the size distribution.

1.5 Apparent Spontaneous Emulsification

Apparent spontaneous emulsification[37] may occur under non-equilibrium conditions when two liquids are brought together. There are three mechanisms by

which this can happen; the diffusion and stranding mechanism[38], interfacial turbulence and transient negative interfacial tension[39]. It is often difficult to determine which mechanism is occurring and to distinguish truly spontaneous emulsification from the one which occurs with very slight mixing.

The diffusion and stranding mechanism involves nucleation and growth of droplets from localised super-saturation near an interface[37, 40]. This happens, for example, when toluene, containing dissolved ethanol, is placed in contact with an aqueous phase. As the water-soluble alcohol diffuses ahead into the water it leaves the insoluble toluene behind. The interface becomes highly irregular in structure. This process is driven by the negative enthalpy of the solution of ethanol in water.

The second mechanism involves the break up of an interface between two liquids by capillary waves to form emulsion droplets. These thermal fluctuations, caused by diffusion of surface-active material to the interface, increase with temperature and change in the interfacial tension. The flow of liquid parallel to the interface also assists emulsification and if interfacial tension gradients are present then droplets may become trapped between the two phases[41].

The third mechanism involves the apparent presence of negative interfacial tensions. This occurs in oil-water systems with a third component in both phases. The interfacial tension is lowered when increasing amounts of surfactant and co-surfactant can apparently extrapolate the tension to negative values. What actually results , (rather than a negative tension), is the expansion of the interface and emulsification at the interface. The interfacial tensions remain low but positive due to the depletion of the monolayer during expansion[39].

This phenomenon can occur when a homogeneous two-component liquid mixture is cooled below its upper consolute temperature. A small temperature quench into a meta-stable region will result in droplets of the minority phase forming by nucleation of monodisperse droplets. Examples where this occurs include mixtures of polyisoprene and polyethylene-propylene[42], isobutyric acid and water, 2-6 lutidine and water [43].

Adjustment of the concentration of a component, or a chemical reaction can also produce a new phase. This last method is commonly used to form solid/liquid dispersions such as Ag sols and polystyrene latices.

1.6 Applications of Emulsions

There are many different classes of emulsions used in both industrial applications and in domestic products. The function of a particular emulsion is often a feature of its stability, concentration, droplet size, viscosity, presence of an emulsifier and rheological behaviour[44, 45] and deposition behaviour. Wetting and spreading characteristics are important.

1.7 PDMS emulsions preparation

Obey et al[12] first described the synthesis of relatively mondisperse silicone O/W emulsions. The droplet size and electrophoretic mobility of the emulsions were studied using dynamic light scattering and electrophoresis. The effect of ammonia and monomer concentration on the droplet size was investigated. The PDMS phase was characterised principally by Si^{29} and ^{1}H NMR, Mass spectrometry and

gel-permeation chromatography. The results showed that the most abundant polymeric species is the cyclic tetramer octamethyltetrasiloxane (D_4). It was shown that the ratio of linear to cyclic polymer in the PDMS phase may be altered by changing the amount of ethanol and / or monomer present in the initial reaction mixture.

Wegener et al[46] investigated the effect of adding cross-linking monomer to the initial reaction mixture together with ethanol. Results showed that at low cross-linker concentrations, emulsions droplets are formed, whilst above 0.4 volume fraction particles were present. Dilution with ethanol indicated that the particles were of a soft "microgel type" nature. Analysis of the PDMS by NMR indicated the formation of cross-linked network structures.

Anderson et al[47] investigated the effect of the addition of surfactant on the eventual average emulsion droplet size and the molecular weight and chemical composition of the PDMS phase. The surfactants used were both ionic and non-ionic. The presence of surfactant indicated that the proportion of linear to cyclic PDMS was increased and the average droplet size decreased. It should be pointed out here that the PDMS emulsion forms spontaneously via a nucleation and growth mechanism. However, mechanical energy is required initially to ensure dissolution of the starting monomer.

1.8 Chemical model of hair

To provide an accurate model of the deposition mechanisms that occur on hair fibres, that is by nature explanatory, it is necessary to relate the components of

the model investigated in this project to the different structures and properties of hair.

1.8.1 Surface chemistry of hair

All mammalian keratin fibres, including human hair, are covered by thin shells of hardened protein, the cuticle cells, which overlap from root to tip along each fibre, providing significant surface heterogeneity, see figure 1.1. Each of these cells is separated from its neighbour and the central core of the fibre by a multilaminated cell membrane complex of an overall thickness ~25μm. As radial distance is increased within the complex, three layers can be identified[48]. The outer α-layer contains 18-methyleicosanoic acid (18-MEA) is covalently-bound to the epicuticle of the cell, an inter-cellular "glue" known as δ-layer and another layer lipid , inner β-layer. The outer β-layer is also close to the fibre surface. Low cohesive forces are expected between the outer β- and δ-layers.

Hair is keratinised tissue, composed of dead cells which are cemented together by a group of proteins called keratins. Lipids account for ~2% of its' total mass. Hairs have a cortex covered by a "cuticle", which is a pile of flat cells that protect and maintain the cortex[50]. Human hair consists of ~80% protein,15% water, inorganic material and 1%-9% lipids[51]. The latter is derived from sebum and consists of free fatty acids; mono-, di-, and triglycerides, wax esters, hydrocarbons and alcohols. The mineral content ranges between 0.25%-0.95%, on a dry ash basis. Its amino acid composition is listed in table 1.1[52], however these values vary from individual to individual due to genetics, diet, cosmetic treatment, medication etc.

Fig 1.1 The layers of keratin on hair surface, (a) Optical microscopy[49], (b) AFM[48]

(a)

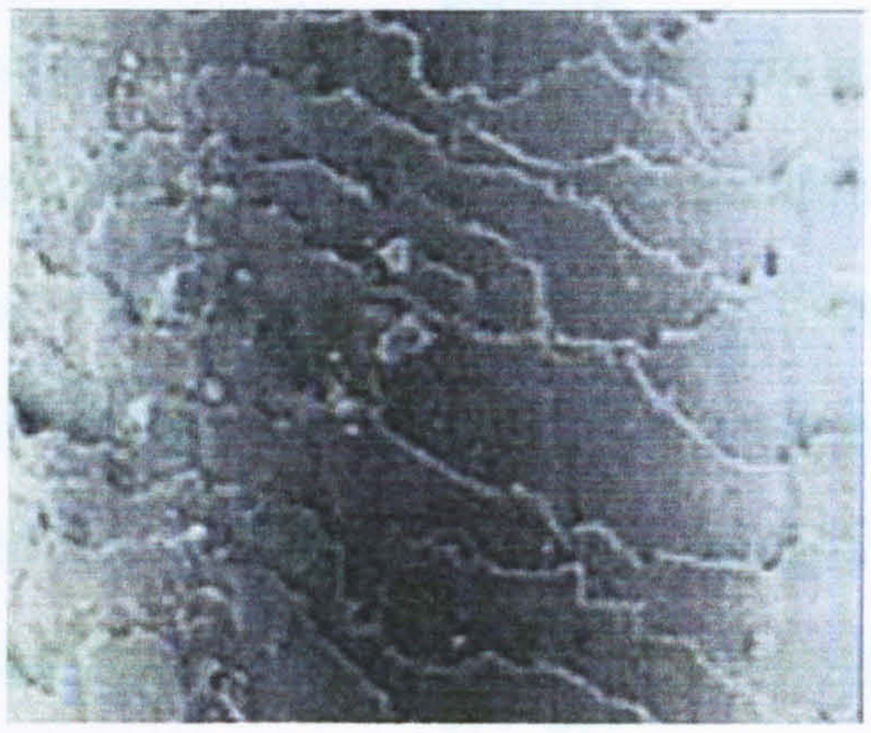

(b)

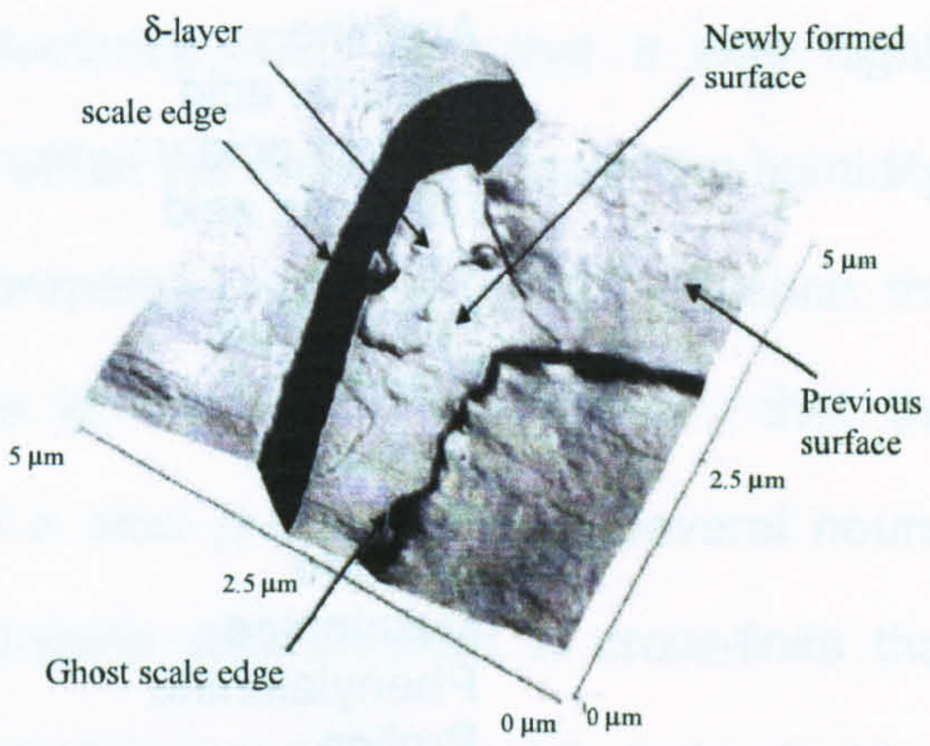

It was initially preferred to investigate deposition directly on to hair or keratin based substrate. However, it would have been necessary to purchase primary human epidermal keratinocytes, (Clonetics, Walkersville, MD) as a frozen stock and culture the thawed cells according to the method of Rheinwald and Green[53].However, it was not possible to sustain the required environment on a substrate to promote keratin development and place in the flow cell designs. The use of samples from a human head was also not possible due to ethical implications and the variation between specimens dependent on individuals, sites of extraction and methods of collection[54].

Table 1.1 Amino acid composition of human hair

Amino acid	µmoles / g^{-1} (dry hair)
Alanine	362-384
Arginine	499-550
Aspartic acid	444-453
Cysteic acid	22-40
Glutamic acid	995-1036
Glycine	463-513
Half cystine	1407-1512
Histidine	64-86
Isoleucine	244-255
Lecuine	502-529
***Lysine**	***206-222**
Methionine	50-56
Phenylalanine	132-149
Proline	646-708
Serine	1013-1091
Threonine	648-673
Tyrosine	177-195
Valine	477-513

** Amino acid chosen to represent hair surface*

1.8.2 Surface roughness of hair

The surface structure of hair is not uniform. It has a "direction" due to its growth and the arrangement of the cuticle envelope, which influences data obtained. Smith and Swift[48] used lateral force (LFM) and force modulation atomic force microscopy (AFM) to examine human hair fibre after non-covalently linked fatty acids have been removed, with a fibre transverse cross-section of 180 Å (54mm). An AFM topographic image of a human hair is shown in figure 1.1(b). Perwulz er al[55] later noted that the nature of the fibre surface played a role in spreading mechanisms.

1.8.3 Surface charge of hair

Martinsen et al[56], investigated the dielectric properties of human hair, noting that there was a significant electrical conductance (DC) and that it was highly dependent on the moisture level present within the fibres. The lower the humidity, the lower the DC conductance. This property was reported to influence the adsorption and desorption mechanisms in the fibres, and noted that the absorption of water into hair fibres was a slow process, lasting several hours. Watt[57] suggested that water absorbed initially was involved in cross-links that strengthened the molecular structure of keratins but did not contribute to electrical conductance. After this period, these cross-links will be broken and molecular mobility increase, enhancing conductivity. The DC conductance was found to increase for several days[56] after the hair had swollen and absorbed more water. This water then formed hydrogen bonds to the polar side chains on the hair shaft. This implied that the steady state hydration of the fibres had been achieved and that the absorbed water molecules regrouped in a way that increased their contribution to conductance.

Desorption was noted to be a much faster process[56] in comparison with adsorption due primarily to the fact that the loosely bound water molecules, which have the largest influence on conductance easily diffuse out of the hair fibres. The entire process was found to last only a few minutes. The more strongly bound molecules provide a slow desorption lasting for several hours.

1.9 PDMS deposition on to hair

Green[8] was the first to observe that the presence of silicone oil in shampoo significantly improved the appearance and texture of hair, and who subsequently influenced manufacturers to include it into personal care products[58-65]. It is clear that silicone oils are useful shampoo components and the deposition and spreading mechanisms continues to inspire considerable theoretical discussion[66-70].

There have been several studies of silicone oil deposition on keratin surfaces using a variety of spectroscopic techniques, including X-ray flourescence (XRF)[71], atomic adsorption[72] and infra-red spectroscopy[73]. Gruber et al[74] utilised XRF spectroscopy to quantitatively determine silicone oil (PDMS) deposition onto Keratin surfaces, (hair) when delivered from a shampoo under standard wash conditions.

Figure 1.2 Oil deposition onto hair shaft

The anionic shampoo developed was a blend of high molecular weight, linear, polydimethylsiloxane gum (PDMS, Dimethicone) and a low viscosity linear PDMS

fluid. The characteristic energy for silicone is 1.74KeV, known as the Kα band. X-ray analysis comes from the first few microns of the surface of the hair. It was noted that the molecular weight of cationic polymer was the largest influencing factor in the deposition rather than polymer composition or charge[74]. This effected the rheology of the shampoo during application, which in turn increased the deposition or retention of silicone droplets onto the keratin. The charge appeared to influence the nature of deposition after multiple shampoo treatments by preventing a build-up of silicone-oil on the keratin fibre. Shampoo containing PDMS displayed significant silicone deposition which continued to deposit after repeated washing. This suggested that silicone was capable of spreading on the hair shaft even though the shampooed hair becomes hydrophilic. This observation is supported by previous studies that observed silicone oils could spread on hydrophilic and hydrophobic surfaces due to a negative spreading parameter[75].

1.10 Objectives of this research

[2]The monodisperse, surfactant-free, PDMS emulsions described in this thesis provide an ideal system for studying the physical and colloidal properties of liquid/liquid dispersions. Since emulsions are extremely important in a number of industrial applications, (see section 1.6), their wetting properties and deposition behaviour is of importance. An understanding of the behaviour and deposition is of practical, as well as fundamental, interest. For example, one should be able to follow droplet deposition as a function of flow regimes and examine whether the emulsion behaves as predicted by DLVO theory.

Depending on the level of added cross-linking monomer in the reaction mixture, (refer to section 1.7), either liquid droplets or microgel-type particles are formed. A microgel particle is a cross-linked particle that can be swollen in size by a good solvent. The study of microgel particles occupies a growing niche in the field of colloid science[76]. Cross-linking will also affect the nature of the PDMS phase. With the addition of cross-linker, it should be possible to change the characteristics of silicone oil, density, viscosity, molecular weight, etc; and hence the emulsion droplets. The effects of the viscosity of the internal liquid phase can alter the motion of a liquid droplet, provided that the O/W interface is fluid in nature. As the PDMS emulsion has no added emulsifier, the droplets present an ideal case for studying droplet motion and impact with a substrate, for example the movement in a stagnation point flow regime.

[2]The PDMS emulsions described above (section 1.7) provide an ideal system for studying the deposition of emulsion droplets onto surfaces. The objective of this thesis was to study the deposition of PDMS emulsion droplets onto solid surfaces by use of the stagnation point flow cell as previously used by Marston[77]. The stagnation point flow cell allows the deposition to be studied under conditions of Brownian diffusion. The solid surfaces used were mica and a variety of chemically modified glass slides. Four specific treatments were investigated, (i) acid cleaned, (ii) 3-aminopropyl trimethoxy silane (APTES) treated glass, to provide a positively charged surface, (iii) Repelcote modified glass to provide a hydrophobic surface and (iv) L-Lysine coated glass to model amino acid composition of hair. The PDMS emulsions were prepared with various diameters and ζ-potentials. The deposition process was studied at various MTMS concentrations, salt

concentrations (different ionic strengths) and substrate chemistry over a period of three hours.

The work presented in this thesis has been motivated by the continuing need to optimise the performance of shampoo formulations. The main objective of this work has been to establish the role that cross-linking density of PDMS, surface charge, surface chemistry and surface roughness play in aiding efficient shampoo adhesion and coating by studying a simple model system. The study of a model system is the best way of gaining an insight into the mechanisms involved in the washing process. The use of rigid substrates, such as glass or mica, can help to eliminate the problems associated with the many surface heterogeneity's found in fibrous materials. Similarly, by using model uniform droplets to represent shampoo emulsion droplets one can remove the issues associated with particle shape and composition. The surface chemistry of glass is such that it can be easily modified to produce a different surface for investigation in the flow cell. The advantage of chemically grafting the polymer to the surface is that the polymer is unable to desorb throughout the course of an experiment, which helps to simplify the system so that the true effects of a polymer coating can be studied. The model droplets chosen for this work were micron-sized cross-linked PDMS droplets. This offers the advantage that their viscosity and cross-linked density can be readily manipulated. This versatility provides the possibility of studying many different particle-substrate systems. Droplets must be large enough to be viewed in the flow cell under the microscope.

Given that the cleaning of hair usually takes place in the presence of an aqueous solution, the most appropriate method for studying the removal of model shampoo

emulsion droplets from a hard surface under liquid flow is the parallel plate flow cell. A flow cell has therefore been developed to provide defined flow conditions under which removal experiments can be carried out. The substrates chosen for this work were glass microscope slides and mica slides. The cell has been specially designed so that the slides can be readily exchanged for each new experiment. The Glass and mica possessed optical transparency which allowed the droplets to be monitored during each experiment

The first objective for the work presented in this thesis was to synthesise model micron sized cross-linked PDMS droplets for use in the flow cell. The second objective was to prepare and characterise the different surface-modified glass and mica substrates. The remaining objectives were to study the deposition and detachment of the model droplets from the different glass and mica substrates in the flow cell, in particular; the effects of substrate chemistry, roughness, droplet cross-linked density, electrolyte and surfactant concentration.

This thesis has therefore been divided into four sections. The first section consists of details of the synthesis and characterisation of cross-linked model droplets. The second section describes the preparation and characterisation of glass and mica substrates. The third and fourth sections describe the stagnation point and horizontal flow cell designs with their corresponding results respectively.

1.11 References

1. Tadros, Th.F, Vincent, B., Encyclopedia of Emulsion Technology (Beecher Ed.), Vol. 1, Chap 3., Marcel Dekker, New York, 1983

2.Schulman, J.H., and Cockbain, E.G., Transactions of the Faraday Society, 36, 651, (1940)

3.Shinoda, K., and Friberg, S.Advances in Colloid and Interface Science, 4, 281, (1975)

4. Prince, L.M.Journal of Colloid and Interface Science, 23, 165, (1967)

5. Prince, L.M., " Microemulsions: Theory and practice, Academic Press, New York, 1977

6. Walstra, P., Encyclopaedia of Emulsion Technology, P. Beecher, Ed., Vol 1, Chap 2., Marcel Dekker, New York, 1983

7. Gopal, E.S.R., Emulsion Science, P. Sherman, Ed., Chap 1., Academic Press, London, 1968

8. Shinoda, K., Journal of Colloid and Interface Science, 24, 4, 1967

9. Shinoda, K., Saito, H. Journal of Colloid and Interface Science, 30, 258, 1969

10. Albers, W., Overbeek, J.Th.G., Journal of Colloid and Interface Science, 14, 501, 1959

11.Boyd, J., Parkinson, C., Sherman, P., Journal of Colloid and Interface Science, 41, 359, 1972

12. Israelachvili, J., Colloids and Surfaces a-Physicochemical and Engineering Aspects 91, 1, 1994

13. Nakashima, T., Shimizu, M., Ceramics, 21, 408, 1986

14. Kandori, K., Kishi, K., Ishikawa, T., Colloids and Surfaces, 55, 73, 1991

15. Peng, S., Williams, R.A., Control of Particulate Processes IV, Delft, Engineering Formulation, New York, 1997

16. Katoh, R., Asano, Y., Furuya, A., Sotoyama, K., Tomita, M., Okonogi, S., Journal of the Japanese Society for Food Science and Technology- Nippon Shokuhin Kagaku Kogaku Kaishi, 44, 44, 1997

17. Nakasima, T. Shimizu, M., Kagaku Kagaku Ronbunshu, 19, 984, 1993

18. Bibette, J., Roux, D., Nallet, F., Physical Review Letters, 65, 2470, 1990

19. McClememts,D.J., Colloids and Surfaces a-Physicochemical and Engineering Aspects 90, 25, 1994.

20. Bibette, J., Roux, D., Nallet, F., Physical Review Letters, 65, 2470, 1990

21. Richetti, P., Kekicheff, P., Physocal Review Letters, 68, 1951, 1992

22. Barchini, R., Saville, D.A., Langmuir, 12, 1442, 1996

23. Bibette, J., Morse, D.C., Witten, T.A., Weitz, D.A., Physical Review Letters, 69, 2439, 1992

24. Calderon, F.L., Biais, J., Bibette, J., Colloids and Surfaces a-Physicochemical and Engineering Aspects 74, 303, 1993

25. Hemar, Y., Herrman, N., Lemarechal, P., Hocquart, R., Lequeux, F., Journal De Physique II, 7, 637, 1997

26. Calderon, F.L., Stora, T., Monval, O.M., Poulin, P., Bibette, J., Physical Review Letters, 72, 2959, 1994

27. Hengelmolen, R., PhD.Thesis, University of Bristol, 1994

28. Tang, K.Q., Gomez, A., Journal of Colloid and Interface Science, 175, 326, 1995

29. Tang, K.Q., Gomez, A., Journal of Colloid and Interface Science, 184, 500, 1996

30. Cloupeau, M., Prunetfoch, B., Journal of Electrostatics, 25, 165, 1990

31. Cloupeau, M., Prunetfoch, B., Journal of Electrostatics, 25, 1021, 1994

32. Panagiotou, T., Levendis, T.A., Journal of Applied Polymer Science, 43, 1549, 1991

33. Stöber,W., Fink, A., Bohn, E., Journal of Colloid and Interface Science, 26, 62, 1968

34. Vanderhoff, J., Journal of polymer Science: Polymer Symposium 72, 161, 1985

35. Goodwin, J.W., Hearn, J., Ho, C.C., Ottewill, R.H., Colloid and Polymer Science, 252, 464, 1974

36. Fitch, R.M., Tsai, C.H., Polymer Colloids, R.M.Fitch, Ed., Vol 1, Plenum Press, New York, London, 1971

37. Davies, J.T., Rideal, E.K., Interfacial Phenomena, 2nd Ed., Academic Press, New York, 1963.

38. Davies, J.T., Haydon, D.A., Procedures of the second International Congress on Surface Activity1, 417, 1957.

39. Vermeulen, M., Joos, P., Ghosh, L., Journal of Colloid and Interface Science, 140, 41, 1990

40. Miller, C.A., Colloids and Surfaces, 29, 89, 1988

41. Kaminski, A., McBain, J.W., Procedures of the Royal Society, London, Series A, 198, 447, 1949

42. Cumming, A., Wiltzius, P., Bates, F.S., Physical Review Letters, 65, 863, 1990

43. Krishnamurthy, S., Goldburg, W.I., Physical Review A 22, 2147, 1980

44. Chapat, M., Colloids and Surfaces a-Physicochemical and Engineering aspects 91, 57, 1994

45.Israelachvili. J., Colloids & Surfaces A; Physiochemical & Engineering aspects, 91, 1, 1994

46. Wegner, M., M.Sc. Thesis, University of Bristol, 1993

47. Anderson, K.R.,Obey, T.M., Vincent, B., Langmuir, 10, 2493, 1994

48. Smith.J.R., Swift.J.A.,J.Microsc., (Oxford) 204(3), 203-211.

49.Minnesota Microscopy Society Web site, maintained by Stuart McKernan

50. Leveque.J.L, Elsner.P, Berardesca.E, Maibach.H.I, (Eds), Bioengineering of the skin: Water and the stratum corneum, (CRC Press, Boca Raton)

51. Chatt.A., Katz.S.A, "Hair analysis; applications in the biomedical and environmental sciences" VCH

52. Robbins, C.R., "Chemical and physical behaviour of human hair", Van Nostrand Reinhold Co., New York, 1979, p.22
53. Rheinwald, J.G., Green.H., Serial cultivation of human epidermal keratinocytes; the cell formation of keratinizing colonies from single cells. Cell, 6, 331, 1975
54. Wester,R.C., Mailbach.H.I., Individual and regional variation with in vitro percutaneous absorption. In: Bronaugh, R.L. (ed.) In vitro Percutaneous Absorption: principles, Fundamentals and Applications, CRC Press, pp 25-30.
55. Perwuelz.A., DeOlivera.T.N., Caze.C., Colloids.Surf.A., 147, 317, 1999
56. Martinsen.G., Grimnes.S., Kongshaug.E.S., Medical & Biological Engineering & Computing, 35, 177-180, 1997
57. Watt.I.C., J.Macromol.Sci.Rew., Macromol.Chem.2, pp.169-245.
58. Green.H.C., United States Patent, 2, 826, 551, 1958
59. Berthiaume,M.D., in Goddard.E.D, Gruber.J.V., (Eds) Principles of polymer science and Technology in Cosmetics and personal care, Marcel Dekker, New York, 1999, pp.275-324
60. Rosen.M.R., Drug Cosmet.Ind. 163,1998,28
61. Larrey.M.D., Quaglino.V., Ricca.J.M, Rogasik.S., Soap.Perf.Cosmet. 33, 1997
62. Lochhead.R.Y., Soap Cosmet.Chem.Spec., 42, 1992
63. Halloran.D.J., Soap.Cosmet.Chem.Spec., 22, 1992
64. Yahagi.K., J.Soc.Cosmet.Chem., 43, 275, 1992
65. Starch.M.S., Soap Cosmet Chem. Spec, 34, 1986
66. Gerdes.S., Cazabat.A.M., Strom.G., Tiberg.F., Langmuir, 14, 7052, 1998
67. Gerdes.S., Cazabat.A.M., Strom.G., Langmuir, 13, 7258, 1997
68. Hill.R.M., Burow.R.F., ASTM Spec.Tech.Publ.STP. 1328, 226, 1997
69. Berthiaume.M.D., Jachowicz.J., J.Colloid.Inter.Sci., 141, 299, 1991
70. Jachowski.J., Berthiaume.M.D., J.Colloid Inter. Sci.133, 118, 1989
71.Smedt.De.A.,Reeth.I.V.,Marchioretto.S.,Glover.D.A.,Naud.Cosmet.Toilet.112, 39,1997
72. Gooch.E.G., Kohl.G.S., J.Soc.Cosmet.Chem. 39, 383,1988
73. Klimisch.H.M., Kohl.G.S., J.soc.Cosmet.Chem., 38, 247, 1987
74. Gruber.J.V., Lamoureux.B.R, Joshi.N., Moral.L., Colloids & Surfaces B: Biointerfaces, 19, 127-135, 2000
75. Cazabat.M.A., Gerdes.S., Valignat.M.P., Villette.S., Int.Sci., 5, 129, 1997
76. Saunders, B.R., Vincent, B., Colloid and Polymer Science, 275, 9, 1997

Chapter 2: O/W emulsions; inter-droplet interactions

2.1 Introduction

There are three classical interactions between colloidal particles[1]. These include; *van der Waals* forces or electromagnetic inter-particle interactions, resulting almost entirely from London dispersion forces present in the charge fluctuations of polarised molecules, *steric forces* created if adsorbed molecules, polymers, at the particle-solvent interface, *electrostatic forces* produced from the interaction of particle electrical double layers.

2.1 Electrical double-layer (EDL)

The surface charge of an oil droplet in water is acquired through the ionisation of groups at the oil/water interface of the droplet. This surface charge will affect the distribution of ions near the surface in the aqueous phase. This arrangement of ions near the surface leads to the formation of an electric double layer, as first described by Gouy and Chapman[2,3].

The "electrical double layer" (EDL) is the name commonly given to the ionic atmosphere in the vicinity of an electrically charged surface which is in contact with an electrolyte. Ions of opposite charge to the surface (counter-ions) are attracted towards the surface and those of like charge (co-ions) are repelled from the surface.

Stern[4] proposed that the EDL consists of two distinct regions. The inner region (or "Stern layer") comprising of tightly bound ions, sufficiently strongly attached to the

surface, by electrostatic and/or van der Waals forces, to be unaffected by thermal motion. In the outer ("diffuse") region the ionic distribution is influenced by a combination of electrostatic and thermal mixing forces. The arrangement of ions in the EDL, along with the resultant electrical potential, ψ, is shown schematically in figure 2.1.

Grahame[5] first proposed the concept of the " inner Helmholtz plane", located at a distance from the surface equal to the radius of the specifically adsorbed ions. These ions are dehydrated (in the direction of the surface) on adsorption. The "outer Helmholtz layer" , or "Stern plane", lies at a distance equal to the radius of adsorbed hydrated ions.

Fig 2.1 Schematic representation of "EDL" structure

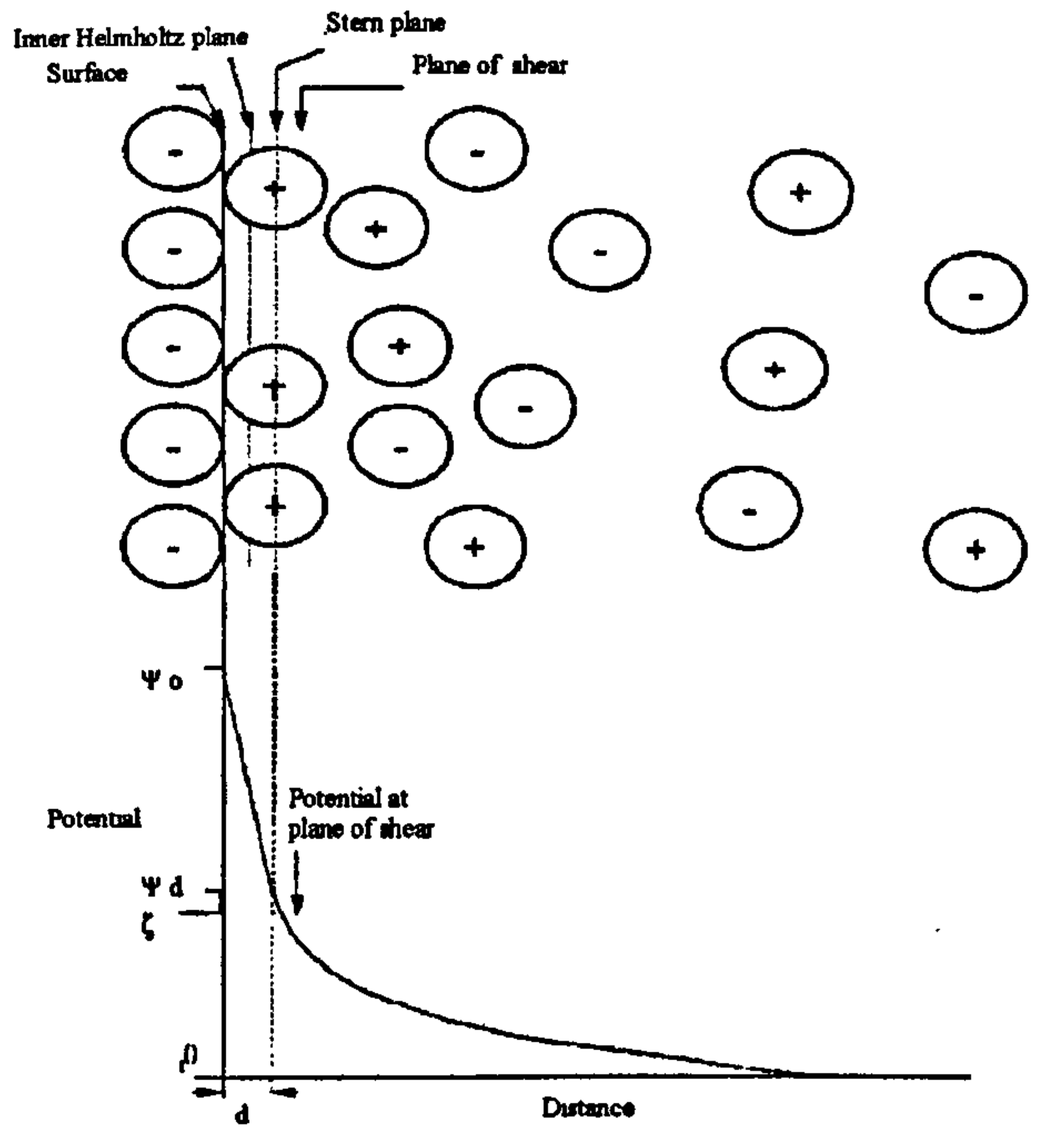

Figure 2.1 depicts the structure of the double layer. The electric double layer has been extensively discussed[5,6], and only a brief description is given here. The double layer is made up of the surface charge (σ_o) giving rise to a surface potential (Ψ_o) and a diffuse layer. There may be a layer of counter ions specifically adsorbed next to the surface in the aqueous phase (the Stern layer). The potential at this point has a value Ψ_d. This is usually experimentally determined as the zeta potential (ζ)[6]. This is the measured potential at the plane of shear as the surface moves in an electric field. The distribution of ions in the bulk phase surrounding the surface forms the diffuse layer. It is assumed that the potential decreases exponentially away from the Stern layer. The potential in the diffuse layer is described by equation [2.1];

$$\Psi = \Psi_d \exp^{(-\kappa x H)} \qquad [2.1]$$

Here H is the distance from the surface, $^1/\kappa$ is the Debye-Hückel length, which depends on the permittivity of the medium and the electrolyte concentration. The Debye-Hückel length is the extension of the double layer and is given by the expression [2.2]:

$$^1/\kappa = \frac{(\varepsilon_r \varepsilon_o kT)\ ½}{(2e^2 N_A c z^2)} \qquad [2.2]$$

where ε_r is the dielectric constant of the medium, ε_o the permittivity of free space, k the Boltzmann constant, T the absolute temperature, N_A Avogadro's number, e the electronic charge, c the bulk concentration of electrolyte and z the valency of the ions. The size of the surface charge and the nature and extent of the electric

double layer determines the electrostatic repulsion between the droplets and also determines many experimental observations , e.g electrokinetic effects, refer to section chapter 5. It could be noted that as the electrolyte concentration increases, the extension of double layer decreases. For 1:1 electrolyte $^1/\kappa$ is of the order of about 1nm for a 10^{-1} mol dm^{-3} solution and 10nm for a 10^{-3} mol dm^{-3} solution.

The interaction energy, V_E, resulting from the overlap of the diffuse parts of the electric double layer of two identical particles of radius a, can be calculated from the following expression, for large κa[7],

$$V_E = 2\pi a\varepsilon\varepsilon_0 2\ln(1+\exp[-\kappa H]) \qquad [2.3]$$

where H is the shortest distance between the two surfaces and ε is the permittivity of the dispersion medium. From equation 2.3 it is apparent that V_E at a distance H depends on the value of κ. Note that this interaction is repulsive for two identical overlapping double layers. The electrical potential decreases across the Stern layer, from Ψ_o at the surface to Ψ_d at the Stern plane itself. The concepts of the plane of shear and ξ-potential will be discussed later in this chapter.

Quantitatively models of the EDL have been presented by a number of authors, most notably Gouy[2] and Chapman[3], Derjaguin and Landau[8], Verwey and Overbeek[9]. However, there will be no discussion here of these classical contributions. The electrical double layer repulsive force for two different spherical particles, V_E, can be expressed as:

$$V_E = \frac{-2\pi \varepsilon r_1 r_2 \kappa}{r_1 + r_2} \frac{\{\Psi_1\Psi_2 + \Psi_1^2 + \Psi_2^2\}}{\{\exp(2\kappa H) - 1\}} \qquad [2.4]$$

where r_1, r_2 are the individual radii, Ψ_1, Ψ_2 are the respective surface potentials, H represents surface-surface distance, ε is the dielectric constant of fluid medium and κ is the inverse of double layer thickness

2.2 London-van der Waals Interactions

Van der Waals forces arise from dipole-dipole (Keesom) interactions, dipole-induced dipole (Debye) interactions, and fluctuations in the electronic fields of atoms and molecules (dispersion or London interactions). The simpler microscopic[10] rather than macroscopic[11] theoretical calculation approach was used in this study to calculate V_A. The attractive interactions in this system mostly result from EDL forces rather than van der Waals forces. This approach was later extended by de Boer[12] and Hamker[6] who assumed that the interactions between the individual atoms or molecules, within each particle, are additive. The total van der Waals energy of interaction, V_A, was therefore calculated by summation (or integration) over all the pairs of molecules in the two interacting particles. Hamaker derived the interaction energy (V_A) between two identical droplets of radii a, provided that the surface to surface distance is small (i.e. H << a) to the following expression[3];

$$V_A = \frac{-A_{12}\, a}{12\, H} \qquad [2.5]$$

A_{12} is the effective Hamaker constant. The Hamaker constant can be calculated

from dielectric data of a material over a wide frequency range[13,14]. In the above equation A is the Hamaker constant, which is related to the polarisability of the molecules comprising of the particles through,

$$A = {}^{4}/_{3}\ \pi^2 q^2 \alpha_o^2 h\, \upsilon_o \qquad [2.6]$$

In this equation, q is the number density of the constituent molecules, α_o is the static polarisability of the molecule, h is Planck's constant and υ_o is the frequency of electronic fluctuations of the material. In the case of like particles, both of material 1, equation [2.6] may be simplified to the form;

$$A = (A_{22}^{1/2} - A_{33}^{1/2})^2 \qquad [2.7]$$

where A_{22} and A_{33} are the Hamaker constants for the particles and for the solvent interactions, respectively.

The van der Waals force for two identical spheres acting across a medium is attractive, as A_{23} is always positive. The first term of equation [2.6] is the zero-frequency term. For media dispersed in water this is the dominant term. This is because water has a high static dielectric constant ($\varepsilon \approx 80$) whereas the dielectric constant for PDMS is much lower ($\varepsilon \approx 1.9$)[12]. This, added to the non-zero (dispersion) frequency term (the second term of equation 2.5), gives a total value of $A_{PDMS\text{-}water}$ of 0.35×10^{-20} J at 300 K. The Hamaker constant for D_4, the major constituent of the silicone phase, is estimated from refractive index data[15] is 5×10^{-20} J. The Hamaker constant decreases with increasing distance from the surface of the droplet. This is known as the retardation effect and is due to a fast

decay in the dispersion energy between two atoms as separation increases. Electrostatic screening can also affect A_{12} by reducing the zero frequency contribution. This is due to the electrostatic fields of the interacting atoms being screened by polarising ionic charges in the medium.

Casimir and Polder[16] and Schenkel and Kitchener[17] later extended the approach to make allowance for the finite time required for propagation of the electromagnetic field between the two particles. This "retardation effect" reduces the attraction and becomes important for $H \geq \lambda$ (the wavelength of the field). Despite this correction, the accuracy of the microscopic approach is limited because of the inherent assumptions. These include the pairwise additivity of intermolecular forces, the dominant contribution of a single characteristic frequency (usually in the ultraviolet region), and the modulation of the electromagnetic radiation in the liquid medium by the inclusion of a single, high frequency dielectric constant.

2.3 Interaction energy, V_T

Derjaguin and Landau[8], Verwey and Overbeek[9] independently proposed that the total interaction energy between two charged particles (no adsorbed polymer), V_T, may be regarded as the sum of the van der Waals interaction energy, V_A, and the interaction energy due to the overlap of the electrical double layers, V_E:

$$V_T = V_A + V_E \qquad [2.8]$$

In the case of PDMS emulsions the forces to consider are the attractive van der Waals forces and the repulsive interaction forces between the two charged

electric double layers. The "DLVO" theory is central to the subject of colloid stability, and is usually interpreted in terms of V_T versus H curves as shown in figure 2.2.

The electrostatic interaction decays exponentially with distance, with a range of the order $1/\kappa$, and the van der Waals interaction decreases as an inverse power of the inter-particle distance. It can be seen that van der Waals attractive predominates at small and at large inter-particle distances. At intermediate distances the electrostatic term dominates, for low electrolyte concentrations

Figure 2.2 Schematic of the potential energy curves for two identical emulsion droplets

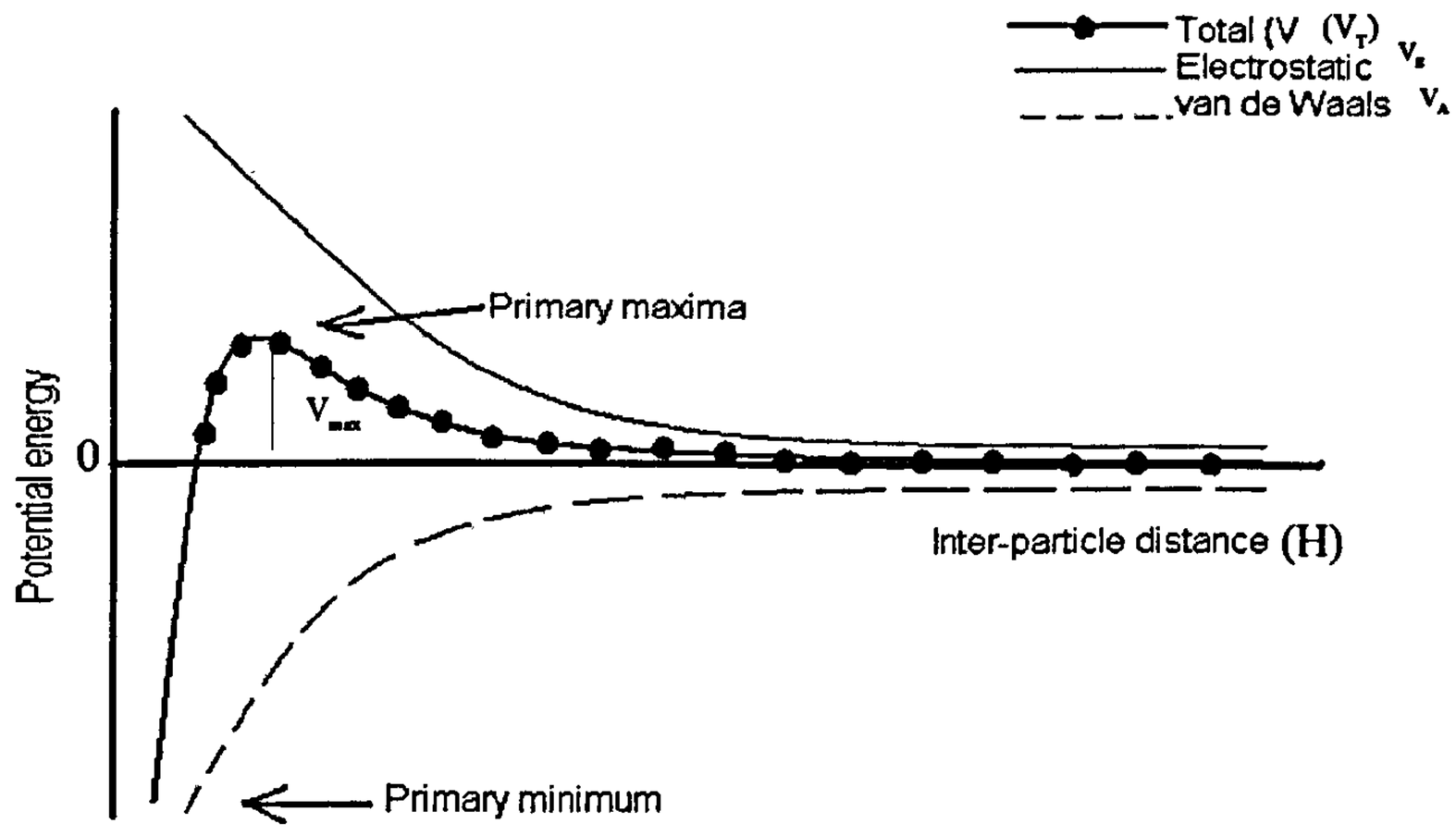

If the primary maximum, shown in the total potential energy curve, is large compared with the thermal energy, kT, of the droplets, the emulsion should be stable. This maximum depends on the value of ψ_0, and upon the range of the

force, i.e. upon 1/κ. If it is not large enough, 25 kT and below, then the emulsion will coagulate and the system will enter the primary minimum (at very small values of H)[18]. Droplets in the primary minimum will be irreversibly coagulated. It can also be noted that there is a secondary minimum at much larger inter-particle distances, which, if it is sufficiently deep, may give rise to reversible coagulation.

An electrolyte acts as a screen for surface charge and so increasing the concentration of electrolyte will decrease the electrostatic repulsion. There exists a critical concentration at which coagulation will occur when the primary maximum is insufficient to ensure droplet stability. Thus, to improve the colloid stability of a dispersion, one needs to increase the surface potential and decrease the electrolyte concentration. The height of the energy barrier, V_{max}, determines the rate constant for particles coagulating in the primary minimum. If $V_{max} >> kT$ (the thermal energy) the particles will not have enough to overcome the barrier, and so the dispersion will be stable in the kinetic sense. If the secondary minimum depth is greater than the thermal energy the dispersion may exhibit weak (reversible) flocculation. The form of the curve will depend upon the size, shape and the material of the particles, and also upon the dispersion electrolyte concentration.

2.4 Steric stabilisation effect on van der Waals and EDL

Emulsions can also be stabilised by adsorbed polymer or surfactant at the O/W interface. At equilibrium, adsorbed molecules may protrude into the continuous phase (all adsorbed polymer layers have a "tails and loops" morphology). When two droplets approach each other a repulsive force is generated when these two layers interact. This stabilising effect is known as steric stabilisation.

The Bancroft rule stated that the stability of an emulsion was dependent on solubility of a surfactant in the continuous phase"[10]. This theory was later developed by Griffen et al [11, 19] who introduced a numerical scale to determine the probability of a surfactant to form W/O or O/W emulsions, referred to as the Hydrophile-Lipophile Balance (HLB).

PDMS / water emulsion droplet stability is provided by a fraction of the oil phase behaving as an in-situ surfactant. This resides in the PDMS droplet with the charged end groups residing at the interface. Thus, two droplets approaching each other will only be subjected to electrical and van der Waals type of interactions. Steric interactions, in this instance, can be ignored.

The adsorption of polymeric species onto either or both surfaces can prevent the close approach of the two bodies, which in turn modifies the van der Waals forces, V_A, and electrostatic interaction energy, V_E, see figure 2.3. Changes in the latter may arise from a combination of effects, including the surface charge density, σ_0, and the displacement of the plane of shear from the surface by a distance, δ, (polymer layer thickness), see figure 2.1. The steric interaction energy term can be incorporated into the total interaction energy expression as follows;

$$V_T = V_A + V_E + V_S \qquad [2.9]$$

Figure 2.3 Simplified schematic representation of interaction curve in the presence of high neutral homopolymer coverage, in a good solvent.

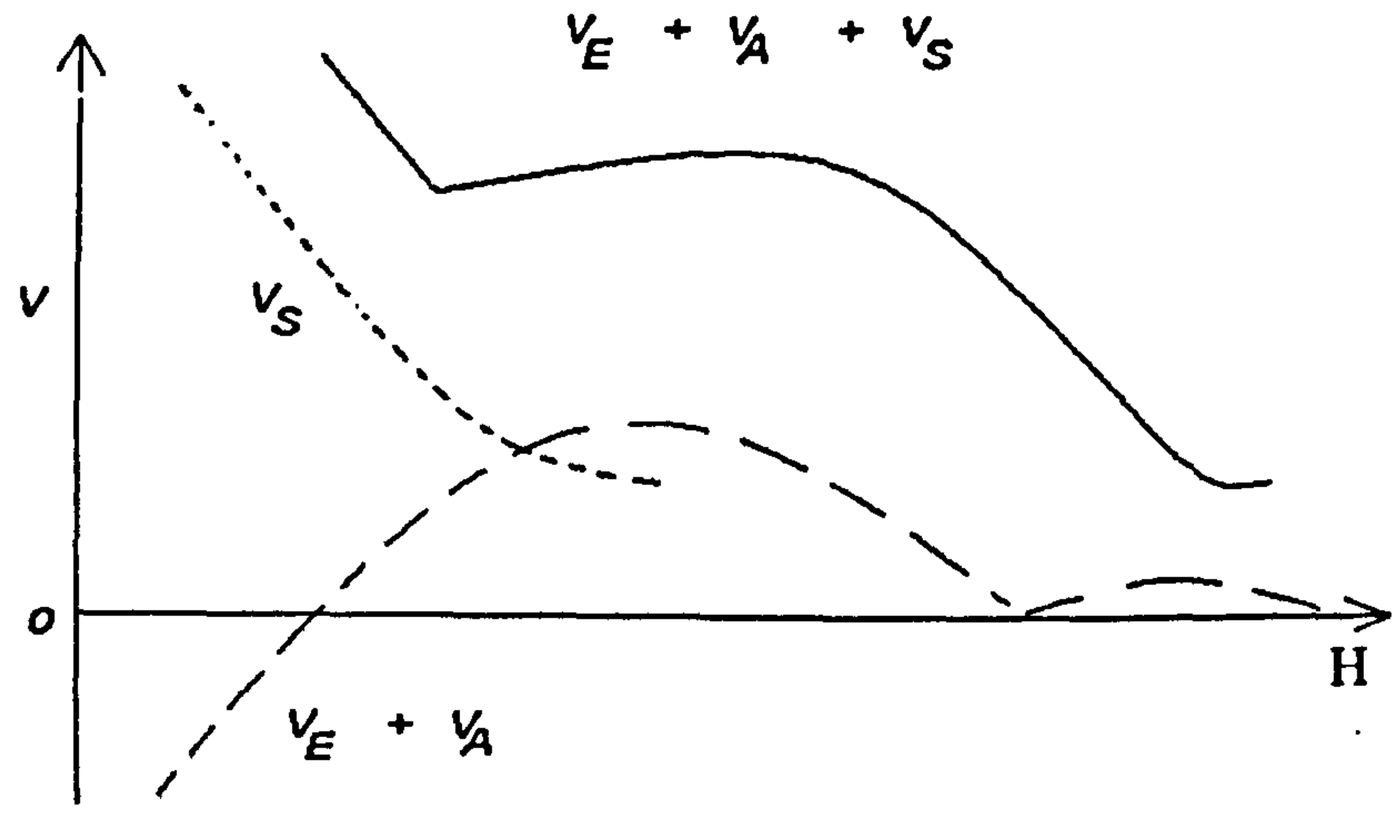

Vincent[18] extended the van der Waals forces theory proposed by Vold[19] for composite particles with an adsorbed polymer layer and its surrounding solvent. This extension assumed that the particles, adsorbed polymer and surrounding solvent have a uniform Hamaker constant, A_{33}. If $A_{33} = A_{22}$, then Vincent suggested that the polymer layer could be treated as a solvent sheet of thickness, δ. However, if A_{33} is < or > A_{22} then V_A is increased in magnitude. It should be noted that this effect was quite small for high molecular weight adsorbed polymers.

In addition, Vincent[20] later calculated V_E for distances of separation $H > 2\delta$, where δ was the thickness of polymer layer. In this case, the potential at the outside of the double layer, ψ_d, which is usually equated with the ζ-potential ζ, replaced ψ_0 or ψ_d in the standard equation 2.3. It should also be noted that $(H - 2\delta)$ was used instead of the inter-particle distance, H. Therefore the previous electrostatic

expression could be extended for two polymer-coated particles with similar double layers as shown in equation 2.10;

$$V^{s}_{E} = 2 \varepsilon \varepsilon \pi_0 (a+\delta) \Psi_\delta \ln (1+\exp[-\kappa (H-2\delta)]) \qquad [2.10]$$

If $H < 2\delta$, the expression for the electrostatic interaction energy is more complex due to "steric" forces. The total steric interaction, V_s, was shown to arise from three effects, V_{el}, V_{ads} and V_{mix} and can be expressed by equation 2.11.

$$V_S = V_{el} + V_{ads} + V_{mix} \qquad [2.11]$$

The "elastic" or "volume restriction" effect, V_{el}, disturbs the conformations of the adsorbed chains, causing a loss of configurational entropy and a repulsive effect, (i.e., V_{el} is positive). The "adsorption" attractive effect, V_{ads}, occurs if the polymer coverage is low as the polymer chains form bridges between two approaching particles, causing the V_{ads} to always be negative. Finally, the "osmotic" or "mixing" effect, V_{mix}, arises as H decreases and displaces the solvent from the interfacial region to the bulk. The V_{mix} value is dependent on the polymer-solvent interaction energy, or Flory-Huggins parameter, c. Therefore V_{mix} is positive in a good solvent, ($c < 0.5$), or negative in a poor solvent ($c > 0.5$). However, when $H < 2\delta$, the V_E value is usually much smaller than V_T and can therefore be ignored. Therefore, no evaluation of these effects on the V_s value will be discussed in this thesis.

2.5 Thin film thinning / Droplet Coalescence

Emulsions have an additional instability, compared with solid colloidal particles,

namely coalescence. When two droplets come into close proximity with one another by Brownian collisions, coagulation or creaming / sedimenting, a thin liquid film of the dispersion medium forms between the two interfaces[21]. This film will drain to a metastable thickness depending on a complex process involving hydrodynamics and interfacial interactions . Disruption and elimination of the film will result in the two droplets uniting together into a single droplet. If the film is unstable then coagulation will always result in coalescence.

Figure 2.4 shows the general features of the lamella between two PDMS droplets. The PDMS-water-PDMS film can be considered as a type B_1 film as defined by Hunter[1]. In the case where the radius of the droplets is large when compared to the separation distance, b, then the Derjaguin approximation[22] is applicable. Under these conditions, elements on each sphere interact as parallel plane elements at the same separations and therefore the total interaction is a sum over the infinitesimal elements. P(b) is defined as the normal pressure in a film of thickness b, and $P(\infty)$ is the normal pressure in a film where the interaction energy across the film is zero. In this case, $P(\infty)$ is equivalent to the isotropic pressure in the adjacent bulk phase P(o). The interfacial layers are the regions of thickness δ in the film where the electrical double layer applies, i.e the presence of an interfacial structure, see figure 2.1.

Fig 2.4 Diagrammatic representation of the thin film and border regions between two PDMS droplets[18]

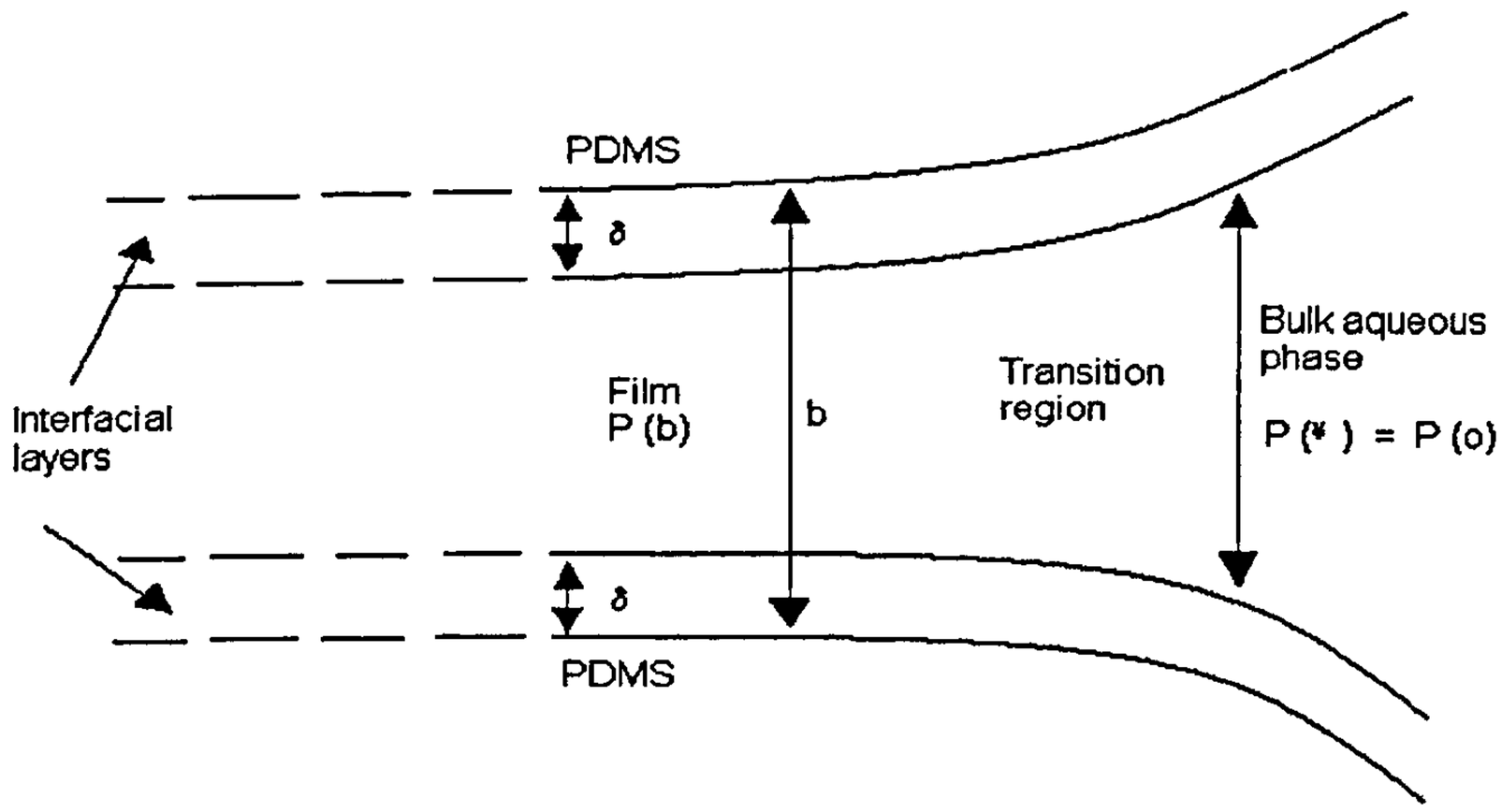

2.6 Thermodynamics of film thinning

Emulsion coalescence is a thermodynamically favourable process (as opposed to emulsion formation). The variation in the free energy of the film is dependent on the interactions described by DLVO theory, see section 2.1, due to the fact that as the film thins, so the surface area of the droplets must increase. If a surfactant is present this results in an increase in the interfacial tension, which is unfavourable to the process. If the approaching droplets have sufficient kinetic energy to surmount this free energy barrier then they will coalesce. If this barrier is sufficiently high then the emulsion droplets will remain in the coagulated state. In addition to the surface forces of intermolecular origin, two colliding droplets in a liquid medium will also experience hydrodynamic interactions due to the viscous friction of the thinning film.

2.7 Forces acting across a thin film: disjoining pressure

For a coagulated pair of droplets there are two stable film thicknesses. These exist when the film is sitting in either the primary or the secondary minimum. The variation of the potential energy of interaction with film thickness is dependent on the van de Waals attractive forces and electrostatic repulsive forces (as for coagulation) with an additional very close range repulsive force. This force is only significant when a film that is in the primary minimum tries to thin further (i.e b< 2δ), see figure 2.3. It is normally a very steep repulsive force, usually associated with the molecules adsorbed in the interfacial areas. In the case of the PDMS/water films, the rigidity without adsorbed polymers or surfactants at the interface is very low. As discussed in section 2.3 there are no steric interactions as such. Most of the hydrodynamic pressure exists in the interior of the film. This pressure, acting normal to the plane of the film is called the disjoining pressure[23].

The excess normal pressure (P(b)-P(o)) in the film is balanced by the disjoining pressure, $\pi(b)$. A film will tend to thin spontaneously until $\pi(b)$ is zero (in the primary or secondary minima). The disjoining pressure can be considered to be made up from the contributions listed in section 2.4:

$$\pi(b) = \pi_A(b) + \pi_E(b) + \pi_S(b) \qquad [2.12]$$

The disjoining pressure is made up of van de Waals (π_A), electrostatic (π_E) and steric (π_S) contributions. A stable film has a positive disjoining pressure, such as $\pi_E + \pi_S > \pi_A$. Other forces, such as gravity, may also act on the film, but , in the case

of a horizontal film, these can be ignored. In the transition zone P(b) < P(o) (π(b) is negative) due to the high interfacial curvature in the region. Here P(b) is lower than P(b) in the film so liquid tends to get sucked into the transition region from the film by a capillary force acting parallel to the flat interfaces. This does not affect π(b) as the disjoining pressure is described normal to the film.

Another method by which the forces acting on a thin film can be described is through the interfacial tension, which contributes to a tangential pressure P_t across the film. It should be noted that the interfacial tension in the film is not the same as for a bulk phase as the film is under stress. As a film thins, the area increases. As the interface expands so the tension increases due to a reduction in absorbed amount. The presence of adsorbed surfactants utilises the Gibbs-Marangoni effect to restore equilibrium. This is achieved by a combination of adsorption of more surfactant from the bulk to replenish the interface (Gibbs effect) and flow of the monolayer along the interface driven by the tension gradient (Marangoni effect).

It should be noted that the mere fact of the existence of a metastable states does not guarantee that the film will actually reach this state. Therefore, the concept of kinetic stability is used to denote the resistance of the film against rupture, the major factor providing kinetic stability of emulsions is the presence of adsorbed surfactant monolayers at the droplet surface.

2.8 Hydrodynamics of film thinning

The rate at which a film flows from between two droplets can affect the rate of

coalescence, however the deformation of the droplets makes hydrodynamic flow difficult to measure. The radial flow of liquid exerts a shearing force, which will lead to internal circulation within the droplet. As a result a phenomenon known as " dimpling" can occur, see figure 2.5.

Fig 2.5 Schematic representation of the "dimple" between two emulsion droplets

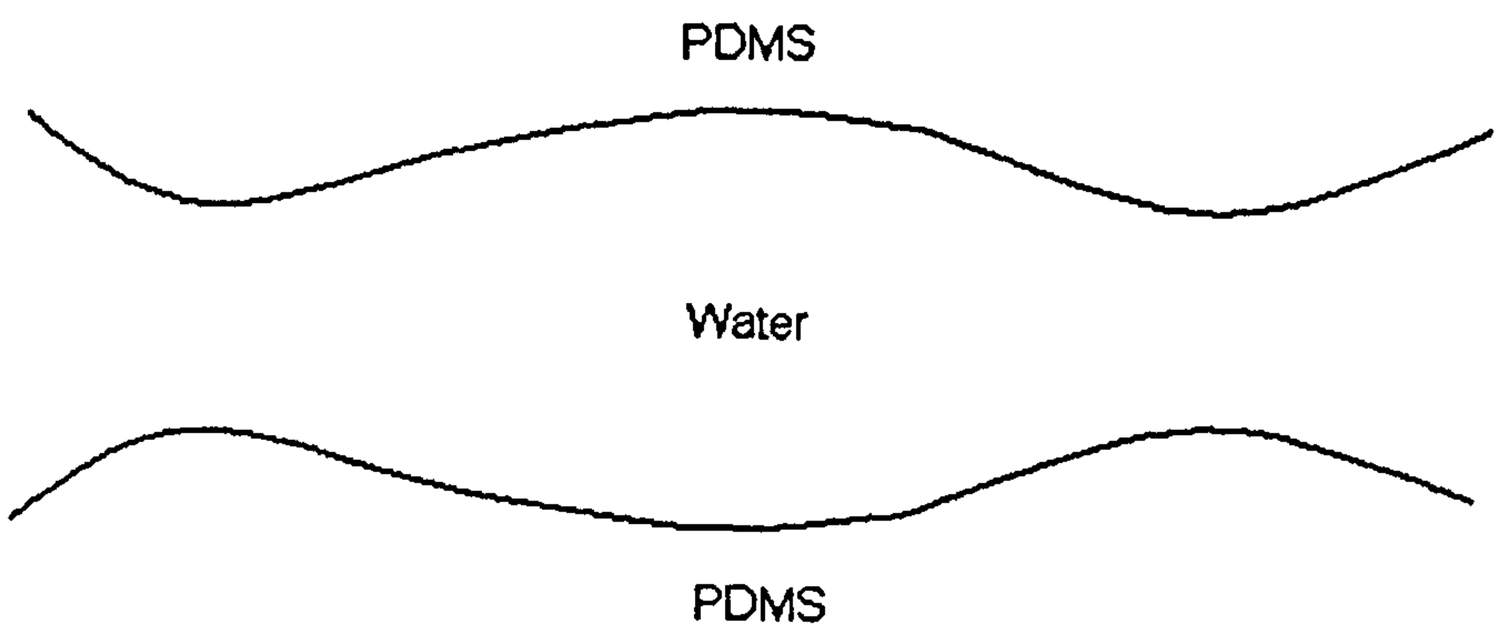

The figure above shows the thinnest region of a dimple does not necessarily occur along the axis of approach. Instead, it may occur at the periphery of the contact zone. Dimpling is lessened by the presence of an adsorbed surfactant or polymer at the interface, which causes increased rigidity. The dimple does not usually occur for small drops (diameter <1 μm) and instead a planar film will form[21]. The rate of film thinning was reported by Reynolds[24] who solved the Navier-Stokes equation and found a relation between the droplet velocity and the driving force, neglecting gravitational and inertia forces. A good summary of this is given by Hunter[1].

2.9 Film rupture

Thermal or mechanical fluctuations in the film thickness may occur in the region of closest approach. These waves can grow in magnitude until, at the point of closest approach the apexes may join, causing coalescence. Reduction in the film thickness results in increased van de Waals attraction, which causes more thinning with the ultimate disruption of the whole film. This will occur if the attractive contribution outweighs the electrostatic repulsion and the opposing increase in the interfacial tension due to expansion, i.e;

$$\frac{d\Pi_A}{db} > \frac{d\Pi_E}{db} + \frac{d\Pi_\gamma}{db} \qquad [2.13]$$

If the condition expressed in equation 2.12 is met then the film is unstable; the fluctuation will grow and rupture occurs. This will tend to occur at a critical film thickness.

2.10 References

1. Hunter, R.J., Foundations of Colloid Science, vol 2, Clarendon Press, Oxford, 1991

2. Gouy, G., Journal of Physical Chemistry, 9, 457, 1910

3. Chapman, D.L., Philosophical Magasine, 25, 475, 1913

4. Stern.O, Z. Electrochem. 30, 508, 1924

5. Grahame.D, Chem.Rev, 41, 441, 1947

6. Hamaker, H.C., Physica, 4, 1058, 1937

7. Hunter, M.J, Hyde, J.P, Warrick E., Fletcher.H, Journal of the American

Chemical Society, 68, 667, 1946

8. Derjaguin, B.V., Landau, L., Acta Physiochem USSR 14, 633, 1941

9. Verwey, E.J.W., Overbeek, J.Th.G., Theory of the Stability of Lyophobic Colloids, Elsevier, Amsterdam, 1948

10. Bancroft, W.D. Journal of Physical chemistry, 17, 514, 1913

11. Griffen.J, Journal of the society of Cosmetic chemists, 1, 311, (1949)

12. J.H.de Boer, Trans Faraday Soc, 32, 10 (1936)

13. Gregory, J., Advances in Colloid and Interface Science 2, 396, 1969

14. Israelachvili, J., Intermolecular and Surface Forces, 2nd Ed., Academic Press, London, 1991

15. Clever, H.L., Taylor, M.L., Journal of Chemical and Engineering Data, 16, 91, 1971

16. H.B.G.Casimir, D.Polder, Nature, 158, 787, (1946)

17. J.H.Schenkel, J.A. Kitchner, Trans. Faraday Soc., 56, 161, (1960)

18. Tadros, Th.F., Advances in Colloid and Interface Science, 46, 1, 1993

19. Griffen, J., Journal of the Society of Cosmetic chemists, 5, 249, (1954)

20. Vincent.B, Obey.T.M, Journal of Colloids & Interface.Science, 163, 454, 1994

21. Ivanov, I.B., Kralchevsky, P.A., Colloids and surfaces A: Physiochemical and Engineering Aspects 128, 155, 1997

22. Derjaguin, B.V., Kolloid – Zeitshrift, 69, 155, 1934

23. Derjaguin, B.V., Obuchar, E.,Journal of Colloidal Chemistry, 1, 385, (1935)

24. Reynolds.O, Philosophical Transactions of the Royal Society, 177, 157, (1886)

Chapter 3: PDMS Emulsions

3.1 Introduction

Silicones are generally synthesised by the hydrolysis of the highly reactive Si-Cl bond[1] as shown in figure 3.1. The silicones made by the reaction in figure 3.1 can be either linear or cyclic. One of the most commonly investigated silicone polymers is polydimethylsiloxane (PDMS). This and other silicone polymers are widely used in the manufacture of cosmetics, food-processing materials and medical preparation. They are highly valued for their lubricity, their low surface energy and their ability to act as antifoaming agents. PDMS has the basic structure shown below.

Fig 3.1: General synthesis of silicones

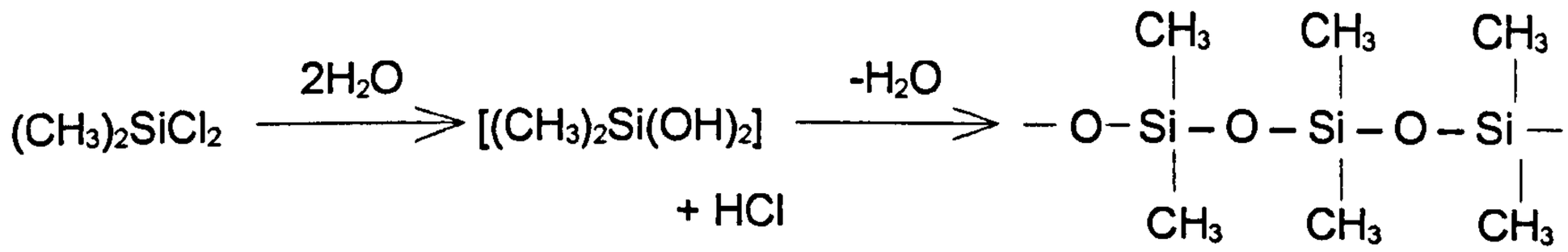

Siloxane components are described using a nomenclature comprising of four letters; *M,D,T,Q,* which represent $R_3Si(O_{0.5})$, $R_2Si(O_{0.5})_2$, $RSi(O_{0.5})_3$ and $Si(O_{0.5})_4$ respectively. R represents a methyl group. Alternative monomers can be used e.g, dimethyldiethoxysilane DMDES, $(CH_3)_2Si(OC_2H_5)_2$ which is the starting monomer used in this work. The hydrolysis and polymerisation of this monomer was first described in 1945[2]. Hydrolysis, in acidic alcohol, results in mainly cyclic polymers

being produced. It was noted that the proportion of cyclic to linear, (from 15%-70% cyclic) polymers could be altered by changing the reaction conditions. The cyclic polymers formed contain a minimum of 3D units linked together in the form shown in figure 3.2.

Figure 3.2 The general structure of cyclic silicones, D_4 unit

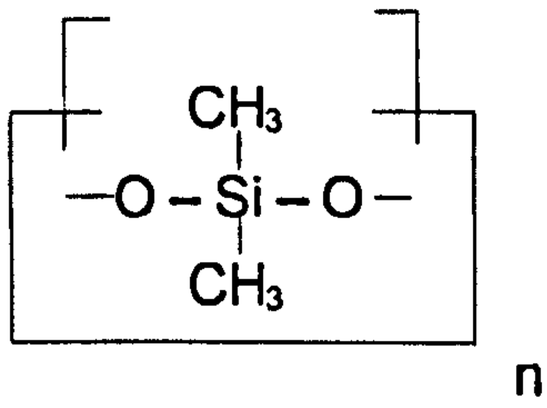

Kippling[3] and later Patnode[1] found cyclo-octamethyltetrasiloxane (D_4, n=4 in figure 3.3) to be the predominant molecule formed in the hydrolysis reaction (~47% of the product). As a result of the larger size of the silicon atom, and the nature of the Si-O bond, larger rings are allowed with silicon compared to carbon chemistry. These cyclic molecules and low molecular weight silanols (PDMS with -OH end groups) are used as intermediates in the synthesis of higher molecular weight polymers. In fact, D_4 is the most commonly used oligomer for the production of higher molecular weight silicones[4,5]. It readily reacts with hexamethyldisiloxane (M_2) in concentrated sulphuric acid at room temperature, or with tetra-alkylammonium hydroxides at 80°c in what is termed "linearisation" of the siloxanes. If D_4 is dispersed in aqueous media by a quaternary ammonium hydroxide, it acts as a catalyst, then very high molecular weight silicones are obtained[6,7]. The resulting silicone emulsion is stable and of a small droplet size. Such silicone emulsions can be employed as released agents or as coating compositions. The silicone polymers can be extracted at the end of the

polymerisation by breaking the emulsion. The use of silicone in personal care products has been well documented. Their low toxicity, low volatility, chemical inertness and excellent spreading properties allow siloxanes to be utilised in several industrial formulations. These include shampoos, conditioners, hair sprays and provided reduce resistance to wet and dry combing, reduce static build up and enhance gloss.

3.2 Monodisperse systems

The monodisperse PDMS emulsion system was first developed in 1994 by Obey and Vincent[8], as a novel and more efficient alternative to the polydisperse emulsions already in use. The preparation of the chemically inert PDMS is surfactant free making it an ideal system with which to gain information on the physical and colloidal properties of an almost ideal liquid / liquid dispersion.

The branching structure of the Si – O bonds within PDMS and control of its molecular weight allows manipulation of the droplets' unique physical properties. These include low surface tension, which provides the droplets with spreading properties reminiscent of liquid films on surfaces, shear stability, thermal and oxidative stability and one of the lowest glass transition temperatures for any polymer. The Si-O bond has enhanced flexibility, with almost no energy barrier for backbone rotation

The introduction of a cross-linking monomer also allows control of the droplets viscoelasticity. The variation in the volume fraction of cross-linking monomer present makes it possible to prepare colloidal systems containing particles ranging

from liquid PDMS droplets at low concentration, increasing to form a microgel region, through to a highly cross-linked, rigid amorphous solid silica at higher concentrations.

3.3 Preparation of Cross-linked PDMS emulsions

A range of di-functional (DMDES) and tri-functional (MTES) monomer mixtures were added to aqueous solutions of Ammonia '880', table 3.1. The emulsion mixtures were diluted with purified *Millipore Millifiltration* water to obtain the required volume fractions and then manually shaken for 2 mins. Each emulsion was then left to equilibrate at room temperature for 18–20 hours. After this time, the system's appearance becomes more and more turbid. The emulsions were then dialysed using cellulose *Visking* tubing against *Millipore Millifiltration* water for 3 hours, changing the water every 30 minutes. Table 3.1 lists the emulsion systems parameters used for a 0.01(v/v) total monomer volume fraction (ϕ) during this study. The emulsion parameters were repeated increasing the total monomer volume fractions to 0.025(v/v) and 0.05(v/v).

Table 3.1 Emulsion preparation parameters

Total monomer (ϕ)	Di-functional monomer DMDES (ϕ)	Tri-functional monomer MTMS (ϕ)	NH_3 (aq) (ϕ)
0.01(v/v)	0.01(v/v)	0.000(v/v)	0.01(v/v)
0.01(v/v)	0.01(v/v)	0.005(v/v)	0.01(v/v)
0.01(v/v)	0.01(v/v)	0.010(v/v)	0.01(v/v)
0.01(v/v)	0.01(v/v)	0.050(v/v)	0.01(v/v)
0.01(v/v)	0.01(v/v)	0.100(v/v)	0.01(v/v)
0.01(v/v)	0.01(v/v)	0.200(v/v)	0.01(v/v)

3.4 Proposed reaction scheme

The synthesis used in this project has been developed from methods previously described[5,6], in which oil-in-water emulsion systems were prepared using di-functional silicone alkoxide monomer (DMDES), tri-functional cross linking MTES and aqueous ammonia solution. The synthesis was originally developed from the Stöber and Fink[7], base catalysed hydrolysis and polymerisation of tetra ethyl siloxane (TEOS) to form micron sized colloidal silica particles. The method used here involves the spontaneous emulsification, via controlled nucleation and growth of the separating phases from an initial single-phase system. This produces monodisperse PDMS, (silicone) oil-in-water emulsions, see figure 3.3.

The initiation of the polymerisation of the siloxane monomer occurs via hydrolysis of ethoxy groups. The formation of small nuclei from a homogeneous phase occurs in the aqueous ammonia phase due to the high degree of solubility of the monomer in water. This generates radical intermediates in the aqueous phase, to which monomer units are attracted until they exceed their solubility and precipitate out. The precipitated molecules then form spherical droplets, which absorb surface-active oligomers also formed in solution, and these can then act as in-situ surfactants.

These then form primary droplets with other monomers. In time these primary droplets expand their interface, but although their negative charge provides a large enough energy barrier to make them kinetically stable, their expanding size eventually makes them colloidally unstable.

Figure 3.3 Proposed reaction scheme

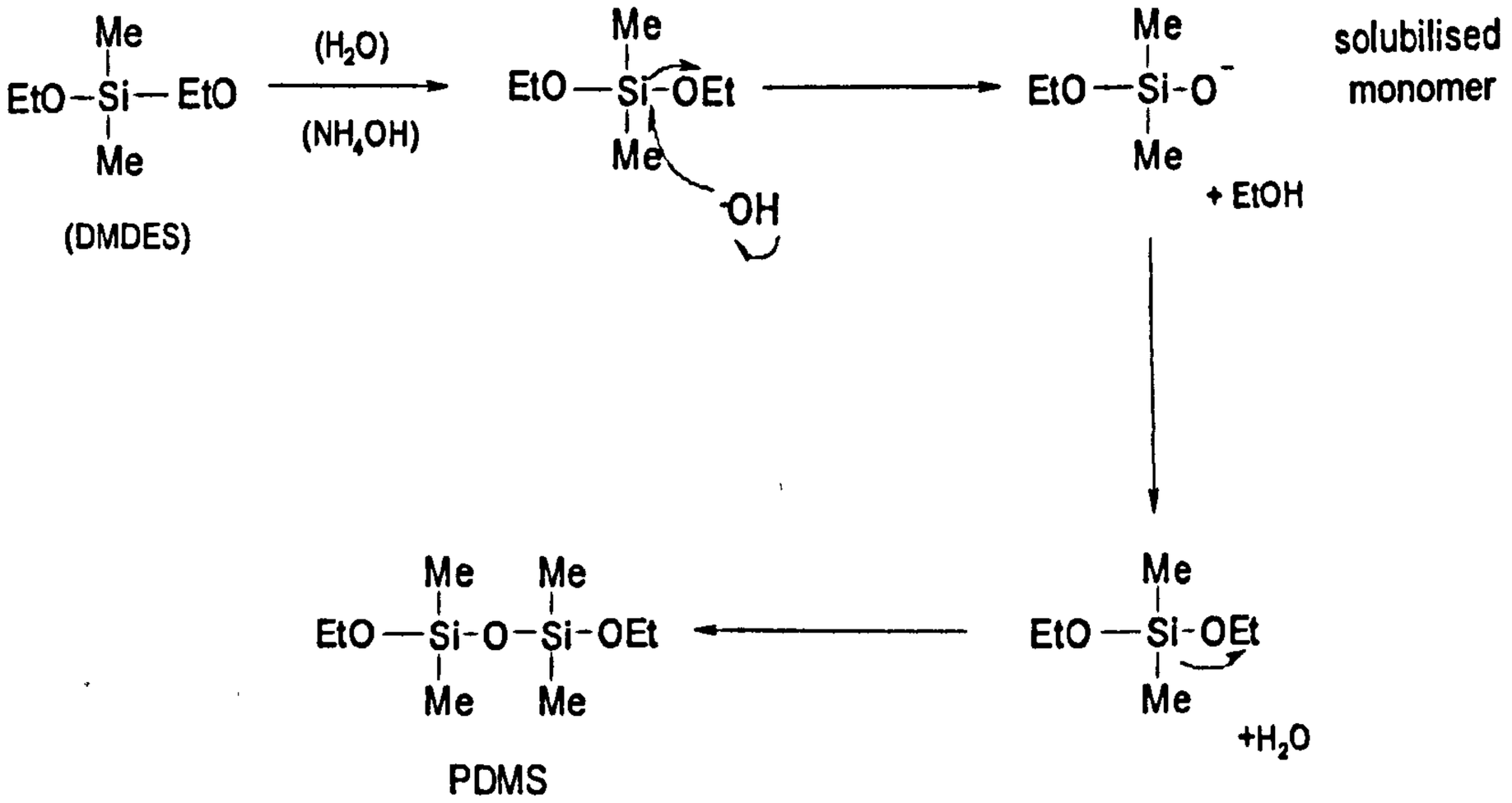

The droplets finally coagulate or coalesce. Droplet nucleation, mature droplet capture and flocculation of oligomeric radicals, continues throughout polymerisation and equilibrium is only reached once the rate of primary droplet nucleation equals the rate of primary droplet capture. Overall there is a spontaneous generation of a new phase from a metastable solution within 24 hours. The advantage of this very simple, fast emulsification process means that it produces emulsions with very narrow polydispersity.

All the PDMS emulsions studied in this investigation were made in the same way through the polymerisation of a silane monomer in aqueous alkali solution. This process proceeds via a nucleation and growth mechanism from a homogeneous aqueous phase. The monomer used in this study was dimethyldiethoxysilane (DMDES),EtO-Si(Me)$_2$-OEt a di-functionally active molecule where Me denotes a methyl group (CH_3) and Et an ethyl group (CH_2CH_3).

Fig 3.4 Structure of PDMS as a function of cross-linker volume fraction.

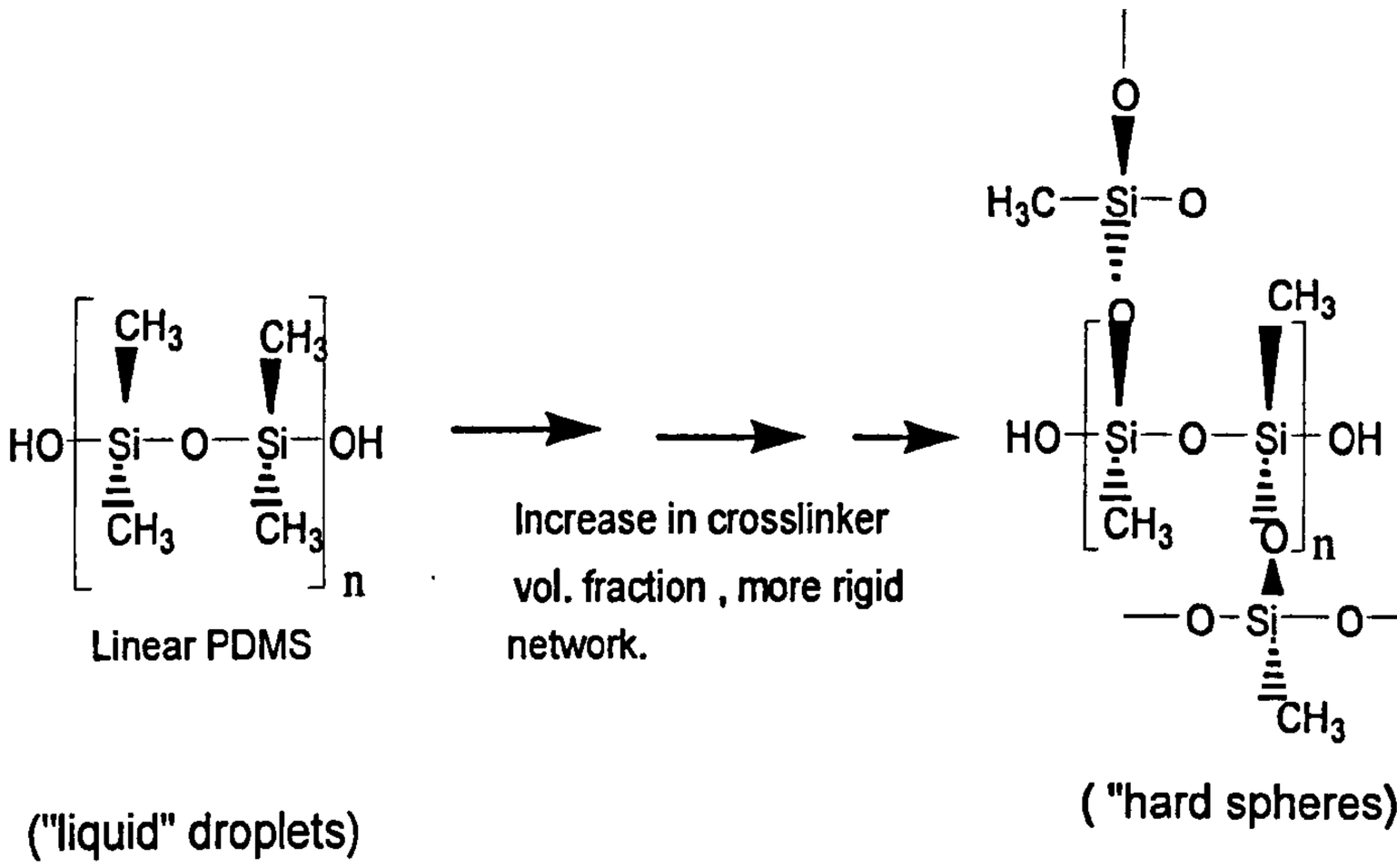

The second monomer was a tri-functionally active cross-linking molecule methyl-triethoxysilane (MTES).

The method of emulsion preparation was as follows: DMDES was added to an aqueous solution of ammonia and vigorously shaken. The volume fraction of monomer and ammonia used was varied to allow a range of particle sizes to be synthesied following the results reported by Goller, Obey and Vincent[9] on the effect of MTMS concentration on emulsion droplet size. Monomer concentrations remained constant at 0.05 v/v with a fixed ammonia concentration of 0.10 v/v was used. For a relatively short period of time, (ranging from approximately 10 mins to 1 hr), the solution remained transparent. A gradual increase in turbidity was observed over the next 12-24hrs. The polymerisation proceeded via initial hydrolysis of the active ethoxy groups to form ionic precursors to the oilgomeric molecules.

3.5 References

1. Patnode,W., Wilcock,D,F., Journal of the American Chemical Soc., 68, 358, 1946
2. McGregor,R,R., Warrick,E,L., United States patent No.2384384, 1945
3. Kipping,F,S., Journal of the Chemical Society, 2125, 1912
4. Scott,D,W., Journal of the American Chemical Soc, 68, 2294, 1946
5. Kantor,S,W, Grubb,W,T., Osthoff,R,C., Journal of the American Chemcial Soc, 76, 5190, 1954
6. De.Grunzbourg,A., Favier,J,C., Hémery,P., Polymer International, 35, 179, 1994
7. Hyde,J,F., Wehrly,R., United States Patent No.2891920, 1959
8. Obey,TM., Vincent,B., Journal of Colloid and Interface Science, 163, 454, 1994
9. Goller, M.I, Obey,TM., Vincent,B., Teare.D, Wegener.M, Coll.Surf.A, 123-124, 183, 1997

Chapter 4: Experimental

4.1 Introduction

This chapter discusses the equipment, chemicals, experimental methods and characterisation techniques discussed in chapters 5, 6 and 8. The techniques are divided into four main categories; (i) emulsion characterisation, (ii) oil phase analysis, (iii) substrate surface characterisation, (iv) deposition and removal techniques.

4.2 Materials

Dimethyldiethoxysilane (DMDES) (97%), methyltriethoxysilane (MTES), aminopropyltrietoxysilane (APTES 99%) were obtained from Aldrich and distilled prior to use. Ammonia 880 solution (35% w/w), hydrochloric acid (37%), hydrogen peroxide (36%), *Repelcote* (2% solution of dimethyldichlorosilane in octamethylcyclotetrasiloxane), n-heptane, ethanol, sodium chloride, sodium dodecylsulphate (SDS, specially pure) were supplied from BDH chemicals(UK). The Visking dialysis tubing (19 mm internal diameter) was obtained from Medicell International (UK), while the water was purified by using a Millipore"Milli-Q" filtration system, (Millipore Ltd.) . The microscope glass slides were bought from BDH and chemically modified using the methods described in chapter 6. Lysine modified glass slides were also obtained from BDH, modified previously with the amino acid. G250-1Mica slides were obtained from Agar in dimensions that simulated glass slides, 3" x 1" .

4.3 Emulsion characterisation

4.3.1 PCS (Photon correlation spectroscopy)

PCS or dynamic light scattering (Brookhaven Instruments) was used to measure the hydrodynamic diameter of the cross-linked colloidal droplets, as discussed in chapter 3, and in a variety of different solutions, see chapter 5. Traditionally, this technique has been based on the concept that the light scattered by droplets moving under Brownian motion, will undergo different frequency shifts and show the phenomenon of "Doppler broadening"[1,2]. If this broadened scattered signal is then compared with the signal from the incident light source, a pattern of beat frequencies is produced which provide information on the velocity of the droplets. These scattered light functions are then studied by a correlation technique.

Modern PCS techniques are capable of measuring time shifts in addition to frequency effects providing more detailed data. The scattered intensity is measured before and after a time interval, and the two intensities obtained are shown to be dependent on the diffusion of the droplets. The dilute, monodisperse systems used in this study contain non-interacting droplets have an intensity correlation time constant which can be related to the diffusion coefficient, D, and can therefore be described by the Stokes-Einstein equation, 4.1.

$$D = \frac{kT}{6\pi\eta a} \qquad [4.1]$$

where a is the particle radius, η is the solvent viscosity, k is the Boltzmann constant, T is temperature.

4.3.2 Electrophoretic Mobility and ζ-Potential

A *ZetaPlus Zetaliser* instrument (Brookhaven Instruments, UK) was utilised to determine the electrophoretic mobility of cross-linked droplets in different surrounding solutions, see chapter 3. The electrophoretic mobility of a charged droplet, u, relative to stationary solvent, in an applied electric field can be defined by the expression [4.2]

$$u = \frac{\upsilon_e}{E} \qquad [4.2]$$

where υ_e is the velocity of the particles in the applied field, and E is the applied field strength. The "zeta-potential", (ζ), term is defined as the electrical potential at the plane of shear between the continuous and discontinuous phases in motion relative with each other. However, it is traditionally difficult to define the exact location of the plane of shear as the viscosity changes continually in this region. In general, the experimentally determined zeta-potential is regarded as a good approximation (or slight underestimate) for the theoretical Stern potential, Ψ_d. Li and de Bruyn[3] reported that ζ–potential is a relatively accurate approximation of the Stern potential ,Ψ_d, especially for the case Ψ_d <100mV and for an electrolyte concentrations $<10^{-2}$ mol dm^{-3}. The electrophoretic mobility and zeta potential are both dependent on κ*a*[4]. For the limiting case κa >>1, the Smoluchoski equation[5] [4.3] can be applied,

$$u = \frac{\varepsilon\varepsilon_0\zeta}{\eta} \qquad [4.3]$$

For κa <<1, the Hückel equation[5] becomes more efficient [4.4], where η is the viscosity of the dispersion medium.

$$u = \frac{\varepsilon\varepsilon_0\zeta}{1.5\eta} \qquad [4.4]$$

Conversion tables for electrophoretic mobility to zeta-potential were computed by Wiersema et al.[6] for a wide range of κa values, and presented graphically by Ottewill and Shaw[7]. O'Brien and White[8] re-analysed the calculation of ζ-potentials from measured electrophoretic mobilities and the results were in agreement with those of Wiersema et al.[6] and cover a wide range of ζ-potentials.

Recent advances in the interpretation of ζ-potential data has included the calculation of the non-electrostatic part of the adsorption free energy of ions, also charged and uncharged surfactant molecules and polyelectrolytes which are used as adsorbable components of the aqueous solution in electrokinetic measurements[9].

Only dialysed samples were analysed using $1x10^{-3}$ mol dm^{-3} KCl (aq) as background electrolyte. 2 cm^3 of the sample emulsions was diluted with 14cm^3 of 10^{-3} mol dm^{-3} Kcl to achieve a suitable turbidity and filled into the cell. Each cell was then flushed with Milli Q water several times between samples.

4.4 Oil phase analysis

4.4.1 Viscosity and density

Viscosity measurements were carried out using a Cannon-Fenske capillary viscometer in a water bath, with the thermostat fixed at 25 +/- 0.5°C, using the procedure described by Matthews[10]. The volume of the sample measured was kept constant at 12ml. The viscometer was calibrated with pure water and cleaned with ethanol and dried between measurements. Errors were estimated at less than 0.5s. Density measurements were carried out using a Paar Densiometer.

4.4.2 Transmission Electron Microscopy, (TEM)

A Jeol Jem 1200 Ex TEM instrument was used to obtain detailed images of cross-liked PDMS droplets in the Microscopy department, University of Bristol. The technique utilised an electron beam to illuminate the sample, emulsion droplet, and obtain accurate droplet dimensions and detailed image[1,2]. The sample was deposited on to a fine copper mesh grid that was coated with a supporting transparent membrane and subsequently dusted with platinum powder. The electron beam and sample are investigated under a high vacuum where the droplet scatters the electrons out of the field of view. The amount of scattering defines the image contrast and is dependent on the atomic number of the sample. The lower the atomic number, (e.g for organic materials), the lower the resolution. However heavy metal atoms create enhanced images. The image is then magnified and focused on to a viewing screen that allows images to be taken and stored. The TEM instrument contained a standard tungsten filament, operated up

to 200KV and a magnification of 500K. The microscope was set up for bright and dark field imaging, selected area and convergent beam electron diffraction and lattice imaging. The instrument was fitted with a MegaView II digital camera, using *Soft Imaging Systems GmbH analySIS 3.0* image analysis software.

4.4.3 Mass spectroscopy (FAB)

All mass spectra discussed in chapter 5 were conducted by the mass spectrometry service in the University of Bristol. A VG Analytical Autospec, a magnetic sector instrument was used which could perform fast atom bombardment (FAB). This is an ionisation technique used for higher molecular weight compounds. The solvent matrix was 3-nitrobenzyl alcohol (3-NOBA). The mass ranges used for FAB was 100-950 Da, 600-1475 Da, 1100-2300 Da and 1900 – 3000 Da. The mean Mw was calculated and the standard deviation determined by the following expression;

$$\text{Std. Dev.} = \sqrt{\frac{\sum (x-\bar{x})^2}{n}} \qquad [4.5]$$

where x is the product of (mass x relative height), $\bar{x}$ is the mean molecular mass (sum of all x divided by n, the sum of relative heights).

4.4.4 Interfacial tension

The surface tension of the colloidal emulsions were measured using a Kruss DVT30 Drop Volume Tensiometer fitted with Drop Shape Analysis (DSA) 10MK2

software, where cross-linked PDMS oil was immersed into an empty cell. The same droplet shape method was used to calculate the interfacial tension by comparing a theoretical drop profile with the measured pendant drop profile, which was created by using a capillary. As a result of the density difference between the aqueous fluorescein continuous phase, higher density, and discontinuous oil phase, lower density, it was necessary to immerse the former as a drop in to the later liquid. This ensured any buoyant forces acted on the drop and not the surrounding phase. The interfacial tension was calculated from a known droplet volume at the moment of release and the density of the two liquid phases using the following expression [4.6];

$$\gamma = \frac{V_{drop} \cdot \delta r \cdot g}{\pi \cdot \delta} \qquad [4.6]$$

where v is the drop volume, δ is the capillary diameter, γ is the interfacial tension, δr is the difference in density and *g* represents the acceleration due to gravity.

A light barrier was used to record the moment at which the drop broke from the capillary, while simultaneously recording the plunger stroke of the syringe used for dispensing the drop. This enabled the volume between two drop signals to be known exactly. Saturation of the two phases was achieved prior to measurement by shaking the two liquids together, and using the separated phases.

4.4.5 High resolution Si^{29} and H^1 NMR

H^1 NMR and Si^{29} NMR spectra were obtained from the high resolution NMR services, University of Bristol. A DELTA /GX 270 instrument was used to obtain H^1 Spectra of the isolated cross-linked PDMS oil phase while a Lambda 300 instrument was used to produce Si^{29} spectra. The spectra were plotted as integrals and the peaks expanded over a range of 10 to 0.5ppm. $CDCl_3$ was used as the dissolving solvent while TMS was introduced as a reference compound. A chemical-shiftless relaxation agent, chromium acetylacetonate [$Cr(acac)_3$], was added to overcome the negative nuclear Overhauser effect, (ratio of double resonance intensity to single resonance intensity in double resonance experiment) and increase signal intensity by inducing a faster relaxation time. Si^{29} NMR spectroscopy was used to identify the silicon environment present in the PDMS phase. A detailed discussion of the theory of NMR will not be given here[11].

4.4.6 Gel Permeation Chromatography (GPC)

A cross-linked PDMS oil phase was isolated from the emulsions and analysed by GPC at RAPRA. A PLgel guard plus 2 x mixed bed-D, 30 cm length, 5µm pore diameter column was used to measure the molecular weight of the PDMS polymers. Chloroform was used as the solvent at a fixed flow rate of 1.0ml min^{-1}. A single solution of each sample was prepared by adding 10 ml of solvent to 20mg of sample and left to dissolve for 4 hours. The solutions were mixed thoroughly and transferred into sample vials, without filtration. The vials were then placed in an autosampler before being introduced into the column which was at a constant

temperature of 30°c. Data capture and subsequent data handling was carried out using Viscotek 'Trisec 2000' and 'Trisec 3.0' software. The GPC system used for this work was calibrated with polystyrene and all of the results were expressed as "polystyrene equivalent" molecular weights. The results obtained are discussed in chapter 5 .

4.5 PDMS- substrate interaction characterisation

4.5.1 Three phase Contact angle

The captive bubble technique was used to measure the three phase contact angle between the substrate surface, the surrounding aqueous phase and the cross-linked oil phase components[12-14]. The apparatus was set up as shown in figure 4.1.

Figure 4.1 (a) Schematic representation of contact angle cell, (b) three phase contact parameters

(a) (b)

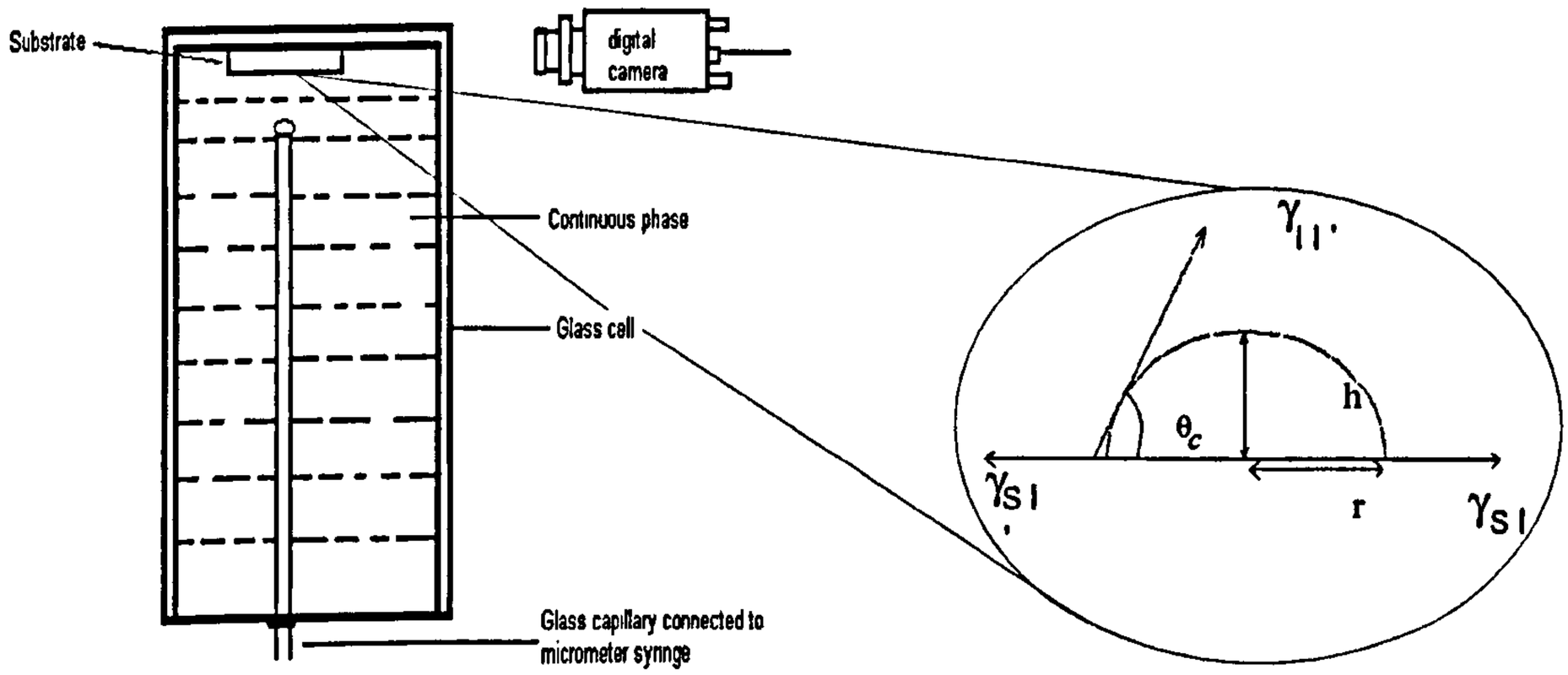

An air-tight glass syringe was attached to a micrometer screw gage which operates the plunger for accurate displacements in both directions. A flexible tube connected the syringe to a glass capillary with a flat ground end which was then immersed in a glass cell containing the surrounding aqueous phase. The end of the glass capillary was fixed at a short vertical distance below and parallel to the surface of the substrate surface. A drop of the oil phase liquid was produced from the glass tube capillary by adjusting the micrometer volume until it was released from the tube and rose to the submerged substrate surface under gravity forces, see figure 4.1 (b).

A CCD camera was focused on the edge of contact between the drop and substrate surface, which was horizontal to the field of view and the image of the three phase contact line was recorded via a digital camera and analysed according to Young and Dupré equations. The balance of forces at the line of contact between the cross-linked PDMS, γ_l, surrounding aqueous fluorescein, γ_r, and the substrate surface was expressed using the Young equation, [4.7];

$$\gamma_{sl} = \gamma_{sr} + \gamma_{lr} \cos\theta_c \qquad [4.7]$$

where γ_{sr} is the surface tension between substrate-aqueous fluorescein, γ_{sl}, is the surface tension between substrate-PDMS drop, γ_{lr} is the surface tension between the surrounding aqueous phase-PDMS drop and θ_c is the three phase contact angle. The Dupré extension [4.8] was then used to calculate the work of the adhesion of the cross-linked PDMS drop to the substrate, including the thermodynamic effects in the system.

$$W_{ad} = \gamma_{sl} + \gamma_{sl'} - \gamma_{ll'} \qquad [4.8]$$

or

$$\cos\theta_c = \frac{W_{ad} - 1}{\gamma_{ll'}} \qquad [4.8]$$

where the γ terms are equilibrium values of surface free energy. The influence of the vertical component of the force on the solid substrate, $\gamma_{ll'} \sin\theta$.

4.5.2 Streaming potential

An Electrokinetic Anlyzer EKA (Paar GmbH), equipped with a home-built measuring chamber was used to investigate the surface potential of each modified substrate. Yiantsios *et al*[15,16] were the first to develop a flat cell micro-electrophoresis apparatus with platinum electrodes. The resulting electrical ζ-potentials were determined as a function of the flow rate and calculated from the slope of the E / P lines[17]. In this study, a rectangular cell was designed to allow the solution to flow along a channel formed from two substrate surfaces at a fixed distance. Ag/AgCl electrodes were positioned at each end of the channel to determine the potential generated by the flow, see figure 4.2. The method is based on the influence of adsorbed ions, from the surrounding solution, on the surface charge at the solid-liquid interface[9]. This charge is balanced by counter ions in the EDL on the liquid side of the interface, see figure 4.3. It is possible to distinguish between adsorbed ions close to the solid surface, the Stern layer, and the mobile ions at a significant distance from the surface where both electrostatic attraction and thermal motion influence their position.

Fig 4.2 Schematic representation of Streaming potential

1. Solution reservoir
2. Squeezed tube valve left
3. Squeezed tube valve right
4. Temperature conductivity sensor
5. Pump
6. Differential pressure sensor
7. Measuring electrode
8. Measuring cell
9.Sample filling

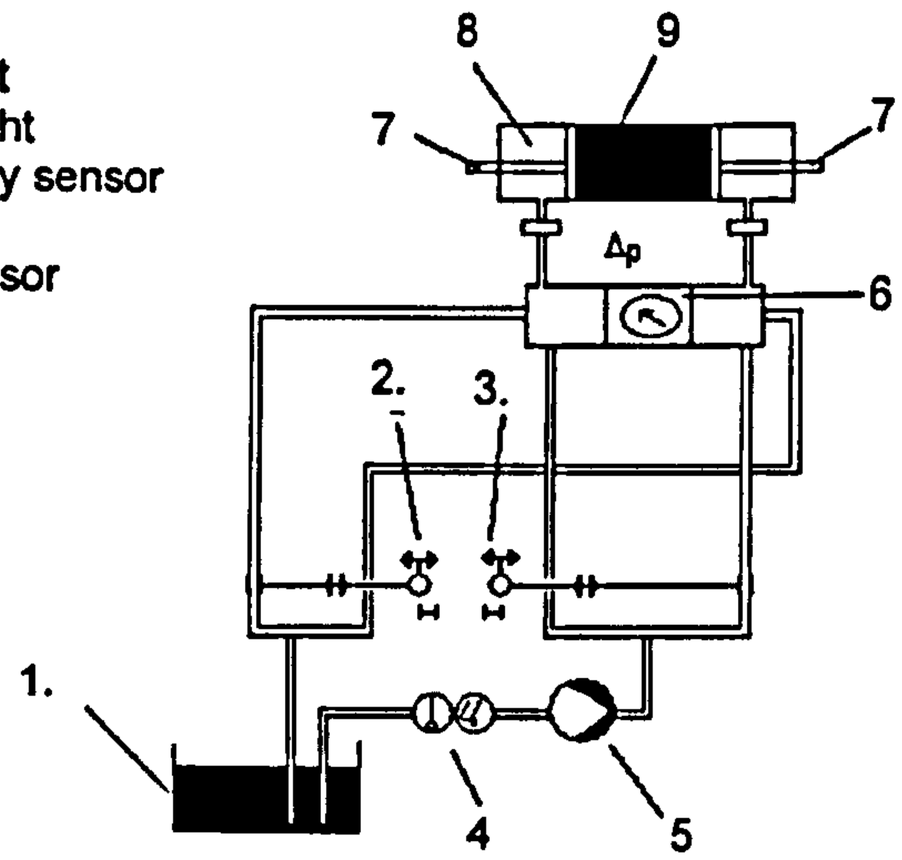

The streaming potential is produced from the application of a tangential shift of an aqueous solution from an applied pressure, across the channel formed by the substrates at a fixed position. This shift causes the displacement of hydrodynamically mobile ions by balancing the surface charge. The ζ-potential, (eg. the electrical potential at the hydrodynamic phase boundary), is calculated from the Smoluchowski equation[18] [4.10]. The mechanisms that occur at the stationary surface is represented schematically in figure 4.3. The ζ-potential is calculated from the following equation;

$$\zeta = \frac{V_s}{\Delta p} \cdot \eta \varepsilon \varepsilon_0 \cdot \frac{L}{A} \cdot \frac{1}{R} \qquad [4.10]$$

where V_s is the streaming potential, Δp the hydrodynamic pressure difference across the sample, L and A are the length and cross sectional area of the sample and R is the electrical resistance across it[15-16,19,20]. $V_s / \Delta p$ can be determined by direct measurement of the potential generated by a constant pressure obtained

from the slope of a plot of potential against increasing pressure difference to give better precision. ε and ε_0 are the viscosity permittivity of the liquid and permittivity of free space respectively, which are constant for a given temperature. The EKA determines R from the ratio $(V_s/\Delta p)/(I_s/\Delta p)$, while L/A is determined by the EKA using Fairbrother and Mastin theoretical model[21], however details will not be discussed here. Further information can be found in reference 21.

Figure 4.3 Schematic representation of the streaming potential; (a) when EDL at rest, (b) when liquid forced over surface, (c) ion accumulation producing a potential difference, E, (d) E causes back-flow current.

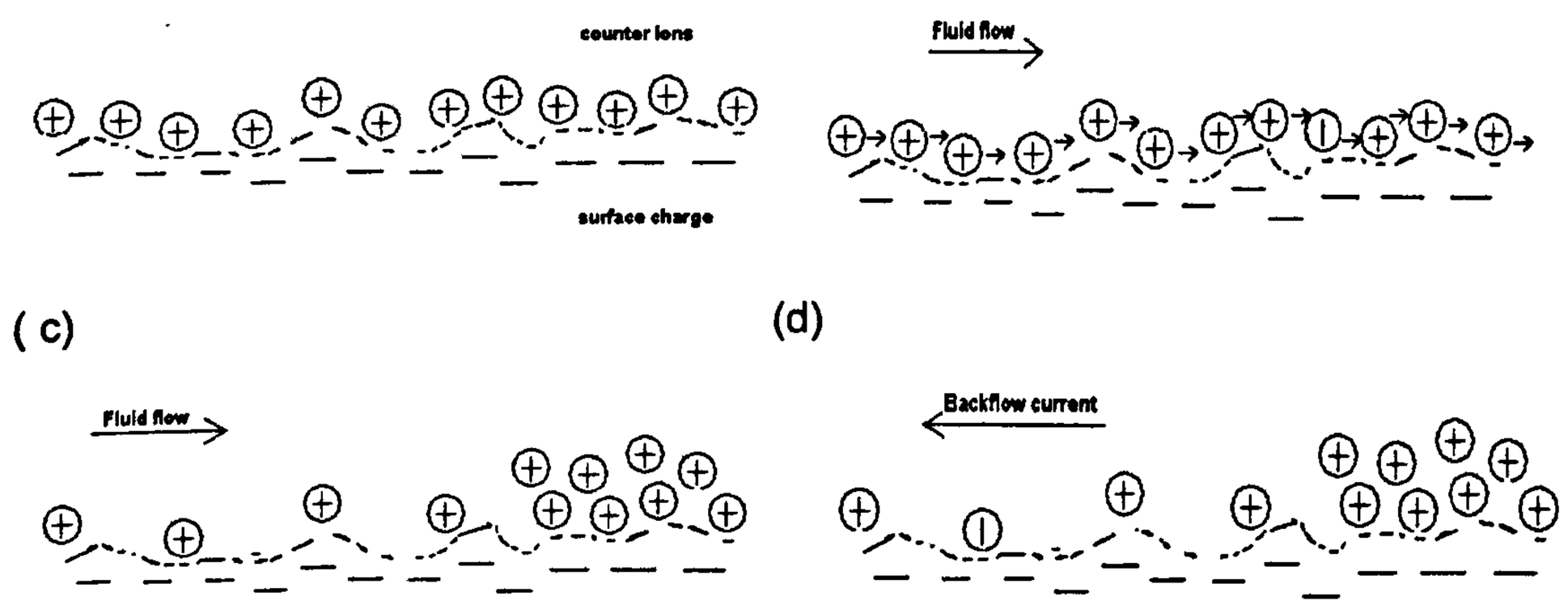

The EKA instrument has been used to investigate colloidal systems where it would otherwise be difficult to obtain results; for example platelets, films, fibres and particles too large and dense for electrophoresis and can be embedded in hydrophobic flat sheet supports and the ζ-potential then measured by EKA. The influence of solution ionic strength, additive concentration and surface chemistry

on the solid-liquid interfacial double layer or ζ-potential, has become significant in many detergency processes. Figure 4.4 illustrates how the Brookhaven-Paar BI-EKA ElectroKinetic Analyser is suitable for use on the macroscopic sample used in this investigation[8].

Fig 4.4 Applicability of ζ-potential determination methods

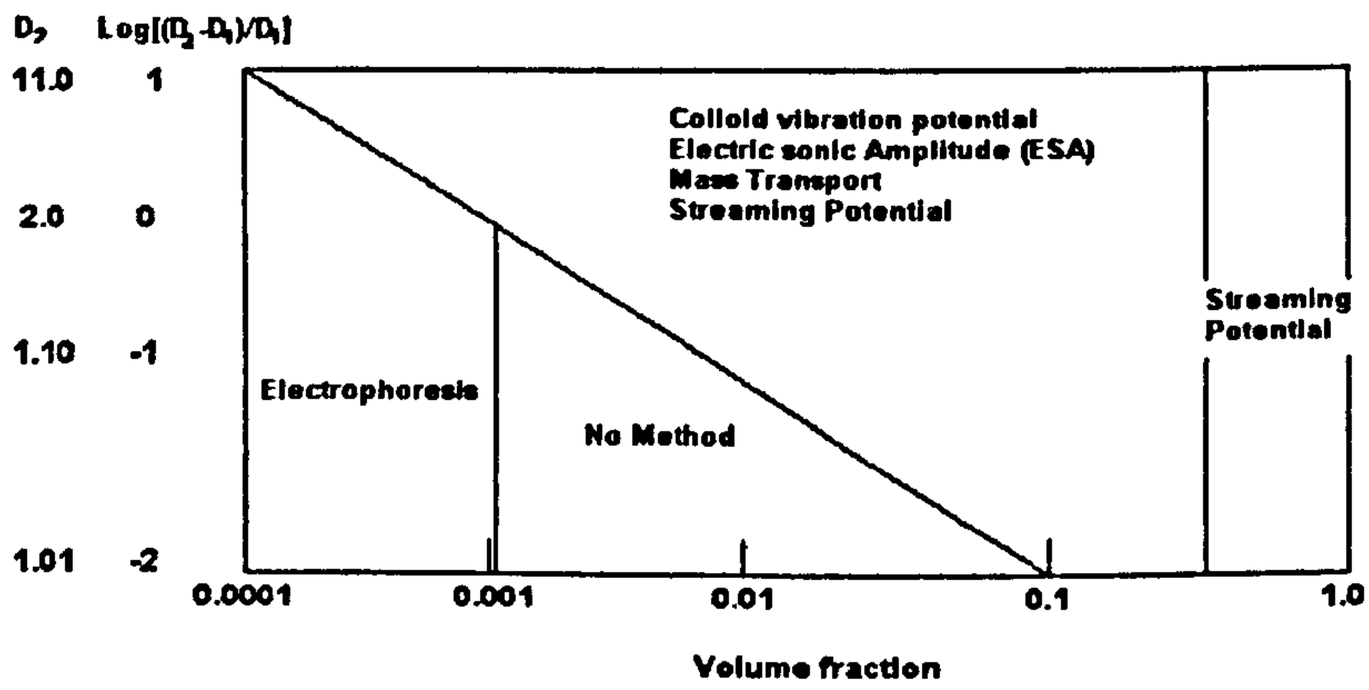

Goddard and Leung[22] measured the surface electrical properties of hair during a simulated wash process using an EKA instrument containing a cylindrical cell. Packed hair beds formed a channel between the two electrodes and the test solutions. The untreated hair in water showed a ζ-potential of -14mV, and -43.1mV in the presence of an anionic surfactant shampoo. After a second rinse with water, the surface potential was reduced to -20.1mV. Once a cationic "conditioner" was introduced into the system, the surface adopted a positive ζ-potential value of +25.7mV, which reduced to +4.9mV after a final rinsing of water. This effect indicated that there were significant physisorption forces present between the particles and substrate, as the hair surface remained positive after several water rinses.

4.5.2.2 Influence of particle deposition on substrate surface potential

It has been shown that the presence of an adsorbed particle with an opposite charge from the substrate surface, decreases the local charge density and so reduces the streaming potential. The streaming current for a particle covered surface can therefore be deduced from the following expression,[4.11]

$$\Delta I_p = I_p - I = \iint_s (\rho^* V^* - \rho V) \bullet dS \qquad [4.11]$$

where I_p is the streaming potential for particle covered surface, I is the current for bare surface, ρ^* and V^* correspond to the perturbed electric charge density and fluid velocity in the S plane respectively, due to the adsorbed particles. An opposite effect was reported for a sphere bearing the same charge sign. The adhered particles decrease the local fluid velocity field at distances greater than its radius, (a), and so decrease the shear rate at the wall, symmetrically relative to the flow direction[23]. This was especially significant for high electrolyte concentration systems, where the double-layer thickness much smaller than the particle radius, (a).

Zembala et al[24] later reported that particle surface coverage could be determined by experimentally measuring the streaming potential. The streaming potential, Es, for bare mica increased and became more positive in the presence of melamine-formaldehyde particles at a fixed pH ~8, and changed from ~10mV to ~120mV. Zembala et al confirmed experimentally that the presence of adsorbed particles influences the streaming potential of interfaces as a result of damping the fluid

motion in the vicinity of particles and the additional charge transport from the ionic atmosphere surrounding particles. For thin double-layers, $^1/\kappa$ a <0.5,and low coverage , the effect is linear and described by;

$$\frac{E_{sp}}{E_s} = \frac{I_p}{I} = \frac{\zeta_a}{\zeta_j} 1 - (10.21 + 6.51 \frac{\zeta_p}{\zeta_j}) Q \qquad [4.12]$$

where E_{sp}, E_s and I_p, I are the streaming potential and streaming current for the particle covered surface and bare substrate respectively, ζ_a, is the apparent zeta potential of the channel in the presence of deposited particles, ζ_j , ζ_p are the zeta potential of the of the particles and interface respectively and Q is the surface concentration defined by pa^2N and N is the particle number.

For neutral or slightly charged interfaces, the effect described by semi-emperical function independent of particle size, ionic strength, and shape of channel.

$$\frac{E_{sp}}{E_s} = \frac{I_p}{I} = e^{c^0{}_i\theta} \qquad [4.13]$$

where $e^{c^0{}_i\theta}$ is the probability of finding an empty surface area over the bare surface.

4.5.3 X-Ray Photo-electron spectroscopy (XPS)

The elemental composition of each of the substrates investigated were analysed by the Interface analysis center, University of Bristol. An ESCA-Lab 220i XPS

was used to obtain quantitative composition data within a sensitivity range of approximately 0.1 atom percentage. The information was gathered from a depth up to 5nm below the surface, with a lateral resolution of a few μm^2.

The method is based on the use of an electron-beam to bombard the substrate surface and capture electrons freed from the atomic orbitals of the sample, see figure 4.5. The kinetic energy of the emitted photo-electron is given by the expression;

$$K_E = h\nu - B_E - f \qquad [4.14]$$

K_E is the kinetic energy of emitted photo-electron, $h\nu$ is the x-ray photon energy, B_E is the binding energy of electron in th atomic orbital and f is the work function of the surface. The quantities measured were the relative number and the kinetic energy of the released electrons.

Each atom species present can therefore be detected by the characteristic binding energies of its electrons and provide information on its chemical environment. The spectral peaks are compared to software models to determine the element's chemical form, while the area under each peak is proportional to the number of elements present. XPS has recently been used to investigate several chemically modified substrates, including protein covered surfaces[18] similar to those prepared in this thesis.

Fig 4.5 (a) Schematic representation of an XPS instrument, (b) photoelectron-beam bombardment of a samples' outer electrons.

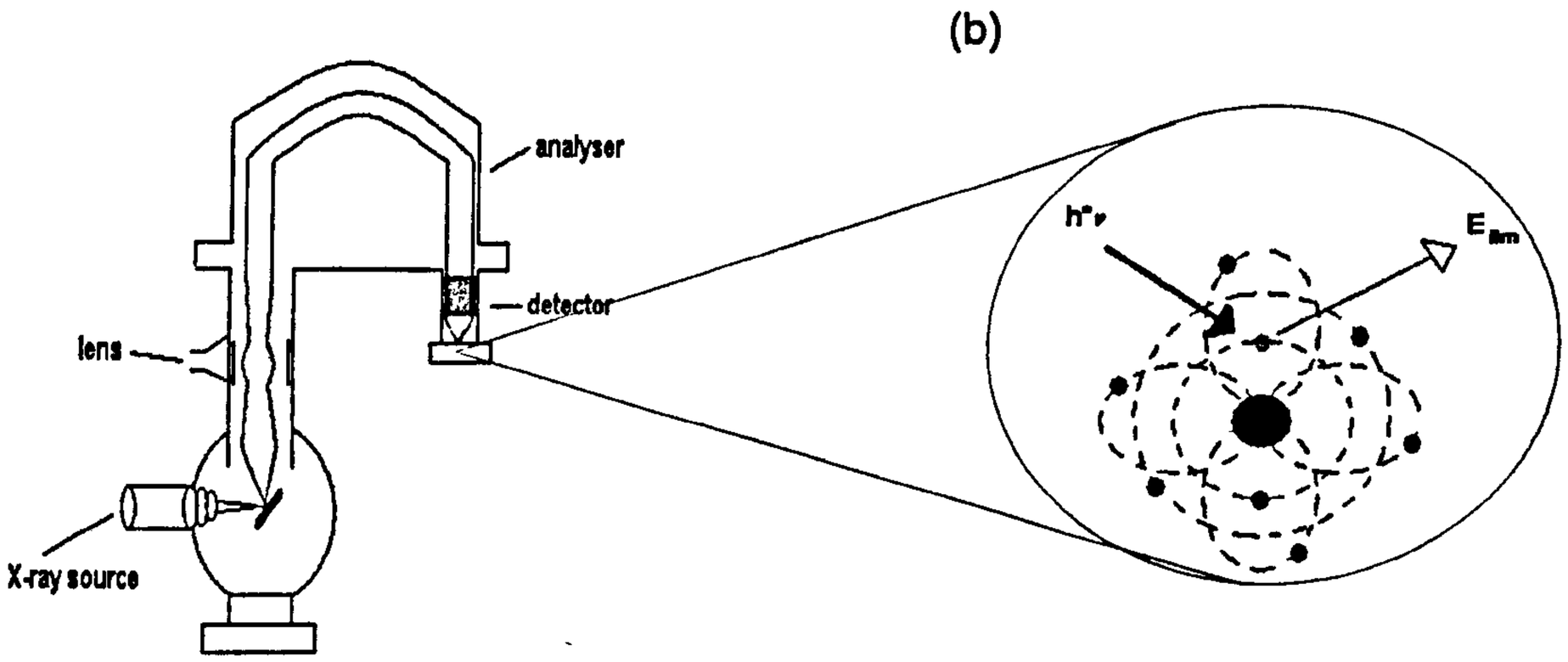

4.5.4 Atomic Force Microscopy (AFM)

Each substrate surface used in deposition and removal studies discussed in chapters 9 and 10 were characterised for surface asperities using a Nanoscope Multimode III AFM(Digital Instruments), Physics department, University of Bristol. This technique was used to provide information on the surface heterogeneity of the chemically modified solid substrates in air. The interaction force between the silicone nitride tip, attached to a low modulus cantilever, and the substrate surface was measured indirectly as the deflection of the micro-cantilever, (see figure 4.6), while peizo-electric scanners maintain the tip at a constant force. A beam-bounce detector(3), developed by Meyer and Amer, was used to measure the positioning diode laser beam(1). This beam is reflected from the mirror surface(2) on the back of the cantilever(7). This signal is then converted (4,5) into a 3-D topographical image with a 5nm lateral and 0.01nm vertical resolution at a fixed at a scan size of

1µm and scan rate of 3.052 Hz. A tapping mode interaction between the cantilever tip and the substrate was adopted in this study at a constant force.

Figure 4.6 (a) Principle of atomic force microscopy, (AFM), (b) Tapping mode

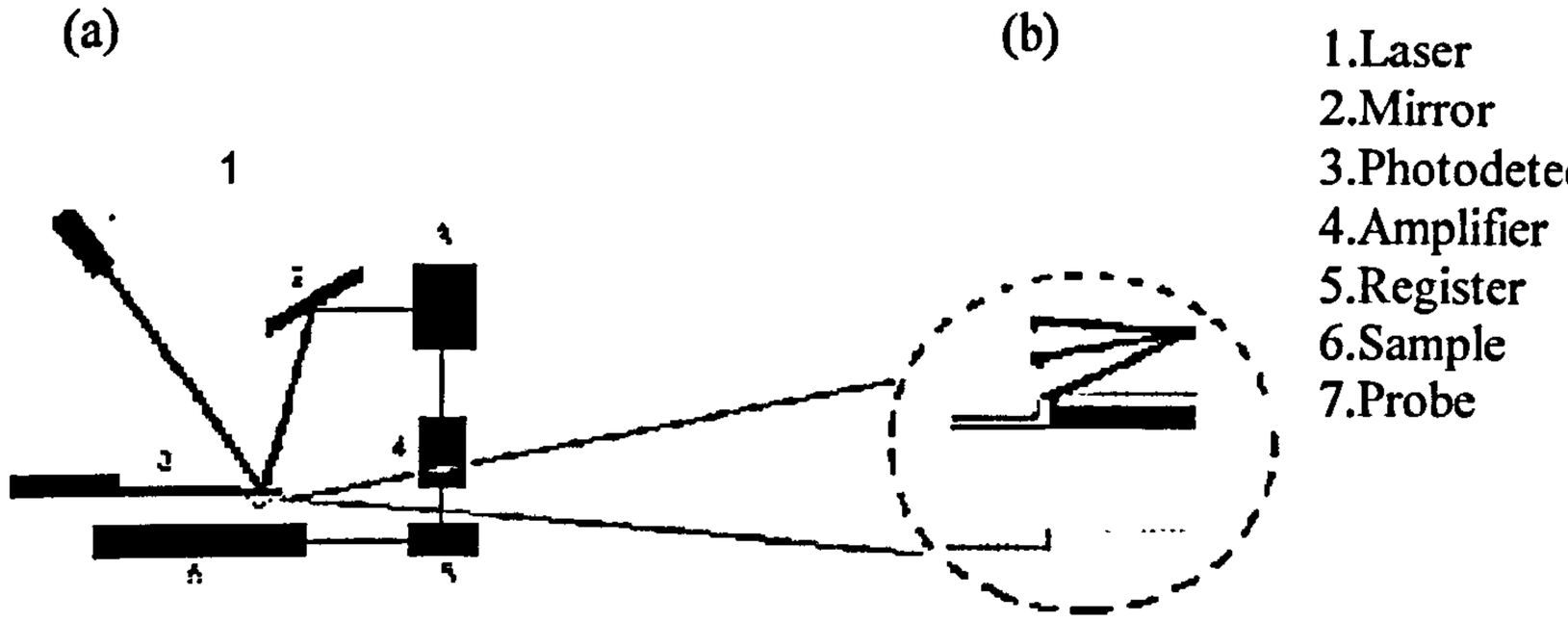

This mode was favoured over the traditional contact and non-contact modes due to its' superior resolution and its non-destructive frictional forces which can overcome adhesion and electrostatic forces present in deformable samples. This mode was especially useful for those samples coated with polymers and proteins such as the APTES and Lysine modified glass used in this investigation.

4.6 Colloidal deposition

4.6.1 Stagnation point flow cell design

The stagnation point flow cell was first developed by van de Ven et al[20] and was constructed from a glass frame with a platinum foil disc bonded to the top of a central column. The cell used in this work only differed from the original design by the use of machined brass but was chosen for the dimensional uniformity and the

advantage of a movable second plate. A detailed schematic representation of the flow cell design is shown in figure 4.7. The stagnation point flow system is based on the concept that a non-rotating symmetrical obstacle in the fluid stream produces a point of zero velocity next to its upstream surface. The flow on each side of the central streamline OX is deflected around the object is illustrated in figure 4.8(a). The streamlines diverge and the velocity along the central streamline OX decreases as the stagnation point, X, is approached, (see figure 4.8 (b)).The flow regimes are characterised by the Reynolds number, which was kept under 5 to ensure flow turbulence was eliminated within the cell. The cell was fed from a reservoir containing 250 cm^3 of cross-linked PDMS emulsion, drawn through the cell to an outlet reservoir by siphoning to this outlet reservoir, (see figure 4.9). The suspension flows, as a result of an hydrostatic pressure difference between the two reservoirs through the circular capillary pipe.

Surfactants, electrolytes or tri-functional monomer were added to the emulsion prior to placing it in the reservoir. A calibrated depth micrometer was used in conjunction with an image analyser, (see section 4.6.5), to ensure that the dimensions of the flow cell were matched as close to the original van de Ven design as possible. The lower plate diameter, L, and radius, R, was fixed at 10mm and 5mm respectively, while the plate separation, h was 1.9mm. The solution being investigated was impinged against the mica plate substrate, and left the cell through the external pipe of radius, R', 1.1mm.

The distance h_c between the top of the capillary and the mica plate was equal to 0.16cm which gives $h_c/R = 1.6$.

Figure 4.7 Schematic representation of stagnation point cell

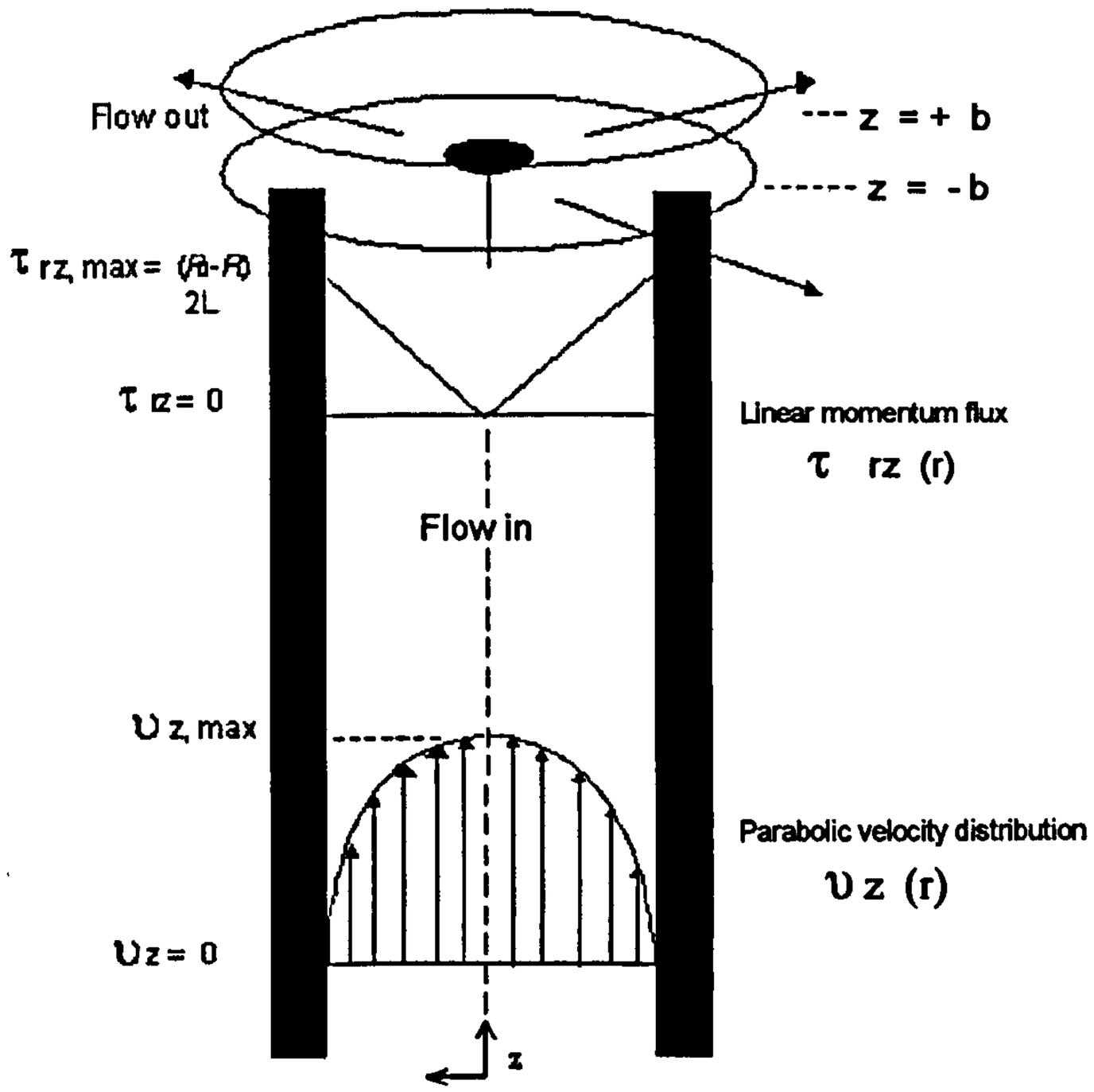

All the chemically modified substrates used were placed in the same position as the mica. The volumetric flow rate Q in the cell was regulated by a peristaltic pump. This allowed the Reynolds number to be adjusted within the range 0.1 to 100. It should be noted that the pressure generated under the mica plate was sufficient to hold it in place next to the external tube without using an adhesive. This reduced the possibility of any cell contamination during the measurement. The use of a siphon ensured that the flow in the cell was uniform, and free from the "surge" associated with mechanical pumps. The reservoirs were set at a height so that the volume of fluid in the inlet reservoir had very little effect on the flow rate obtained.

Figure 4.8 (a) schematic representation of Stagnation Point formation, (b) schematic representation of fluid streamlines at the substrate surface

(a) (b)

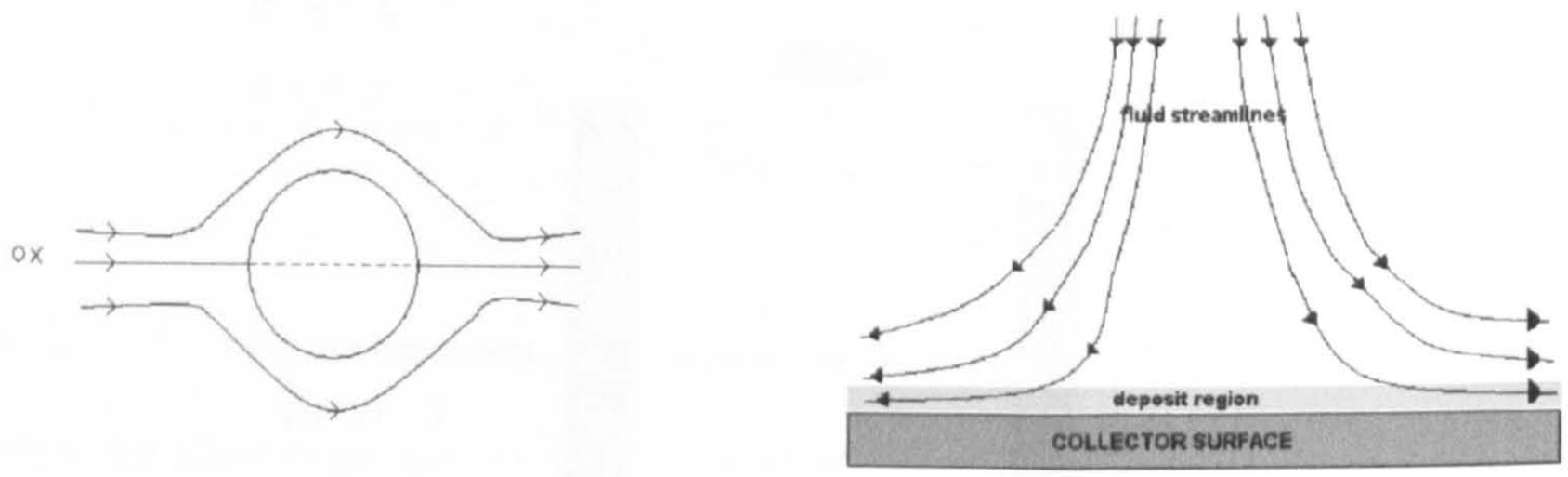

The height difference between the reservoirs was large in comparison to the depth of fluid in them. The flow rate was measured, and was found to be 7.5 cm^3 min^{-1}. The peristaltic pump was set so that the outlet reservoir remained completely empty for the duration of the experiment. For these reasons no return pipe was needed to control the fluid depth in the inlet reservoir as the dispersion was recycled almost immediately upon the exiting cell. Adsorbed particles were observed *in situ* under an optical microscope, coupled with a CCD camera and an image processor / analyser software. All the fluids[19] and flow cell parts used were carefully cleaned to ensure any contamination was kept to a minimum. This was maintained by performing a number of measurements such as water conductivity, flow rate, interfacial tension and rising velocities in quiescent water. The presence of minute impurities can induce variations of several orders of magnitude in droplet adhesion.

Figure 4.9 The flow cell setup

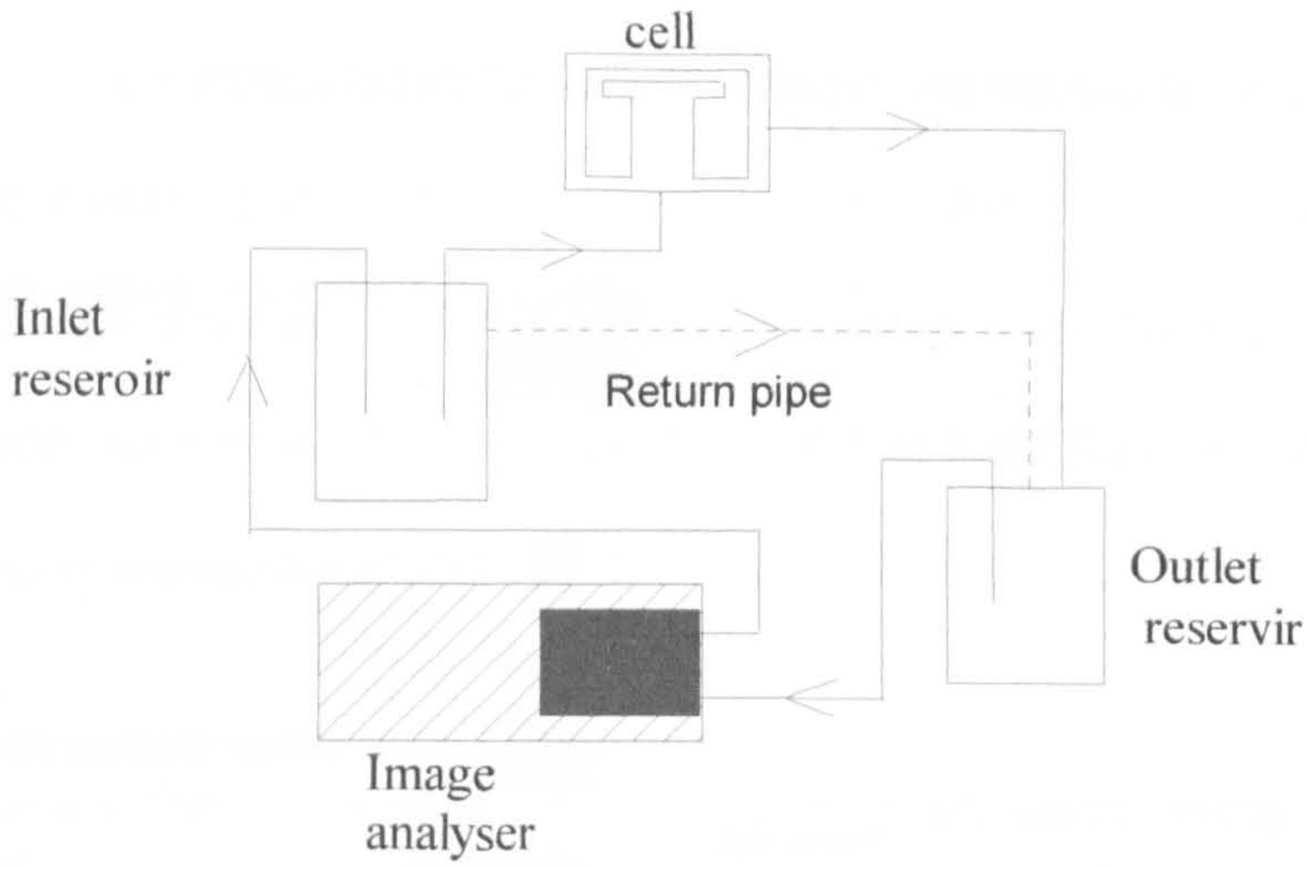

4.6.2 Observation System

Particle deposition experiments were performed directly on the stage of a Nikon Optihot epi-illuminating Microscope fitted with dark field illumination, and using the direct microscope observation method[25], shown schematically in Fig 4.10. An aluminium mounting plate fixed the cell into position in the stage sample holder, which was kept constant for each experiment. A Sony CCD camera attached to the microscope and connected to a PC was fitted with image analysis software, *Noesis Visilog 5.0,* which allowed user observation and simultaneous image capture, see section 4.6.5. The moment the dispersion was seen to be emerging from the impinging jet, a stopwatch was started using the image analysis software. The microscope was focused and aligned to view directly above the stagnation point and the experiments were then performed *in situ* on the stage. Image capture and analysis began as soon as this process was completed, with images being captured every 3mins for the first hour of deposition and then every 10 min

for the remaining 2 hrs for a total of 3 hrs.

Figure 4.10 Schematic representation of observation

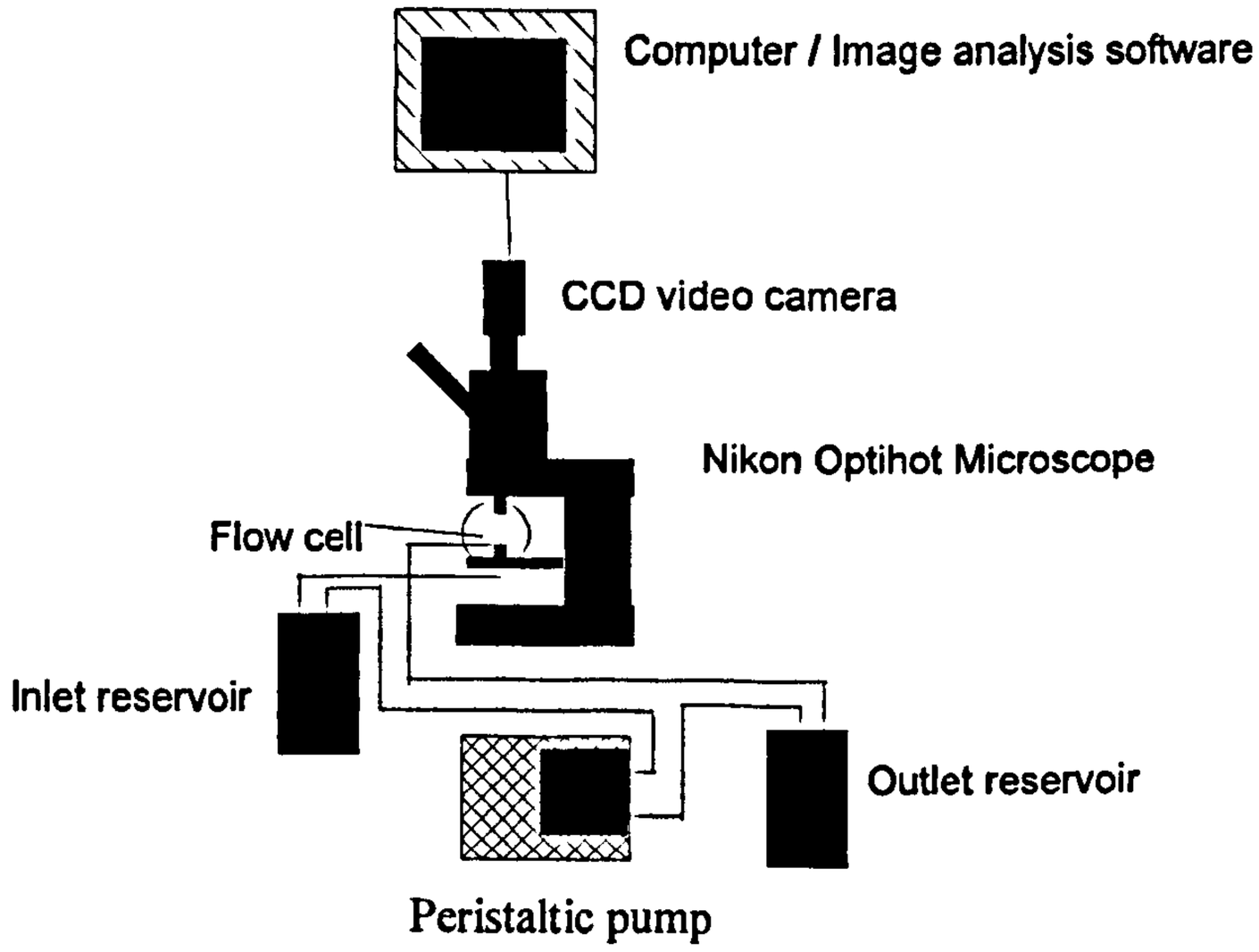

4.6.3 Imaging software

The *Visilog 5.2* image analysis software was developed to capture and record images using camera compatible software and simultaneously analysing each image to obtain the information commanded through the creation of macros. The macro used in this study were devised in conjunction with the manufacturers Noesis SA, France[26] and is shown in full in figure 4.11. The macro analysis script firstly enabled the droplets to be counted by performing a threshold function on the image. The black and white picture is made up of pixels that are each assigned a number between 0 and 256 on the grey scale. The number '0' depicts

black, whereas '256' depicts white, and all the numbers in between are varying shades of grey. The threshold value was chosen so that all the pixel numbers above that value were selected. In this way, the particles were selected over the dark background resulting in a binary image. Once this operation had been carried out, the image analysis software could determine where the edges of the particles were, and subsequently could also count the total number of particles present in the image.

The macro illustrates the main operations performed on each image and they were recorded during either stagnation flow cell or horizontal flow cell experiments. The initial operation displays the image in full screen mode without stretching to allow the image to be observed as large as possible. The calibration parameters are set and the image to be analysed is opened to remove the white particulates within the boundary of each droplet in the image. The contrast between the droplets and the rest of the image is then enhanced and the background removed. The pixelated image grey scale is extended from 0 to 255 to enhance the image resolution. A smoothing operation is then performed on the enhanced image to remove any "noisy" contrast within each droplet area. Operations to enhance and erode were performed to remove contaminants in the background were then performed to smooth the boundary between droplets and the background which subsequently created a distinct separation between the droplets. This separation analysis is then subtracted from the original image to provide a binary image and removes any droplets touching the image border so that only whole droplets are included in a subsequent analysis. These operations created an image in which the droplet number, contact area and distribution could be more accurately obtained.

Fig 4.11 Droplet detection and analysis macro

```
Function 1
[RmSendMessage("visilog",TOP_SET_STATE,0,"ProcessRight1");
P_image.MIP_VIEWCONSTR();
M_scrollzoom.GUI_SETVAL(0);
input=ImageManager.AUTO_INPUT_IMA(0," ");
IpSetCurCal("test emulsion 1");
opening(Input,12,"ima1");
substract(input,"ima1","ima2");
normalize("ima2",0,0,{0,255},"ima3");
lowpass_3x3("ima3","box",1,"ima4")
highpass_3x3("ima4","high",0,"ima5");
auto_threshold("ima5",{0,200},1,"ima6");
erode("ima6",3,"ima7");
reconstruct("ima6","ima7","ima8");
opening("ima8",3,"ima9");
separate("ima9",0,"bindist",3,"extmerge","labmark",0,"ima10");
logical_sub("ima9","ima10","ima11");
hole_fill("ima11","ima12");
border_kill("ima12","ima13");
label("ima13","ima14");
RmSendMessage("visilog",TOP_SET_STATE,0,"Analysis");
analyze("ima14","none","adjust","none",1,a1");
visilog.MIP_DISPLAY(input);
P_image.IO_LOAD_IMA("ima14");
P_image.IO_SHOW_HIDE();
P_image.IO_SHOW_HIDE();
P_image.IO_SHOW_HIDE();
P_image.IO_SHOW_HIDE();
P_image.IO_SHOW_HIDE();
```

4.7 Colloidal detachment

Particle removal forms the dominant feature in all cleaning processes, which is illustrated by the many techniques that have been developed to study the detachment of colloidal particles from a variety of substrates[27-30]. Recent publications on particle removal could be divided into three main techniques; (i) centrifugal methods using a force, equal to the force of adhesion perpendicular to the flat substrate[31], (ii) atomic force microscopy (AFM) in which a colloidal particle cantilever is used to measure the adhesion force from its deflection[32-35], while the

most common removal technique has been by (ii) liquid flow .

The second main objective in this study is to determine the magnitude of the critical force required to achieve detachment. Although the stagnation point technique has previously been used to observe detachment mechanisms[30,36-38] by increasing the wall shear stress outside the stagnation point, an horizontal flow cell has been employed in this study to observe detachment mechanisms *in situ*.

A particle deposited on one of the substrate surfaces is subjected to an hydrodynamic force parallel to the plate. The magnitude of the critical force is dependent on the liquid flow rate, fluid viscosity, particle radius, and the distance between parallel plates.

4.7.1 Horizontal flow cell design

There are numerous literature examples of techniques that involve the measurement of a controlled force, which promotes particle or droplet detachment. The particular type of technique investigated in this project uses a liquid flow with which to encourage droplet detachment from chemically modified surfaces in a parallel plate flow. This technique has been studied in detail by many sources including, Yiantsios[15] et al, and Sharma et al[54].

Preliminary flow cell studies were performed on the optical microscope , using direct visual observation and simultaneous picture analysis with a Visilog 5 imaging programme[26]. Horizontal flow cell particle detachment was studied and

droplet behaviour of various PDMS emulsion compositions were observed as a function of time. The adhesive strength distribution of particles are presented in the form of the percentage of particles adhering versus the applied wall shear stress. The latter can be converted to hydrodynamic force applied on the particles, F_H, through equation [4.15][1].

$$F_H = 8 \sigma d^2 \qquad [4.15]$$

where σ is the hydrodynamic wall shear stress, d is the particle diameter. Most experiments were repeated to test reproducibility satisfactorily. As was expected from similar experiments in literature, particles were not removed at once from a single-valued force but from a continuous distribution of forces overcoming adhesive bonds. Previous literature has regarded the shear stress wall force to remove 50% of the adhered species , F_{H50} , to be representative of the average particle strength adhesion.

The cross-linked PDMS droplets investigated in this study were allowed to settle on the substrate for a fixed period of 3hrs to simulate deposition period experienced during stagnation point investigations described in section 4.6. A fixed cross-linked PDMS emulsion was analysed, 0.05(v/v) total monomer, DMDES: MTMS, 0.01(v/v) NH_3, observing their adhesion/ removal properties by using a flow rate of 0 – 353 ml/min^{-1}. Pictures were obtained after a deposition period of 3 hrs and taken at increments of 5 flow rate from 0-100, over a constant area of observation, 14 mm^2 .

The horizontal flow cell experiments conducted in this study have been used as an extension of the stagnation point flow deposition investigations. The technique was used to observe the removal mechanisms of the droplets deposited on the substrate and their detachment by liquid flow. There have been several different flow cell designs and experimental conditions reported as a function of flow rate. However the cell used in this study consisted of two sample plates clamped together with a spacer between to create a channel through which the detachment solution flowed[15,40-42].

Niida et al[43] developed this design to include a rectangular glass tube in which particles were deposited on the bottom substrate plate, which could not be removed and had to be used repeatedly. Additional substrates had to be placed on top of the bottom glass plate of the cell , creating the potential for disturbed laminar flow lines and eddies through the cell[40,41,48]. These conditions forced particles to detach and provided false hydrodynamic and adhesion force data.

The cell design utilised in this work is shown in figure 4.12. It differs from the format described above in that it is constructed from machined brass with two rectangular plates screwed to the cell walls and the substrate to be studied formed the top plate . A black mirror-finished perspex trapezoid block, fixed to the center of the bottom plate, acted as background to the flowing solution. This reduced the number of surface asperities and so disturbed the flow and ensured that the surface provided significant contrast with the cross-linked droplets in the emulsion. The two plates were fixed at a gap ~ 0.5-1.0 mm to allow the solution to maintain a laminar flow through the cell. O-rings[41] were placed between the two plates to seal the cell assembly from leaks and pressure fluctuations. The

substrate from which detachment was observed directly was positioned in the indentation in the top plate, which was in turn placed directly on the microscope stage. The cell allowed the variety of different substrates to be investigated to be studied in situ, easily cleaned and fresh surfaces replaced to its original position after each experiment. Laminar flow was maintained throughout the investigations. The particles are deposited onto the underside of the top substrate from where they are washed off by the flow of the wash solution. The remaining experimental parts, including pump, flow cell, flow meter and three-way taps, were connected using Portex translucent, PVC tubing, 3.5mm internal diameter, as discussed in *Sharma et al* [39]. All solutions used in the flow cell were prepared using Milli Q water, de-gassed by boiling ,which ensured that the formation of air bubbles in the flow cell was reduced. The presence of bubbles in any part of the experimental set-up effects the flow rate and in extreme cases can remove droplets from the substrate.

Figure 4.12 Schematic representation of Horizontal flow cell

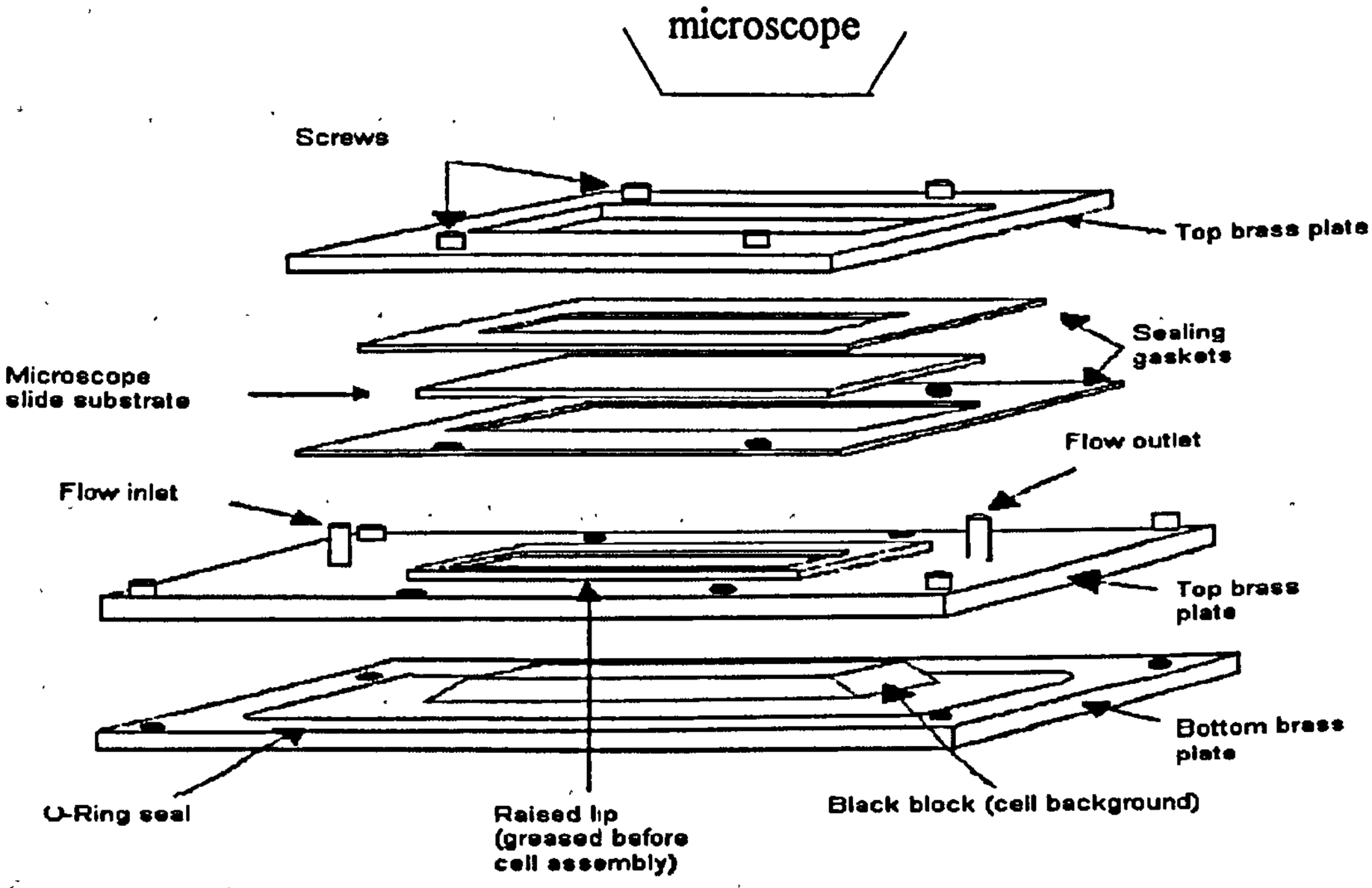

4.7.2 Experimental set up

The horizontal flow cell was constructed as shown in figure 4.12 and secured on the microscope stage. Milli Q water, 250ml, was pumped using a Cole Parner variable flow stainless steel gear pump, (0-2500 ml min^{-1} range), through the cell from a reservoir and flushed to waste at the start of each experiment. 100ml of cross-linked PDMS emulsion was introduced from a second reservoir, containing the colloidal emulsion ,through the inlet tube. The flow rate was regulated via a Gilson Instruments flow meter, GF-1460, fitted with a glass ball, capable of measuring liquid flow between 0-945ml min^{-1}. Air bubbles caught in the system were initially expelled by using a high flow rate, this was reduced to 150ml min-1 as the colloidal dispersion circulated through the system for 5 minutes. The cell flow remained stationary for 3 hours, to simulate the deposition time utilised during the stagnation point deposition experiment, (see section 4.6). This time was utilised to allow droplets to deposit on to the underside of the treated glass / mica substrate. This was a direct result if the density difference between the continuous and discontinuous phases. After this period, the pump introduced the removal solution for 60 seconds at 10 ml min^{-1}, to expel excess droplets away from the substrate and into waste.

This procedure ensured only droplets that had adhered to the substrate remained in the observation area. 250ml of the wash solution to be investigated was used to re-circulate through the cell during the detachment experiment, reducing the interaction of flowing droplets with those remaining on the substrate. During an experiment the liquid was re-circulated by placing the outlet pipe from the flow meter back into the liquid reservoir. A three-way tap was placed between the

pump and the cell to allow the flow to be diverted away from the cell when it was being cleaned and the flow meter outlet pipe was removed so that the liquid could be flushed to waste.

The same image capture and analysis equipment was used for the horizontal flow system as described in the stagnation point flow system, see section 4.6. The first picture was taken at an initial flow rate of 37ml min^{-1}. The solution was allowed to flow through the cell at this rate for 3 minutes until the system reached a removal equilibrium. The pump flow rate was increased and another picture was recorded. This procedure was repeated, in increments of 35ml min^{-1} until the maximum flow rate, 747ml min^{-1} was reached producing a total of 11 images. Various wash solutions were used during removal studies, including aqueous fluorescein, electrolyte solutions, SDS solutions and PDMS emulsions of various cross-linker volume fraction, see chapter 10. Particular care was taken to avoid air bubbles in the system particularly when using surfactants and therefore it was not possible to exceed an SDS concentration of 0.25M. The cell was cleaned by flushing 1l of Milli Q water through to waste at the end of each run and each substrate was removed. The spreading and strong adhesive properties of the cross-linked droplets on contact with the substrate surface rendered them non-reusable and data was compared between batches of the same substrate. However, results from the same substrate batch were found to be reproducible.

4.8References

1.Hunter, R.J., "Foundations of Colloid Science", Oxford University press, Oxford, 1989

2.Shaw, D.J., "Introduction to Colloid and Surface chemistry", Butterworth-Heinemann Ltd., Oxford, 1989

3. H.C.Li, P.L.de Bruyn, Surface Sci., 5, 203 (1966)

4. R.J.Hunter, "Zeta Potential in Colloid Science: Principles and Applications", Academic Press, London (1981).

5. M. von Smoluchowsk, Bull.Acad.Sci., Cracovie, 184 (1903)

6. P.H.Wiersema, A.L.Loeb, J.Th.G.Overbeek, J.Coll.Int.Sci., 22, 78 (1966)

7. R.H.Ottewill, J.N.Shaw, J.Electroanal.Chem., 37, 133 (1972)

8. R.W.O'Brien, L.R.White, J.Chem.Soc., Faraday Trans. 2, 74, 1607 (1978)

9. Werner,C., Jacobasch,J., Internationial journal of artificial organs, vol.22, 3, 160-176, 1999.

10.Mathews

11.Adamczyk, Z., Szyk, L., Langmuir, 16, 5730, 2000

12.Billet and Ottewill, "Wetting", Soc.Chem.Ind.Monograph, 25, 253, 1967

13.Jaycock and Ottewill, Trans.Inst., Mon., Met., 72, 497, 1963

14.Ter-Minassian-Saraga, "Contact Angle Wettability and Adhesion", Ad. In Chem.Ser. 43, 232, 1964

15.Yiantsios, S.G., Karabelas, A.J., J.Colloid Interface Sci., 176, 74, 1995.

16.Van Wanegen, A.R., Andrade, J.D., J.Colloid Interface Sci., 76, 305, 1980.

17.Ball, B., Fuerstenau, D.W., *Miner.Sci.Eng*. 5, 267, 1973

18.Baty,A,M., Suci,P,A., Tyler,B,J., Geesey,G,G., J.Coll.Int.Sci, 177, 307-315, 1996

19. M.Y.Boluk, T.G.M.van de Ven, Physicochemical Hydro., 11, 113 (1989)

20.T.Dabros, T.G.M. van de Ven, Colloid & Polymer Science, 261, 694 (1983)

21.Serizawa, T., Kamimura, S., Akashi.M., Colloids. Surf. A., 164, 237, 2000

22.Johnsonm.C.A., Lenhoff, A.M., J.Colloid.Interface.Sci., 179, 587, 1996

23.Hull.M., Kitchener, J.A., Trans. Faraday. Soc., 26, 3093, 1969

24. Zembala.M, Adamczyk.Z, Warszynski.P, Langmuir, 20, 24, 10517, 2004

25.Dabrós, T., van de Ven, T.G.M., J.Colloid.Interface Sci. 89, 232, 1982

26.Noesis, 6-8 Rue de la Réunion, Les Ulis, 91955 Courtabœf,

27.Visser.J., in "Surface and Colloid Science", (E.Matijevic, ed.). Vol.8, p.3., John Wiley & Sons, New York, 1976

28. Podczeck.F, J.M.Newton, Journal of Pharmaceutical Sciences, 84, 1067, (1995)

29. Visser.J. Journal Of Colloids and Interface Science, 34, 26, (1970)

30.Varennes.S, van de Ven.T.G.M., Physicochemical Hydrodynamics, 9, 537, (1987)

31.Krupp.H., Adv. In Colloid and Interface Sciences., 1, 111, (1967)

32.Binning.G., Quate.C.F., Gerber.C., Physical Review Letters, 56, 930, (1986)

33. Marti.O., Drake.B., Hansma.P.K., Applied Physics Letters, 51, 484, (1987)

34.Mizes.H., Eklund.Ott.E., Hays.D. Colloids and Surfaces A: Physicochemical and Engineering Aspects, 165, 11, (2000)

35. Schaefer.D.M., Gomez.J., Journal of Adhesion, 74, 341, (2000)

36.Varennes.S, van de Ven.T.G.M., Colloids and Surfaces, 33, 63, (1988)

37.Varennes.S, van de Ven.T.G.M., Physicochemical Hydrodynamics, 10, 415, (1988)

38. van de Ven.T.G.M., Colloids and Surfaces, 39, 107, (1989)

39.Sharma, M.M., Chamoun, H., Sarma, Sita Rama Sarma, D.S.H, Schechter, R.S.,J.Coll.Int.Sci., 149, 121 (1992)

40. Elzo.D., Schmitz.P., Houi.D., Joscelyne.S., Journal of Membrane Science.,109, 43, (1998)

41.Das.S.K., Schechter.R.S., Sharma.M.M., Journal of Colloid and Interface Sci., 164, 63, (1994)

42.Das.S.K., Sharma.M.M., Schecter.R.S., Particulate Science and Technology, 13, 227, (1995)

43.Niida, T., Kousaka,Y., Furukawa, T., Particle & Particle systems characterisation, 6, 69, 1989

Chapter 5 Cross-linked PDMS emulsion characterisation

5.1 Introduction

A range of cross-linked PDMS emulsions were prepared in accordance with the method described in chapter 3, section 3.3. These emulsions were then subjected to a range of characterisation techniques to obtain the optimum features necessary to observe the deposition, adhesion, spreading and removal properties of cross-linked PDMS colloidal systems under optical microscopy. These properties include stable colloidal emulsions, containing droplets of low viscosity and with diameters >1μm.

5.2 Emulsion characterisation

5.2.1 Emulsion turbidity

The turbidity of dialysed cross-linked PDMS emulsions, at a fixed total monomer, 0.05(v/v) volume fraction,as described in chapter 3, was observed using an *Olympus Camedia* digital camera, C-860L, 1.3 million pixels. Figure 5.1 illustrates the increase in emulsion turbidity and the simultaneous decrease in phase stability as the volume fraction of tri-functional cross-linker, MTMS, increases. The visual appearance of the systems also indicates the change from low viscosity, low refractive index deformable droplets to white highly cross-linked rigid particles. The amount of light scattered by the colloidal matter increases with the increasing cross-linker density. It was noted that those samples containing MTMS ϕ under 0.5(v/v) showed increasing phase separation and/or sedimentation with time and with the upper clear phase more apparent towards 1.0(v/v). Those emulsions dialysed against Milli Q water were found to be more stable with time than

undialysed systems extending the shelf life from a few weeks to over a month.

Fig 5.1 Turbidity change as a function of MTMS, ϕ, 0.01 -1.0 (v/v)MTES,left – right

In addition any sediment or creamed phases could be re-dispersed by simple aggitation. This observation was in good agreement with previous findings[1,2] which suggested that the traces of NH_3, still present in undialysed systems, propagate further reactions and increase the cross-linked networks, or they act as background electrolyte and reduce the EDL repulsion between the droplets. This feature accelerates the aggregation / coagulation processes and increases the average droplet size and polydispersity simultaneously.

5.2.2 TEM

Cross-linked PDMS droplets were isolated from the dialysed emulsions above with MTMS ϕ 0.05-0.8 (v/v)and the images recorded using a Joel JEM TEM, see chapter 4. It was not possible to observe isolated PDMS droplets containing less than 0.05(v/v) ϕ MTMS as the droplet shell was not able to withstand the sample

preparation for TEM analysis. At low MTMS ϕ, 0.05 (v/v) – 0.2 (v/v), emulsion droplets are formed, and they collapse under the pressure of the sample grid and the cross-linked PDMS liquid phase that was contained inside the droplets is now outside a PDMS shell, plate I (a-c). As the MTMS ϕ was increased from 0.2-0.4 (v/v), the average droplet diameter decreased as the cross-linking network becomes more densely packed and PDMS oligomer chains were brought closer together, see plate I (c-d). The droplets are observed to deform under low pressure but remain structurally intact. This is in agreement with the findings reported by Wegener[3] who suggested that a microgel structure is adopted inside the droplets. The highest MTMS ϕ observed, 0.4(v/v) – 0.8 (v/v) MTMS ϕ, displayed some aggregation, irregular droplet shapes and a wider polydispersity, see plate I (e). The cross-linked network became so rigid that "particle-like" spheres were formed with average diameters 90% lower than the 0.05(v/v) MTMS droplet diameters. All the synthesised emulsion droplets investigated showed enhanced stability to coalescence, in accordance with previous reports[3-6] who attributed this property to the high density of surface-ionised hydroxyl groups, similar to those reported for Stőber[7] silica particles. This was confirmed by the negative surface potentials measured and discussed in section 5.2.5. These emulsions were also found to have enhanced stability with respect to commercially produced PDMS[8], and were therefore chosen as model systems to observe droplet deposition and removal behaviour without interference from bulk phase droplet-droplet interactions.

Plate I: TEM images of PDMS droplets, fixed total monomer 0.05(v/v) as a function of MTMS ϕ; (a) 0.05(v/v), (b) 0.1(v/v), (c) 0.20(v/v), (d) 0.4(v/v), (e) 0.8 (v/v)

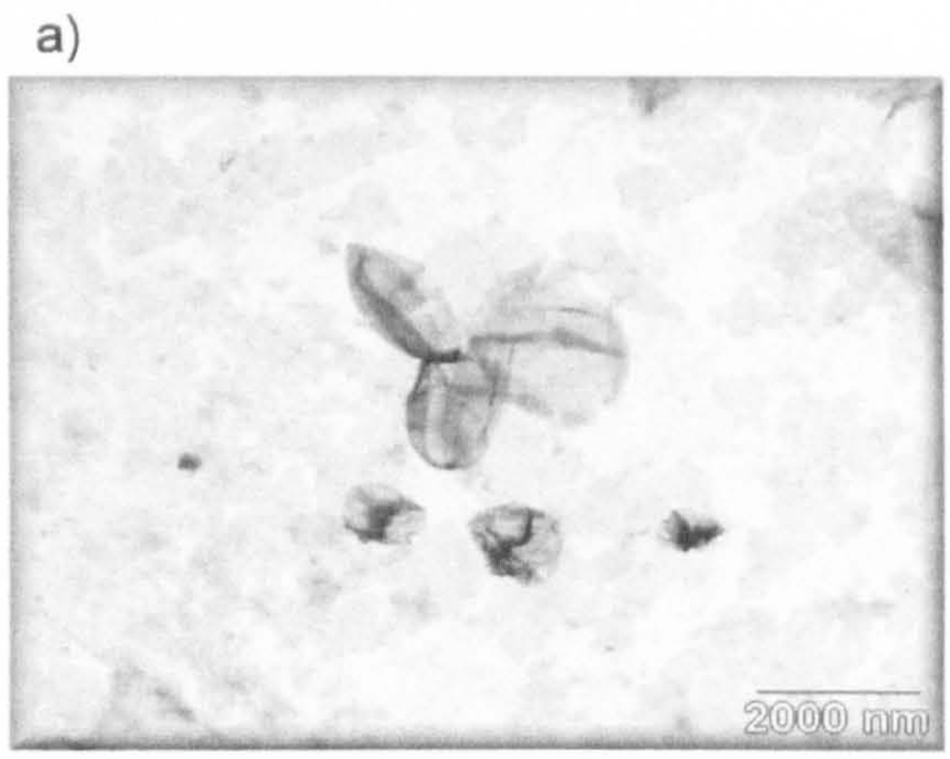

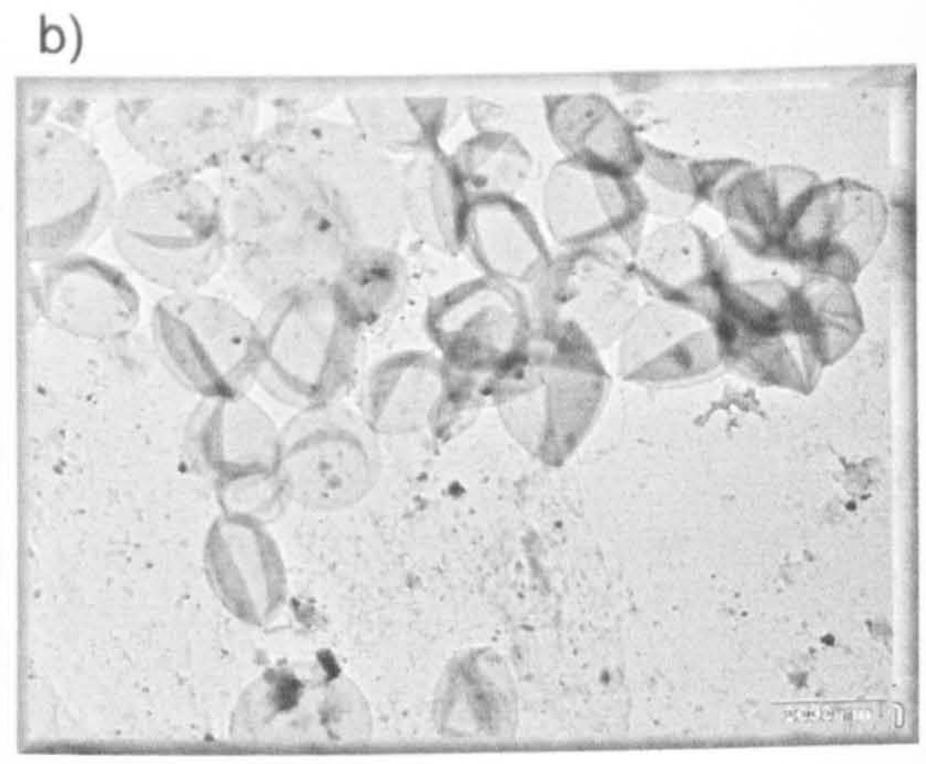

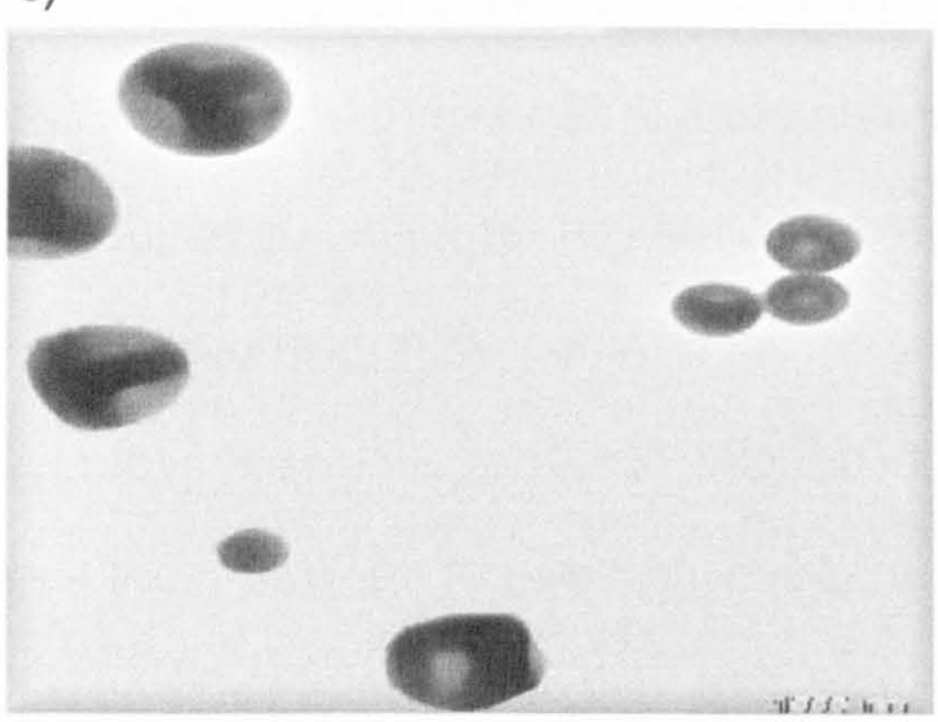

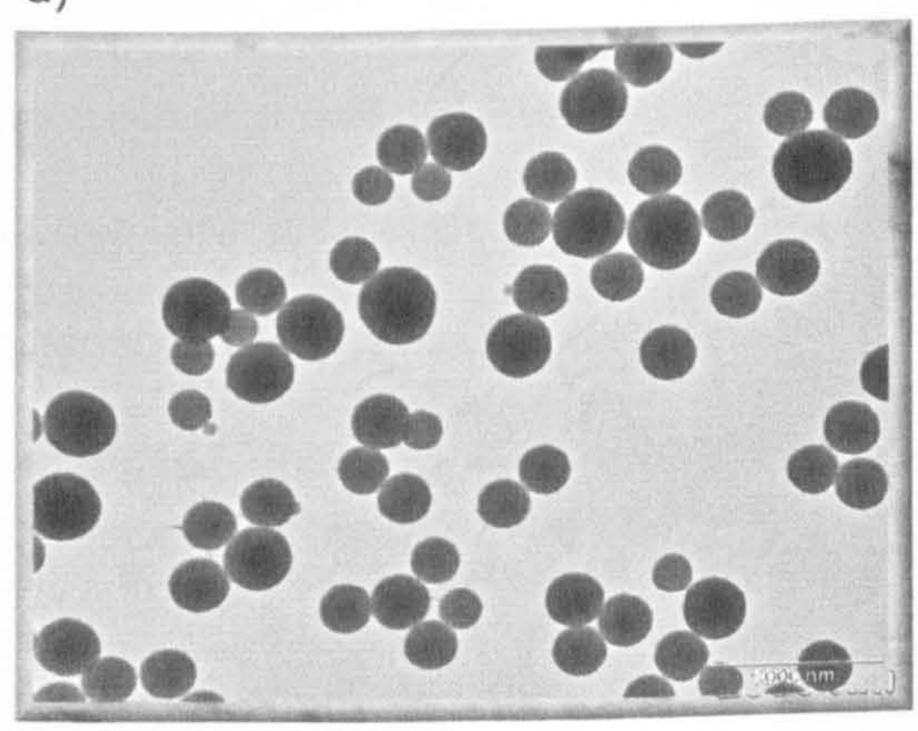

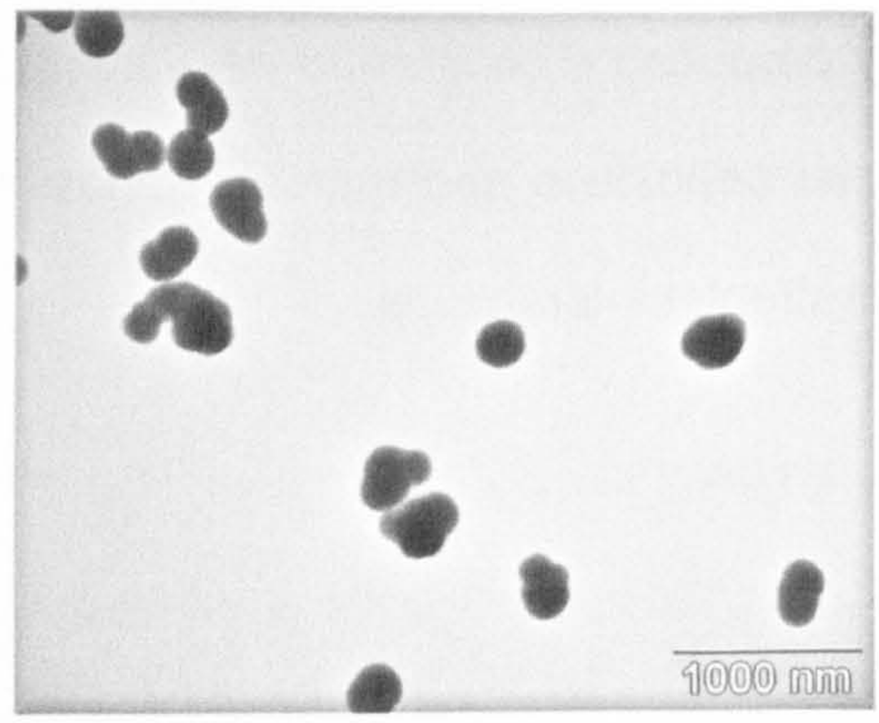

5.2.3 Influence of NH_3 concentration

The influence of NH_3 concentration on the formation of cross-linked PDMS emulsions has been the subject of previous studies by Goller et al[2]. In this study, the presence of NH_3 was observed to significantly effect the polydispersity and surface tension of the droplets. TEM images of dialysed emulsion samples of 0.01 (v/v) fixed total monomer and fixed cross-linker 0.2 (v/v) are shown in figure 5.3 containing (a) 0.01(v/v) NH_3 and (b) 0.3(v/v)NH_3. In image (a), the cross-linked droplets appeared relatively monodisperse and remained structural intact. The dark "ring" surrounding each droplet suggests that there is a deformable outer shell with an approximate thickness of ~100nm. In comparison, image (b) illustrates that an increase in NH_3 concentration leads to a decrease in droplet shell thickness. Droplet flocculation and a range of droplet sizes is also observed as a result of fluctuating surface potentials and a reduction in the inter-droplet separation through diminished electrostatic repulsive forces. This observation is in agreement with Goller et al[2] who attributed the increase in average droplet diameter to the presence of higher NH_3 concentration and therefore an increase in ionic strength.

A Brookhaven zetaliser was used to measure the surface charge of the fixed cross-linked PDMS emulsion above as a function of increasing the ammonia concentration without the presence of background electrolyt . An increase in the presence of NH_3 ϕ from 0.01(v/v), 0.1 (v/v), 0.2 (v/v) to 0.3 (v/v) showed a steady decrease in the droplet surface charge, and is less negative, from -3.0, -1.75, -1.23 to -1.55 $10^{-8}m^2s^{-1}V^{-1}$ respectively. The electrophoretic mobility analysis was found to be in agreement with TEM images which showed a simultaneous

increase in droplet size and polydispersity.

Fig 5.2 TEM images of fixed total monomer,ϕ , 0.01(v/v) (a)0.01(v/v) NH_3, (b)0.3 (v/v) NH_3

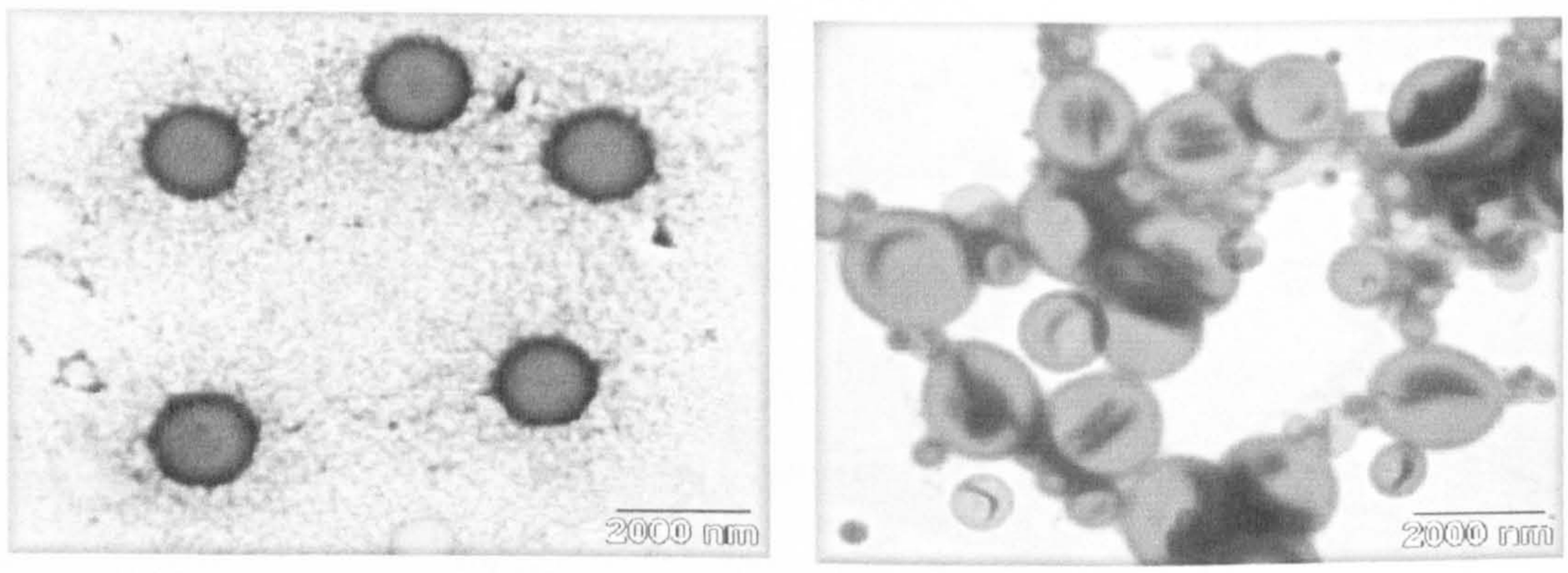

5.2.4 PCS

Photon Correlation Spectroscopy, PCS, was used to determine the effect of total monomer concentration, cross-linker ϕ, electrolyte and surfactant concentration on the cross-linked droplet hydrodynamic diameter D_{hyd}. At least three sets of measurements were made for each sample to obtain reliable average diameter values. Figure 5.3 illustrates the gradual decrease in the average hydrodynamic diameter as the MTMS volume fraction, ϕ, was increased using an emulsion system of a fixed 0.01(v/v) total monomer and 0.01(v/v) NH_3(aq), (● data points). This trend is in excellent agreement with the observations reported by Obey and Vincent[1] for similar fixed monomer emulsion systems (● data points). The difference in the diameter magnitude between the two data sets and can be attributed to the variations in experimental procedure.

The steepest decrease in the average droplet size was evident at low MTMS ϕ , 0.0(v/v) - 0.4(v/v), from approximately 1.6 μm to 0.5 μm. It was suggested that the increased presence of cross-linker decreased the solubility of the PDMS oligomers in the system[1]. This behaviour increased the rate of nucleation sites available and led to the formation of a large number of nuclei during the emulsion growth and this resulted in smaller droplets. A sharp decrease in the droplet diameter can be observed between 0.4 (v/v)-0.6(v/v) MTMS ϕ and has been attributed to the enhanced rate of production of nucleation sites for emulsion growth which resulted from the reduced solubility of cross-linked PDMS oligomers[9].

Fig 5.3 Effect of cross-linker ϕ (v/v) on droplet diameter at fixed 0.01 (v/v) total monomer

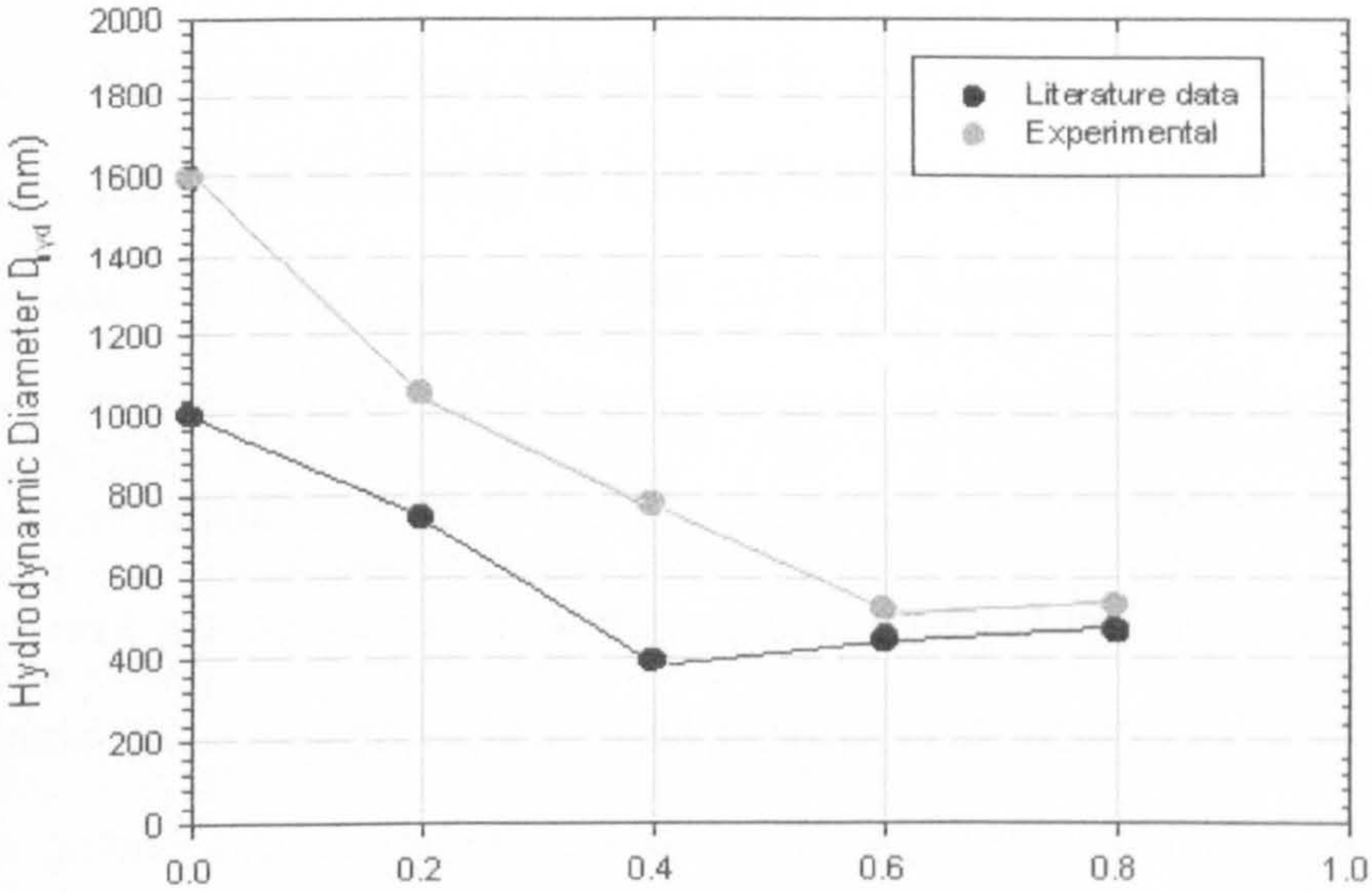

The droplet size then remains fairly constant at 900nm due to the elastic nature of

the "microgel" transition phase. This meta stable equilibrium state allows cross-linker to be absorbed into the network structure without significant changes in volume or diameter. The size stability is also influenced by density matching, where the motion of the droplets is restricted by the similarity between the density of the continuous and discontinuous phases, see chapter 3, and reduces the tendency for droplet coalescence. Above 0.8(v/v), the cross-linked network becomes so dense, the oligomers present form rigid, silica-like, solid particle which accommodates an increase in ϕ MTMS by adding it to the existing structure and therefore a rapid droplet size increase is observed. The higher ratio of tri-functional to di-functional material in solution increases the probability of cross-linking reactions and produces irregular shaped particles with increased polydispersity and increased ϕ MTMS. It became difficult to obtain accurate PCS measurements[3].

One of the main objectives of this study was to investigate the spreading behaviour of cross-linked PDMS droplets on rigid substrates, see chapter 1. As a result of the data obtained from the TEM images and PCS measurements, only dialysed emulsion systems containing under 0.2 (v/v) ϕ MTMS were found to possess sufficiently large diameters and low viscosity enabling their adhesive and spreading properties to be observed under optical microscopy. Previous literature[9] has shown that above pH4 cross-linked PDMS emulsions are stable and show very little effect on the physical properties. Based on this finding all emulsions used in this study were kept at a fixed pH7-8 throughout the investigations.

The influence of MTMS volume fraction, ϕ, on cross-linked PDMS droplet diameters was observed to increase proportionally with 0.01(v/v), 0.025(v/v),

0.05(v/v) total monomer ϕ, see figure 5.4. The highest starting concentration of monomer displayed in the greatest droplets size increase due to the increased availability of nucleation sites. No Ostwald ripening processes was observed in any of the emulsion systems investigated, including 0.05(v/v)MTMS and they remained stable through every measurement.

Fig 5.4 D_{hyd} as a function of total monomer volume fraction, ϕ,

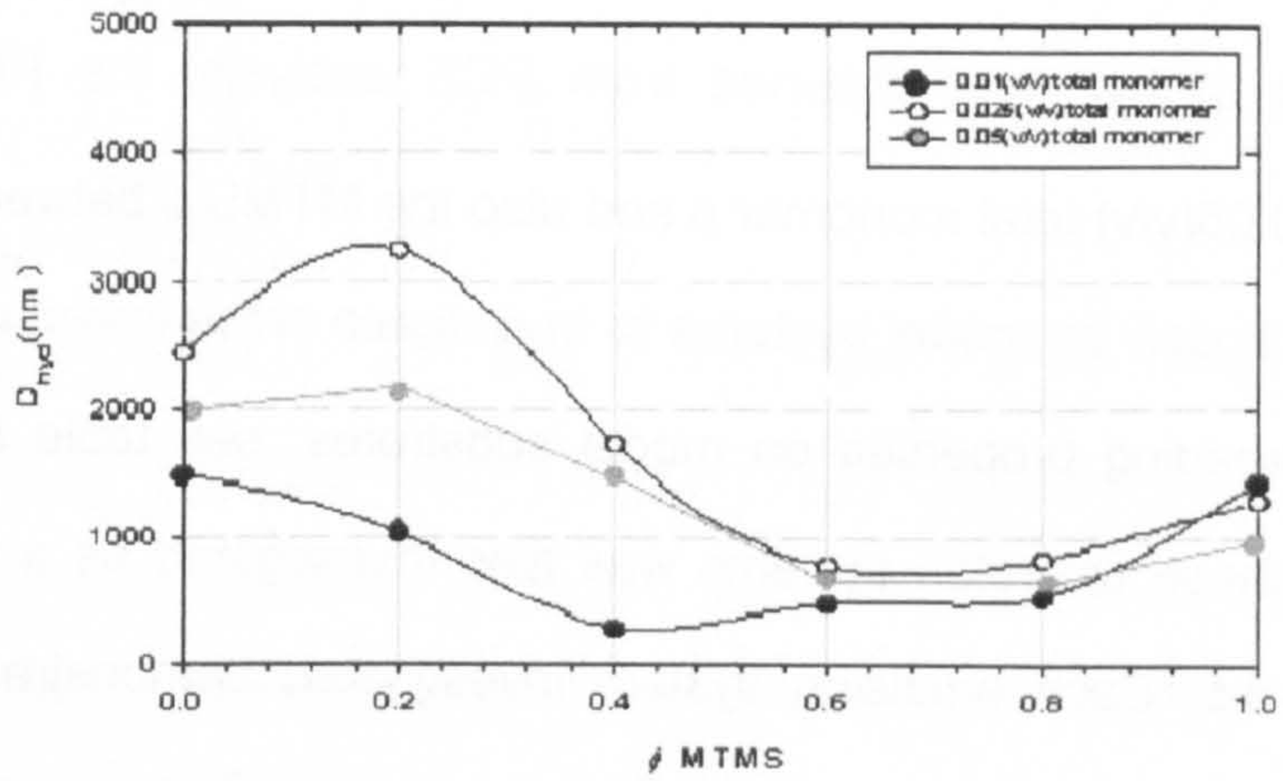

Overall the average droplet size and polydispersity was enlarged with the increasing total monomer ϕ present, and this was expected with the larger amount of monomer available for the polymerisation process. Emulsion systems containing >0.07(v/v) total monomer were not investigated as it was above the solubility limit of DMDES in aqueous medium and any unreacted monomer that solubilised inside, forming PDMS droplets, increased the polydispersity further[9]. The largest stable cross-linked droplet diameters were recorded for those emulsions systems containing 0.05(v/v) total monomer and were visible within the range of the optical microscope.

Table 5.1 Influence of MTMS ϕ on D_{hyd} at fixed 0.05(v/v) total monomer

MTMS ϕ (v/v)	0.05 (v/v) total monomer D_{hyd} (μm)	Error (+/-)
0.000	2.0	0.25
0.005	1.7	0.31
0.01	1.9	0.10
0.05	2.4	0.10
0.1	1.7	0.20

As a result of the data obtained from PCS analysis, the PDMS emulsions containing 0.05(v/v) total monomer ϕ and also the MTMS ϕ between 0.0(v/v) – 0.2 (v/v) were chosen as model systems to investigate cross-linked droplet adhesion and the spreading properties on model substrates, see table 5.1. The droplet stability of these emulsion systems was also investigated as a function of time, see figure 5.5. Each emulsion system investigated demonstrated a significant droplet size increase immediately after preparation. Those systems containing less than 0.05(v/v) MTMS ϕ, showed the largest droplet growth as they reached an hydrodynamic diameter almost four times that of the original. However the rate of nucleation and growth during polymerisation was relatively slow. The phase stability of the systems deteriorated after four weeks as the droplets reduced to their original size. The emulsion systems containing 0.05(v/v)-0.1(v/v) displayed similar changes as the droplet size increased to over three times the original diameter.

Fig 5.5 Hydrodynamic diameter, D_{hyd}, as a function of time at fixed 0.05(v/v) total monomer

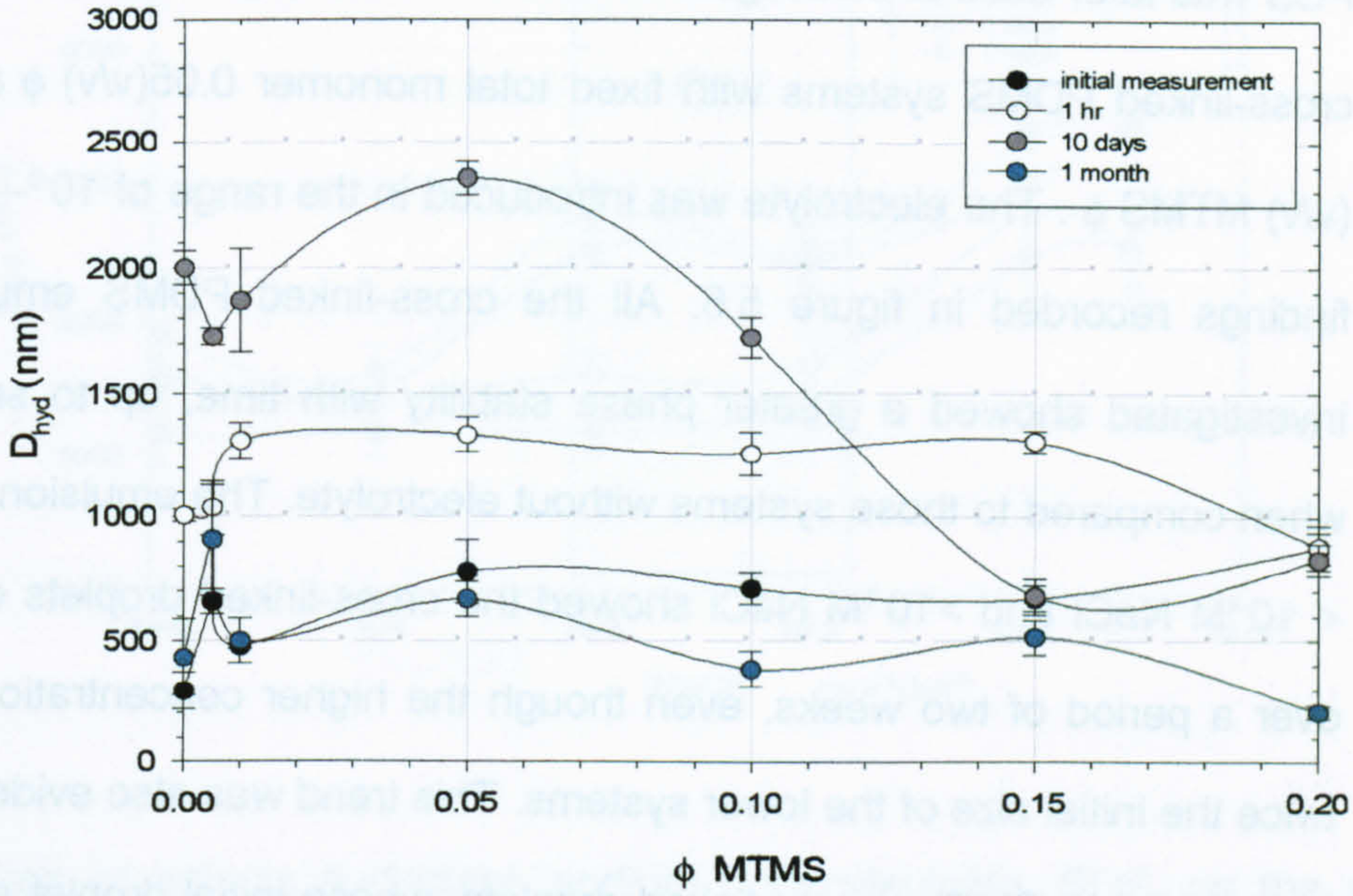

Emulsions that contained above 0.15(v/v)-0.2(v/v) MTMS ϕ reached an equilibrium size in a few hours which suggested rapid nucleation and growth of the di-functional and tri-functional monomers and they remained stable as a result of the greater presence of cross-linking within the network. The loss of phase stability after a few days was accompanied by the final droplet diameter being much smaller than the initial measurement. This trend was also observed by Wegener[3] for emulsion systems containing 0.4(v/v)-0.6(v/v) MTMS ϕ who related it to density matching effects, see chapter 3.

The differences in particle size values shown by TEM and PCS measurements could be attributed to the drying processes and deformation that droplets under go during TEM sample preparation. The polydispersity was approximately below 8% and could therefore be considered monodisperse. Above 0.5(v/v) MTMS ϕ,

polydispersity increases between 10%-20%.

PCS was later used to investigate the effect of electrolyte, NaCl, concentration on cross-linked PDMS systems with fixed total monomer 0.05(v/v) ϕ and fixed 0.05 (v/v) MTMS ϕ . The electrolyte was introduced in the range of 10^{-5}– $3x10^{-1}$ and the findings recorded in figure 5.6. All the cross-linked PDMS emulsion systems investigated showed a greater phase stability with time, up to several months, when compared to those systems without electrolyte. The emulsion that contained < 10^{-4}M NaCl and >10^{-1}M NaCl showed the cross-linked droplets doubled in size over a period of two weeks, even though the higher concentration systems had twice the initial size of the lower systems. This trend was also evident between 10^{-3} M –10^{-2}M NaCl. The cross-linked droplets, whose initial droplet size was similar to those of lower electrolyte concentration, swelled to triple the size after one week. This happened through coalescence and they remained at this size for one month.

This would suggest that the CCC lies between these values. This is in good agreement with Teare[9], who determined the critical electrolyte coagulation (CCC) for KCl at $5x10^{-3}$ mol dm^{-3} by using 0.01(v/v) total monomer, 0.01(v/v)NH_3 and without MTMS, 5 days after preparation. At KCl > $7.5x10^{-3}$ coalescence occurred after 4 hrs, while those systems that contained KCl < $5.x10^{-3}$ showed a stable emulsion. However the kinetics of coalescence decreases with increasing cross-linker ϕ, e.g 0.2(v/v) had slower coalescence. The presence of even low ϕ MTMS makes these emulsions resistant to coalescence. However, no difference was observed in the CCC as MTMS ϕ was increased from 0.0(v/v), 0.1(v/v) to 0.2(v/v).

Fig 5.6 D_{hyd} of cross-linked PDMS emulsions as a function of [NaCl]

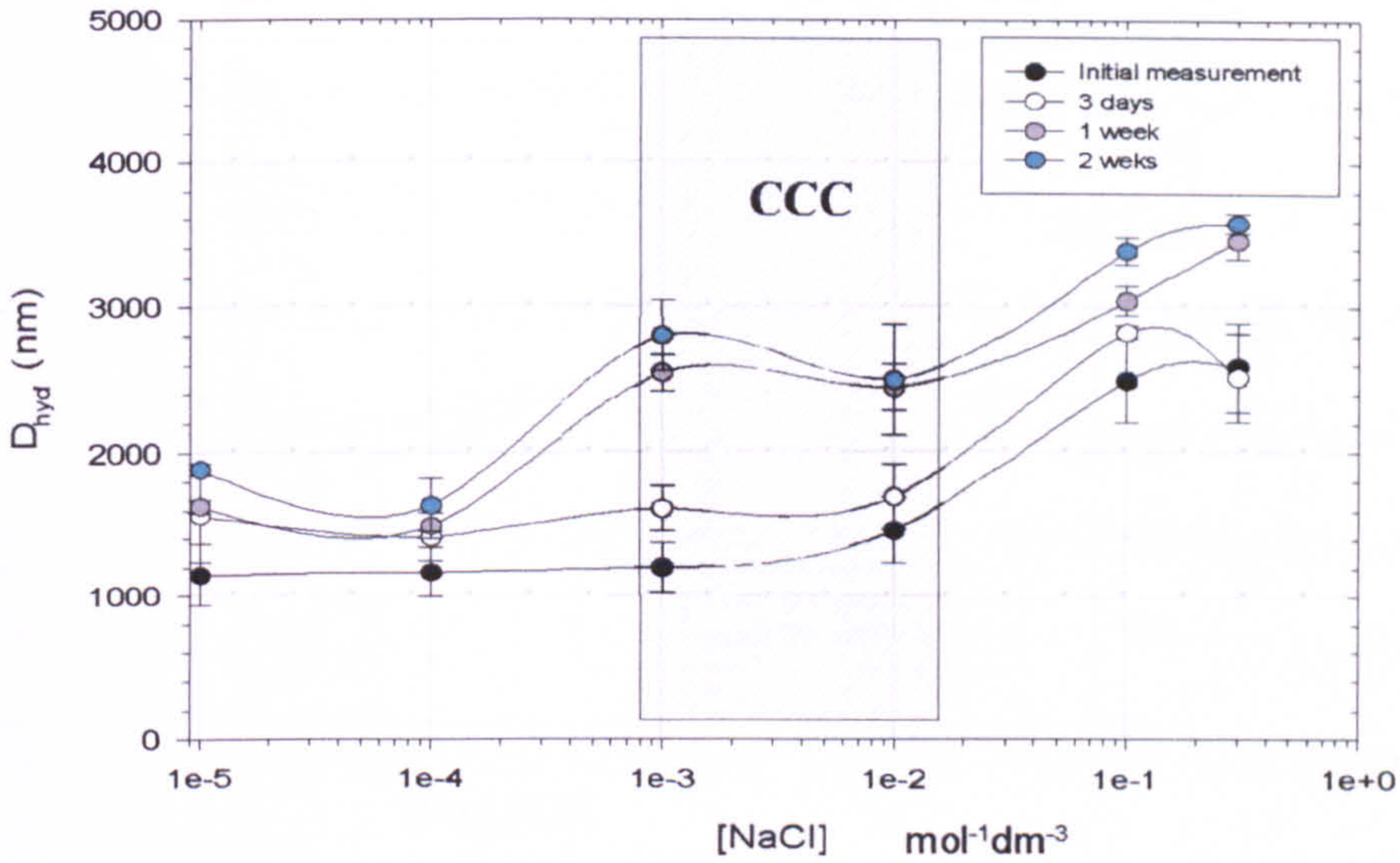

The addition of anionic surfactant, sodium dodecylsulpate, SDS, on the same fixed parameter emulsion as above but without the presence of electrolyte was investigated. A variety of SDS solutions concentrations, 0.08mM -8.0mM, were introduced into the systems and the changes in droplet hydrodynamic diameter were monitored as a function of time. The results displayed in figure 5.7. The system investigated with the lowest surfactant concentration, 0.08mM, indicated that the SDS molecules preferentially adsorbed onto the droplet surface due to the presence of surfactant-like cross-linked PDMS chains. The droplet hydrodynamic diameter was observed to swell almost immediately after the surfactant was introduced and was measured to be more than three times that of cross-linked droplets without the presence of surfactant. The swelling mechanism continued steadily over several weeks, after which the droplets swelled to almost twice their original size. As the surfactant presence was increased, 0.8mM SDS, there was a less pronounced effect on the droplet growth and appeared to stabilise after one week.

Fig 5.7 Effect of adsorbed SDS effect on cross-linked PDMS emulsion droplets.

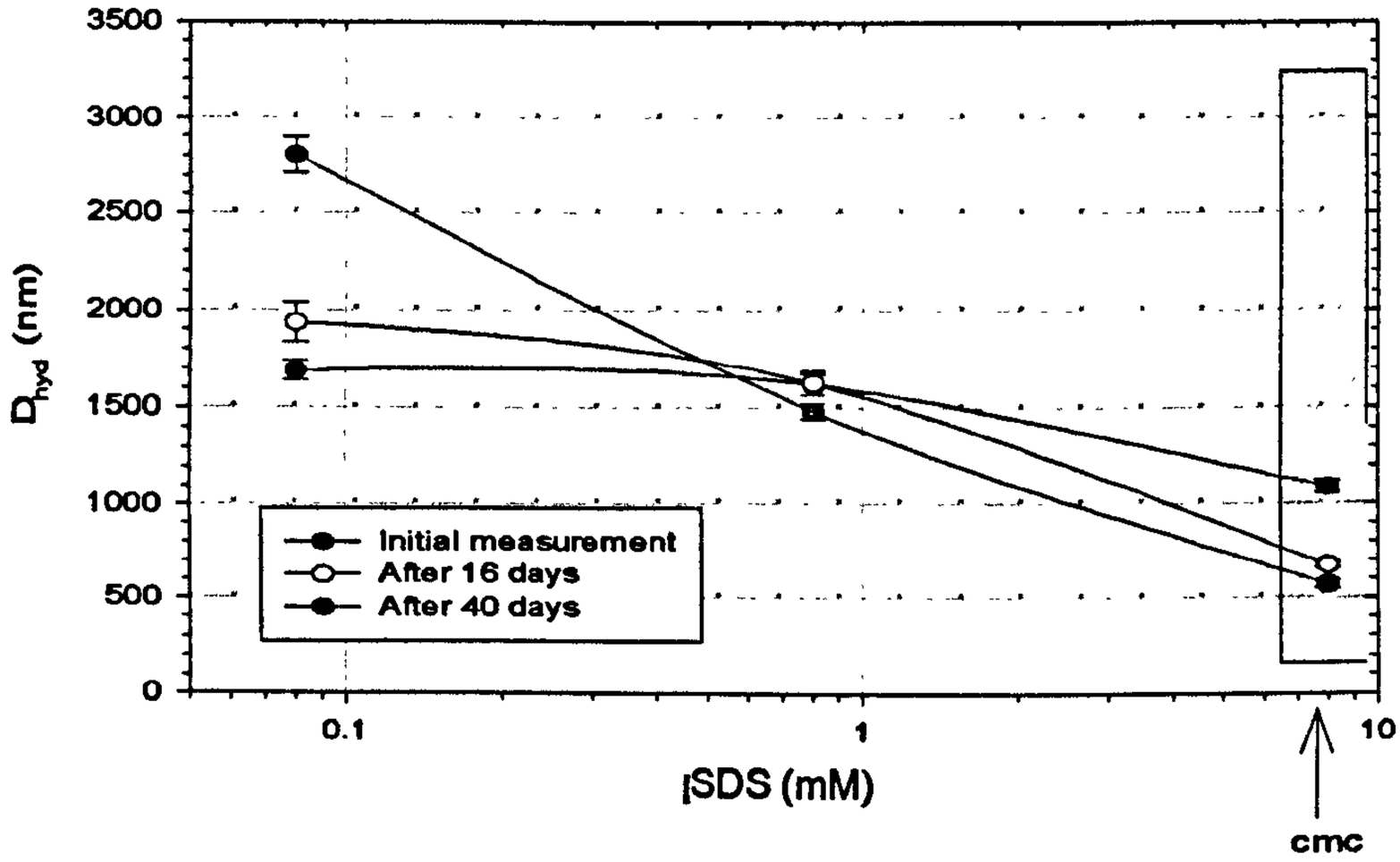

However as the SDS concentration neared the cmc point, > 8.0mM, the droplets appeared to have become saturated with SDS almost immediately after its introduction and actually began to contract with time. These observation were in direct agreement with those noted by Anderson[10], who reported that the addition of surfactant into these emulsion systems produced smaller droplet sizes due to the lowering of the interfacial tension and the reduced amount of energy required to increase the interfacial area.

5.2.5 ζ-potential measurements

The cross-linked PDMS emulsions used in this study are prepared without the presence of surfactant and are stabilised by functionalised linear PDMS and therefore have a fluid interface. These droplets are deformable and their motion in an applied electric field are influenced by the internal flow of polymer chains contained inside. Previous studies[9] have suggested that droplets are affected in

the same manner as solid particles of the same surface potential or κa value in electrophoretic theory[11], especially when an adsorbed surfactant monolayer is present[8], as there is no significant momentum transfer across the oil/water interface for moving droplets. This assumption has not been proven or disproven for synthesised cross-linked PDMS emulsions. The samples investigated by Teare[9] were dispersed in $1x10^{-3}$ mol dm^{-3} KCl as a background electrolyte, and a series of five experiments were conducted for each sample. Only small fluctuations in the electrophoretic mobility were reported for the PDMS droplets containing MTMS ϕ 0.0(v/v), 0.1(v/v) and 0.2(v/v), $0.5x10^{8}$, in solutions greater than pH5.

Electrophoretic mobility measurements made for this study, were conducted on a Malvern ZetaPlus Zetaliser, using dialysed PDMS emulsion systems with varying total monomer ϕ and cross-linking density under 0.2(v/v). Each sample contained $1x10^{-3}$ mol dm^{-3} KCl as background electrolyte. All the systems indicated that the cross-linked droplets particles were negatively charged, resulting from the dissociation of surface groups, (HO^{-}) which are present at the ends of mobile PDMS chains at the oil-water interface.

The surface charge provides the emulsion system with an electrostatic and kinetic surface energy barrier against coagulation. This stability has been attributed to the high density of surface-ionised hydroxyl groups[3-6], similar to those observed for the Stöber silica particles[7]. It has been suggested that the synthesised PDMS emulsions, used in this study, have enhanced stability, against coalescence, with respect to similar commercially produced PDMS. This property has been attributed to the preferential adsorption of linear PDMS chains at the oil/water

interface[8], see section 5.2.2. This provides the droplets with enhanced Gibbs elasticity and is not evident in homogeneous commercial PDMS. The surface ζ-potential of the cross-linked droplets was measured as a function of tri-functional cross-linker (MTES) ϕ at total monomer volume fractions 0.01(v/v), 0.025(v/v) and 0.05(v/v), see figure 5.8.

Fig 5.8 Effect of total monomer, ϕ, on droplet surface ζ- potential as a function of MTMS ϕ

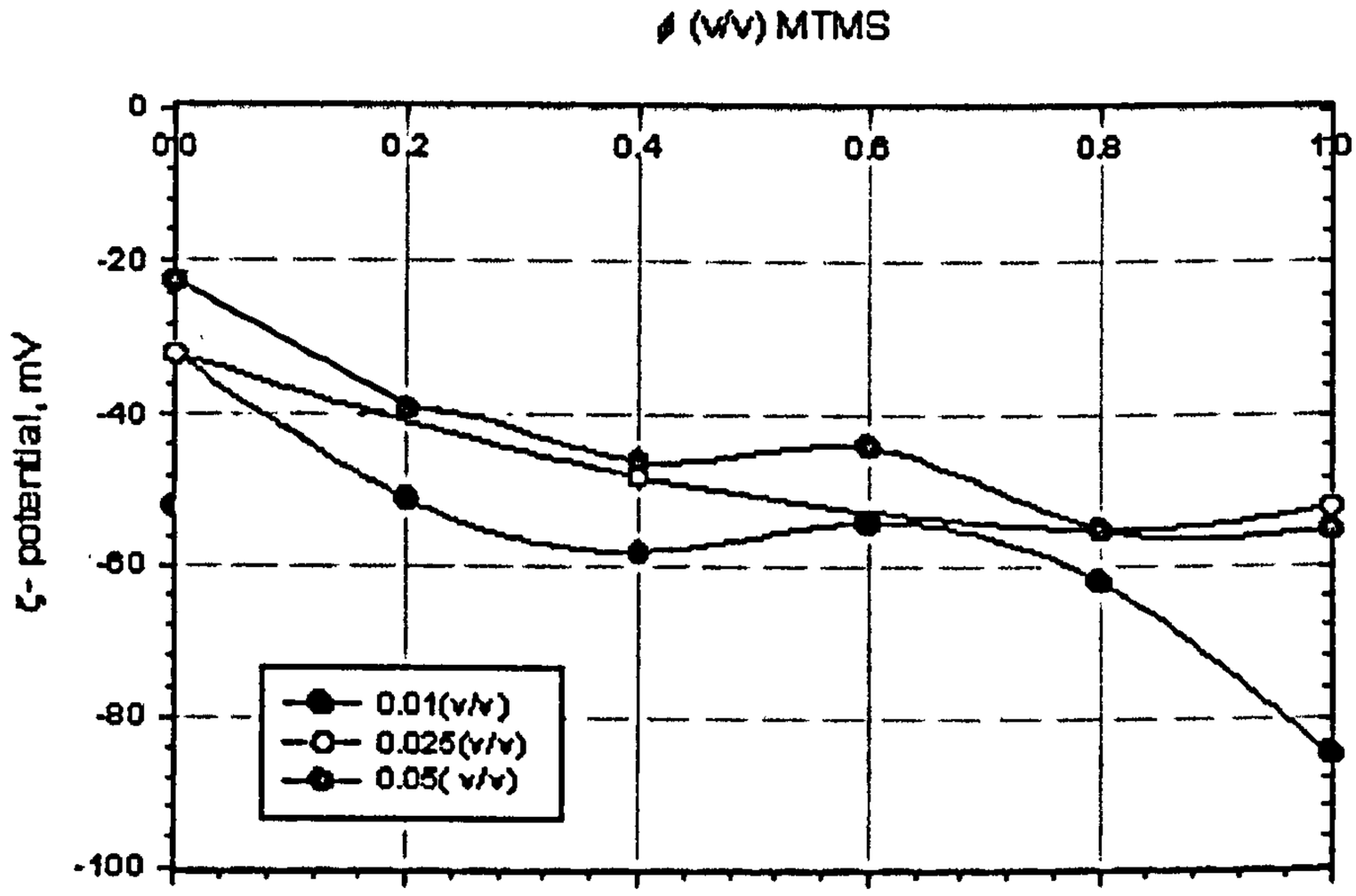

Overall there was an increase in surface negativity as MTMS ϕ was increased from 0.0(v/v) – 0.2(v/v),corresponding to the sharp decrease in droplet diameter. The presence of greater cross-linking density combined with the increased surface potential provides enhanced stability against coalescence. These measurements were in excellent agreement with Wegener[3] who also noted that increasing MTMS ϕ of the PDMS droplets simultaneously decreased the average electrophoretic mobility and particle size.

Similar trends were observed as the total monomer ϕ was increased from 0.01(v/v) – 0.05(v/v) with varying MTMS ϕ. There was gradual decrease in surface negativity as the total monomer ϕ was increased from 0.01(v/v) -0.05(v/v), with -10mV difference between emulsions. The measurements confirmed that it was possible to use the highest total monomer ϕ 0.05(v/v) systems to obtain stable cross-linked droplets observable under optical microscopy and not loose surface negativity. The surface properties of the droplets are presented in table 5.2 as a function of MTMS ϕ.

Table 5.2 MTMS ϕ effect on surface potential of PDMS droplets, 0.05(v/v) total monomer

MTMS ϕ (v/v)	ζ-potential (mV)	Error (+/-)	Mobility ($10^{-8}m^2s^{-1}V^{-1}$)	Error (+/-)
0.000	- 22.3	0.6	-3.24	0.08
0.005	- 29.7	2.7	-0.74	0.49
0.01	- 25.2	2.5	-1.36	0.20
0.05	- 25.4	2.1	-1.85	0.17
0.1	- 41.8	1.4	-1.58	0.11

The surface charge stability of cross-linked droplets was investigated as a function of time and illustrated in figure 5.9. Dialysed emulsion systems were used with fixed 0.05(v/v) and varying MTMS ϕ from 0.0(v/v)-0.2(v/v). The increase in surface charge negativity corresponded to the reduction in cross-linked PDMS droplet diameter that was observed after several weeks. This behaviour was also reported by Teare[9] where droplets of low viscosity, i.e. low MTMS ϕ, from emulsions of similar composition displayed the least negative mobility. In addition, the rate and magnitude of surface potential change decreased with increasing MTMS ϕ. The

most significant surface charge changes over time and occurs at the lowest cross-linker densities, between 0.0-0.1(v/v). This trend could be as a result of the mobility of PDMS chains which migrate more slowly to the droplet interface. Above 0.1(v/v), the increased cross-linked network restricts the movement of the anionically terminated chains and therefore the magnitude of the surface charge is determined by the chains present initially.

Fig 5.9 Droplet surface ζ-potential as a function of MTMS ϕ

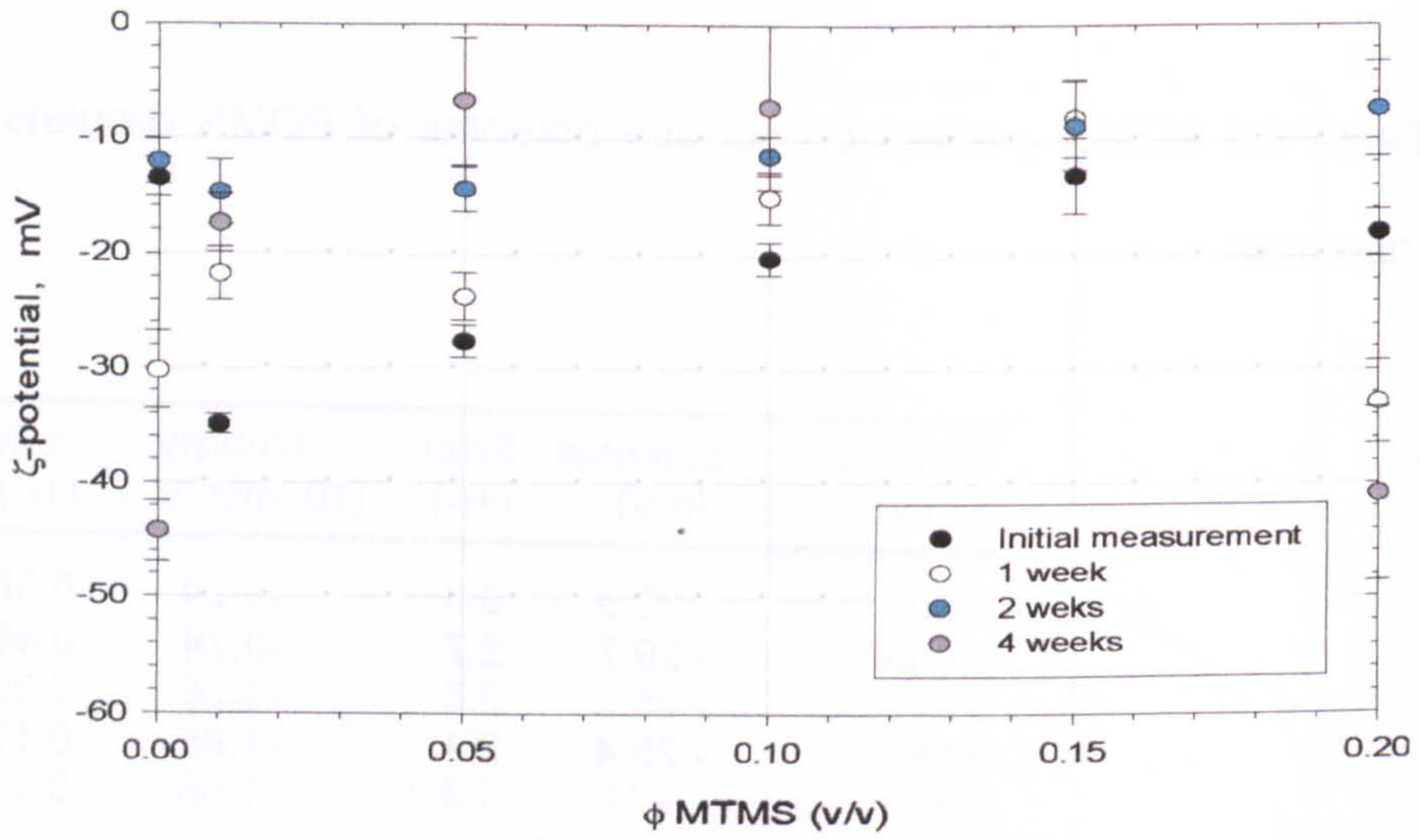

A range of NaCl electrolyte concentrations were added to cross-linked PDMS emulsion systems with fixed total monomer 0.05(v/v)ϕ and MTMS 0.05(v/v)ϕ. The resulting effects were recorded using a Malvern *ZetaPlus Zetaliser* without the presence of KCl, see table 5.3. An increase in electrolyte concentration resulted in a significant decrease in droplet surface charge negativity as shown in table 5.3.

Table 5.3 ζ-potential of cross-linked droplets as a function of NaCl concentration

[NaCl] (*M*)	ζ-potential (mV)	Error (+/-)	Mobility ($10^{-8}m^2s^{-1}V^{-1}$)	Error (+/-)
10^{-5}	-35.9	1.45	-2.8	0.11
10^{-4}	-29.9	0.91	-2.3	0.07
*10^{-3}	-31.6	1.17	-2.5	0.09
10^{-2}	-27.1	0.54	-2.1	0.04
10^{-1}	-16.2	0.89	-1.3	0.07
$3x10^{-1}$	- 5.7	2.75	-0.4	0.21

*value close to CCC

However, it was noted that the lowest electrolyte concentration produced a lower or more negative droplet surface potential than those droplets measured without the presence of electrolyte. This behaviour can again be related to the droplet size increase with electrolyte presence. Even above the CCC 10^{-3} – 10^{-2} mol dm^{-3},there is a significant amount of negative surface potential, approximately -30mV. Teare[9] and Neuman et al[8] also observed this trend for PDMS systems without MTMS in the presence of KCl and NaCl electrolyte respectively. The same emulsion systems of fixed 0.05(v/v) total monomer and 0.05(v/v) MTMS ϕ was investigated in the presence of the anionic surfactant SDS and its' influence on the droplets' surface charge was again measured by *Malvern ZetaPlus Zetaliser, see* table 5.4

Table 5.4 Surface charge of cross-linked droplets as a function of [SDS]

[SDS] (mM)	ζ-potential (mV)	Error (+/-)	Mobility ($10^{-8}m^2s^{-1}V^{-1}$)	Error (+/-)
0.08	-37.9	5.9	-2.9	2.2
0.8	-34.2	0.7	-2.7	0.1
8.0	-34.2	0.3	-2.7	0.1

The addition of 0.08mM SDS dramatically increased the negative surface ζ-

potential of the droplets from -23.0mV, without the presence of surfactant, to -37.0mV. The anionic head group from the SDS surfactant in the continuous phase adsorbs onto the droplet surface which adds to the negative charge already present from the Si-O$^-$ PDMS end groups. The presence of adsorbed SDS produces a strong inter-droplet electrostatic repulsive force and causes the overall ionic strength of the system to increase. This leads to a contraction of the EDL so that the ζ-potential, measured at the shear plane, is reduced. The potential for further surfactant adsorption on to the PDMS droplet surface is reduced as the SDS concentration is increased from 0.08mM to 0.8mM. The negative surface potential reaches a plateau, which corresponds to the constant droplet size shown in figure 5.8 at the same surfactant concentration.

5.3 Characterisation of cross-linked PDMS oil

5.3.1 Isolation of oil phase

It was difficult to isolate cross-linked PDMS liquid from the emulsions as they are very closely phase density matched and gravity was an insufficient force to separate the two phases. A range of dialysed 1 dm^3 emulsions of 0.05v/v DMDES and 0.0(v/v)-0.2(v/v) ϕ MTMS was produced and 6.0 mol dm^3 NaCl was added to saturate each system and induce phase separation through coalescence and rapid creaming. Typically 10ml of cross-linked PDMS oil could then be removed from the top via careful pipetting, which corresponded to approximately 40% yield from the starting total monomer volume. The isolated oil was shaken with Milli-Q water several times to remove excess NH_3 and other aqueous soluble impurities.

5.3.2 Determination of PDMS ϕ

The initial total monomer ϕ was fixed at 0.05(v/v), however it was not possible to extract the final ϕ of the cross-linked PDMS formed. Several techniques were investigated but none of the traditional methods were successful. The dry weight could not be determined as both liquid phases evaporated, freeze drying resulted in the sublimation of the emulsion system and high temperature distillation was not accurate as the PDMS phase was too difficult to separate and absorbed onto the glass surface. It was also not possible to extract the creamed PDMS phase in a more volatile diethyl ether as it evaporated with the solvent. Even though the emulsions behaved as Newtonian fluids, it was not possible to calculate the volume fraction ϕ of the dispersed phase from the viscosity of the emulsion[12,13] using Einstein's equation[14] for systems containing ϕ <0.01;

$$\eta_r = 1 + 2.5\phi \qquad [5.1]$$

This only applied to hard spheres dispersions, where η_r was the relative viscosity. In addition the internal viscosity of the droplet was not significantly different from the continuous phase and therefore it was not possible to obtain an accurate value. The isolation of ~ 15ml of PDMS from 1dm-3 0.05(v/v) total monomer emulsion represents ϕ ~ 0.019. The change in density of DMDES, ρ = 0.865g cm^{-3} to PDMS, ρ = 0.955g cm^{-3} results in a yield 41%.

5.3.3 Mass spectra

The mass spectra of cross-linked PDMS phases was obtained from emulsions containing fixed total monomer 0.05(v/v) ϕ with 0.0(v/v)–0.2(v/v) MTMS ϕ, see chapter 4, to determine sample's composition from the mass fragments. The average molecular weight was determined by summing the products of mass fragment x relative intensity and then dividing this total by the sum of relative intensities as described by Teare[10]. The spectra shown in figure 5.10 illustrates the fragments and constituent ions present in each sample. A single D unit has a mass of 74 $D\overline{P}$ and therefore any ions below 222 $D\overline{P}$, three siloxane units (D_3), were considered to be fragments and therefore not included in calculations. The calculated mean molecular weights as a function of MTMS ϕ and their standard deviation are tabulated below, table 5.5.

The general increase in molecular weight with increasing MTMS ϕ provides additional evidence of cross-linking density within the droplets and correlates to the more rigid structures observed with TEM, see section 5.2.2.

Table 5.5 Calculated average molecular weight as a function of MTMS ϕ

MTMS ϕ (v/v)	Mean Mw	Std. Dev +/-
0.00	194	0.1
0.01	220	0.4
0.05	220	0.4
0.10	254	0.6
0.20	930	1.2

Fig 5.10 Mass spectra of isolated PDMS oil, at fixed 0.05(v/v) total monomer; a)0.0(v/v) MTMS, b) 0.01(v/v) MTMS, c) 0.05(v/v)MTMS, d)0.1(v/v) MTMS, e) 0.2(v/v) MTMS

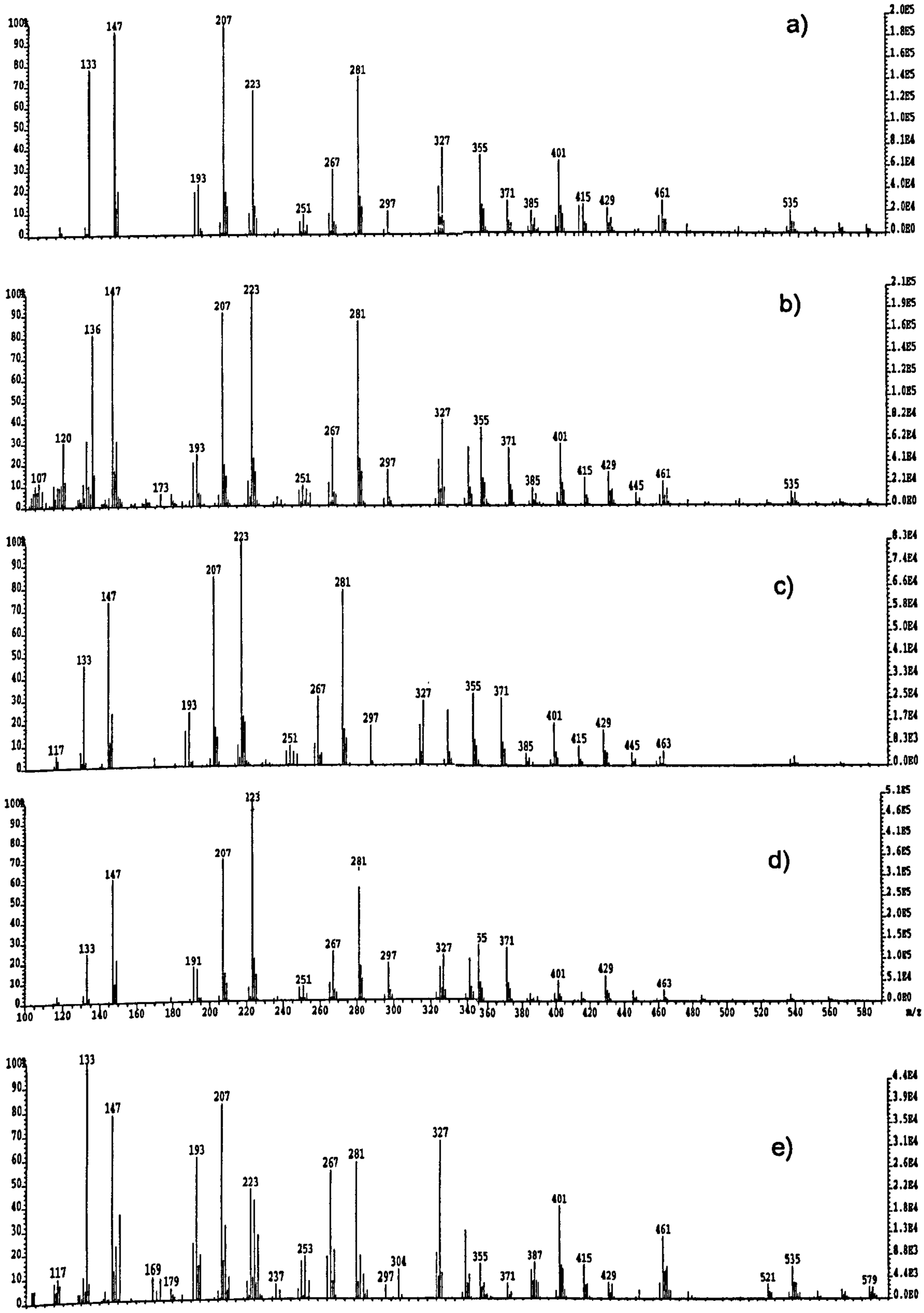

The only significant difference between the 0.00(v/v), 0.01(v/v) and 0.05(v/v) spectra was the height ratio of the most abundant peaks at 223 $D\overline{P}$ and 281 $D\overline{P}$. These represent a trimer with an additional H and a D_4 tetramer unit minus a methyl group respectively. As the MTMS ϕ increases from 0.05(v/v)-0.2(v/v), the relative height of these two peaks diminished, corresponding to the decrease in linear PDMS chains and increase in cyclic siloxane units. Other oligomeric species present included 207 $D\overline{P}$ D_3 unit, 327 DP which related to , 281 $D\overline{P}$ represented a tetrameter, 461 $D\overline{P}$ corresponding to an hydroxy terminated hexamer, 283 $D\overline{P}$ and 654 $D\overline{P}$. These fragments corresponded to a tetramer and octamer based fragments and the distance between the peaks created a large standard deviation. The range of stable oligomeric species observed were in good agreement with those reported by Obey and Vincent[1]. The influence of NH_3 ϕ on oligomeric species was not investigated in this study as no variance in sample composition was reported previosly[1,8]. The abundance of oligomeric species was found to be more effected by the ratio of di-functional to tri-functional monomer ϕ. Emulsion samples containing above 0.5(v/v) MTMS were not analysed as the extent of cross-linking produced species whose molecular weight was too large to be calculated by mass spectrometry. In addition large molecular weight samples contain bonds that easily fragment and would invalidate the measurement. Obey et al[9] noted a number of averaged molecular weight 320 $D\overline{P}$, and detected trimers and heptamers.

5.3.4 Elemental analysis

The influence of MTES ϕ on the C, H, N composition was obtained for the same dialysed cross-linked PDMS emulsion, as described previously in section 5.3.1,

and the experimental values were recorded in the table 5.6. The presence of methyl groups on the PDMS backbone aids the formation of a cross-linked network and traditionally gives a C:H ratio of 1:3. This was illustrated for those emulsion systems containing no tri-functional MTMS and 0.05 (v/v) di-functional DMDES.

Table 5.6 Experimental elemental composition of fixed 0.05(v/v) total monomer PDMS oil phase

MTMS ϕ (v/v)	C (%)	H (%)
0.00	5.9	12.2
0.01	3.8	12.0
0.05	2.8	11.5
0.10	1.8	10.0
0.20	1.6	10.0

However, the ratio was observed to decrease with increasing MTES ϕ, possibly as a result of the physical transition from lightly cross-linked liquid PMDS oil to an increasingly dense network within the droplets. The simultaneous decrease in the C while the H presence remains fairly constant could be an indication of a shift in cyclic to linear PDMS chains as the cross-linker presence ϕ increases.

5.3.5 GPC

Gel permeation chromatography (GPC) was carried out, by RAPRA, on an isolated cross-linked PDMS oil phase at a fixed 0.05(v/v) total monomer with varying MTMS ϕ to confirm the molecular weight variations shown by the mass

spectra measurements, see section 5.3.3. The columns were calibrated with polystyrene, see chapter 4, and all of the results were expressed as the "polystyrene equivalent" molecular weight averages and polydispersity as summarised in the table 5.7 below.

Table 5.7 Cross-linked PDMS at fixed 0.05(v/v) total monomer with increasing MTMS ϕ

MTMS ϕ	Mw	Mn	Polydispersity
0.000	200	180	1.10
0.005	210	180	1.15
0.010	220	190	1.20
0.050	280	200	1.40
0.100	940	240	3.85

The increase in average molecular weight as a function of cross-linker ϕ follows the same trend as that observed in the mass spectra results, +/- 10 $\overline{DP}$, see section 5.2.2. The difference noted between the two techniques could be attributed to the fact that only the lower Mw PDMS species can be analysed by GPC as they dissolve in the solvent. Therefore any higher Mw chains remain insoluble and are not able to be detected by the column. Figure 5.11 illustrates; (a) the molecular weight against a function of weight fraction for each MTMS ϕ, and (b) the retentive volume chromatogram with respect to the detector response and both were normalised with respect to area.

Fig 5.11 (a) Overlay of computed Mw distribution, b) DP chromatograms

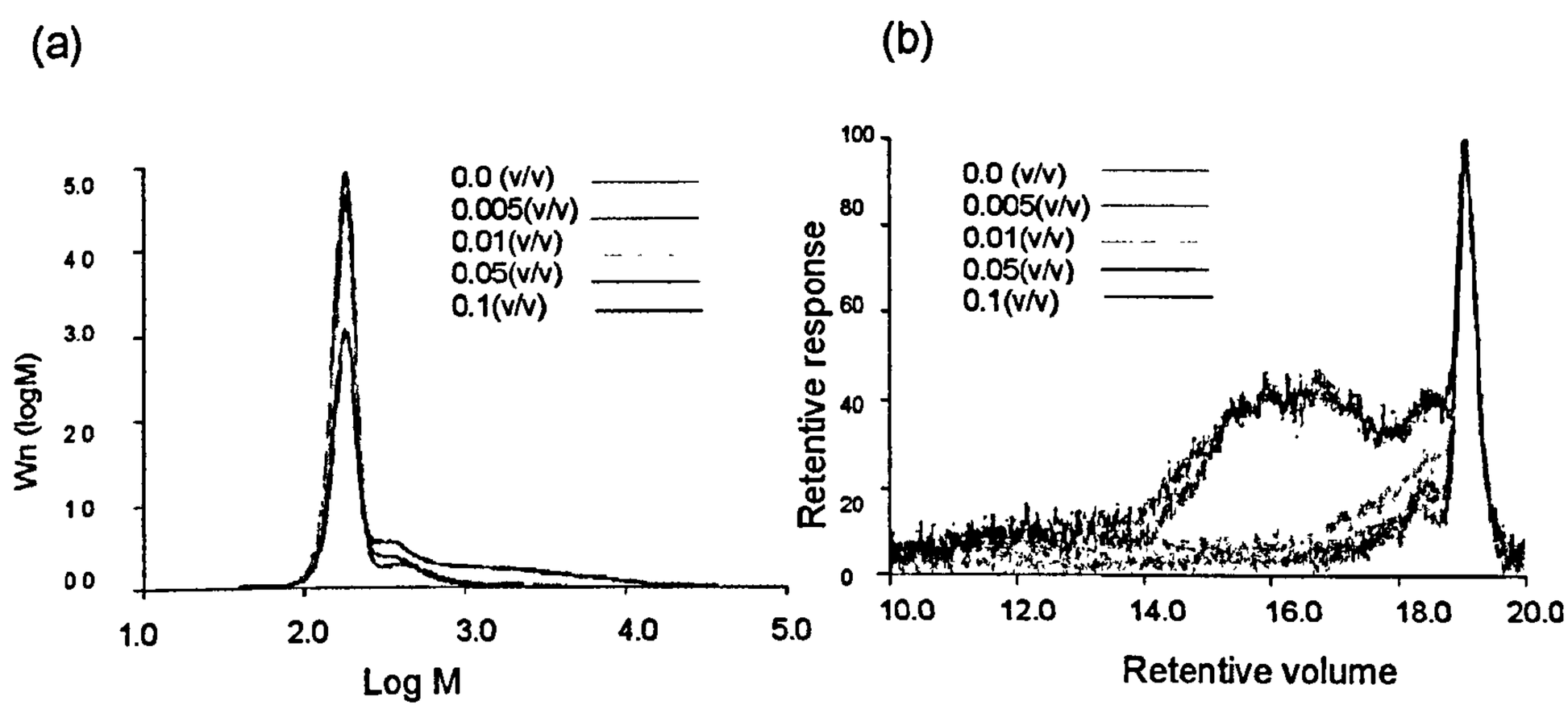

Each emulsion system analysed showed a similar major peak at approximately 180 mass units with an increasing contribution for the high molecular weight "tail" as MTMS ϕ increased, fig 5.11 (a). This produces a simultaneous increase in the calculated weight average molecular weight and a decrease in the chromatogram peak areas as the more highly cross-linked chains were not able to pass through the GPC columns. The response from the refractive index (concentration) detector, the differential pressure (viscosity) and the light scattering detectors confirmed that higher molecular weight material was not present in any of the samples. This was also observed from the peaks that appeared at the right hand side of the molecular weight distributions fig 5.11(a) and also from the high retention volume on chromatogram fig 5.11(b). The level of noise in the plots reflected the weakness of the signal from the samples. Obey et al[1] noted GPC gave a number and weight-averaged molecular weight at 420 DP which corresponded to a predominance of five or six repeating units[2].

5.3.6 High resolution H^1 NMR and Si^{29} NMR

The ^1H NMR spectra presented in fig 5.12 were obtained from the isolated cross-linked PDMS phase of identical emulsion systems described in section 5.3.1, to identify the end-groups present. Once the baseline had been magnified, due to the poor signal intensity, several sharp signals could be observed. Every spectra contained a set of sharp methyl peaks which corresponded to cyclic polymers, e.g D_4 and D_6, at 0.00ppm, (methyl, protons). These peaks occur in every spectra and comprise over 90% of the total signal, therefore only subtle changes in peak height were observed as the MTMS ϕ was increased from 0.0(v/v) to 0.2(v/v). The majority of the linear PDMS chain end groups present were either ethoxy / hydroxy or oxide groups. The former were observable as a weak methylene quartet at 3.65ppm and an adjacent quartet at 3.68ppm, while the oxide ion end groups are not observable in a H^1 spectrum. The increase in intensity of these peaks and the absence of a broad hydroxy peak indicates that the end groups are mostly ethoxy. No significant peaks could be attributed to unreacted DMDES monomer residues. Overall, emulsions containing MTMS $\phi < 0.2$(v/v) showed very little change in H environment implying the systems consisted of over 90% cyclic PDMS species.

These results were in good agreement with those reported by Obey et al[1] and Wegener[3], who noted that non cross-linked 0.05(v/v) emulsion systems consisted of 88.6% cyclic D_4, 11% linear PDMS, 0.4% D_3 units out of the total oil phase. It was suggested that the high dilution of the monomer, present during polymerisation, reduced the probability of oligomers reacting with each other. Therefore intra-oligomeric cyclisation was favoured over inter-oligomeric reaction.

Fig 5.12 H^1 NMR spectra of isolated PDMS oil; a) 0.0(v/v) MTMS, b) 0.01(v/v) MTMS, c) 0.05(v/v) MTMS, d) 0.1(v/v) MTMS, e) 0.2(v/v) MTMS

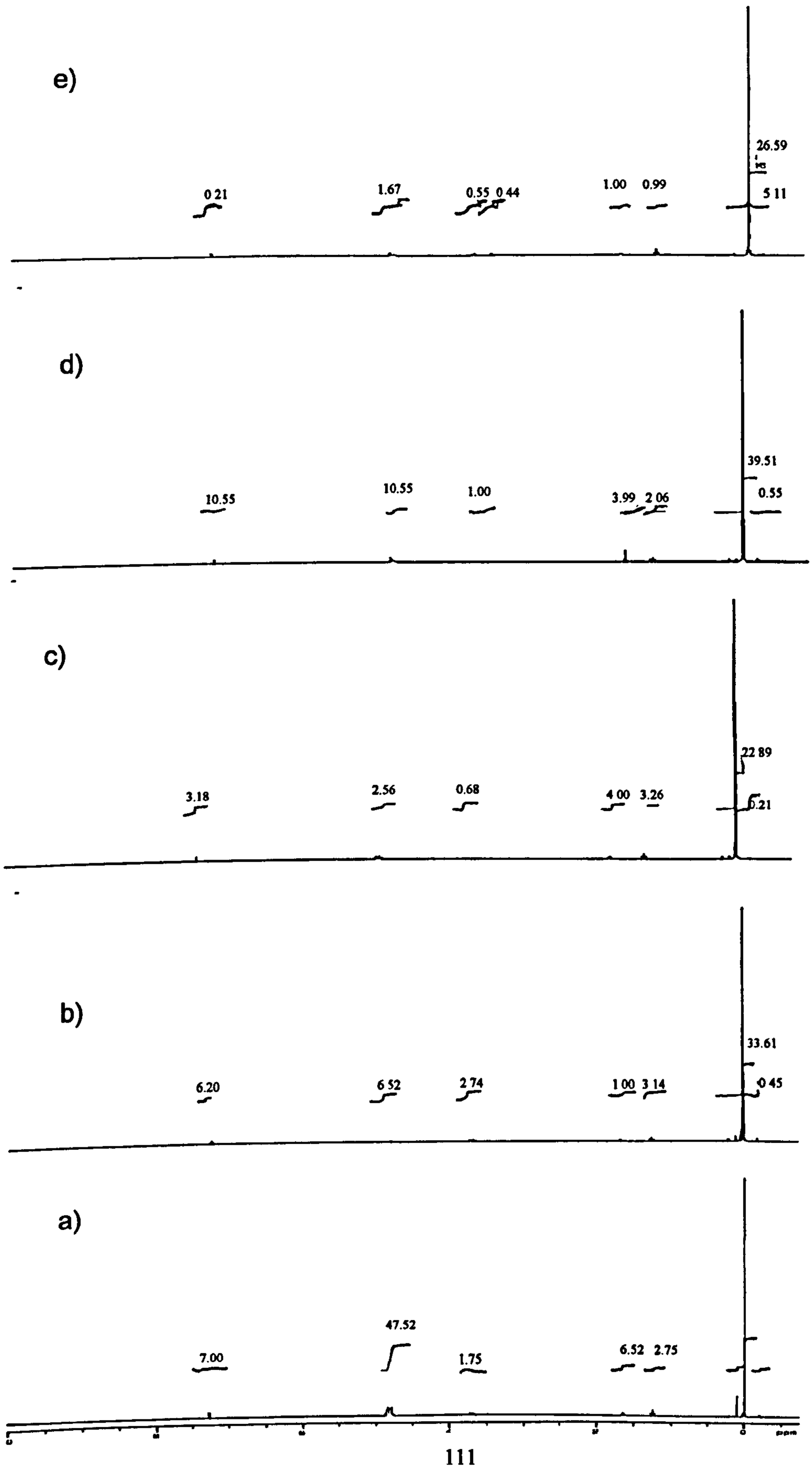

Si^{29} NMR has successfully been used to determine the composition of Si compounds by Harris[15] and Williams[16], while Janke et al[13] utilised the technique to characterise cyclic DT compounds. This technique has been used in this study to assign the ratio of linear to cyclic composition within the cross-linked PDMS phase from identical emulsion systems described in section 5.3.1. The spectra displayed in fig 5.13 illustrate the difficulty in assigning the peaks to cross-linked PDMS structures due to the presence of tri-functional MTMS, which complicated the signal intensity. However several peaks can be assigned to the cross-linked PDMS structure. The peak at -8.32pm can be assigned to D_3 cyclic as reported by Levy et al[17] and Alexenrod[12], or a D unit in a more complex cross-linked structure as shown in figure 5.14. The signals that occur at 11.6ppm could correspond to end groups, e.g M^{OH}.

Figure 5.14 Possible DT networks structural combinations

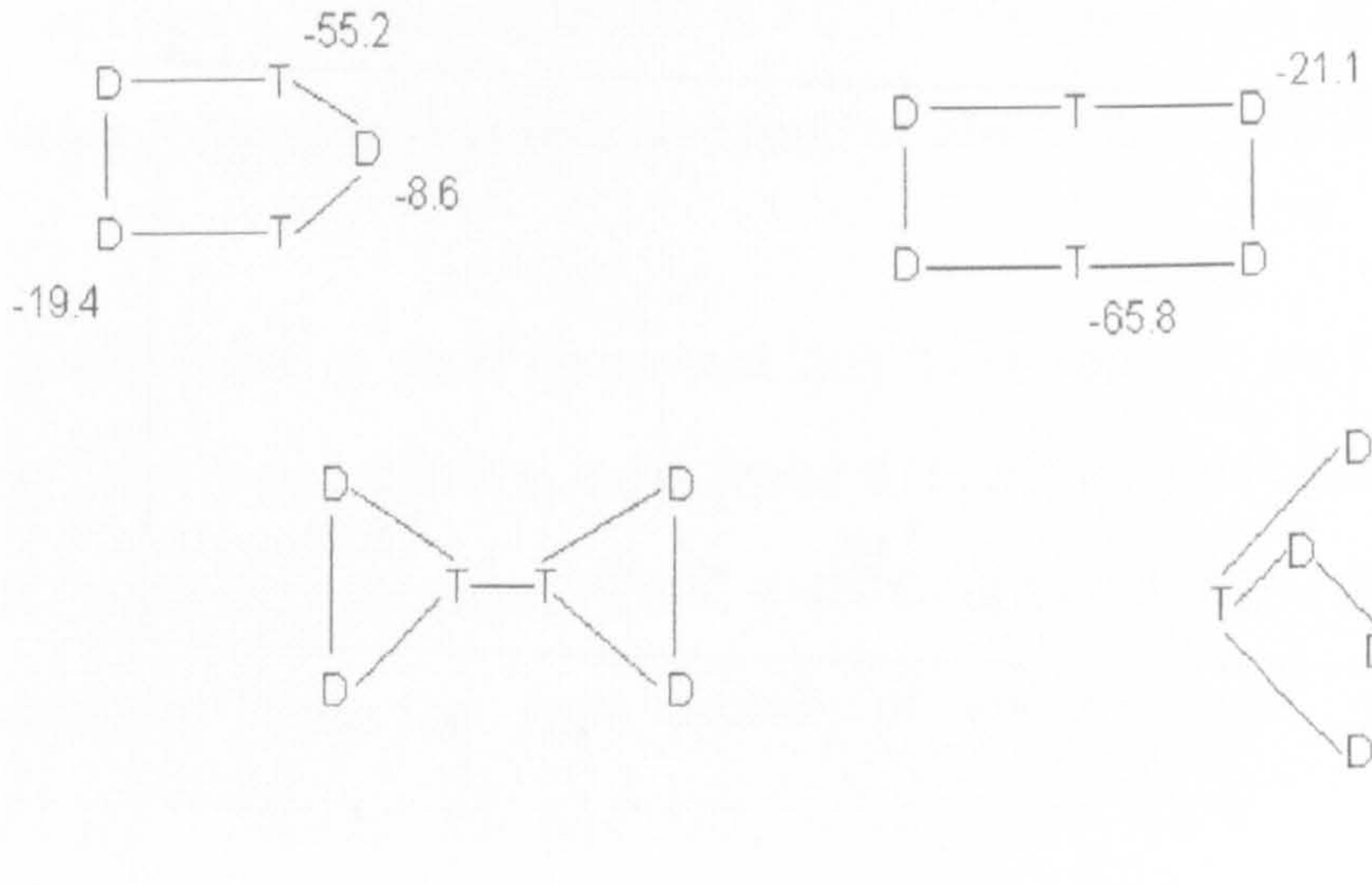

Fig 5.13 Si^{29} NMR spectra of isolated PDMS oil; a) 0.0(v/v) MTMS, b) 0.01(v/v) MTMS, c) 0.05(v/v) MTMS, d) 0.1(v/v) MTMS, e) 0.2(v/v) MTMS

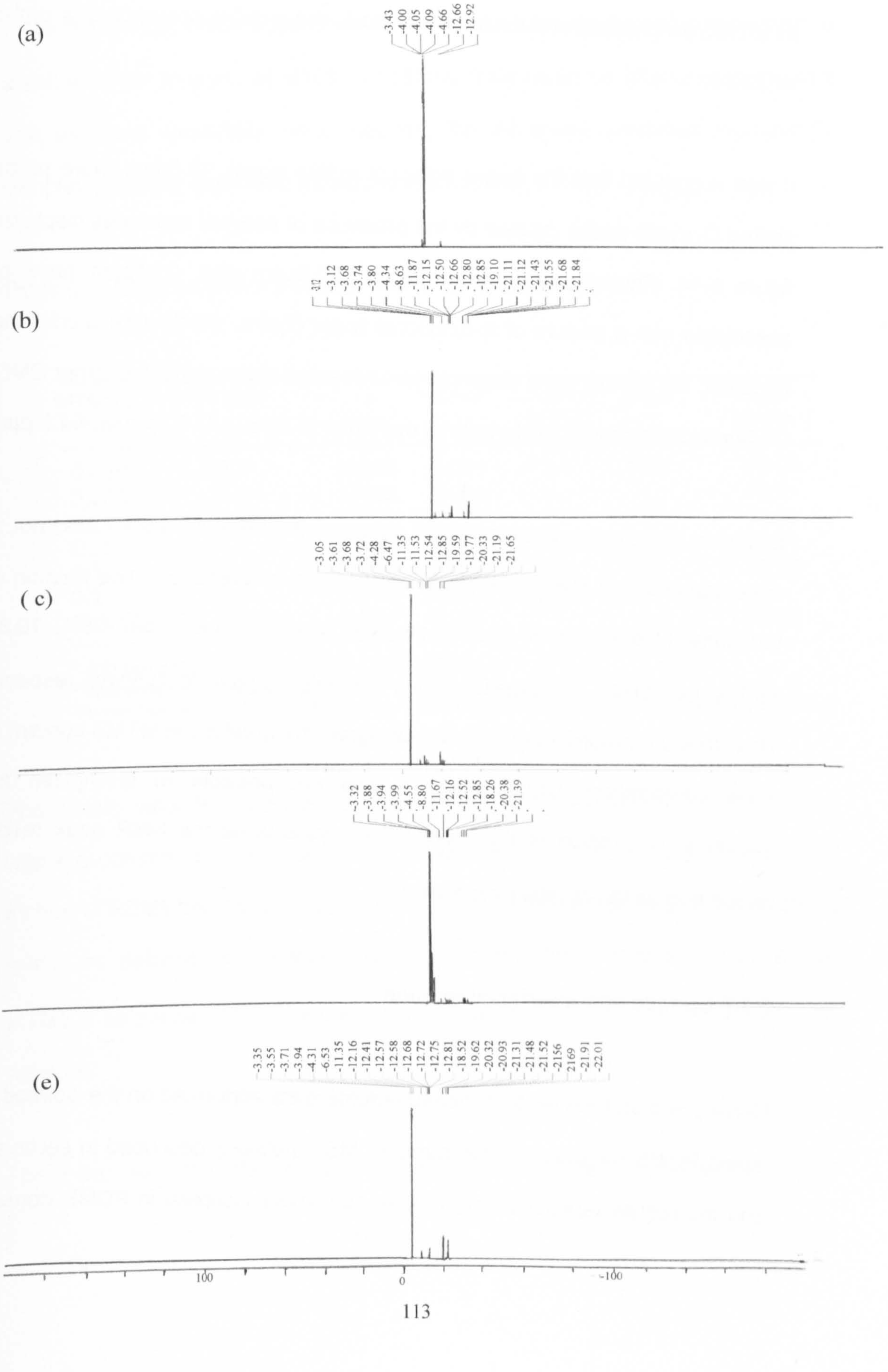

The di-functional signal region occurs between -18.7ppm and -21.1ppm with the strongest peak at -19.1ppm. Wegener[3] observed this peak increased in intensity as MTMS ϕ increased and could be related to the growing presence of a cyclic D_4 structure.

It was suggested that the peaks adjacent to this signal, 19.0ppm, were probably shifted D_4 cyclic peaks caused by the presence of network structures displayed in figure 5.14. Those peaks that occur at -20.8ppm and -21.1ppm have been associated with a mixture of di-functional linear chains, which were shorter than a decamer. No signals were observed for unreacted di-functional monomer DMDES, (-3.0ppm) or unreacted tri-functional monomer MTMS, (-43.5 ppm or -64.5 ppm).

Emulsion systems containing MTMS ϕ greater than 0.5(v/v) were found not to be measurable which also agreed with the findings of Wegener[3]. The fraction of tri-functional to di-functional resonance peak area increases from 4.8%, 10.3% to 45.3% as MTMS ϕ increases from 0.1(v/v), 0.2(v/v) to 0.5(v/v) respectively. Therefore the greater the tri-functional signal, the greater the MTMS content in the initial composition. Unfortunately it was not possible to distinguish further structural information of the cross-linked systems as the NMR peak resolution diminished as the MTMS ϕ increased.

5.3.7 Surface and interfacial tension

Density and surface tension measurements were performed on the isolated cross-linked PDMS oil phase of the same PDMS emulsions described in section 5.3.1, and the results tabulated below. A steady, linear increase in PDMS density with

increasing MTMS ϕ was observed and in agreement with those values reported by Obey et al[1]. At low MTMS ϕ, the density values were measured to be close to the value of pure D_4, which is the dominant species. However, the value increased to a value similar to water at MTMS >0.15(v/v). This could be attributed to the fact that as more cross-linker is introduced, the oil phase becomes increasingly complex as larger oligomeric molecules are formed.

Table 5.8 PDMS oil phase characterisation as a function MTMS ϕ

MTMS ϕ (v/v)	T (°c)	ρ (g/cm³)	Error (+/-)	υ** (mPas)	Error (+/-)	$\gamma_{o/w}$ [mN/m⁻¹]
0.000	26.0	0.948	0.001	2.6	0.003	18.06
0.005	26.4	0.969	0.001	-	-	18.51
0.01	26.6	0.966	0.001	2.7	0.005	19.67
0.05	27.7	0.967	0.001	3.0	0.005	20.01
0.1	26.1	0.982	0.001	6.5	0.006	19.97
0.2	26.3	0.999	0.001	20.1	0.007	-
Std. PDMS*	25.0	0.944	0.001	-	-	19.26

* 220 Mw, (Aldrich), OH terminated PDMS chains
** viscosity values obtained from Tear PhD thesis
Neuman[13] synthesised PDMS(0% MTMS), $\gamma_{o/w}$ = 14.2 +/-0.2, ρ= 0.956+/-0.002, υ =3.8+/-0.3mm²s⁻¹, ρ_c = 68Nm⁻²

The density value for 0.05(v/v) total monomer and 0.2(v/v) MTMS ϕ corresponded with the commercial non cross-linked PDMS* oil, Fw 770, 5.0 cSt. The internal motion of PDMS chains has been shown to influence the viscosity of the oil phase within the deformable droplets[3]. The oil becomes more viscous with increasing MTMS ϕ as the mobility of the linear chains becomes inhibited by the cross-linking network.

There was very little effect on the surface or interfacial tension of the cross-linked

oil phase as MTMS ϕ was increased from 0.0(v/v) to 0.2(v/v). Wegener[3] attributed this property to the efficiency of PDMS at adopting low energy methyl groups at the air-water interface. This property would otherwise influence hydrodynamic properties of other equivalent deformable droplets or hard spheres[2,8,10,18]. It was not possible to extract sufficient quantities of 0.2(v/v) MTMS ϕ to analyse its' interfacial tension. The 0.05(v/v) total monomer with 0.2(v/v) MTMS ϕ oil has a interfacial tension value similar to the commercial PDMS described above. These measurements have shown that the presence of tri-functional MTMS below 0.2 (v/v) ϕ, utilised in this study, has a significant influence on the cross-linked droplet size and surface ζ-potential, while the properties of the bulk oil phase properties remained fairly constant.

5.4 References

1. Obey,T.M, Vincent .B, J.Coll.Int.Sci., 163, 454, 1994
2. Goller, M.I, Obey,T.M, Teare, D.O.H, Vincent,B, Wegener.M.R; Coll.Surf.A, 123-124, 183, 1997
3. M.R.Wegener, PhD thesis, University of Bristol, 1993
4. Scott D.W., Journal of the American Chemical Society, 68, 2294, (1946)
5. Kantor S.W., Grubb W.T., Osthoff R.C., Journal of the American Chemical Society, 76, 5190, (1954)
6. De Gunzbourg A., Favier J.C., Hémery P., Polymer International 35, 179, (1994)
7. Stöber.N, Fink.A, Bohn.E, Journal of Colloid and Interface Science, 26, 1, 62, 1968
8. Neuman.B, Vincent.B, Krustev.R, Hans-Joachim.M, Langmuir, 20, 4336-4344, 2004
9. Teare.T, PhD thesis, University of Bristol,
10. Andersen.K.R, Obey.T.M, Vincent, B, Langmuir, 10, 2493, 1994
11. Hunter.R.J., Zeta Potential in colloid science, Academic press, London, 1981
12. Alexnrod.T, G.A.Webb, Webb Eds., Wiley, NY, 1974, pg 251
13. Janke.H, G.Englehardt, M.Magi, E.Lippmaa, Z.Chem, 13,435, 1973
14. Einstein.A, Investigations on the theory of brownian movement, Dover, NY, 1956
15. Harris.R, "NMR and the periodic table", Acc. Press, London, 1978, Chp.10

16. Williams.E, Annual reports on NMR spec., 15, 1983, 235.

17.Levy.G, J.D.Cargoli, NMR spectra of nuclei other than Protons

18.Barnes.T.J, Prestidge.C.A, Langmuir, 2000, 16, 4116

CHAPTER 6: Introduction of a fluorescent dye

6.1 Refractive index contrast

The main objective in this project is to investigate the deposition, spreading and removal behaviour of cross-linked PDMS emulsion droplets within flow cell systems. However, low MTES ϕ, 0.00(v/v) -0.2(v/v) have a refractive index, in the range of 1.3335 – 1.334, which is very similar to the aqueous continuous phase, 1.333. This made it almost impossible to distinguish between those oil droplets present in the flow solution and those deposited on substrate surfaces. A water soluble fluorescent dye, fluorescein, was added at a fixed concentration, $1x10^{-3}$ mol dm^{-3}, to enhance image resolution and subsequent image analysis.

6.2 Fluorescence

The phenomenon of fluorescence is the result of a three stage process which begins with excitation, a process where an external source, e.g light, produces a photon of energy, $\acute{\imath}_{EX}^{1}$. The second stage involves the absorbence of the photon energy by the fluorophore which in turn creates an excited electronic singlet state(S_1') with a typical excited-state lifetime of 1-10 x 10^{-9}s. The final process results in a fluorescence emission of a photon of energy $h\acute{\imath}_{EM}$.

The presence of the polyaromatic hydrocarbon dye, fluorescein, at low concentrations 0.001mol dm^{-3}, increased the refractive index of the aqueous phase from 1.33 to 1.4 and aided the detection of droplet-droplet and droplet-substrate interactions.

6.3 Fluorescein

Fluorescein is an important *xanthene* dye with a large variety of technical applications, especially in biosciences industry[2,3]. The molecule, $C_{20}H_{12}O_5$, (Mw 332.31) contains a carboxyl phenyl perpendicular to but conjugated to the xanthene ring[4]. The presence of an O-bridge links the benzene rings and leads to the rigidity of the fluorescein structure which makes it highly fluorescent[5]. The dye has a large absorption in the visible range with a high fluorescence quantum yield, ~92%[5], as fluorescence emission is the dominant process during the deactivation of the fluorescein excited state. The synthesis of the dye has been discussed in detail by Mastalerz[6] but will not be discussed in this work.

The photo-physical properties of fluorescein are dependent on its environment, e.g pH[7-9], the hydrogen-bonding power[10]and the polarity of the surrounding solution[11,12]. In fact its pH sensitive fluorescence can be used as a physiologocal pH indicator[13,14] due to the reconfiguration of the pi-electron system after the fluorophore is protonated. Song et al[15] reported that fluorescein adapts to changes in the environment by adopting at least six different structural configurations which are illustrated in figure 6.1. These derivatives have different quantum yields and lifetimes and produce variations in the absorption and fluorescence spectra. The fluorescein used in this study exists mainly as the dianion (f) in polar water up to pH 8.5 [7,12].

A study of the fluorescence intensity / absorption behaviour of fluorescein was carried out with a HP 8452 UV-Vis Spectrophototmeter in the range of 430-800nm. Fluorescein can be excited at wavelengths >500nm[16], (485nm) and therefore minimises fluorescence distortion by the background emulsion.

Figure 6.1 Structural configurations of Fluorescein in aqueous solution, (a) protonated cation, (b) a transition ampho-ioni molecule, (c) a trans neutral quinoid molecule, (d) neutral lactonic molecule, (e) a monoanion, (f) a dianion*.

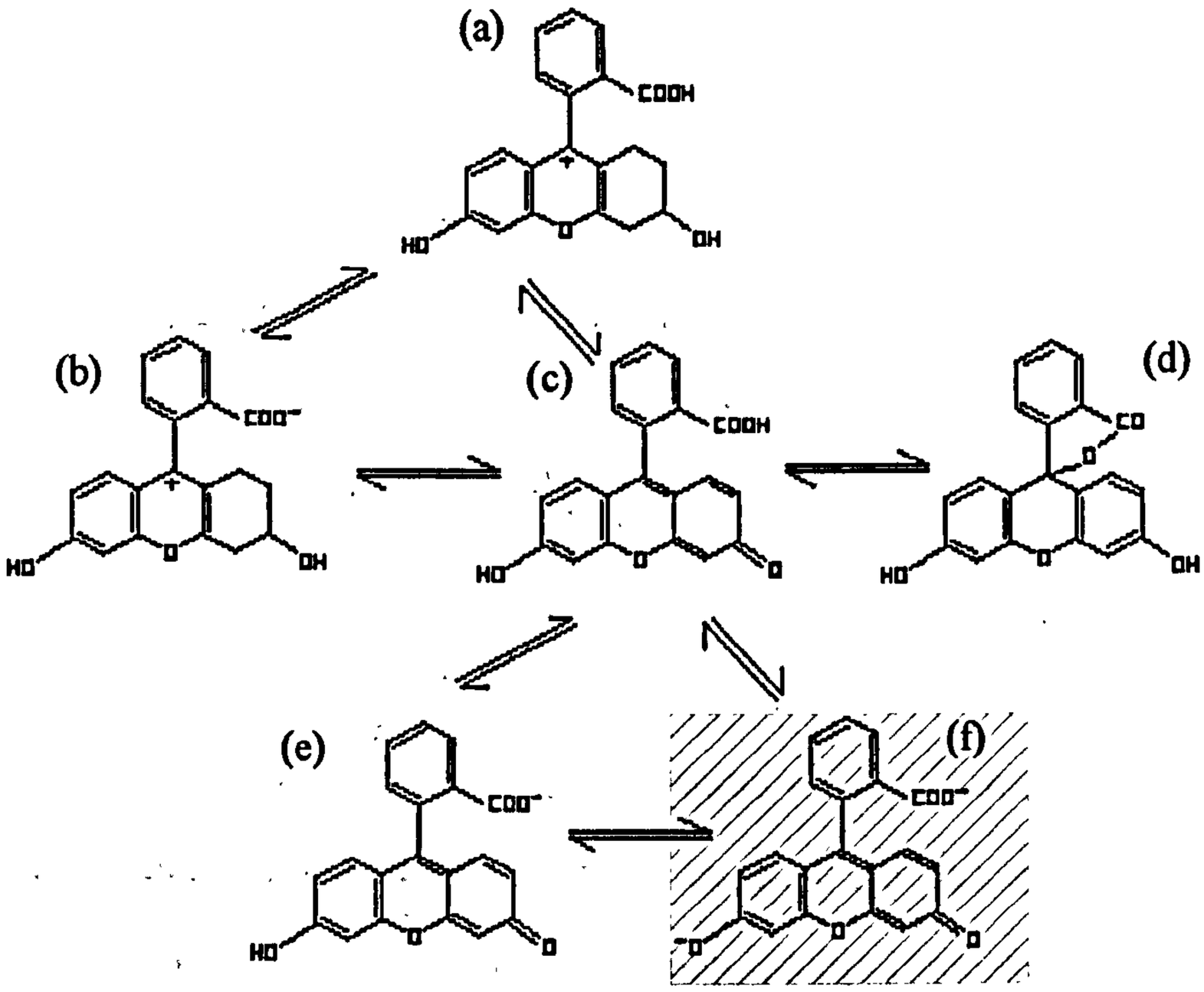

At longer wavelengths, light scattering by dense media such as cross-linked PDMS oil droplets is reduced and results in greater penetration of the excitation light. The intensity is quantitatively dependent on the Beer-Lambert law as the product of the molar extinction coefficient, the optical path length, the solute concentration, the fluorescence yield of the dye, the extinction source intensity and the fluorescence collection efficiency of the instrument. It was noted that there was a significant increase in absorption as the fluorescein concentration was increased from 0.001mol dm^{-3} to 0.1mol dm^{-3}. The fluorescence intensity remained stable for over 3hrs when measured at a fixed fluorescein concentration 0.01mol dm^{-3} and a fixed wavelength, 480nm, see figure 6.2.

Figure 6.2 Absorption intensity as a function of time, at fixed λ = 480nm and fluorescein 0.01mol dm^{-3}

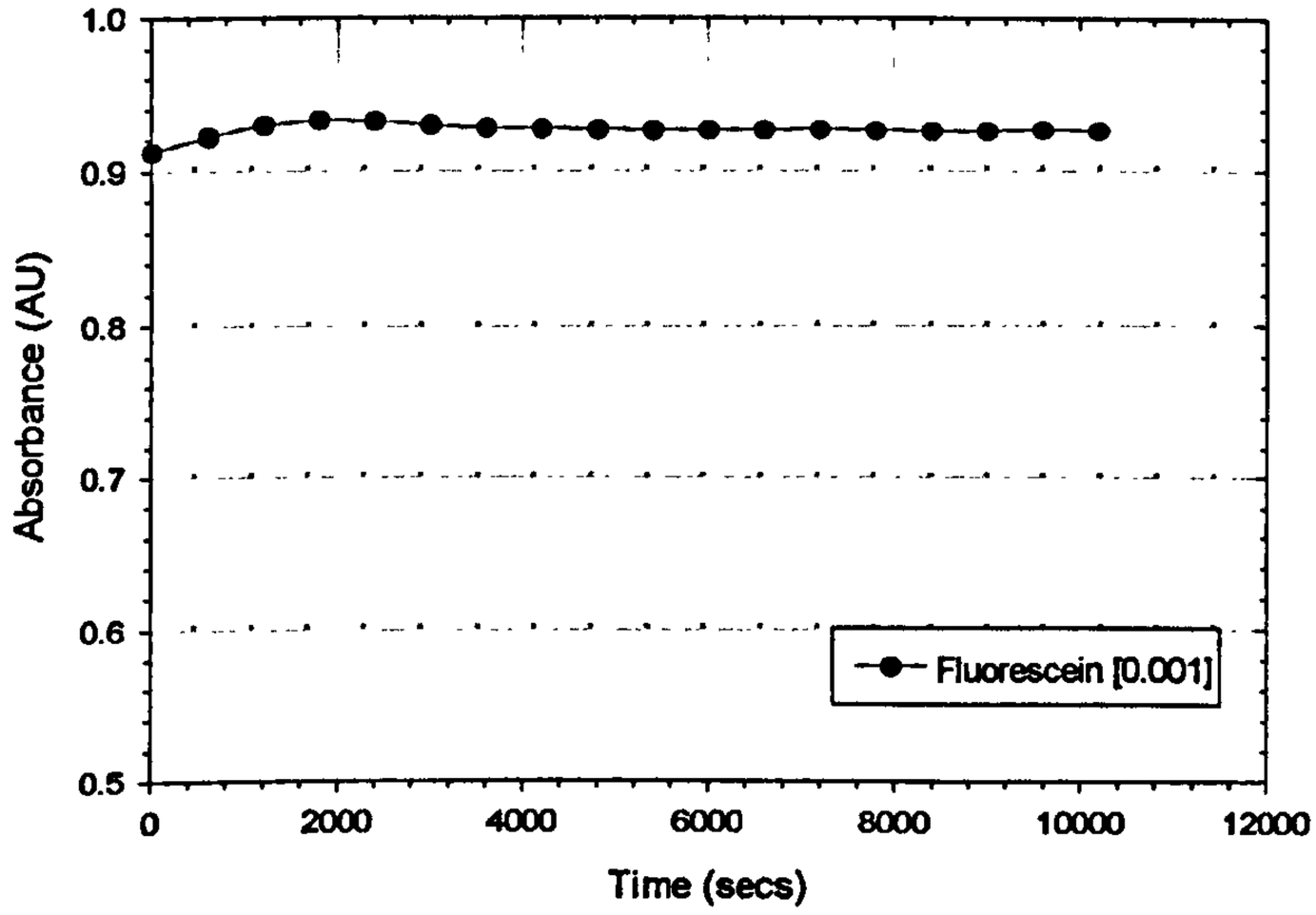

This confirmed that the fluorescence intensity would remain stable for the duration of the deposition and removal flow cell experiments, see chapter 4. The occurrence of photo-bleaching was minimised during experiments by the flow cell designs which blocked excess incident light penetrating the flow solution and by the use of a low light detection CCD camera with a high-numerical aperture objective.

The surface active property of the water soluble dye was investigated by measuring the surface tension of aqueous fluorescein as a function of solution concentration, see chapter 4. Figure 6.3 shows that the higher the concentration of fluorescein, the greater the deterioration of the surface tension of the aqueous solution. However, the lowest concentration of fluorescein investigated, 0.001mol dm^{-3}, retained a surface tension value very similar to pure distilled Milli Q water. Therefore every cross-linked PDMS emulsion used for flow cell experiments contained a fixed concentration of 0.001 moldm^{-3}

fluorescein to minimise the interference from the dye at the oil / water and oil / substrate interfaces.

Figure 6.3 The influence of Fluorescein concentration on surface tension of an aqueous solution.

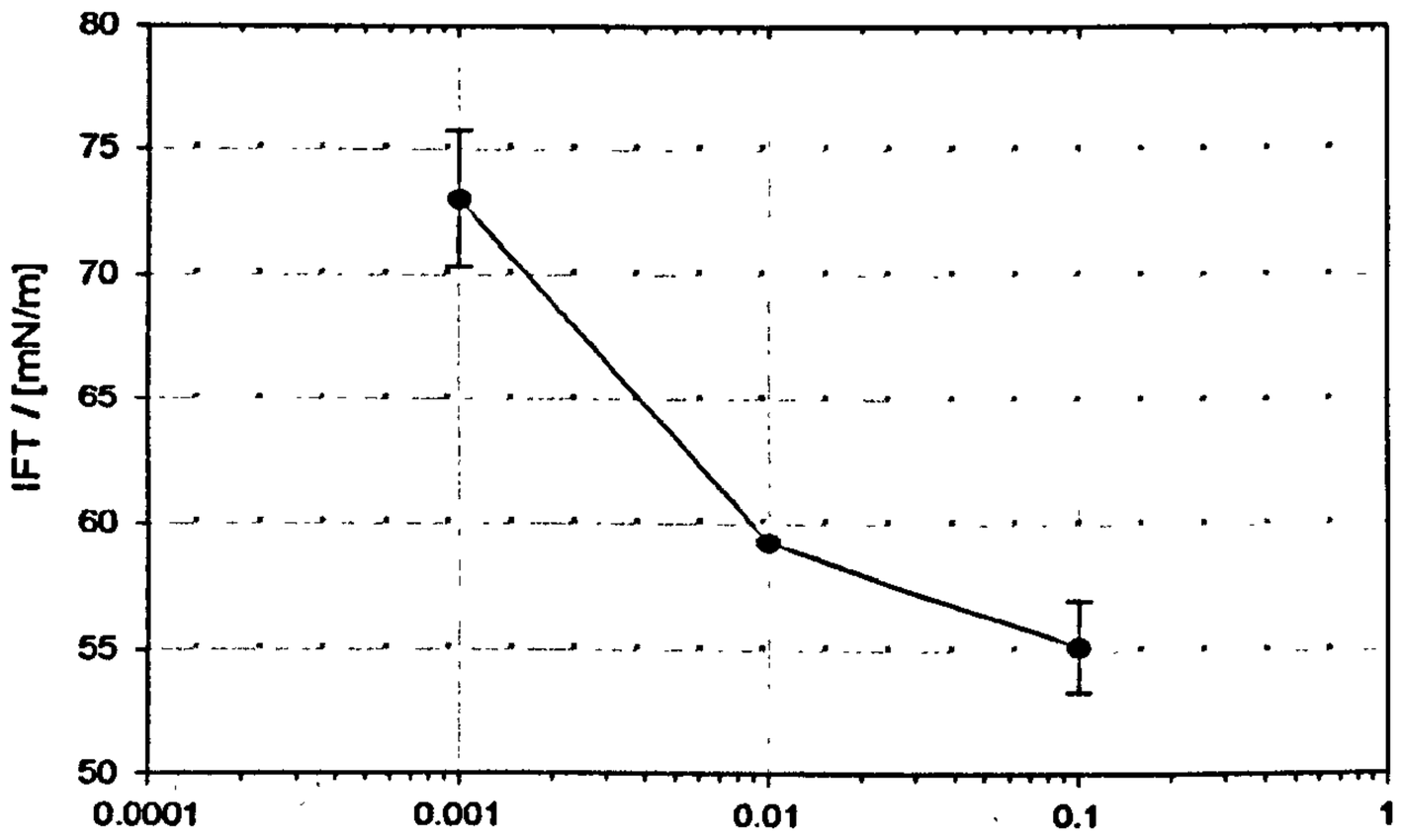

Sang et al[15] also reported on the absorption lifetime of the fluorescence dye, 0.01moldm^{-3}, in the presence of SDS. This was determined by using an Horiba NAES-1100 single -photon counting apparatus. The values are listed in table 6.1, where Φ_{AQ}, Φ_{SDS} are the fluorescence quantum yield of the dye in aqueous and SDS solutions respectively and τ_{AQ}, τ_{SDS} are the fluorescence lifetime of aqueous and SDS solutions respectively.

Table 6.1 Fluorescence quantum yields and lifetimes of fluorescein in aqueous and SDS solutions

ρ	γ (mN/m^{-1})	λ_{max} (nm)*	$\varepsilon \bullet 10^3 \left\lvert \frac{1}{M \bullet cm} \right\rvert$*	Φ_{AQ}*	Φ_{SDS}*	τ_{AQ}* (ns)	τ_{SDS}* (ns)
0.995 +/- 0.01	72.11	496	4.6	0.76	0.74	4.28	4.25

** vales obtained from Sang et al[11]*

The spectral properties or fluorescence lifetime of fluorescein showed little or no change in the presence of SDS. It can be assumed therefore that there is little or no binding between the dye and SDS micelles due in part to to the solubility of fluorescein in aqueous solutions and the electrostatic repulsion between the anionic dye and the anionic SDS micelles. It is also possible to assume that the presence of low concentrations of fluorescein in cross-linked PDMS emulsions. This would have negligible effect on deposition or removal flow cell studies.

6.4 References

1. Shriver, Attkins, Physical chemistry

2. Stanton.S.G., Kantor.A.B., Petrossian.A., Owicki.J.C., Biochim,Biophys.Acta, 766,228,1984

3.Thelen.M., Petrone.G., O'Shea.P.S., Azzi.A., Biochim, Biophys.Acta, 766, 161, 1984

4. Osborn.S, D.Rogens, Acta Crystallogr.Sect., B, 31, 359, 1975

5. Birks.J.B., Organic Molecular Photophysics, vol.1&2, Wiley, New York, 1973, 1975.

6. Mastalerz.P, Chemica Organiczna, PWN, Warszawa, 1986

7. Abdel-Halim.F, R.M.Issa, M.S.El-Ezaby, A.A.Hasanein, Z.Phys.Chem.(Frankfurt am main), 73, 59, 1970

8. Martin.M, L.Lindqvist, J.Lumin, 10, 381, 1975

9. Diehl.H, R.Markuszewski, Talanta 36, 416, 1989

10. Martin.M, Chem.Phys.Lett., 35, 105, 1975

11. Sang.A, T.Wu, S.Chen, M.Zhang, T.Shen, Dyes Pigments, 39, 371, 1998

12. Zhao.Z, T.Shen, H.Xu, Spectrochim.Acta, 45A, 1113, 1989

13.Handbook of Fluorescent probes and research chemicals, Haugland, Molecular probes, 1992

14.Parker, C.A., Photoluminescence of solutions, Elsevier 1968

15. Sang.A., Zhang,J., Zhang.M., Shen.T., Tang.J., Coll.Surf.A: Physicochemical and Engineering Aspects,167,253-262, 2000

16. Boguta.A., Wróbel.D., Journal of Fluorescence, vol.11, 2,

Chapter 7: Droplet deposition and removal

7.1 Colloidal deposition

Droplet deposition is a dynamic process that occurs due to capture in a primary energy minimum and is effected by the flow field near the collector surface with a finite probability of escape from the surface[1,2]. Vincent and Harley developed a particle hetero-aggregation theory[3-8] to explain high affinity particle adsorption isotherms by analysing the total interaction energy of a particle approaching a surface partially covered with adsorbed particles. The three main limiting conditions that occur during colloidal deposition are illustrated in figure 7.1. The initial stage of colloidal approach to a clear solid surface is similar to the attractive droplet-droplet interaction aggregation, (a-b). Rapid deposition follows due to barrier-less capture into a potential well dependent on particle flux to surface. Finally, deposition slows or reaches an equilibrium plateau (coating)[9] as the number of particles near to the substrate surface increases. This in turn enhances the mutually repulsive interactions between adsorbing and adsorbed species on the substrate. The arrangement of adsorbed particles on the collector surface is dependent on the strength and balance of the normal and lateral interactions, in which the total energy of interaction for an approaching particle may be expressed as;

$$V_T = V^{ps}{}_T + nV^{pp}{}_T \qquad [7.1]$$

where n is the coordination number of the adsorbed droplet; $V^{ps}{}_T$ is the interaction between the approaching droplet and the surface and $V^{pp}{}_T$ is the interaction with

droplets already adsorbed. As a droplet approaches the surface, attraction to the surface is reduced by a repulsive interaction with other already adsorbed droplets.

Fig 7.1 Schematic representation of the net interaction of a droplet approaching; (a) a clear flat surface, (b) a clear large particle, (c) a surface with adsorbed droplets

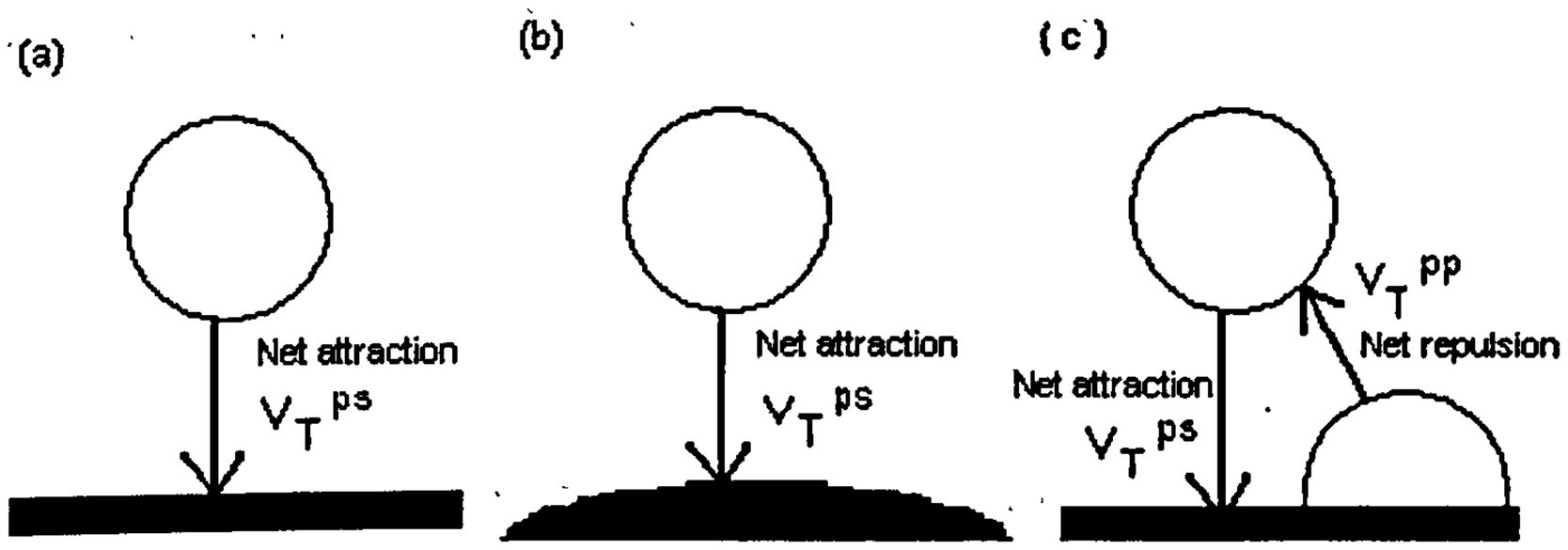

The interaction energy - distance profile contains a maximum, V_{max} or energy barrier to the additional adsorption whose magnitude is dependent on the surface charge of both the substrate and particle interface and on the number of particles already adsorbed. An equilibrium adsorption state is reached at a specific surface coverage for each system, at which further droplet adsorption is prevented as a result of the approaching-adsorbed particle repulsive interaction force. The equilibrium coverage value is greatly influenced by the solution electrolyte concentration, the substrate surface composition, the surface charge and the number concentration of the depositing dispersion.

A series of calculated potential energy profiles was generated for the total interaction energy for a PDMS - mica - water as a function of separation distance (H), assuming constant surface potential, see Appendix A1, A2. However, it must

be noted that the model chosen for the DLVO calculations does not account for the deformability of the droplets in the system, or the presence of substrate surface roughness, as discussed in chapter 8. Both these features can greatly influence the contact area between droplets and substrates and therefore any calculated forces of adhesion given in this study can only be a rough estimate of the actual values and only provide a qualitative trends in the force profiles. It should also be noted that the Hamaker constant used in these calculations is based on pure PDMS and does not take the presence of cross-linker into account. Therefore there could be a significant error in the final values.

7.2.1 Interaction forces between approaching droplet and flat plate

The total van der Waals interaction force between a particle and planar surface, as shown in figure 7.1 a-b, was derived by Boer[10] and Hamaker[11] who extended the microscopic approach discussed in chapter 2, equation [2.5]. The following expression calculates V_A from the summation of over all pairs of molecules in the two interacting surfaces.

$$V_A = \frac{-Aa}{6H}\left[1+\frac{H}{2a+H}+\frac{H}{a}\ln\left(\frac{H}{2a+H}\right)\right] \qquad [7.2]$$

where a is the particle radius, H is the separation distance and A is the Hamaker constant for the entire system shown listed in table 7.1.

Table 7.1 Substrate-PDMS-water Hamaker constant, A_{123}

Substrate	A_1 (substrate)	A_{123} (substrate-PDMS-water)	A_{123}^* (substrate-D_4-water)
Glass	6.5×10^{-20} J	2.6×10^{-20} J	-9.8×10^{-22} J
Mica	10.0×10^{-20} J	5.4×10^{-21} J	3.9×10^{-21} J

The interaction between water and a glass or mica surface, with PDMS oil as the medium, is shown to be attractive (+ve), which implies the oil will wet the surface. However, the interaction between water and a glass surface, with D_4 as the medium, is repulsive which would cause the oil drop to contract on the surface.

In this work, the equations of Hogg et al[12], Bell et al[13] and Prieve et al[14] were used to model the sphere and planar surface interaction from their extension of the expression for spheres with unequal electrical double layers or potentials, for $a_2 \sim \infty$.

$$V_E = \frac{a_1 a_2}{a_1 + a_2} \frac{128 \pi n_o kT}{\kappa^2} \Psi_1 \Psi_2 \exp(-\kappa H) \qquad [7.3]$$

Hogg, Healy and Fuerstenau[12] used the Derjaguin approach[15,16] to derive expressions which gave agreement with exact results for low potentials (<60 mV). The expression for two unequal spheres with potentials Ψ_1 and Ψ_2, respectively, is found to be;

$$V_E^S = \pi \varepsilon \varepsilon_o a_1 a_2 \frac{(\Psi^2_1 + \Psi^2_2)}{(a_1 + a_2)} \left[\frac{2\Psi_1 \Psi_2}{(\Psi^2_1 + \Psi^2_2)} \ln \frac{1 + \exp[-\kappa H]}{1 - \exp[-\kappa H]} + \ln(1 - \exp[-2\kappa H]) \right] \qquad [7.4]$$

This equation is only valid for small and constant Ψ_1 and Ψ_2, for κa_1, κa_2 >10 and small *H* (<a_1, a_2). This model for the interaction between electrical double layers uses the boundary condition of constant surface potential, implying that the surface charge, Ψ_o changes as κ changes, or as two surfaces approach, H. The deformability of fluid drops with solid surfaces determines the behaviour of numerous systems such as emulsions, foams and mineral flotation processes.

Dabros et al[17] derived the van der Waals interaction component of the above equation from [2.5], while the electrostatic potential energy for the sphere-flat plate geometry was determined from the expression[7.5] for the interaction between two spheres[18]. This was achieved by setting the radius of one sphere to infinity.

$$V_{el}\Psi = \pi\varepsilon a(\Psi_1^2 + \Psi_2^2)\left[\frac{2\Psi_1\Psi_2}{\Psi_1^2 + \Psi_2^2}\left[\ln\frac{1+\exp(-\kappa H)}{1-\exp(-\kappa H)}\right] + \ln(1-\exp(-2\kappa H))\right] \quad [7.5]$$

where Ψ_1, is the potential of the particle, Ψ_2 is the potential of the surface, ε is the permitivity of the medium, κ is the reciprocal Debye length given by equation [2.2]. Miklavcic et al[19] reported several deviations from the Laplace equation and the subsequent DLVO theory, for the case of a liquid mercury drop subjected to a repulsive double-layer force across a mica substrate in an aqueous solution. These deviations included; the deformation of one surface during interaction and the exponential decay length which was was no longer the Debye length under,

due to the repulsive double-layer pressure. The force behaviour diverges from DLVO if the internal pressure of the drop matches the external surface pressure. In addition, there is an exponentially attractive "hydrophobic" force between the two immiscible liquids and a solid.

Horn et al[20] used a Derjaguin approximation to report the influence of disjoining pressure, exerted by a planar mica surface, on the deformation of a sessile mercury drop surface across an aqueous electrolyte solution.

$$\Pi(r) = \Pi(D(r)) = \Pi(D_0 - z(r)) \qquad [7.6]$$

The case of disjoining pressure at the radial distance, r, is to the equal to the pressure between flat plates at the separation D(r), since $z = 0$ for a convex sessile drop. At large separations, the drop was shown not to be significantly deformed by the disjoining pressure, while at intermediate separations, the pressure became repulsive, producing some flattening of the drop. At small separations the surface force becomes attractive, the apex of the drop is drawn towards the solid and the drop shape becomes elongated.

7.2.2 Interaction forces between approaching droplet and adsorbed species

The interaction of two flat plates with similar double layers has been used to represent the approach of particles to the adsorbing surface as the number of deposited particles increases, as shown in figure 7.1(c). As two similar charged

surfaces approach in an electrolyte solution, the diffuse parts of their electrical double layers overlap causing a repulsive force to be created between the approaching surfaces.

Derjaguin[21], Verwey and Overbeek[22], independently, derived expressions for the electrostatic potential energy interaction (V_E^{fp}), between flat plates of identical, constant surface potentials as a function of the separation (H), equation [7.7];

$$V_E^{fp} = \frac{64\pi n_o a k T \gamma^2}{\kappa^2} \exp(-\kappa H) \qquad [7.7]$$

where n_o is the bulk concentration of counter-ions, κ is the Boltzmann constant and T is the temperature. In the above expression,

$$\gamma = \frac{\exp\left[ze\Psi_0/2KT\right] - 1}{\exp\left[ze\Psi_0/2KT\right] - 1} \qquad [7.8]$$

and

$$\kappa = \frac{\{2e^2 n_o z^2\}^{1/2}}{\varepsilon\varepsilon_0 KT} \qquad [7.9]$$

in which e is electron charge, ε_o is the permitivity of free space, e is the dielectric constant of the medium and z is the valency of the counter-ions. Derjaguin[22] extended this theory for the approach of identical spheres by considering each sphere to be made up of infinitely small concentric rings which are treated as a flat plate. The energy of approach of the spheres for small double layer

extensions, V_E^S, is relative to the particle radius ($\kappa a > 10$), and the separations ($H_o < a$) and surface potentials, $\Psi_o < 25$ mV was then given by

$$V_E^S = 2\pi\varepsilon\varepsilon_o a \Psi_o 2\ln(1+\exp[-\kappa H]) \qquad [7.10]$$

7.2.3 Droplet Bond number

The Bond number, *Bo*, can indicate the shape of the droplet in close proximity to a rigid substrate surface, e.g the smaller the $Bo < 10^{-2}$ the more spherical the droplet, equation [7.11], where σ is obtained from a tensiometer. It can be noted that the diameter of the film, d_c is typically 10% of the size of d_p.

$$B_o = \frac{\Delta\rho\, g\, d_p^2}{\sigma} \qquad [7.11]$$

The shape of the droplets can also be predicted from the Laplace equation, as it corresponds to a "contact" angle equal to zero and a plot of d_c against the droplet diameter d_p gives a linear relationship.

Fig 7.2 Schematic side view of a droplet deposited under a substrate.

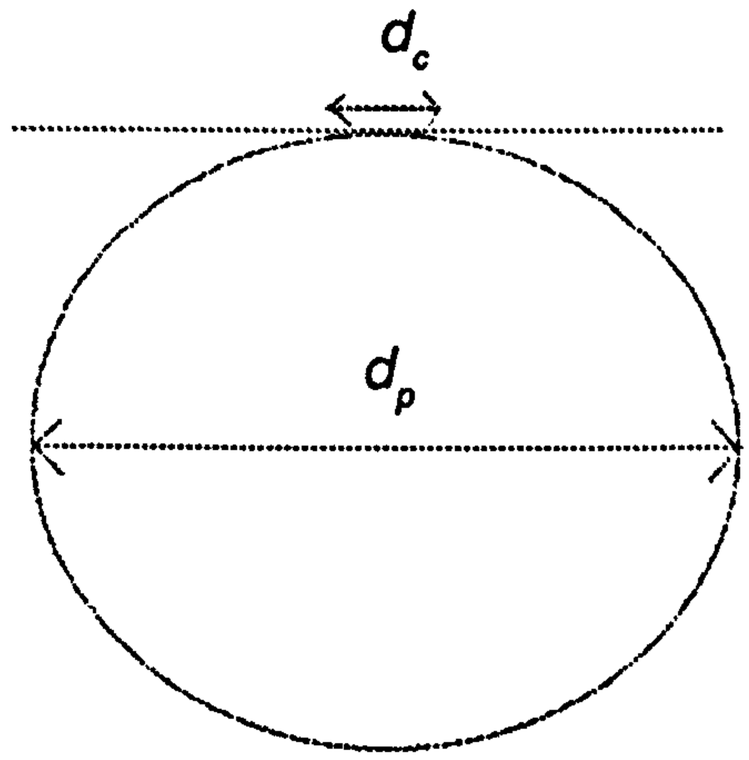

7.2.4 Stagnation point deposition parameters

Although a detailed discussion of the flow within the stagnation point cell is not within the scope of this thesis, several flow characteristic parameters have been included in this chapter[9]. The Peclet number, Pe, characterises the dependence of the droplet motion on the Brownian motion and the fluid flow as defined as;

$$Pe = \frac{2\alpha v a^3}{R^2 D_0} \qquad [7.12]$$

where D_0 is the diffusion coefficient of the droplets in the bulk medium as expressed by equation [4.1] in chapter 4. The value of the flow intensity for this system $\alpha = 3.06 m^{-1}s^{-1}$, the Reynolds number Re = 4 Vm, and h/R = 1.6 The Peclet number for the systems used in this investigation is < unity, $4x10^{-3}$, therefore the brownian motion predominates rather than the hydrodynamic forces. The transport of droplets within the flow cell can also be characterised by the

dimensionless particle flux at the collector, the Sherwood number (Sh);

$$Sh = \frac{J_0 a}{D_0 n_0} \qquad [7.13]$$

where J_0 is the initial flux towards the collector surface;

$$J_0 = n_0 k_d \qquad [7.14]$$

where k_d is the rate constant for the deposition process, from equation [7.22]. The theoretical maximum flux at the surface, Sh_{max}, can also be derived, using the Smoluchowski-Levich approximation. This makes the assumption that hydrodynamic interactions are canceled by specific interactions in the vicinity of the collector and corresponds to fast deposition;

$$Sh_{max} = \frac{Exp\left[-\frac{Pe}{6}(\delta+1)^3 - \overline{F_g}\,\delta\right]}{\int_{\delta}^{\infty} Exp\left[-\frac{Pe}{6}(H+1)^3 - \overline{F_g}\,H\right] dH} \qquad [7.15]$$

In this equation δ is the distance from the surface at which droplets are irreversibly captured and F_g is the gravitational force acting on the particles, given by equation [7.16];

$$\overline{F_g} = \frac{4\pi \Delta\rho\, a^4 \cos\theta}{3kT} \qquad [7.16]$$

where $\Delta\rho$ is the apparent density of the droplets, and ($\theta = 180^\circ$) is the angle between the gravitational field and the direction of the flow. The ratio of the

experimentally derived flux to the maximum flux is referred to as the "stability ratio", W.

$$W = \frac{Sh_{max}}{Sh} \qquad [7.17]$$

Fast deposition can be predicted when the experimental flux to the collector exceeds the maximum flux, e.g $W \leq 1$. The nonlinearity of the flux of droplets to the surface can be described in hydrodynamic terms by invoking the concept of a "blocking coefficient", b_m^2. This term can be used to express the number of droplet cross sections blocked by each adsorbed particle, referred to as the "blocking factor". The coating density found at a time t, S (t) may then be expressed as;

$$S(t) = \frac{J_0}{\beta_m}\left(1-\exp^{(-\beta m t)}\right) \qquad [7.18]$$

where

$$\beta_m = J_0 A_1 = J_0 \pi a^2 \gamma \qquad [7.19]$$

In this equation A_1 is usually of the order of the particle cross-section, the lowest possible value of γ was used, 1.1 (close packing).

The value of this blocking factor may be derived directly from the experimentally determined coating density / time plot, and its value is related at a fundamental level to the accessibility of the collector surface to approaching particles.

7.2.5 Deposition coverage

The optimum uniform particle coverage and the hexagonal close packing ratio was expressed by Hansen et al[23] to predict the theoretical maximum adsorbed amount, S_{max},

$$S_{max} = \frac{[2\pi]}{[\sqrt{3}]} \frac{[a_1 + a_2]}{[a_1]} \qquad [7.20]$$

where a_1, a_2 are particles diameters and $a_1 << a_2$.

The total droplet coating density on the flat collector surface, (θ), or the adsorbed amount , developed from the adsorption experiments conducted by Vincent et al[24-28], was derived from the coating density (the number of particles per square meter), S, and the maximum number of particles that would hexagonally close pack per unit area, S_{hcp}, calculated from PCS data, see chapter 5 and equation [7.11];

$$\theta = \frac{S}{S_{hcp}} \qquad [7.21]$$

The change in coating density, S, or adsorbed amount, was then plotted as a function of time and created an exponential curve, see figure 7.3. The initial rise in coating density, (i), is due to the barrierless deposition onto the substrate. As the coating density increases, the repulsive contributions from depositing particles present on the substrate increases correspondingly. This effect becomes

increasingly significant until a plateau coating density, S_{pl}, is reached and no further particle deposition is observed. Experimental data has been fitted[16] using a first order rate equation, [7.22];

$$S(t) = S_{pl}\,(1\text{-}exp^{-kd\,t}) \qquad [7.22]$$

where k_d is the first order rate constant that is characteristic for each deposition condition. Here k_d is the combined blocking and detachment rate, where Spl = J_o / k_d and J_o is the initial deposition rate. At short times the above equation reduces to $S = J_o t$ [29].

Fig: 7.3 Schematic representation of coating density, S, and derived adsorbed amount, θ, as a function of time,

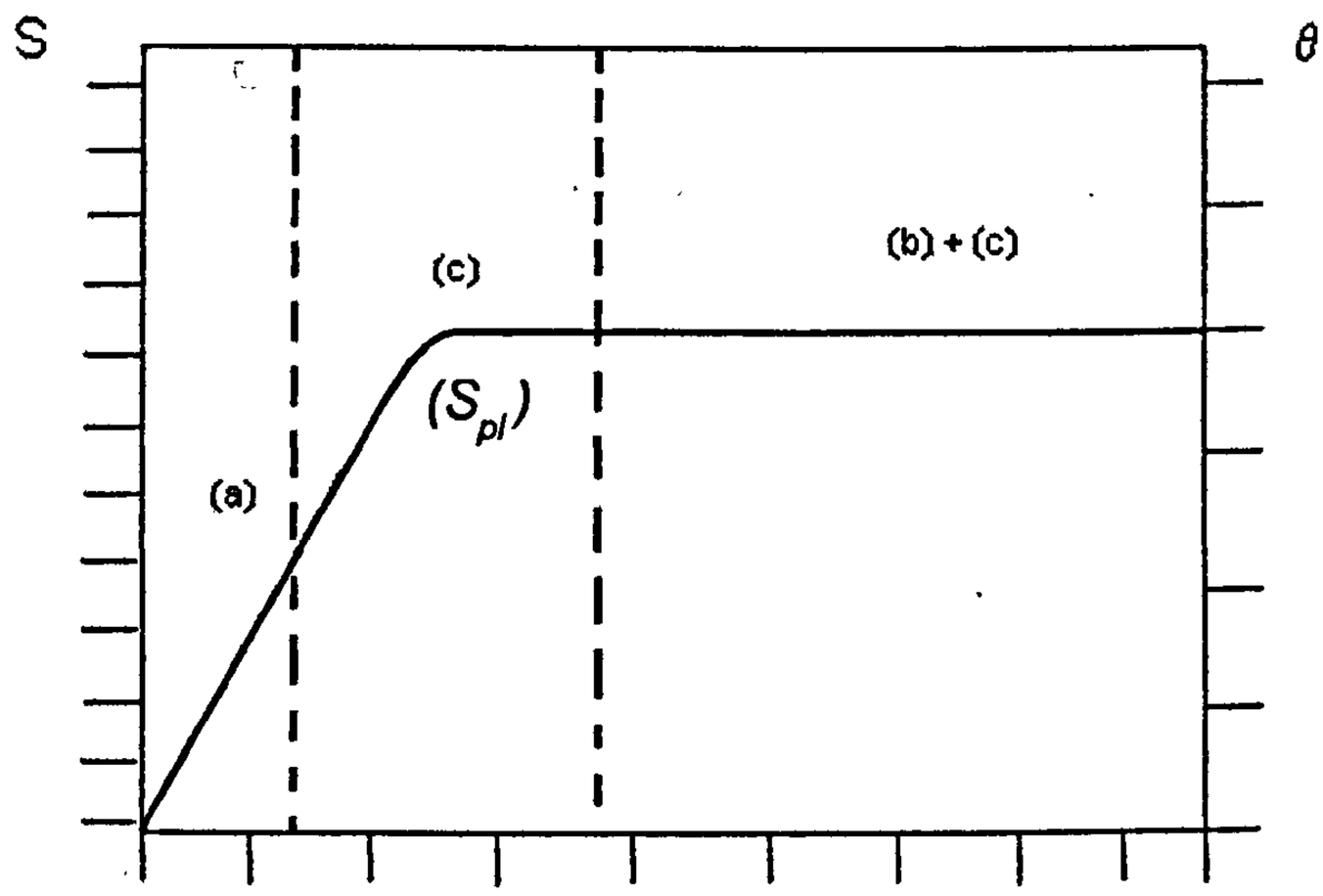

The three deposition stages in the above diagram refer to the droplet-substrate interactions described in figure 7.1, section 7.1. Stage (a) describes the

barrierless attractive interaction between a droplet and bare flat substrate. Stage (b) indicates the deposition rate reduces as the deposition substrate coverage increases caused by the build up of repulsive forces between deposited and approaching droplets. The final stage (c) is a complex combination of attractive forces between the droplet and substrate together with repulsive droplet-droplet interactions . At high coverage regimes the flat substrate surface can be distorted to resemble the curved deposited droplet surface.

The high coating density deposition regimes have been defined as surface coverage where the mean particle-particle separation distance is smaller than the average particle radius[30]. This classical definition has previously only applied to solid, rigid particles but can also be used for the coverage regimes of deformable droplets observed in this study.

Adamczyk et al[31] reported on high surface coverage regimes observed in stagnation point flow methods, at a fixed Re < 4. It was noted that as the surface coverage of depositing rigid particles becomes non-uniform and the surface blocking effects become more significant and the precision of experimental results lowers.

7.2.6 Tubular pinch effect

Segré et al[32] first reported the "tubular pinch" (Segré and Silberberg effect) in which particles were subjected to lateral forces, resulting in the migration of particles to an equilibrium distance located at approximately 60% of the distance

from the tube axis to the tube wall. Four main mechanisms were reported for this effect; (i) wall repulsion due to lubrication forces, (ii) inertial lift related to shear slip, (iii) lift due to particle rotation, (iv) lift force due to the curvature of the undisturbed velocity profile. There is a constant competition between the Brownian motion and migration due to shear forces, which results in different concentration distributions under different flow conditions. Cao et al[18] report the use of the Peclét number to determine the dominant force in each system. Systems with Pe <1000, showed that particles migrate with uniform concentration in regions >10 particle diameters from the channel wall, due to the wall effects. The migration effect became progressively stronger as the Pe number increased, with the transition in the range of Pe 10^3 -10^5 .

7.2.7 "Blocking" effects

Dabros et al[30] extended the deposition theory to include blocking effects present on partially coated surfaces, which resulted from modified fluid flow field and repulsive particle-particle interactions. Interactions between adsorbed and approaching particles were reported to change the mass transfer conditions near the collector surface as the coating process increased and the inter-particle repulsive forces reduced the particle flux to the collector surface. This resulted in a non-linear increase of the coating density as a function of time as the trajectories of flowing particle were modified, making sections of the collector surface inaccessible and further increase of the blocked area[33-35].

The adhesion kinetics over the duration of the stagnation point flow experiments

conducted in this study was used to obtain the characteristic adhesion time, τ, which is composed of a desorption and blocking component[36];

$$1/\tau = \beta + j_0 A \qquad [7.23]$$

in which β is the desorption rate and A is the area blocked by an adhering particle. The blocked area A can be derived from the radial pair distribution g(r) as can be calculated from the spatial distribution of the adhering particles. Radial pair distribution functions describe the relative density of adhering particles around the stagnation point as a function of their separation distance[37].

$$g(r) = \frac{\rho\,(r, dr)}{\rho_0} \qquad [7.24]$$

where ρ (r, dr) is the density of adhering particles in a shell with width *dr* at a distance r from the stagnation point center. Each adhering particle is taken once as a center particle. As an example, the spatial arrangement of adhering particle and the resulting distribution function g(r) are given in fig7.4. The blocked area was calculated from the region $g(r) < 1$[38], where small blocked areas with a relatively high density of adhering particles correspond to attractive inter-droplet forces and large blocked areas imply repulsive interactions between droplets.

Previous models[39] and experimental results have suggested that collector surface properties, which change before and during particle deposition, can create significant "blocking effects"[9,39-42]. The extent of this "blocking effect" was shown to be dependent on the range of repulsive double-layer interactions and Péclet

number. Collector surface heterogeneity can create deposition "active sites" that once they become saturated can make sections of the substrate inaccessible to flowing particles[39,42]. In addition, the chemical nature of the collector surface can be altered in the vicinity of deposited particles by enhancing the repulsive interaction forces with approaching particles and by the colloidal forces exerted on the particles in the suspension[43]. It has also been shown that a single deposited particle is able to block an area which is many times larger than its geometrical cross-section. All of these effects can significantly reduce the particle flux to the substrate which was assumed to diminish linearly with the growing number of particles on the surface[44] and also the cross-sectional area of the deposited particles, all of which influences the magnitude of the blocking coefficient.

Dabros et al[44] reported that as the density of uniform coating increases, the flow diminishes in the deposition region and at total coverage, the flow decreases to 10% of its original value. However, the velocity never drops to zero as the fluid can penetrate the space present between rigid deposited particles. This study has attempted to directly observe these effects, where it has previously not been possible, and to extend these hypothesises for deformable droplets.

Fig 7.4 Spatial arrangement of adhering droplet,(a), g(r)<1 region with blocked area, A, (b)

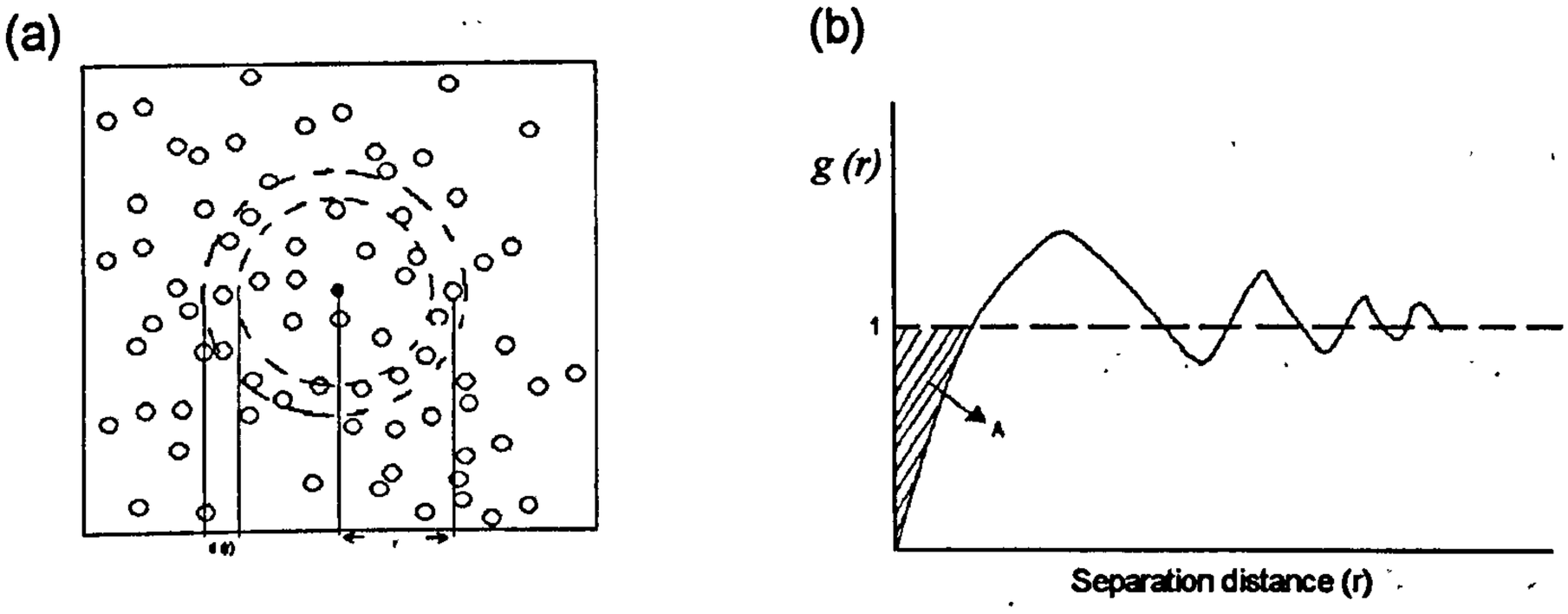

7.2.8 Adhesion

The adhesion forces exerted by an oil droplet on a plane wall can be defined as the van der Waals attraction at the equilibrium separation distance, and will exist as long as the hydrodynamic forces exerted on the droplet are smaller than the adhesion forces[44]. Therefore adhesion is a balance between hydrodynamics and interfacial forces. Adhesion is a physical balance between hydrodynamic and interfacial forces in which a droplet will adhere to a substrate in a flow cell as long as the latter force is not exceeded by the former. Das et al[45] extended the theory developed by Goldman et al[46] for the case of a deformable particle on a rigid substrate by studying shear or frictional stresses. Mahé et al[47] observed that as an alcane droplet came into close proximity with the glass substrate in an aqueous solution, it slowly deformed and the water film between the two interfaces was drained under the action of gravity. The presence of impurities or additional components prevented the droplets to adhere to the substrate. Yiantsios et al[48] reported that the deposition time for particles, < 2μm, was related

to a balance between gravity effects and electrostatic force barriers. However once this barrier is overcome, the time taken for the maximum adhesion strength to be reached is dependent on the viscous resistance from molecular water layers between the two interfaces.

7.2.9 Contact deformation

The contact region between a droplet and rigid substrate has been modeled by several different authors, with JKR and DMT theories being the most significant. Johnson, Kendall, Roberts (JKR theory)[49-51], derived from Hertz[52] theory, predicted the compressed stress at the contact area of deformation from a model of two elastic spheres, of infinite radius, pressed against each other by an external load with a specific surface energy at the region of interaction. It was suggested that the stress present at the contact region between two sphere becomes tensile with increasing distance from the center of contact In addition, it was predicted that the sphere surface approached the substrate at right angles near the edge of the contact region.

In contrast, Derjaguin, Muller and Toporov (the DMT theory)[53] predicted that an interaction between the sphere and the substrate surface existed beyond the contact region by assuming that the attractive force between the two solids was finite. The DMT theory predicted a lift force 4/3 times that of the JKR model and suggested that there was a finite tensile load at the edge of the contact area between the sphere and the substrate.

It was concluded that the contact deformation of the interacting solid particle

colloidal systems in a liquid medium, with $E>10^{10}$ dyn/cm^2 and μ is smaller than unity, can be accurately described by the DMT theory with certain modifications[54,55]. These modifications were presented by Sharma et al.[56] who suggest that deformation of the solids must be calculated using the forces of interaction in both the contact and non-contact regions. However, for the softer more deformable spheres, with $E<10^{10}$ dyn/cm^2 and μ is larger than unity, the JKR theory better describes the interactions observed within the cross-linked PDMS emulsion systems in this study[49-51,53]. Sharma et al[56] also argued that the magnitude of the surface force inside the contact region is a direct function of the radius of the contact zone, while the extent of deformation is dependent on the total force of interaction. This interaction force contains repulsive components which act in response to the attractive van der Waals force. Das et al[57] calculated that the contact area radius of a deformable particle on a rigid substrate reaches an equilibrium separation distance and the interacting forces distribute symmetrically about the center of the contact region.

Das[57] reported the deformation of contact area caused by the action of the hydrodynamic force on an adhered particle and rigid substrate was negligibly small and did not provide a large enough restraining torque. In addition, the mechanism of detachment of colloidal particles from a surface could not be explained on the basis of friction alone. The presence of surface roughness was found to be a necessary condition for the existence of a large enough restraining torque. The magnitude of this restraining torque can be determined by the surface roughness of the particles, the substrate and the extent of the elastic deformation. If the substrate contains asperities that are much larger than those on the

particles (e.g. glass substrate), then it is these asperities on the substrate and the extent of elastic deformation that primarily determine the restraining torque. On the other hand, if the particles possess much larger asperities than those on the substrate (e.g. a mica substrate), then it is the characteristic height of these asperities that primarily determines the magnitude of the restraining torque. Therefore work on the mechanism of hydrodynamic detachment of particles should be focused primarily on characterising the surfaces in terms of the distribution of asperities.

7.2.10 Film thinning and rupture

The stability of the film to rupture is dependent on the magnitude of the hydrodynamic forces operating across it and the physico-chemical properties of the cross-linked oil[58], e.g. viscosity[59], interfacial rheology[60] and surface electrostatic potential[61]. There are two main mechanisms of coalescence in thin liquid films.

Slow coalescence is observed in metastable emulsion films and can take years for the process to be completed, due to the nucleation of thermally activated holes in the film[62]. The faster film rupture mechanism occurs in the first minutes of the film formation, however. These interfacial undulations are reduced by the high Gibbs elasticity values. The droplet-droplet lifetime, t, has been shown to be proportional to the droplet diameter[63], d, equation [7.25], while the CCC required to induce coalescence decreases as the interfacial contact area between the droplets increases.

$$t \propto d^2 \qquad [7.25]$$

When the film is thin, e.g a few nm, the van der Waals forces become predominant and the pressure exerted on the film, P, is equal to the opposite of the disjoining pressure,

$$P = \frac{A}{6\pi h^3} \qquad [7.26]$$

where h is film thickness, and $A = (\sqrt{A_2} - \sqrt{A_1})(\sqrt{A_3} - \sqrt{A_1})$, where A_1, A_2, A_3 are the Hamaker constants for the water film, the solid wall and the oil phase respectively. P has more complex expressions if double layer forces are present or film thickness fluctuates.

Mahé et al[47] reported that high Mw oil phases, with corresponding high Hamaker constants, were more likely to display contact film thinning or even rupture. It was found that the time taken for film rupture, t_r , was found to decrease as the capillary pressure, P_c , increases. The film stability has been studied using a variety of systems, including air-water-air[64], oil-water-silica[65] and water-oil-glass systems[47]. Film rupture occurred slowly, a few minutes, in the latter system when the film thickness was a few nm and the van der Waals forces become significant. The rupture point was located in either the peripheral or central zone of the film due to the relative weakness of the van der waals and double layer forces. Substrate surface heterogeneity was also shown to effect the contact zone giving it an irregular shape.

Mahé et al[47] reported the influence of the chain length on film stability between a droplet and smooth glass surface in the presence of a slow shear flow of water. The water film created between oil droplets, consisting of < C10 and a solid substrate surface drained under the action of gravity[44], after which, van der Waals forces create an equilibrium film stability. However, it was observed that the film ruptured more quickly for the drops of C15 and above.

7.2.11Spreading dynamics on smooth and rough surfaces

A liquid drop can wet a smooth, rigid surface by either forming a well-defined contact angle, *partial wetting*, or by spreading to a create continuous film across the substrate, *complete wetting*[33]. Recent theories[66-70] and experimental studies[67,70,71] have reported on the particle-substrate wetting dynamics and suggested that the dominant forces involved are gravity,liquid-air surface tension, γ, and long- range van der Waals forces[66]. If the surface tension of the drop is the dominant force, Tanner's spreading law[67] can be used to model the wetting dynamics, giving an approximate solution of the hydrodynamic equation in the complete wetting regime;

$$a \alpha t^n \qquad [7.27]$$

where *a is* the radius of the liquid-substrate contact area and *t* represents time. Recent ellipsometry measurements of PDMS on bare silicon[72] confirmed the prediction by de Gennes[73] of the presence of a "pancake" precursor film that

proceeds the macroscopic spreading front, the drop contact angle is given by :

$$\tan \theta = 2ha / (a^2-h^2) \qquad [7.28]$$

As film spreads from a partial to a complete wetting transition, h << a;

$$\theta = 2h / a \qquad [7.29]$$

Pérez, Schäffer and Steiner[74] predicted a new spreading regime for the case of a small spherical PDMS cap height on a substrate, at a constant volume ranging from $\Omega = 1 \times 10^{-9}$ to $1 \times 10^{-6} cm^3$, suggesting VW forces would become dominant.

However, if the substrate surface becomes roughened , the wetting behaviour moves from Young's equation to Wenzel's modification of Young's model, which includes the ability of the drop to penetrate the gaps between surface asperities;

$$\cos \theta = r \cos \theta \qquad [7.30]$$

where cos θ is the contact angle for smooth surfaces. The modification predicts the contact angle magnitude is dependent on the surface asperity.

Lundgen et al[75] recently extended this theory through a molecular dynamic simulation of the variation in contact angle between a deformable droplet and substrates containing controlled surface asperities, see figure 7. (a-b). At low roughness regimes, <10Å , the droplet diffuses into the gaps between asperity

peaks, completely filling the hollows, and the θc is independent of the substrate surface (a). However, above a critical roughness, >20 Å, the gaps between the peaks create air pockets preventing the droplets from penetrating the asperity hollows, (b). The drop spreads over the top of the peaks as they are more wettable than the sides and maximises contact with the top of the peaks.

Figure 7.5 Droplet spreading mechanisms on rough substrate (a) diffusion into gap, (b) no gap penetration,

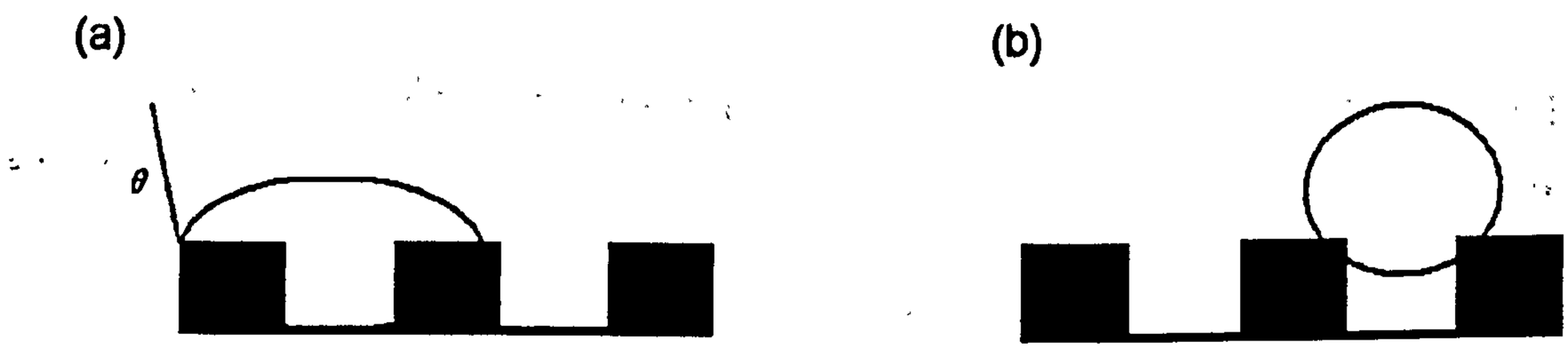

7.3 Colloidal removal

Das et al[57] reported that once a drag or hydrodynamic force is exerted on a particle in a single direction of flow, an opposing frictional force arises to balance the force. The shear stress resulting from the frictional force deforms the contact region so that the opposite points on the surface become closer, see figure 7.6.

Deformation of the contact region between a droplet and a rigid substrate causes the short range Born forces to become concentrated near to the substrate, which results in an asymmetric distribution of surface forces at the contact area. This

asymmetry gives rise to a net restraining torque until it reaches a critical value at which the particles are detached by a rolling motion.

Fig 7.6 The hydrodynamic and frictional forces acting on a deformed particle

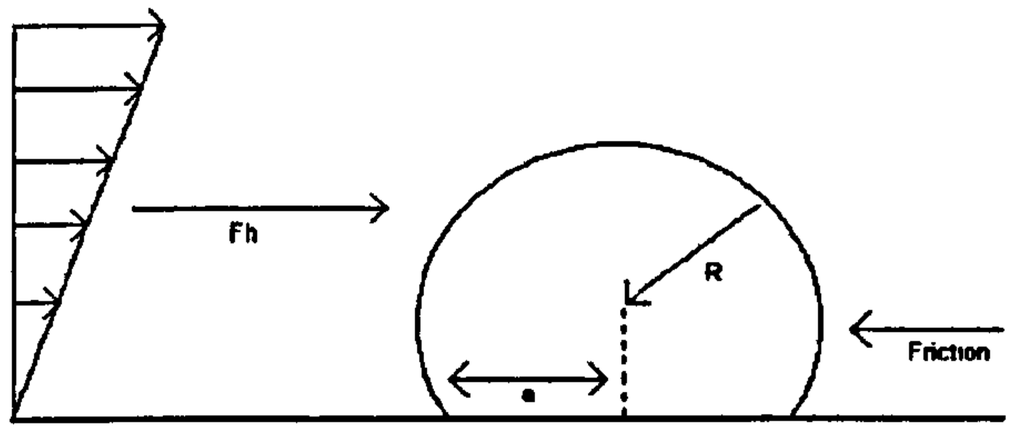

where R is droplet cap radius, a is contact radius and Fh is the drag force acting effectively at a point above the particle center.

The critical shear force was predicted by JKR theory[49-51] to be more dependent on the sphere radius and specific surface energy than the elastic properties of the sphere. Das et al[57] noted that the restraining torque, acting on a deformable sphere at rest on a rigid substrate, could be determined by the relative magnitudes of their elastic constants. Surface asperities localize Born forces around the point and they have been found to affect contact deformation. The height of the particle and substrate asperities were found to influence the magnitude of the restraining torque more than the force of adhesion. Therefore the dominant factor in the hydrodynamic detachment of particles was the determination of the lever arm in the restraining torque. The critical force of mica substrate in the presence of 10^{-2}M NaCl was obtained from the point of intersection of a plot of the hydrodynamic force against the restraining force. The

critical force was found to be smaller than the theoretically calculated values, while results for glass substrates were larger. Hubbe[76] reported elastic properties played a secondary role on the restraining torque. Sharma et al[56] noted that although the elastic deformation property of a particle of the dictated the contact radius size, it was not responsible for the resistance to rolling. It was observed that the critical hydrodynamic force was larger for glass particles on molecularly smooth mica substrate, than polystyrene particles. In addition the hydrodynamic drag force required to remove particles was ~2 orders or a magnitude smaller than the lift force and the maximum slope (force) of the net potential energy curve. However Hubbe[64] compared the magnitude of contact deformation with the height of the asperity, determined the lever arm and concluded the magnitude of the restraining torque was dependent on the contact radius. It was suggested calculations of Born force should be modified to include non-localised force distribution and surface roughness differences.

The critical hydrodynamic force, γ_c, can be calculated by equating the hydrodynamic force, exerted on the droplet by the external water flow, to the adhesion force[77];

$$\gamma_c \sim \frac{\sigma}{\mu} (\cos\theta) \frac{\phi_p}{\phi^2} \qquad [7.31]$$

where γ_c is the critical shear rate, σ is the interfacial tension, ϕ_p is the contact zone diameter, θ is the contact angles respectively, μ is the viscosity of water. The critical shear stress, γ_c, was observed when the near part of the contact zone moves upstream in the direction of the flow it gradually decreases while the front

part of the zone remains static. The droplet finally detaches when the contact zone disappears[46]. For a given shear rate, the droplet reaches an equilibrium shape, independent of the initial conditions. The critical hydrodynamic force is defined as the force required to displace 50% of the particles deposited, (F_{H50}).

O'Neil et al conducted removal experiments with glass and polystyrene particles, 10μm, on mica substrates and a flow solution of water and 10^{-2}M NaCl aq. The following expression was used to calculate the hydrodynamic force, equation [7.32],

$$F_H = 1.7(6\,V_R)\,\mu R V_R \qquad [7.32]$$

where μ is fluid viscosity, V_R is fluid velocity at center of the particle ($V_R = 6(Q/A)(R/l)(1-R/l)$, Q is the flow rate, A is the cross sectional area and l is the thickness of the flow area.

The flow cell results given in this work are presented as plots of F_{H50} as a function of flow rate, for each flow solution or substrate as presented in previous studies[19-21]. However, there is not often a single-valued force that removes the majority of particles but a continuous distribution of force that exceeds adhesive bonds. This distribution is directly related to the non-uniformity of the surfaces of substrates and colloidal droplets[31,39-42].

7.4 Horizontal flow parameters

It is widely considered that detachment occurs in a horizontal flow cell when a torque is exerted on a hard sphere in contact with a flat surface[78-81]. This value exceeds the restraining torque and a critical value is obtained. Once rolling has commenced, the particle rapidly acquires enough lift to detach it fully from the surface. The origin of the restraining torque is thought to be a result of the surface roughness and contact deformation that occurs in real systems[78,82].

Hubbe[76] developed this theory by suggesting that a particle can be slid, rolled or lifted away from its initial site of deposition and many processes can lead to time-effects in the release of particles from surfaces exposed to shearing flow. Dahneke[83,84] derived an expression for the rate of escape of Brownian particles from a deep minima of potential energy, which can be used to predict detachment in the presence of flow, but is only relevant when it is larger than the adhesive forces or the hydrodynamic forces present and is therefore not relevant to this system. The viscosity and inertia of a fluid gives rise to forces acting on immersed stationary particles based on Re and the velocity of stream-wise velocity. The simple shear flow streamwise velocity is given by;

$$u = H\sigma/\eta \qquad [7.33]$$

where H is the distance from the wall, σ is the shear stress, and η is the dynamic viscosity, and can be related to the particle Reynolds number in the form;

$$Re_p = a^2 \tau p / \eta^2 \qquad [7.34]$$

where υ is the kinematic viscosity of the fluid, a is the radius of the particle.

Visser[80] related the critical hydrodynamic force (F_H) for particle removal and its force of adhesion (F_A) to surface roughness, particle shape and deformation, through a material coefficient (γ);

$$F_H = \gamma F_A \qquad [7.35]$$

Hubbe[76] evaluated the coefficient, γ, for a rolling particle release mechanism based on a torque balance. This led to a new expression involving the particle radius, R, and the radius of the contact area, a, equation [7.36].

$$F_A a = 1.3999 F_H a \qquad [7.36]$$

O'Neil[85] theoretically calculated the critical hydrodynamic force as the tangential force acting on the center of the particle, for particle of radius, a, in contact with a plane wall underwent laminar shear flow, equation [7.40].

$$F_H = 1.7(6\pi)\eta a V_x \qquad [7.37]$$

where, η, is the fluid viscosity and V_x, is the flow velocity at the center of the particle. The flow velocity at the particle center, V_x, is dependent on the cell dimensions and can be related to the experimental flow rate, Q, using equation

[7.38].

$$V_x = 6\left(\frac{Q}{A}\right)\left(\frac{a}{h}\right)\left(\frac{1-a}{h}\right) \qquad [7.38]]$$

where, A is the flow cross sectional area, and h is the horizontal cell depth. These equations are only relevant to flow regimes under Re ~2000-2500, at which point there is a transition from stable streamline to stable turbulent flow[85]. Turbulence is characterised by the Reynolds number (Re), which represents the ratio of the inertial to the viscous forces, equation [7.42].

$$Re = \frac{h\rho Q}{\eta A} \qquad [7.39]$$

where, ρ, is the liquid density. The maximum flow rate attained in the experimental set up used in this work was 353mL min^{-1}, which equates to a Reynolds number of 4, using the parameter listed in table 7.1. Removal experiments often illustrate how particles detach with a distribution of critical hydrodynamic forces rather than a single value. This behaviour is especially pronounced when substrate surface roughness is not uniform as some particles are exposed to larger asperities and consequently require larger hydrodynamic forces for detachment than those in contact with smaller asperities. Previous literature studies[77-79] have overcome this problem by adopting the method of calculating the hydrodynamic force required to remove 50% of particles, F_{H50}, from the surface area of observation and then compared this value with other experiments. However due to the adhesive properties of the cross-linked PDMS droplets, it was only possible to quote F_{H40} for

the detachment studies carried out in this project.

Table 7.1 Parameters used for calculating hydrodynamic force

Viscosity of water 'η' (N s m^{-2})	Density of water 'ρ' (g m^{-3})	Particle radius 'R' (μm)	Cell depth 'h' (mm)	Flow cross sectional area (mm^2)
0.001	1	3.05	0.5	7.75

7.4.2 Removal data and analysis

Each image recorded using the *Visilog 5.2* software was analysed as discussed previously in chapter 4. The droplet number, individual droplet contact area and radial position was determined. The number of particles remaining for each scan, was set as a percentage of the number measured at the initial flow rate of 37mL min^{-1}, this was then presented as a plot of the percentage of particles remaining on the substrate as a function of flow rate. The plot produced a 'S' shaped graph that could be fitted with a sigmoidal function curve and used to identify the flow rate that caused 50% of the particles to be detached, F_{H50}.

The total number of particles deposited initially varied slightly between substrate batches , as well as their distribution across the slide. Consequently the flow rate required to remove F_{H50} of the particles also showed a slight variation between slides of the same batches.

Data was normalised to compare experiments carried out between slides of the same batch and also between different substrates. A baseline standard was

established by conducting five flow cell runs for each slides, using pure water as the wash solution. The average flow rate for F_{H50} particle removal was obtained and all other flow cell runs conducted for each substrate were then normalised against this average. This procedure gave a correction factor for each wash solution.

The accuracy of the results from both the stagnation point and Horizontal flow cell experiments was effected by the accuracy with which the concentration of the flow solutions were determined, the flow rate measurement, and the calibration of the image capture software. However, the most obvious influence error would have been the non-uniformity of the substrate surfaces investigated. In order to quantify this error, the standard deviation was calculated for the average removal force obtained from each of the separate runs carried out with a water wash solution. This was done separately for the different substrates used in the flow cell and the results are shown as error bars on the plots of critical hydrodynamic removal force (F_{H50}). In addition, the influence of surface asperities was investigated as part of the general deposition and removal study.

7.5 References

1. Cleaver, J.W, B.Yates, J. Coll. Interface.Sci. 44, 464 (1973)
2. Dabros, T, Van de ven, T.G.M, J.Colloid.Interface Sci, 89, 232, (1982)
3. Adamczyk, Z, Zembala, M, Siwek, B,Czarnecki, J, J.Colloid Interface Sci., 110, 188, (1986)
4. Vincent.B, C.A.Young, Faraday Disc.Chem.Soc., 65, 296, 1978
5. Vincent.B, C.A.Young, J.Chem.Soc, Faraday Trans. 1, 76, 665, 1980
6. Vincent.B, P.F.Luckham, Colloids & surfaces, 1, 281, 1980

7. Vincent.B, M.Jafelicci, P.F.Luckham, Th.F.Tadros, J.Chem.Soc, Faraday. Trans.1, 76, 674, 1980

8. Vincent.B, P.F.Luckham, Colloids & Surfaces, 6, 83, 1983

9. Dabros.T, Van de ven, T.G.M, Colloid Polymer Sci. 261, 694(1983)

10.de Boer.J, Trans Faraday Soc, 32, 10 (1936)

11.Hamaker.H, Physica, 4, 1058 (1937)

12.Hogg.R, T.W.Healy, D.W.Fuerstenau, Trans.Faraday.Soc., 62, 1638 (1966)

13. Bell.G, S.Levine, L.N.McCartney, J.Coll.Int.Sci., 33,335, (1970)

14. Prieve.D, E.Ruckenstein, A.I.Ch.E.J, 22, 276, (1976)

15. Derjaguin, Kolloid Z., 69, 155 (1934)

16. Devereux.O, P.L.de Bruyn, "Interaction of Plane Parallel Double Layers", MIT Press, Cambridge, Mass, (1963).

17. Dabros.T, T.G.M., van der Ven, Coll.Polym.Sci., 261, 694, 1983

18.Adamczyk.Z., Siwek.B., Zembala, M., J.Coll.Int.Sci, 151, 351, 1992

19. Bachmann D J, Miklavcic S J, 1996 Langmuir, 12, 4197

20. Horn, R.G, Bachmann, D.J, .N, Connor, J,Phys: Condens. Matter S (1996) 9482-9490,

21. Derjaguin.B, Disc.Faraday Soc., 18, 85, (1954).

22. Verwey.E, J.Th.G.Overbeek, "Theory of the Stability of Lyphobic Colloids" Elsevier (1948)

23.Hansen

24. Langbein.D, Phys. Rev., B2, 3371, (1970).

25. Parsegian.V, B.W.Ninham, J.Coll.Int.Sci, 37, 332, (1971)

26. Winterton.R, Contemp. Phys., 11, 559, (1970)

27. Israelachvili.J, D.Tabor, Prog. Surf.Memb.Sci., 7, 1, (1973).

28. Richmond.P, "Colloid Science", Spec.Per.Rep.Chem.Soc., London, 2, 130, (1975)

29. Dabros.T, van de Ven.T.G.M, Journal of Colloid and Interface Science, 89, 1, 232, 1982

30. Dabros,T., van de Ven T.G.M., Colloids & Surfaces A: Phys.Eng.Aspects, 75, 95-104, (1993)

31.Adamczyk, Z., Siwek, B., Zembala, M., J.Colloid Int.Sci., 151, 351, (1992)

32. Segré.G, Silberberg.A, Journal of Fluid Mechanics, 14, 1, 115, 1962

33. Vincent.B, S.Whittington, in E.Matijevic (ed.), "Surface and Colloid Science", Vol.12, p.I., Wiley, New York (1980)

34.Ruijter, M.J., Charlot, M., Voué. M., de Coninck, J., Langmuir, 16, 2363, 2000

35.Marmur, A., Adv. Coll.Interface Sci. 19, 75, 1983

36.Elimelech, M; Sep. Teachnology, 4, 186-212, 1994

37. Kamiti, M, van de Ven.T, Coll.Surf.A, 100, 117-129, 1995

38. Sjolems.J, van der Mei.H, Uyen.H, Busscher.H, FEMS Microbiol.Lett, 69, 263-270.

39. Dabros.T, Colloids Surfaces, 39, 127,(1989)

41.Meinders, M.J., Nordmans, J., Busscher, H.J., J.Colloid Int.Sci. ,152, 265, (1992)

42. Sjollema, J., Busscher.H.J., Colloids Surfaces, 47, 337, (1990)

43.Wnek.W.J, Gidaspow.D., D.T.Wasan, J.Colloid InterfaceSci., 59, 1, (1977)

44.Mahé.M, M.Vignes-Alder, A.Rousseau, C.G.Jacquin, P.M.Alder, Journal of Colloid and Interface Science, Vol. 126, No.1, 314-328,Nov 1988, I.Pure systems

45.Das, S.K., Schechter, R.S., Sharma, M.M., J.Coll.Int.Sci. 92,92, 1983

46..Goldman, A.J., Cox.R.G., Brenner.H., Chem.Eng.Sci., 22, 653, 1967

47. Mahé.M, M.Vignes-Alder, A.Rousseau, Journal of Colloid and Interface Science, Vol. 126, No.1, III. Contaminated systems

48. Yiantsios.S.G., Karabelas.A.J., Journal of Colloid and Interface Science, 176, 74, (1995)

49. Roberts, A.D, PhD dissertation, Cambridge University, England, 1968,

50.Kendall, k.Ph.D, dissertation, Cambridge University, England, 1969

51.Johnson, K.L., Kendall, K., and Roberts, A.D., Proc.R.Soc., London., A 324, 301 (1971)

52. Hertz, H., in "Theory of Elasticity" (S.P.Timoshenko and J.N.Goodier, Eds) p.409, McGraw-Hill, New York, 1970

53.Derjaguin, B.V., Muller, V.M., Toporov, Yu, P., J.Coll.Int.Sci., 53, 314, (1975)

54. Muller, V.M, Yushchenko, V.S., Derjaguin, B.V., J.Coll.Int.Sci., 77, 91, (1980)

55..Muller, V.M, Yushchenko, V.S., Derjaguin, B.V., J.Coll.Int.Sci., 92, 92, (1983)

56.Sharma, M.M., Chamoun, H., Sarma, Sita Rama Sarma, D.S.H, Schechter, R.S.,J.Coll.Int.Sci., 149, 121 (1992)

57. Das.S, Schechter.R, Sharma.M, Journal of Colloid and Interface Science, 92, 1983

58.Neuman.B, Vincent.B, Krustev.R, Hans-Joachim.M, Langmuir, 20, 4336-4344, 2004

59.Stoyanov.S, Dushkin.C, Langevin.D, Weaire.D; Verbist.G, Langmuir,14, 4663, 1994

60.Jayalakshimi.Y, Ozanne.L, Langevin.D, J.Coll.Int.Sci, 170, 358, 1995

61.Karraker.K.A, Radke.C.J, Adv.Coll.Int.Sci., 96, 231, 2002

62.Kabalanov.A., Modern Aspects of Emulsion Science, Binks.B., Ed., The Royal Society of Chemistry, London, 1998

63. Vincent.B, Kiraly.Z, Obey.T.M, Modern Aspects of Emulsion Science Binks, B.P., Ed,: The Royal Society of Chemistry:, London, 1998

64. Read.A.D., Kitchener,J.A., J.Coll.Int. Sci.30, 391, 1969

65. Aronson,M.P., Petko,M.F., Princen.H.M., J.Coll.Int.Sci. 65, 296, 1978

66. de Gennes, P.G., Rev.Mod.Phys. 57, 827 (1985)

67. Tanner, L.H., J.Phys.D 12,1473, 1979

68.Lopez, J., Miller, C.A., Ruckenstein, E., J.Coll.Int.Sci. 56, 460, 1976

69.Huh, C., Scriven, L.E, J.Coll.Int.Sci., 35, 85, 1971

70.Ruijter, M.J., Charlot, M., Voué. M., de Coninck, J., Langmuir, 16, 2363, 2000

71.Pérez. E, Schäffer.E, Steiner.U; J.Coll.Int.Sci. 234, 178-193 (2001)

72.Hogg.R, T.W.Healy, D.W.Fuerstenau, Trans.Faraday.Soc., 62, 1638 (1966)

73.de Gennes, P.G., Rev.Mod.Phys. 57, 827 (1985)

74.Pérez. E, Schäffer.E, Steiner.U; J.Coll.Int.Sci. 234, 178-193 (2001)

75.Lundgen.L, Svedinch.P, Beckman.O, Phys.Review.B, 26, 3990, 1982

76.Hubbe, M.A., Colloids Surf. 12, 151 (1983)

77.Yiantsios.S.G., Karabelas.A.J., Journal of Colloid and Interface Science, 176, 74, (1995)

78.Marti.O., Drake.B., Hansma.P.K., Applied Physics Letters, 51, 484, (1987)

79.Yamamoto.T., Periasamy.R., Donovan.R.P., Ensor.D.S., Journal of Adhesion Science and Technology, 8, 543, (1994)

80.Visser.J., Particulate Science and Technology,13,169,(1995)

81.Hubbe.M.A., Colloids and Surfaces,12,151,(1984)

82.Niida.T., Kousaka.Y., Furukawa.T., Particle and Particle systems characterisation, 6, 69, (1989)

83.Visse.J., Journal of Colloid and Interface Science,55,664, (1976)

84.Dahneke, B., J.Colloid Interface Sci., 50, 1975, 194,

85.O'Neill.M.E., Chemical Engineering Science, 23, 1293, (1968)

Chapter 8: Substrate preparation and characterisation

8.1 Introduction

One of the main objectives of this project was to manipulate and record the deposition behaviour of PDMS droplets on different solid substrates by altering the substrate surface heterogeneity, the surface charge and the chemical composition. Various characterisation techniques were used to investigate the surface properties of the substrates. These included; AFM, XPS, streaming potential and three phase inverted contact angle measurements.

Previous studies that investigated controlled particle deposition on to chemically altered substrate surfaces, include Elimelch et al[1] who deposited amine functionalised positively charged polystryene latex particles onto silanised micro-patterned glass slides within a stagnation point flow cell. The alternate negatively and positively charged glass was used to control colloidal deposition through the manipulation of hydrodynamic and repulsive and attractive electrostatic double layer interactions

This study used mica substrates to represent molecularly smooth model surfaces, and compared results with chemically modified glass substrates. The glass substrates were modified in several ways to represent the complexity of the surface chemical composition of hair, see chapter 1. These modifications included; untreated glass as a standard glass model; acid cleaned glass slides (hydrophilic model

surface), Repelcote coated glass (hydrophobic model surface), APTES coated glass (positively charged model surface) and L-Lysine coated glass (amino-acid model of hair surface).

8.2 Substrate surface modification

8.2.1 Preparation of acid cleaned glass slides

BDH low iron clear glass 0.8-1.0 mm thick microscope slides were sonicated in a 2% aqueous solution of *Micro 90* for 30 mins[2-4]. They were then thoroughly washed with Milli Q water to remove all surfactant residue, after which they were heated in a solution of 1:1:1 HCl, H_2O, H_2O_2 , at 80 °c for 30 mins. The slides were washed repeatedly and stored under water until required.

8.2.2 Adsorption of 3-Aminopropyltriethoxysilane onto glass slides

Previous literature has shown how aminoalkyl-substituted silanes, e.g APTES, has been used to chemically modify silica surfaces to investigate the influence of colloidal deposition on the structure of the altered surfaces[5-8].

Glass substrates were coated with a layer of 3-aminopropyltriethoxysilane (APTES) using the method described by Vandenberg et al[5]. Glass substrates were pre-cured at 120°c and immersed in a solution of, 0.4% by weight, of APTMS in toluene in an

atmosphere below 10% humidity, using a glove box, for 24hrs. The substrates were then washed three times in an excess of ethanol and dried in air. The use of a toluene solution rather than an aqueous solution to deposit APTES onto the substrate, ensured that the silane functional groups adhered to the glass surface hydroxyl groups through covalent and hydrogen bonds, rather than the protonated amine groups[8]. This procedure ensured that the amine functional groups moved freely in the surrounding solution and created a net positive charge on the substrate surface at low pH. The adsorbed polymer structures and the presence of polysiloxane bonds between adjacent APTES molecules on the surface[6] adopted in both solutions are compared in figure 8.1.

Fig 8.1 Structures formed from the deposition of APTES onto a clean glass surface , (i) from an aqueous solution, (ii) from a toluene solution with the formation of polysiloxane bonds

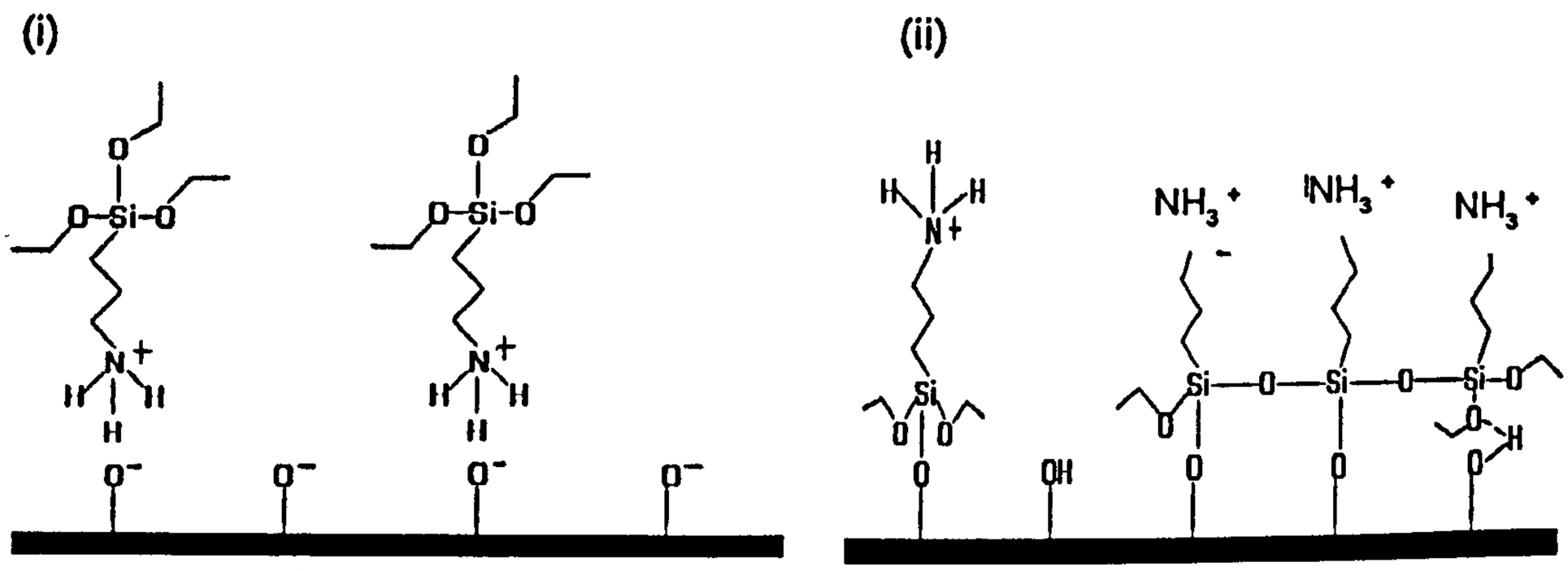

Characterisation studies of the structure of deposited APTES on solid substrates in similar conditions to those discussed above have been conducted previously.

Reported APTES layer thickness have varied from 1.9 nm[5] to multilayers with variable thickness, 6-100Å, depending on the time the substrate is in contact with the solution[9]. It has also been reported that the silanised solid substrates contained ionic polymers[10], transitional metal complexes[11] and non linear optical chromophres[12] on the surface which aided the formation of self-assembled molecular layers.

8.2.3 Preparation of Repelcote modified glass slides

Glass substrates, microscope slides or coverslips, were soaked in a solution of Repelcote, a commercial hydrophobing agent, for 30 minutes at room temperature[4]. As Repelcote solution, 2% dichlorodimethylsilane in octamethylcyclotetrasiloxane, reacts with the hydroxyl groups present on the glass surface, HCl is released and the substrate becomes coated with non-polar, hydrophobic methyl functional groups, see figure 8.3. The slides were then rinsed with n-heptane and the ethanol.

Fig 8.2 Reaction of dichlorodimethylsilane with the hydroxyl groups on a glass substrate resulting in a hydrophobic surface.

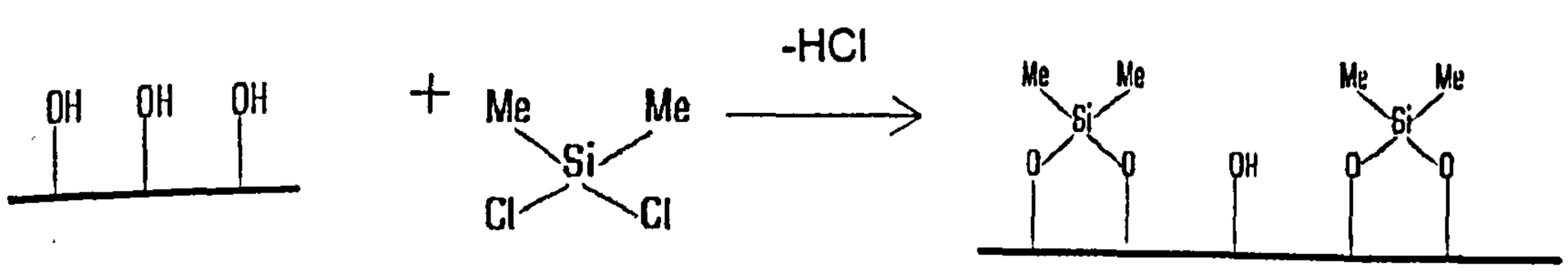

8.2.4 Mica substrate

Commercially prepared G250-1 Mica slides were obtained from Agar in dimensions that simulated glass slides, 3" x 1". Mica, $KAl_2(AlSi_3O_{10})(F,OH)_2$ is an aluminosilicate mineral which consists of layers of symmetrically opposed tetrahedra bases that create two opposite hexagonal cavities which create a single twelve coordinated potassium atom[13,14]. The presence of potassium ions neutralize the negatively charged sheets as they substitute the Si^{4+} within the silica tetrahedra. The magnitude of the negative surface of the mica is dependant on the degree of Al / Si substitution in the silica tetrahedra.

Figure 8.3 Muscovite mica structure[13]

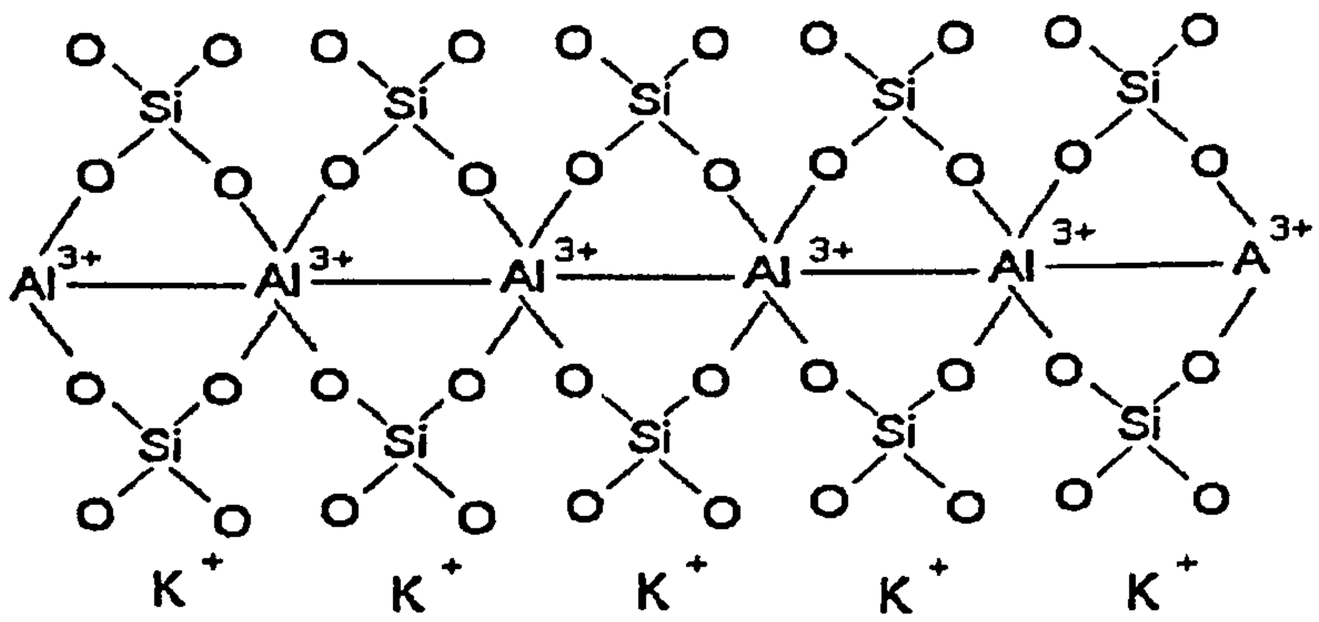

8.2.5 L-Lysine coated glass

Premodified poly L-Lysine microscope glass slides were obtained from BDH. The poly-cation amino-acid adheres to the surface hydroxyls through the carboxyl

functional groups and allows the highly reactive primary amine tail to move freely in the surrounding solution, which creates a net positive surface charge, see figure 8.4. This makes the protein one of the few basic amino acids, while the high pKa value results in the side chains being less effective with significant hydrophobic character.

Figure 8.4 L-Lysine molecular structure

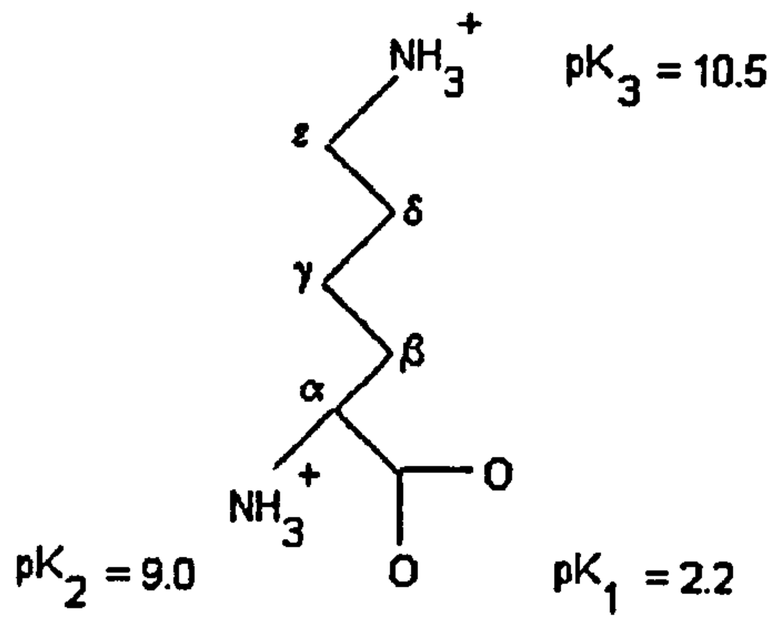

8.3 Substrate characterisation

8.3.1 Substrate surface topography characterisation (AFM)

The interaction between colloidal particles and heterogeneous surfaces is directly influenced by the magnitude and distribution of surface charge heterogeneity[15]. Despite the obvious influence of surface and charge heterogeneity on colloidal interaction forces, few direct measurements have been conducted[16-18] especially in comparison with theoretical investigations. The "Lotus effect"[19] observed in nature can also be observed on fabric surfaces[20] in which water droplets retain their spherical shape on impact with a rough surface and even remove particulates from the

substrate as they roll off. This suggests that an increase in surface roughness enhances the hydrophobic property of the substrate surface.

Each substrate surface used in this study was characterised by using Atomic Force Microscopy, AFM, to obtain detailed quantitative data on its individual topographical roughness and heterogeneity properties. The results were obtained in air by using the tapping mode as described in chapter 4. Graphical representations of each substrate are presented in plate I and the data in table 8.2 below. It is important to note that the lateral and vertical measurements, e.g valleys and peaks 0.01-8nm, were negligible to the particle diameter 2μm-5μm.

The mica is almost molecularly smooth and is therefore an appropriate surface with which to observe model substrate-droplet interactions. Although the untreated glass substrate has the lowest surface heterogeneity value, it has a significant inherent roughness, 10 times the value of mica, which increases the more it is chemically modified. It is possible to note that each chemical modification that was performed on identical glass surfaces produced a different surface heterogeneity pattern, see plate I. This is evident from the distinctive "doughnut" or "crater" marking present on the glass surface after acid cleaning. The irregular surface etching could not only influence to movement of a droplet over the surface but also creates air pockets between the deposited droplet and the crater shape. These three substrates provide distinctively different surface roughness to manipulate droplet deposition and removal.

Table 8.1 AFM substrate surface topography

Substrate	Mean roughness (Ra) nm	Error	RMS (Rq) nm	Error
Mica	0.06	0.01	0.08	0.01
Untreated-glass	0.56	0.01	0.41	0.01
Lysine-glass	0.65	0.01	0.79	0.01
Acid cleaned glass	1.60	0.01	2.80	0.01
APTES-glass	2.60	0.01	5.40	0.01
Repelcote-glass	2.70	0.01	7.40	0.01

It was also possible to distinguish between each of the three polymers used to chemically modify the glass substrate. L-Lysine coated glass displayed a uniform roughness consisting of peaks and troughs which could correspond to an even distribution of the amino-acid solution during manufacture at BDH. In contrast the APTES and Repelcote coated substrates, created in the laboratory, displayed extremely tall "pillars" randomly positioned on the already roughened surface. These pillars could correspond to the presence of bridging bonds between adjacent polymer molecules on the surface[6] as discussed in section 8.2.2. The difference in the average height between the uniform surface asperities and the random "pillars" would account for the higher Ra values. The influence of these different surface topographies, induced by chemical modifications, on colloidal droplet deposition and removal was investigated in chapter 9.

PLATE II: Substrate AFM topographical; (a) acid cleaned glass, (b) APTES modified glass, (c) Repelcote modified glass, (d) Lycine modified glass, (e) Mica

(a)

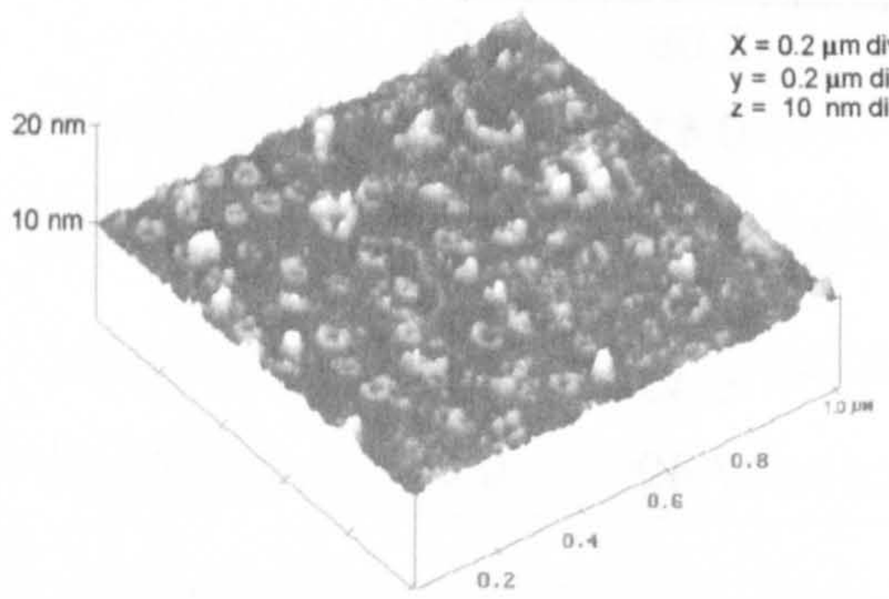

(b)

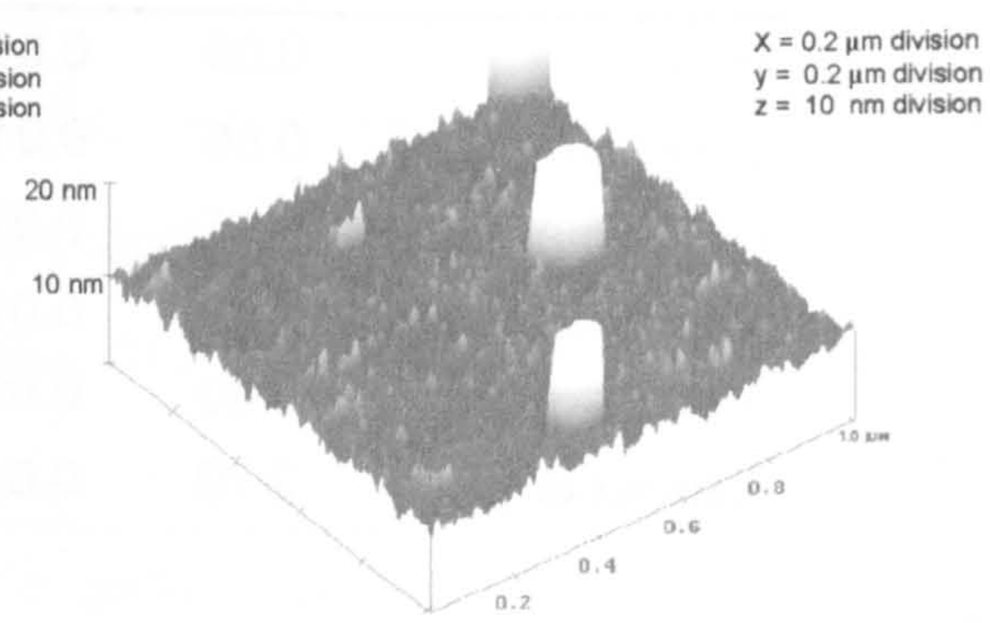

(c)

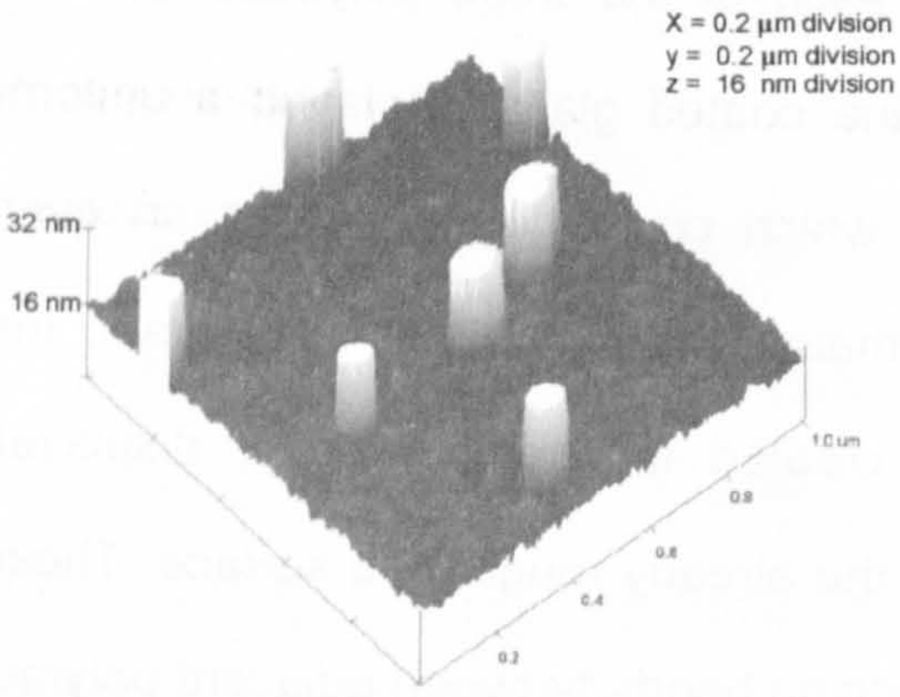

(d)

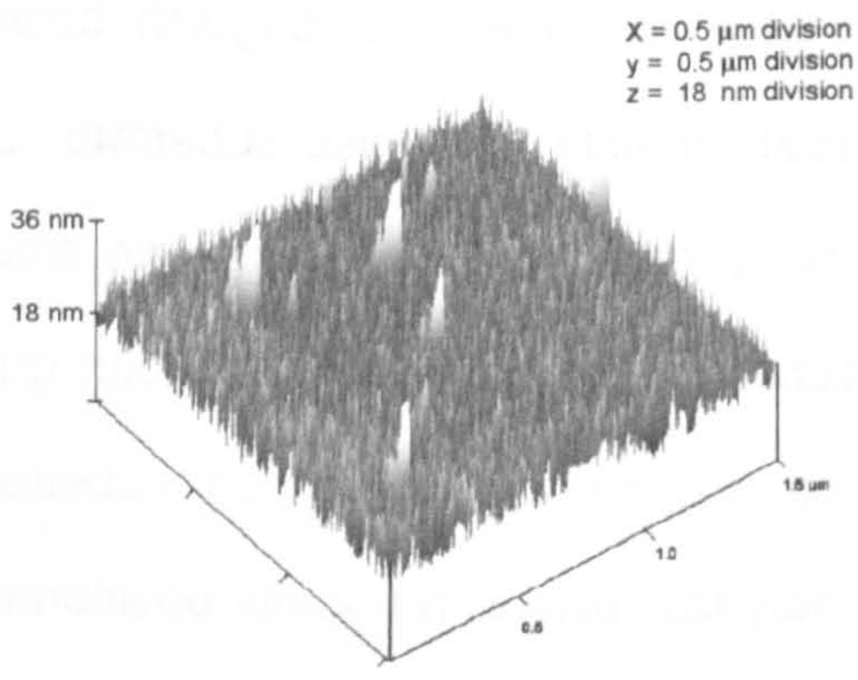

(e)

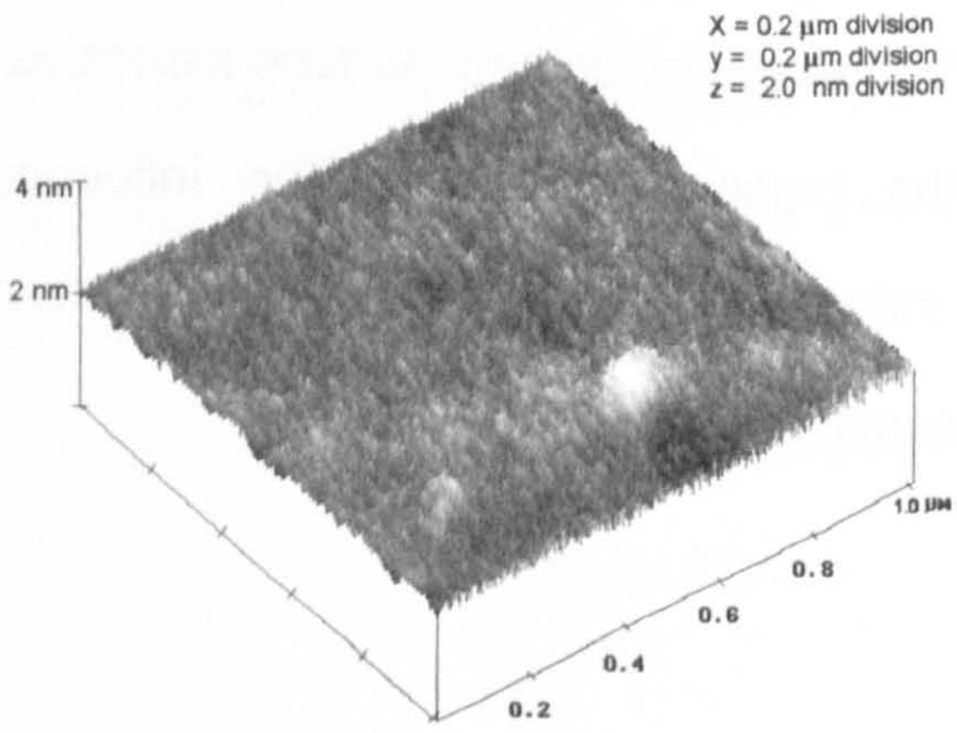

8.3.2 Streaming potential characterisation of substrates surfaces

The use of streaming potential measurements to obtain surface charge values from planar surfaces has been proven to enhance the understanding interfacial electric double layer phenomenon in aqueous solutions, e.g adsorption, surface forces and the structure of surfactant micelles on flat surfaces[13,21-23]. Amongst the many theories and experimental procedures for obtaining the ζ-potential from streaming potential memasurements[24-26] the Helmholtz-Smoluchowski approach, traditionally applied during electrophoresis measurements, is applied for smooth flat plates. However, the ζ-potential calculated from the streaming potential measurements has been reported to be slightly lower than that obtained from electrophoretic mobility techniques[27,28], due to the fact that the exposed surface atoms on a planar surface have different orientations from particles.

The Brookhaven-Paar Bl-EKA ElectroKinetic Analyser streaming potential instrument, described in chapter 4, was used to obtain the surface ζ-potential of each of the substrates investigated. Each surface was analysed in the presence of pure water and aqueous Fluorescein solution, 0.001M, at fixed pH 7-8, and the results listed in table 8.2.

Mica-water systems displayed the lowest negative surface charge from surface Si-O$^-$ functional groups, see table 8.2, which compared well with previous studies

conducted through micro-electrophoresis[29] and streaming potential instruments[13,30] and remained constant over the pH range investigated[13].

Table 8.2 Streaming potential of modified substrates

Substrate	H_2O (mV)	Error (+/-)	Fl (aq) (mV)	Error (+/-)
APTES glass	6.6	2.1	4.5	1.2
Mica	0.4	1.8	-0.9	0.9
Lysine glass	6.6	2.0	5.9	2.6
Acid cleaned glass	-16.1	1.9	-15.9	1.8
Repelcote glass	-18.7	1.5	-18.5	2.4
Untreated glass	-33.9	1.5	-35.0	1.5

The charge that occurs at the mica surface can be generated by several mechanisms, e.g. dissociation of surface acid groups[31,32], lattice substitution[33,34], orientation of dipoles, surface polarization or even preferential hydration of surface lattice ions[35,36].

The untreated glass substrate displayed the most negative surface charge at a fixed pH 7-8 due to the presence of surface hydroxyl functional groups which was consistent with previously observed measurements[37]. The presence of unreacted hydroxyl groups dominate the surface ζ-potential especially above the iso-electric point (IEP) pH3 where the surface has been shown to become more negative with increasing pH.

It is interesting to note that the ζ-potential of the glass decreased dramatically, more negative, as the surface was chemically modified with non-polar Repelcote and by acid cleaning the glass substrate at fixed pH 7-8. The ζ-potential values displayed almost half the negative magnitude of the untreated glass surface in aqueous solutions[3]. This behaviour can be attributed to the uneven coating allowing unreacted surface hydroxyls on the glass surface and therefore created a lower residual negative charge. The net positive charge measured on the APTES confirms that the polymer had adhered to the glass substrate in the expected orientation, see figure 8.1. The L-Lysine coated substrate gave a slightly negative surface charge similar to the charge measured for mica which could imply that some of the amine functional groups were hydrated in the aqueous solution. The same trend was observed for every substrate in an aqueous fluorescein solution and the values remained in the error margins, +/- 2mV.

The mica and unmodified glass substrate were investigated as a function of electrolyte concentration and were observed to maintain a negative surface charge over the entire range, 10^{-5} mol dm^{-3}– $3x10^{-1}$ mol dm^{-3} as shown in figure 8.5. The substrate surfaces maintained a near constant surface potential in the presence of 10^{-5} mol dm^{-3}– 10^{-2} mol dm^{-3} NaCl, +/- 0.6mV and +/- 1.3mV for mica and unmodified glass respectively, which were similar to those measured without the presence of electrolyte. The mica substrate demonstrated a sharp increase in surface charge negativity to 42 mV, in the presence of $>10^{-3}$ mol dm^{-3} NaCl. There is currently no explanation for this observation however it could be suggested that excess solid

electrolyte deposited on the mica surface through electrostatic interaction and created an increase in negative surface charge through its presence on the surface.

Fig 8.5 Streaming potential of Mica and unmodified glass as a function of [NaCl]

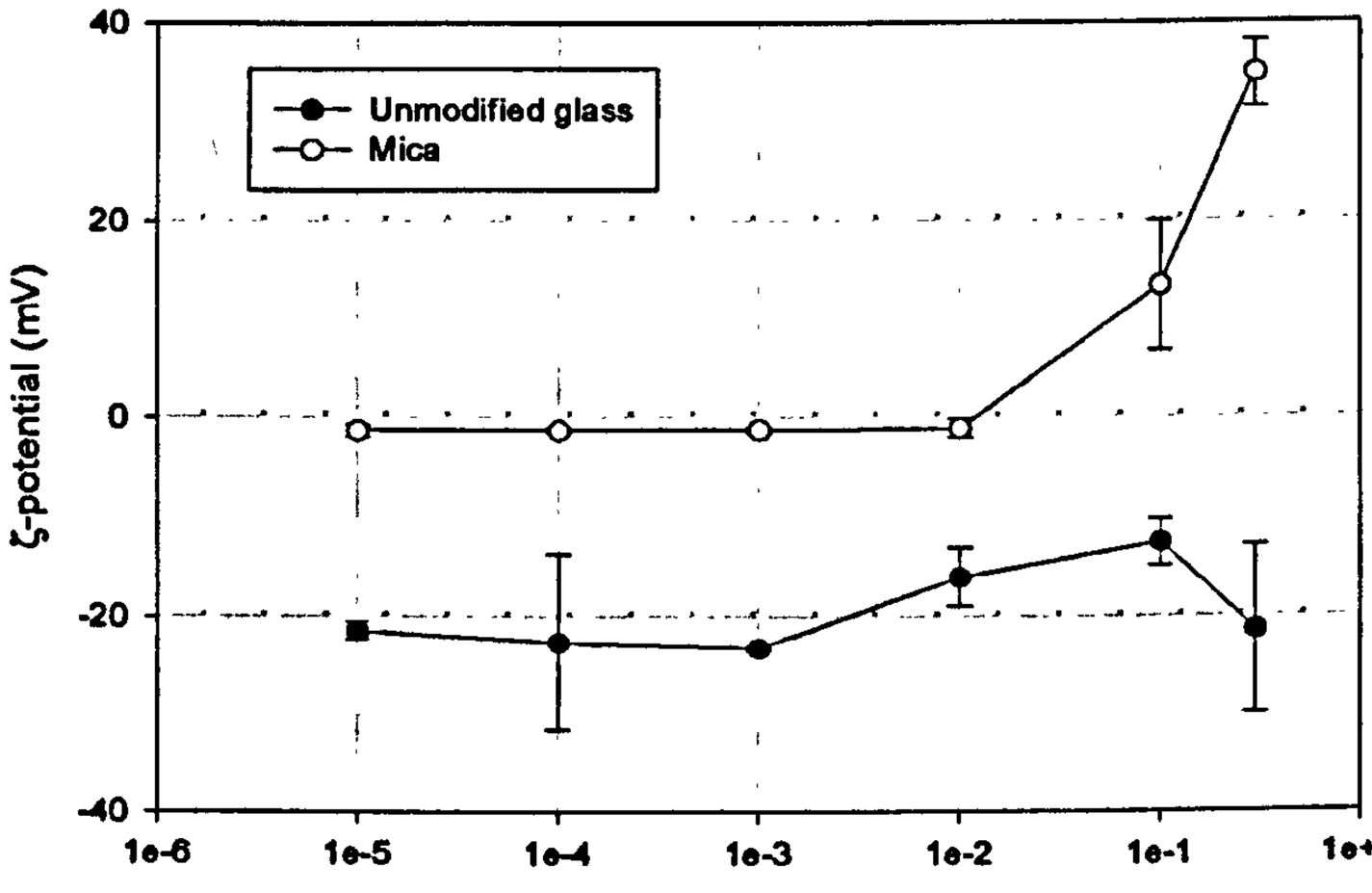

Laskowski[38] reported that the adsorption of ionic surfactants onto solid surfaces could induce surface charge changes and hydration forces. In addition, Stigter[39] and Wiesema[40] reported that the ζ-potential of micelle covered graphite surface, -80mV, adopted a similar value to the surface charge of the micelle formed in the bulk phase. The streaming potential of the mica substrate was determined in this work as a function of SDS concentration at a fixed pH 6-8 and the results displayed in figure 8.6. The mica surface showed a negative surface potential overall SDS concentration ranges investigated.

Fig 8.6 Streaming potential of Mica substrate as a function of SDS

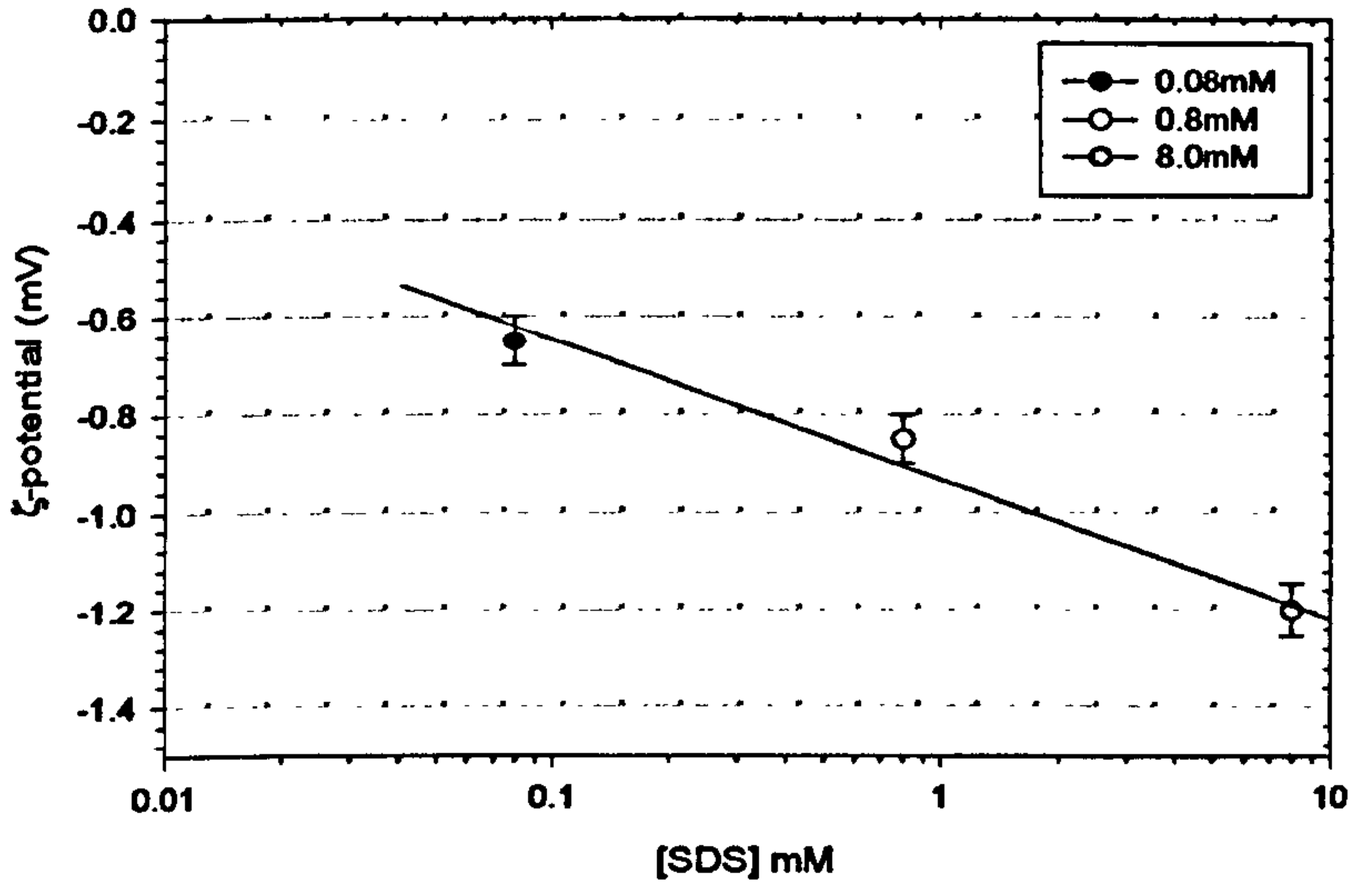

It could be noted that at low SDS concentration, < 0.08mM, the surface charge of the mica was similar to that measured in an aqueous solution water condition, ~0.65mV. At this concentration, the unfavourable electrostatic conditions that occur between the slightly negative mica surface potential and the anionic head group of the surfactant dominate the surface charge of the substrate. However there is a significant increase in surface charge negativity as the SDS concentration increases from below c.m.c, < 0.8mM to above 8.0mM, see chapter 5. This suggests that there is a slow build up of anionic surfactant molecules on the mica surface when the substrate is in the presence of SDS solution >0.8mM. This result agrees with the deposition results observed during stagnation point flow cell experiments, see chapter 9. The images obtained above 0.8mM SDS indicate the presence of self-assembled linear structures, i.e surface micelles, on the surface of the mica substrate, with a surface c.m.c occurring between 0.08mM and 0.8mM.

One hypothesis could be that as the mica surface is only slightly charged compared with the surfactant, the hydrophobic tails adsorb on the substrate surface to minimise unfavourable interactions with water molecules. This leads to a monolayer of surfactant forming on the surface with the head groups pointing into solution[7]. Therefore negatively charged head groups dominate the ζ-potential magnitude of the slide and so become more negative with increasing surfactant adsorption. As the concentration of surfactant is increased, bilayers of surfactant build up at the surface as the hydrophobic tails associate to minimise water contact[5].

This trend was also observed for the electrophoresis measurements of 0.05(v/v) total monomer ϕ, 0.05(v/v) MTMS ϕ surface charge, see chapter 5. The cross-linked PDMS droplets displayed a surface ζ-potential of -23mV without the presence of surfactant which then rose to -35mV above 0.8mM SDS, even though the negative charges on both the PDMS droplet surface and the mica substrate create unfavourable electrostatic repulsive conditions for adsorption.

The use of streaming potential instruments to investigate the effect of protein and polymer adsorption onto various substrates has been reported previously[41,42,43]. However very few studies have been conducted on the influence of colloidal particle coverage on changes in the surface charge of solid flat substrates due to the lack of established theory[44-46].

Zembala et al[16] suggested a two part model for the change in streaming current as a result of solid-particle adsorption on mica; (i) "damping" of fluid velocity in the vicinity of deposited particles, resulting in decreased charge transport from the double-layer at the interface, (ii) a transport of charge from the double-layer surrounding adsorbed particles.

In this study, the change in the streaming potential of a mica surface was measured as a function of deposited cross-linked PDMS droplets from a dialysed solution of fixed 0.05(v/v) total monomer ϕ, 0.05(v/v) MTMS ϕ.

The emulsion solution was introduced into the streaming potential cell, using the method described in chapter 4 and allowed to rest over the substrate surface for 30 mins. The mica surface potential was then measured as more solution was washed over the substrate, see figure 8.7. However, it was observed that the mica surface charge did not appear to alter significantly with an increased deposition of negatively charged PDMS droplets as a function time. The surface in fact remains almost neutrally charged even though the average surface potential of the depositing cross-linked droplets is ~24mV.

This observation could be explained by the fact that the strength of the force of adhesion between the droplets and the molecularly smooth mica surface is weaker than the hydrodynamic shear force created within the streaming potential cell. The droplets would therefore be easily removed from the lifting force and there would be no transfer of surface charge from the droplets to the substrate surface.

Fig 8.7 Streaming potential of mica surface adsorption as a function of time.

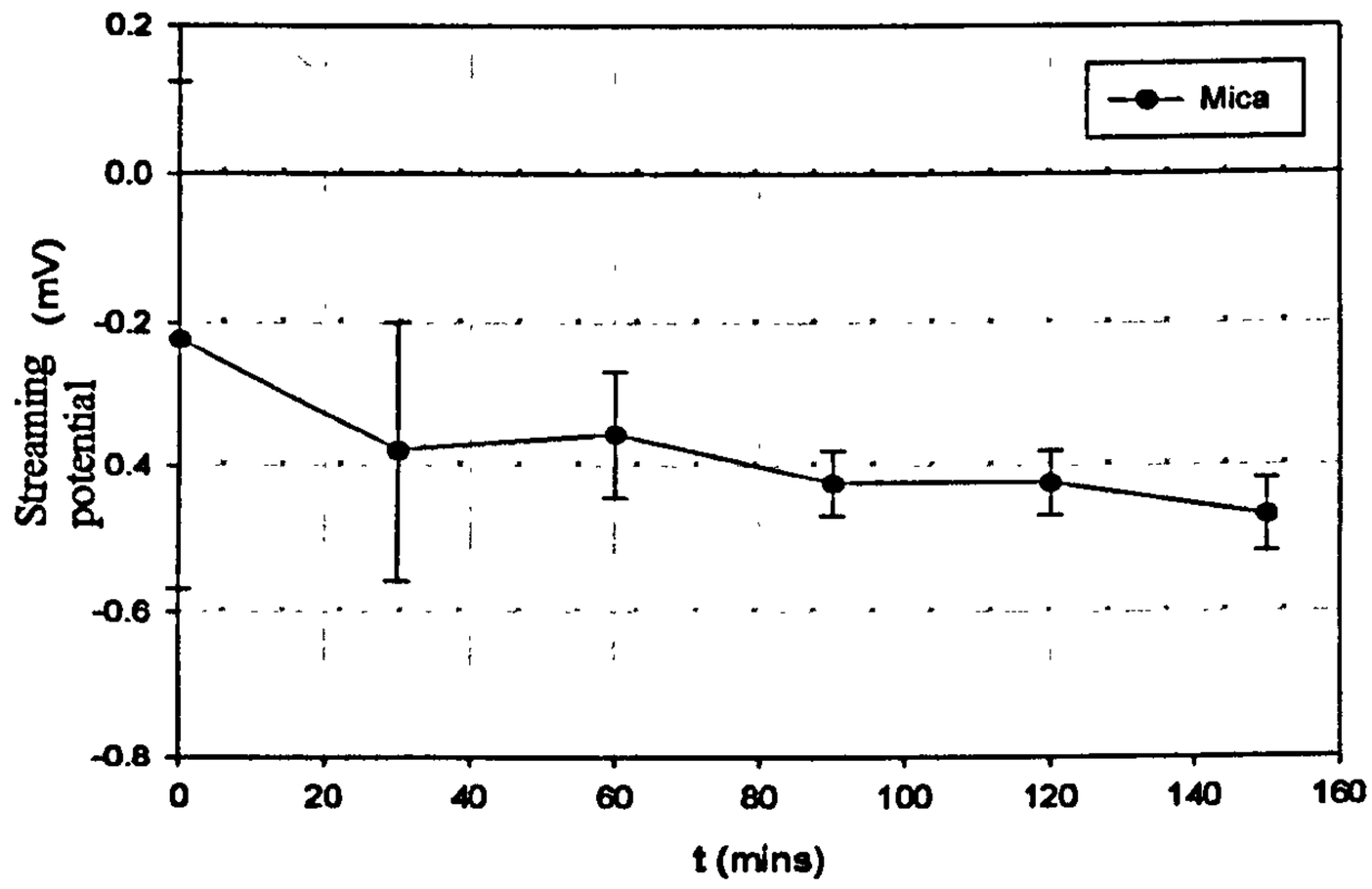

8.3.4 XPS Spectra of substrates

The surface elemental composition of each substrate used in this project was estimated using XPS , Image analysis centre, Bristol. The method described in chapter 4 was used to determine the identity of the surface functionalities which could be preferential sites for adsorption surface and the presence of modification effects on each substrate, see table 8.3. Global XPS spectra was obtained for each substrate, including electrons with binding energies between 0 – 1100eV. The presence of oxygen, carbon, nitrogen and aluminium was detected for all the glass based substrates. In addition iron, potassium and silicon were measured for the mica surface. The binding energies of the peaks were determined by setting the C_{1s} component at a value of 284.2eV.

Figure 8.8 XPS spectra of Mica

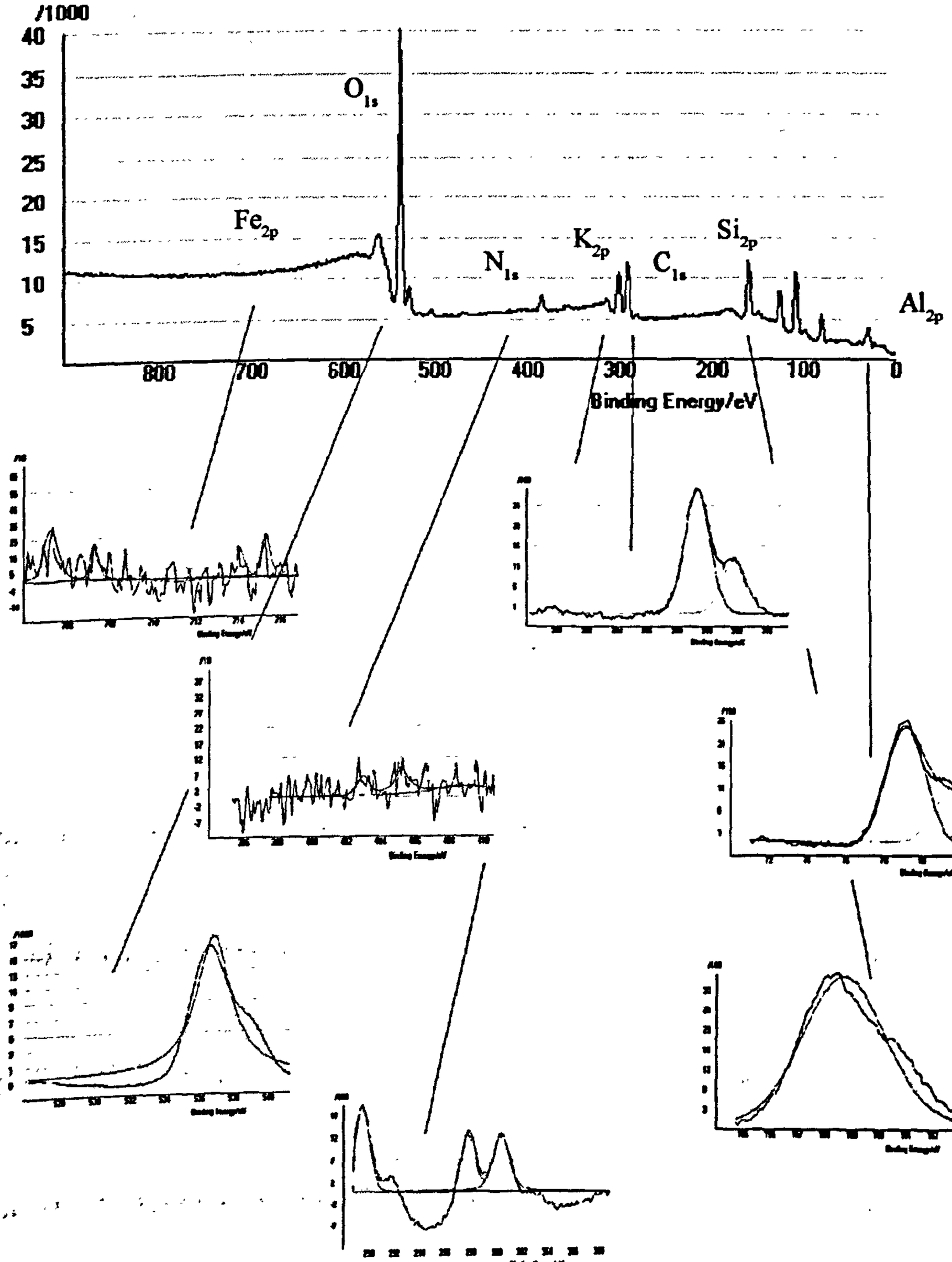

Figure 8.9 XPS spectra of Acid cleaned glass

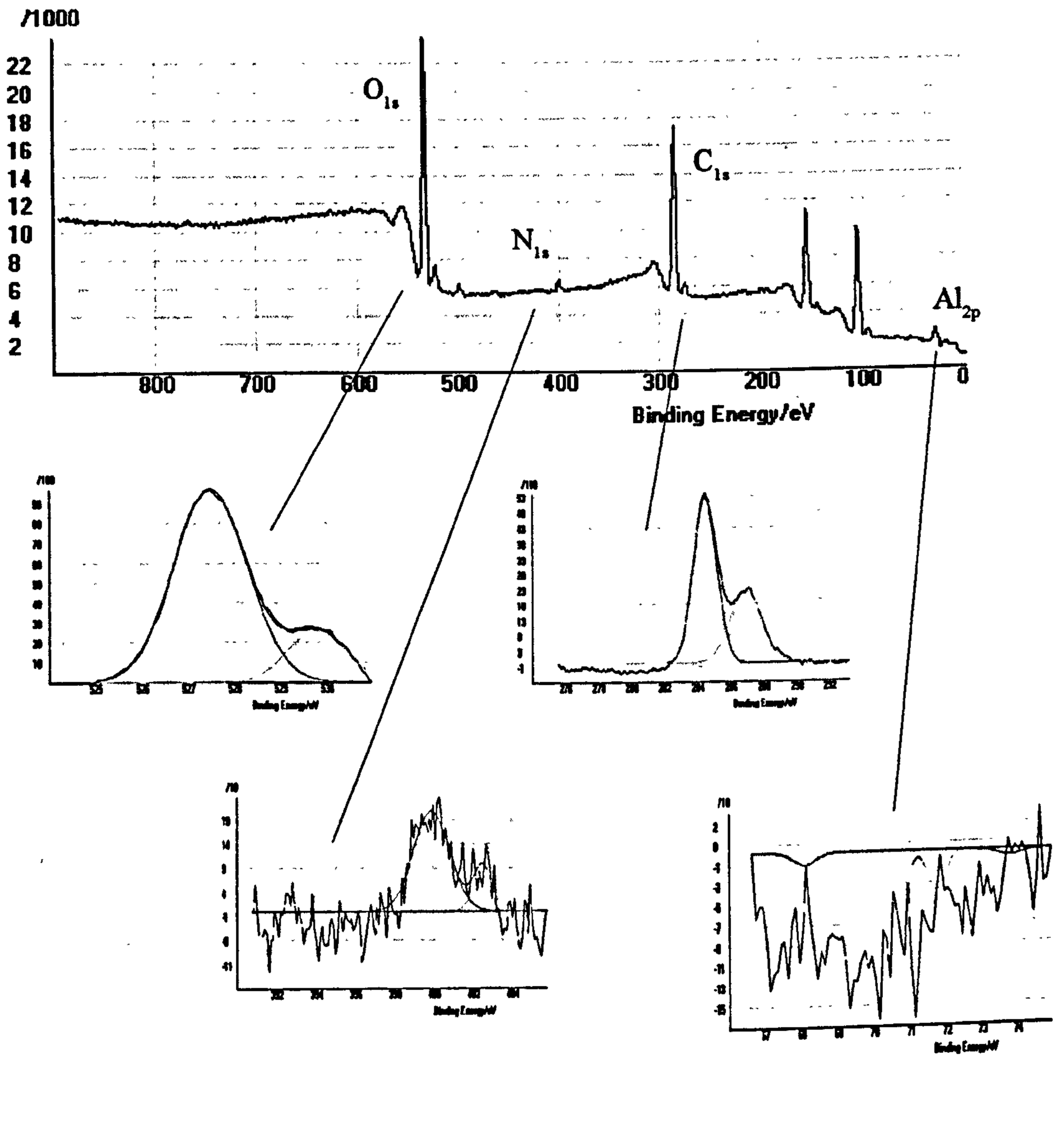

The peak areas were determined with a non-linear background subtraction. Intensity ratios were converted into atomic concentration ratios by using the SSI ESCA 8.3D software. The peaks were curve fitted using a non-linear least squares routine and assumed a Gaussian/Lorentzian (85/15) function. Typical global spectra obtained for mica and acid cleaned substrate surfaces are shown in figure 8.8 and 8.9 respectively. The total surface % composition of element investigated for each substrate is tabulated below, table 8.3.

The major elemental species present on the mica surface was shown to be O-Si species (29%), silicates groups (18%), Al containing (16%) of which 10% were Al-Si species and 0.1% of the global spectra related to the positively K_{2P} ion. These corresponded to the layers of alumino-silica tetrahedra structure, 2:1:1 ratio, illustrated in figure 8.3.

Table 8.3 XPS chemical composition of modified glass substrates

Substrate	Functional group type, total % (wt)				
	C_{1s}	O_{1s}	Si_{2P}	Al_{2P}	N_{1s}
Mica	34.2%	28.9%	17.7%	15.7%	3.4%
Untreated glass	51.9%	35.2%	7.6%	4.5%	0.8%
Acid cleaned glass	36.2%	43.2%	10.8%	8.5%	1.3%
APTES modified	64.0%	28.2%	5.4%	0.2%	2.2%
Lysine modified glass	69.7%	20.3%	5.5%	0.9%	3.6%
Repelcote glass	72.8%	21.3%	4.0%	0.9%	0.0%

The presence of over 34% C (28% carboxyl / carbonate groups), and 2.8% N (nitrate species) could be related to atmospheric contaminants at the mica surface. As expected, the untreated and acid cleaned substrates were measured to have similar surface compositions. However a far higher presence of carboxyl / carbonate C species, 40.5% compared with 66% respectively, and nitrate N species, 0.7% compared with 2.1% respectively from the atmospheric condition was recorded on the latter substrate. The greater adsorption of these species on the acid modified substrate could be attributed to the larger surface area created by the etched "doughnut" shaped indents that occur during the cleaning process. It is also possible to suggest that the majority of Al species within the aluminoborosilicate glass structure is present within the surface layers, few nm. The abundance of these species are therefore observed to decrease from 11% to 0.2% as the top few nm are etched away during the acid cleaning process. However, the same etched markings also allowed the x-ray photon beam to penetrate deeper into the substrate structure which is evident from the relatively high presence of metal-oxide species, e.g 32% Fe_2O_3, which are the main components of the glass structure.

The L-lysine modified glass substrates showed relatively a higher presence of N_{1s} than APTES modified glass. This was expected due to the two primary amine groups present on the alcane chains which adhere to the OH functional groups on the glass surface. However the increase in carboxyl C_{1s} surface species for both substrate, 64% and 79% compared with untreated glass 52%, could suggest that some of the APTES and lysine molecules had adhered to the surface in reverse formation, see figure 8.1 (i) and figure 8.4, with the carboxyl end groups remain free in solution. The

effect on the increased electrostatic repulsive forces between the substrates and the negatively charged PDMS droplets will be discussed in chapters 9 and 10. The highest level of C_{1s} species was present on the Repelcote substrate and could be attributed to the CH_3 functional groups adhered to the surface via SiO bonds, see figure 8.2. The decrease in SiO_2 O_{1s} species compared with unmodified glass would indicate high surface coverage during the APTES, L-Lysine and Repelcote chemical modification processes.

8.3.5 Three phase contact angle characterisation

The static contact angle of PDMS droplets was investigated as a function of cross-linker ϕ and substrate surface heterogeneity. A PDMS emulsion system was used with 0.05(v/v) ϕ total monomer. A three phase captive bubble apparatus was constructed as discussed in chapter 4, and filled with an aqueous fluorescein solution, $1x10^{-3}$ $moldm^{-3}$ to simulate the deposition conditions in a stagnation point flow cell. An image of the inverted contact angle was captured after the droplet had reached an equilibrium position on the substrate and measured with a calibrated image software, Visilog 5, see chapter 4. Images of the three phase static contact angles are shown in plates II-III.

Table 8.4 below illustrates the influence of MTES volume fraction, ϕ, on the three phase contact angle between PDMS oil phase drop at fixed 0.05 (v/v) ϕ total monomer and a fixed mica substrate, see plate III.

PLATE III Three phase contact angle as a function of MTMS ϕ; (a) 0.00(v/v), (b) 0.005(v/v), (c) 0.01(v/v), (d) 0.05(v/v), (e) 0.1(v/v)

(a)

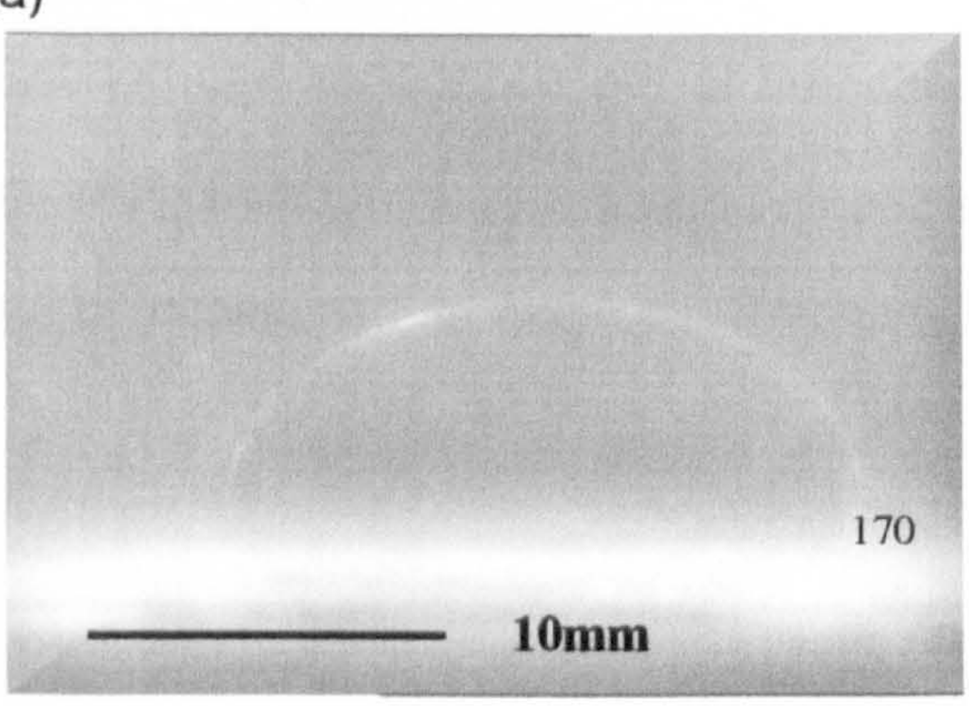

(b)

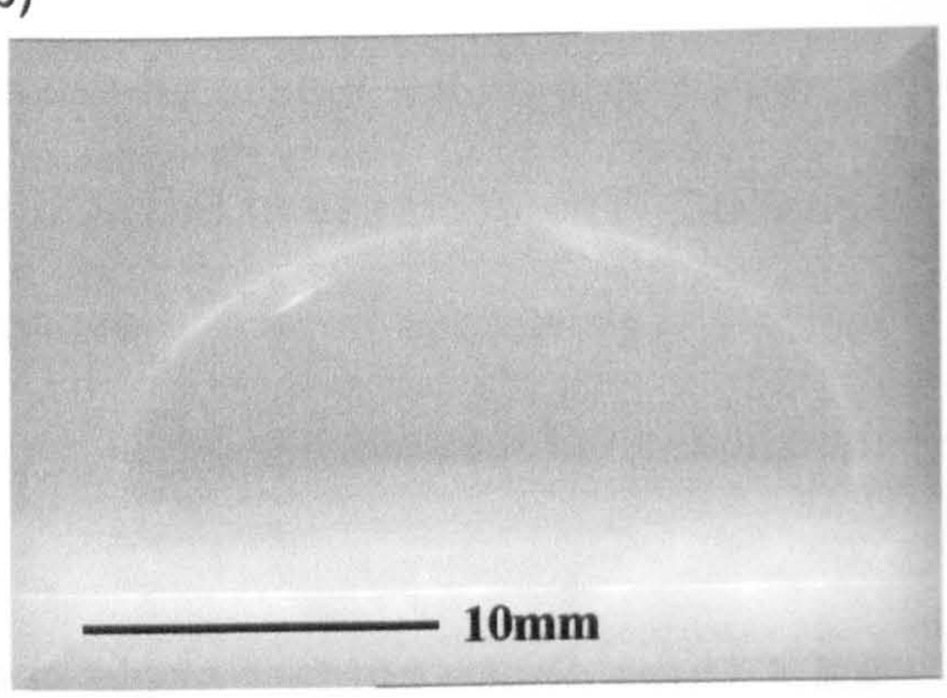

(c)

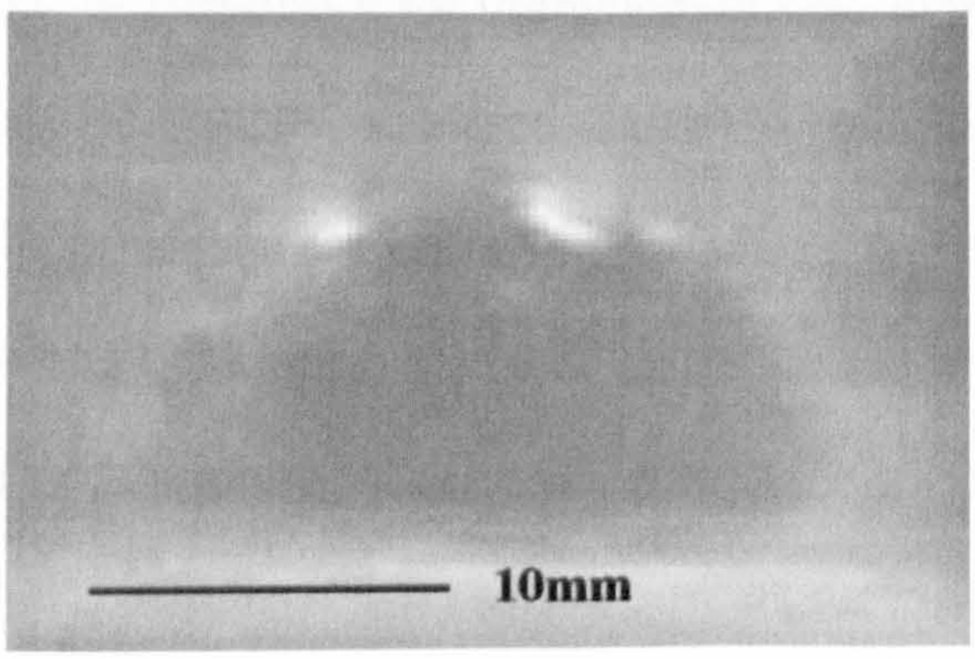

(d)

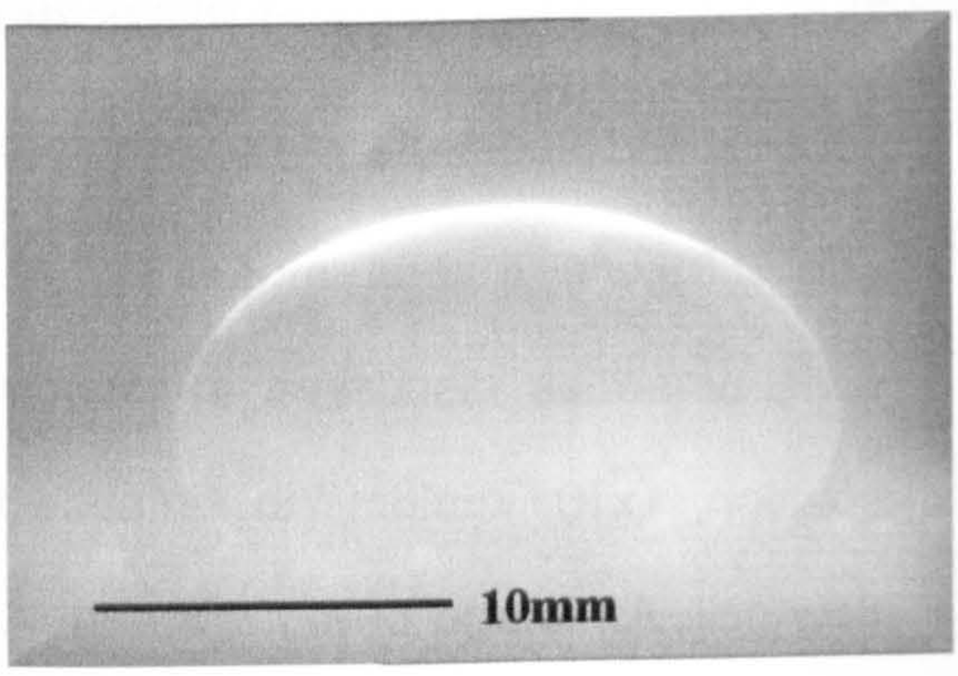

(e)

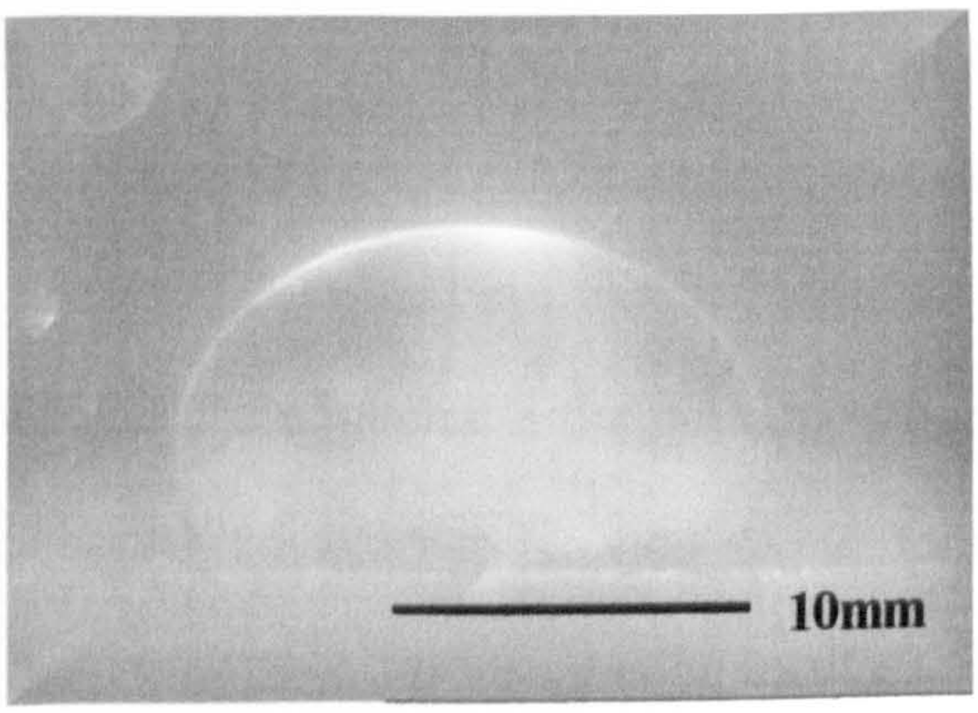

The wetting property of the droplet was observed to decrease with increasing MTMS volume fraction, ϕ. This behaviour is consistent with the increase in cross-linking density within the network structure of the PDMS oil and the presence of strong cohesive forces. As a result, the droplets' surface becomes more rigid, less susceptible to spread and the interfacial work of adhesion, $W_{ad,}$ is reduced. This was illustrated by the increase in surface tension, see chapter 3 section, and plate II.

Table 8.4 Three phase contact angle as a function of cross-linker ϕ, on mica

MTMS ϕ (v/v)	θ_c	Error (+/-)	r (mm)	h (mm)	W_{ad}
0.00	121.8	8.2	4.2	6.8	0.47
0.005	105.7	17.5	4.2	1.4	0.73
0.01	111.0	21.1	3.4	4.1	0.64
0.05	117.4	11.1	3.6	3.6	0.54
0.1	120.1	4.2	3.6	4.9	0.50

Contact angle investigations were extended to observe the influence of substrate surface charge and heterogeneity on droplet spreading properties. A fixed PDMS droplet systems was used 0.05(v/v) total monomer and 0.05(v/v) MTES and a constant droplet volume, 0.5ml. The results obtained for mica and modified / unmodified glass surfaces are summarised in table 8.5, while the contact angle images are shown in plate IV.

PLATE IV Three phase contact angle as a function of substrate surface modification; (a) APTES modified glass, (b) Mica, (c) L-Lysine modified glass, (d) acid cleaned glass, (e) Repelcote glass

(a)

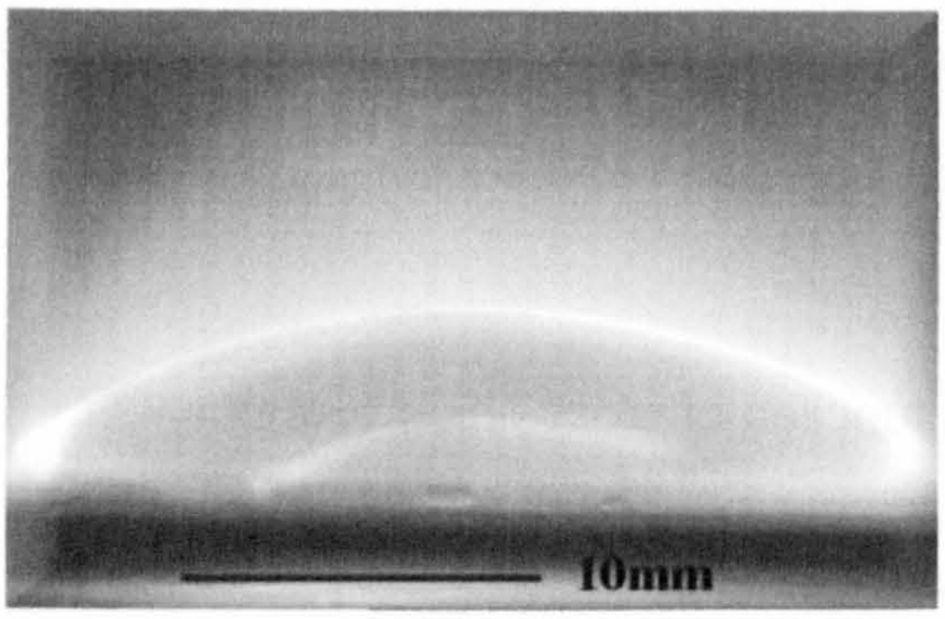

(b)

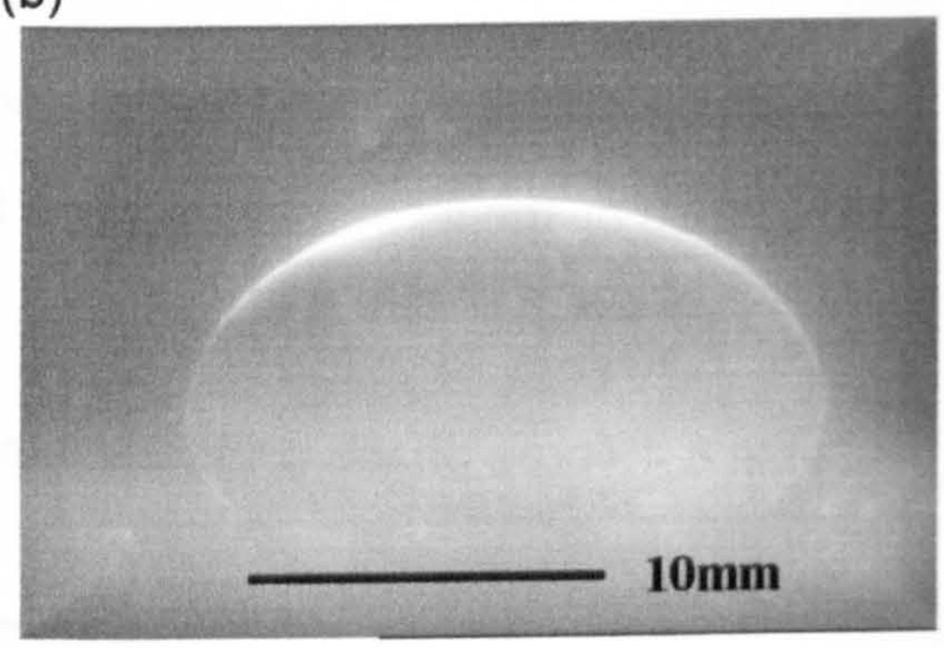

(c)

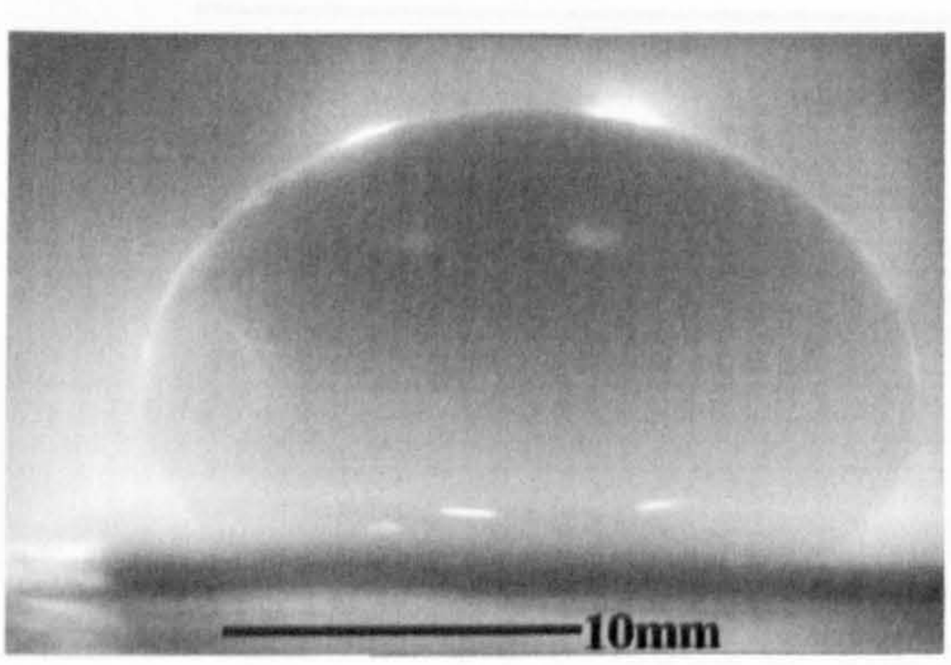

(d)

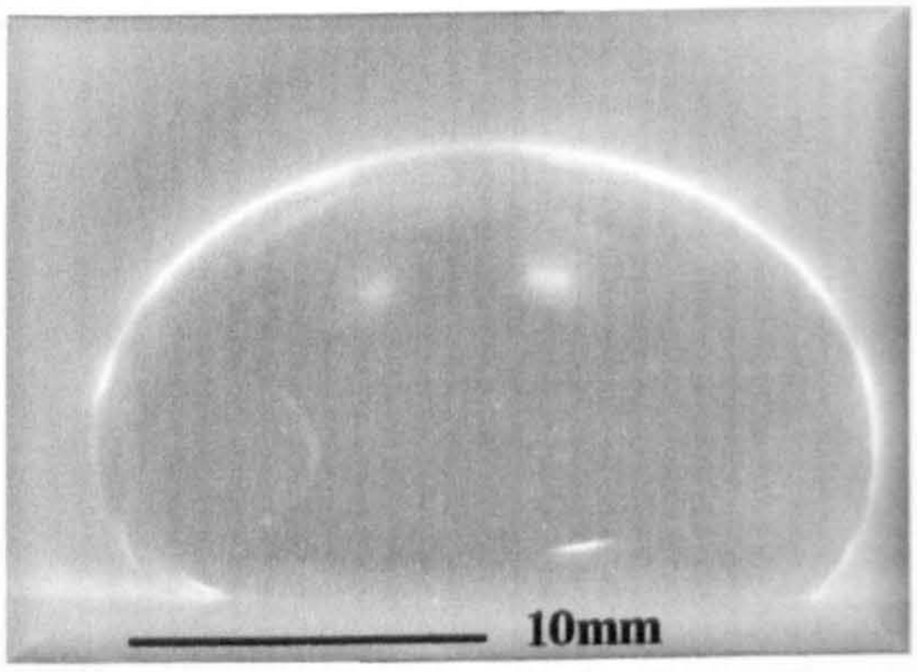

(e)

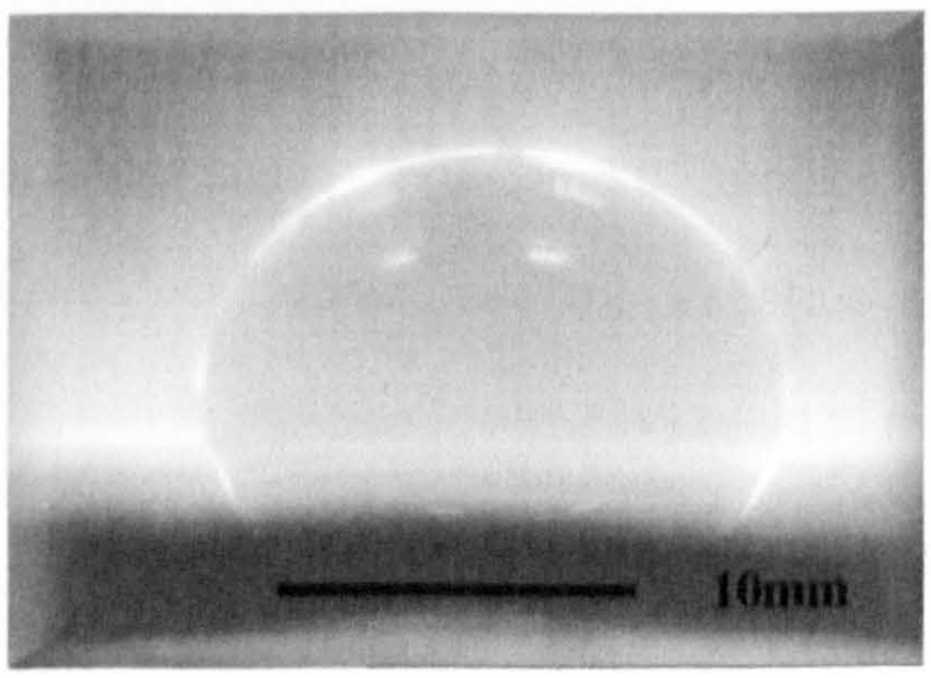

The APTES modified glass substrate and PDMS droplet interfacial interaction created the lowest contact angle $\theta_c < 90^\circ$, wetting the surface. This is in direct contrast with the rest of the substrates, where $\theta_c > 90^\circ$, which indicated a relatively low work of adhesion between the oil drop and substrate interfaces, $W_{ad} < \gamma_{lr}$ and γ_{sl} $> \gamma_{sl}$, see equation [4.7] chapter 4. This trend is shown to decrease with increasing contact angle. In contrast to previous studies, the data obtained for the chemically modified substrates suggested that the extent to which the cross-linked PDMS droplet "wetted" the surface was dominated by the surface charge rather than the surface heterogeneity of the substrate.

Table 8.5 Contact angle data as a function of surface roughness

Substrate	θ_c	Error (+/-)	r (mm)	h (mm)	W_{ad}
APTES glass	42.5	10.2	5.6	2.1	10.65
Mica	114.0	20.2	3.6	5.3	3.61
Lysine glass	121.8	8.2	4.2	6.8	2.88
Acid cleaned glass	125.2	8.9	3.7	6.4	2.57
Repelcote glass	127.6	4.0	4.5	6.7	2.39

The APTES modified substrate, which displayed a net positive surface charge, 6.6mV, while simultaneously possessing one of the highest surface asperities, 2.6μm, created a contact angle with the droplet three times lower than the mica surface, see table 8.1 and 8.2. In fact the molecularly smooth mica surface, Ra 0.06μm, with an almost neutral charge created a contact angle similar to the remaining chemically altered glass substrates, -10°. The increase in three phase contact angle values

observed by the L-lysine, acid cleaned and Repelcote modified glass substrates reflected the increase in surface asperity while the surfaces increased in repulsive droplet-surface interaction as the substrates become increasingly negatively charged. It is interesting to note that this substrate showed one of the least negative surface charge. In this situation it appears that the spreading properties of the oil on the APTES substrate is dominated by the attractive substrate-droplet surface interaction rather than surface roughness. The remainder of the substrates were observed to have similar contact angle values, +/- 4.3, irrespective of the change in surface heterogeneity, chemistry or surface charge.

Choi et al[12] reported that the relaxation processes present within the cross-linked PDMS structure together with the formation of hydrogen bonds caused the PDMS chains to be tethered by the substrate surface heterogeneities. This in turn resulted in contact line between the substrate and droplet to become distorted during adhesion hysteresis.

8.4 References

1. Elimelech.M, Chen.J, Kuznar.Z, Langmuir, 2003, 19, 6594-6597
2. Marsden.N, MSc thesis, University of Bristol, 1995
3. Lovelock, MSc thesis, University of Bristol, 1997
4. Harnett.L, PhD thesis, 1996, University of Bristol
5. Vandenberg.E, L.Bertilsson, B.Liedberg, K.Uvdal, R.Erlandsson, H.Elwing, I.Lundstrom, Journal of Colloid and Interface Science, 147, 103, 1991
6. Carajaval.G, D.E.Leydon, G.R.Quintin, G.E.Maciel, Analytical Chemistry, 60, 1776, 1988
7. Goodwin.J, R.S.Harbron, P.A.Reynolds, Colloid and Polymer Science, 268, 766, 1990

8. Naviroj.S, S.R.Culler, J.L.Koeing, H.Ishida, Journal of Colloid and Int. Sci, 97, 308, 1984

9. Moon.J, Shin.J, Kim.S, Park.J; Langmuir, 1996,12, 4621-4624

10. Decher.G, Hong.J, Schmit.J, Thin Solid films, 1992, 211, 831

11.Petrucci.M, Kakkar.A, J.Chem.Soc., Chem.Commun, 1995, 1577-1578

12. Choi.J, Lim.C, Kim.J, Chung.T, Moon.J, Hahn.J, Kim.S, Park.J, Synth.Met, 1995, 71, 1729-1730

13. Fa.K, Paruchuri.V.K, Brown.S.C, Moudgil.B, Miller.J, Phys.Chem, Chem.Phys, 7, 678-684, 2005

14. Wanless.E, Ducker.W, J.Phys.Chem, 1996, 103, 3207

15. Chen, J,Y., Klemic, J, F., Elimelech,M., Nano Letters, vol.2, No.4, 393-396, 2002

16. Koopal, L, Dukhin, S, Colloid Surf.A, 73, 201, 1993

17. Khachatourian, A, Wistrom, A, J.Phys.Chem, B, 102, 2483, 1998

18.Sader, J, Gunning, J, Chan, D, J.Colloid Interface. Sci, 182, 516, 1996

19. Barthlott.W, Neinhuis.C, Planta, 1997, 202, 1-8.

20.He.B, Patankar.N, Lee,J, Langmuir 2003, 19, 4999

21. Hunter.R, Foundations of Colloid Science, Oxford University press, NY, 2nd edn, ch.1, 2001

22. Bersa.L, Sengupta.D, Roy.S, Int.J.Miner. Process., 59, 89, 2000.

23.Johnson.S, Franks.G, Scales.P, Scales.P, Bogrer.D, Healy.T, Int.J.Mineing process, 58, 267, 2000

24.Walker.S, Bhattacharjee.S, Hoek.E, Menachem Elimelech. Langmuir, 2002, 18, 2193

25.Childress.A, Elimelech, J.Membr.Sci, 1996, 119, 253

26.Erickson.D, Li.D, Werner.C, J.Coll.Int.Sci., 2000, 232, 186

27. Hunter.R, z-potential in Coll.Sci, principle and applications, Academic Press, London, 1981

28.El-Gholabzour.O, Cabreizo-Vilchez.A, Hidalgo-Alvarex.R, J.Coll.Int.Sci., 2003, 261, 386

29.Debacher.N, Ottewill.R, Colloids Surf.A, 1992, 65, 51

30.Zembala,M, Adamczyk.Z, Langmuir, 16, 1593, 2000

31.Quast.K, Readett.D, Adv.Colloids.Int.Sci., 17, 169, 1987Quast.K, Readett.D, Adv.Colloids.Int.Sci., 17, 169, 1987

32.Yoon.R, Salman.T, Donnay.G, J.Coll.Int.Sci, 70, 483, 1979

33.Aplan.F, Fuerstenau.D, Froth Floatation-50th Anniversary, vol, ed.,M.Fuerstenau, AIME, NY, p.g.91, 1962

34. De Bruyn.P, Agar.G, Froth Floatation-50th Anniversary, vol, ed.,M.Fuerstenau, AIME, NY, p.g.91, 1962

35 .Iwasaki.I, Cooke.S, Colombo.A, US Bureau of mines, R15593; US Department of the interior, 1960, 1

36. Iwasaki.I, Cooke.S, Choi.H, Trans.AIME, 1960, 217, 238

37. R.K.Iler, "The chemistry of Silica", John Wiley and Sons Inc., New York, 1979

38. Laskowski.J., Kitchener,J.A., J.Coll.Int.Sci., 29, 670, 1969

39. Stigter.D, Mysels.K, J.Phys.Chem., 1955, 59, 45

40. Wiersema.P, Loeb.A, Overbeek.J, J.Coll.Int.Sci., 1966, 22, 78-99

41. Norde, W., Rouwendal, E., J.Coll.Int.Sci., 1990, 139, 169-177

42. Schurz,J., J.Macromol. Sci.-Chem,1990, A27(13, 14), 1673-1692

43. Jacobasch,H-J., Angewaandte Makromolekulare Chemie, 1984, 128, 47-69

44. Zembala.M, Adamczyk.Z, Warszyski.P, Coll.Surf.A:Phys and Eng Aspects 195, 2001, 3-15

45. Hayes,R.A, Coll.Surf.A, 146, 89, 1999

CHAPTER 9 Stagnation point flow cell results and discussion

9.1 Colloidal deposition on Stagnation point flow cell

The high surface coverage deposition regimes and spreading behaviour of cross-linked PDMS emulsions were investigated as a function of; tri-functional cross-linker ϕ (MTMS), electrolyte concentration, NaCl, anionic surfactant concentration, SDS and substrate surface chemistry / charge. A stagnation point flow cell method was used to observe the deformable droplet deposition mechanisms. Images were recorded directly over the stagnation point, every 3 mins for a duration of 3 hrs, using Visilog 5.6 imaging software, as described in chapter 4. A fixed observation area of 14000μm^2 was maintained and the position of each droplet center in this area was obtained as a x, y Cartesian coordinate . The data was then used to investigate the adsorbed array structure of the PDMS droplets on the collector surface and the data was then presented as the partial radial distribution function g(r) as a function of separation distance from the stagnation point, see chapter 7.

Each experimental variation was repeated three times, using a different substrate each time due to the adhesive properties of the cross-linked PDMS oil and the results were found to be accurate and reproducible. Results were rationalised in terms of the balance that exists from the normal attraction between the collector surface and the adsorbed droplet, and also the lateral repulsion between the flowing and adsorbed droplets.

9.2.1 Deposition of cross-linked PDMS droplets

The deposition of cross-linked PDMS droplets from stable emulsions was studied as a function of cross-linker ϕ. The emulsion system parameters used in this study are listed in table 9.1, with a dialysed PDMS emulsion system of fixed 0.05(v/v) total monomer, varying MTMS ϕ, 0.0(v/v) – 0.1(v/v),and fixed pH 7-8. The flow solution was then introduced into the cell at a fixed flow rate of 5ml min^{-1}. The droplet number concentration was shown not to vary significantly between the emulsions investigated, $6.1x10^{12}$ – $2.8x10^{13}$ dm^{-3}. Agar scientific G250-1 mica sheets were used as the collector surface and positioned perpendicular to the capillary opening, see chapter 4. The average surface potential of the mica substrate was found to be -0.9mV, see chapter 8. Typical deposition images obtained for each emulsion system investigated are shown in plates V-IX.

Table 9.1 Cross-linked PDMS emulsion parameters

MTMS ϕ (v/v)	D_{hyd} (μm)	ζ-pot. (mv)	n_0 (droplets dm^{-3})
0.000	2.0	-22.3	$1.19x10^{13}$
0.005	1.7	-29.7	$2.83x10^{13}$
0.010	1.9	-25.2	$1.19x10^{13}$
0.050	2.4	-23.4	$6.12x10^{12}$
0.100	1.7	-41.8	$2.83x10^{13}$

**Emulsion system used for further investigations in sections 9.2.2– 9.2.4*

All of the PDMS emulsions investigated showed that the cross-linked droplets deposited individually, with a random distribution across the observed collector surface area, while the deposition coverage increased with time.

PLATE V: 0.05(v/v) total monomer, 0.00(V/V) MTMS on Mica substrate; (a) 3 mins, (b) 60 mins, (c) 120 mins, (d) 180 mins

(a)

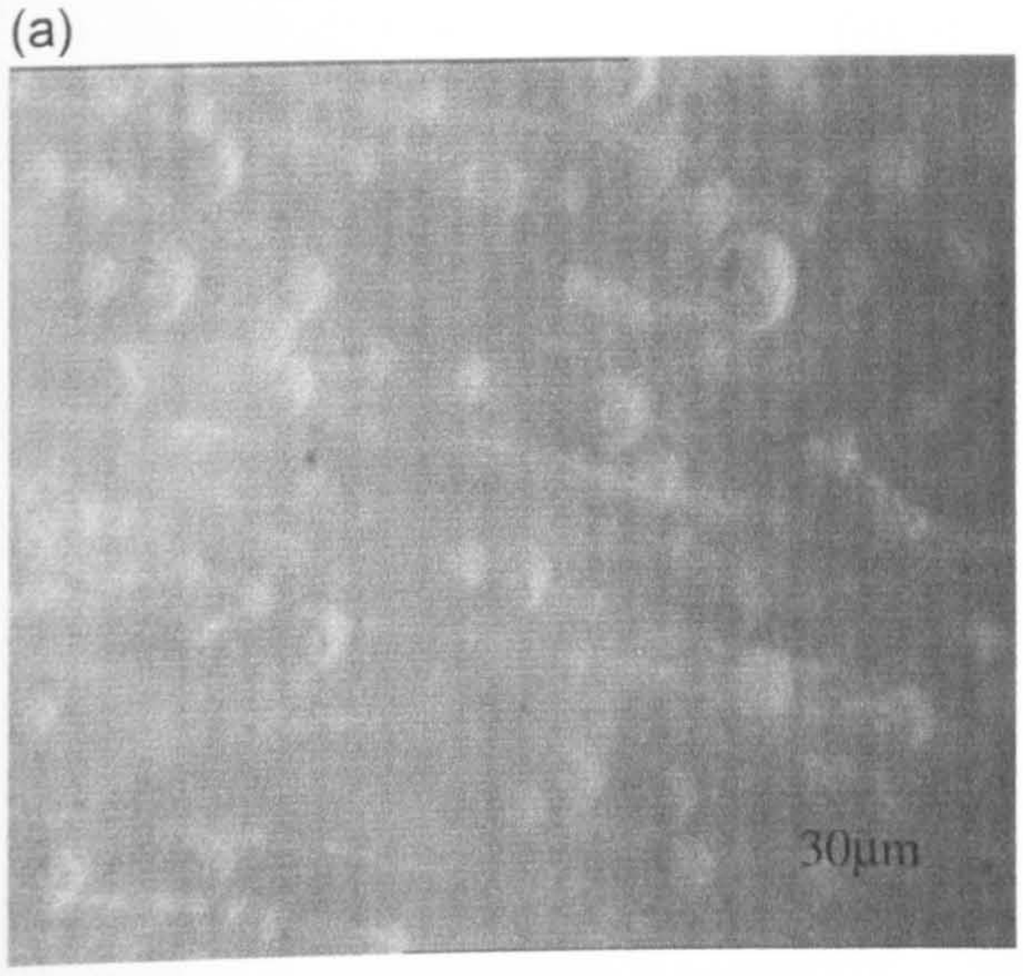

(b)

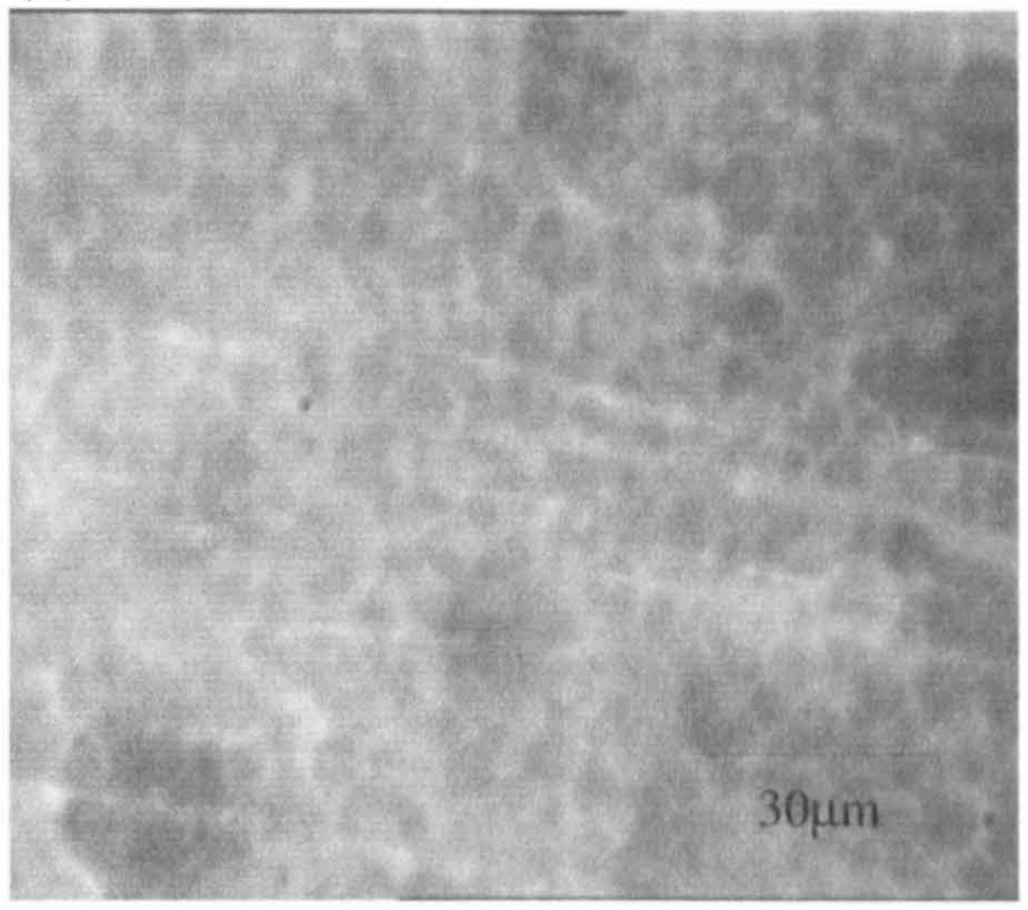

(c)

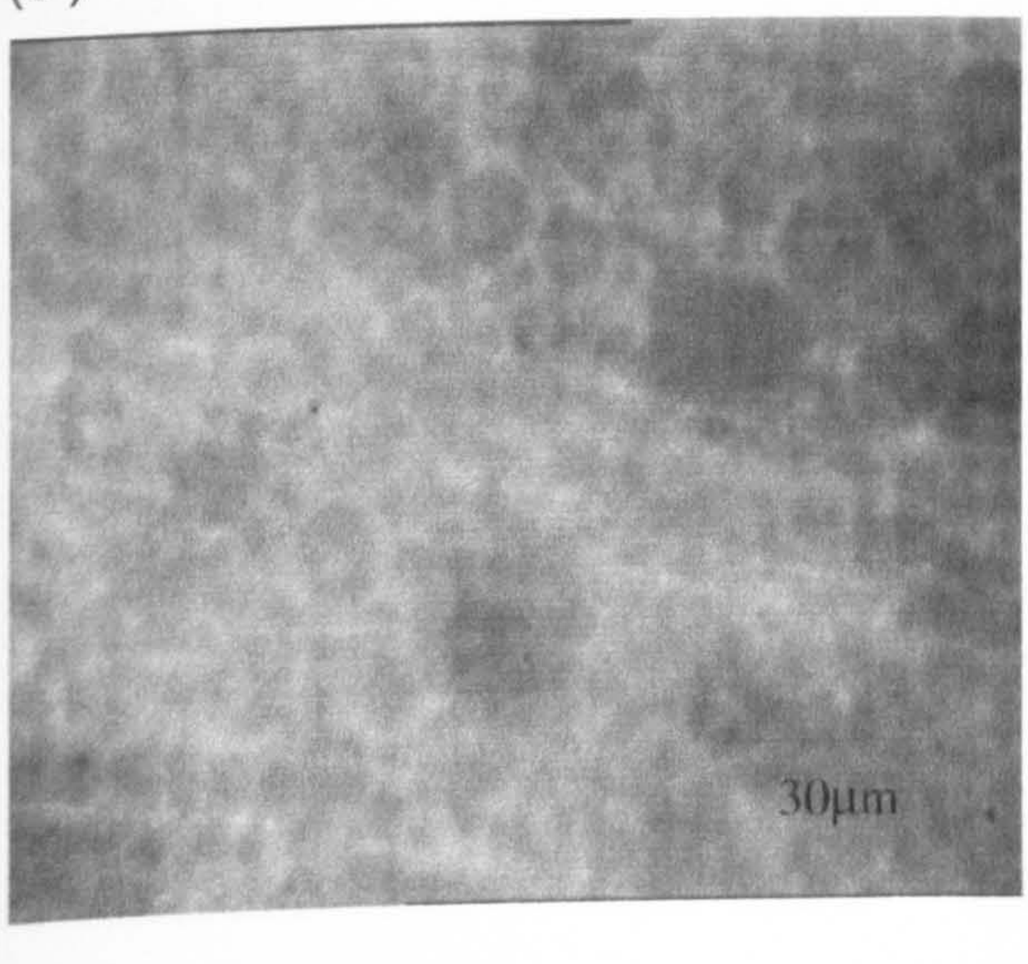

(d)

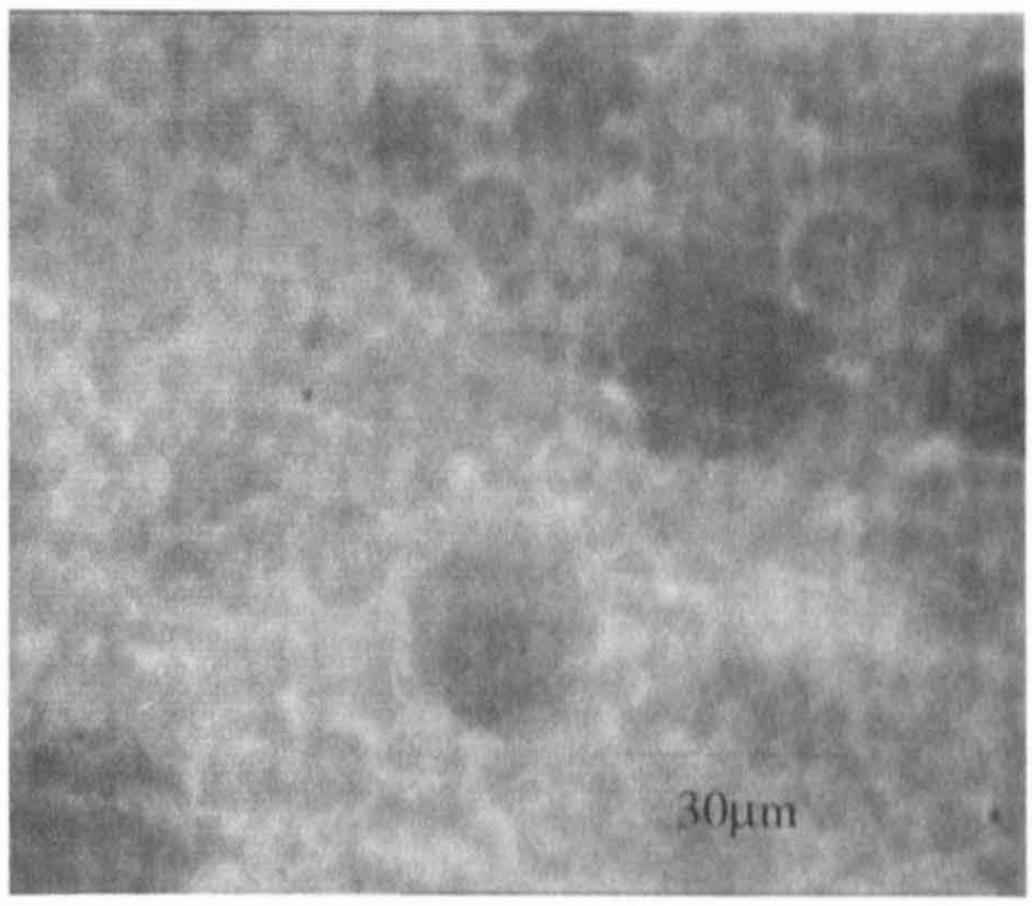

PLATE VI: 0.05(v/v) total monomer, 0.005(v/v)MTMS on Mica substrate:
(a) 3 mins, (b) 60 mins, (c) 120 mins, (d) 180 mins

(a)

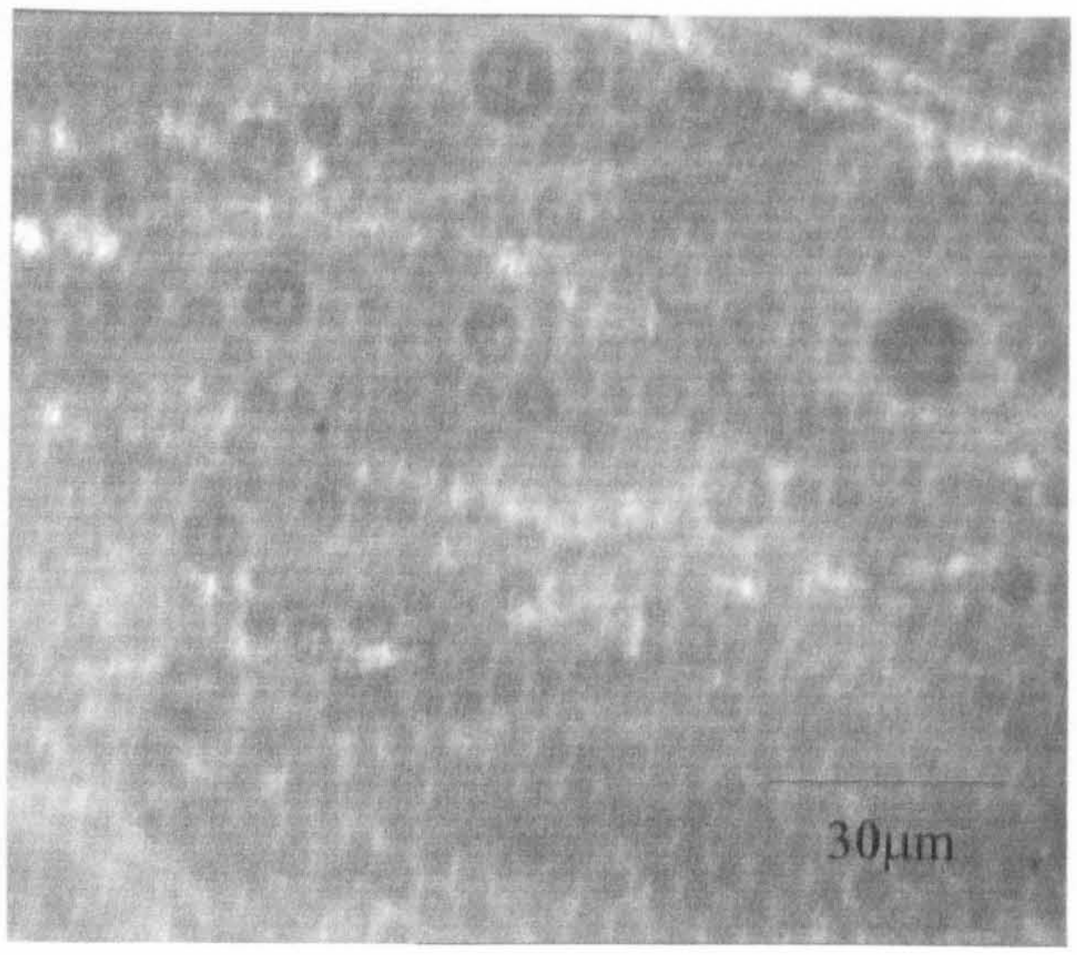

(b)

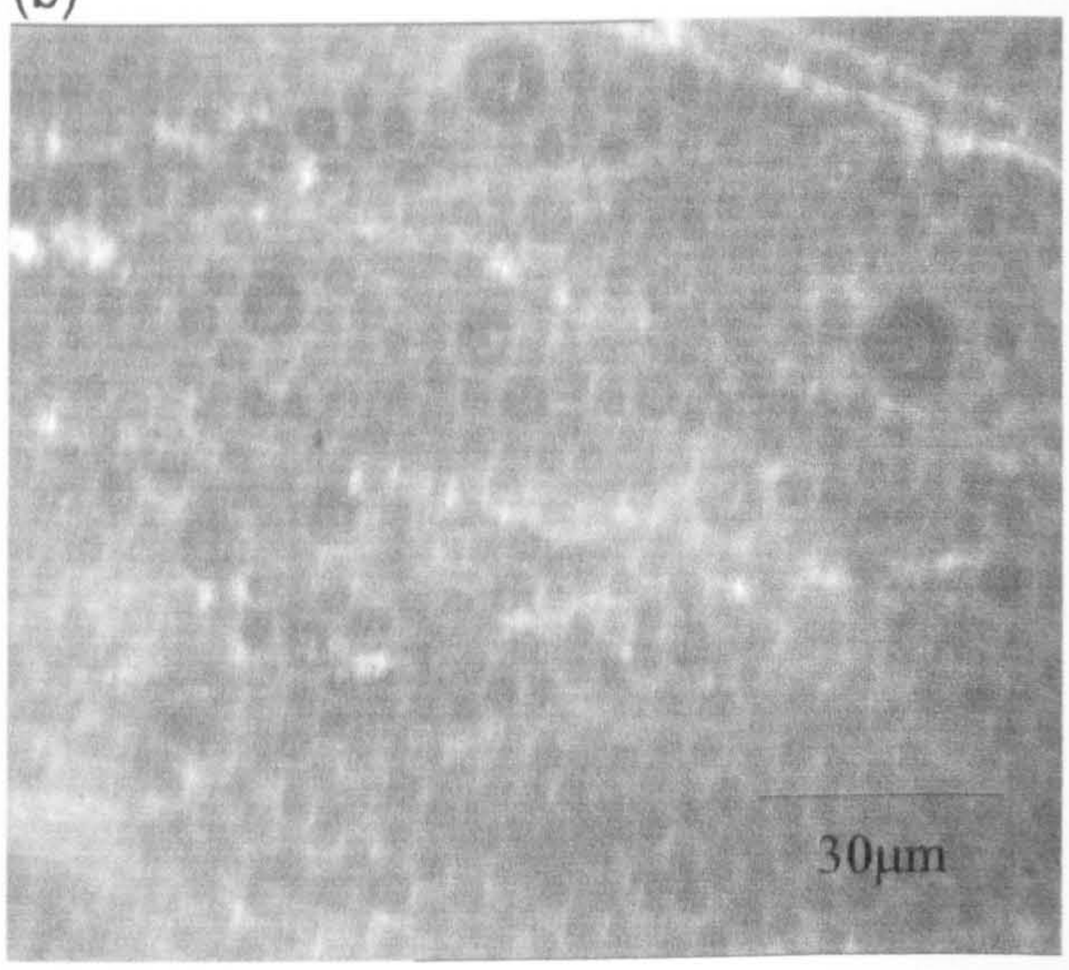

(c)

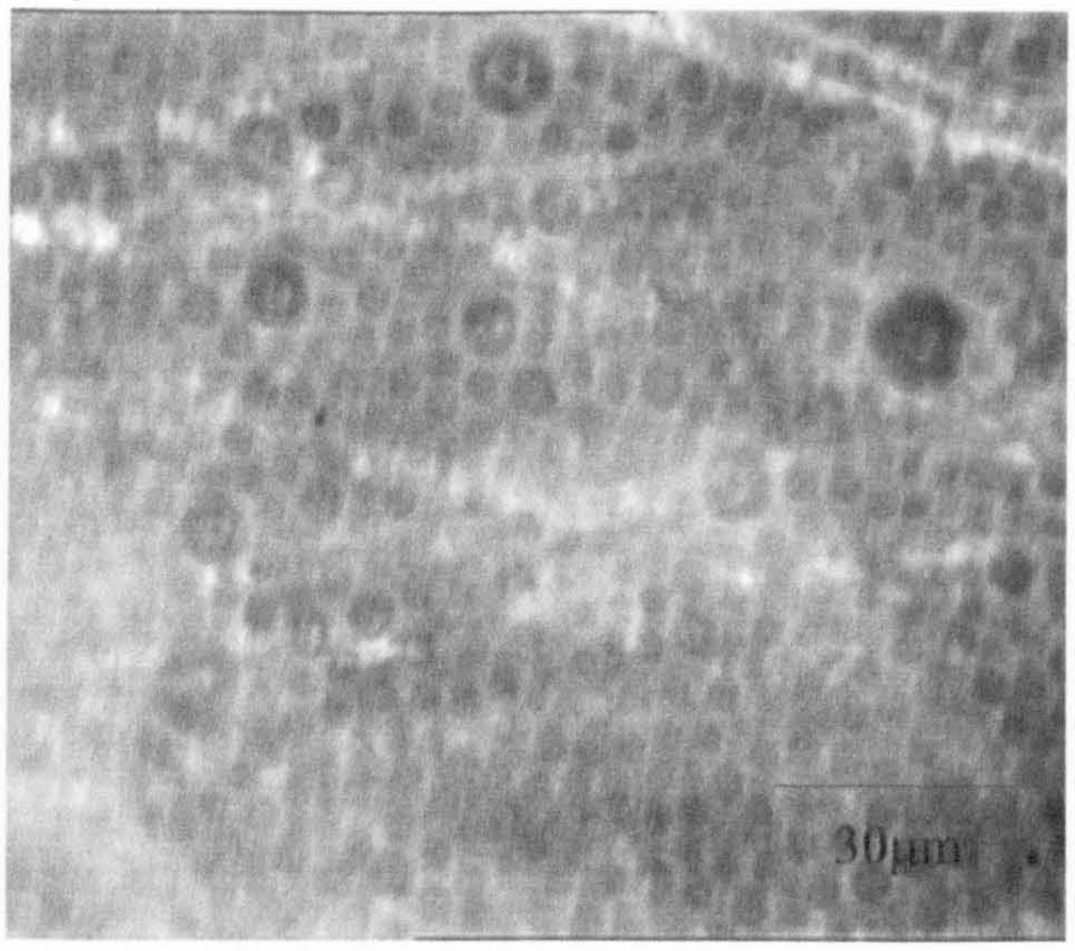

(d)

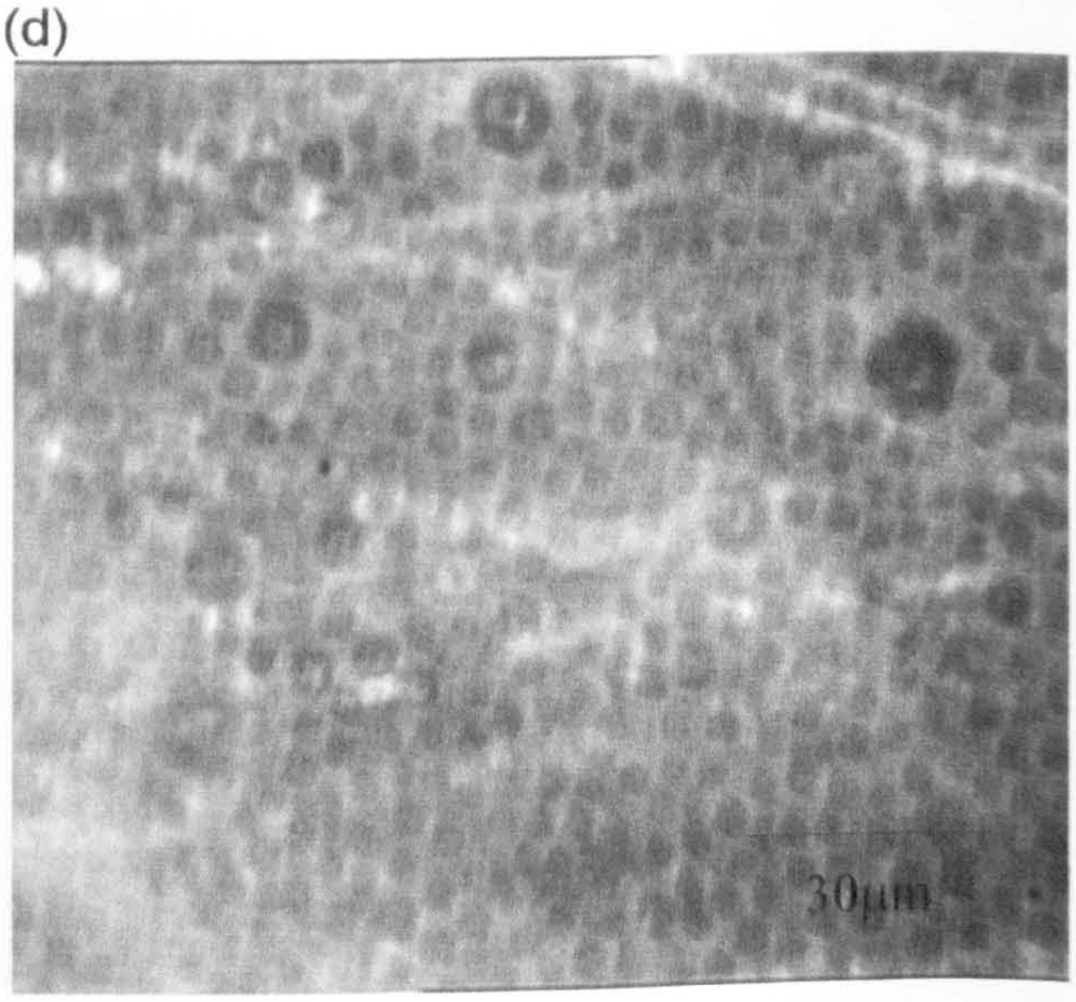

PLATE VII: 0.05(v/v) total monomer, 0.01(v/v) MTMS on Mica substrate:
(a)3 mins, (b) 60 mins, (c) 120 mins, (d) 180 mins

(a)

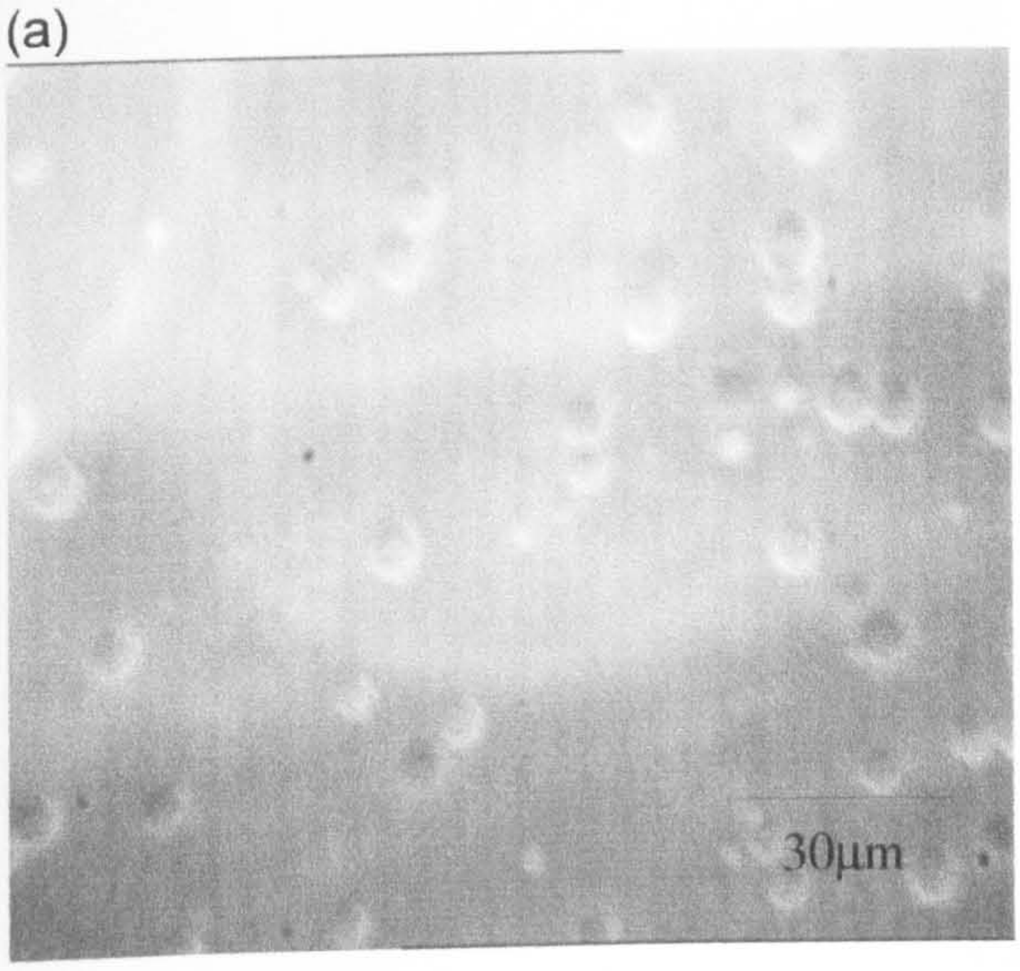

(b)

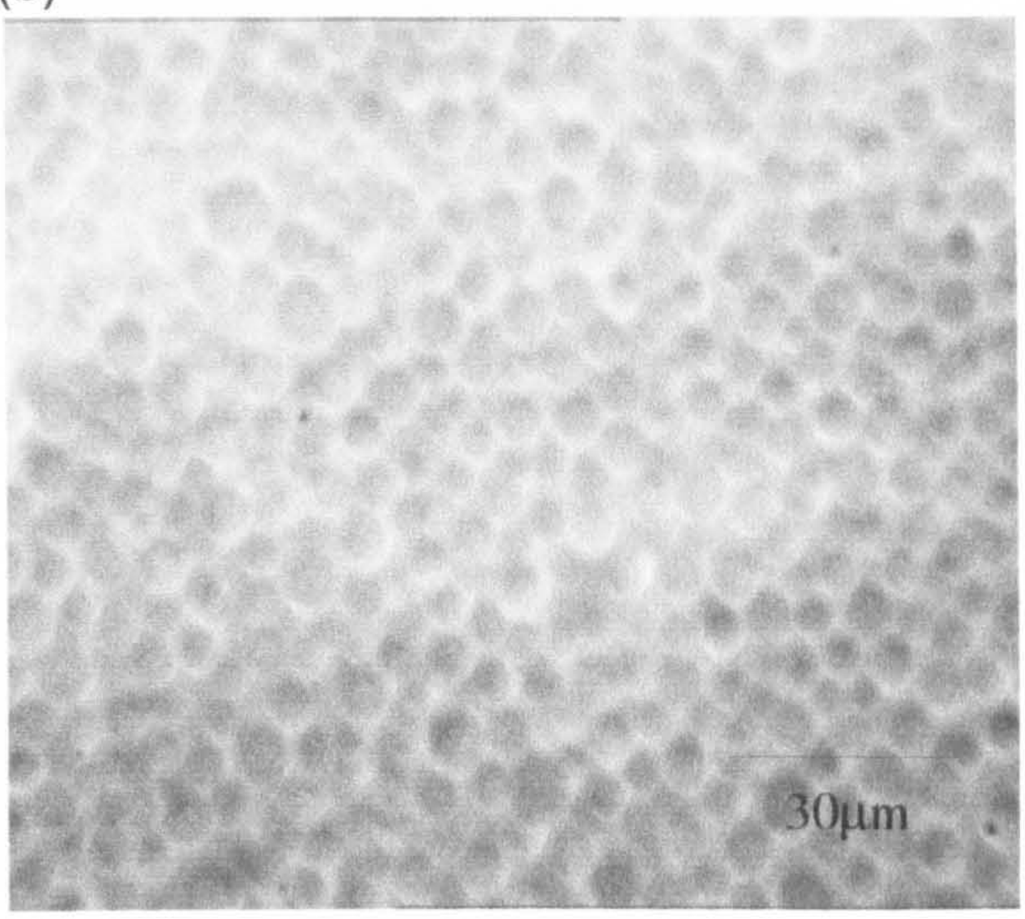

(c)

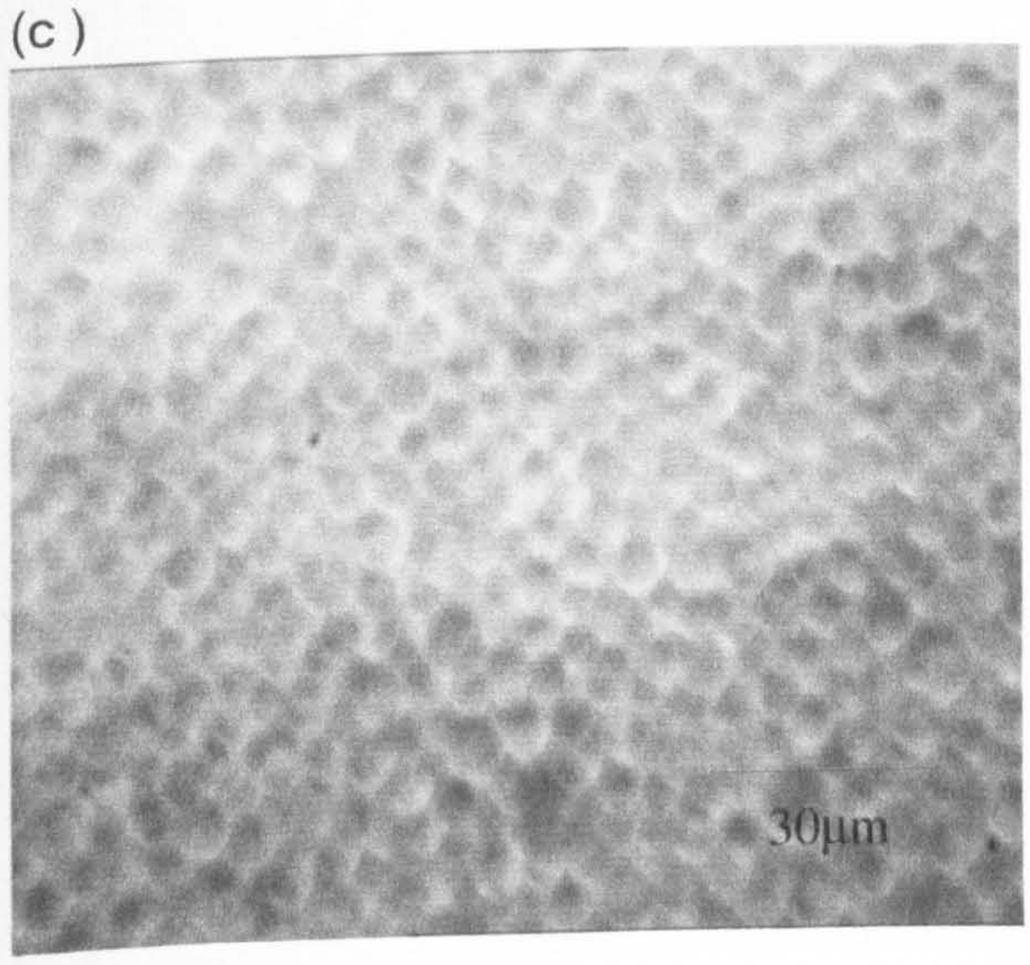

(d)

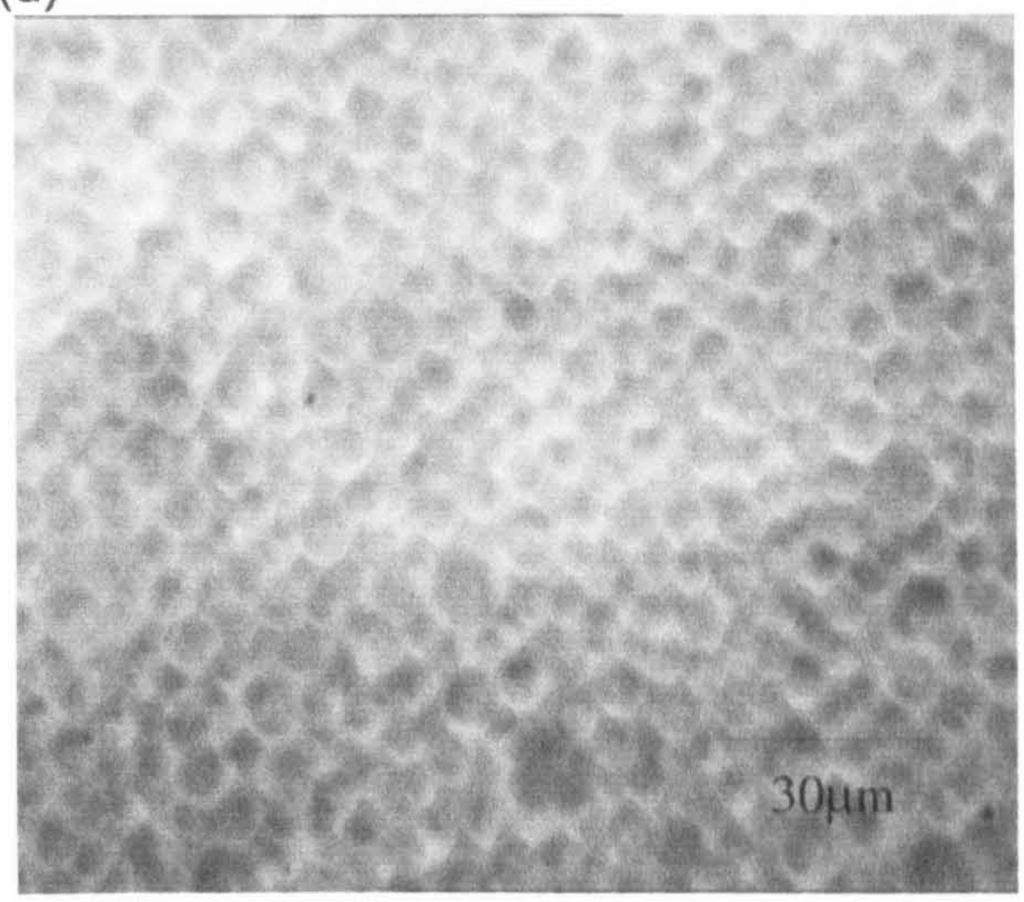

PLATE VIII: 0.05(v/v) total monomer, 0.05(v/v) MTMS on Mica substrate:
(a) 3 mins, (b) 60 mins, (c) 120 mins, (d) 180 mins

(a)

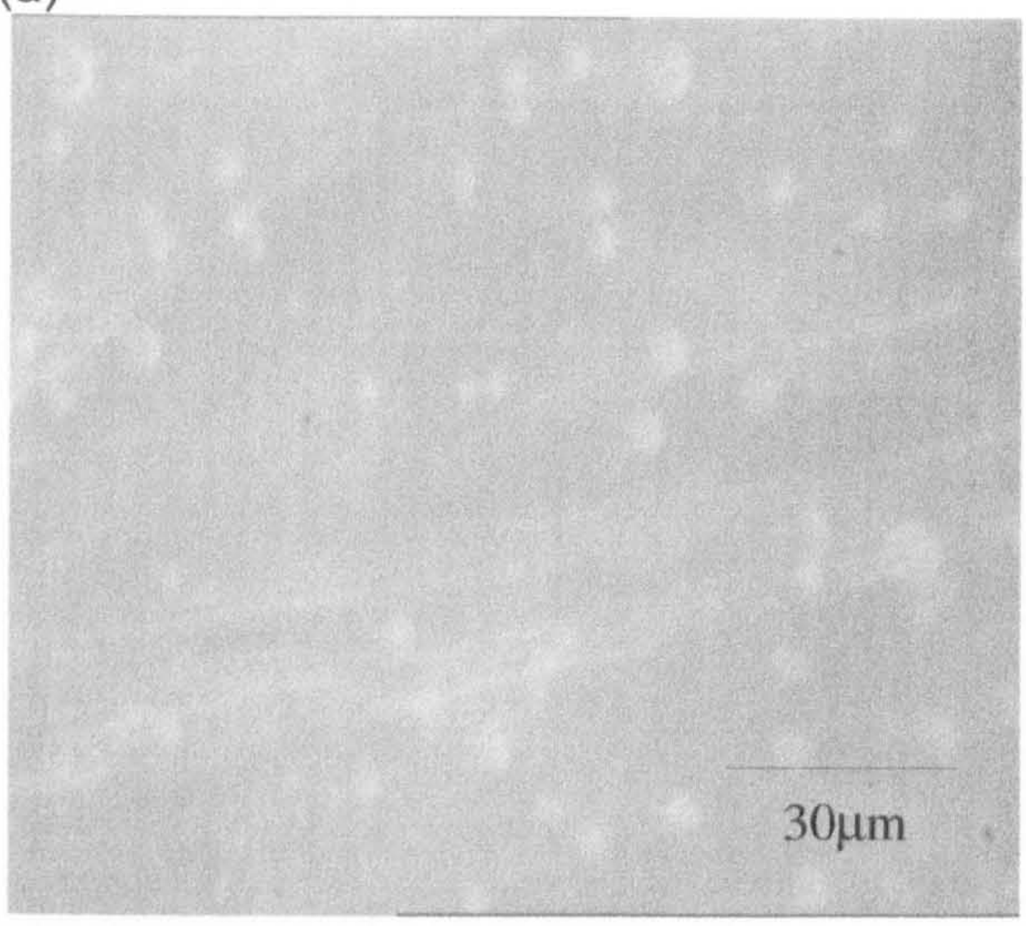

(b)

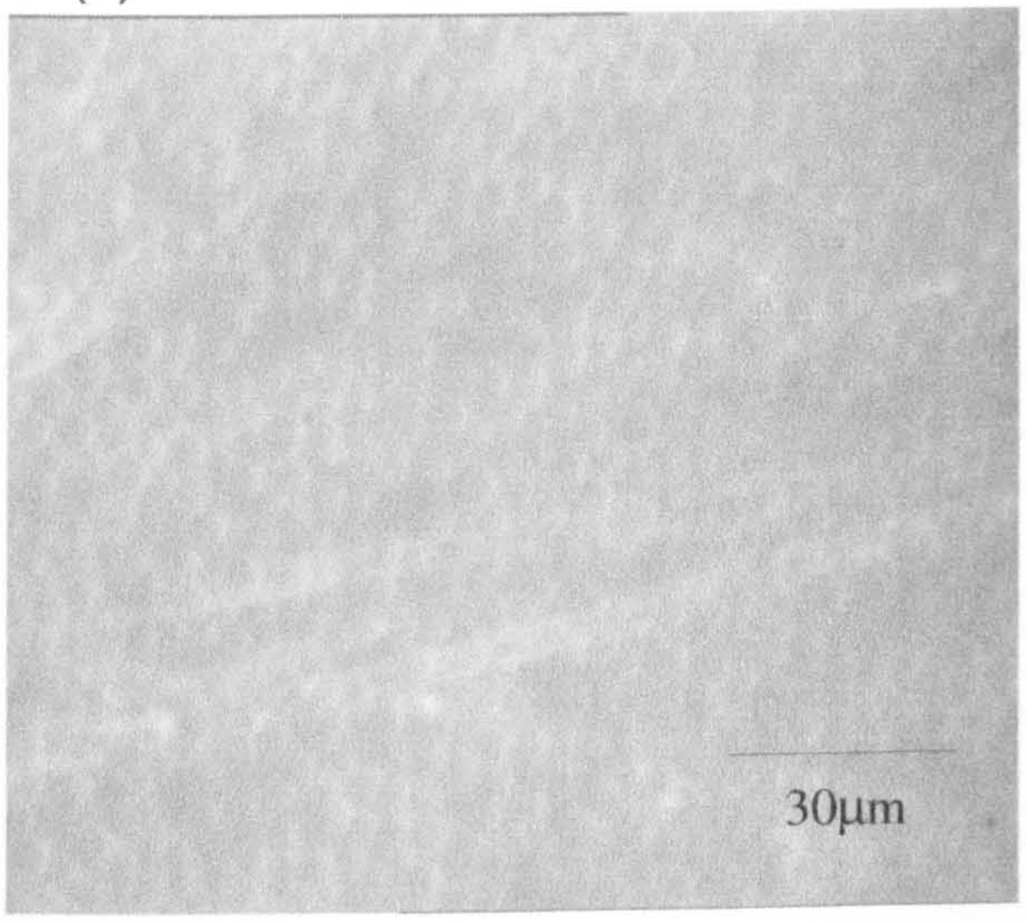

(c)

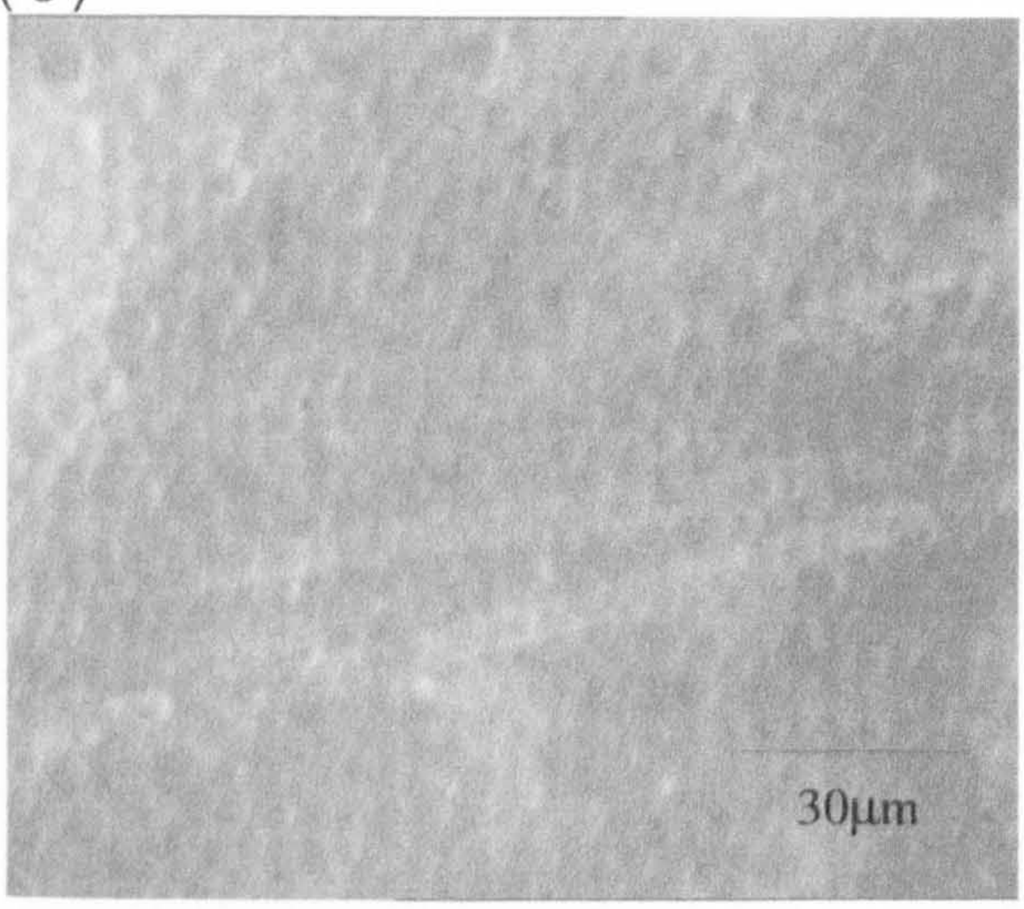

(d)

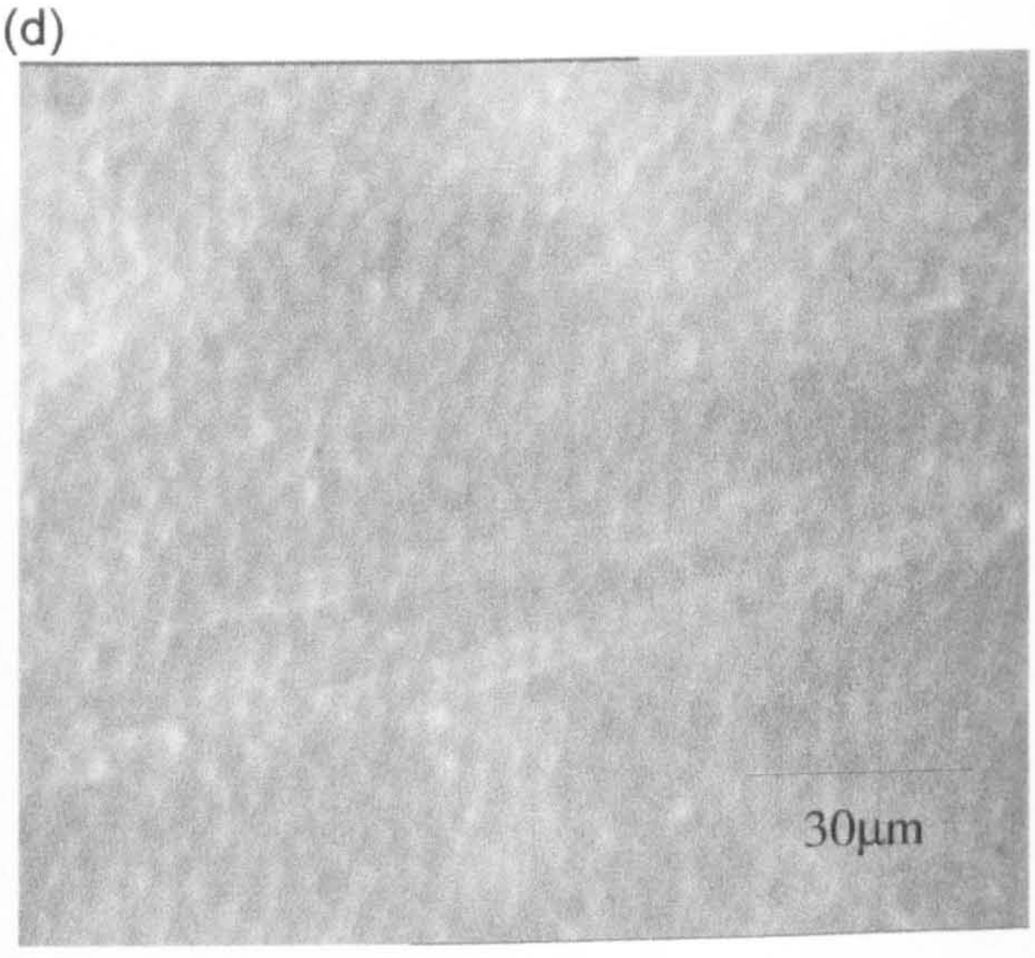

PLATE IX 0.05(v/v) total monomer, 0.1(v/v) MTMS on Mica substrate:
(a)3 mins, (b) 60 mins, (c) 120 mins, (d) 180 mins

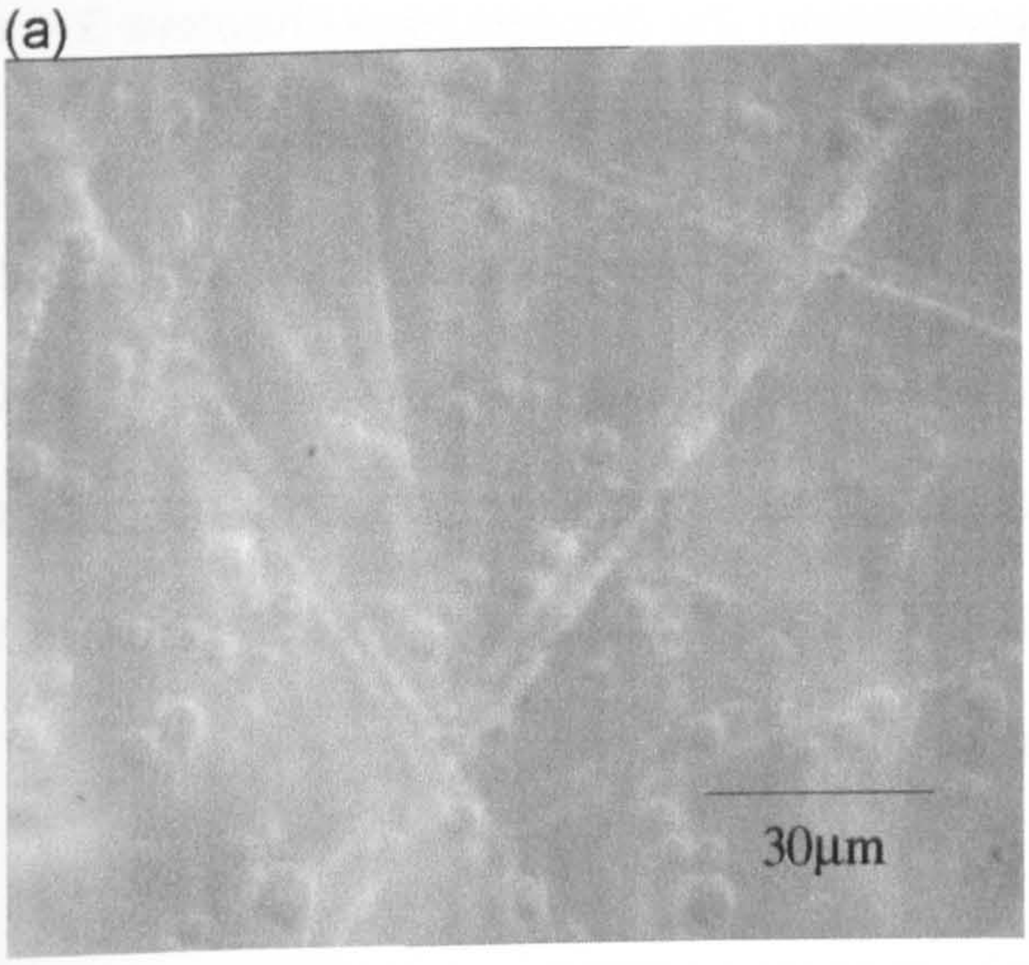

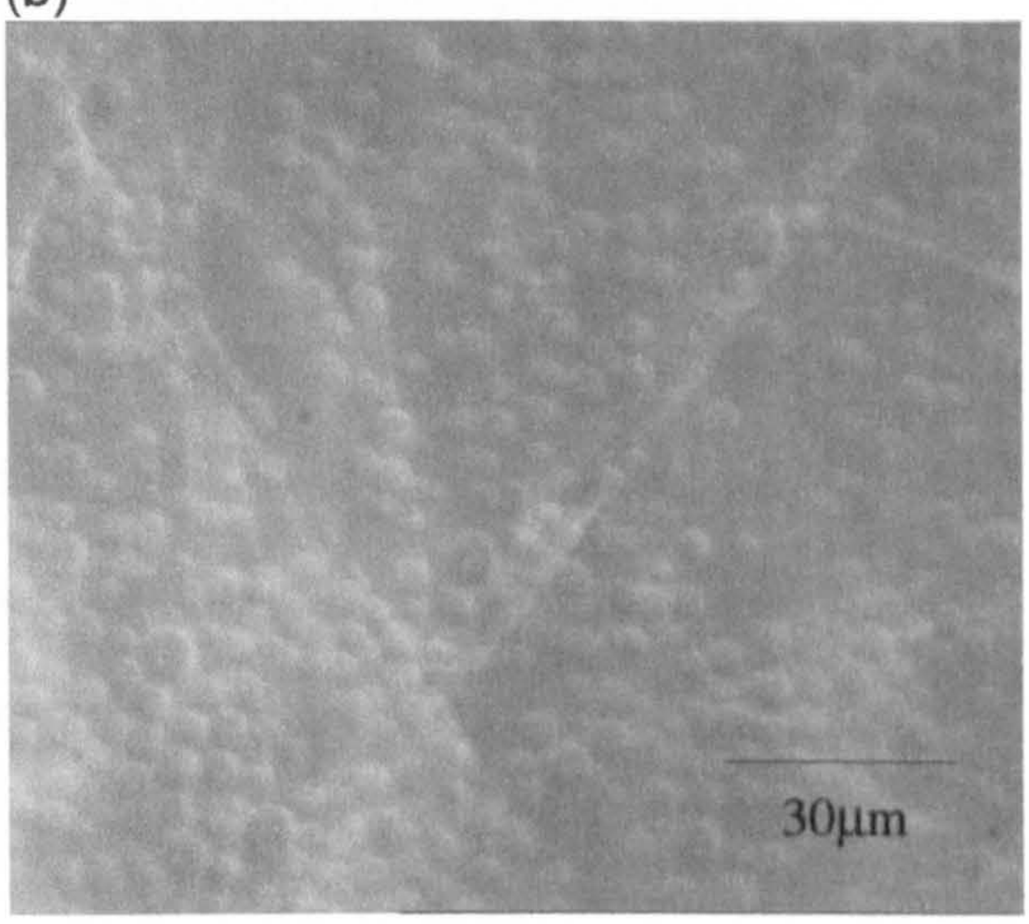

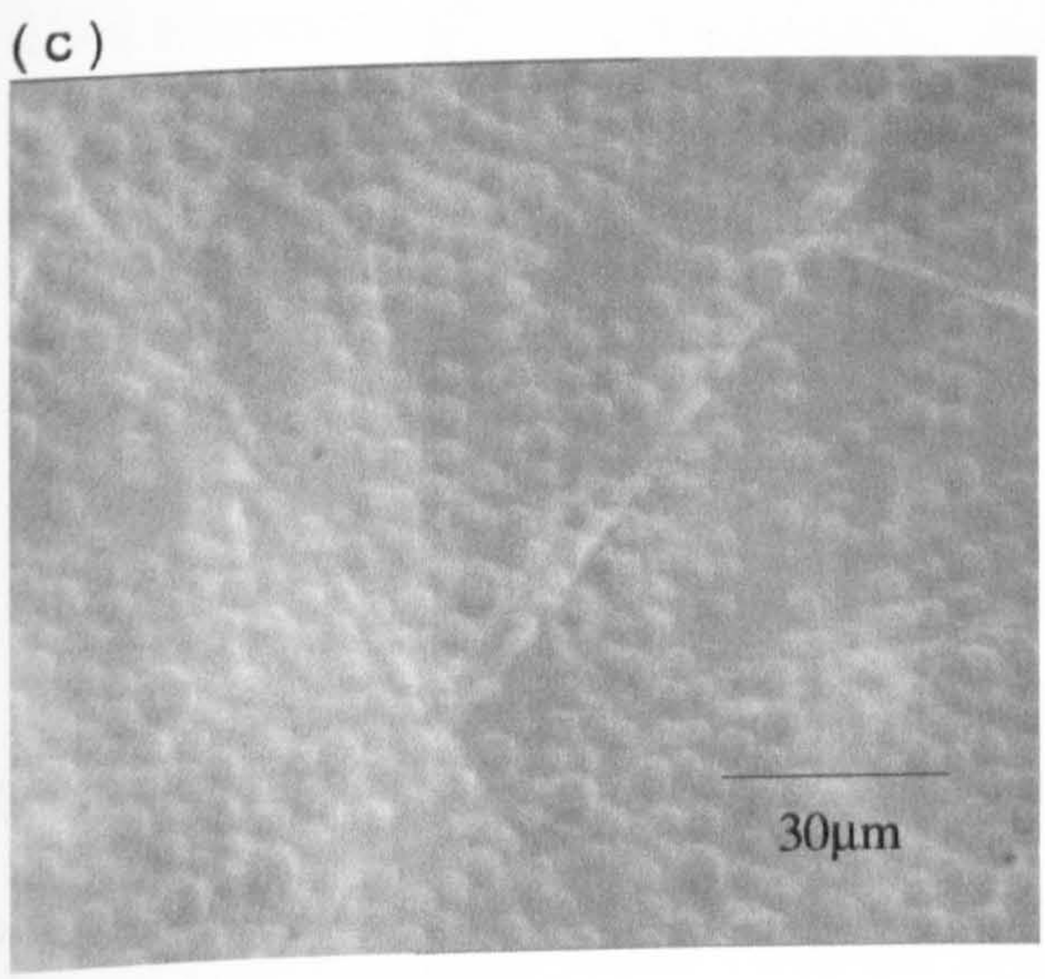

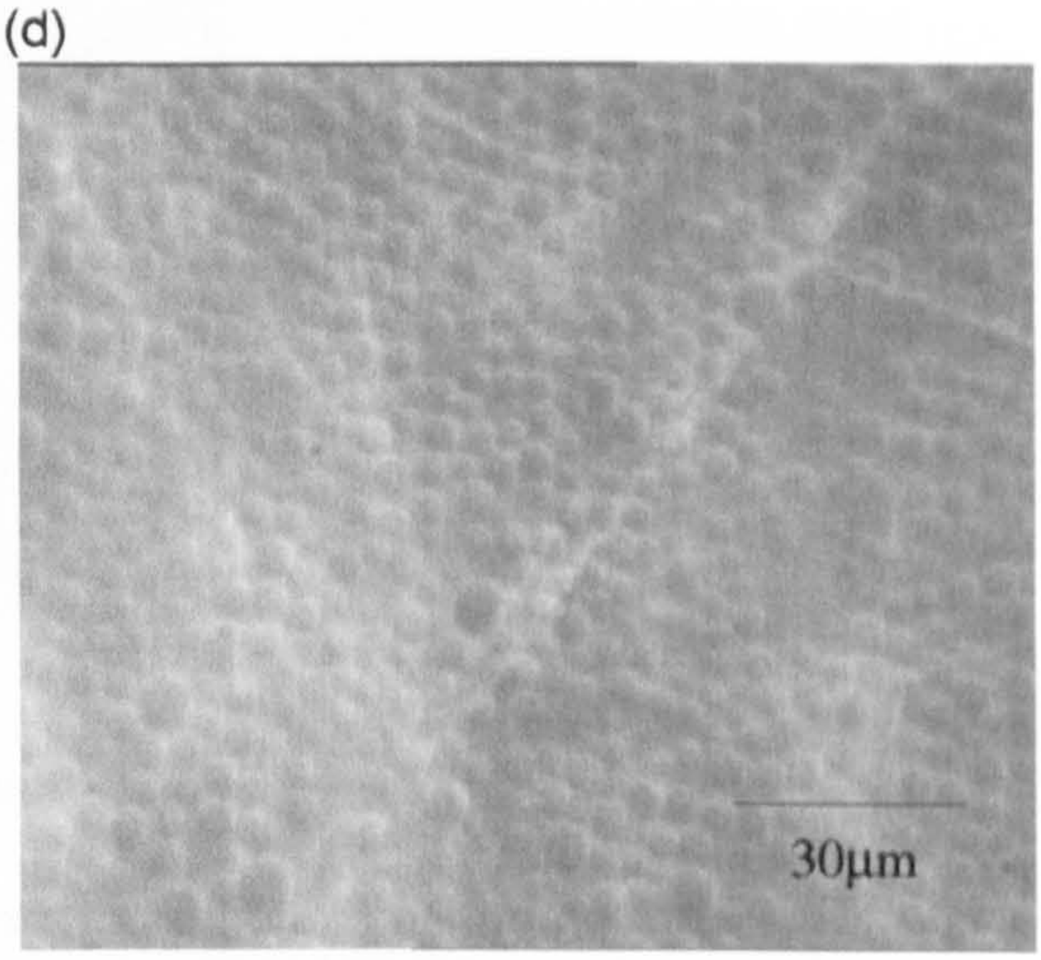

There was no evidence of droplet coalescence on the collector surface during this investigation even at high surface coverage. This behaviour can in part be attributed to the presence of surface ionised OH^- groups and the development of increasingly rigid cross-linked networks within the droplets, see chapters 3 and 5.

All of the cross-linked PDMS emulsion systems investigated showed no evidence of an aqueous film between the droplet and collector surface. It was possible to observe a static contact area which remained intact throughout the duration of the deposition experiments. The contact area was indicated by a lighter circle within the outline of the deposited droplet see figure 9.1.

Figure 9.1 Detail of contact area from 0.01(v/v) MTMS– mica system, after 1 hr.

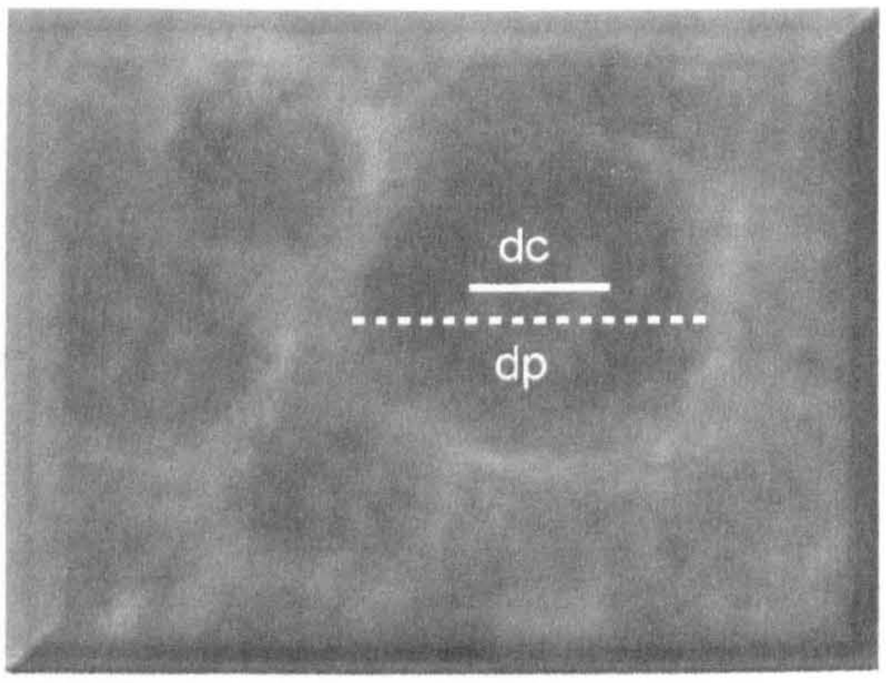

The measured contact area diameter, d_c was observed to decrease from ~32% to 10% of the droplet hydrodynamic diameter, d_p in the bulk solution as the ϕ of cross-linker increased from 0.0(v/v)-0.1(v/v) respectively, see chapter 7.

It has previously been suggested that the droplet-substrate contact angle hysteresis should increase with increasing cross-linker density[1]. This was

attributed to the oxidation of unreacted cross-linker which produce hydrogen bonds, from surface Si-OH groups, between the two surfaces. However, recent development of the JKR theory by Choi et al[2], for the adhesive forces between two elastomers, suggested that the elastic properties of the droplet are dynamic. Therefore the movement of free polymer chains at the interface would enhance its adhesive properties via entanglement mechanisms between tethered and free chains. Therefore, the work of adhesion would decrease as the MTMS ϕ increased as the transfer of polymer chains from one side of the interface to the other is significantly reduced.

The deposited amount and surface coverage ratio, θ, was derived using the equations [7.20] – [7.22], described in chapter 7, which assumed the droplets were hard, solid and non-deformable. The results were presented in figure 9.2 (a-e) as a function of time and also in table 9.2. In addition the calculations assumed the depositing charged particles had a fixed separation distance and a constant contact area with a substrate, independent of time and coverage regimes. However, this model was modified slightly for this system to reflect the dynamic contact area changes that occur during the deposition process. This ensured that a greater precedence was given to the surface area occupied by each droplet rather than the deposited number. This was achieved by using the radius of the contact area between the droplet and the collector surface rather than the hydrodynamic droplet radius obtained from PCS measurements, see chapter 5. All of the deposition profiles showed an initial rapid deposition which then slowed to form a "plateau" or equilibrium deposition value, (*Spl)* , see table 9.2.

Fig 9.2 Deposition profiles as a function of cross-linker ϕ on Mica substrate; (a) 0.0(v/v), (b) 0.005(v/v), (c) 0.01(v/v), (d) 0.05(v/v), (e) 0.1(v/v)

(a)

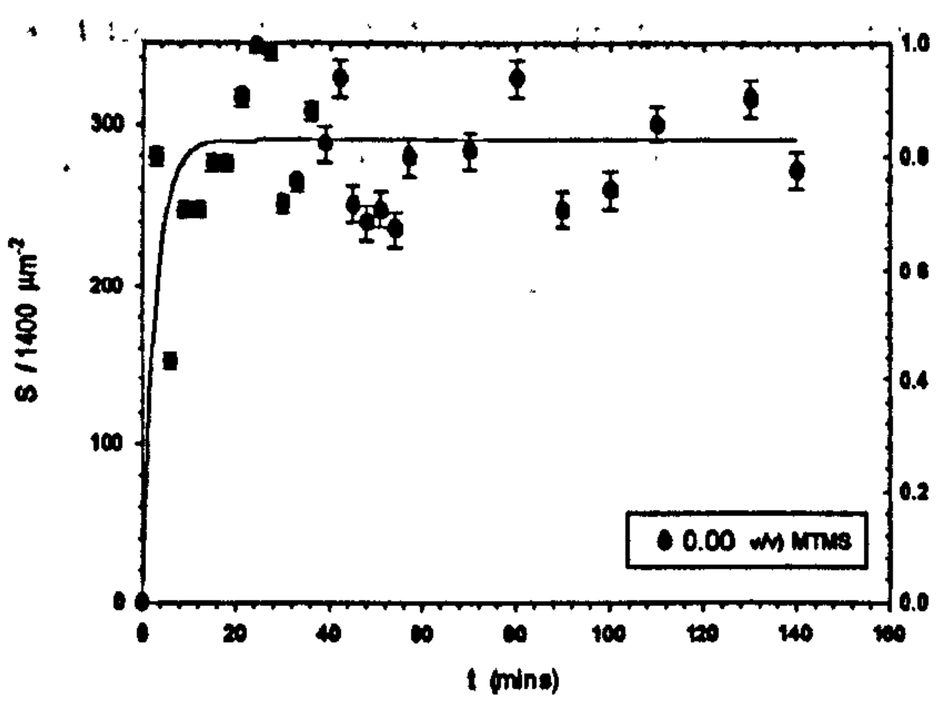

(b)

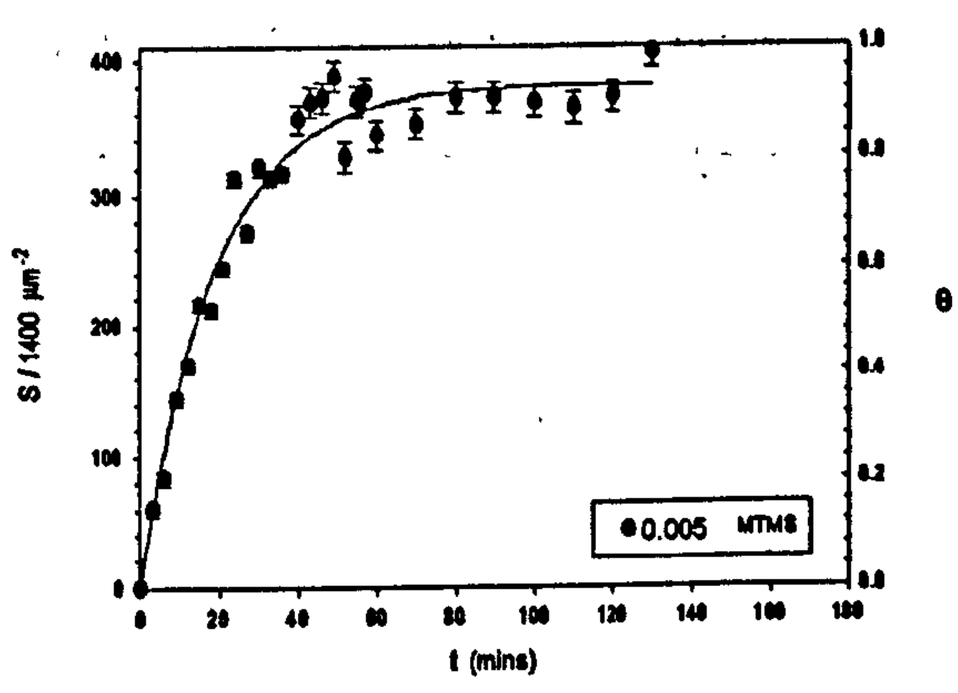

(c)

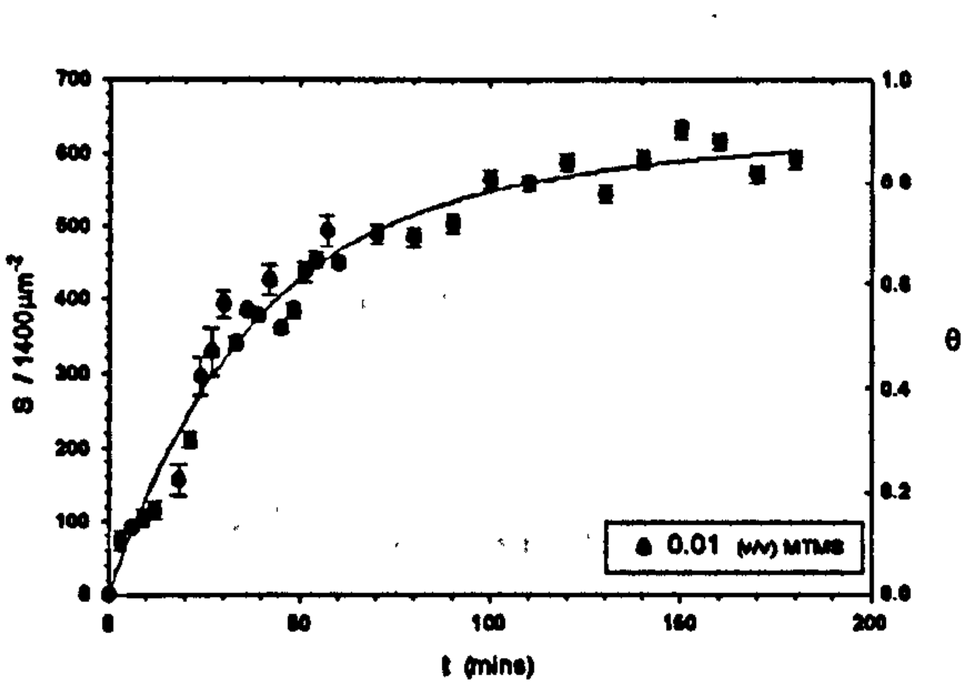

(d)

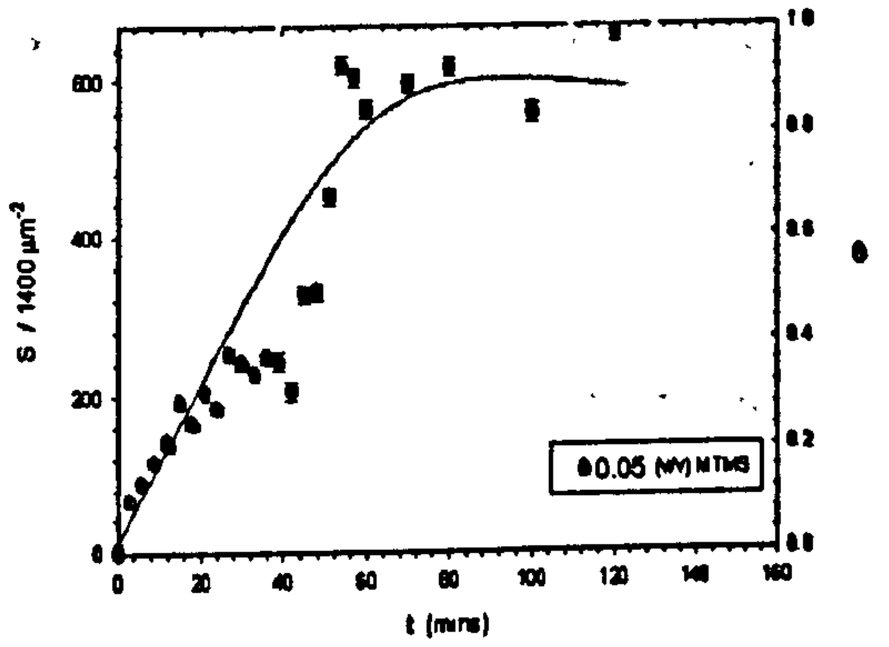

(e)

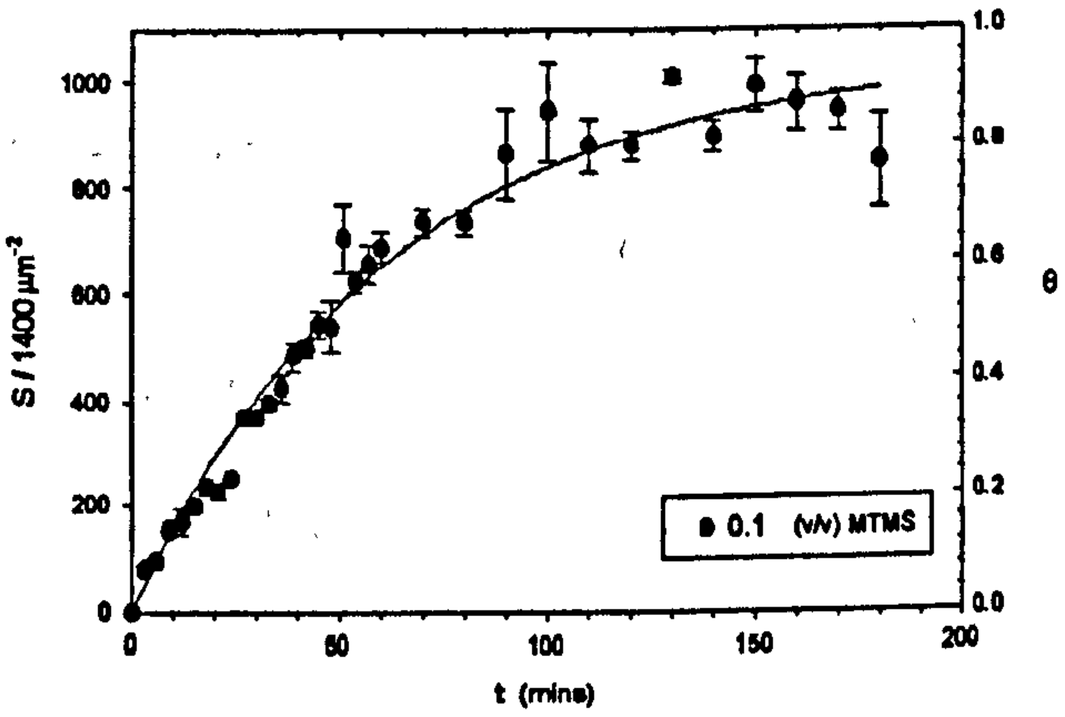

Table 9.2 Deposition parameters with varying MTMS ϕ

MTMS ϕ (v/v)	Spl N_d 1400μm^{-2}	Error (+/-)	t_{spl} (mins)	θ_{max}	K_d / s^{-1}	R^2	% max. surface coverage
0.000	408	21.5	15	1.00	4.00x10^{-3}	0.85	100.0%
0.005	472	19.1	40	1.00	1.70x10^{-3}	0.86	100.0%
0.010	632	11.4	70	0.96	4.76x10^{-4}	0.83	95.8%
0.050	660	11.1	90	0.88	3.96x10^{-4}	0.94	76.0%
0.100	848	25.2	120	0.76	3.50x10^{-4}	0.93	73.9%

The rate of deposition was observed to become gradually slower as the ϕ MTMS was increased. This was evident as the time required to reach the equilibrium deposition plateau, *Spl* increased from 15mins to 120 mins for 0.0(v/v)MTMS and 0.1(v/v)MTMS respectively. In addition, the magnitude of the Spl value and the subsequent deposited amount, S, simultaneously doubled with cross-linker volume fraction, ϕ.

These findings were in direct contrast to the droplet-substrate interaction potential, V_T, calculated previously in chapter 5 and to those presented by Wegner[3]. Classical DLVO theory has previously predicted that as the ϕ MTMS was increased from 0.0(v/v) to 0.1(v/v), the repulsion barrier, $V_{T\,max}$, would decrease from730 KT to 535 KT as a result of the decrease in droplet hydrodynamic diameter. However, this behaviour is accompanied by a significant increase in droplet surface negative potential which would enhance the electrostatic repulsive forces between the surface. Although the number of droplets was observed to increase the θ and surface coverage decreased by ~20%. This would suggest that in addition to classical van der Waals attractive, V_A, and electrostatic repulsive forces, V_{EDL}, blocking effects become more significant with increased cross-linking

density. These blocking effects were observed to increase the droplet-droplet separation distances on the collector surface and also seen to influence the deposition of subsequent droplets in close proximity to the substrate. These deviations from the classical assumptions, which resulted in values outside normal parameters have previously been predicted theoretically[6-8], but as yet have not been observed experimentally. In general, those systems containing <0.1(v/v) MTMS, showed that the droplet-droplet electrostatic repulsive forces were overcome and the inter-droplet separation distances were reduced to a minimum. However, those emulsion systems containing >0.1(v/v), maintained a distinct separation similar to that predicted by the hard-sphere DLVO model.

A more detailed study of the spreading behaviour of the cross-linked PDMS droplets on the mica surface as a function of time is shown in figure 9.3. It was observed that those emulsion systems containing <0.005(v/v) MTMS showed the most significant contact area spread. The average droplet-substrate contact area expanded to over twice the initial contact area after 10 mins and an almost total surface coverage was achieved in 30 mins after the initial deposition. The dramatic initial spreading property of the droplets not only physically reduced the amount of collector surface available for further deposition but also altered the surface charge of the collector surface, which artificially enhanced the electrostatic repulsive forces between the substrate and flowing droplets. As the ϕ MTMS was increased 0.005(v/v)>0.05(v/v), the average initial contact area decreased reflecting the increase in droplet surface tension due to the increase in cross-linked density. However, the contact area was also observed to decrease with time as the droplets adopted a more structured packing order similar to HCP. This feature was less pronounced for those systems containing >0.1(v/v) MTMS, where

there was no discernible change in average contact area over time and displayed behaviour close to that predicted by DLVO hard sphere theory, see chapter 7.

These findings were in contrast with those reported by Neuman et al[1] for two approaching deformable PDMS droplets, where those systems < 0.05(v/v) MTMS, showed the greatest film stability between the two surfaces. The repulsive hydration forces were reported to decrease with increasing surface tension and therefore MTMS ϕ. Differences in film stability / lifetimes were related to fluctuations in the adsorbed amount of charged end groups on mobile PDMS chains which preferentially adsorb at the oil / water interface.

Fig 9.3 Droplet contact area as a function of time with varying cross-linker ϕ

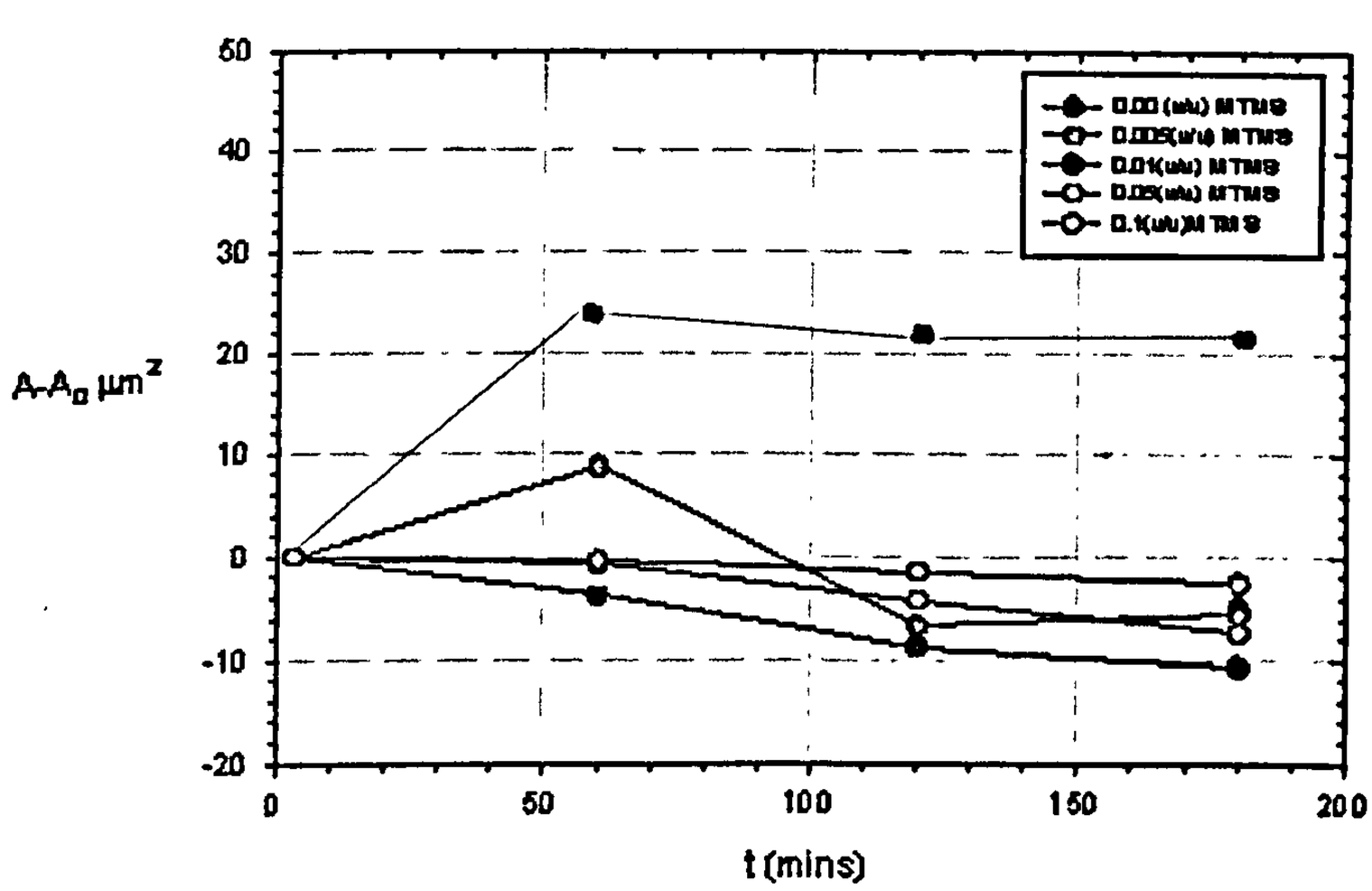

The cross-linked PDMS droplets initially adopted a random distribution which became a more uniform, "close packed" structure as the coating density increased, > 50% and the inter-droplet repulsive forces of separation were

overcome. The average relative location of deposited droplets on the collector surface was presented in figure 9.4 (a-c) as the partial radial distribution function g (r) as a function of the distance from the stagnation point. The graphs show a series of peaks indicating the locations of high droplet density which continue out to the edge of the observed collector surface. Initially, all of the cross-linked systems showed a single maximum peak, indicating that the most significant deposition coverage occurred at distances >20μm from the stagnation point. It could be observed that as the ϕ MTMS increased from 0.0(v/v)-0.1(v/v), the height of the density peaks decreased while their width increased. This trend corresponded to the increase in the number of droplets that could pack on to the collector surface due to a decrease in droplet spreading property and the subsequent reduced blocking effect exerted on approaching droplets. In addition, the enhanced cross-linked density within the droplets allowed them to deposit further from the stagnation point. It is interesting to note that the lowest cross-linked density, 0.0(v/v), displayed the highest and broadest peak which indicated that the enhanced spreading property of the PDMS droplets prevented any significant deposition below 40μm from the stagnation point.

As the deposition time increased, figures (b -c) showed that the distribution peak heights diminished steadily towards unity for all the cross-linked systems investigated, as the total coverage increasing over the observed collector surface.

Fig 9.4 Comparison of radial distribution functions for varying MTMS ϕ on Mica substrate; (a) 3 mins, (b) 60 mins, (c) 180 mins.

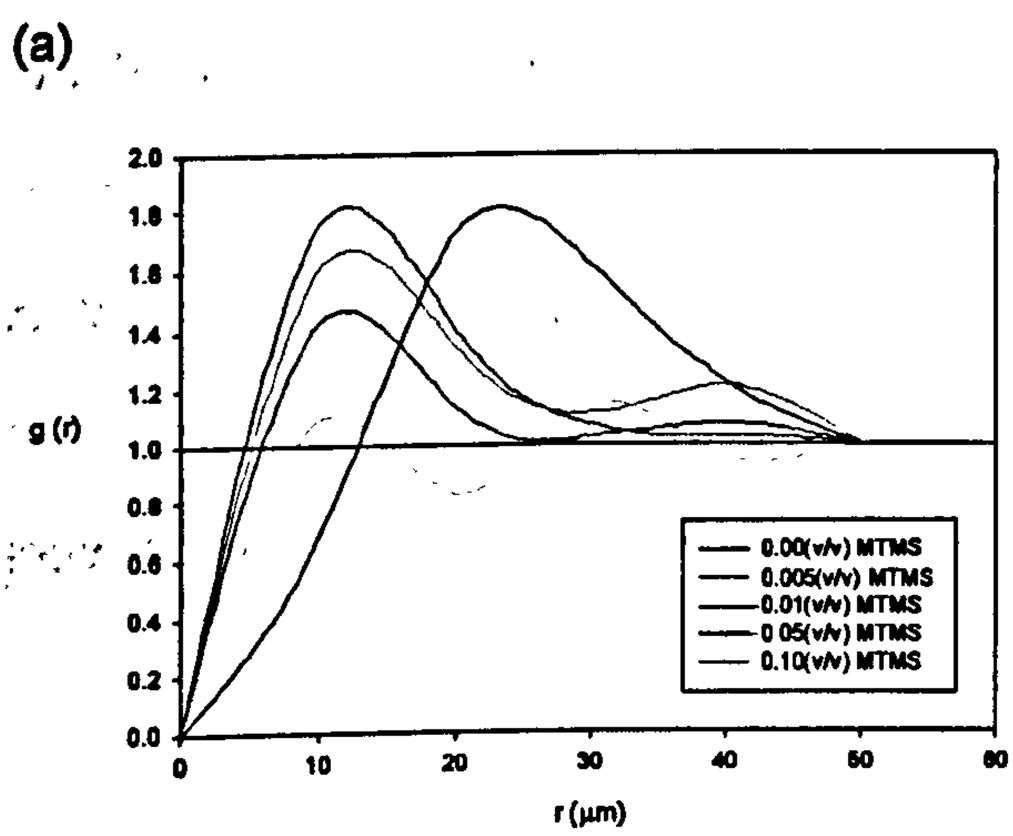

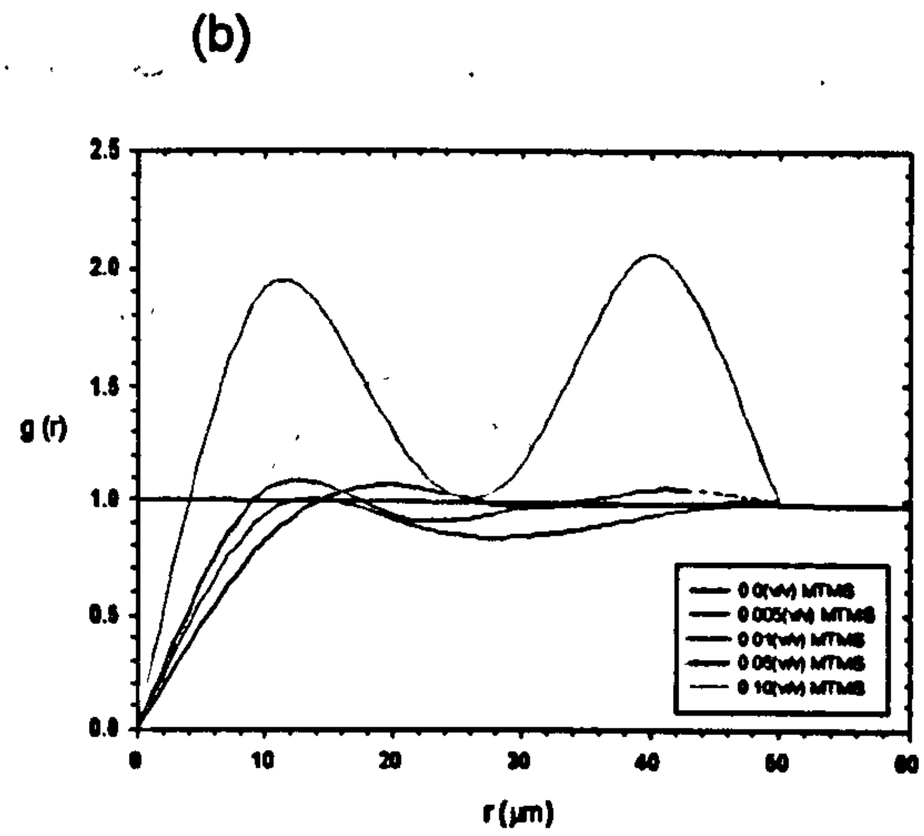

(c)

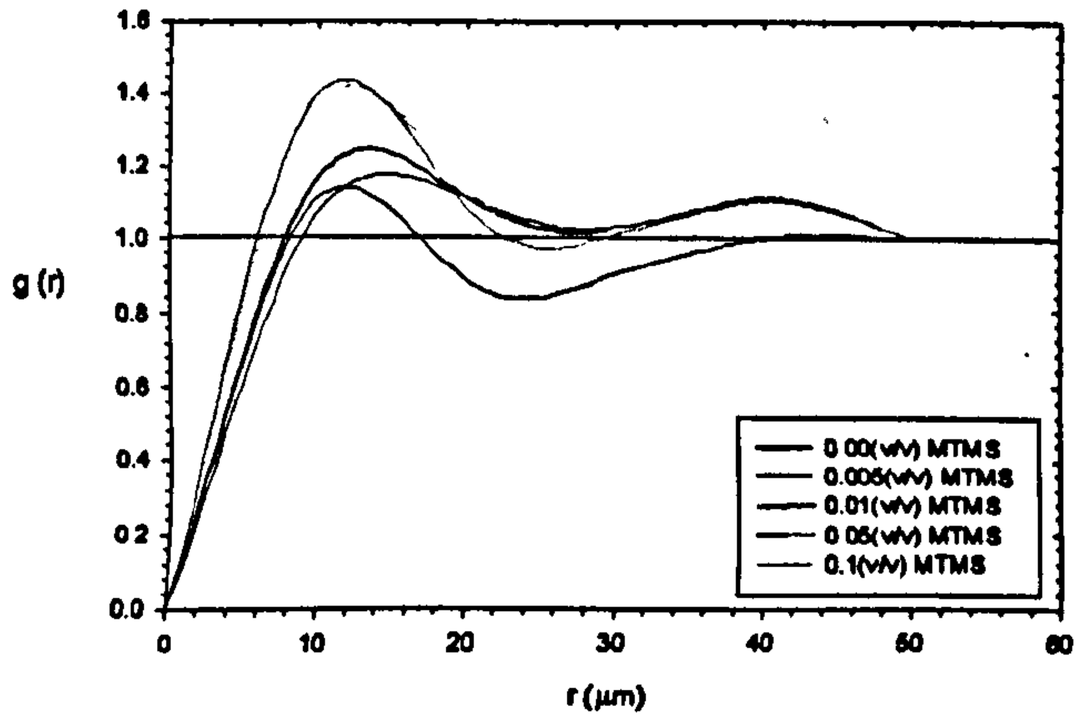

9.2.2 Deposition as a function of electrolyte concentration

An identical investigation to that described in section 9.2.1 was conducted with a fixed 0.05(v/v) total monomer ϕ and 0.05(v/v) ϕ MTMS in the presence of a varying electrolyte concentration. The emulsion and substrate parameters were presented in table 9.3. The examination of PCS and electrophoretic mobility studies in chapter 5 showed that the droplet-droplet coalescence occurred with the increasing concentration and the CCC value was found to occur between 10^{-2} $moldm^{-3}$ – 10^{-3} $moldm^{-3}$.

It was previously discussed in chapter 5 that the droplet surface ζ-potential negativity decreased with increasing electrolyte concentration, due to the preferential adsorption of Na+ ions at the surface in conjunction with an increase in the droplet surface area. The simultaneous increase of the mica negative surface charge resulted in the reduction of the electrostatic repulsive forces between droplet and substrate. These surface charge effects occurred in the same order of magnitude as each other. It could therefore be assumed that the electrostatic repulsive forces and the van der Waals attraction remain almost constant.

Plates X – XV illustrate the influence of NaCl concentration on the deposition of cross-linked PDMS droplets on a mica surface. All of the droplets in the dispersions were observed to deposit individually across the mica surface, while the deposition increased over time and with increasing electrolyte concentration.

PLATE X 10^{-5} mol dm^{-3} [NaCl]: (a)3 mins, (b)60 mins, (c)120 mins, (d)180 mins

(a)

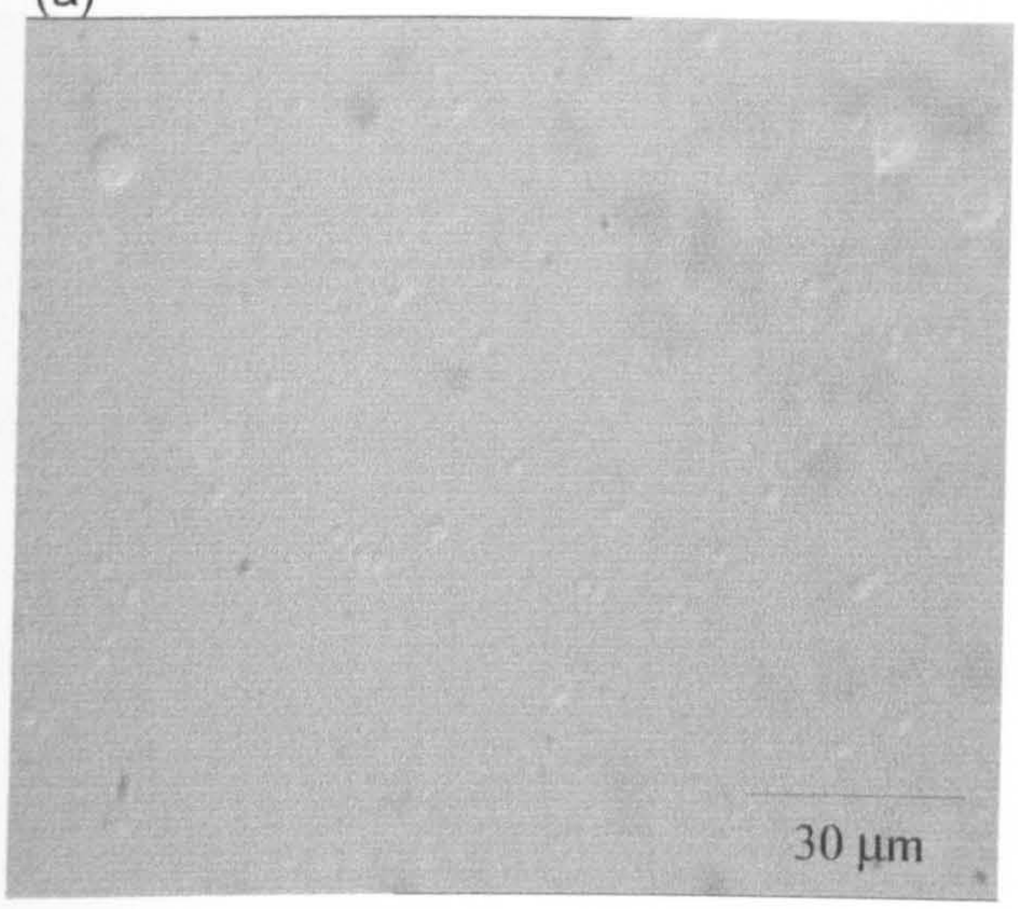

(b)

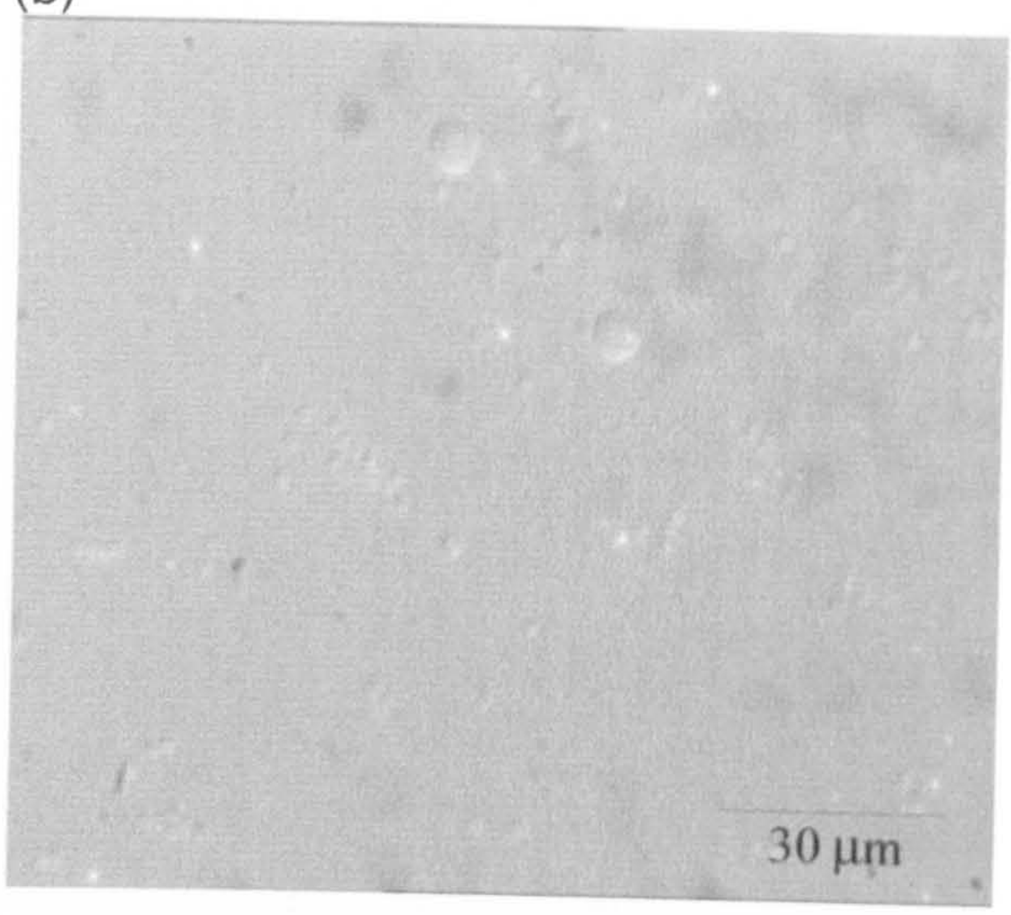

(c)

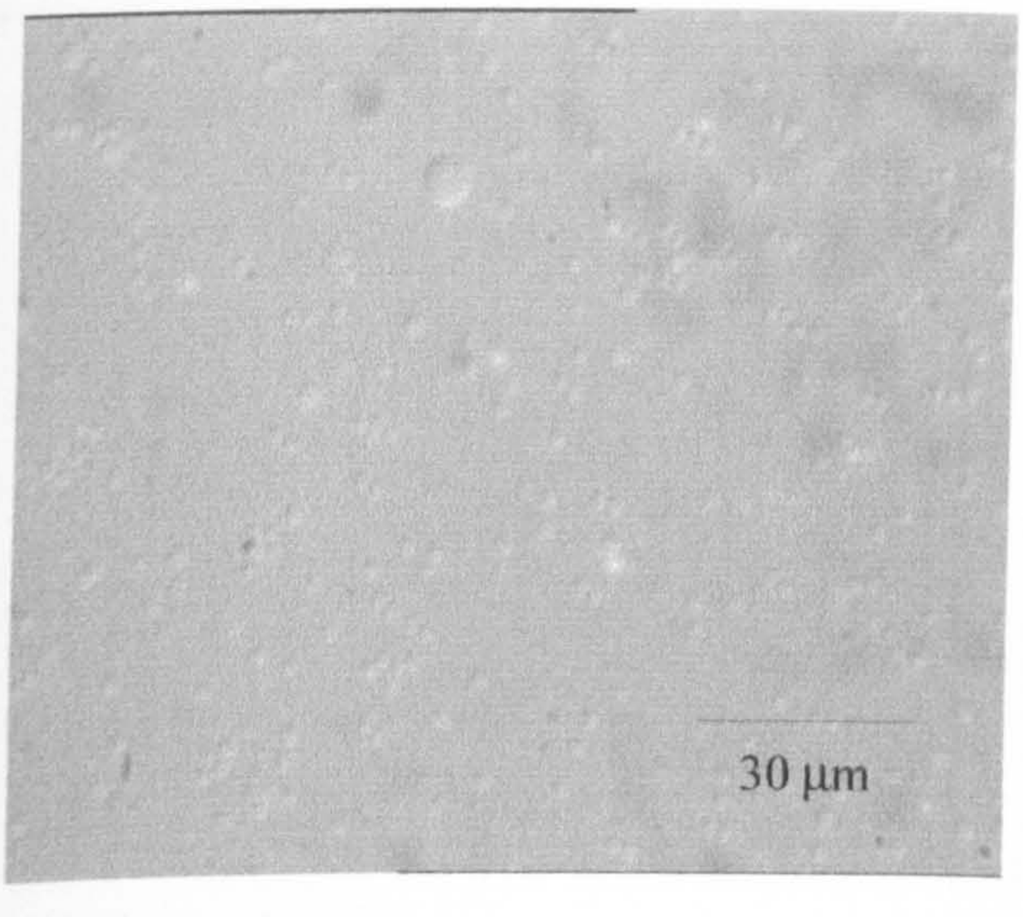

(d)

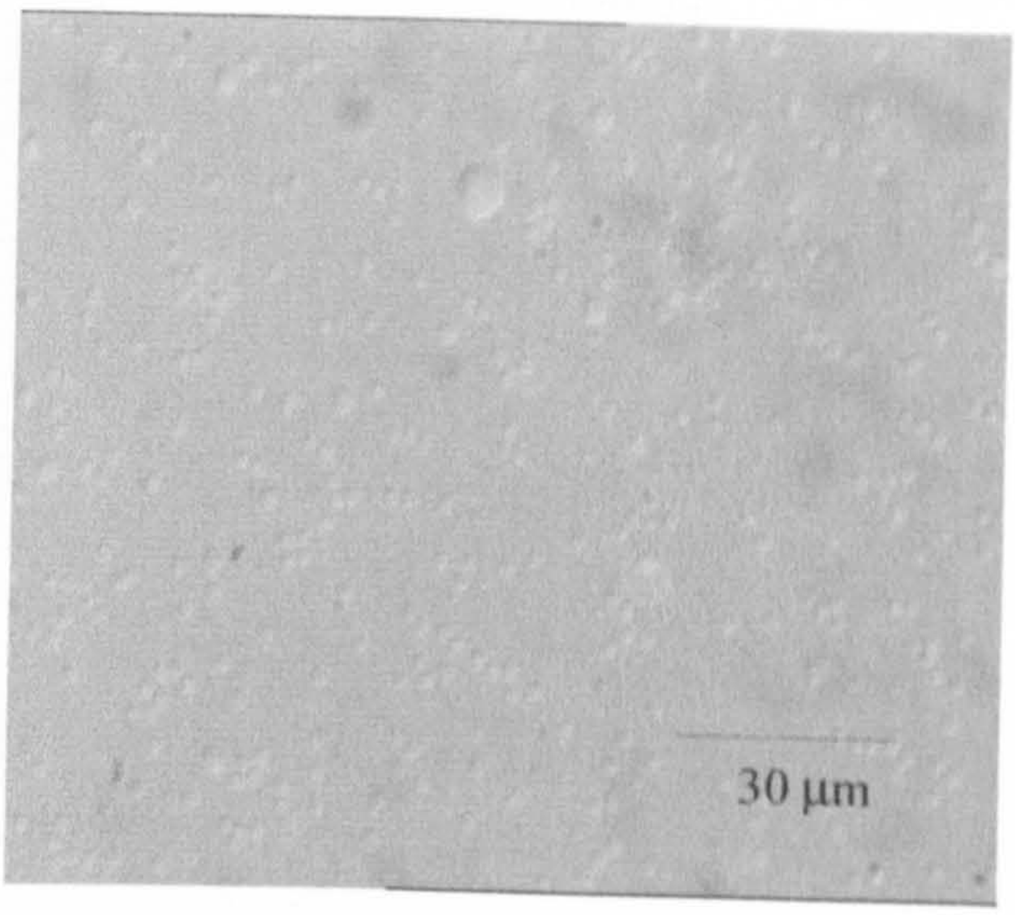

PLATE XI 10^{-4} mol dm^{-3} NaCl: (a)3 mins, (b)60 mins, (c)120 mins, (d)180 mins

(a)

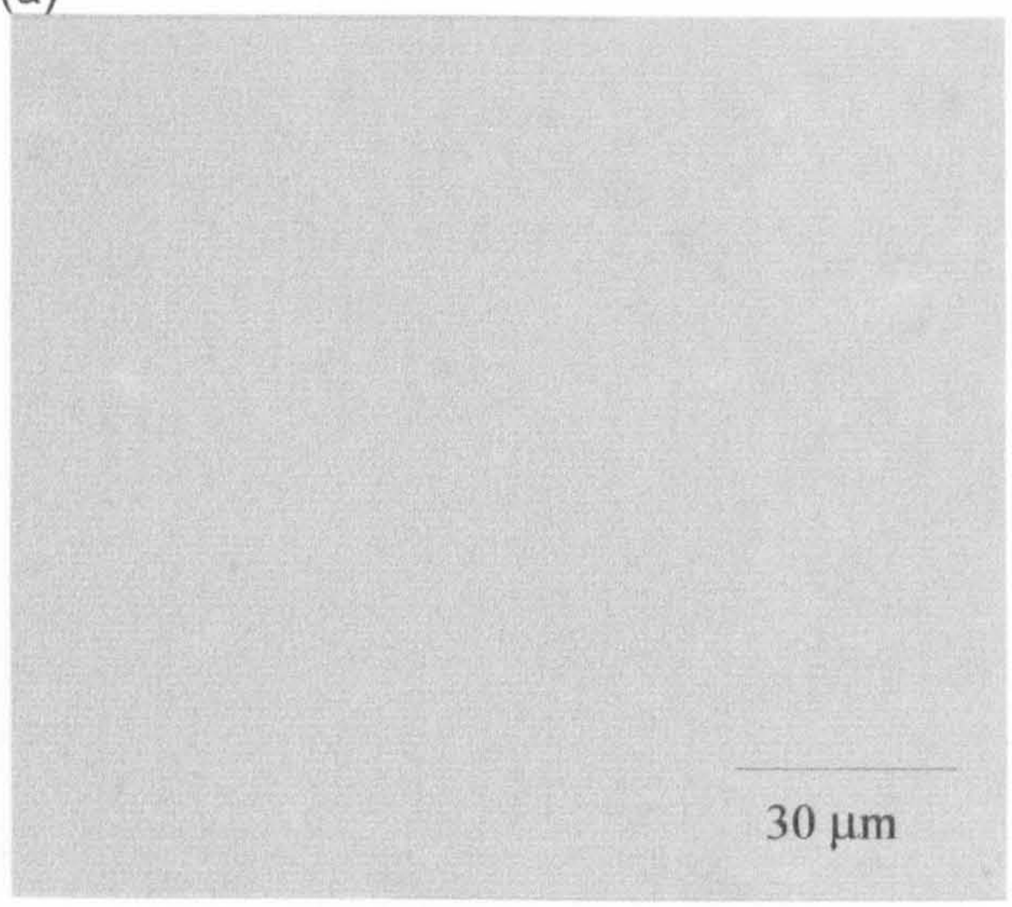

(b)

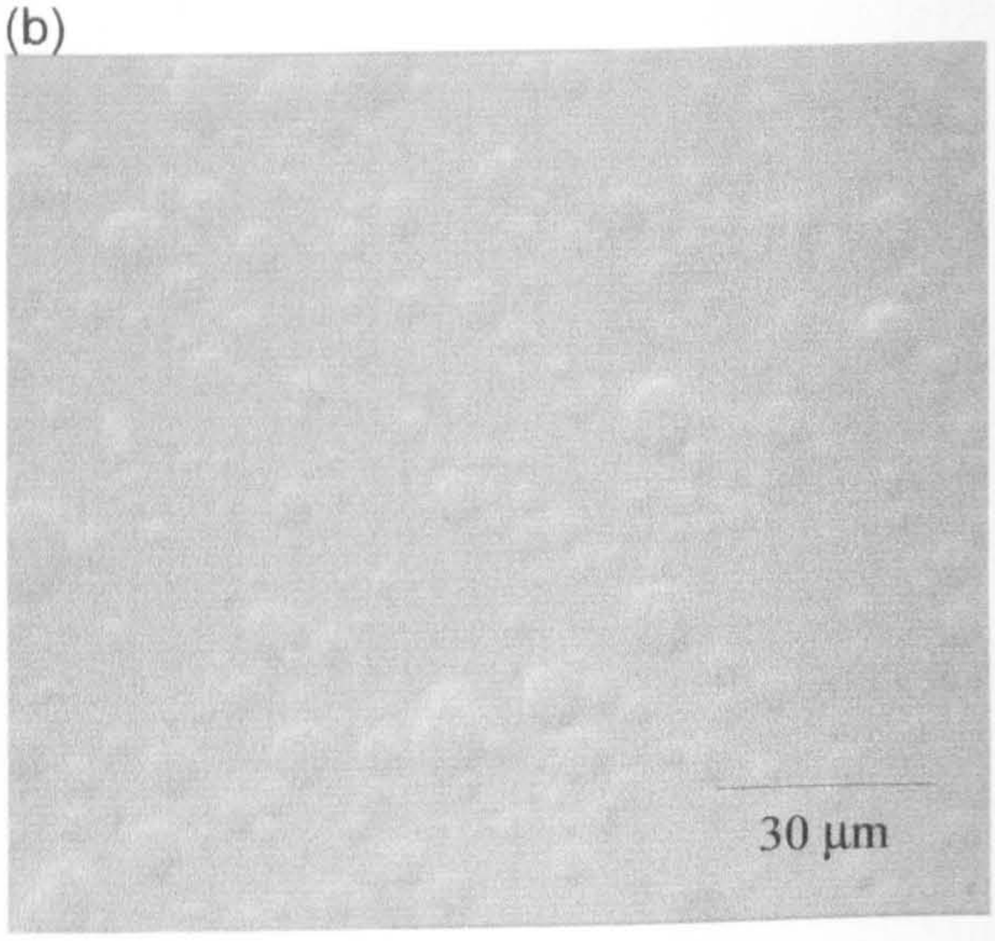

(c)

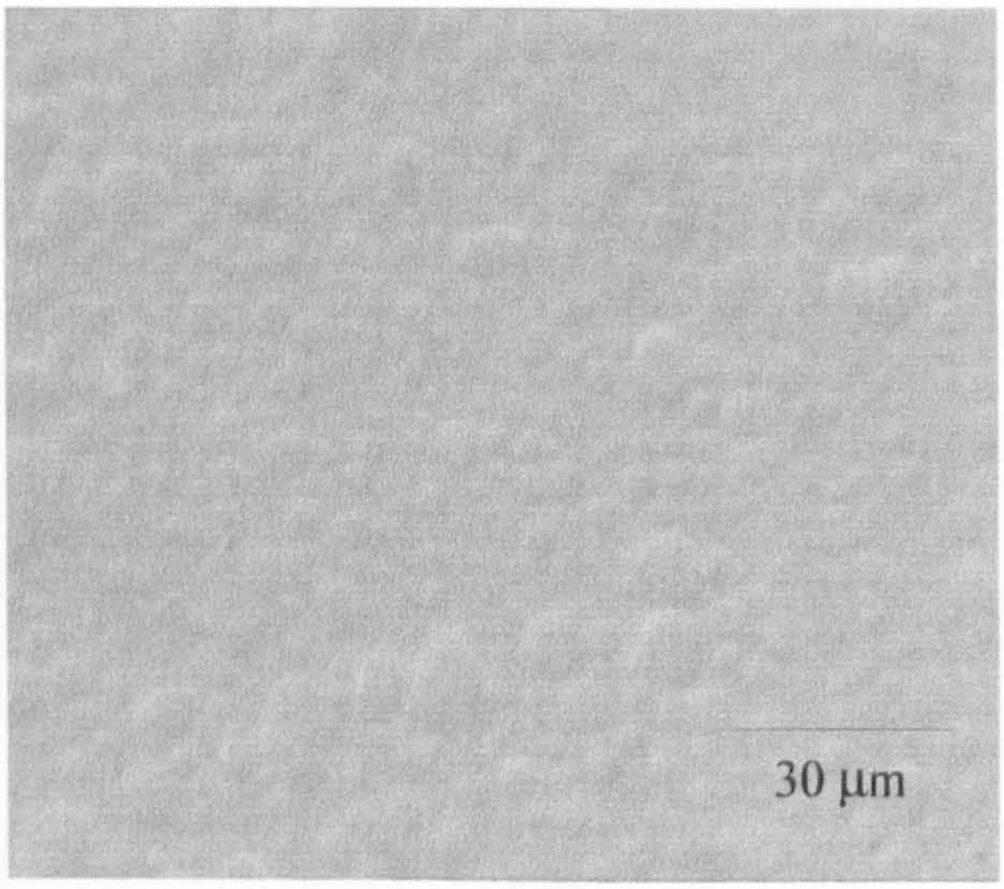

(d)

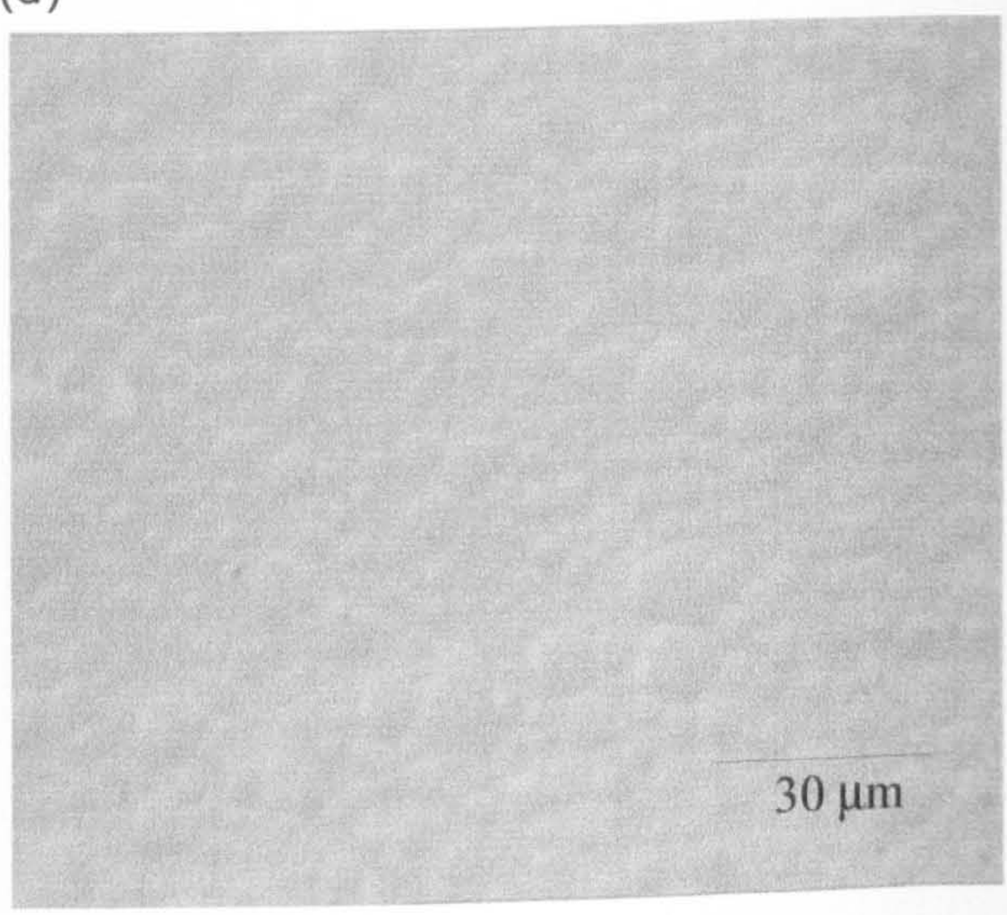

PLATE XII 10^{-3} NaCl:(a)3 mins, (b)60 mins, (c)120 mins, (d)180 mins

(a)

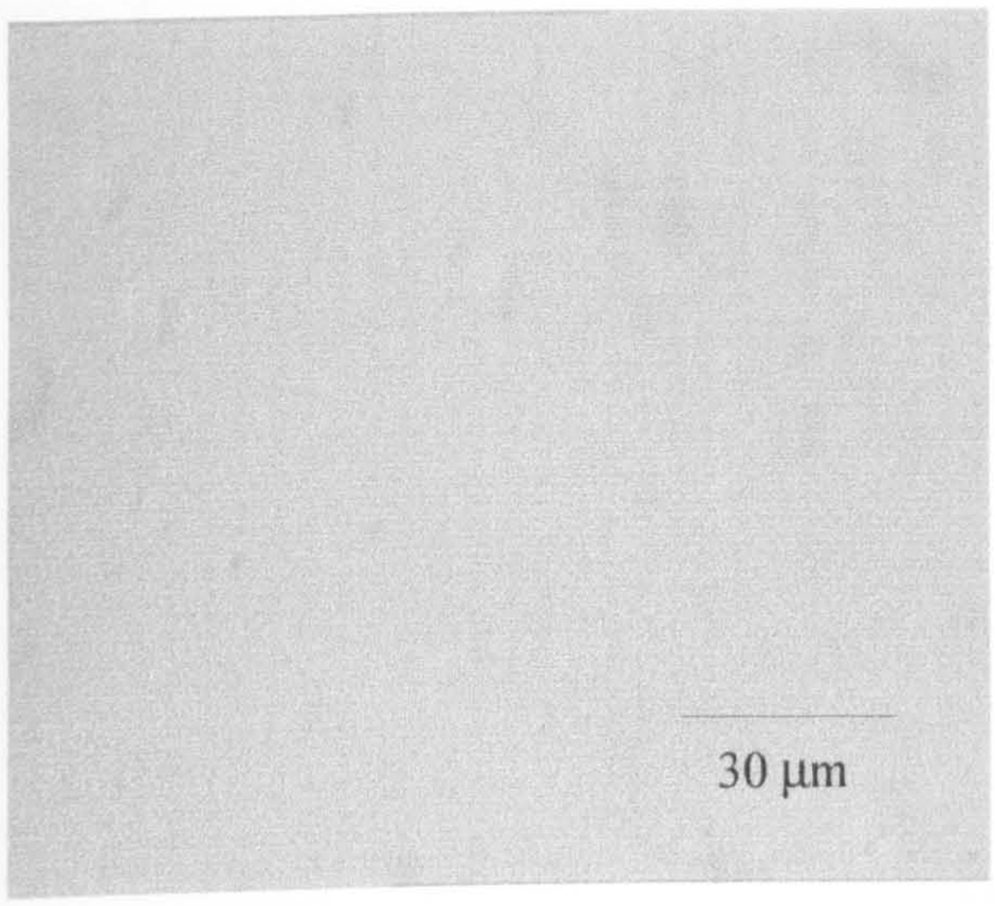

(b)

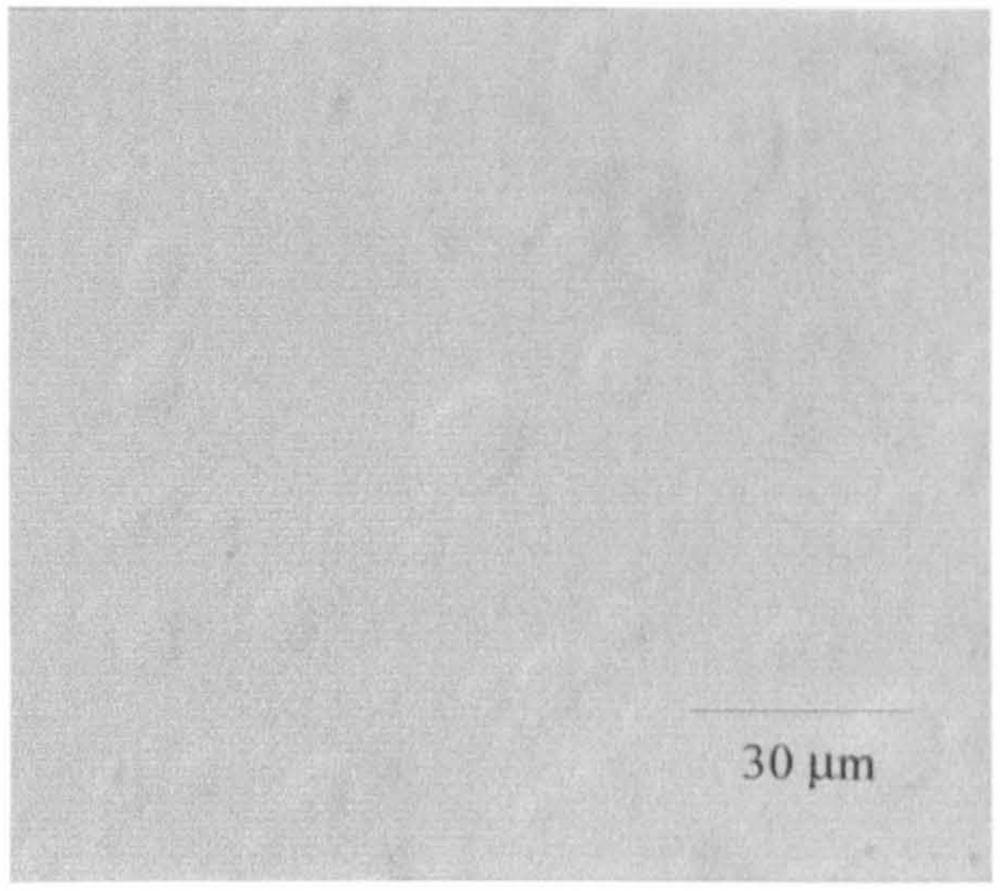

(c)

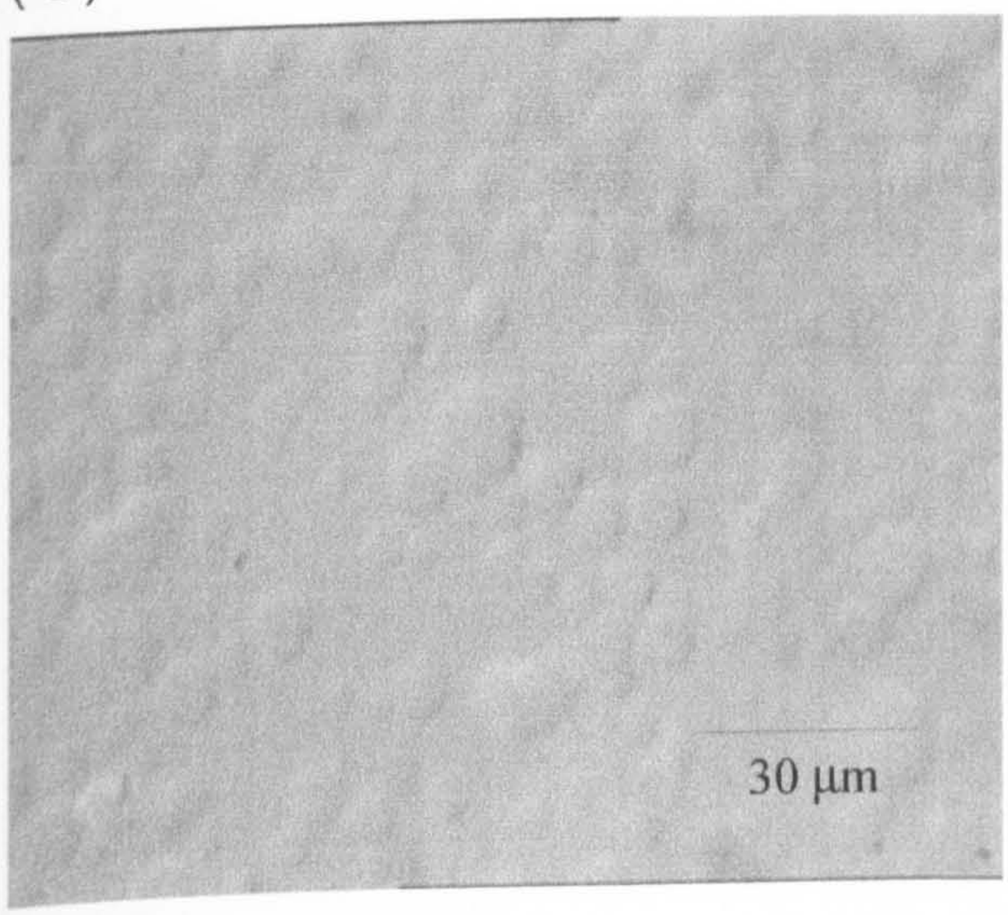

(d)

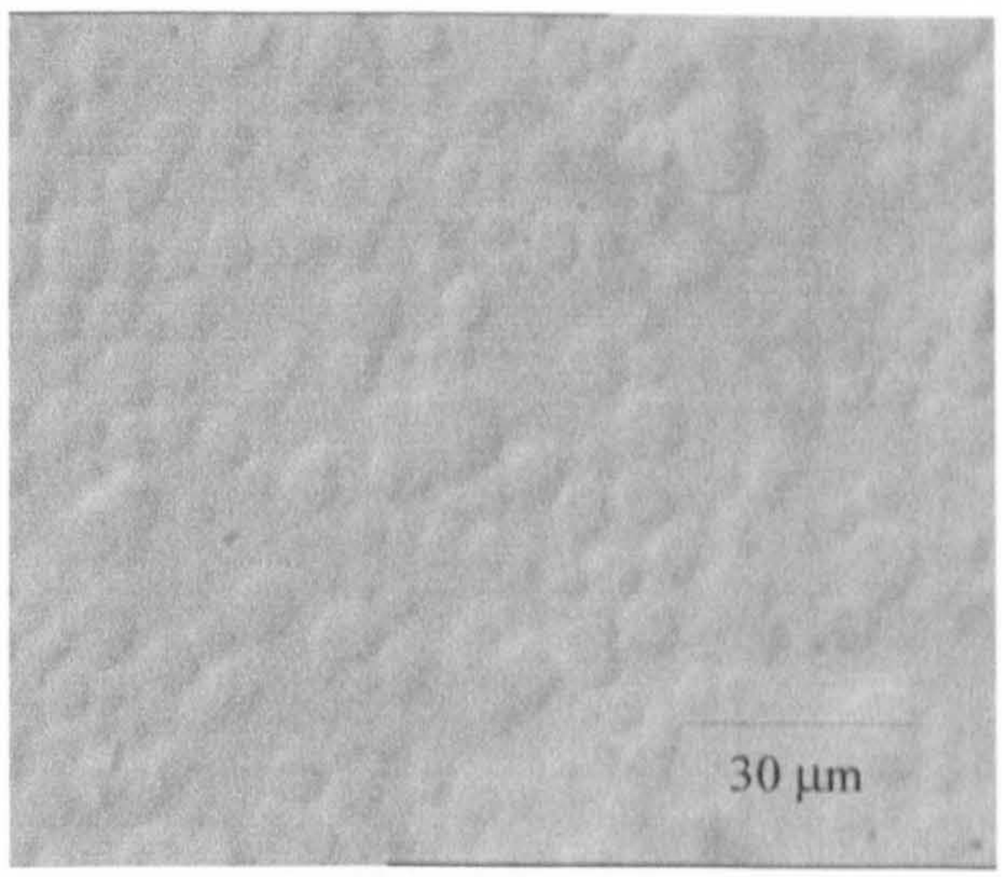

PLATE XIII 10^{-2} mol dm^{-3} NaCl: (a)3 mins, (b)60 mins, (c)120 mins, (d)180 mins

(a)

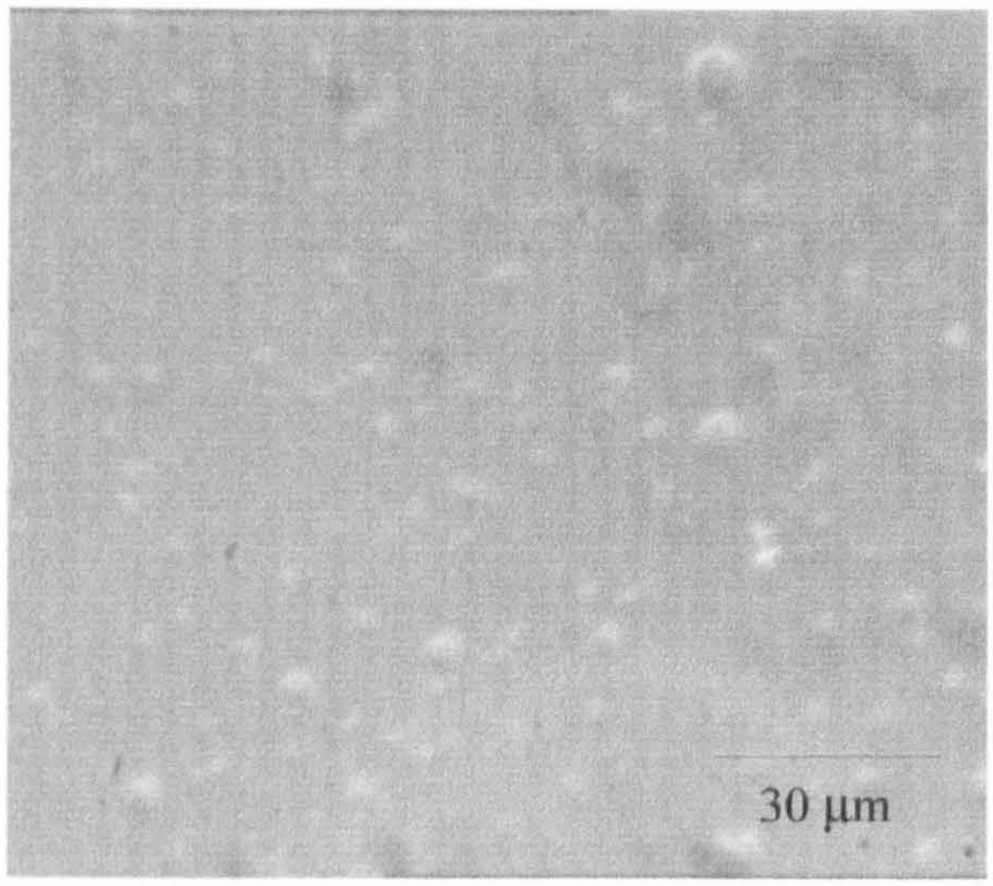

(b)

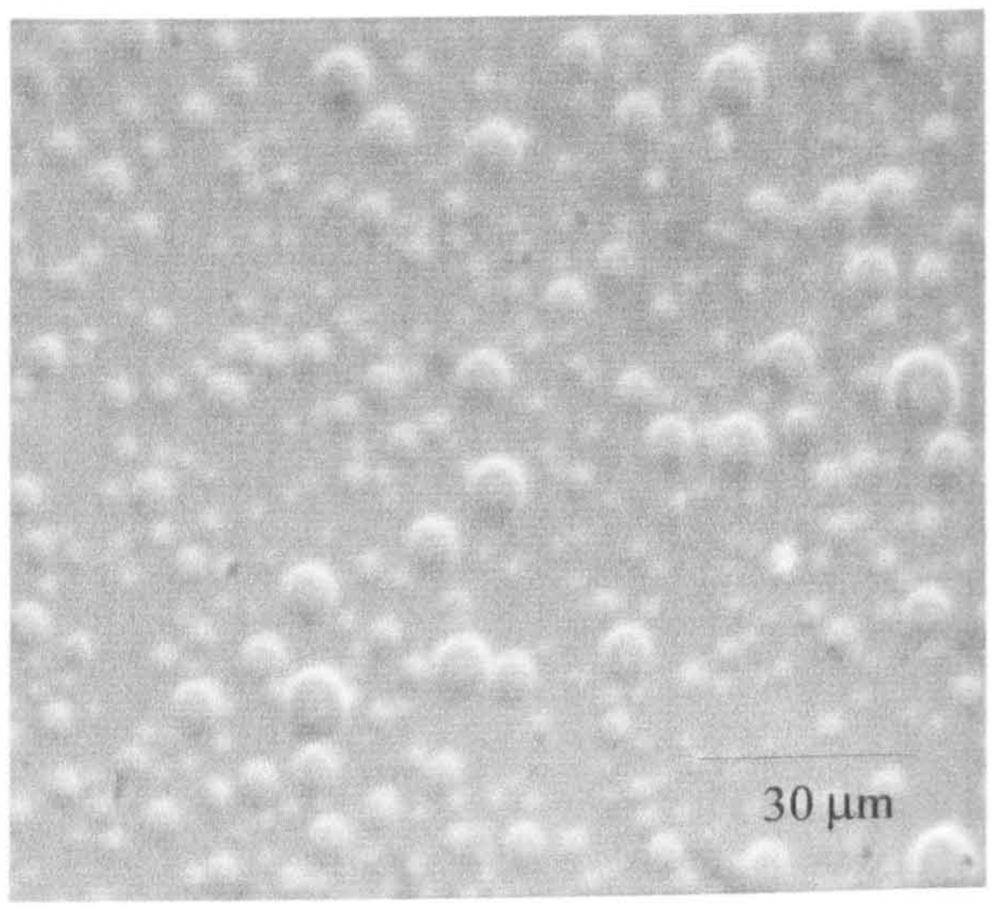

(c)

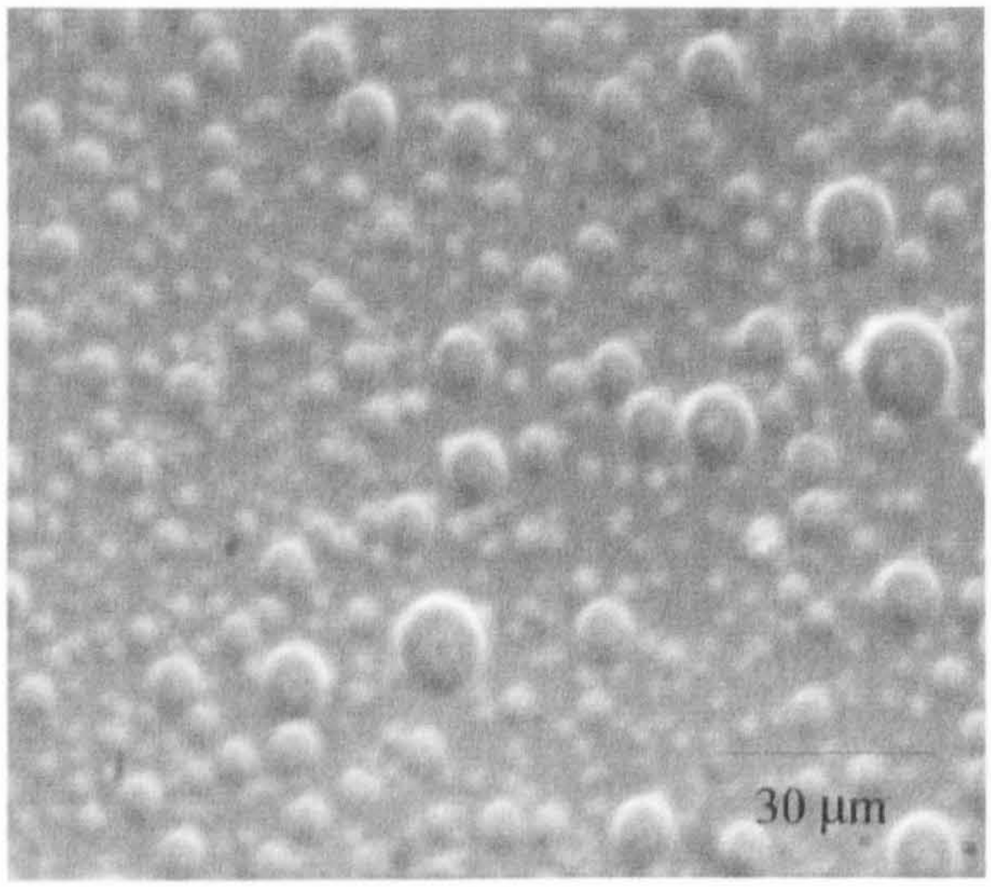

(d)

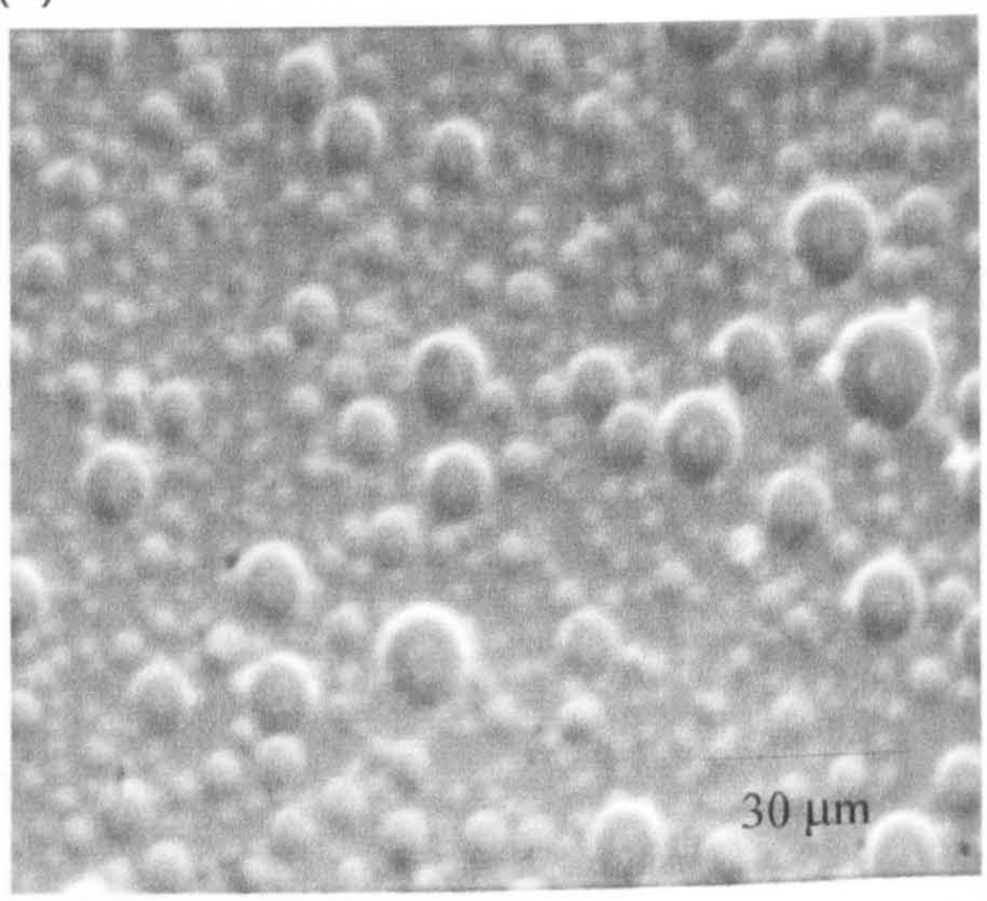

Plate XIV: 10^{-1} mol dm^{-3} [NaCl]: (a)3 mins, (b)60 mins, (c)120 mins, (d)180 mins

a)

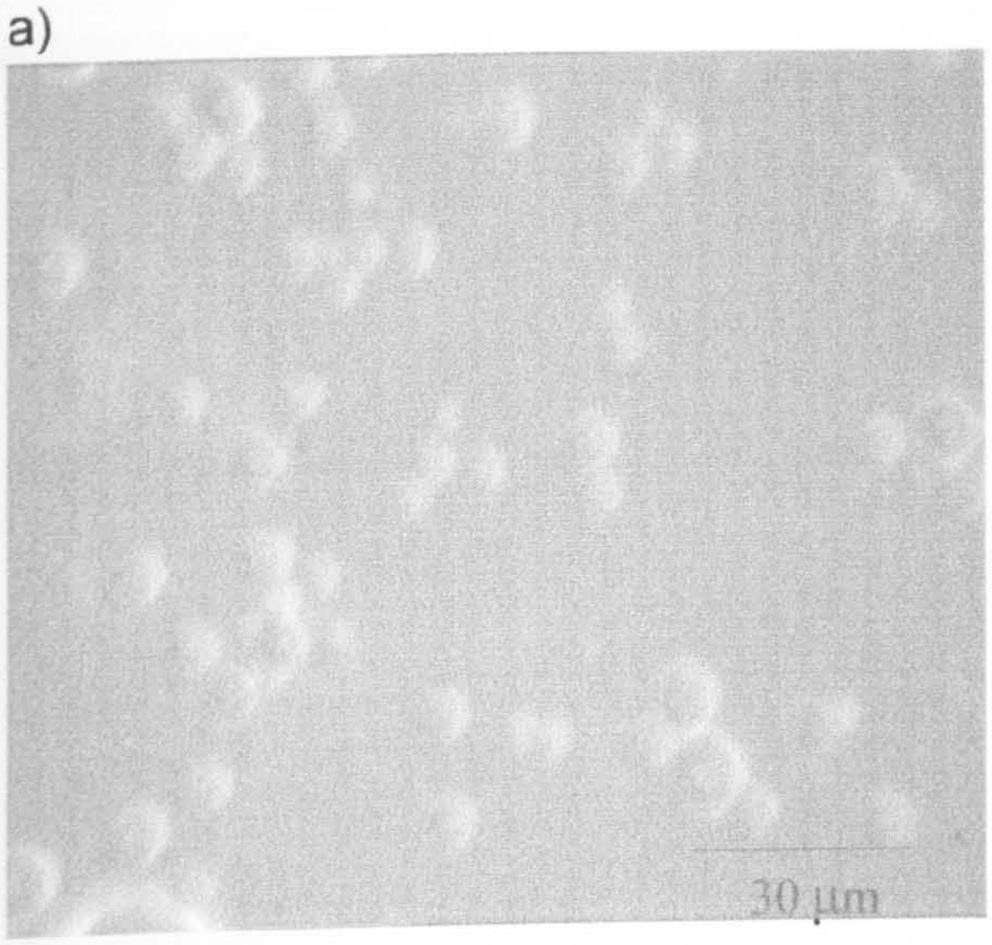

(b)

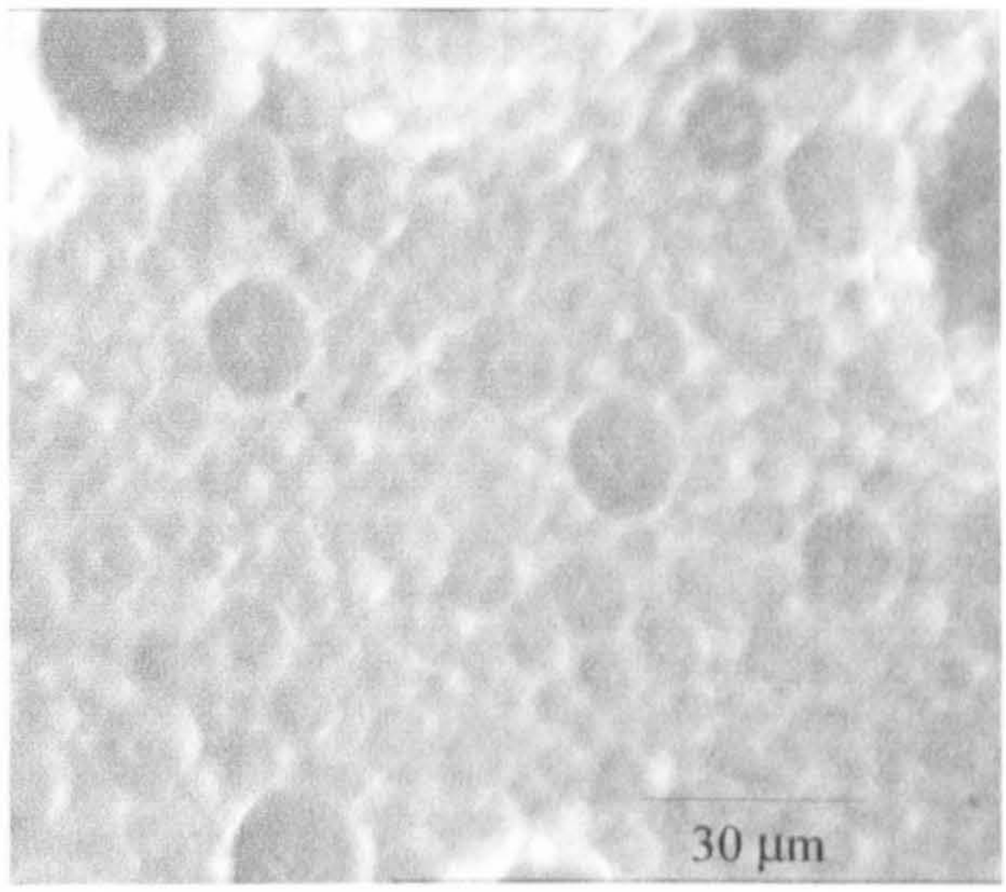

(c)

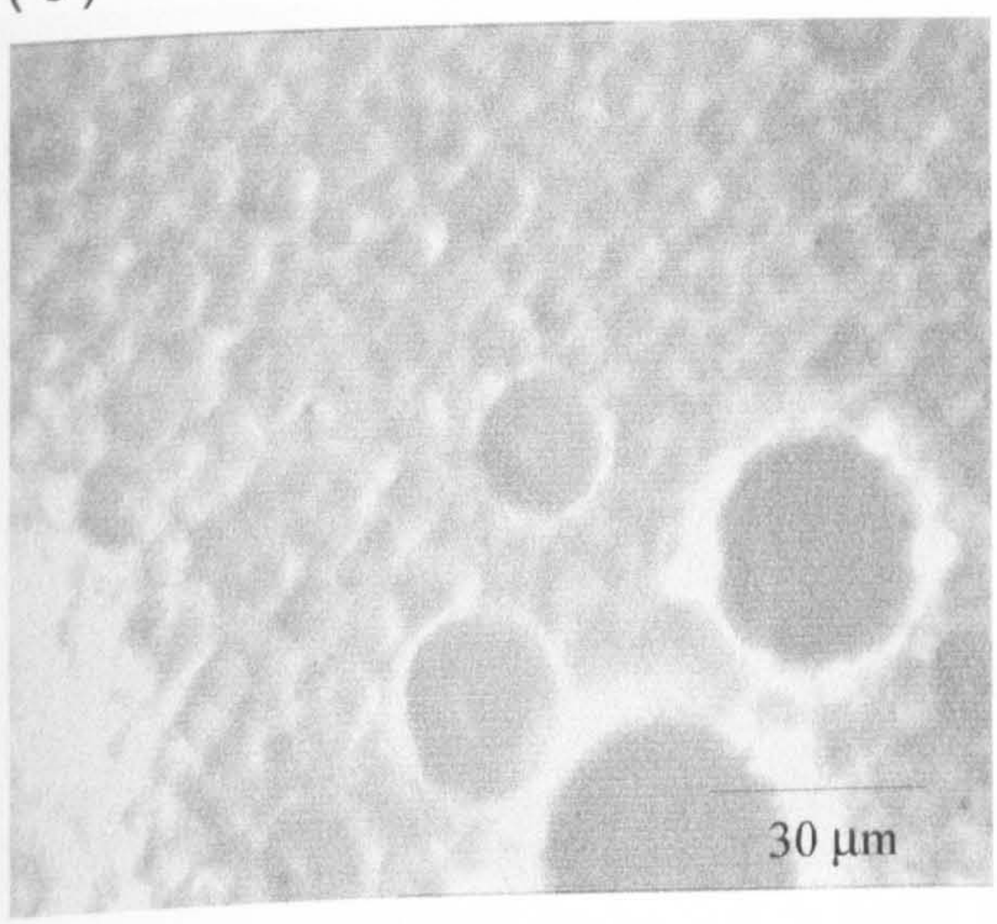

(d)

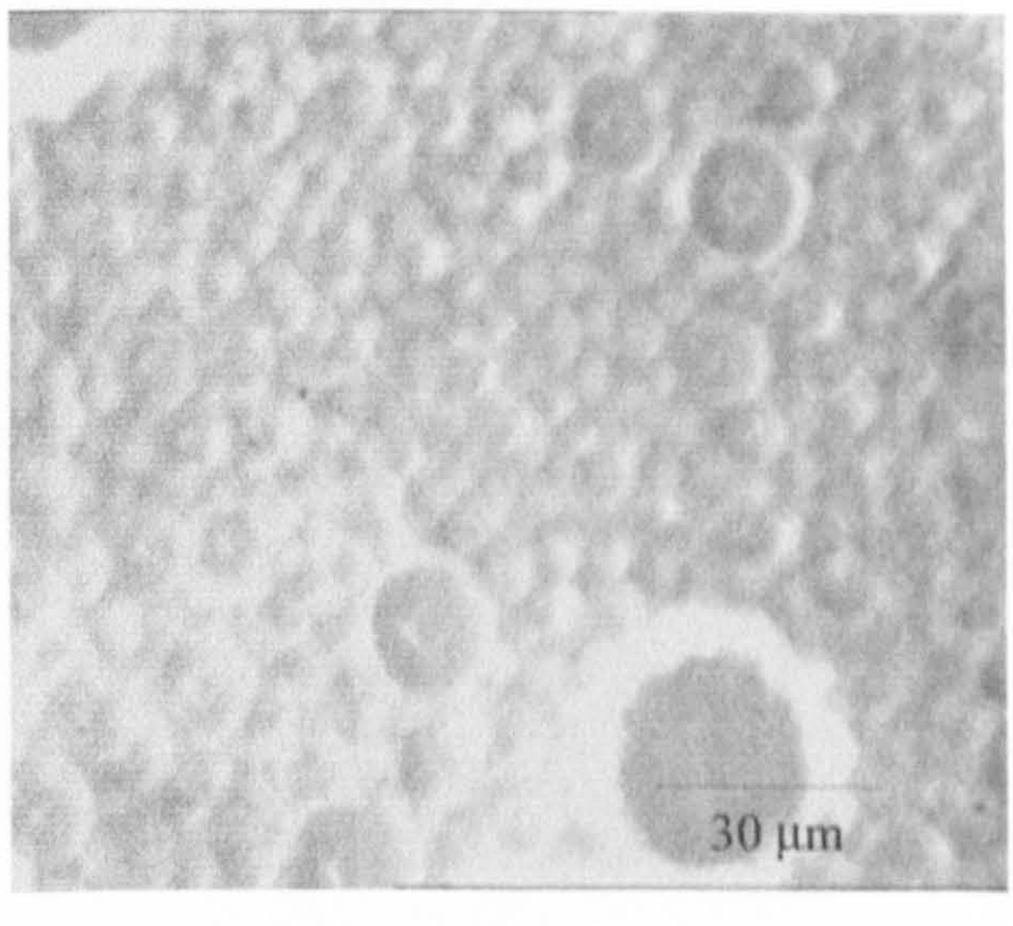

PLATE XV: $3x10^{-1}$ mol dm^{-3} [NaCl]: (a) 3 mins, (b) 60 mins, (c)120 mins, (d) 180 mins

(a)

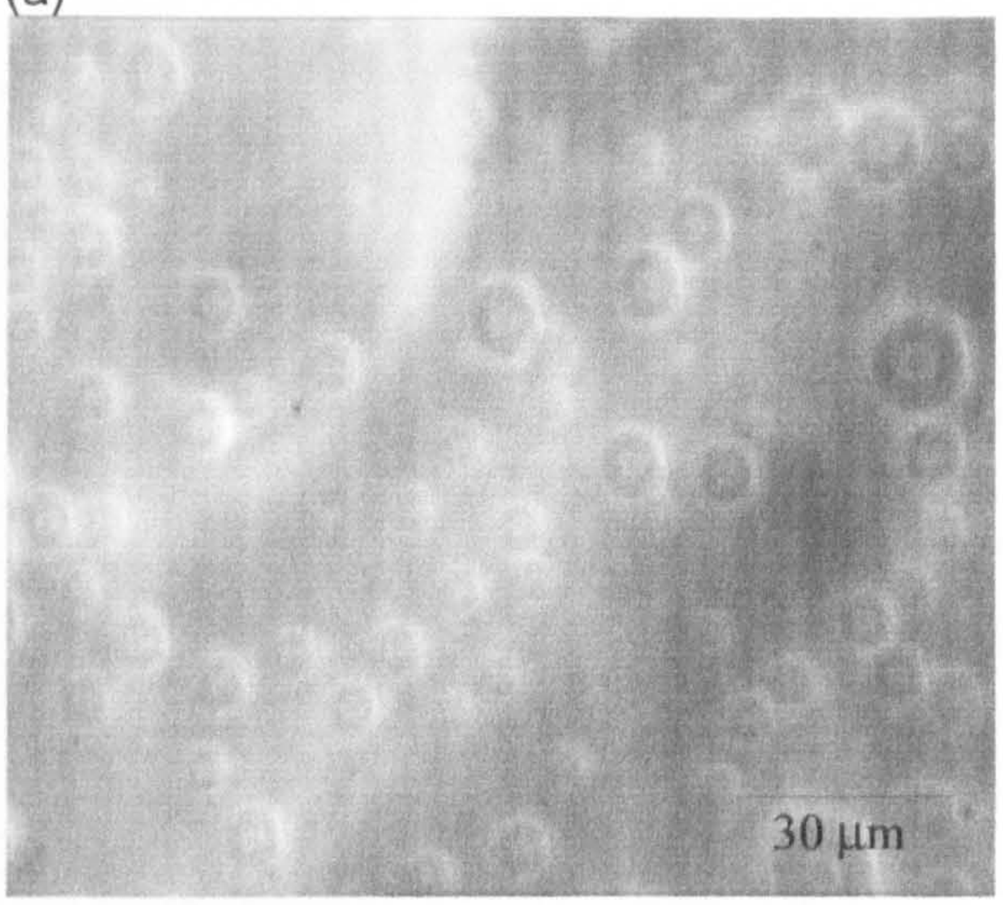

(b)

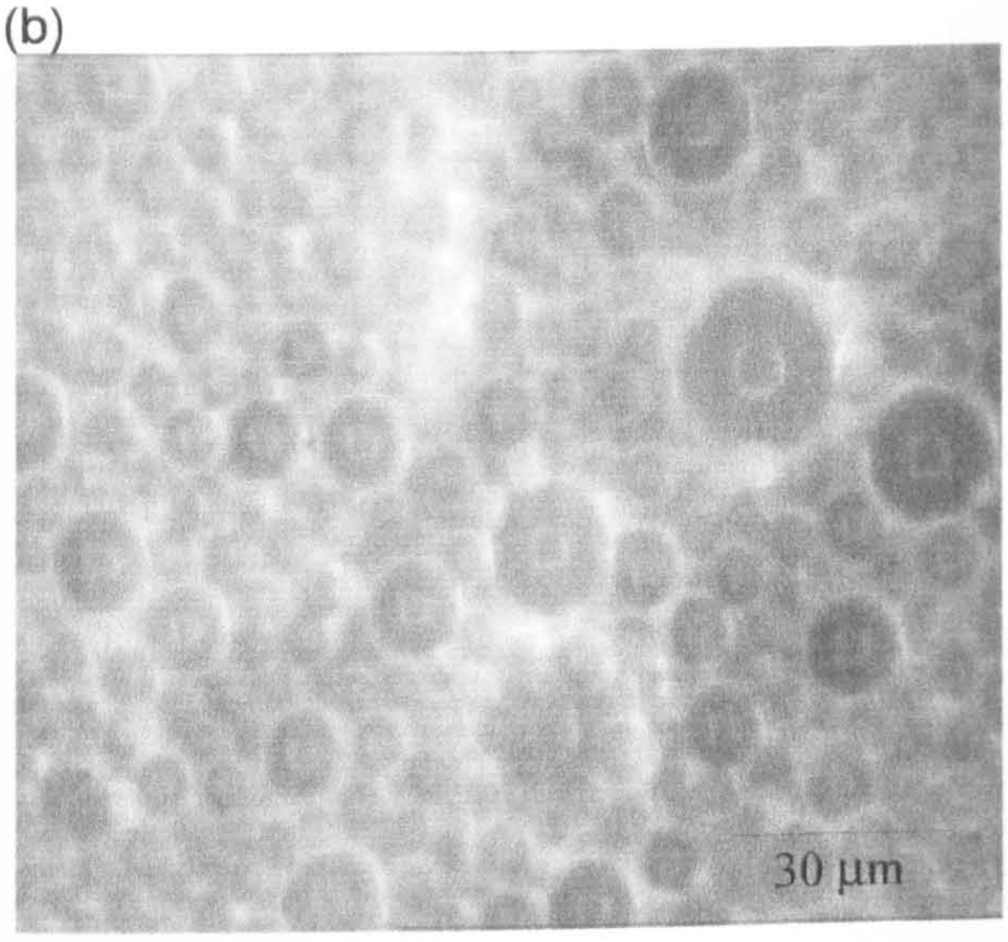

(c)

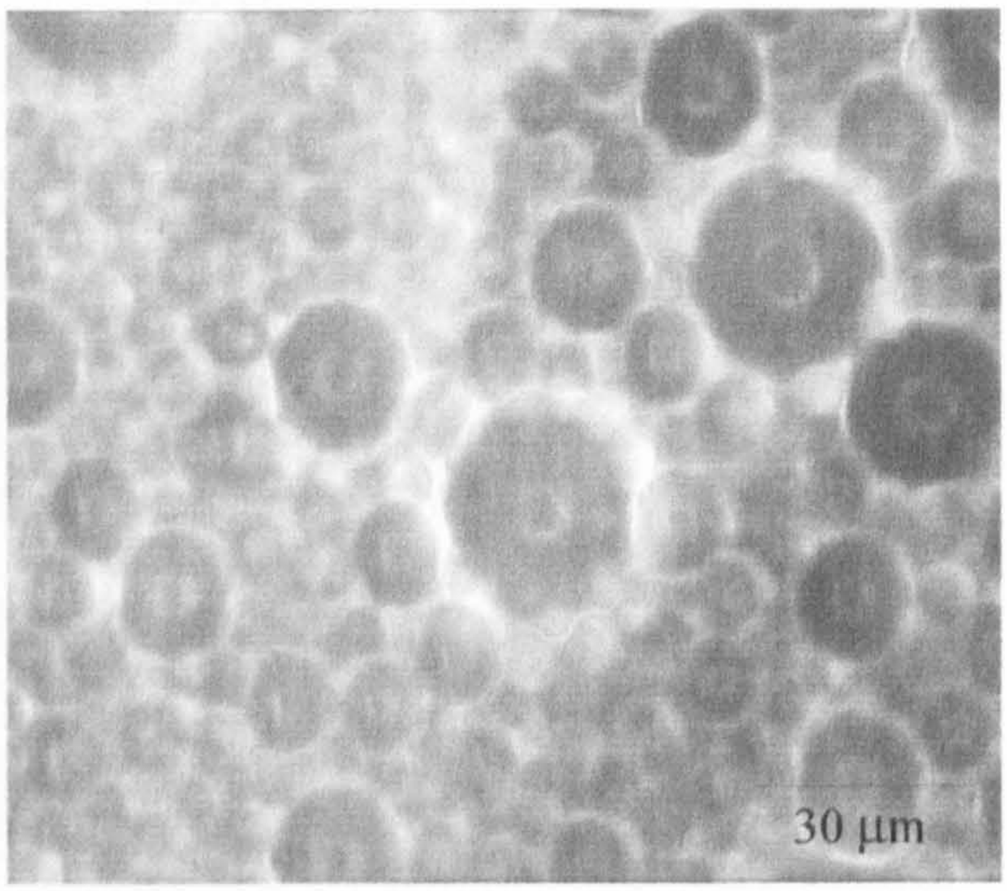

(d)

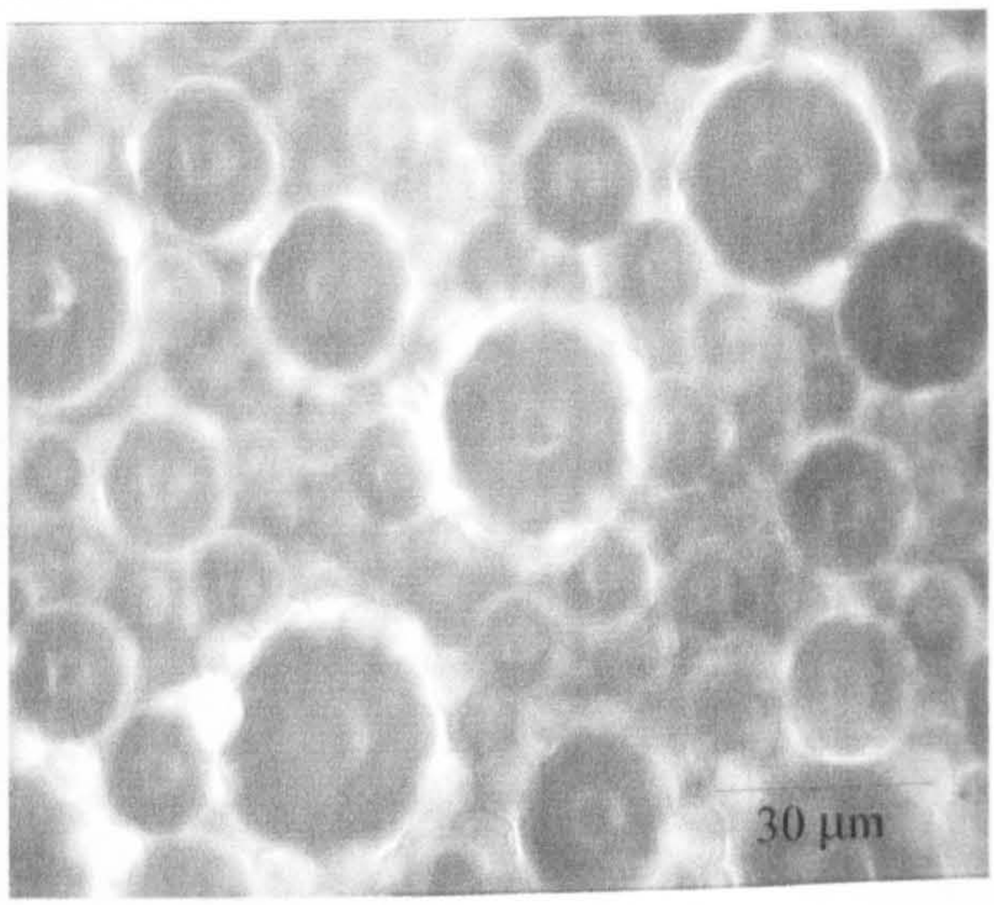

Table 9.3 Cross-linked PDMS emulsion parameters as a function of electrolyte

[NaCl] mol/dm^{-3}	D_{hyd} (μm)	ζ- potential (mv)	Mica ζ-potential (mV)
10^{-5}	1.6	-35.89	-4.26
10^{-4}	1.4	-29.89	-3.70
10^{-3}	2.4	-31.59	-3.36
10^{-2}	2.4	-27.06	-4.84
10^{-1}	3.1	-16.18	-18.19
$3x10^{-1}$	3.3	-5.68	-42.19

Below the CCC, (10^{-3} moldm^{-3}), the deposition images shown in plates X – XV, indicated there was no evidence of direct contact between the droplet and substrate surface the investigations. The presence of a stable aqueous film between the two surfaces, is in agreement with the observations reported by Mahé et al[7-9] who reported that the presence of [KCl] 10^{-3} mol dm^{-3} stabilised an aqueous film between a decane droplet and a substrate surface. It is interesting to note however, that even at these low electrolyte concentrations, some droplet-droplet coalescence could be observed for those droplets in close proximity to the substrate. This behaviour created irregular distribution patterns across the collector surface, which was not previously observed for similarly cross-linked PDMS droplets without the presence of electrolyte, see figure 9.5.

Above the CCC, >10^{-2} mol dm^{-3}, rapid film thinning was observed between the droplets and collector surface as they come into direct contact. An example of this behaviour is shown in figure 9.6, a detail from $3x10^{-1}$mol dm^{-3} , where the contact area was observed as a light coloured "ring" inside the image of the deposited droplet and was similar to that reported previously for cross-linked systems without the presence of electrolyte in section 9.2.1.

Figure 9.5 Evidence of aqueous film and droplet coalescence, detail from investigation using 10^{-4} mol dm^{-3} NaCl, 3hrs after deposition

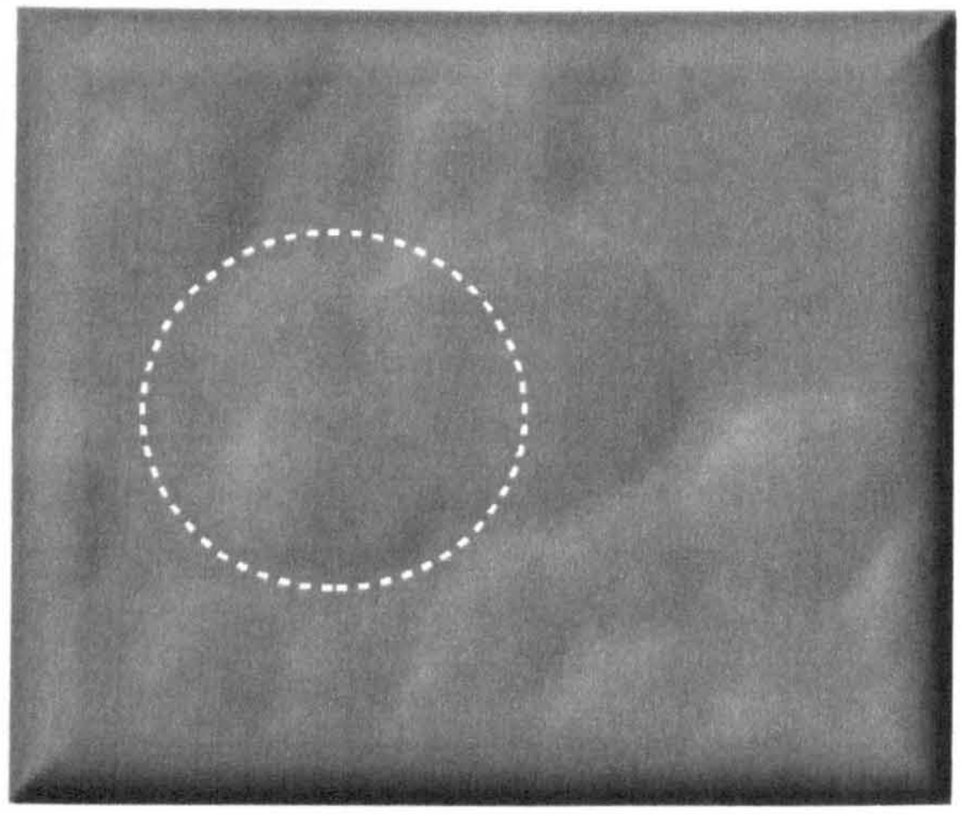

This behaviour was in agreement with that predicted by the calculated V_T profiles. It was shown that as the electrolyte concentration was increased, so the energy barrier on the close approach of two droplets, and also of a droplet with a substrate, decreased as a result of a reduction in electrolyte double layer of the droplet. A large primary maxima was observed at electrolyte concentrations just above the CCC, due to the dominance of electrostatic repulsive forces over van de Waals attractive forces. DLVO calculations predicted emulsion stability even at high electrolyte concentrations and therefore droplet-droplet coalescence was not observed for systems $>10^{-3}$ ml dm^{-3} and the droplet shape was maintained after deposition.

The derived coating density profiles in the presence of electrolyte were presented in figure 9.7 (a-f) as a function of time and the data is listed in table 9.4. All the deposition studies showed an increase in derived coating densities, θ.

Figure 9.6 Evidence direct contact between cross-linked PDMS droplet and mica surface 2hrs after initial deposition using $3x10^{-1}$ mol dm^{-3}

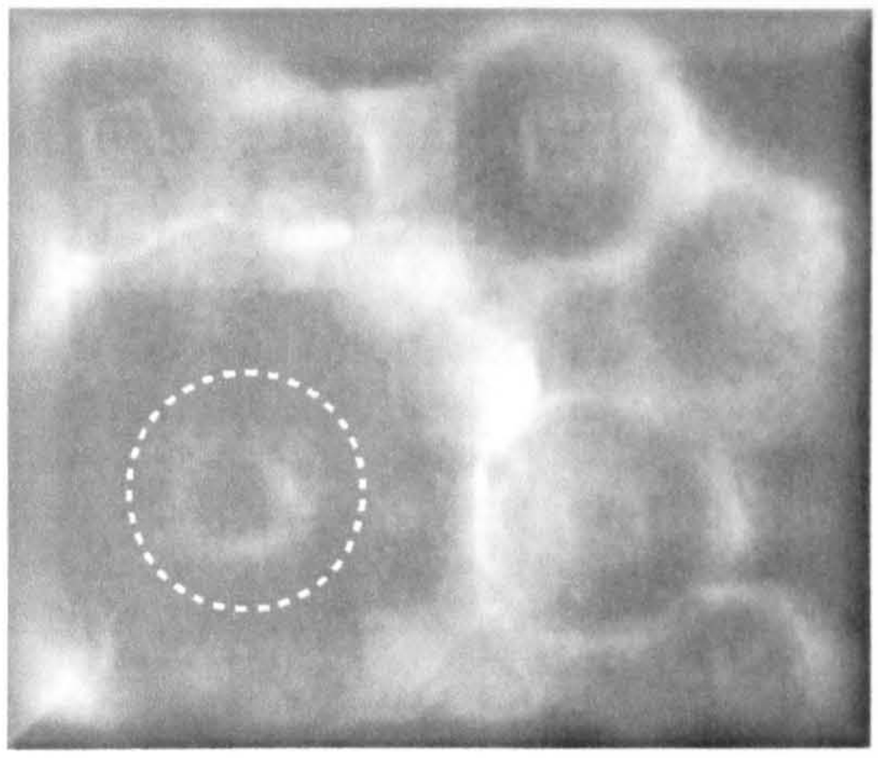

However the magnitude of the equilibrium deposition coverage and the time taken to reach the *Spl* plateau differed from what was observed without the presence of NaCl. The deposition investigations performed at low NaCl concentrations, $<10^{-2}$ mol dm^{-3}, reached a plateau coating density value, θ, lower than that observed in section 9.2.1, which took 10-70 mins longer for the same number of droplets to deposit. This behaviour corresponds to the slight decrease in droplet surface charge negativity, while the mica surface charge remains almost constant.

Table 9.4 Comparison of deposition profiles rates, Spl^{1} as a function of electrolyte

[NaCl] mol dm^{-3}	Spl_{Nd}	t_{Spl} (mins)	θ_{max}	K_d / s^{-1}	R^2	% max. surface cov.
10^{-5}	383	160	0.38	$5.2x10^{-4}$	0.97	13.2%
10^{-4}	512	140	0.81	$5.3x10^{-4}$	0.97	47.6%
10^{-3}	587	100	0.72	$4.1x10^{-4}$	0.96	68.3%
10^{-2}	*265	*180	*0.85	*$3.6x10^{-4}$	*0.94	*83.1%
10^{-1}	368	41	1.00	$7.0x10^{-4}$	0.86	99.4%
$3x10^{-1}$	231	55	1.00	$1.0x10^{-3}$	0.97	100.0%

* Spl plateau not reached after 3hrs

As the presence of electrolyte was increased above the CCC, $>10^{-3}$ mol dm^{-3}, the droplet-collector attractive forces were increased. This was observed to dominate over the lateral droplet-droplet repulsive forces, as the EDL thickness, (1/k), decreased and the range of interactions was reduced. The reduction in lateral repulsion forces during deposition was evident in the simultaneous droplet-droplet coalescence of the flow solution and subsequent droplet spread on the collector surface.

Those deposition investigations performed near the CCC, 10^{-2} $<10^{-3}$ mol dm^{-3}, showed a deposition rate, and derived a coverage similar to that observed without the presence of electrolyte. However, the almost linear deposition failed to reach an equilibrium value after 3 hours indicating that, close to the CCC region, the normal van de Waals attractive forces between the droplets and collector surface dominate over the lateral droplet-droplet repulsive forces.

Above the CCC, $>10^{-3}$ mol dm^{-3}, the deposition became increasingly rapid with an equilibrium value obtained at a rate in the order of magnitude faster than that observed without electrolyte. The smaller droplet deposition number and the high packing order observed across the collector surface was a direct result of the increase in droplet diameter in the bulk solution, together with the decrease in mica surface potential. The investigations performed at these electrolyte concentrations showed the most significant droplet spreading behaviour on the collector surface and corresponded to some of the highest force of adhesion values measured in chapter 10.

Fig 9.7 Deposition profiles as a function of [NaCl] on Mica substrate; (a) 10^{-5} mol dm^{-3}, (b) 10^{-4} mol dm^{-3}, (c) 10^{-3}mol dm^{-3}, (d) 10^{-2} mol dm^{-3}, (e) 10^{-1} mol dm^{-3}, (f) $3x10^{-1}$ mol dm^{-3}

(a)

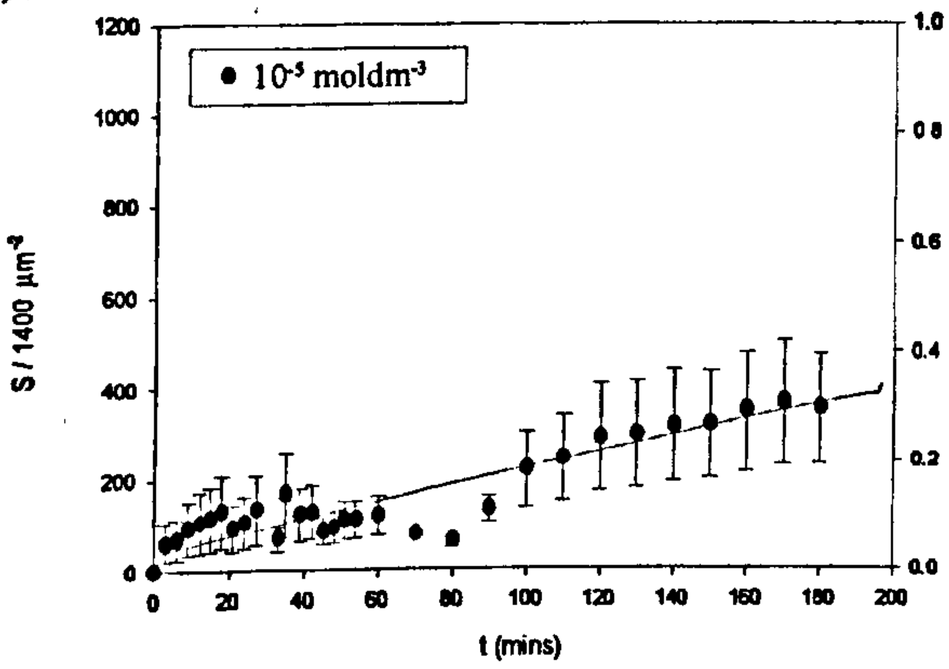

(b)

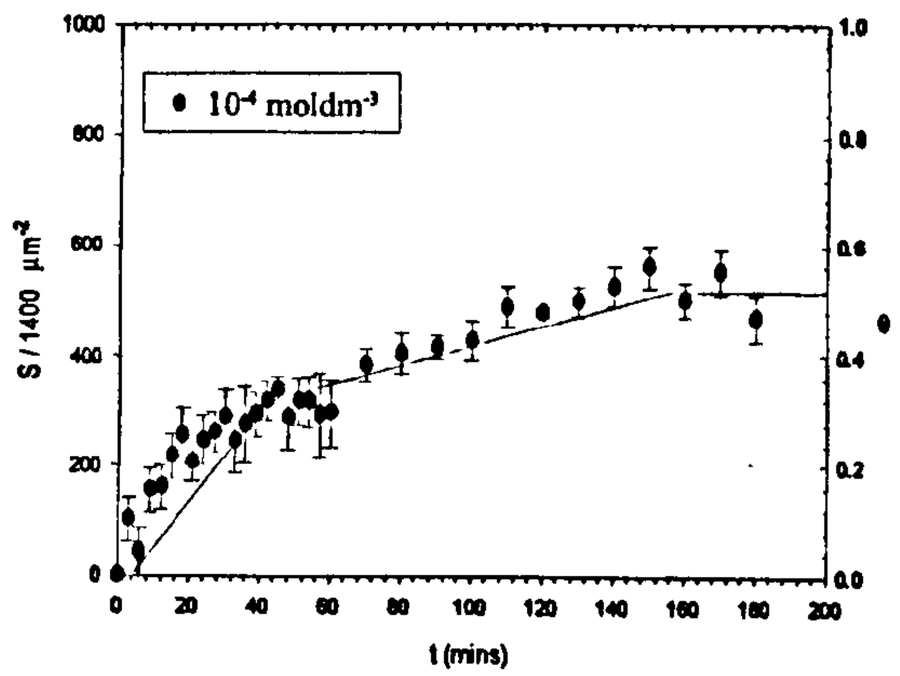

(c)

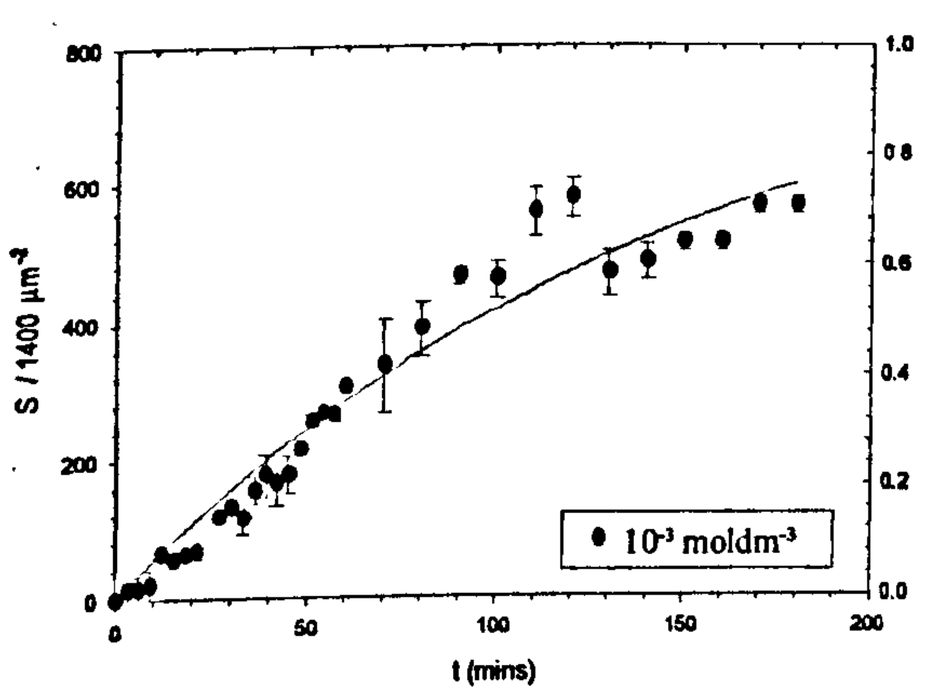

(d)

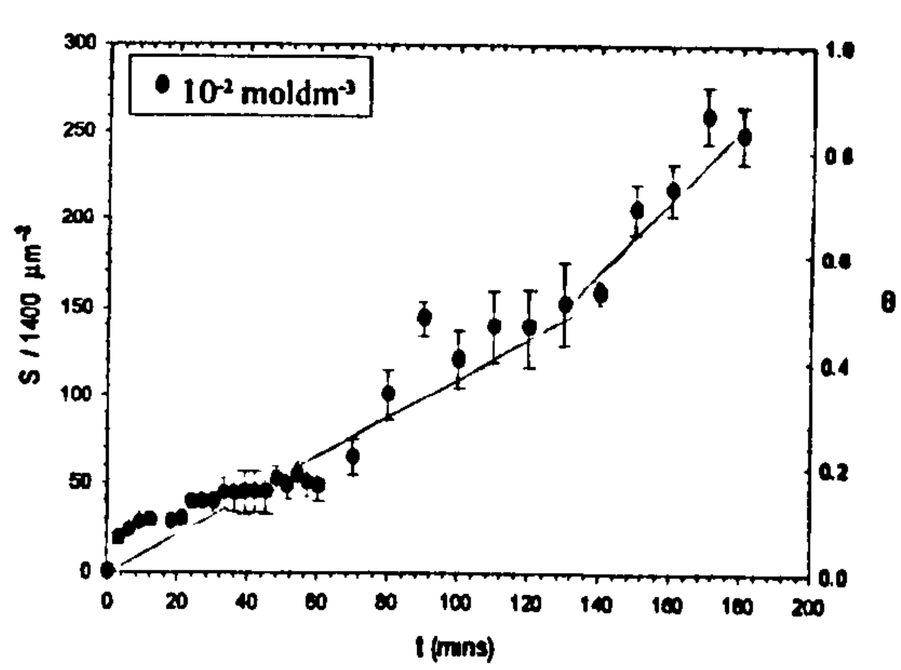

(e)

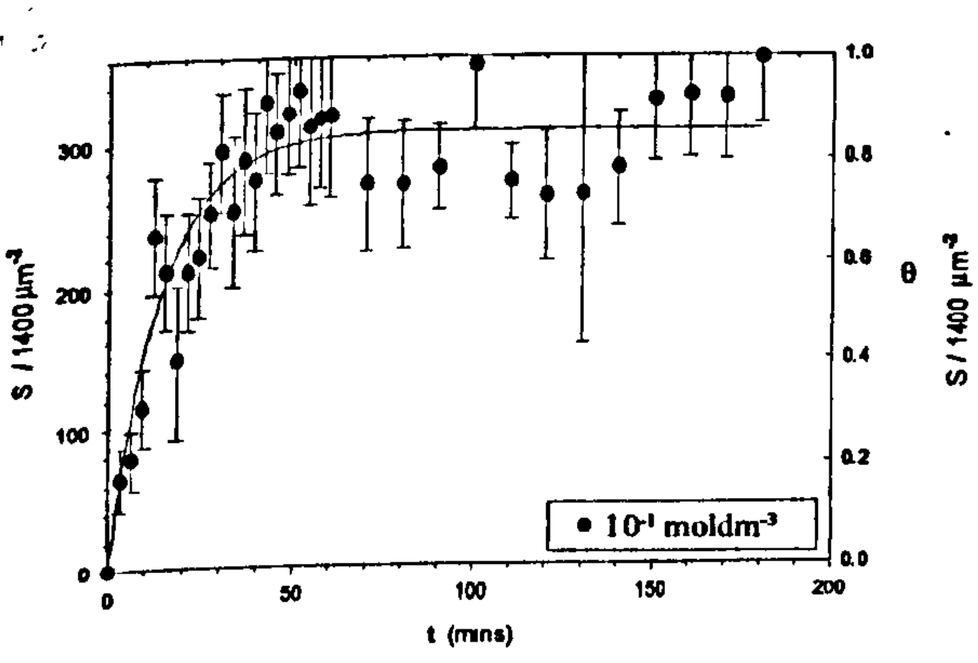

(f)

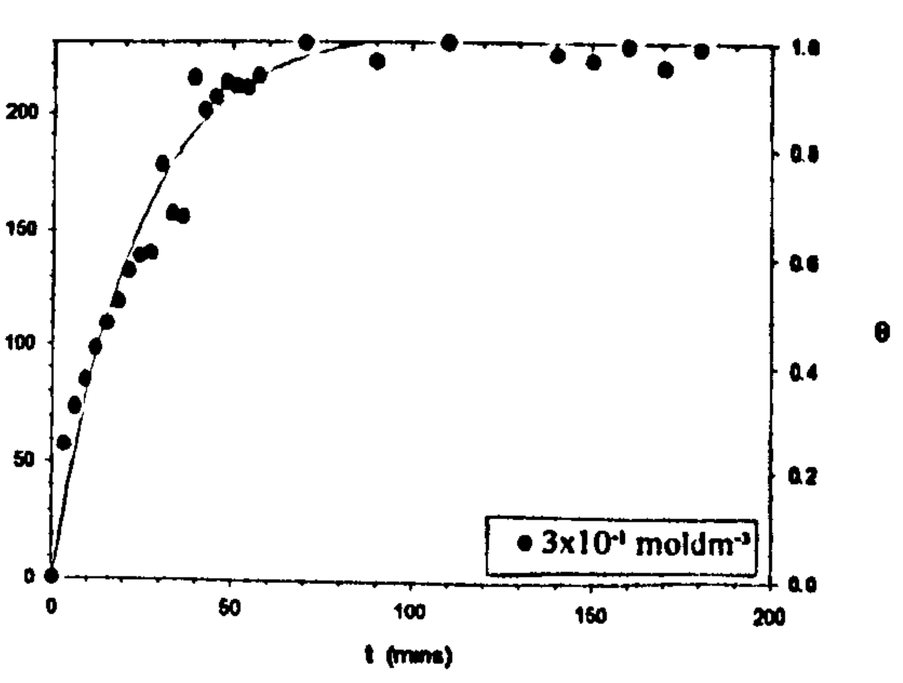

Table 9.4 illustrates how the % coverage dramatically increased with increasing electrolyte concentration, even though fewer droplets deposited compared with those experiments without the presence of electrolyte. A clear transition could be observed between low surface coverage systems, <50% that occur below CCC $<10^{-3}$ mol dm^{-3}, and the high surface coverage deposition, >70% that is displayed by those systems $>10^{-2}$ mol dm^{-3}. It is interesting to note that as electrolyte concentration is increased above 10^{-2} mol dm^{-3} droplet structural integrity is maintained even after deposition.

The average contact area spread for droplets deposited in the presence of electrolyte is presented in figure 9.8. It was observed that those deposition regimes that contained $10^{-5} > 10^{-3}$ mol dm^{-3} displayed almost no droplet spread after contact with the collector surface, with an average contact area, similar to that observed for 0.05(v/v) MTMS systems without electrolyte, 18.5μm^2 (+/- 6.0). As the NaCl concentration exceeded the CCC, the droplet spread became more significant even on initial contact with the substrate. Deposition regimes containing between 10^{-2} moldm^{-3} and $3x10^{-1}$ moldm^{-3} displayed initial contact areas twice or even three times that measured without electrolyte. This feature increased to almost five times the initial contact area, after 3 hours deposition, for the highest NaCl concentration investigated.

This observation corresponded to the simultaneous swell in droplet size and decrease in droplet surface charge negativity as discussed in chapter 5, while the decrease in EDL thickness allowed the droplets and substrate to come into contact. Irrespective of the direct contact between the two surfaces, the deposited droplets were observed to "slip" across the observation area.

Fig 9.8 Droplet-substrate contact area spread as a function of NaCl concentration

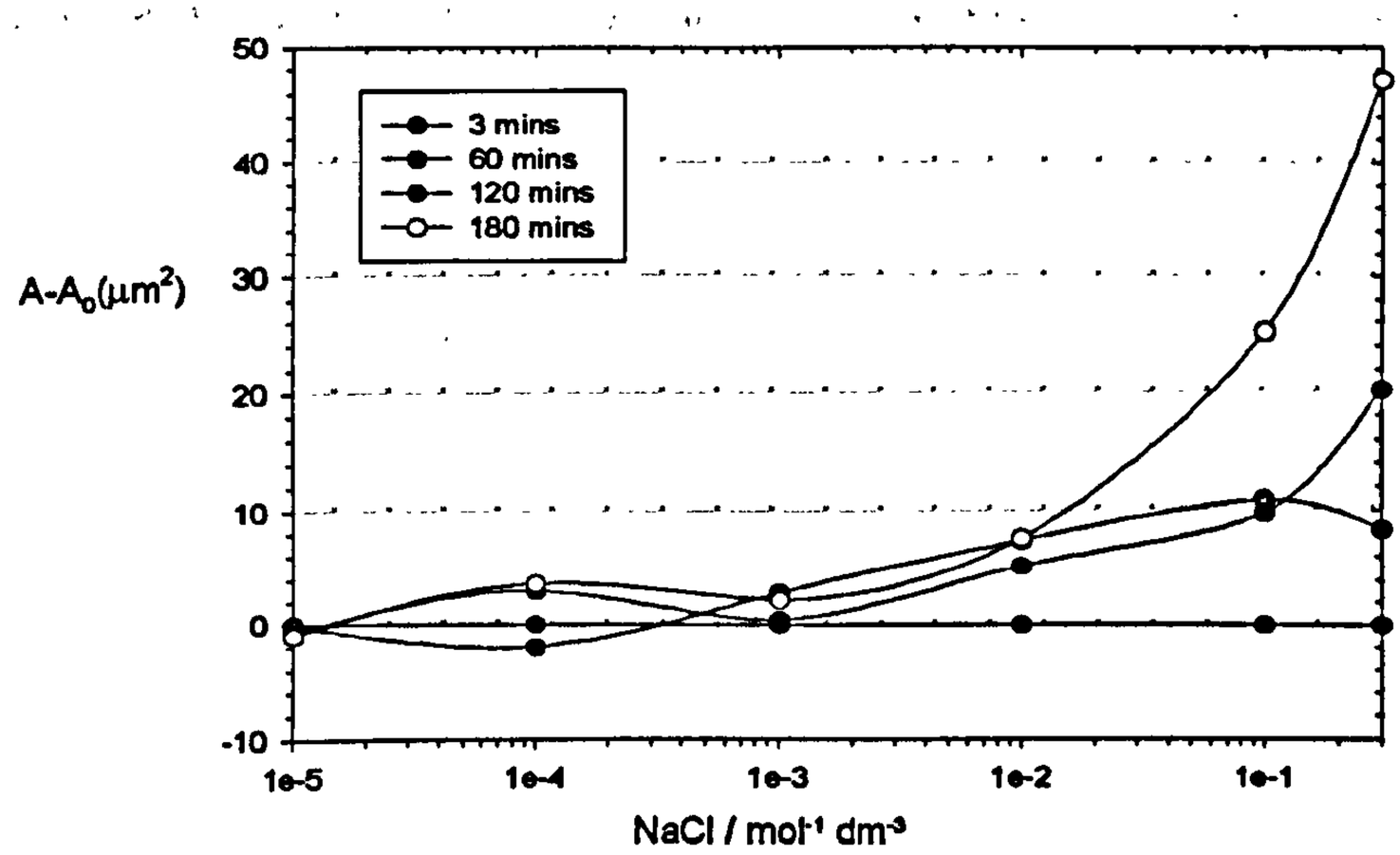

This could be attributed to the force exerted by the high number of depositing droplets on the already densely packed deposited droplets and the low frictional force present on the substrate surface.

Figure 9.9 (a-c) showed that all of the depositing fixed cross-linked systems containing electrolyte showed that the droplets adopted a random distribution across the observed area of the mica surface. However, the solutions with an electrolyte concentration >10^{-3} mol dm^{-3} showed that the normal inter-droplet repulsive forces were overcome almost immediately on contact with the substrate due to the accelerated droplet spreading behaviour. The average relative location of the deposited droplets on the substrate is presented as the partial radial distribution function, g(r), as a function of the distance from the stagnation point. The highest distribution peaks occurred on initial deposition, but there was no discernible trend. However, it was interesting to note that those systems investigated close to the CCC, 10^{-3} – 10^{-2} mol dm^{-3}, displayed the lowest and

Fig 9.9 Comparison of the radial distribution functions of cross-linked PDMS droplets on mica for varying [NaCl] after; (a) 3 mins, (b) 60 mins, (c) 180 mins,

(a)

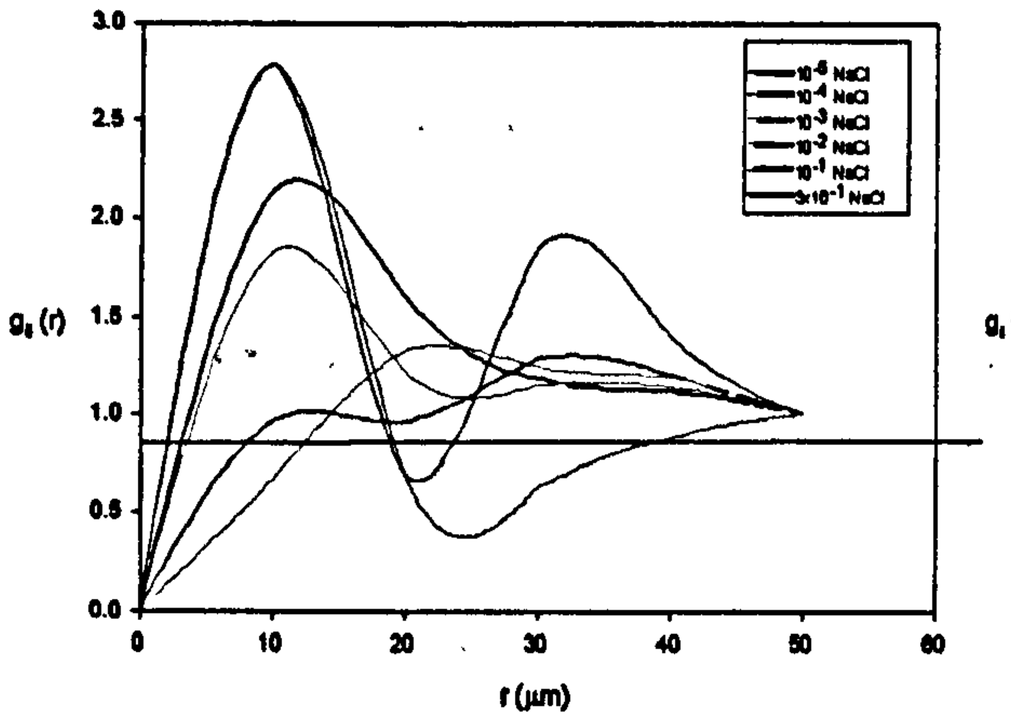

(b)

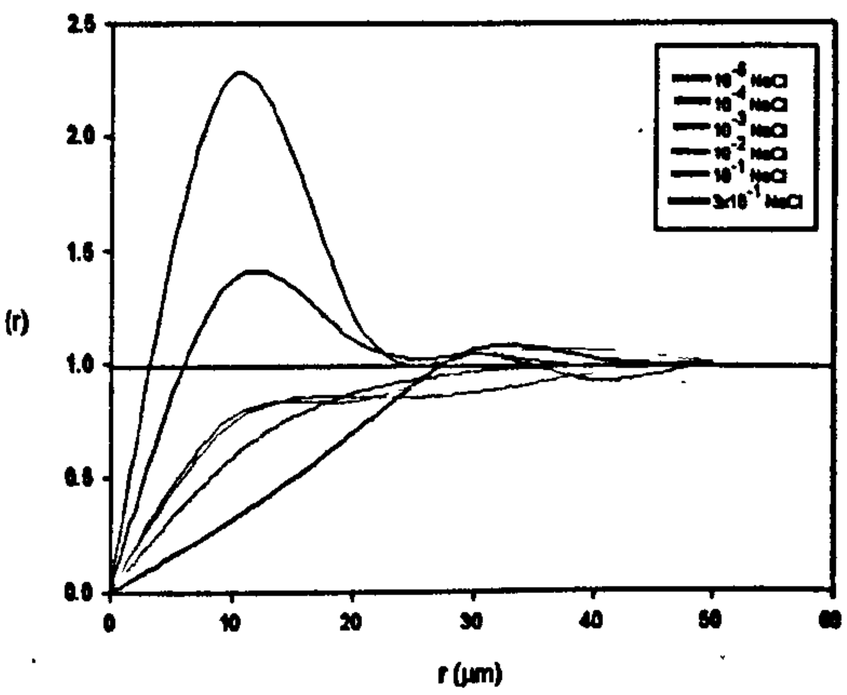

(C)

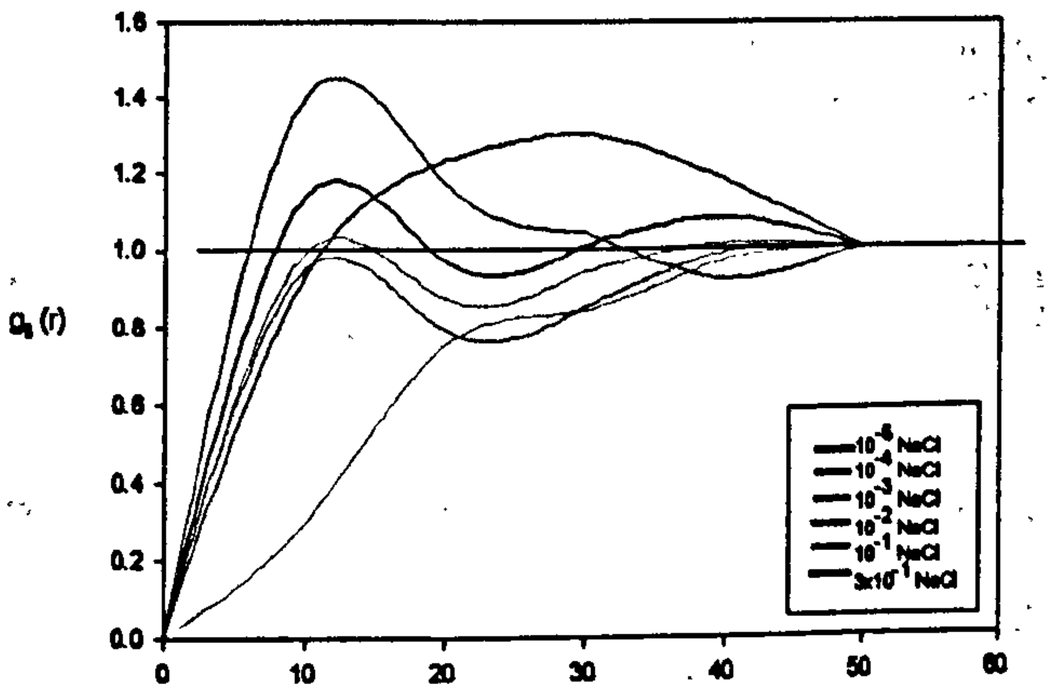

broadest peak height which corresponded to the high deposition coverage on initial contact with the substrate.

As the deposition time increased, the distribution peak height decreased with increasing electrolyte concentration. This trend was exaggerated as the presence of electrolyte increased. Above 10^{-3} mol dm^{-3}, there was no discernible distribution peak and the g(r) value became closer to unity. This behaviour corresponded to the increase in droplet spread on contact with the substrate, which in turn ensured the droplets became densely packed and evenly distributed across the entire collector surface.

9.5 Deposition as a function of SDS surfactant concentration on mica

The same experimental procedure described in section 9.2.1 was used to investigate the influence of anionic surfactant, SDS, on the deposition of PDMS droplets at fixed 0.05(v/v) MTMS on a mica substrate. The parameters of the emulsion and substrate used in the investigations, as previously discussed in chapter 5, are listed in table 9.6.

Table 9.5 Cross-linked PDMS emulsion parameters in the presence of SDS

[SDS] (mM)	D_{hyd} (μm)	ζ- potential (mv)	Mobility (μ/s)/(V/cm)	Mica ζ-potential (mV)
0.08	1.9	-37.9	-2.96	-0.7 (+/-0.05)
0.80	1.6	-34.2	-2.67	-0.9 (+/-0.05)
8.00	0.6	-34.2	-2.67	-1.2 (+/-0.54)

Predictions from calculated V_T profiles indicated that the adsorption of SDS molecules onto the droplet surfaces stabilised the emulsion. This mechanism also prevented the fast deposition of the droplets on to a substrate surface, as the presence of the surfactant prevented the two surfaces from coming into close proximity. In addition, the van der Waal's attractive forces and electrostatic forces would be modified by the polymer chains via a loss of configurational entropy. This in turn produced a greater repulsive effect between the charged surfaces. The relatively low SDS coverage created additional attractive effects. These effects included the interaction of surfactant molecules between the two surfaces and the displacement of solvent from the interfacial region to the bulk as the separation distance between the droplet and substrate decreased. In general, the adsorption of surfactant displaced the plane of shear from the surface by a distance of the SDS surfactant layer thickness (δ), creating a barrier against the two surfaces touching which increased with increasing SDS concentration.

The influence of the anionic surfactant on the system appeared to equilibrate below the cmc, 8.0mM. This was indicated in the fact that although the average hydrodynamic droplet diameter almost trebled in size, the surface charge remained fairly constant over the range of SDS concentration. There was a simultaneous electrostatically induced adsorption of SDS molecules at the mica surface. This increased the negativity of the substrate streaming potential from -0.6mV to -1.2mV, as the mica surface adopted the charge of the micelle surface in bulk solution phase[11,12] and reached an optimum surface adsorption structure.

Fa et al[13] suggested that the electrostatic attraction between an hydrophobic substrate and the SDS head group dictated the packing arrangement of the

surfactant at the surface. At low presence, <0.08mM, it was suggested that surfactant tails adsorbed onto the surface via hydrophobic interactions, see figure 9.10(a). As more SDS was introduced, < 0.8mM, the polymer chains were reported to reverse the position as the polar heads faced the surrounding aqueous solvent, (b) and bilayers built up at the surface as the hydrophobic tails associated to minimise water contact[14].

Figure 9.10 Surfactant packing arrangement on an hydrophobic surface; (a) low concentration, (b) moderate concentration, (c) high concentration

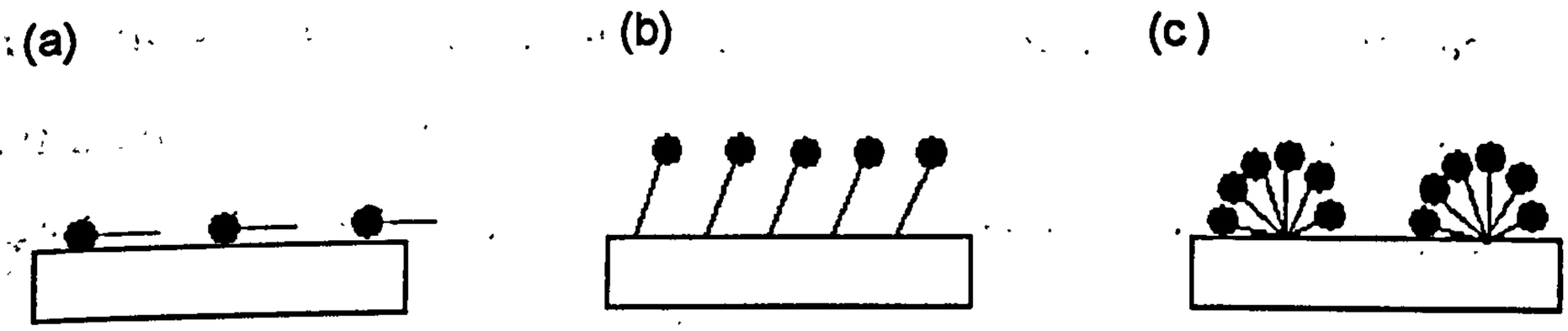

At high SDS levels, close to or above the cmc, >8.0mM, the surfactant chains form a "hemi-micellar" and semi-cylindrical structures are adopted at the substrate surface, (c). Fa et al[13] went further to suggest that formation anionic surfactant structures on a slightly negative surface was due to a combination of hydrophobic attraction and VDW forces, in which the hydrophobic alkyl chains had a more dominant influence on micelle formation than the electrostatic interaction.

It has been assumed in this study that there is sufficient ζ-potential difference between the droplet and substrate to allow normal VDW attraction forces to exist. In addition once the droplet surface is saturated with the surfactant molecules it adopts a more rigid shell and the wetting property is significantly reduced.

The deposition images obtained from systems with SDS concentrations between 0.08mm – 8.0mm are displayed in plates XVI – XVIII. All the systems investigated showed that the droplets deposited individually, without coalescence, and evenly across the collector surface. During the deposition process, the droplets were observed to rapidly overcome the electrostatic repulsive forces and the inter-droplet separation distance was reduced to a minimum as they became densely packed.

Droplets deposited from systems containing < 0.08mM SDS, were observed to deform and undergo rapid film thinning as they came into close proximity with the collector surface. Evidence of direct contact between the two surfaces is shown in figure 9.11, and is shown to be similar to that observed for systems containing < 0.01(v/v) MTMS and > 10^{-2} mol dm^{-3} NaCl described previously in sections 9.2.1 and 9.2.2 respectively.

Figure 9.11 Evidence of direct contact between cross-linked PDMS droplet and mica surface in the presence of SDS 0.08mM, 2hrs after initial deposition

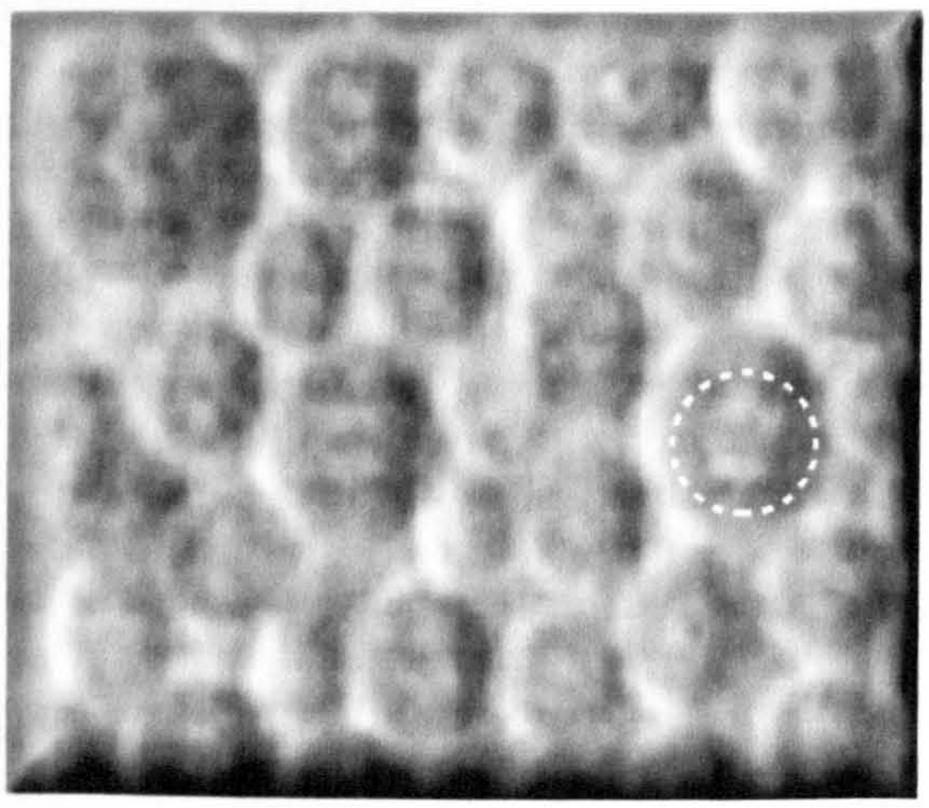

Evidence of direct contact between droplet and substrate indicated by a broken line (- - - - - - - - - - -)

PLATE XVI: 0.08mM SDS; (a) 3 mins, (b) 60 mins, (c) 120 mins, (d) 180 mins

(a)

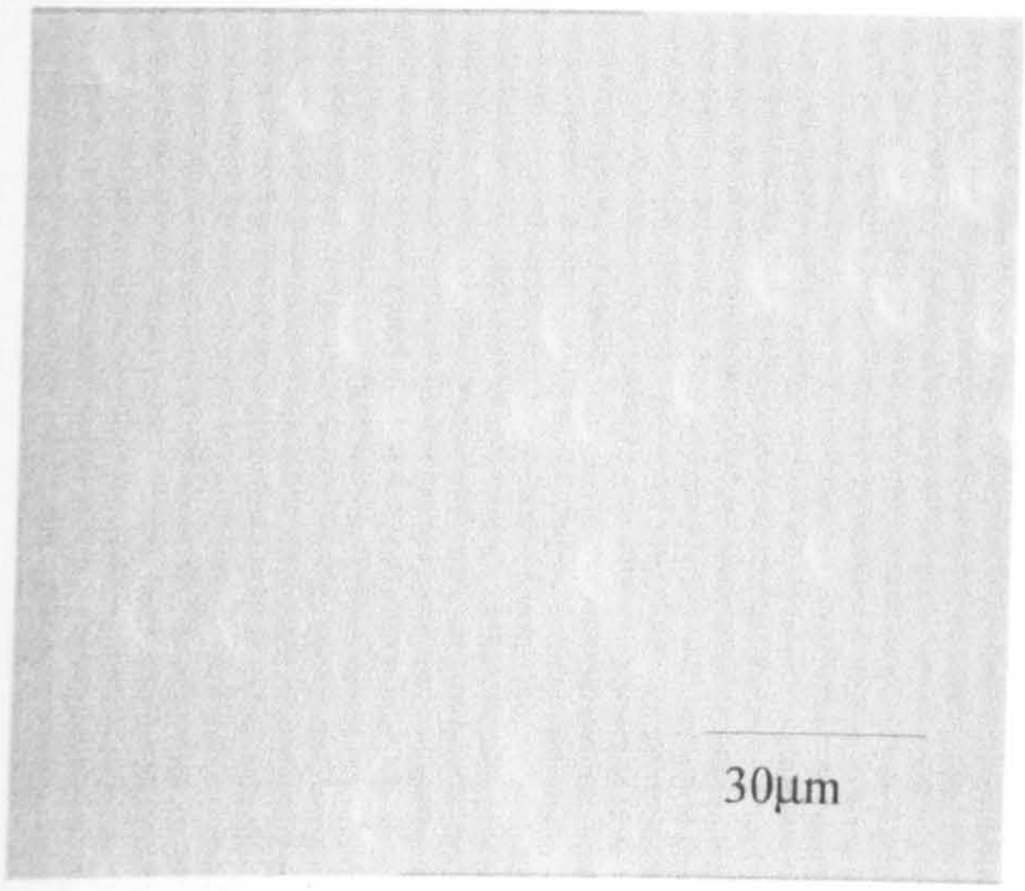

(b)

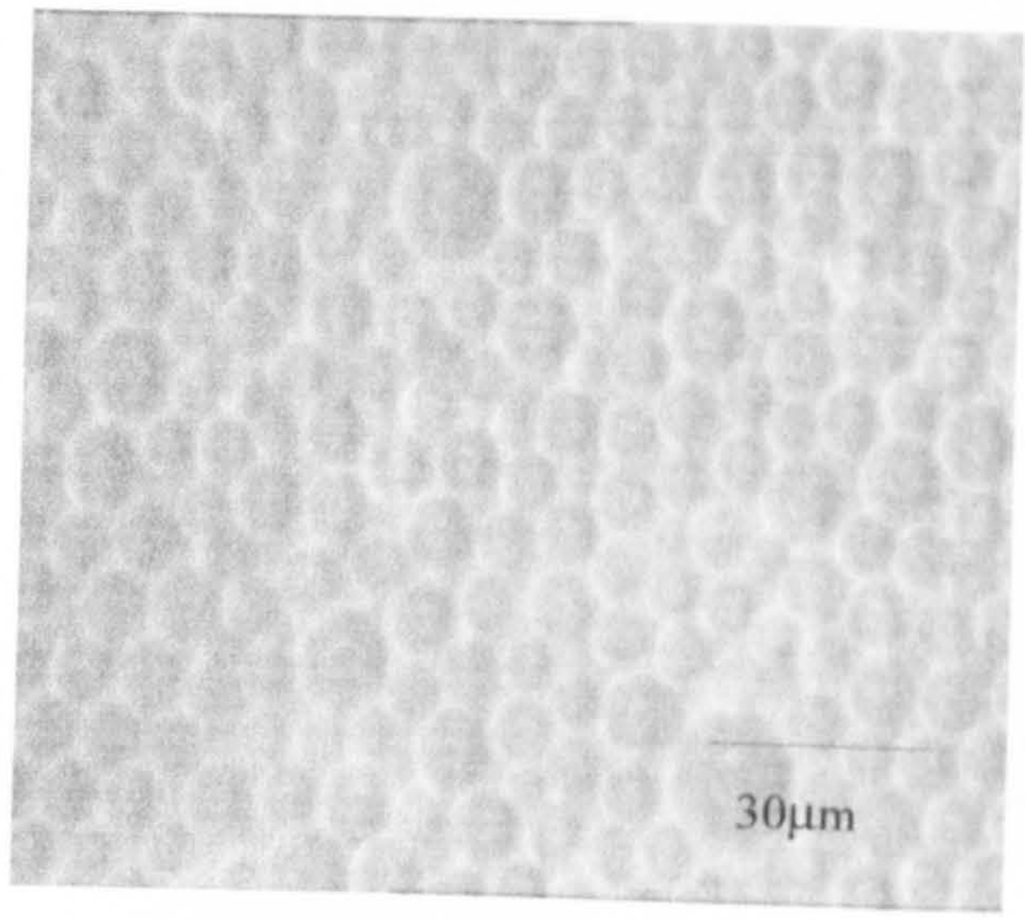

(c)

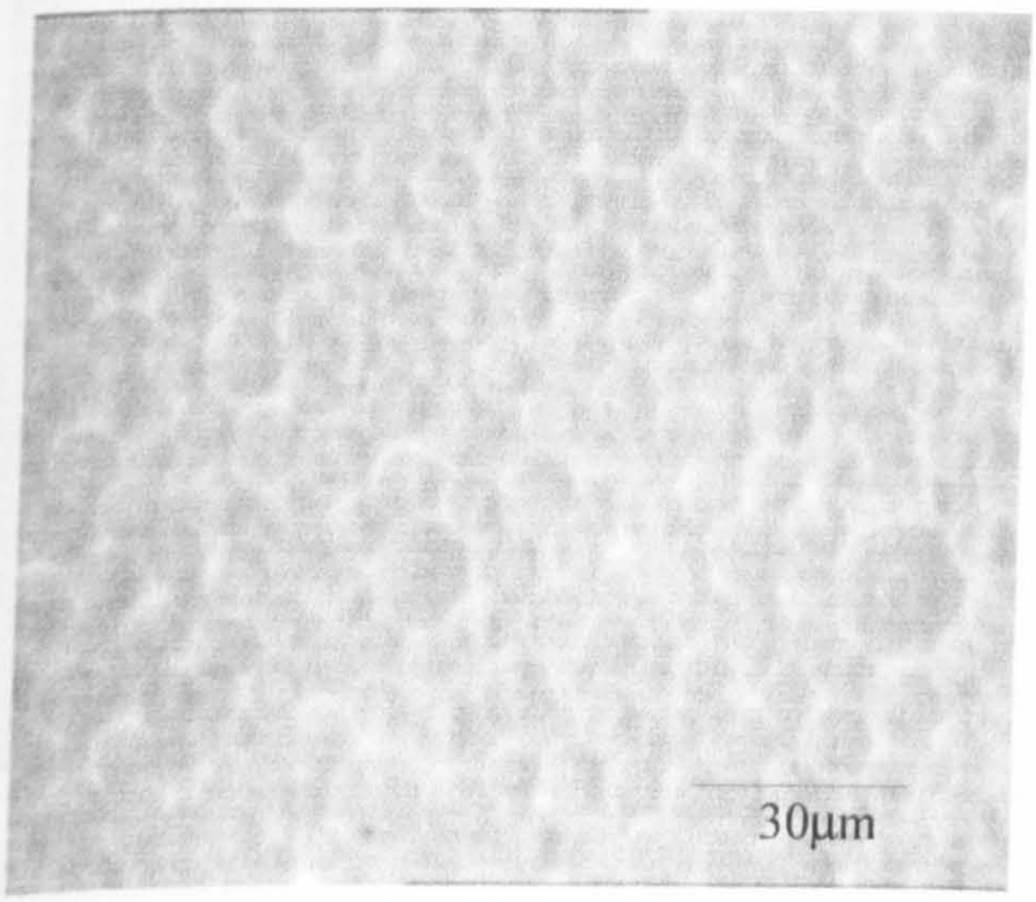

(d)

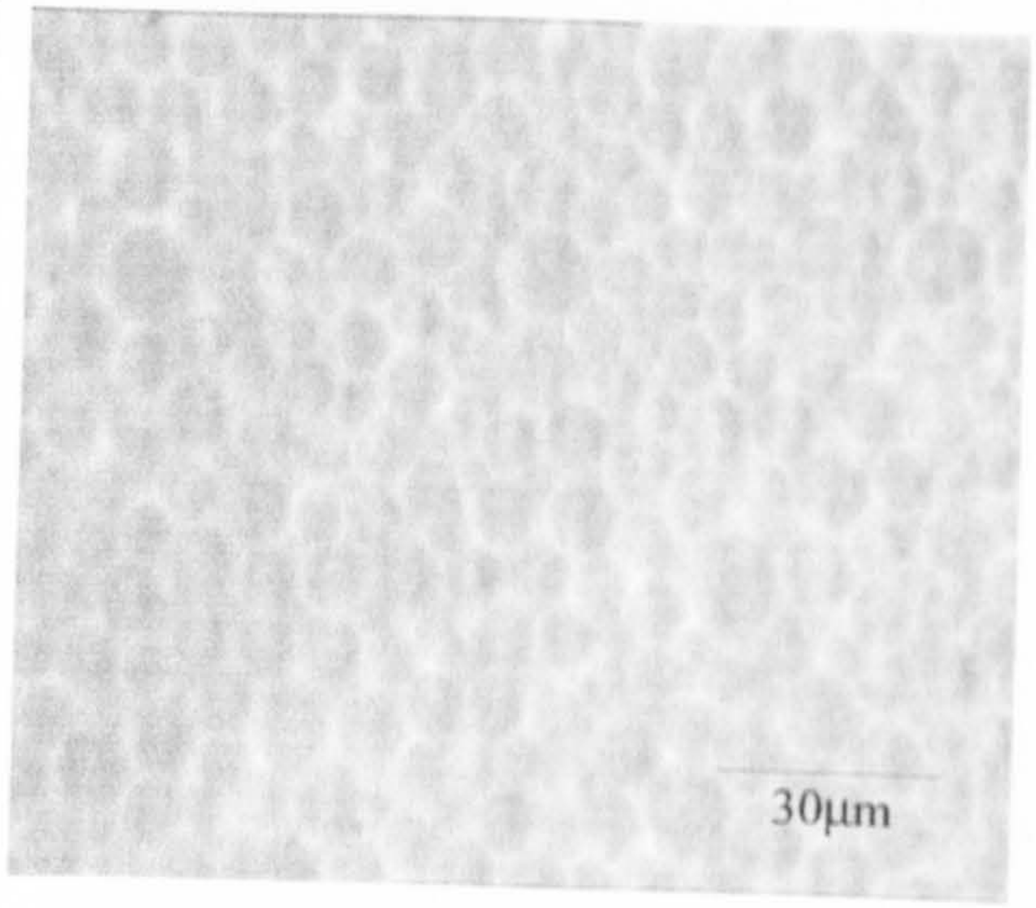

PLATE XVII: 0.8mM SDS on Mica; (a) 3 mins, (b) 60 mins, (c) 120 mins, (d) 180 mins

(a)

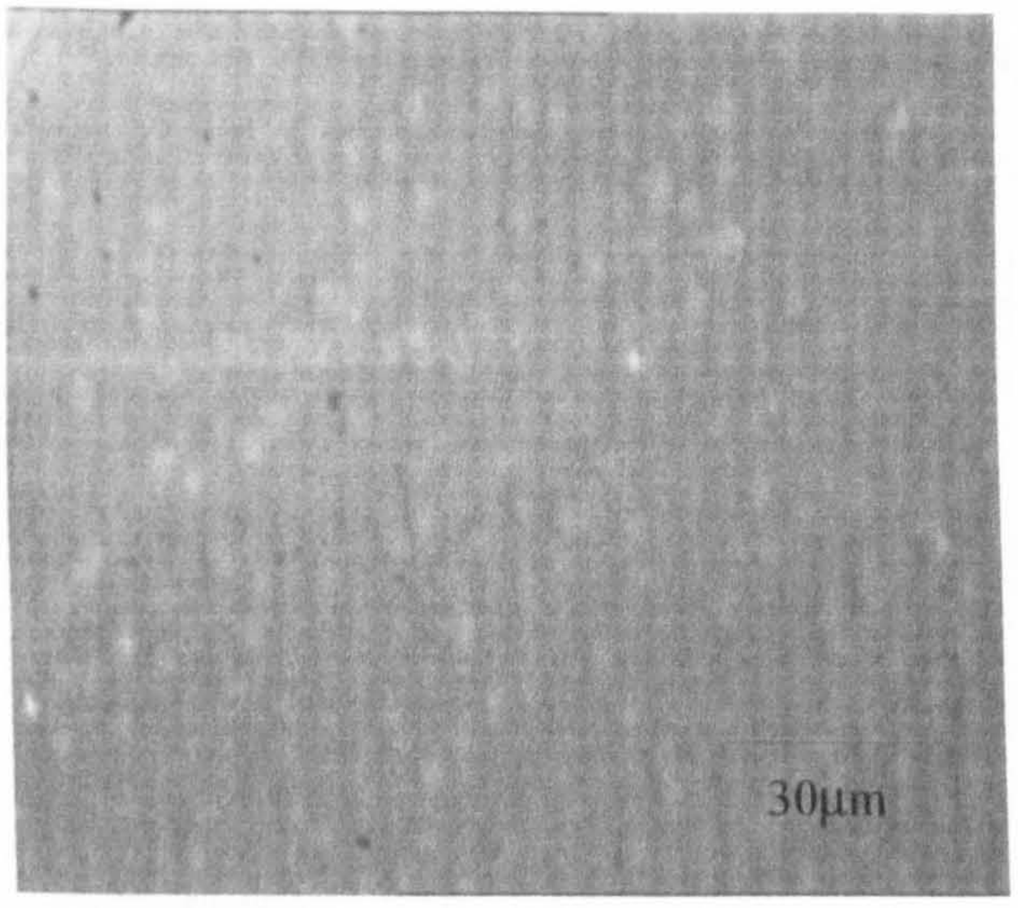

(b)

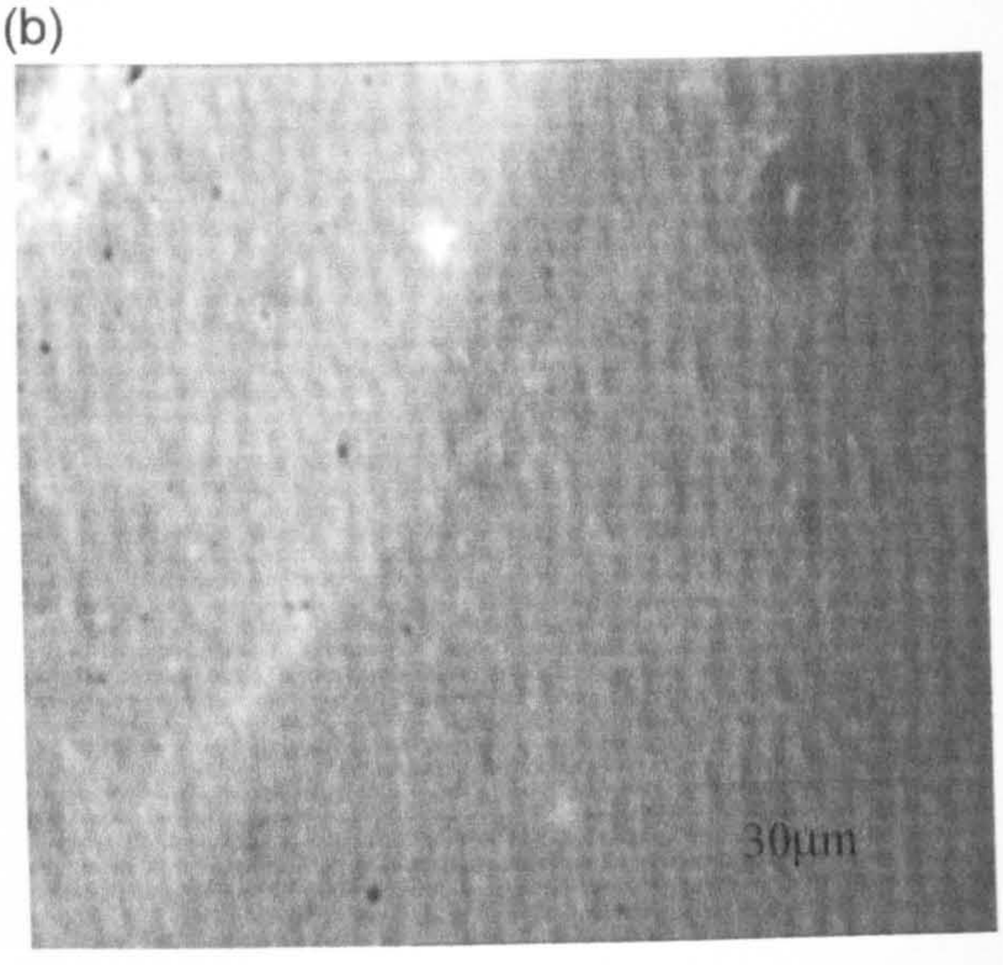

(c)

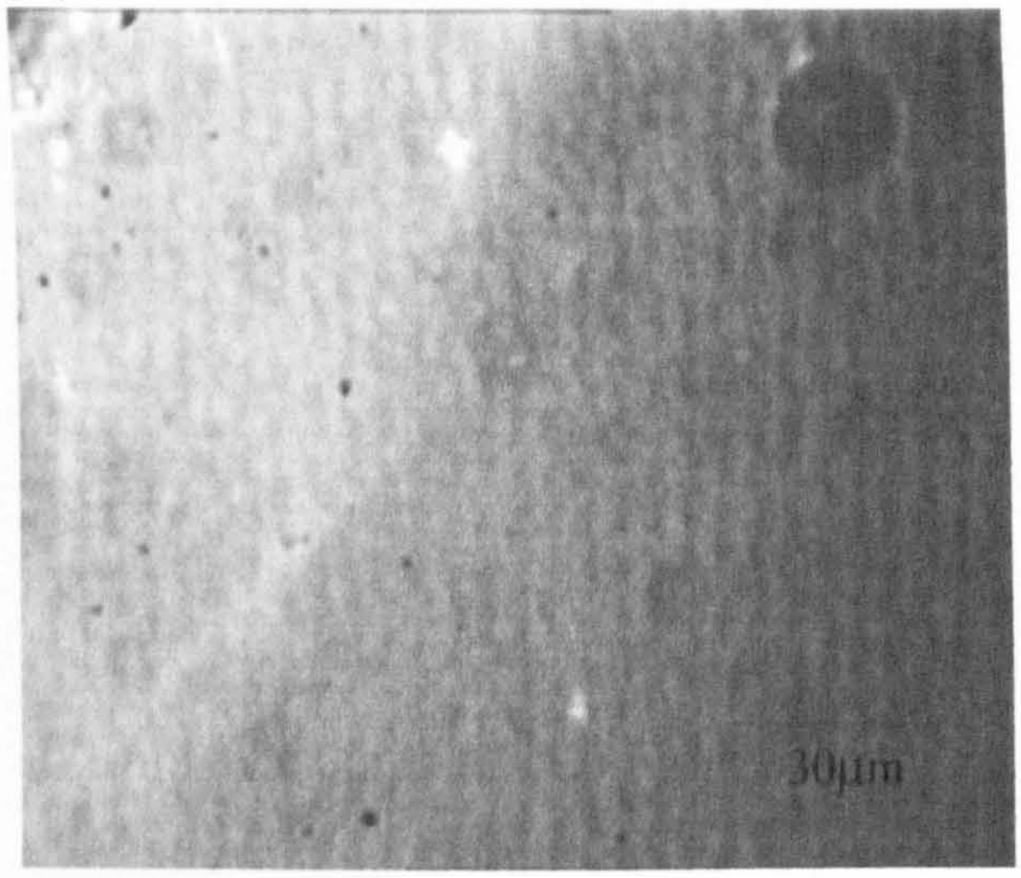

(d)

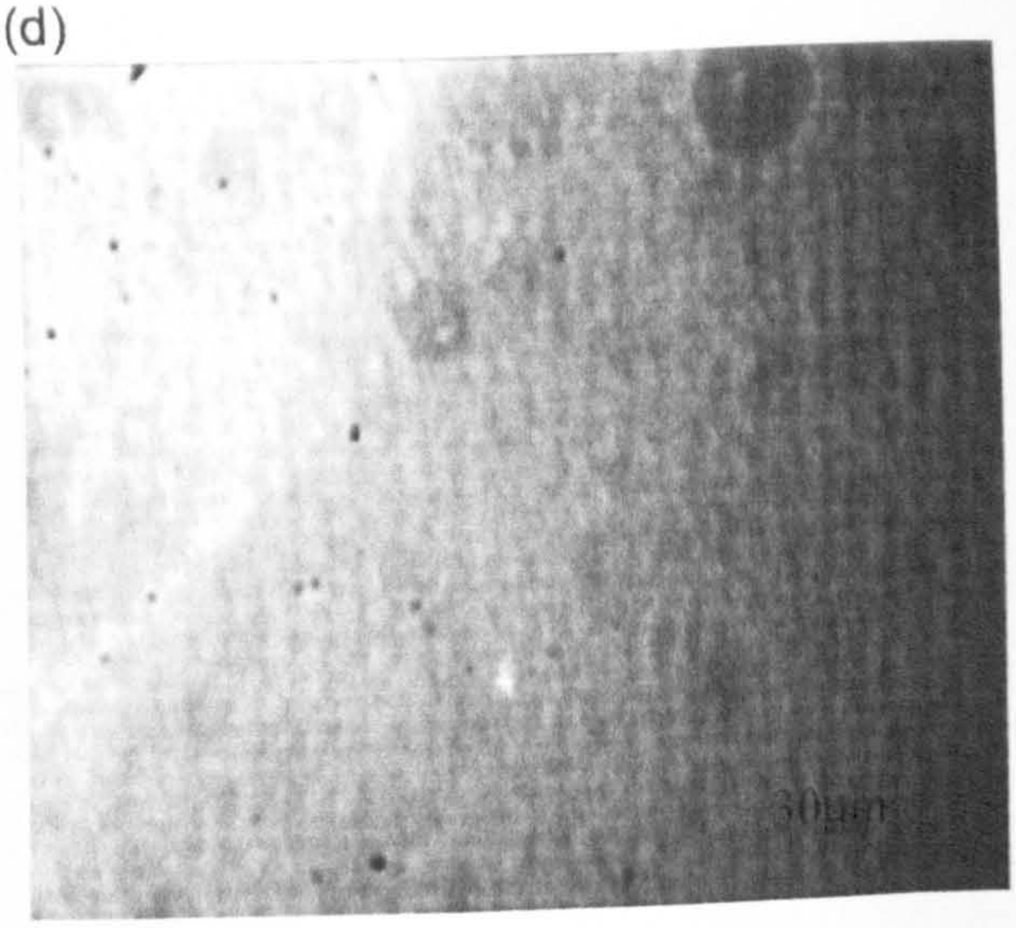

PLATE XVII:I 8.0mM SDS on Mica: (a) 3mins, (b) 60mins, (c) 120mins, (d) 180 mins

(a)

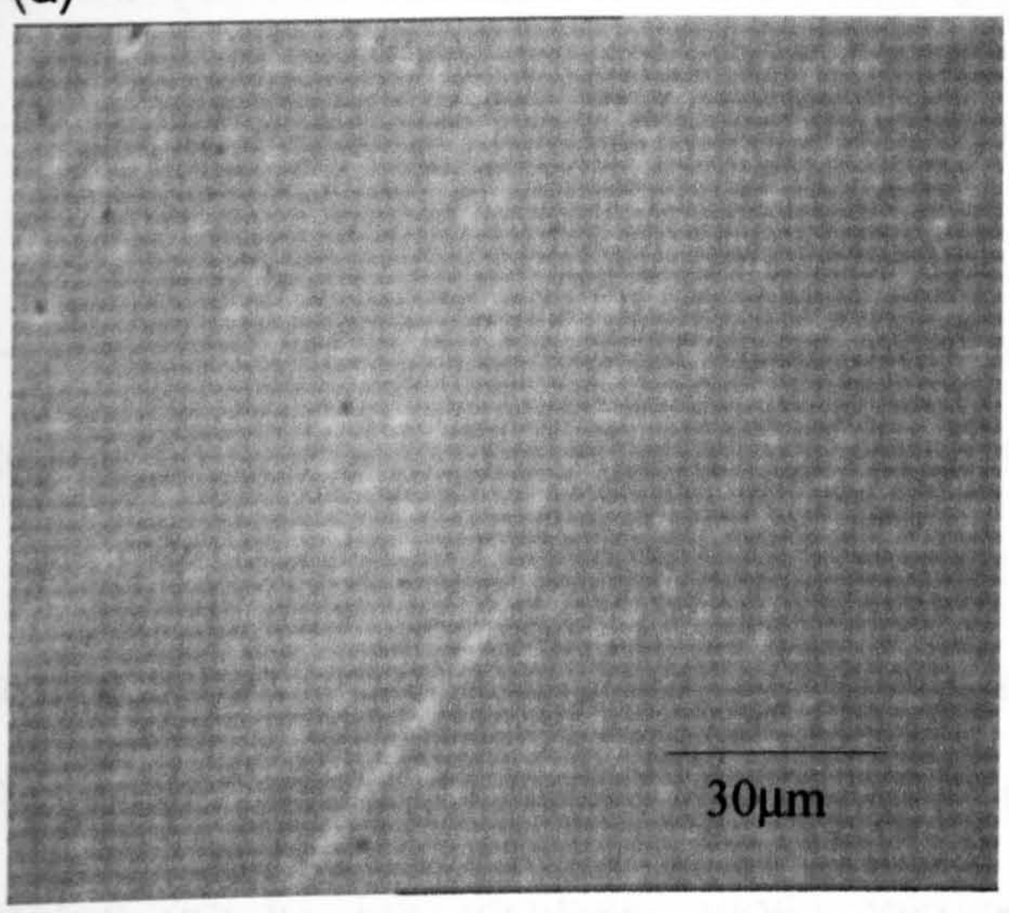

(b)

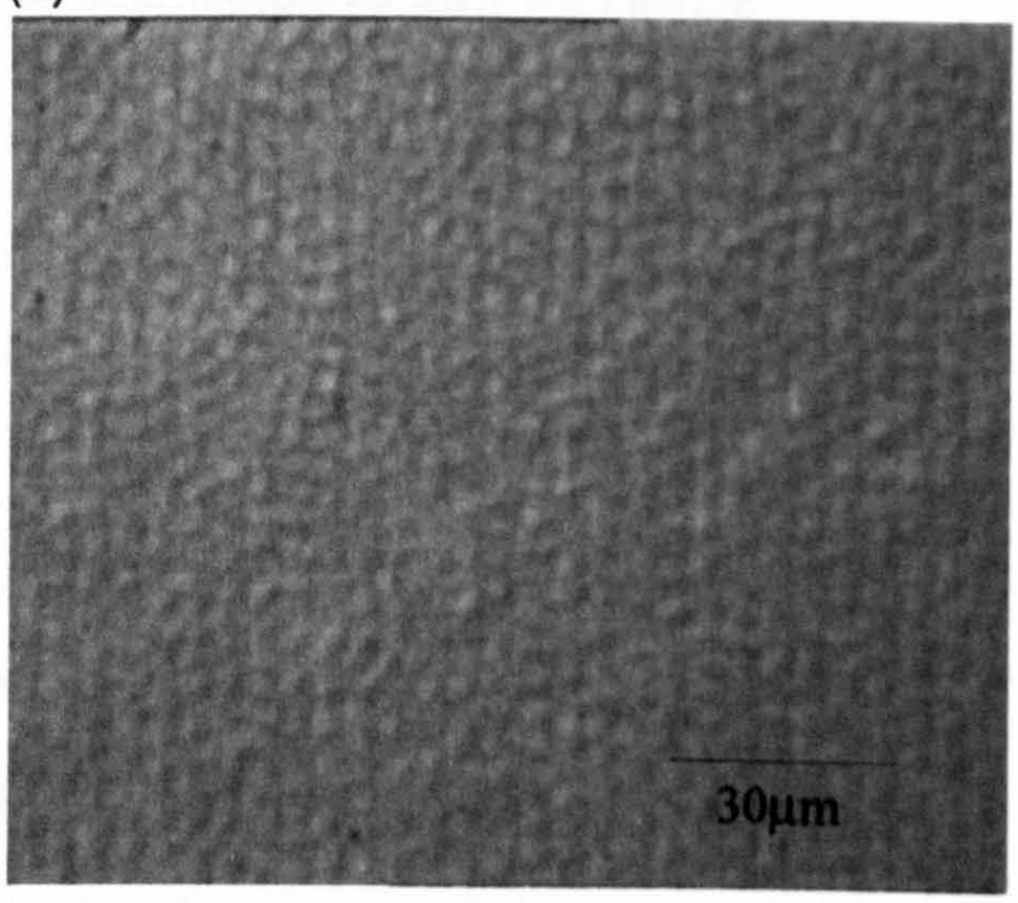

(c)

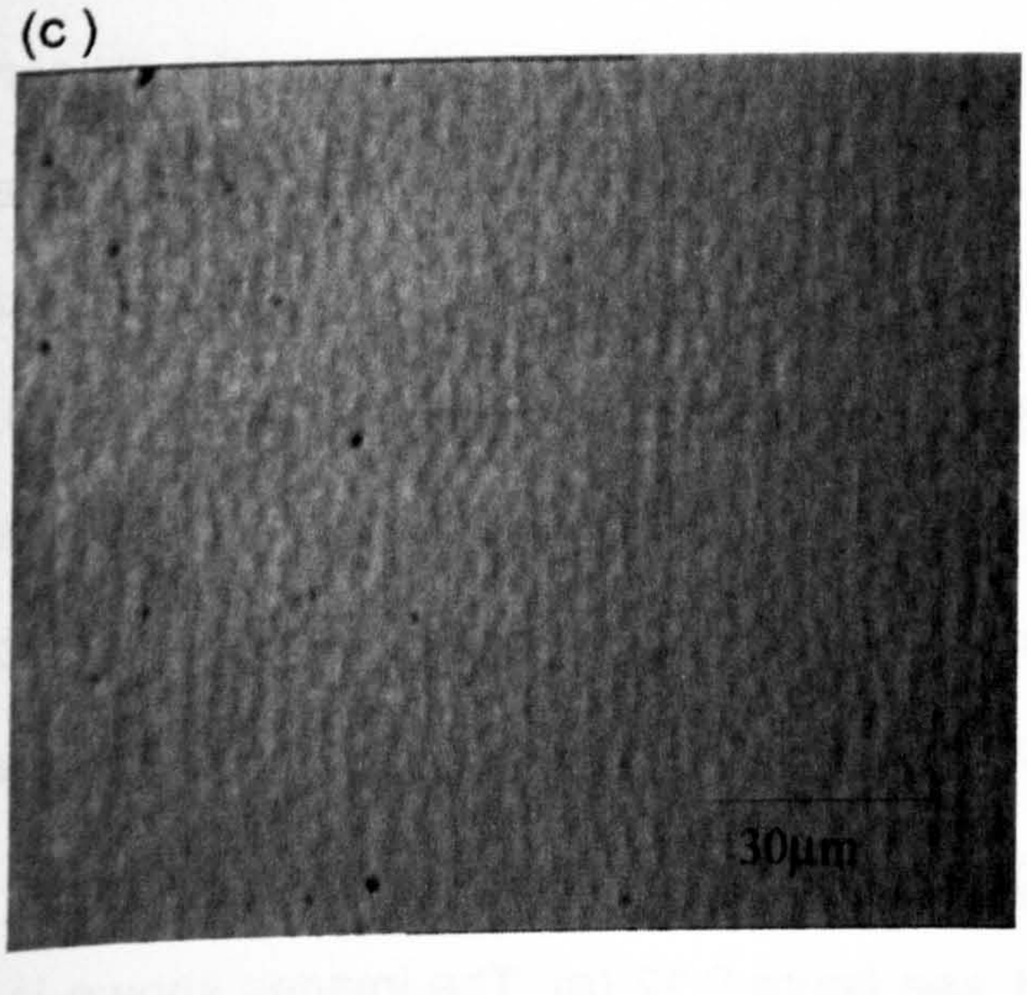

(d)

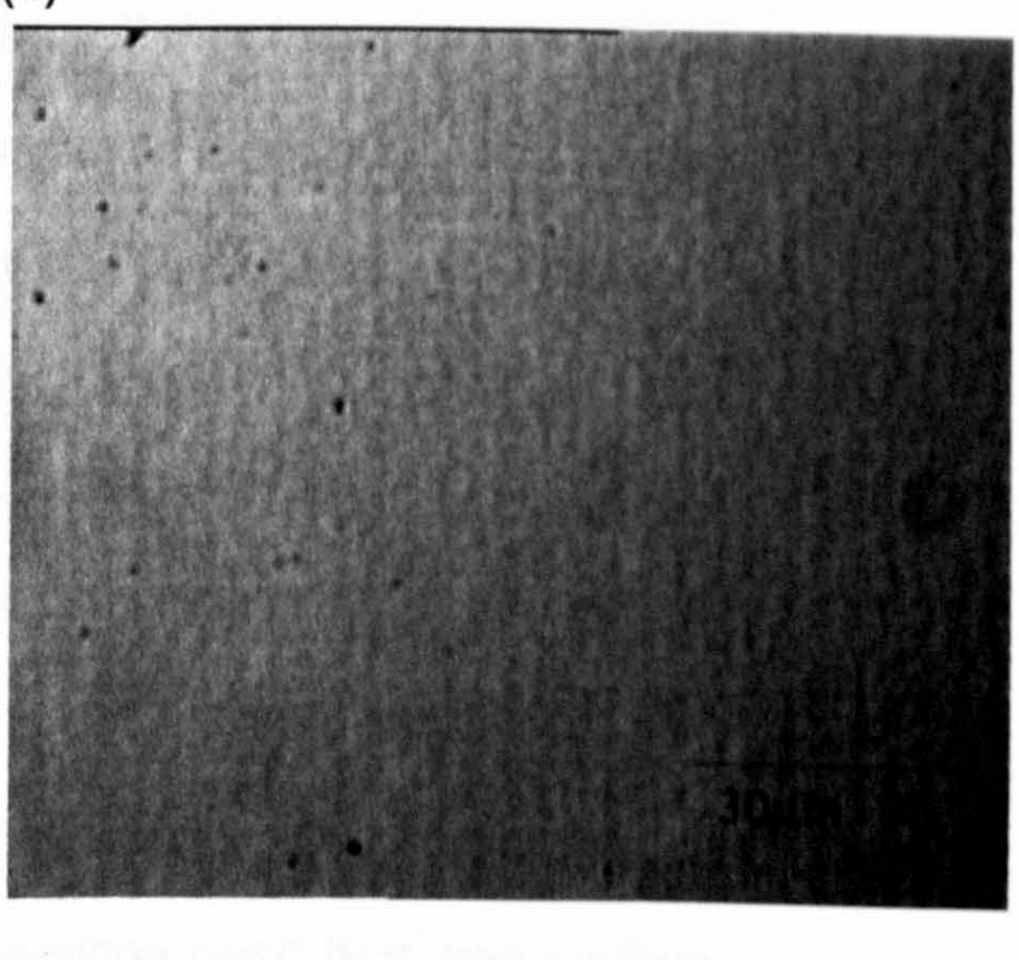

The rapid aqueous film rupture observed in this study was in agreement with those reported previously[15,7-9]. Wiersema et al[16] reported that the rate of the hydrodynamic film drain was increased by a factor of four, when compared with surfactant free systems, due to the destabilisation aqueous film by the charge increase at the interfaces.

However, as the presence of SDS was increased to 0.8mM- 8.0mM, the aqueous film appeared to become more stable between the two surfaces, similar to that observed in those systems containing MTMS >0.1(v/v), see section 9.2.1. Recently, Neuman et al[17] commented on this behaviour and noted that the high amount of SDS required to create a stable film between two approaching PDMS droplet surfaces was due to the high Gibbs elasticity, εG, of the deformable droplet and subsequent repulsive hydration forces. The increased concentration of SDS appeared to reduce the droplets' degree of wetting on the mica substrate and is in agreement with the previously reported observations that the presence of higher surfactant concentrations made the liquid-liquid interface behave as a rigid surface[16]. In addition, the SDS molecules also adsorbed onto the mica surface, forming the packing arrangements described previously in figure 9.10. The presence of surfactant molecules on both surfaces caused the approaching droplets to align in highly ordered, self-assembled micellular structures on the collector surface, see plates XVII-XVIII. This deposition behaviour was only observed for systems containing SDS concentrations >0.8mM and indicted that a surface cmc had been achieved, see figure 9.12 (a). The images shown in figure 9.12 illustrate the similarity between the highly ordered PDMS droplet packing arrangements on mica and those reported by Fa et al[11] and Wanless et al[18]. They produced AFM images of SDS hemi-cylindircal micelles adsorbed on negatively

charged graphite surface below the cmc, <8mM. This was later attributed to the VDW and/or hydrophobic attraction between the non-polar substrate and the hydrophobic alkyl chain of the surfactant molecules.

Figure 9.12 Aqueous film between cross-linked PDMS droplet -mica surface, (a) SDS 8.0mM, 3hrs after deposition, (b) AFM of SDS micelles on graphite[13,15]

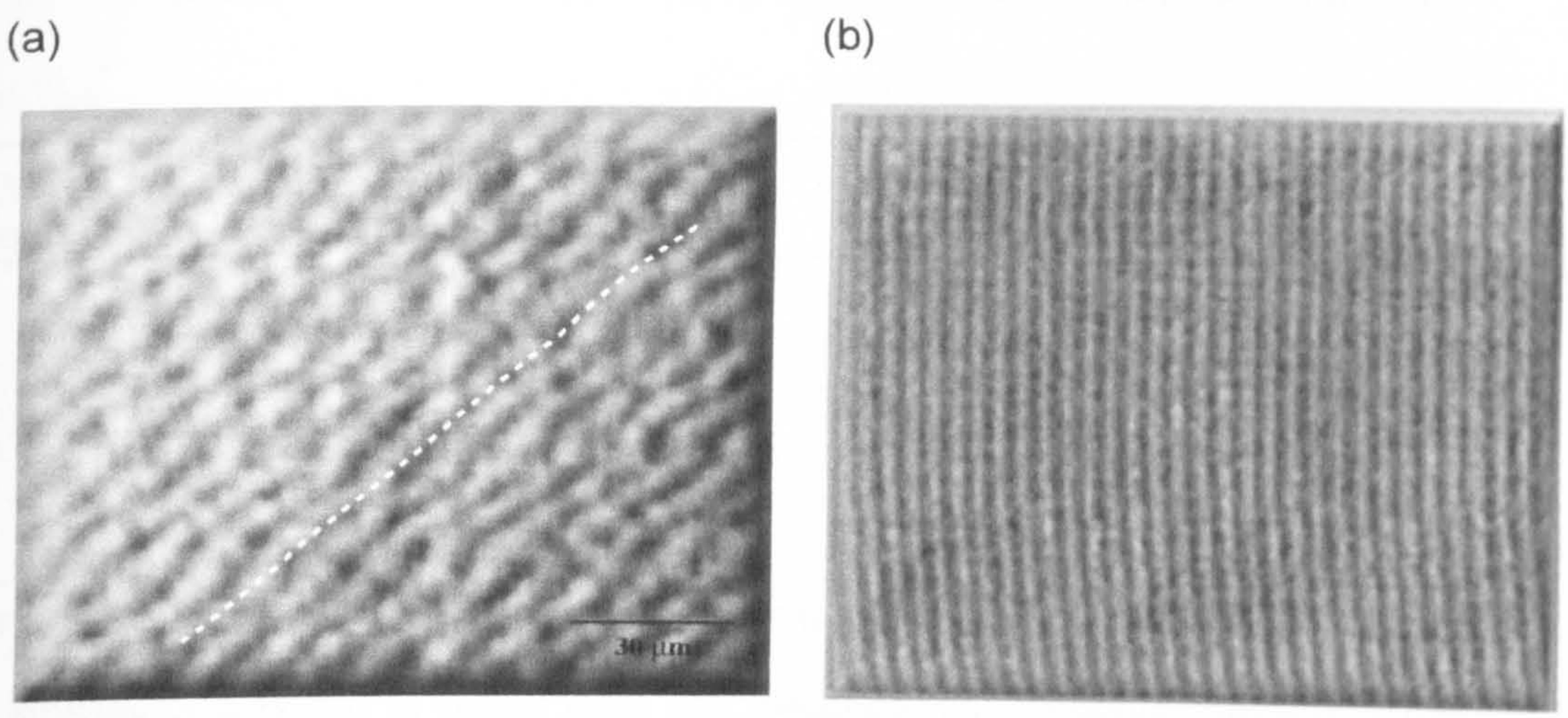

Broken line denotes ordered alignment of droplets (- - - - - -)

Deposition profiles were obtained for fixed cross-linked PDMS emulsion system as a function of time, in the presence of increasing SDS concentration 0.08mM, 0.8mM, 8.0mM and displayed in figure 9.13(a-c) and in table 9.6. It could be noted that the number of deposited droplets present on the mica surface increased with the increasing surfactant concentration. The number required to reach a deposition equilibrium, *Spl,* for systems containing <0.08mM SDS was under half that observed for systems without the presence of surfactant. However, the number of deposited droplets increased to twice that value in the presence of 8.0mM. This trend could be attributed to the spreading property of the PDMS droplets at low surfactant concentrations, which reduced the amount of substrate

surface available for deposition. This property decreased as the increased amount of adsorbed SDS caused the droplet surface to become more rigid. In addition, the average droplet diameter decreased to over half that observed for systems without the presence of surfactant, which in turn allowed more droplets to pack onto the substrate surface.

Table 9.6 Comparison of deposition profiles as a function of [SDS]

[SDS] mM	Spl_{Nd}	t_{Spl} (min)	θ_{max}	K_d /s^{-1}	R^2	% max. surface cov.
0.08	268	48	0.99	$1.06x10^{-3}$	0.89	100%
0.80	572	20	0.97	$1.08x10^{-3}$	0.92	100%
8.00	1040	33	0.97	$2.34x10^{-3}$	0.95	100%

It is interesting to note, that despite the variation in droplet deposition number for the surfactant systems investigated, the time taken to reach a coverage plateau and the rate of deposition was relatively independent of the surfactant concentration. The rate of deposition was found to be an order of magnitude faster than that recorded for the same system without the presence of surfactant and similar to those observed for emulsions containing NaCl $> 3x10^{-1}$ mol dm^{-3}.

Figure 9.14 shows a detailed study of the spreading behaviour of cross-linked PDMS droplets in the presence of increasing anionic surfactant concentration. It was observed that systems containing <0.08mM displayed the largest droplet spread on contact with the mica surface.

Figure 9.13 Deposition profiles as a function of time on Mica substrate with varying SDS concentration; (a) 0.08mM SDS, (b) 0.8mM SDS, (c) 8.0mM SDS

(a)

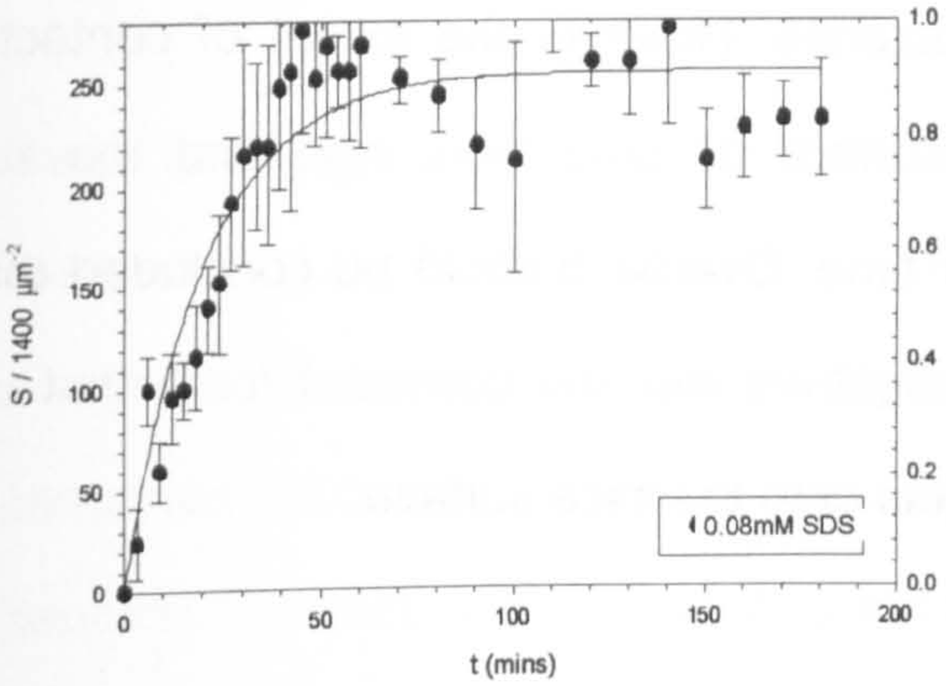

(b)

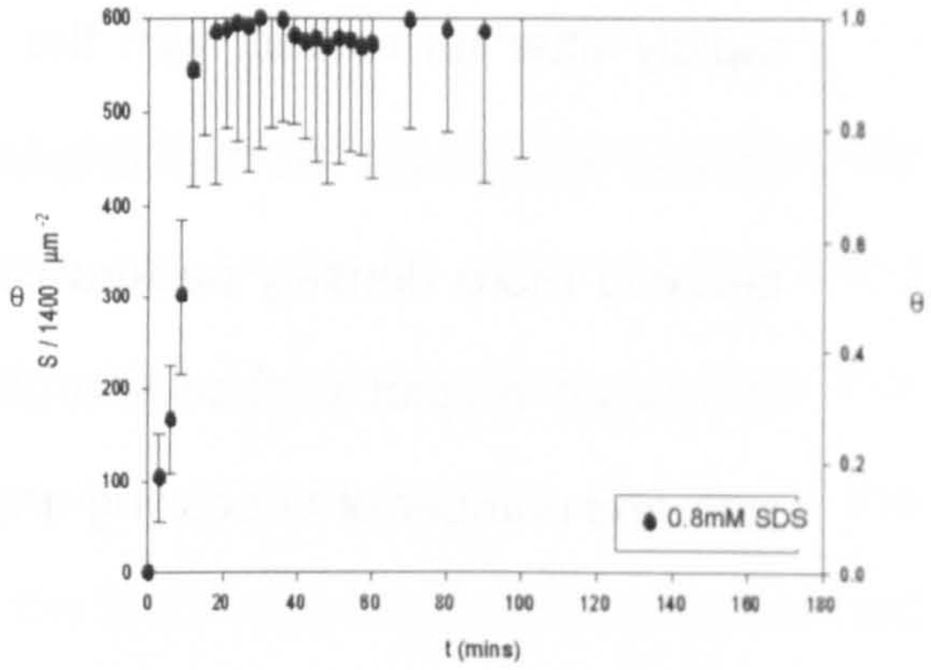

(c)

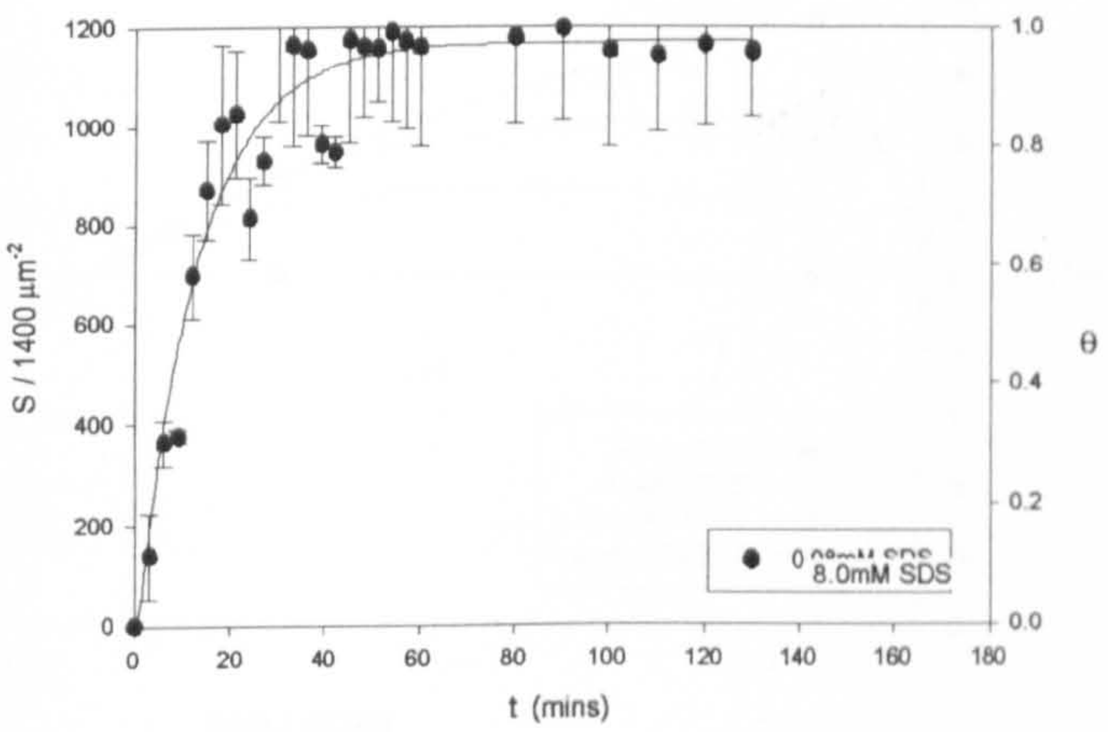

Each droplet occupied an average 55μm² on the mica surface which was similar to that observed for high electrolyte systems but was three times the contact area shown by cross-linked PDMS droplets without the presence of surfactant, see section 9.2.1. It could be noted that an equilibrium droplet spread was obtained rapidly after its contact with the substrate. However the extent of contact area spread decreased as the droplet surface became more rigid and the surface became more densely packed over time. Overall, it could be concluded that the increased droplet surface charge negativity was the dominant force that on the rate and number of depositing droplets onto the mica surface.

Fig 9.14 Deposition contact area as a function of time on Mica substrate with increasing [SDS]

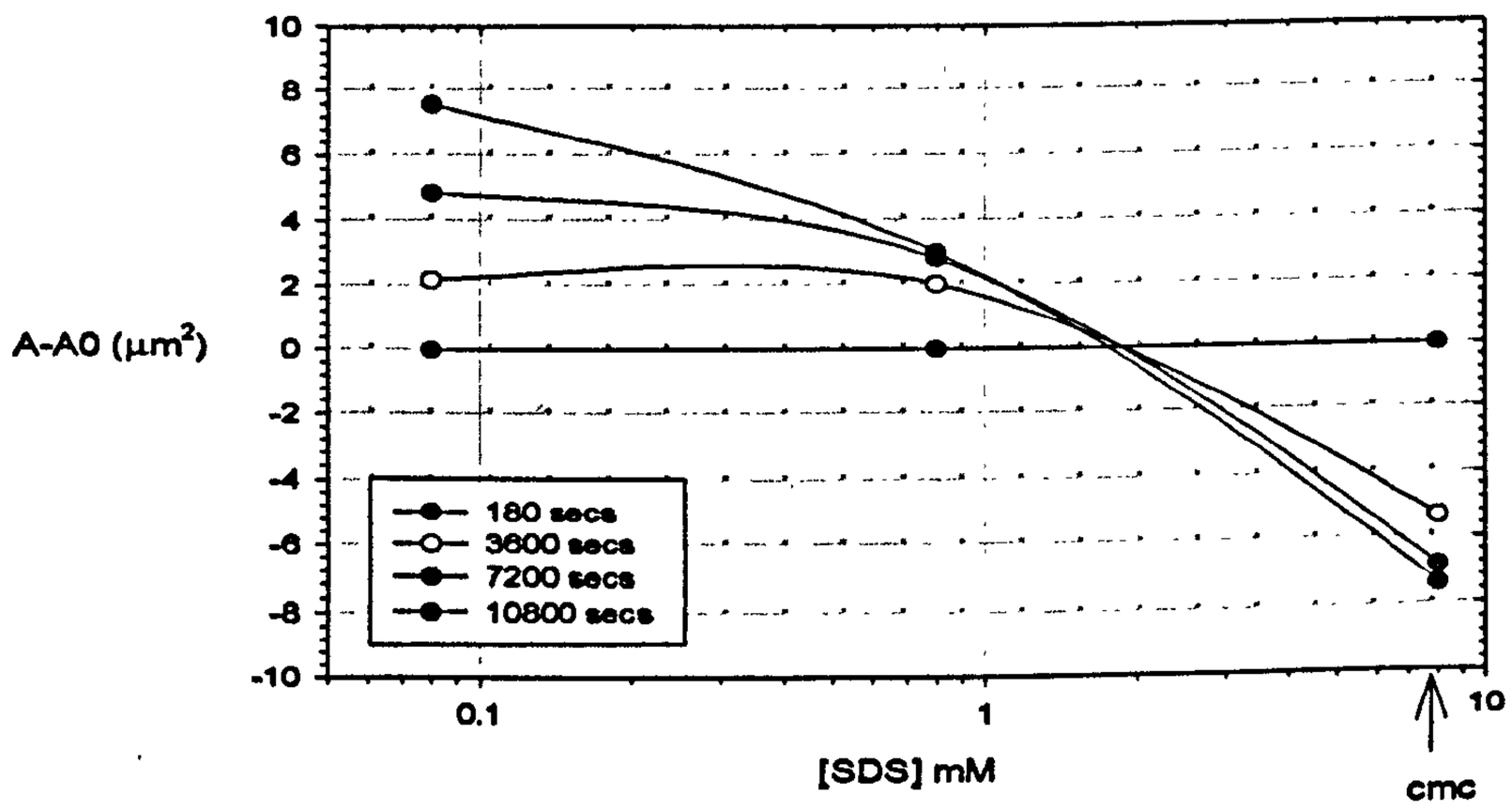

The partial radial distribution g(r) function as a function of time in the presence of anionic surfactant is presented in figure 9.15 (a-c). It is interesting to note that the distribution peak height decreased with increasing SDS concentration corresponded to the reduction in average droplet size and spreading function.

Initially, the fixed cross-linked systems investigated with surfactant concentrations <.0.8mM showed a very broad distribution peak which indicated that the most significant deposition occurred at distances greater than 30μm from the center of the stagnation point.

It was observed that the average distribution peak height did not alter significantly over time for any of the investigated systems, but it could be observed that there was a simultaneous narrowing of the peak width. Those emulsion systems that contained <0.08mM SDS reached unity or an optimum packing density of the deposited droplets after 60 minutes due to the fact that the spreading droplets had an enhanced force of adhesion from polymer chain entanglement mechanisms. to deposit closer to the stagnation point center than was observed previously for systems without the presence of SDS. However, below 0.08mM the

Fig 9.15 Comparison of radial distribution functions for cross-linked PDMS droplets on mica with varying [SDS] after; (a) 3 mins, (b) 60 mins, (c) 180 mins,

(a)

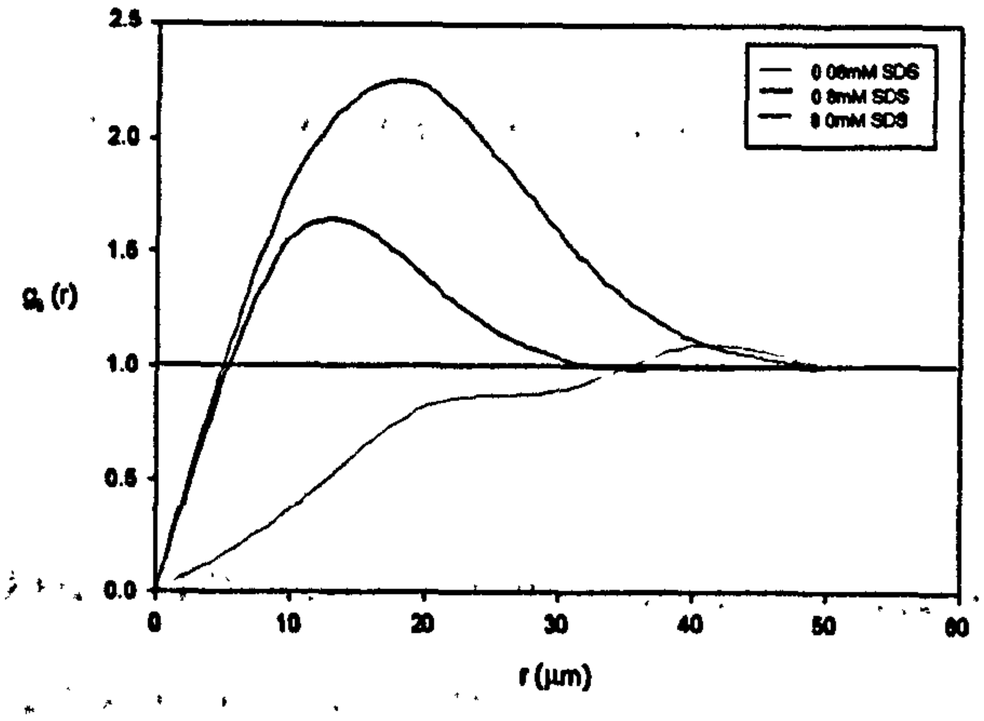

(b)

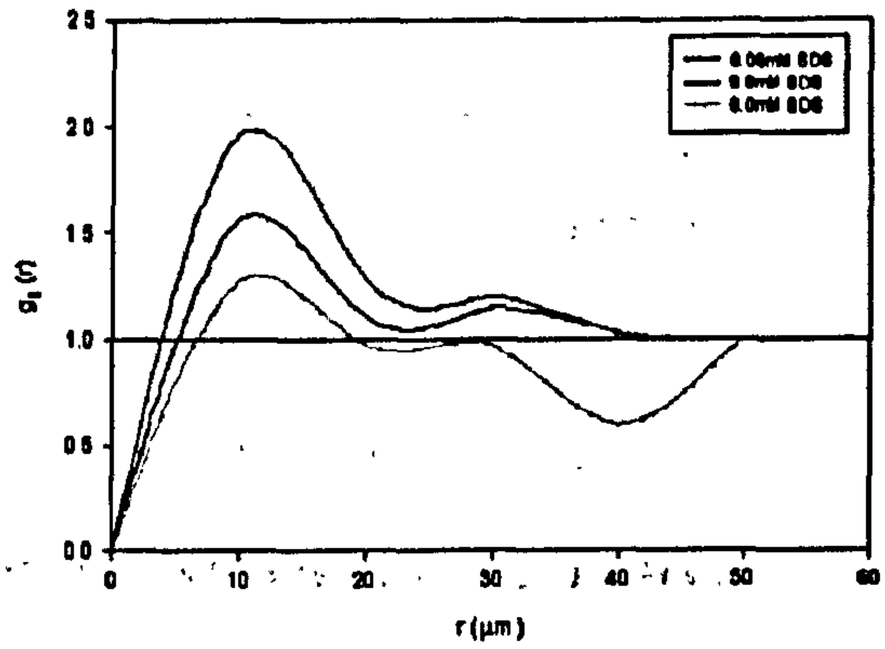

(C)

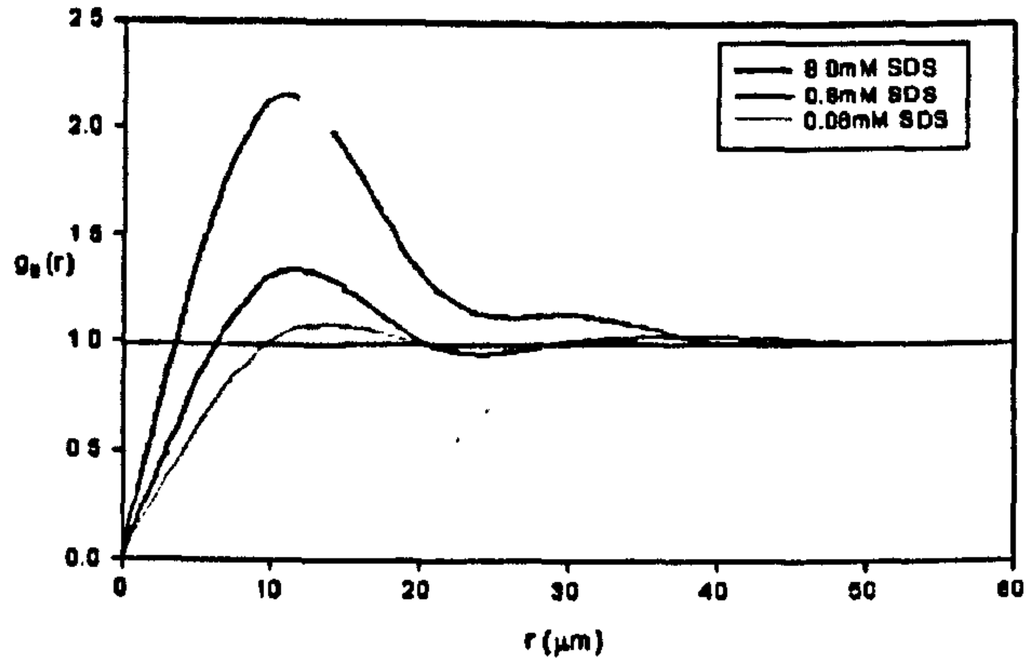

9.6 Deposition as a function of substrate chemistry and roughness

Yiantsios et al[19] reported that the contact angle hysteresis of oil droplets on rough systems decreased as a function of increasing surface asperity and was double that of smooth systems. They concluded that there was a critical surface roughness value, 0.1mm, below which aqueous films are stable and above which they are unstable.

The influence of the collector surface properties on the deposition of fixed cross-linked PDMS droplets was investigated by altering the surface charge, surface asperities and chemical composition of glass substrates. The results obtained from chemically modified glass was then compared with those obtained previously from mica. The glass collector surfaces were altered to produce an acid cleaned surface, an hydrophobic surface (Repelcote), an hydrophilic surface (APTES) and an amino acid model surface (L-Lysine) using the methods described in chapter 8. Identical emulsion parameters were used as in previous sections, 9.2.2-9.2.3 with fixed 0.05(v/v) total monomer and 0.05(v/v) MTMS. In addition a constant flow rate was maintained during the entire investigation.

A summary of the modified substrates surface properties discussed previously in chapter 8 is presented in table 9.7. All of the substrates investigated contained surface asperities with heights <10Å, so it could be assumed that the deposited droplets obeyed the Wenzel regime, discussed in chapter 7. Therefore, the ability of the cross-linked droplets to wet each substrate was dependent on its' surface asperity height, Rq.

It could be noted that overall as the substrate surface roughness increased, so the contact angle created by the cross-linked PDMS droplet also increased.

Table 9.7 Substrate surface properties

Substrate	$\theta\ ^{\circ}_{c}$	Rq (nm)	Streaming potential (mV)	Error (+/-)
APTES mod. Glass	42.5°	1.60	4.5	1.2
Mica	114.0°	0.06	-0.9	0.9
Lysine mod glass	121.8°	0.65	- 5.9	2.6
Acid cleaned glass	125.2°	1.60	-15.9	1.8
Repelcote mod glass	127.6°	2.70	-18.5	2.4

However, there was very little difference between the θ_c value obtained from L-Lysine, acid cleaned and Repelcote modified glass substrates irrespective of the fact that the substrate surface roughness and surface chemical composition varies significantly, see chapter 8. It could therefore be suggested that the magnitude of the collector surface charge was the dominant influence on the droplet-substrate interaction. The APTES modified glass substrate was the most significant example of this hypothesis. Although the substrate surface roughness was similar to the acid cleaned glass surface, the θ_c value obtained from the deposited PDMS droplet was under half that measured for the molecularly smooth mica substrate. It can therefore be concluded that the higher degree of wetting measured between the droplets and the substrate was dominated by the surface charge generated by chemical composition of the APTES chains present on the glass surface.

The deposition images obtained for the chemically modified substrates are presented in plates XIX-XXII.

PLATE XIX: Acid cleaned substrate; (a) 3 mins, (b) 60 mins, (c) 120 mins, (d) 180 mins

(a)

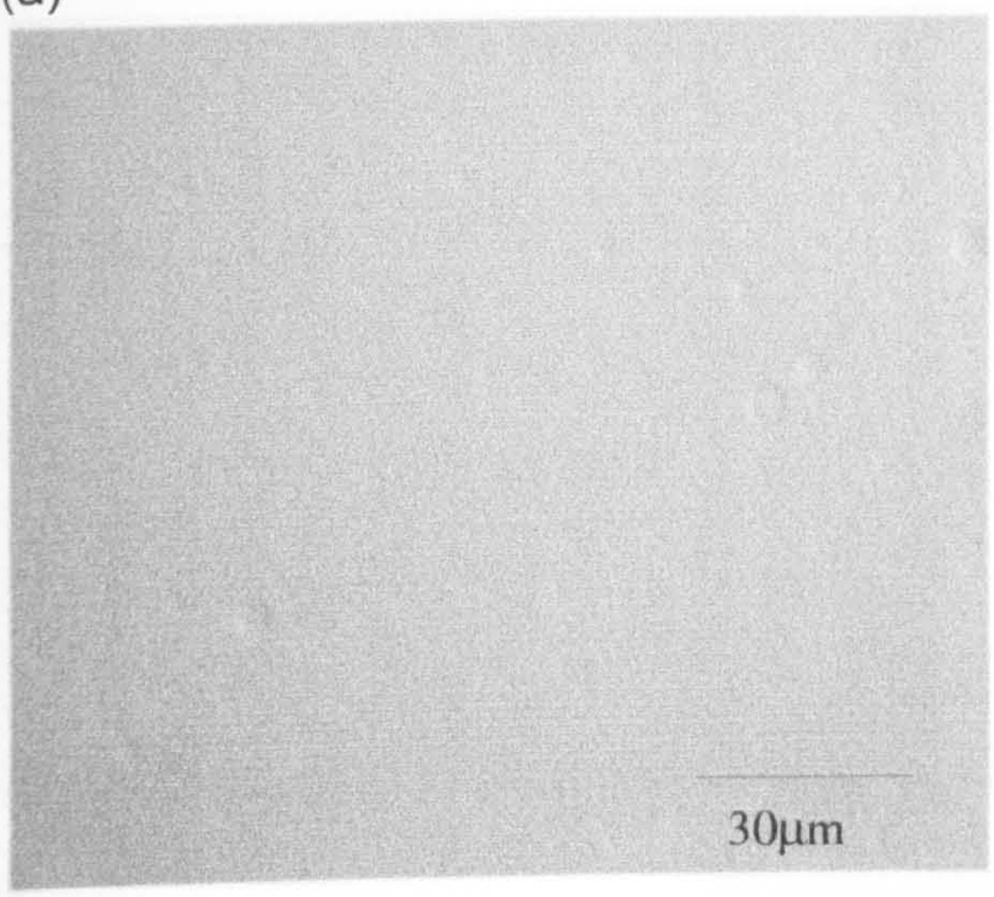

(b)

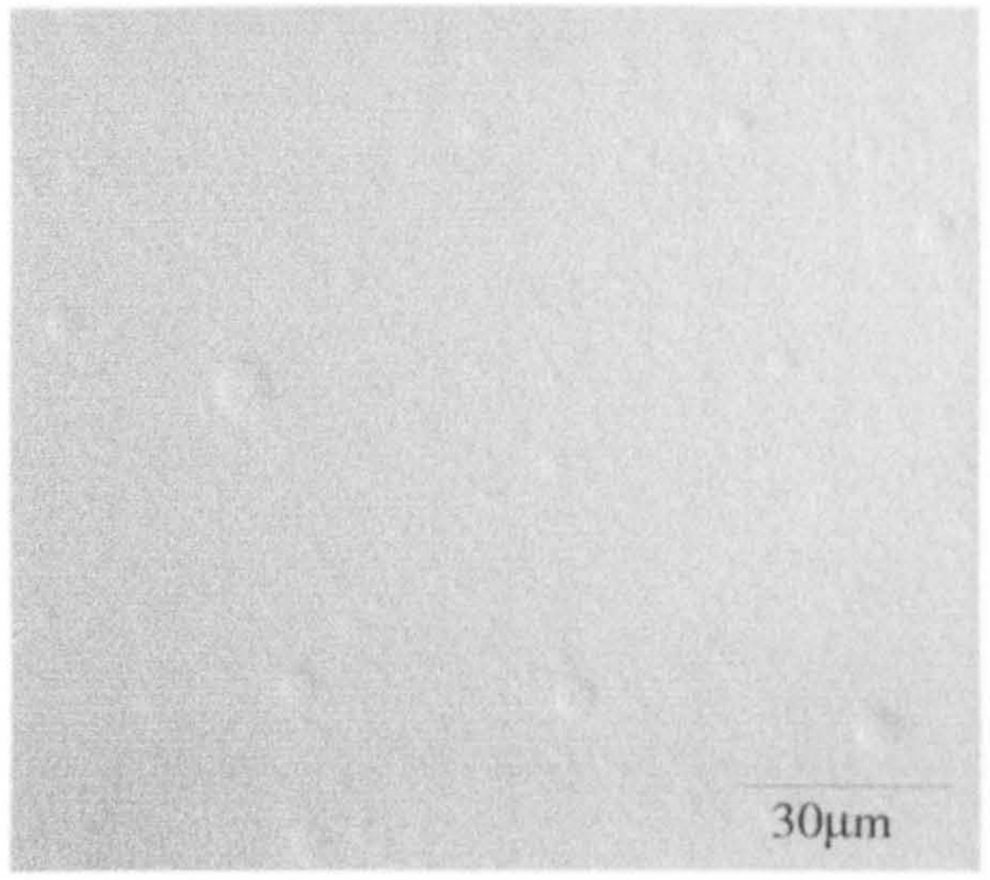

(c)

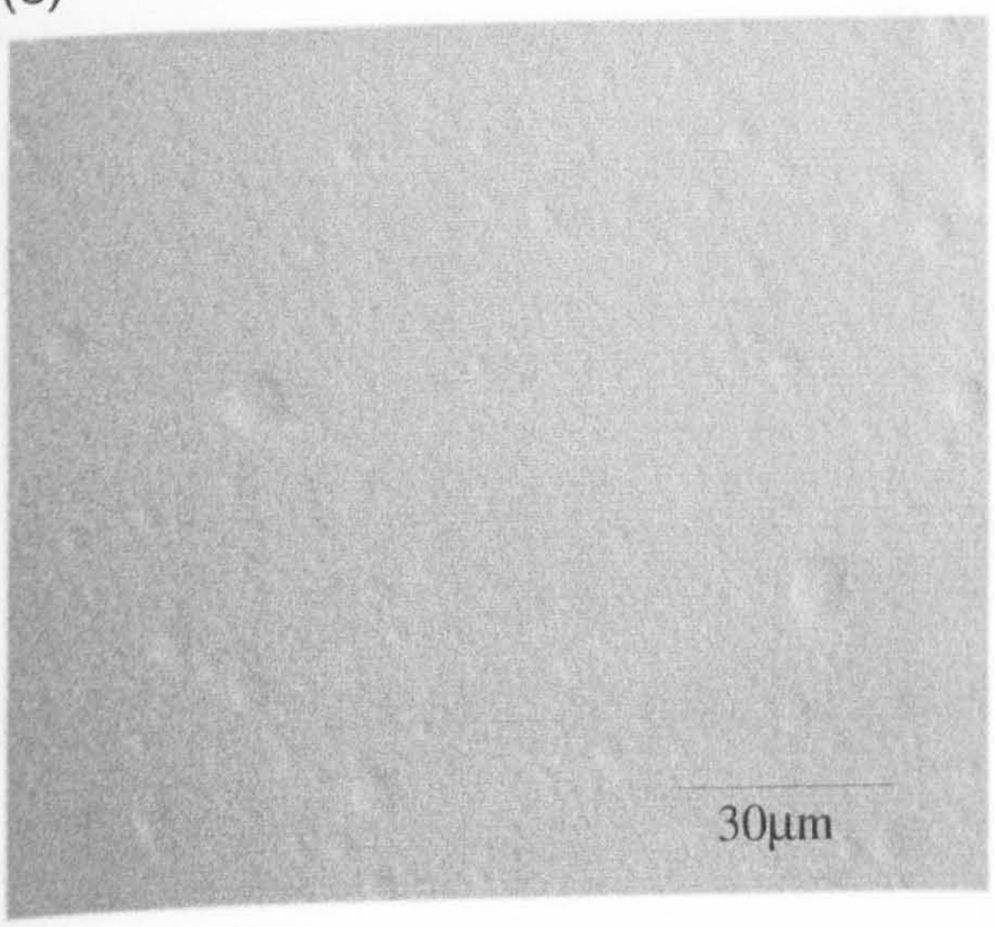

(d)

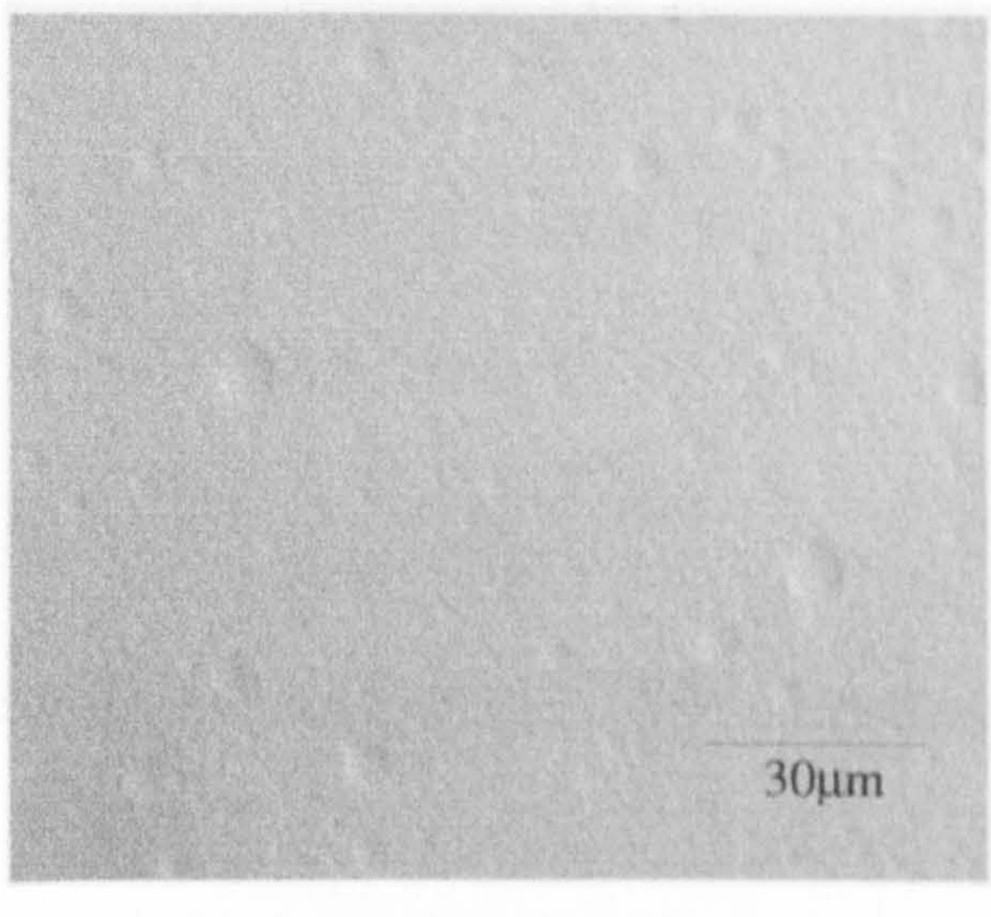

PLATE XX: APTES glass substrate; (a) 3 mins, (b) 60 mins, (c) 120 mins, (d) 180 mins

(a)

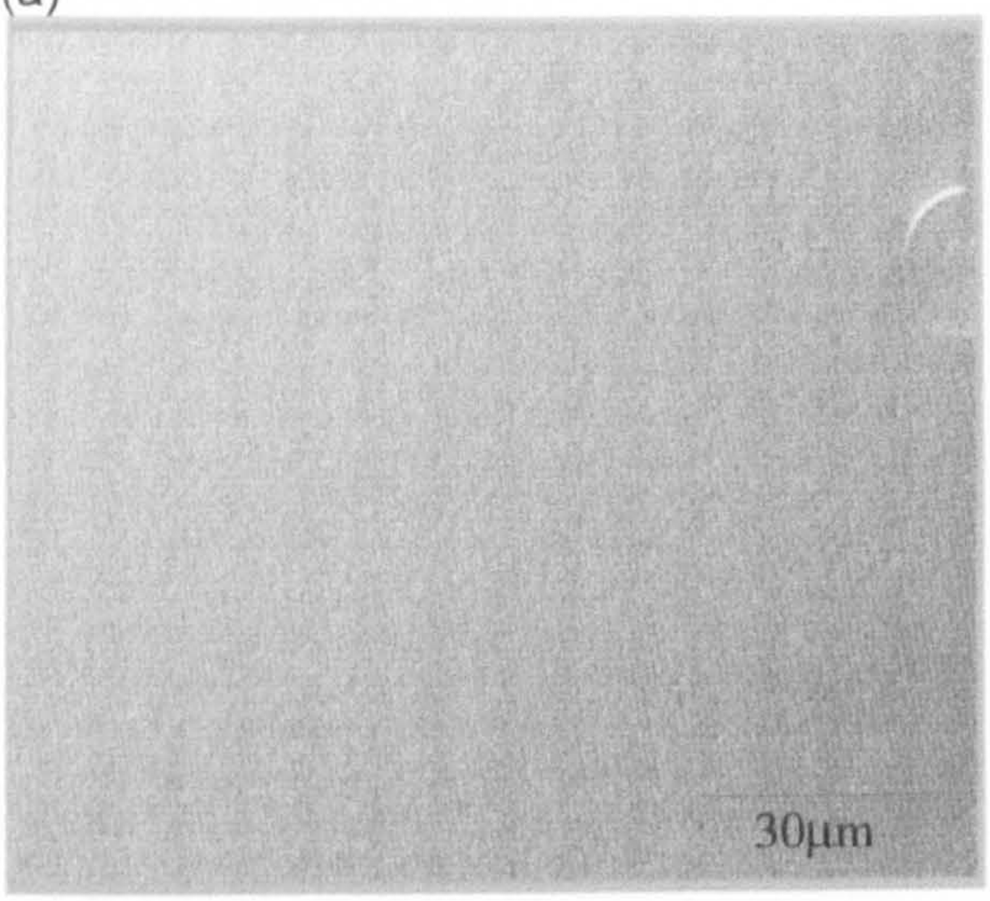

(b)

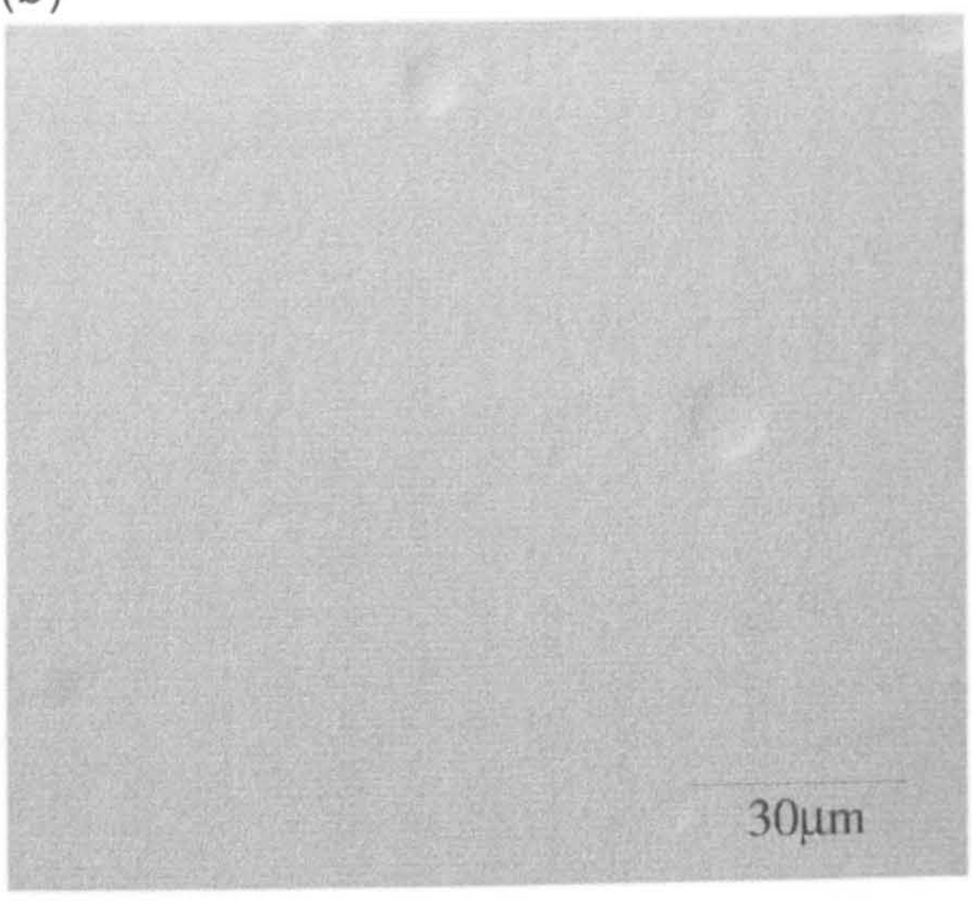

(c)

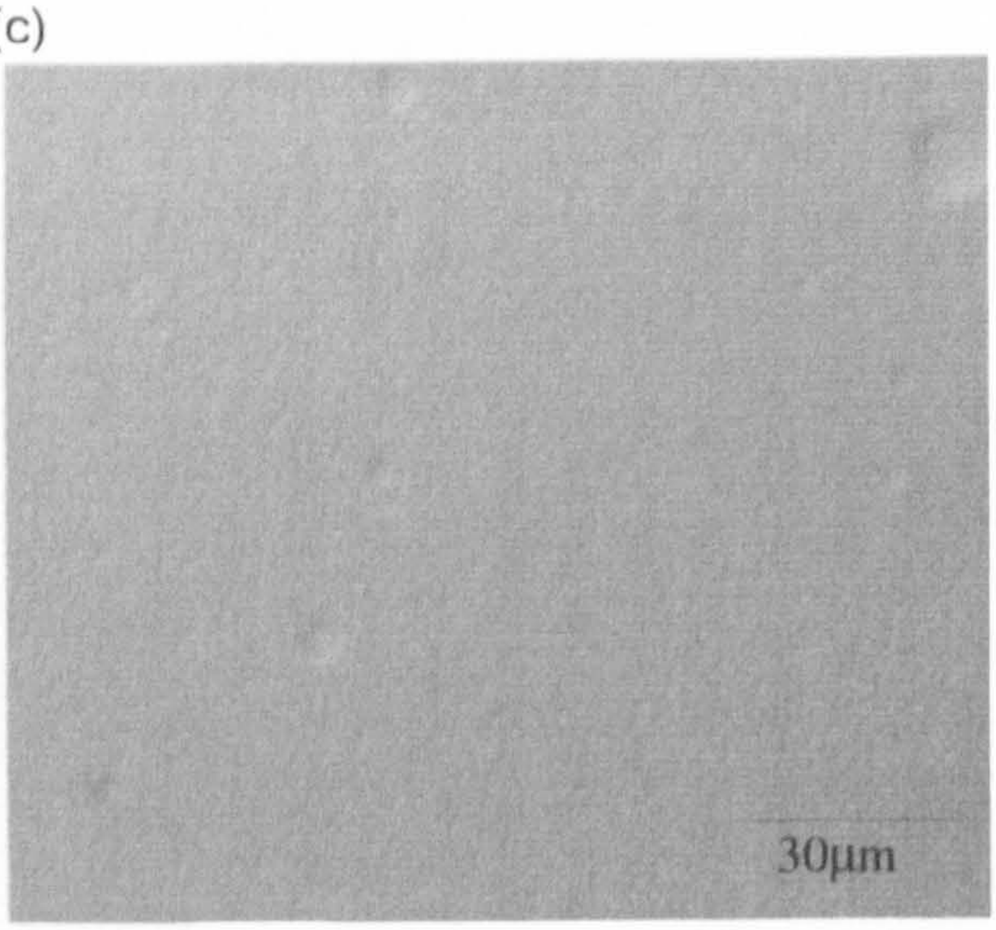

(d)

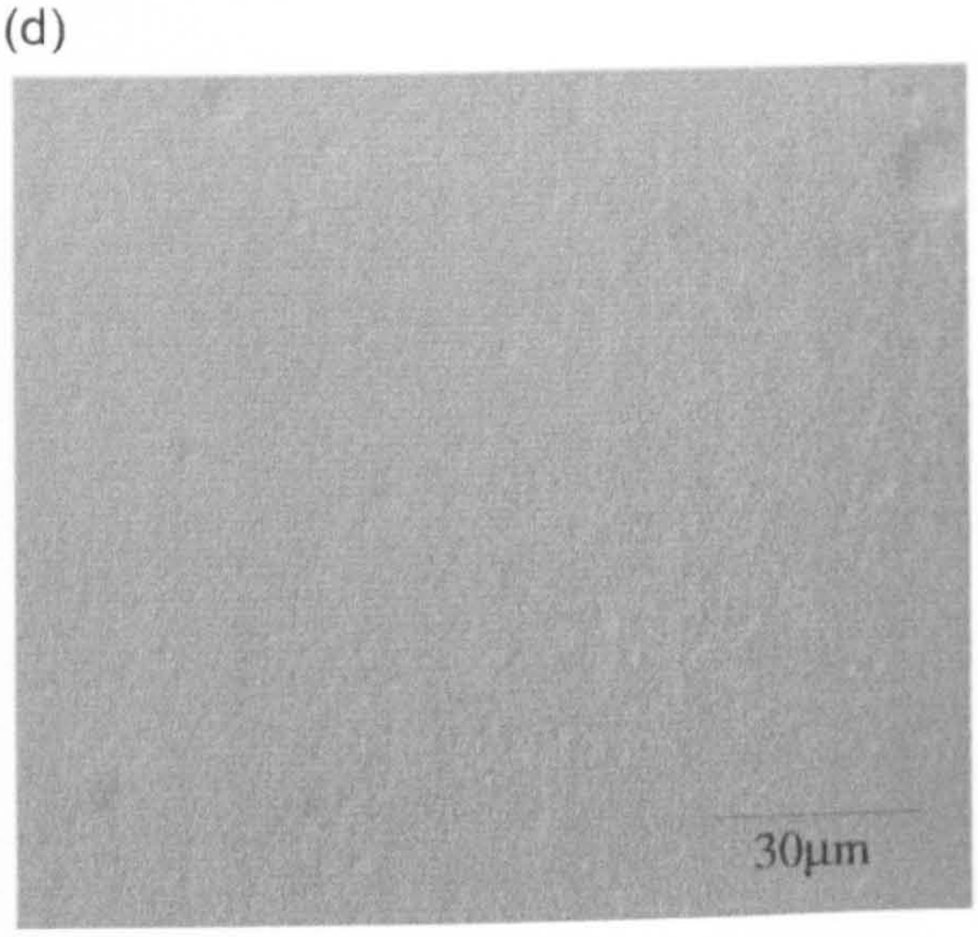

PLATE XXI: Repelcote glass substrate; (a) 3 mins, (b) 60 mins, (c) 120 mins, (d) 180 mins

(a)

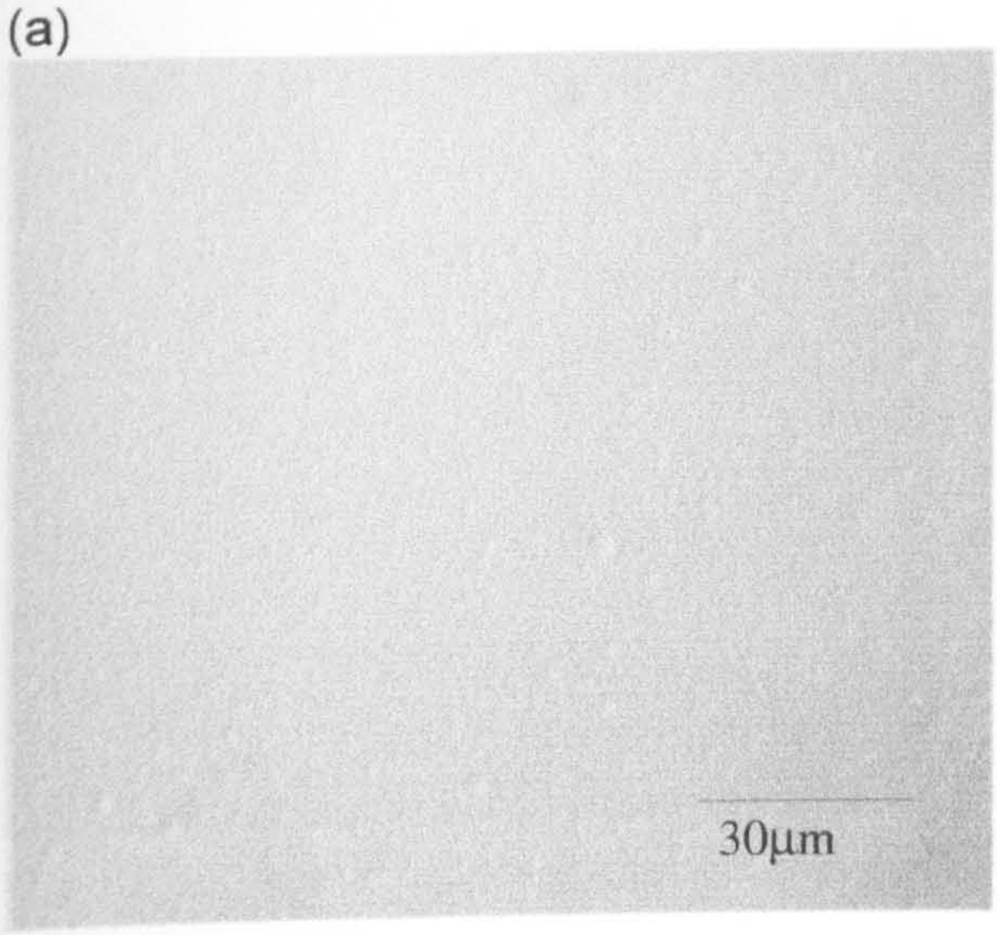

(b)

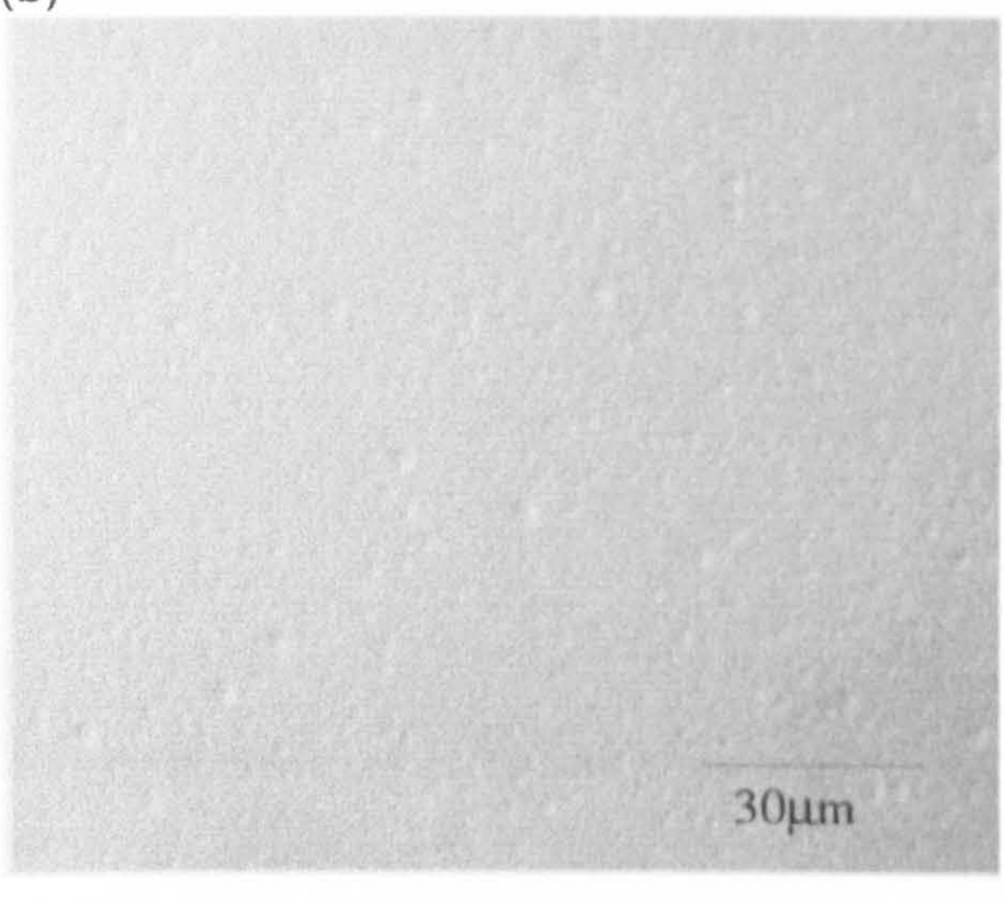

(c)

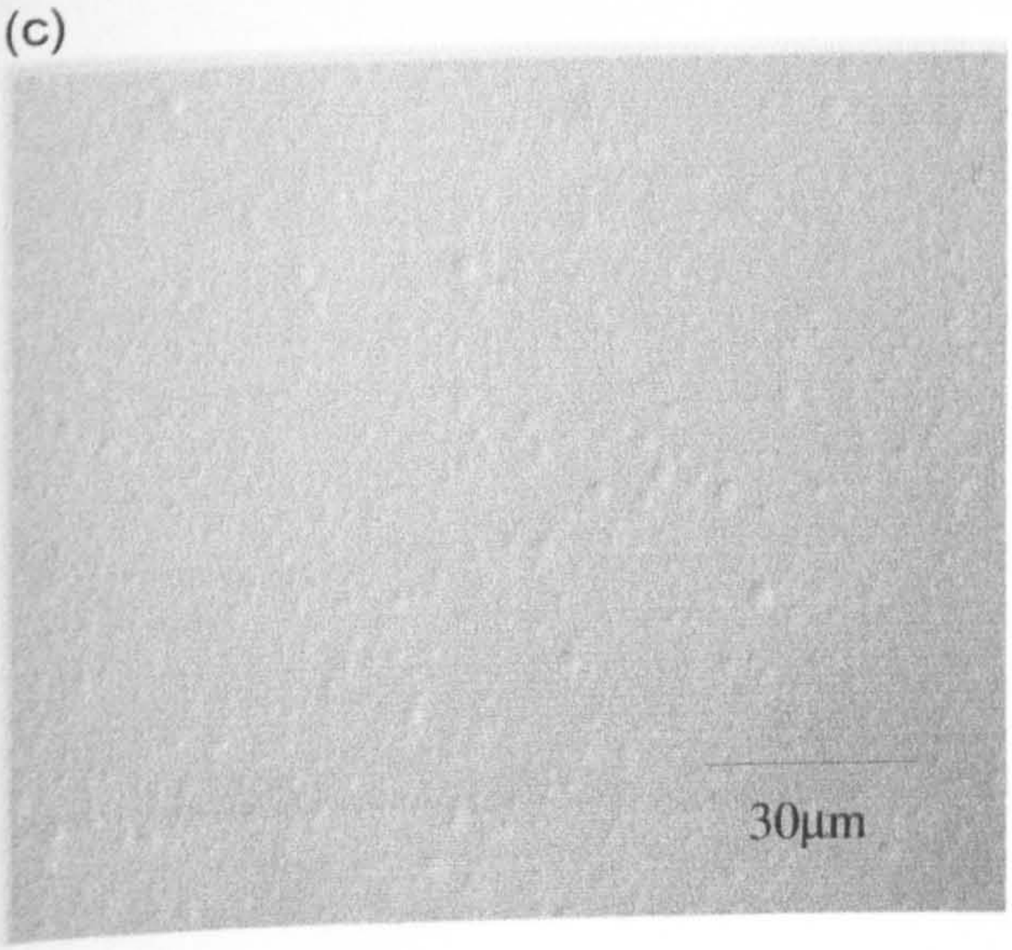

(d)

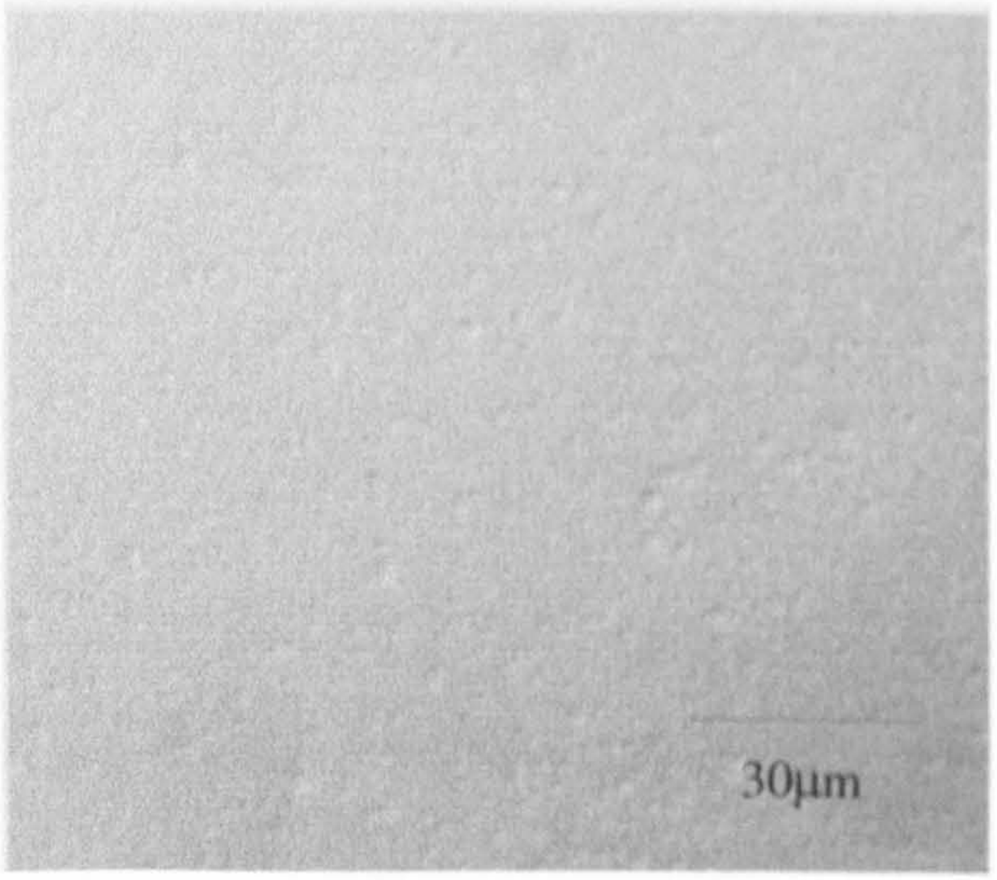

PLATE XXII: Lysine modified glass; (a) 3 mins, (b) 60 mins, (c) 120 mins, (d) 180 mins

(a)

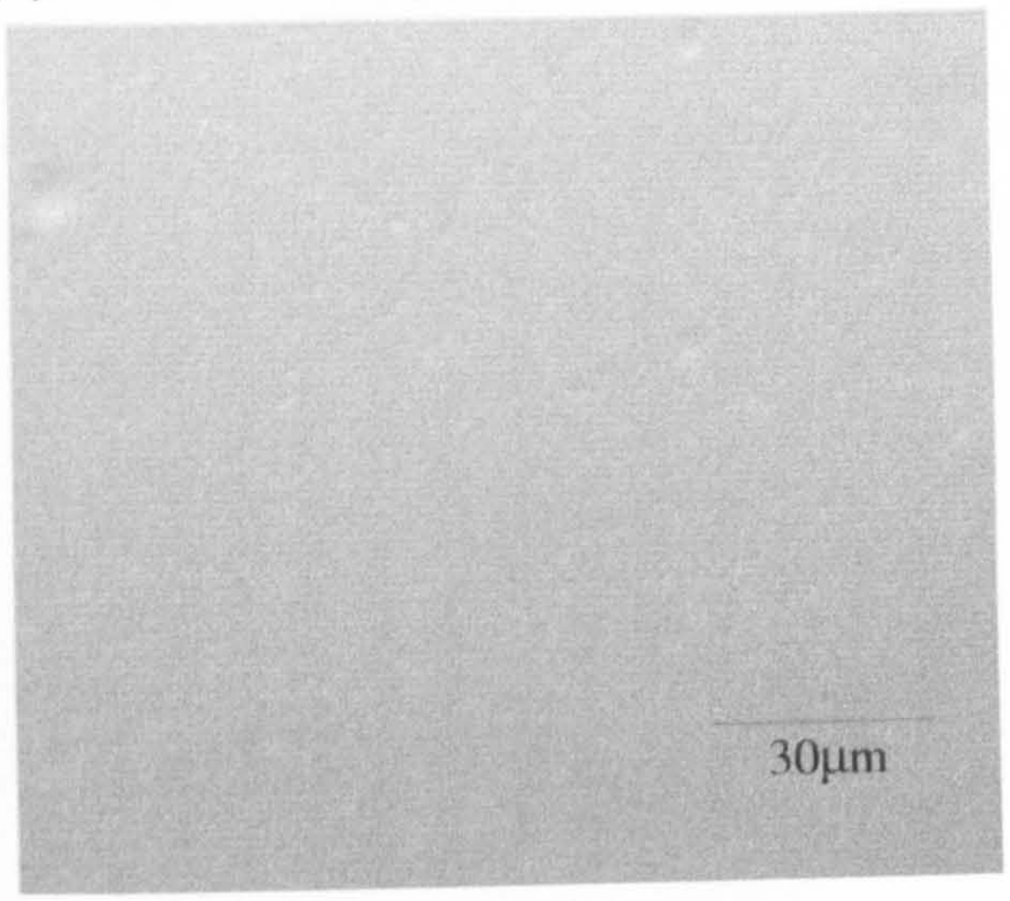

(b)

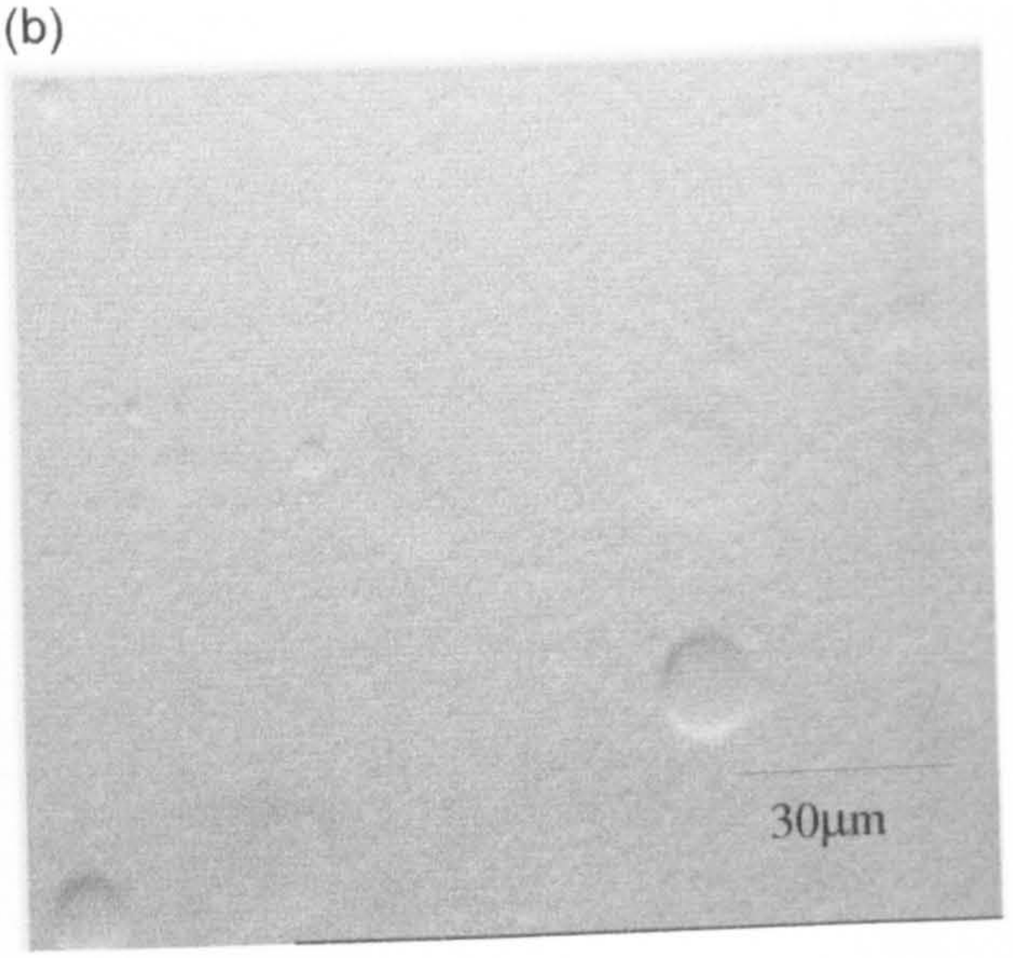

(c)

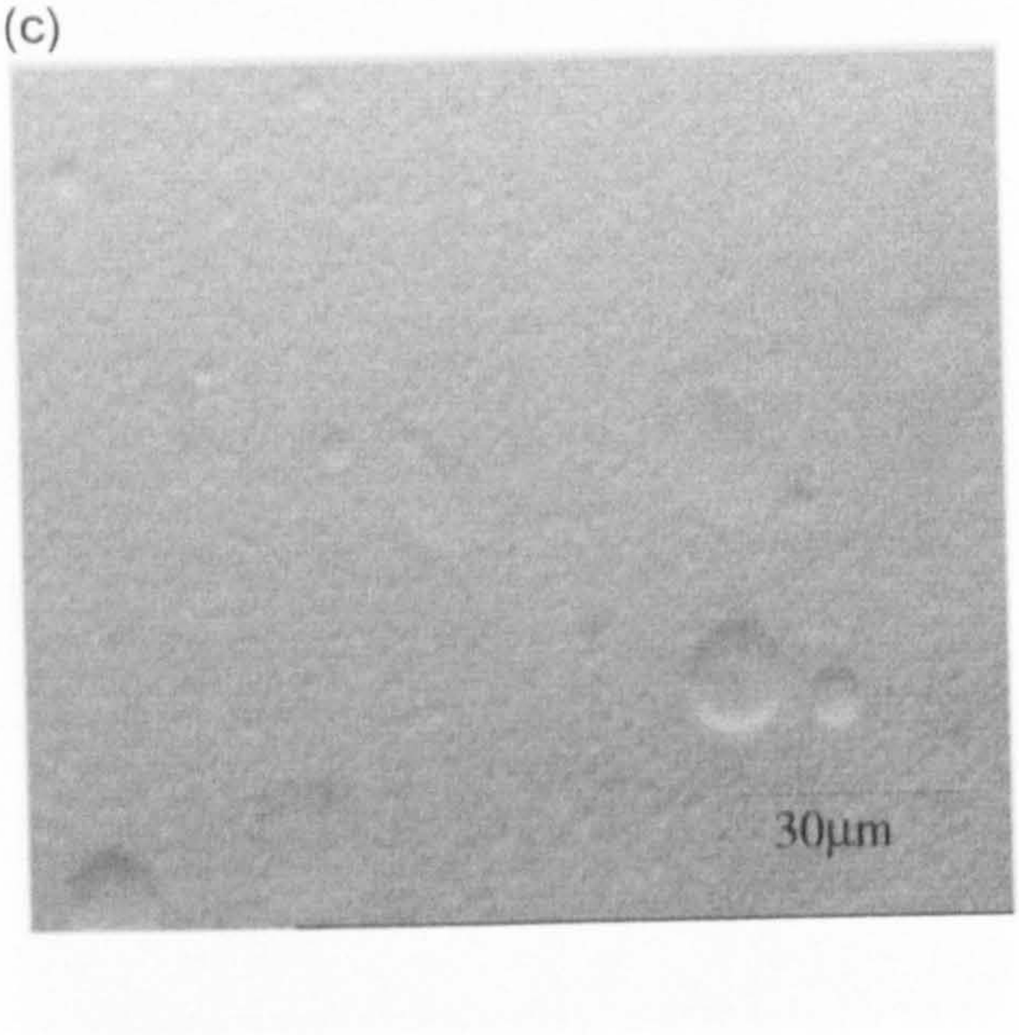

(d)

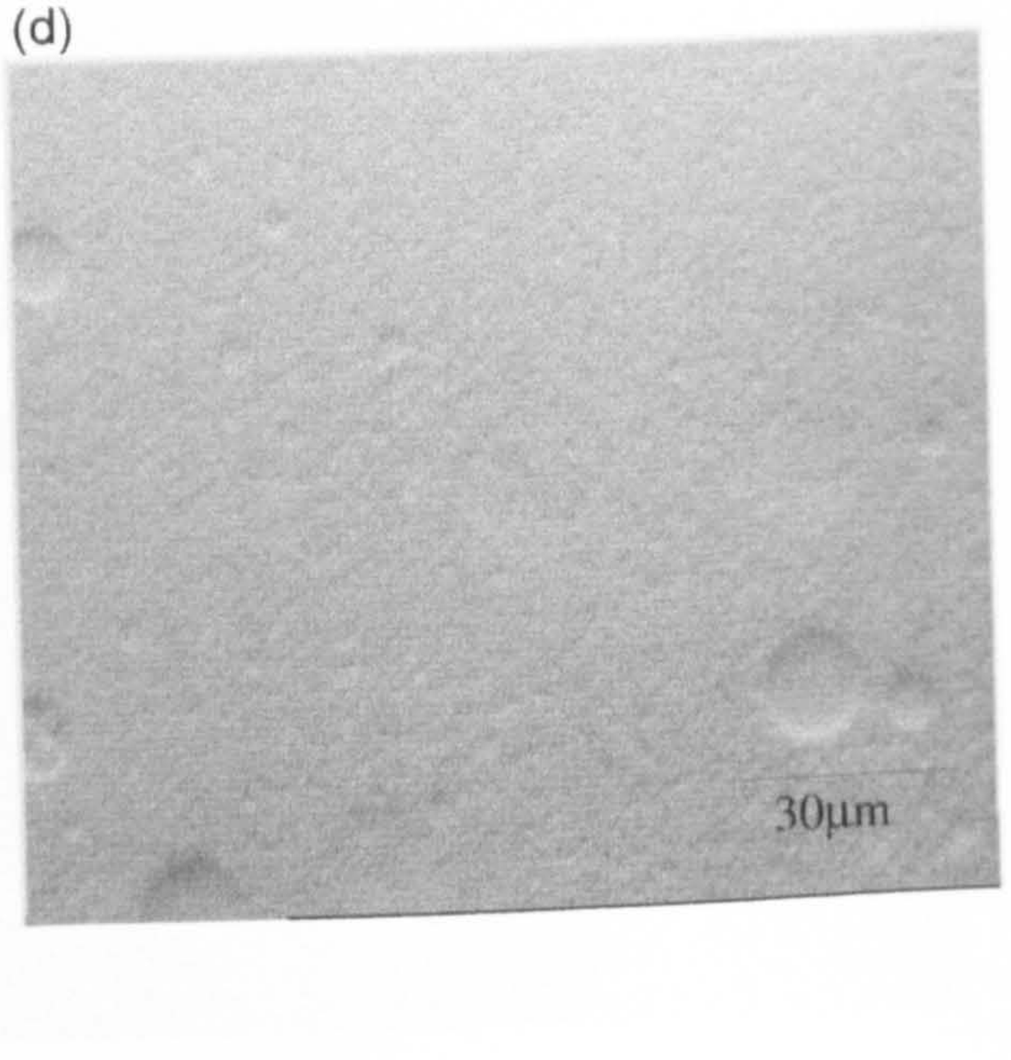

All of the substrates showed that the fixed cross-linked PDMS droplets deposited individually across the substrates, without any evidence of droplet-droplet flocculation or coalescence.

Deposition profiles were obtained for each substrate as a function of time using a fixed cross-linked PDMS emulsion containing 0.05(v/v) total monomer and 0.05 (v/v) MTMS in figure 9.16(a-d) and the data listed in table 9.6. The deposition profile obtained for mica surface from the investigations discussed in section 9.2.1 were denoted with (*) and were included as a comparison for the the other substrates.

The most significant feature of the deposition profiles was the high number of droplets that were observed to deposit on each of the substrates. The APTES modified surface showed the highest number of deposited droplets, was over 40% more than that observed for the mica surface, while the rate of deposition was almost a magnitude faster. This can be partially attributed to the efficiency of the surface heterogeneity to capture the depositing droplets but also the surface topography that held them into position. However, the average surface roughness is lower than the acid cleaned and the Repelcote modified substrates. Therefore, it could be suggested that the accelerated droplet adhesion was dominated by the chemical modification of the glass by the positively charged primary amine groups present on the APTES chains. This in turn created an attractive coulombic interaction between the negatively charged droplet and the positive substrate surface.

Fig 9.16: Deposition profiles as a function of time; (a) APTES modified glass, (b) Repelcote modified glass, (c) Mica*, (d) Acid cleaned glass,(e) Lysine modified glass,

(a)

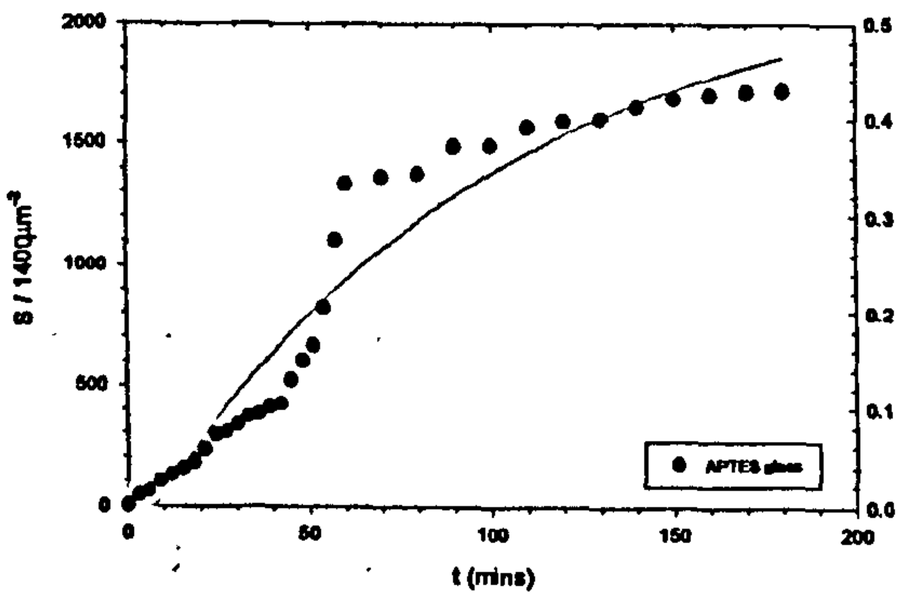

(c)

(b)

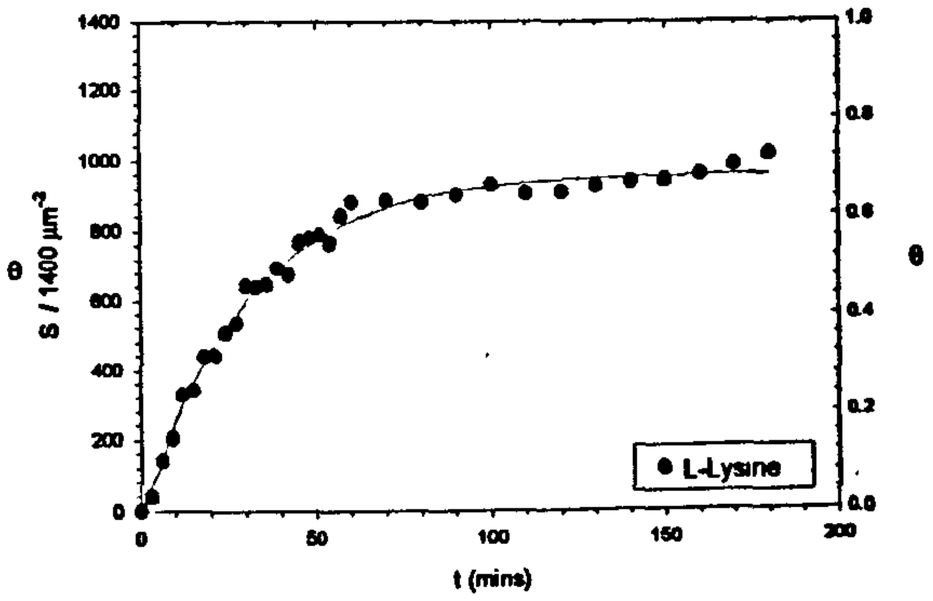

(d)

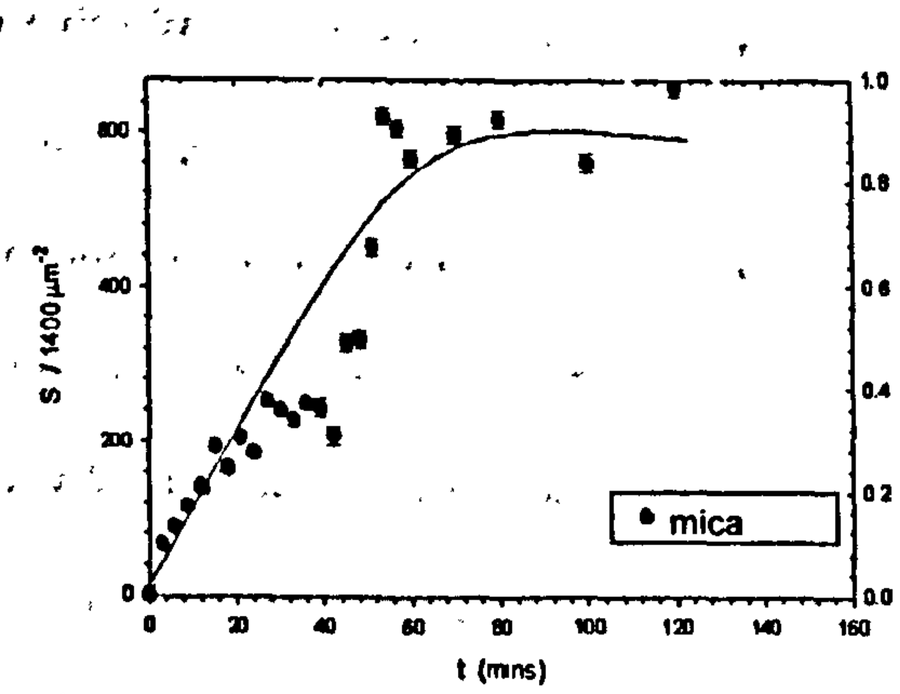

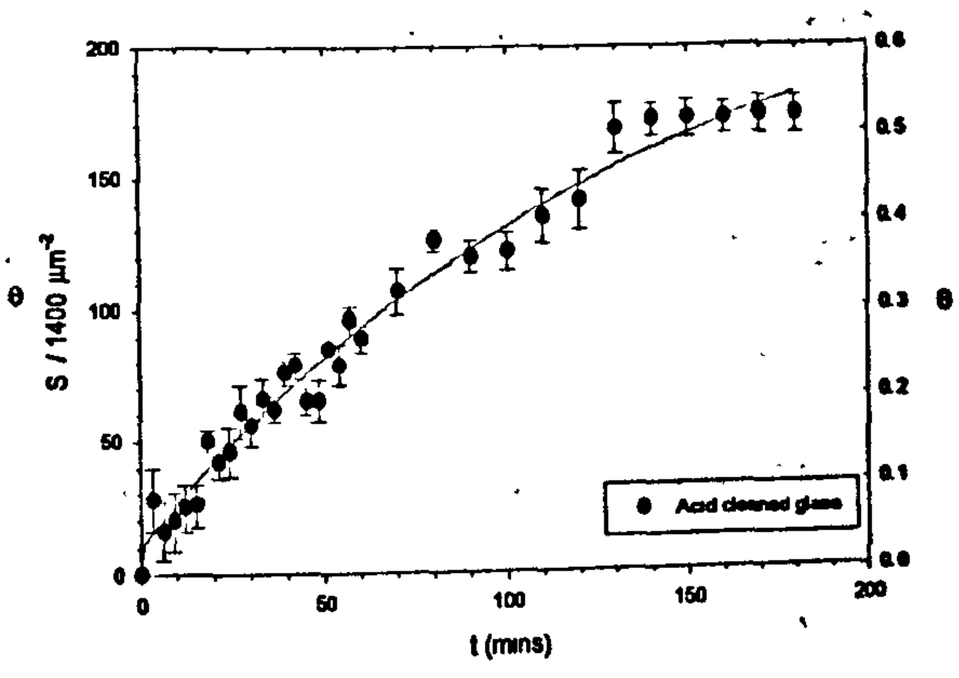

(e)

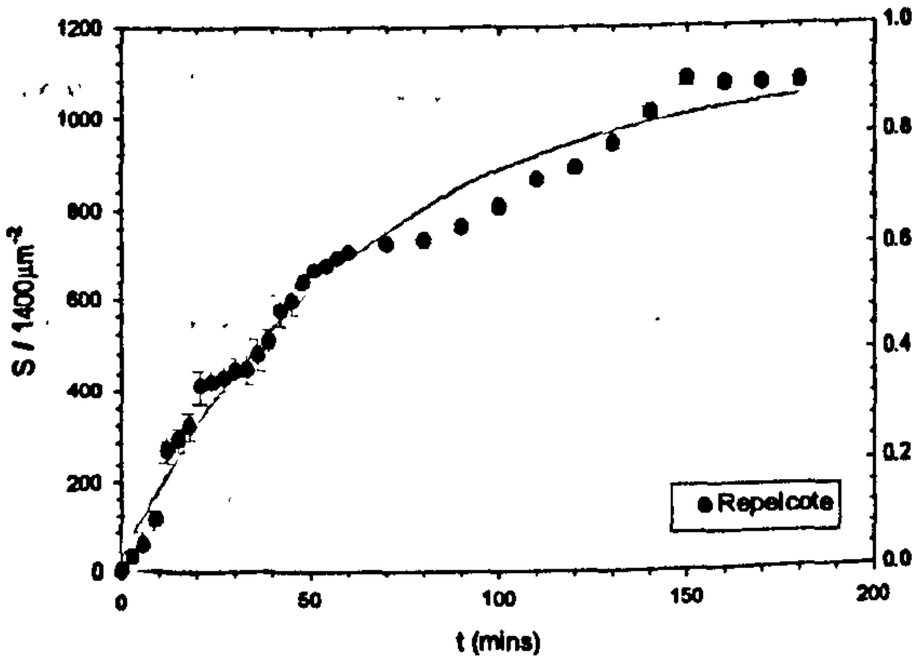

Table 9.8 Comparison of rate values on different substrates

Substrate	Spl $_{Nd}$	Error (+/-)	t_{Spl} (mins)	θ_{max}	k_d/s^{-1}	R^2
APTES mod. Glass	1600	54.5	50	0.39	$2.02x10^{-3}$	0.90
Mica*	*660	11.1	*90	*0.90	*$3.96x10^{-4}$	0.94
Lysine mod. Glass	900	27.1	50	0.86	$5.67x10^{-4}$	0.87
Acid clean glass	175	4.3	130	0.38	$2.79x10^{-4}$	0.91
Repelcote mod. Glass	1100	22.9	150	0.75	$3.25x10^{-4}$	0.52

* Data obtained from section 9.2.1

The L-Lysine and Repelcote modified glass substrates showed 30% and 35% greater droplet deposition number than that observed for mica investigations, respectively. The presence of surface heterogeneity prevented the ability of the droplets to spread on the substrate surface, which reduced the blocking effects and allowed a greater number of droplets to approach the surface. Further more, the L-Lysine substrate was observed to have a lower deposited droplet number than the Repelcote substrate and reached an equilibrium deposition value in half the time. Therefore an increase in droplet deposition could not be entirely attributed to the increase in surface roughness. Results obtained from the three phase contact angle experiments showed little change in the spreading behaviour of the droplets between the surfaces, regardless of the surface chemical composition, see chapter 8. However, the L-Lysine modified glass substrate possessed a much lower negative surface potential than that measured for the acid cleaned and Repelcote glass. This property would reduce the repulsive electrostatic forces between the substrate and approaching droplets and is reflected in the rapid deposition rate. This is in good agreement with the predictions from calculated pair potential curves, which showed a steep increase in the energy barrier as the droplets came into close proximity to substrates with

increasingly negative surface potential.

It is interesting to note that although the acid cleaned glass substrate possessed a similar surface roughness and negative potential to the Repelcote substrate, the droplet deposition number was significantly lower than any of the substrates investigated. This observation could be attributed to the uneven surface topography. The AFM images included in chapter 8 show the unusual "pit" or "crater" pattern created from the harsh acid cleaning conditions used to produce the substrate surface. The height of the surface heterogeneities could create large potential differences and unpredictable eddy currents which would effect approaching droplets.

A detailed study of the spreading behaviour of the cross-linked droplets on contact with the modified substrates is shown in figure 9.17. It was possible to note that the contact area made by the droplets after initial deposition was maintained throughout the duration of the experiments, without any significant contact angle hysteresis observed on any of the substrates investigated. In fact, the presence of surface roughness on the Repelcote substrate, acid cleaned substrate and L-Lysine modified substrate caused the contact angle to contract slightly after deposition as the edge of each droplet adjusted to fill the hollows created by the substrate heterogeneity. The APTES modified glass displayed the largest contact area between the deformable droplet and the substrates due to the attractive coulombic interaction forces. However, the contact angle was pinned in position and prevented from spreading by the high level of surface roughness.

Fig 9.17 Droplet area spread as a function of time

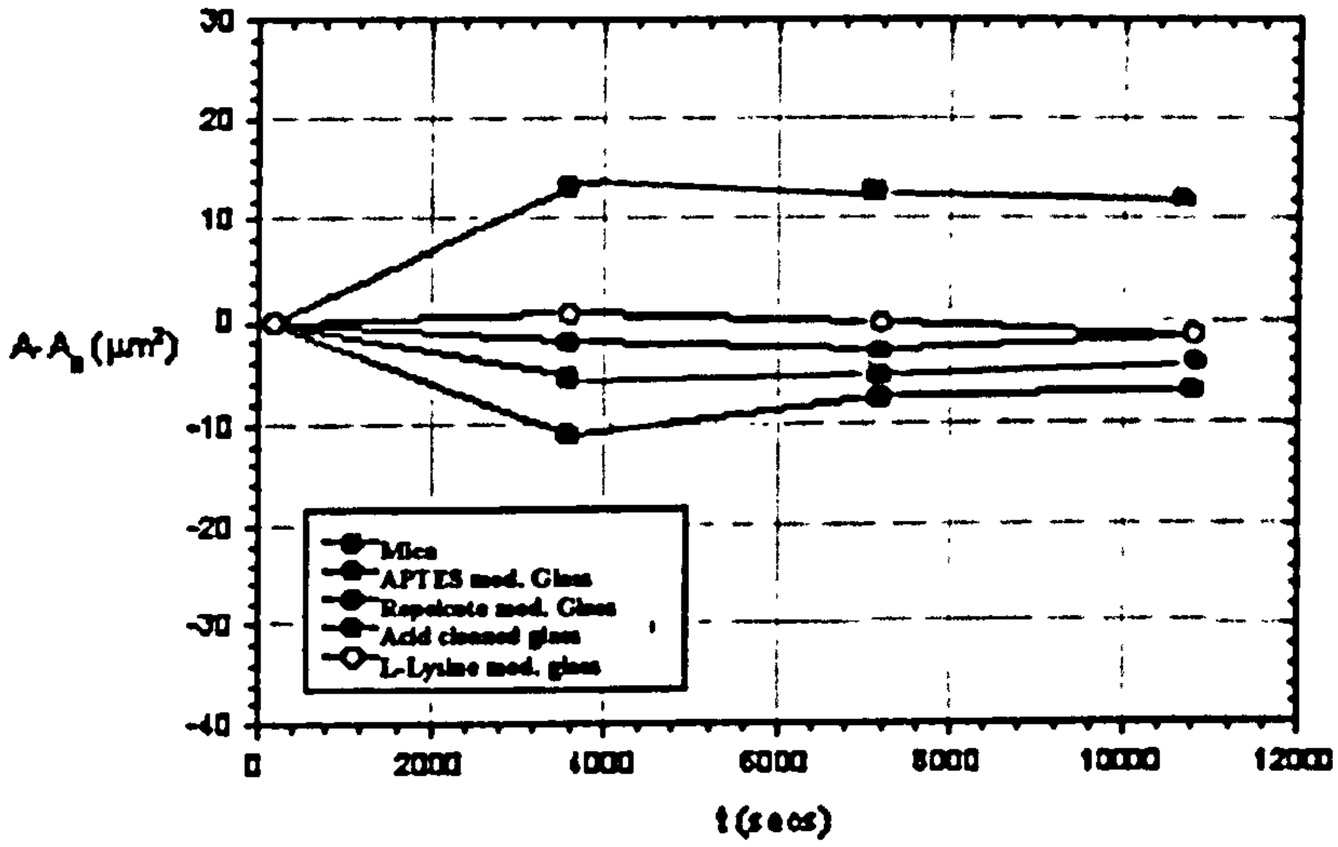

The partial radial distribution function g(r) of deposited fixed cross-linked PDMS droplets was plotted for each chemically modified substrates and compared over time in figure 9.18 (a-c). The deformable droplets were observed to deposited randomly and evenly across each of the collector surfaces, similar to that previously discussed fro mica , section 9.2. However, all of the chemically modified glass substrates displayed far longer average separation distances between the deposited droplets, which in turn corresponds to the relatively high deposition number discussed in figure 9.16. This behaviour can be observed for all of the substrates investigated, irrespective of surface composition. It could therefore be suggested that the surface roughness played a dominant role over the distribution of the the droplets on the collector site than chemical or electrostatic interactions through contact line "pinning" mechanisms.

It could be observed that the overall distribution pattern did not change significantly over time for any of the substrates investigated. The radial distribution obtained after initial contact with the roughened surfaces was maintained even

Fig 9.18 Deposition radial distribution as a function of substrate chemistry;

(a) 3 mins, (b) 60 mins, (c) 180 mins,

(a)

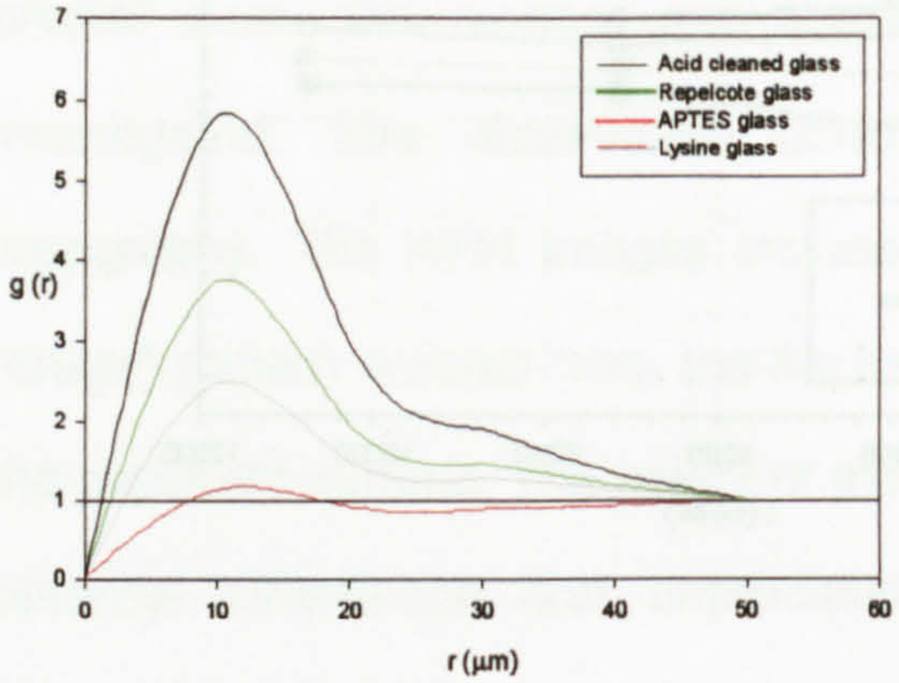

(b)

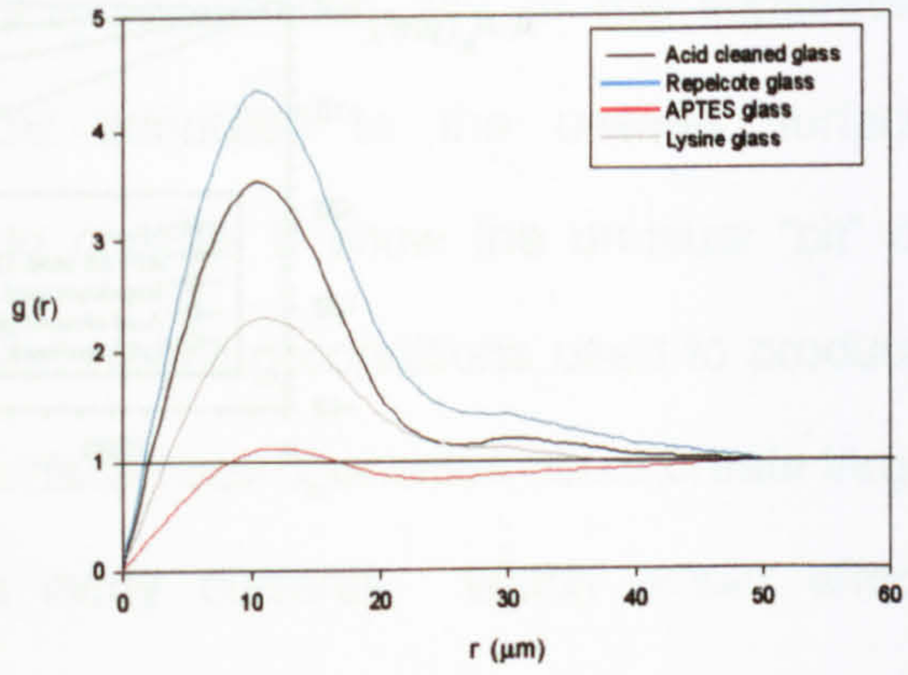

(c)

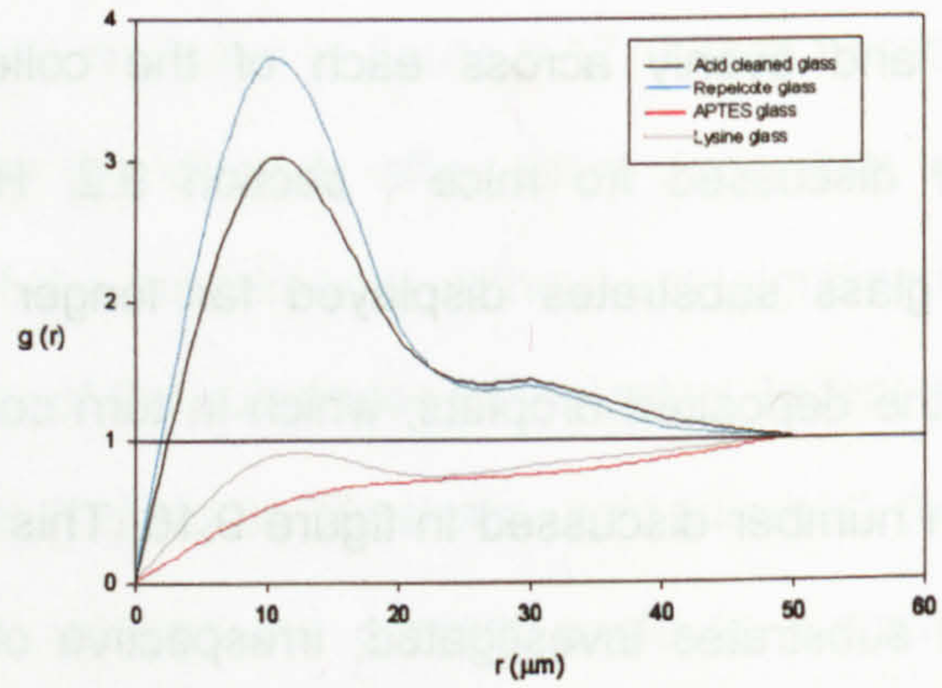

after 3 hours of deposition. However, there was a distinct difference in the location and magnitude of high deposition coverage. The acid cleaned glass and Repelcote modified glass surfaces displayed the highest partial radial distribution peaks, with the greatest deposition coverage at distances over 25μm from the stagnation point center. One suggestion could be that the deformable droplet is not sufficiently captured on contact with these two surface due to the presence of a significant electrostatic repulsive force. However, the droplet inertia is slowed further away from the stagnation point by the presence of surface asperities.

In contrast, the L-Lysine modified glass and APTES coated glass substrates displayed almost immediate optimum deposition coverage shown by the proximity of the partial radial distribution to unity. This behaviour corresponds to the low contact angles formed between the substrates and deformable droplets despite their relatively high surface asperity value, see chapter 8. In addition, uniform surface coverage over the entire collector surface appears to be achieved almost immediately after initial contact with the substrate. It could therefore be suggested that the distribution of deposited droplets was dominated by surface charge. However, presence of surface roughness, induced contact angle pinning, allowed a greater number of droplets to pack onto the surface.

9.3 References

1. Siberzan.P, Perutz.S, Kremer.E, Chaudy.M, Langmuir, 10, 2466, 1994
2. Choi.G, Soojin.K, Ulman.A, Langmuir, 13, 6333-6338, 1997
3. Wegner PhD thesis , University of Bristol, UK, 1993
4. Elimelech, M; Sep. Technology, 4, 186-212, 1994

5. Kamiti, M, van de Ven.T, Coll.Surf.A, 100, 117-129, 1995
6. Sjolems.J, van der Mei.H, Uyen.H, Busscher.H, FEMS Microbiol.Lett, 69, 263-270.
7. Mahé,M., Vignes-Alder, M., Adler, P.M., J.Coll.Int.Sci., 126, 1, 337, 1988
8. Mahé,M., Vignes-Alder, M., Adler, P.M., J.Coll.Int.Sci., 126, 1, 329, 1988
9.Mahé,M.,Vignes-Alder, M., Adler, P.M., Rousseau,A., Jacquin, C.G., J.Coll.Int.Sci., 9126, 1, 314, 1988
12. Yiantsios, S.G., Karabelas, A.J., J.Colloid Interface Sci., 176, 74, 1995.
13. Fa.K, Paruchuri.V.K, Brown.S.C, Moudgil.B, Miller.J, Phys.Chem, Chem.Phys, 7, 678-684, 2005
14. E.T.Vandenberg, L.Bertilsson, B.Liedberg, K.Uvdal, R.Erlandsson, H.Elwing, I.Lundstrom, Journal of Colloid and Interface Science, 147, 103, 1991
15.Aronson
16.Wiersema.P, Loeb.A, Overbeek.J, J.Coll.Int.Sci., 1966, 22, 78-99
17.Neuman.B, Vincent.B, Krustev.R, Hans-Joachim.M, Langmuir, 20, 4336-4344, 2004
18. Wanless.E, Ducker.W, J.Phys.Chem, 1996, 103, 3207
19.Yiantsios, S.G., Karabelas, A.J., J.Colloid Interface Sci., 176, 74, 1995.

Chapter 10 Horizontal flow cell removal results and discussions

10.1.1 Removal from Mica with varying ϕ MTMS

The hydrodynamic forces required to remove adhered cross-linked PDMS droplets from mica substrate was investigated using the horizontal flow cell method described in chapter 4. An aqueous solution was introduced to observe the colloidal removal mechanisms and measure the critical hydrodynamic shear flow for each system. The removal data from a series of emulsion droplets consisting of a fixed total monomer 0.05(v/v) and varying MTMS ϕ were compared with the data obtained from an uncross-linked PDMS system. The spreading properties of the cross-linked PDMS droplets meant that it was not possible to use the same substrate more than once. Therefore the data obtained from different batches of the same substrate have been plotted and shown in figure 10.1(a-g), where F_{H50} value is denoted by the broken line (----------).Images from each removal experiment are shown in plates XXIV – XXX.

Table 10.1 F_{H50} removal data as a function of MTMS ϕ

ϕ MTMS (v/v)	F_{H50} (nN)	γ_c (ml min^{-1})	% removed total	F_A (N)	ϕ_p (μm)
0.000* (v/v)	*>1.4x10^{-2}	>353	*26.4	4.5x10^{-8}	5.1
0.005 (v/v)	1.3x10^{-2}	350	43.2	3.7x10^{-8}	4.6
0.010 (v/v)	4.8x10^{-3}	240	50.6	1.5x10^{-8}	4.7
0.050 (v/v)	2.9x10^{-3}	226	60.6	9.6x10^{-9}	4.0
0.100 (v/v)	3.6x10^{-4}	200	63.5	4.5x10^{-10}	3.8
0.150 (v/v)	1.5x10^{-4}	126	78.1	3.5x10^{-10}	3.6
0.200 (v/v)	<7.2x10^{-5}	<30	88.3	6.2x10^{-11}	3.5

It should be noted that while the mica surface has an almost constant surface potential of -0.4mV throughout these investigations, there is a simultaneous

Plate XXIV: 0.0(V/V) MTMS (a) After 3hrs (b) 100ml/min^{-1}, (c) 200ml/min^{-1}, (d) 350ml/min^{-1}

(a)

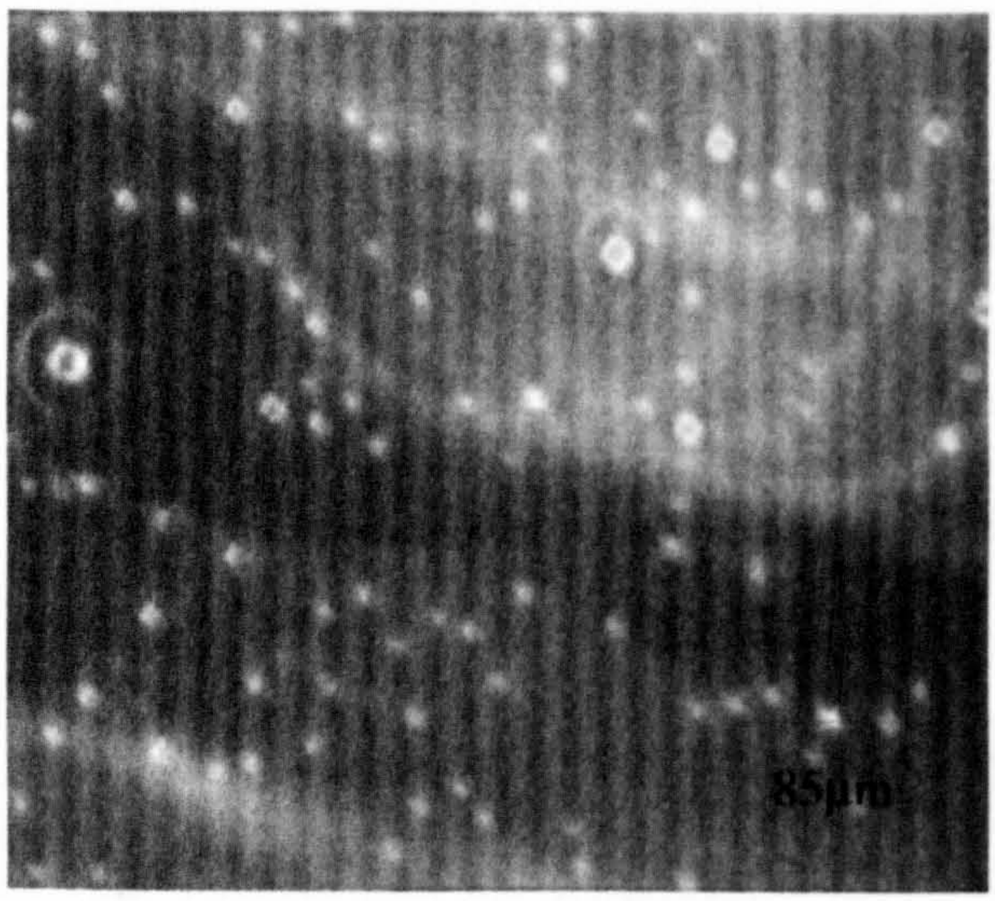

(b)

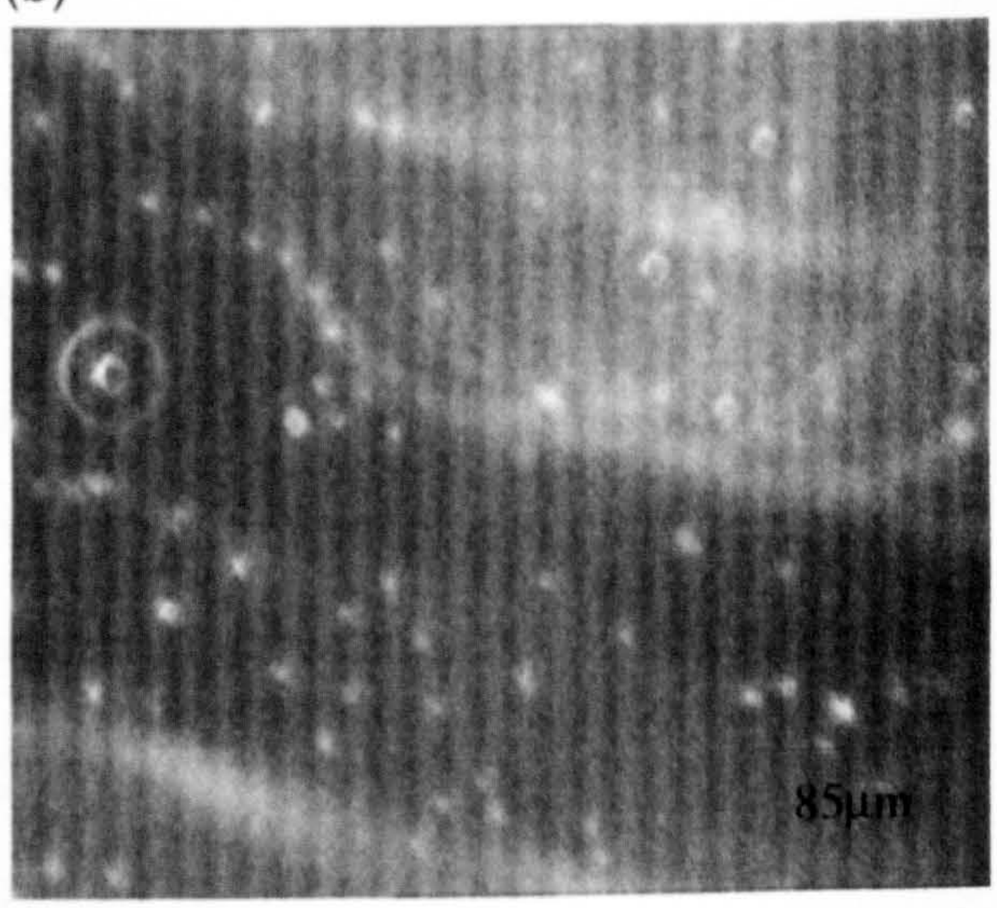

(c)

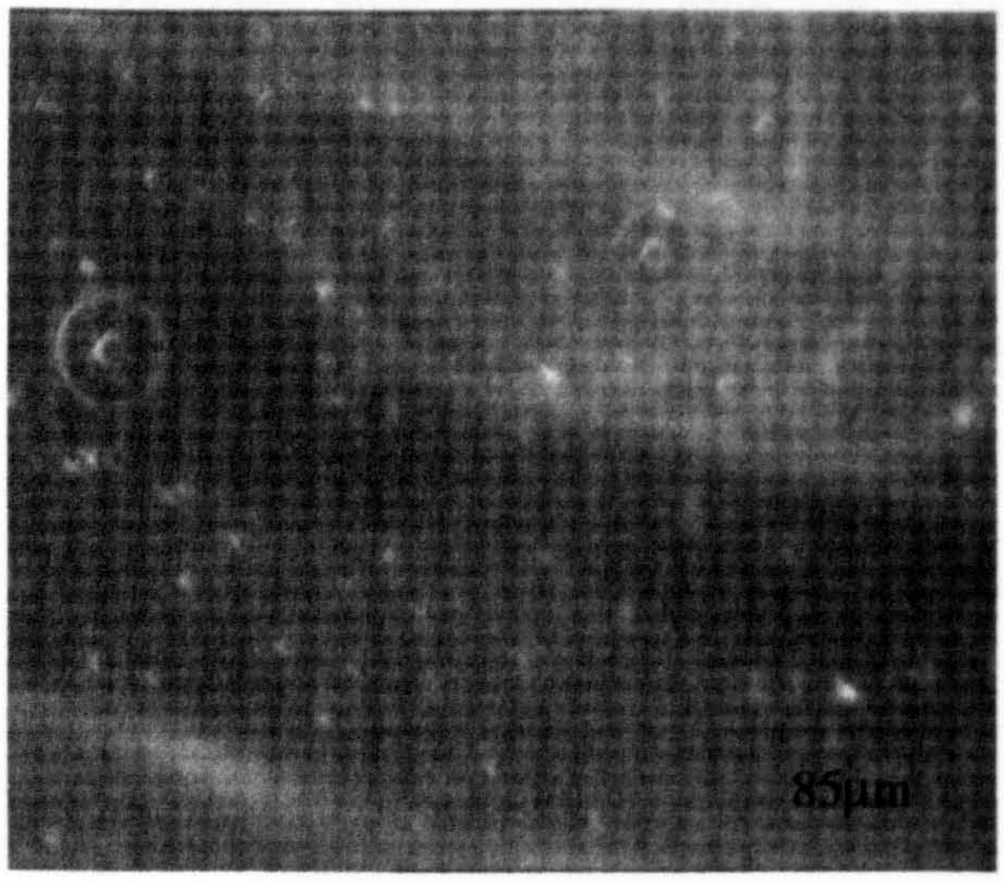

(d)

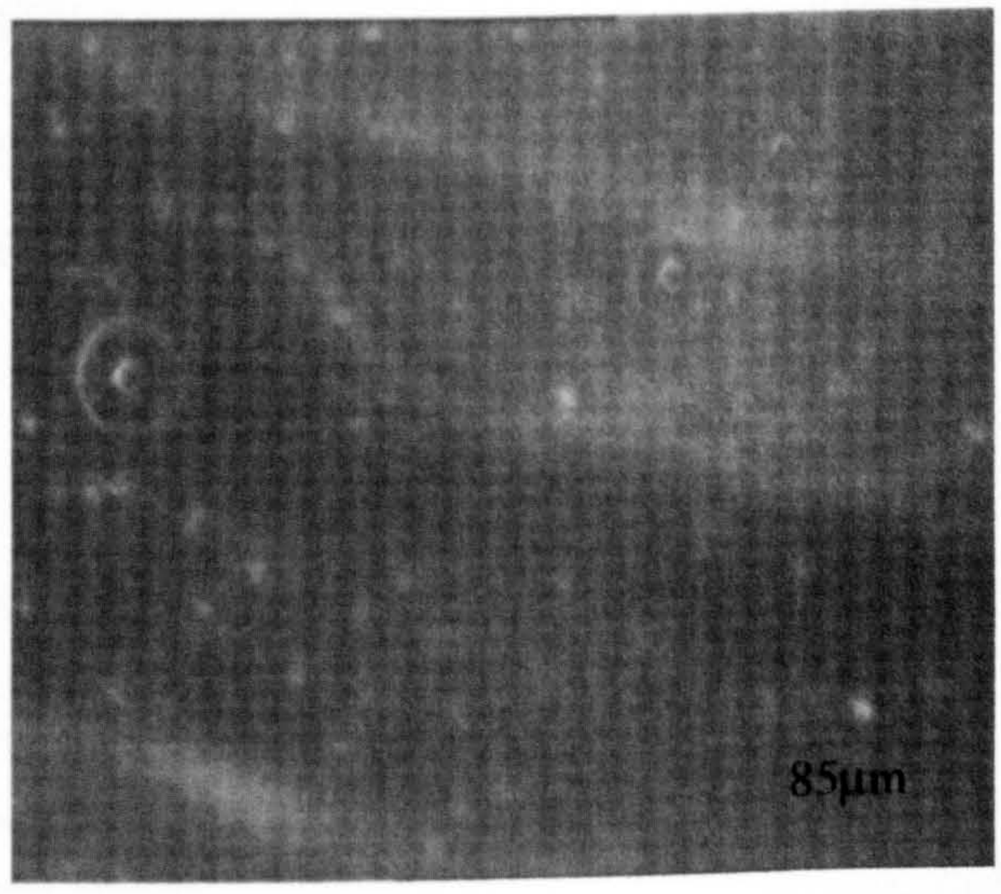

Plate XXV: 0.005(v/v) MTMS (a) After 3hrs, (b) 100ml/min^{-1}, (c) 200ml/min^{-1}, (d) 350ml/min^{-1}

(a)

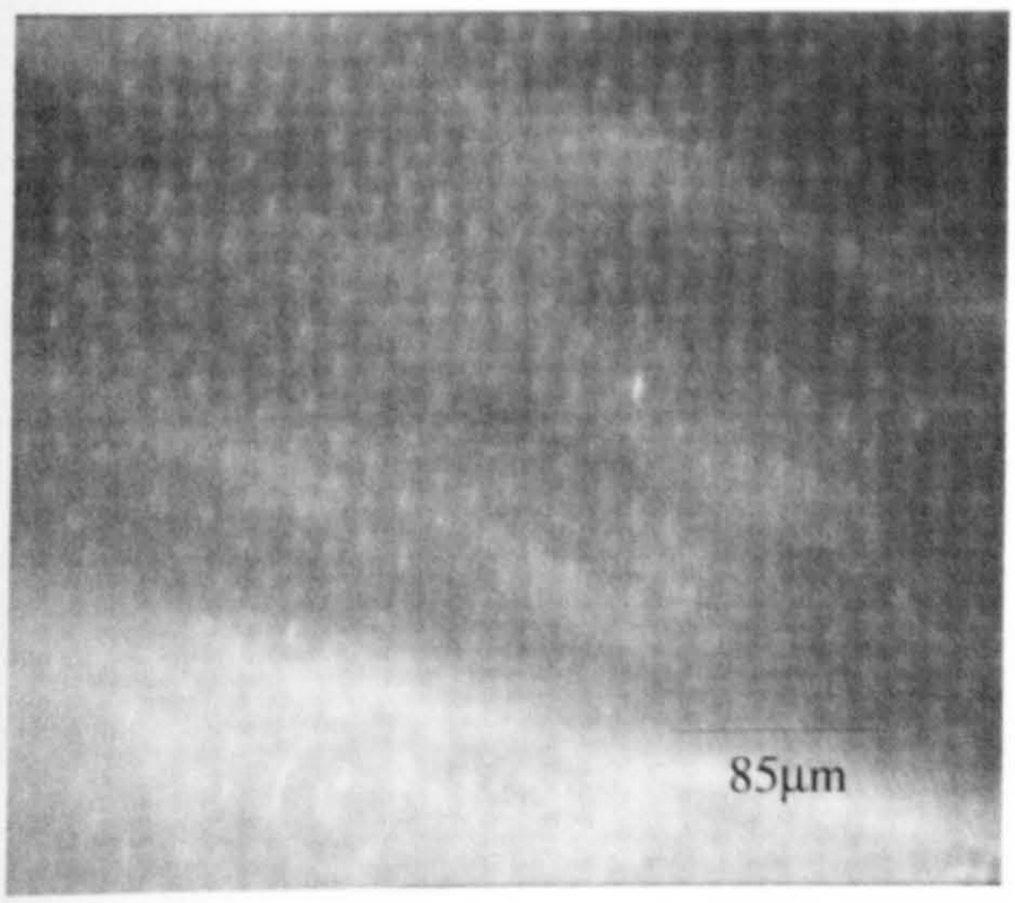

(b)

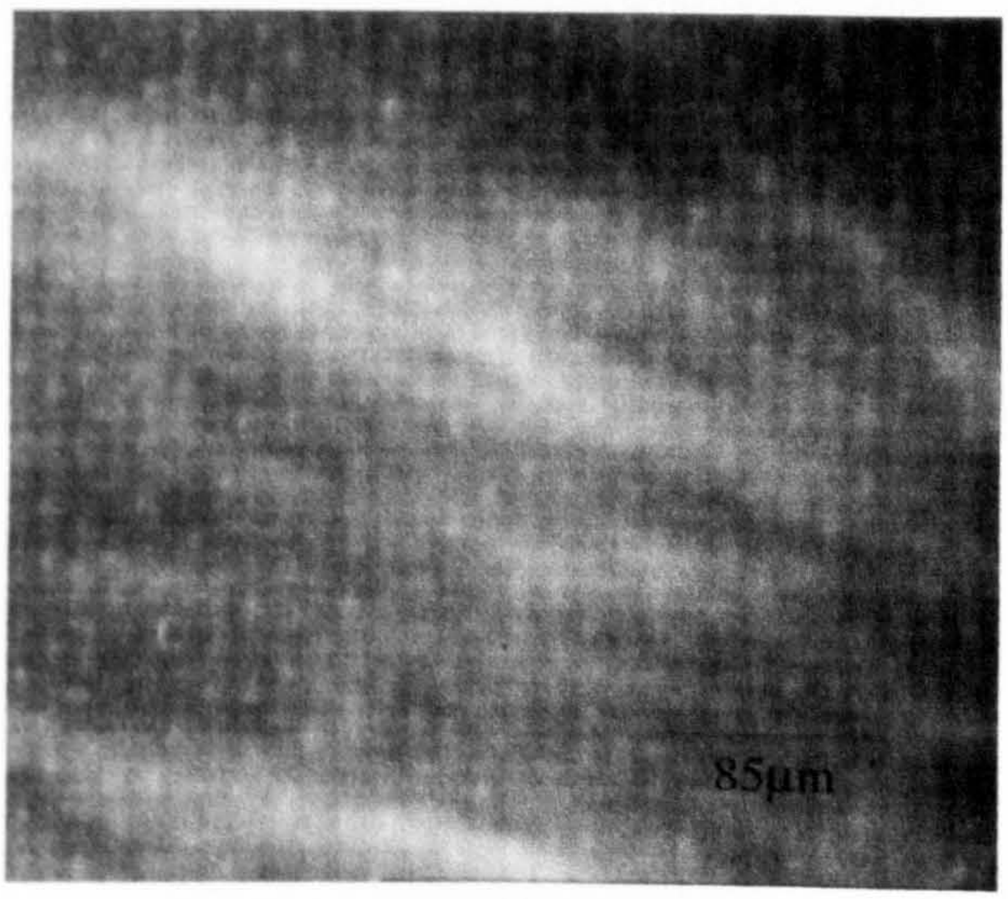

(c)

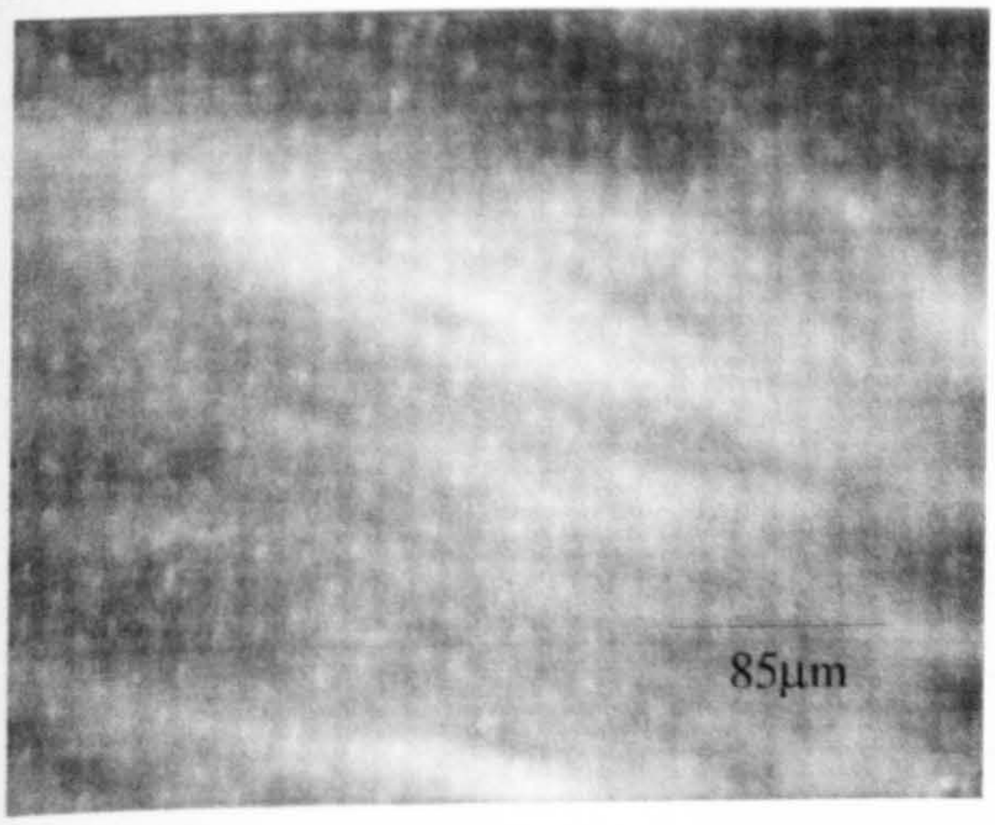

(d)

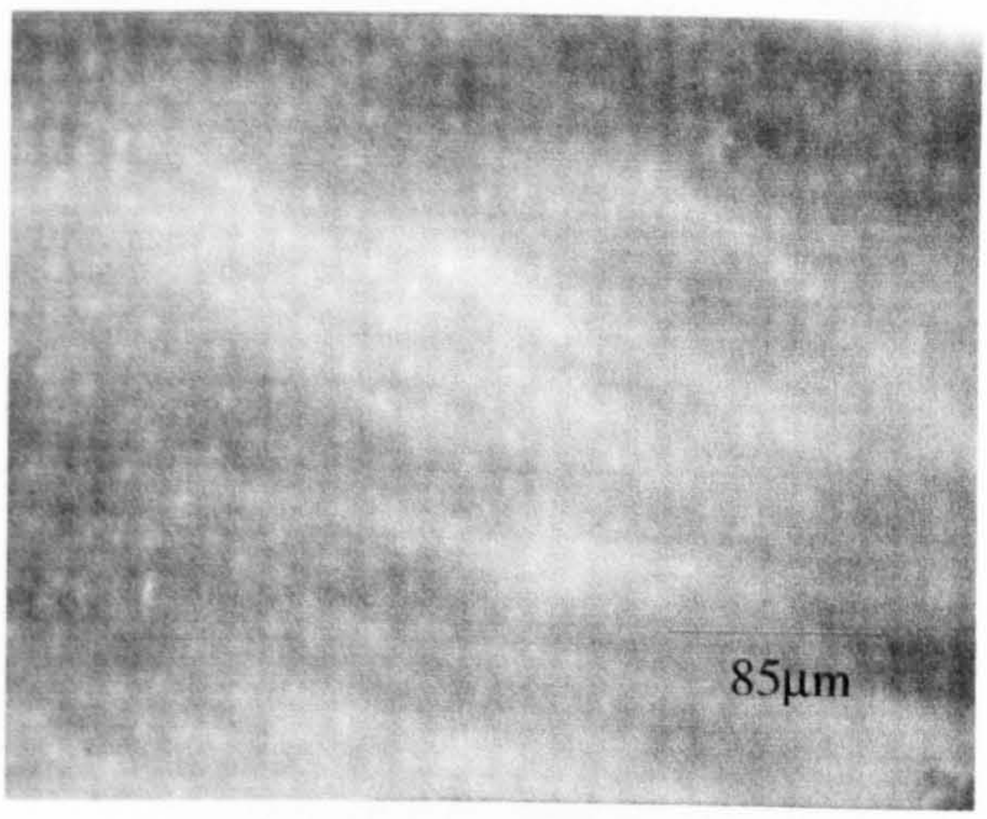

Plate XXVI: 0.01(v/v) MTMS (a) After 3hrs, (b) 100ml/min^{-1}, (c) 200ml/min^{-1}, (d) 350ml/min^{-1}

(a)

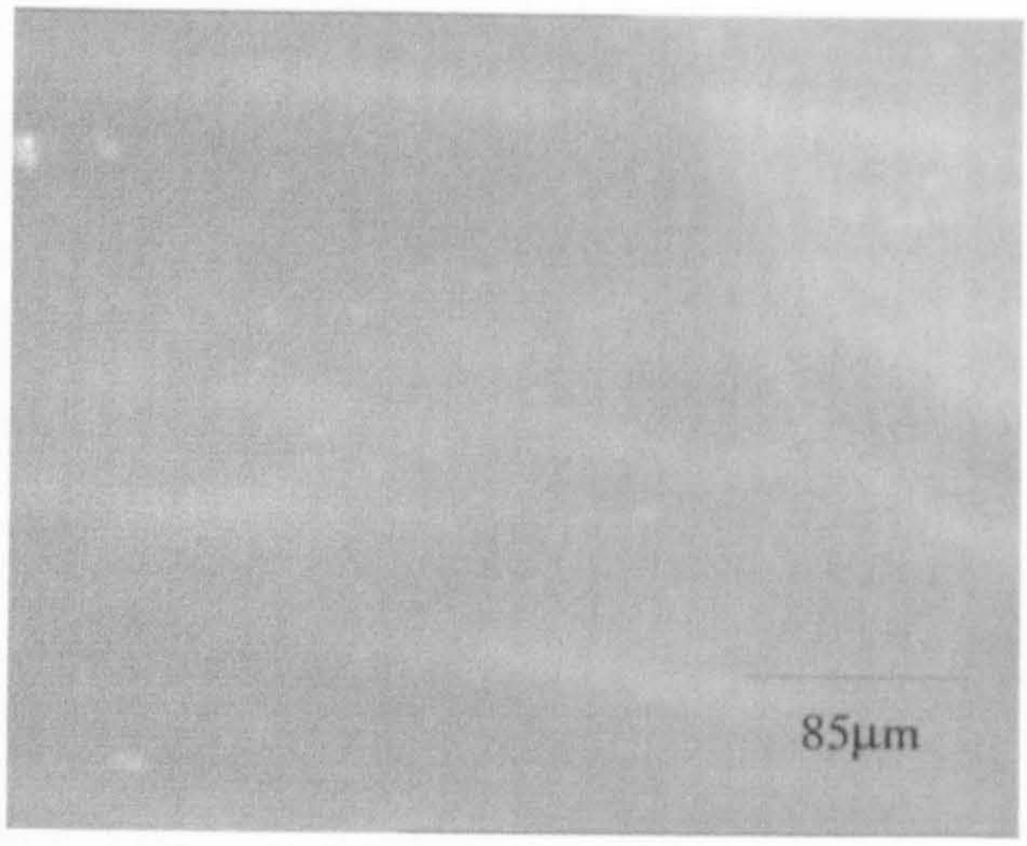

(b)

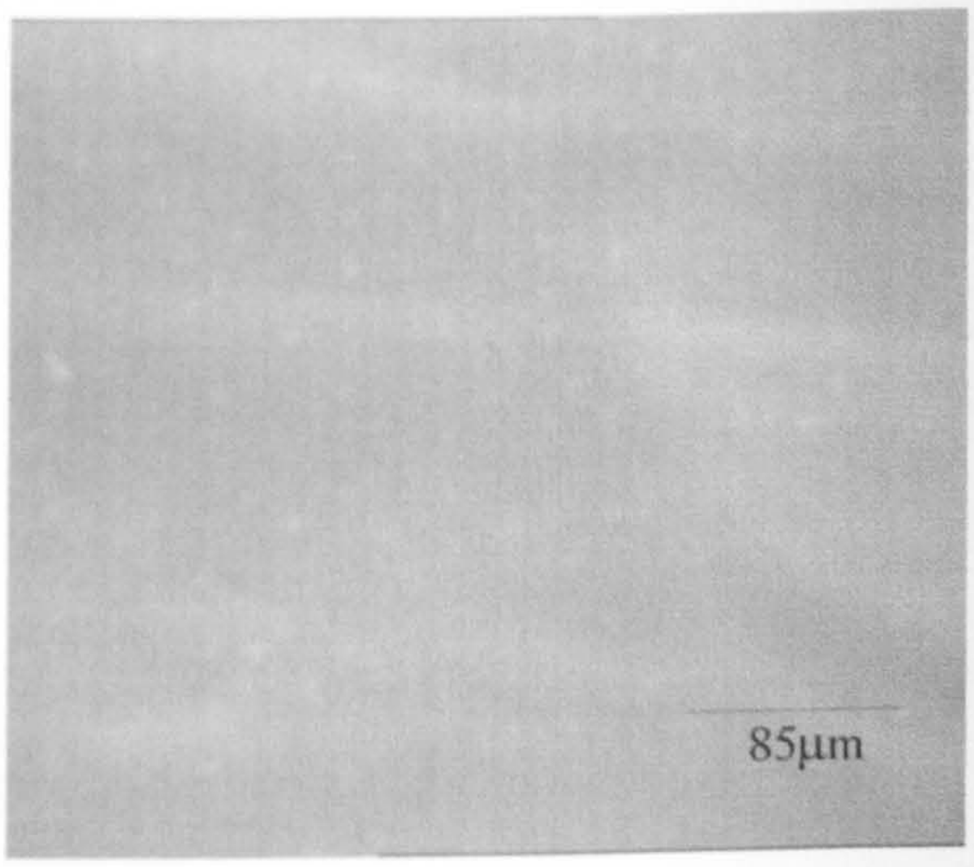

(c)

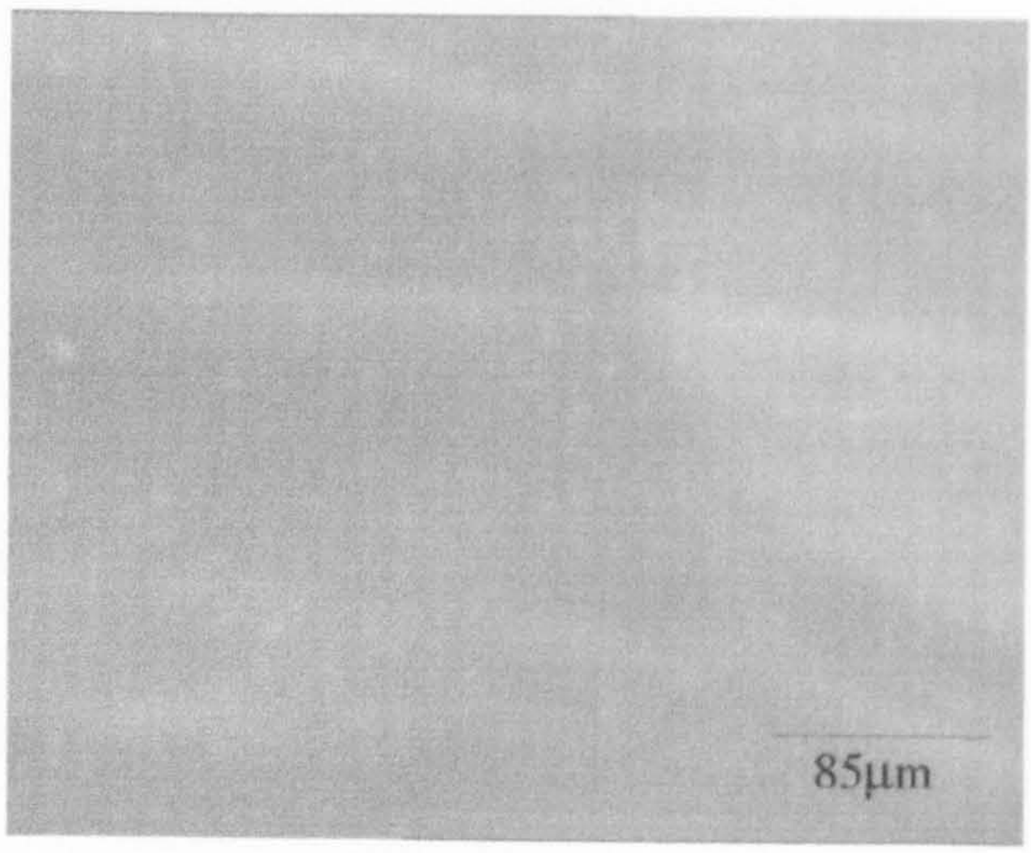

(d)

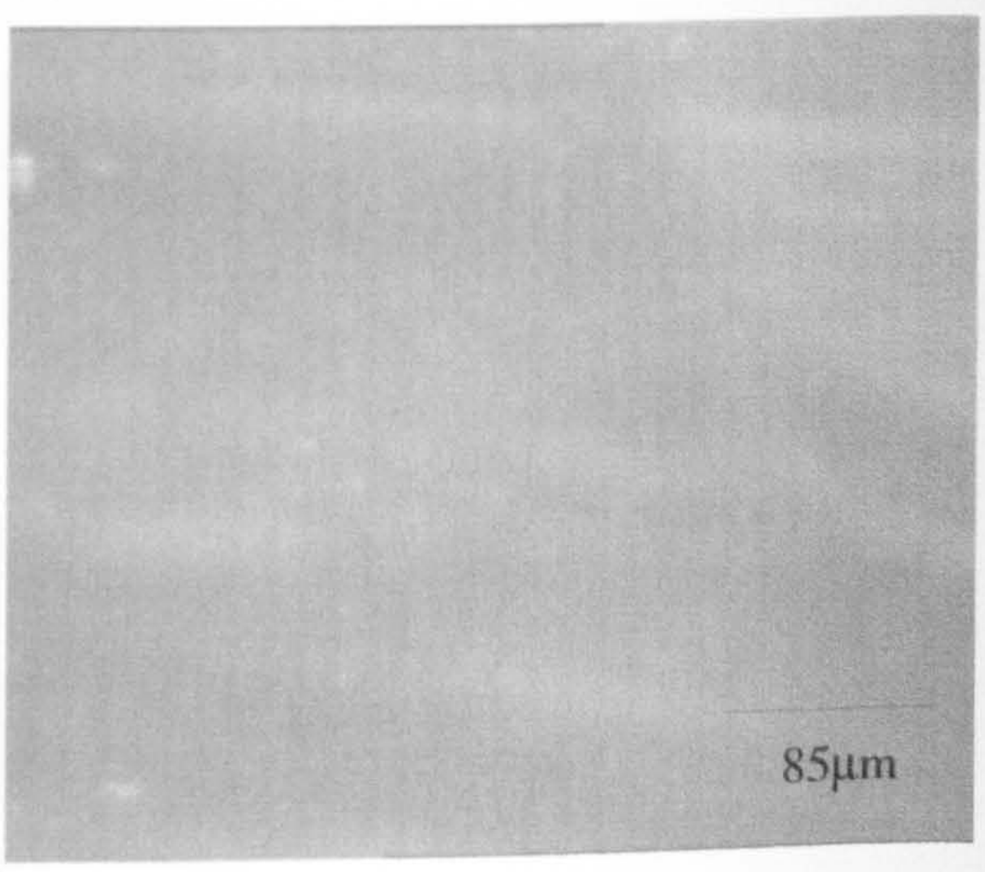

Plate XXVII 0.05(v/v) MTMS (a) After 3hrs, (b) 100ml/min-1, (c) 200ml/min-1, (d) 350ml/min-1

(a)

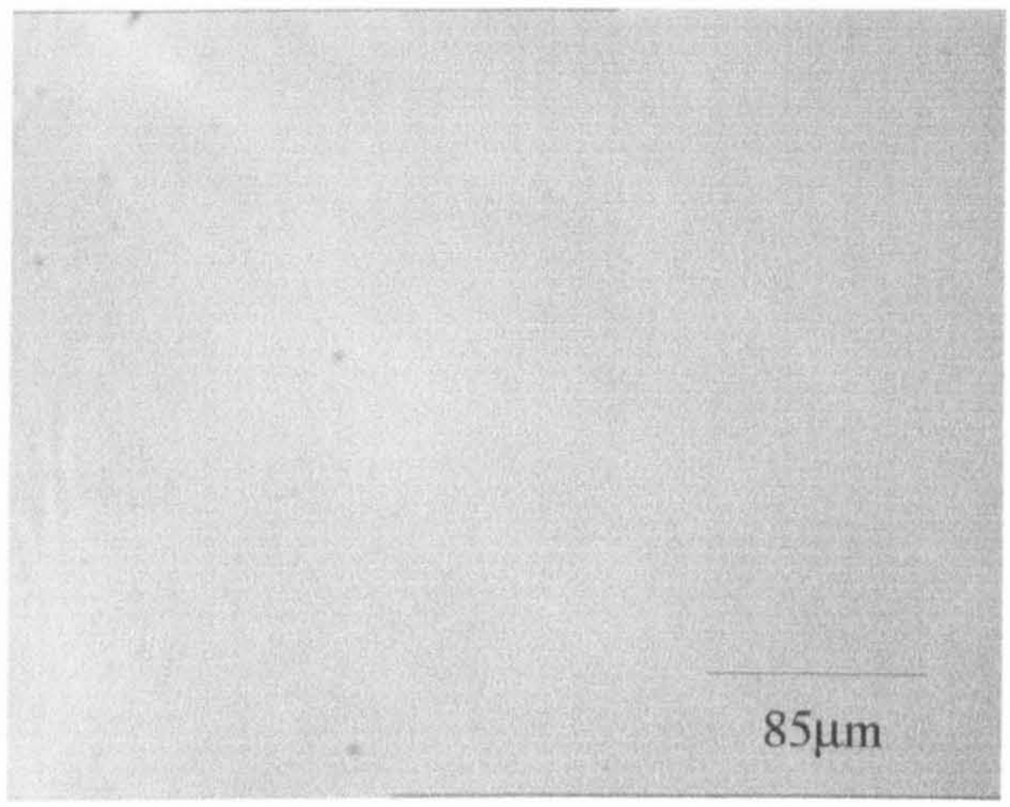

(b)

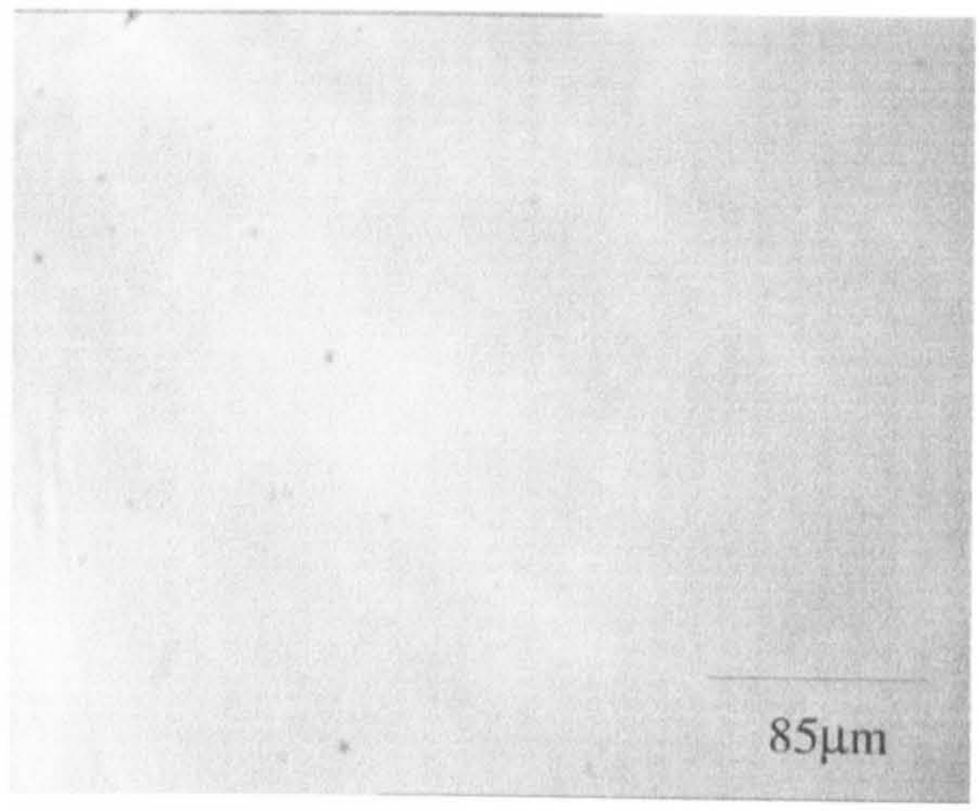

(c)

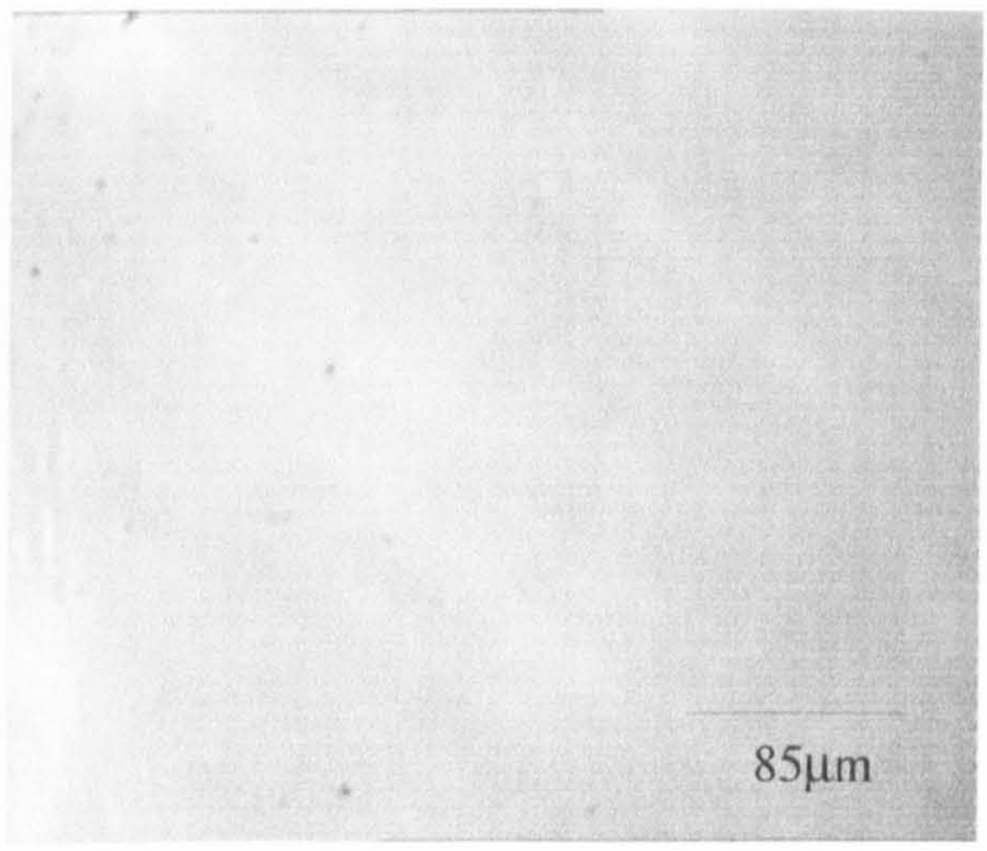

(d)

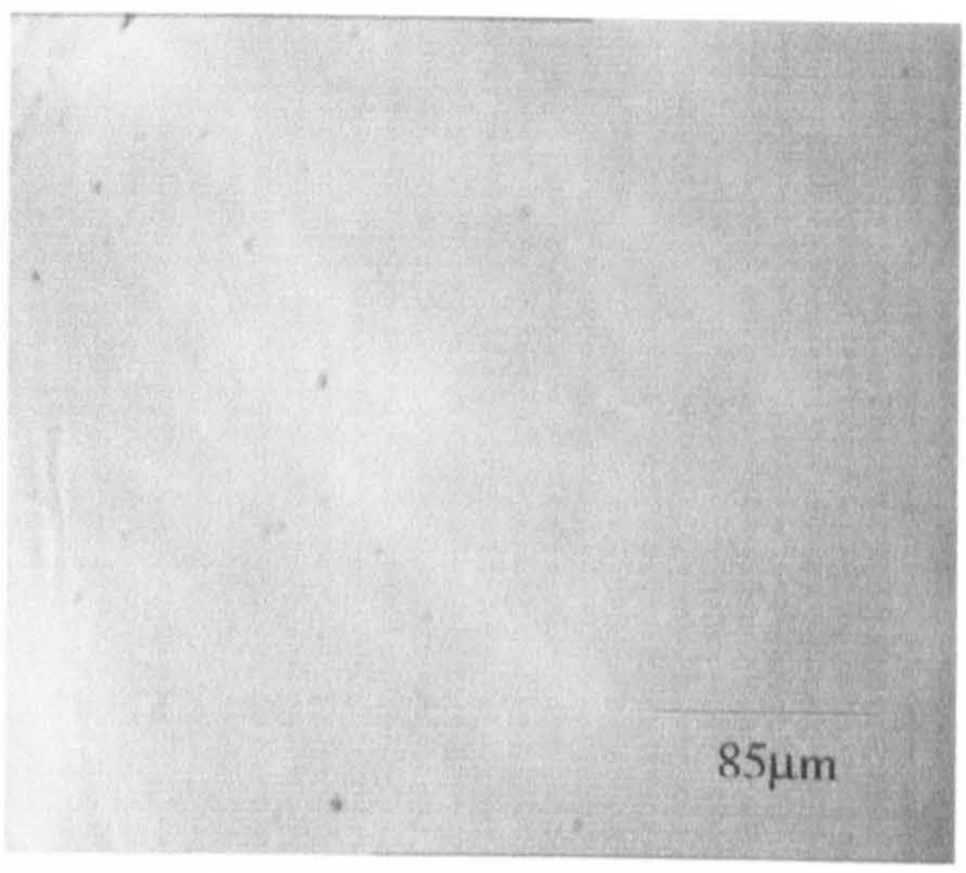

Plate XXIX: 0.15(v/v) MTMS (a)After 3hrs, (b) 100ml/min^{-1}, (c)200ml/min^{-1}, (d) 350ml/min^{-1}

(a)

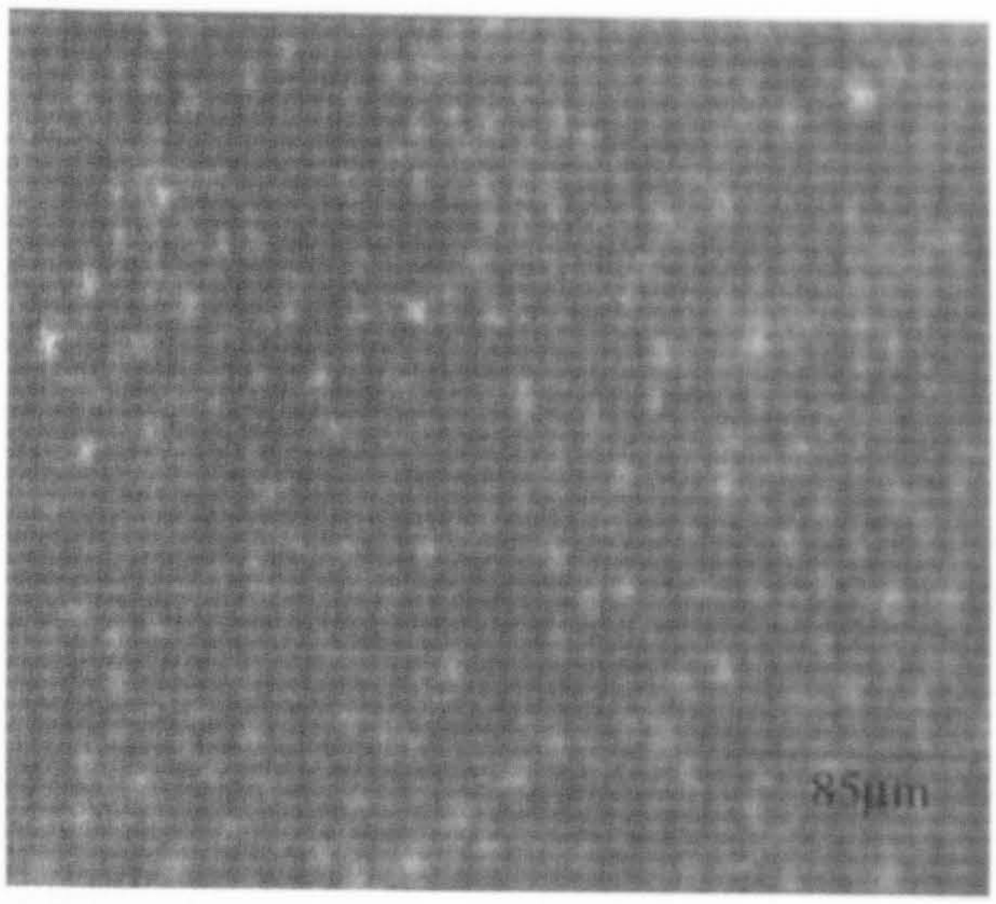

(b)

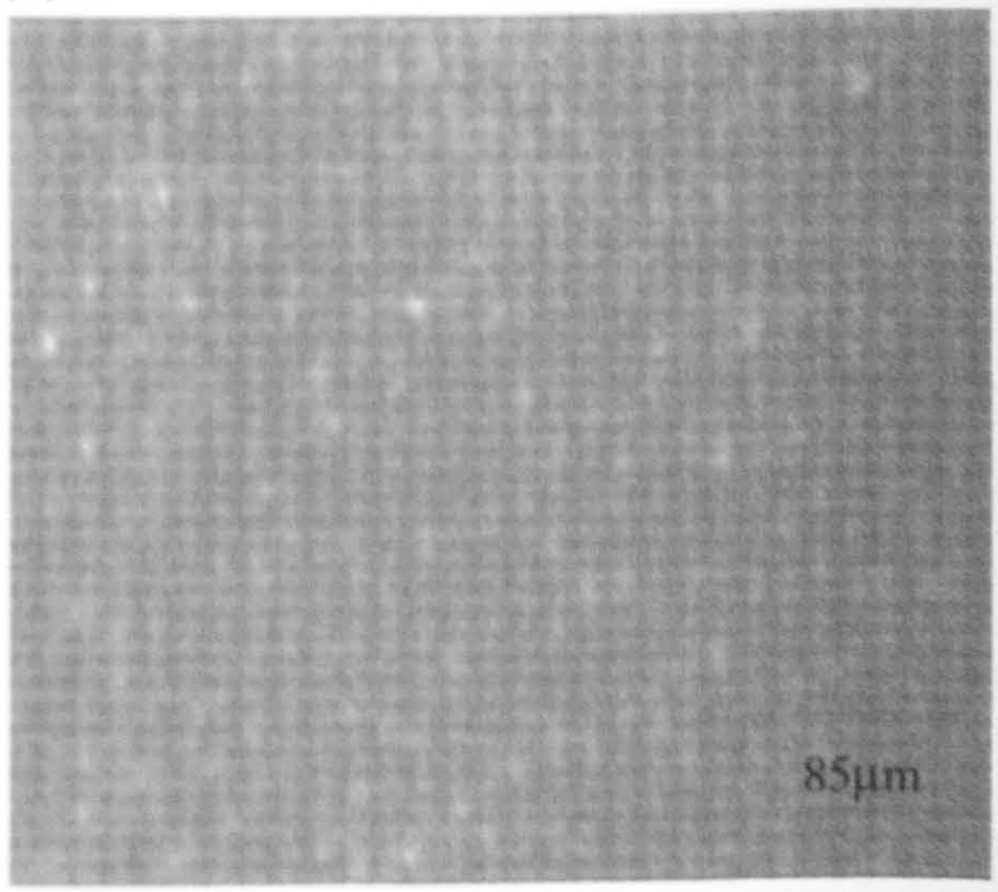

(c)

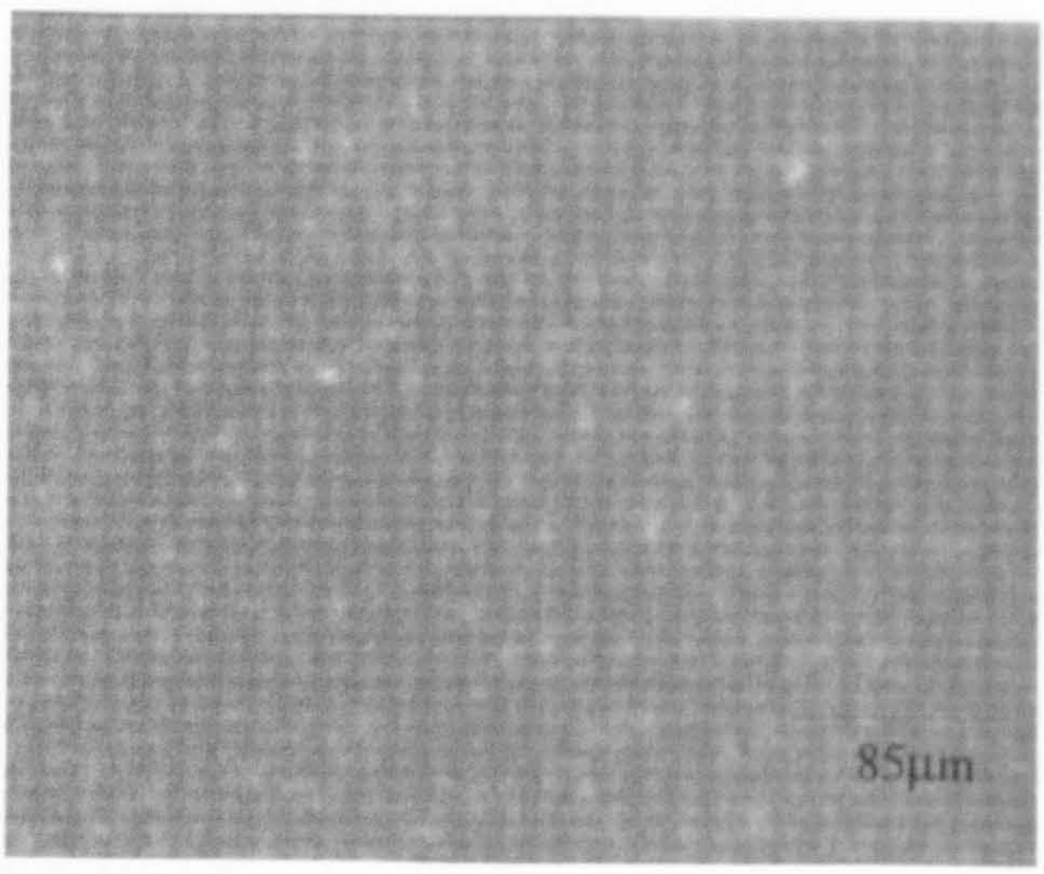

(d)

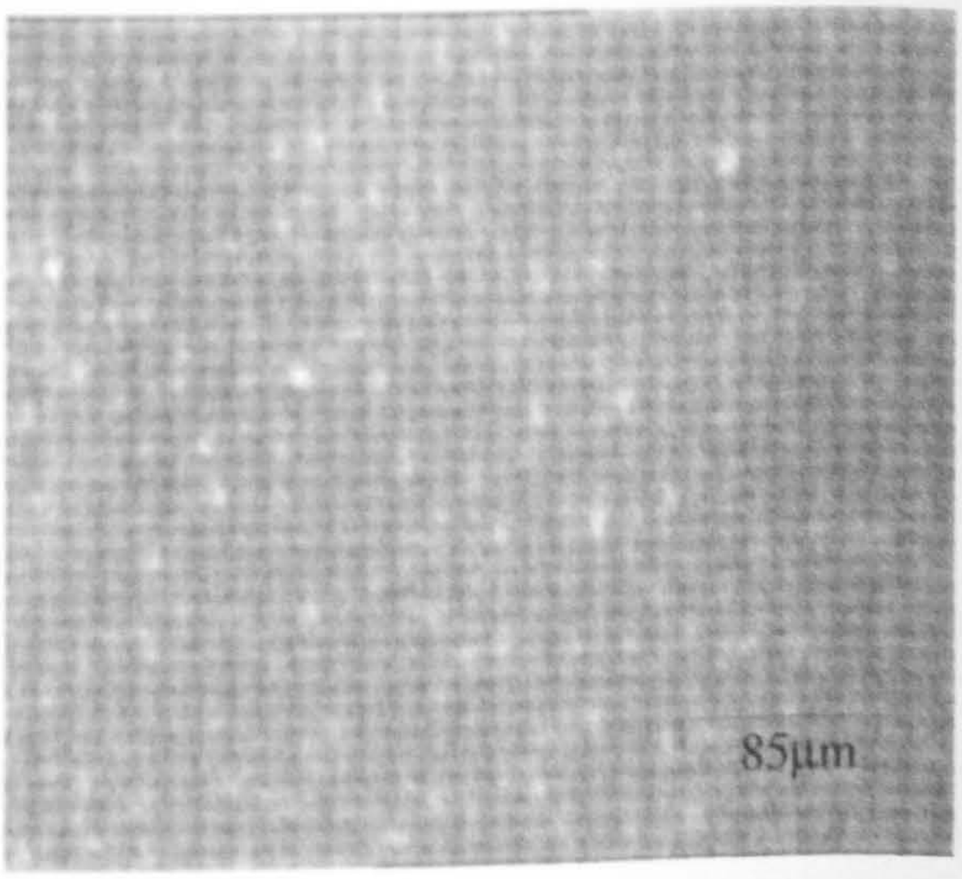

Plate XXX 0.20(v/v) MTMS (a)After 3hrs, (b) 100ml/min^{-1}, (c)200ml/min^{-1}, (d) 350ml/min^{-1}

(a)

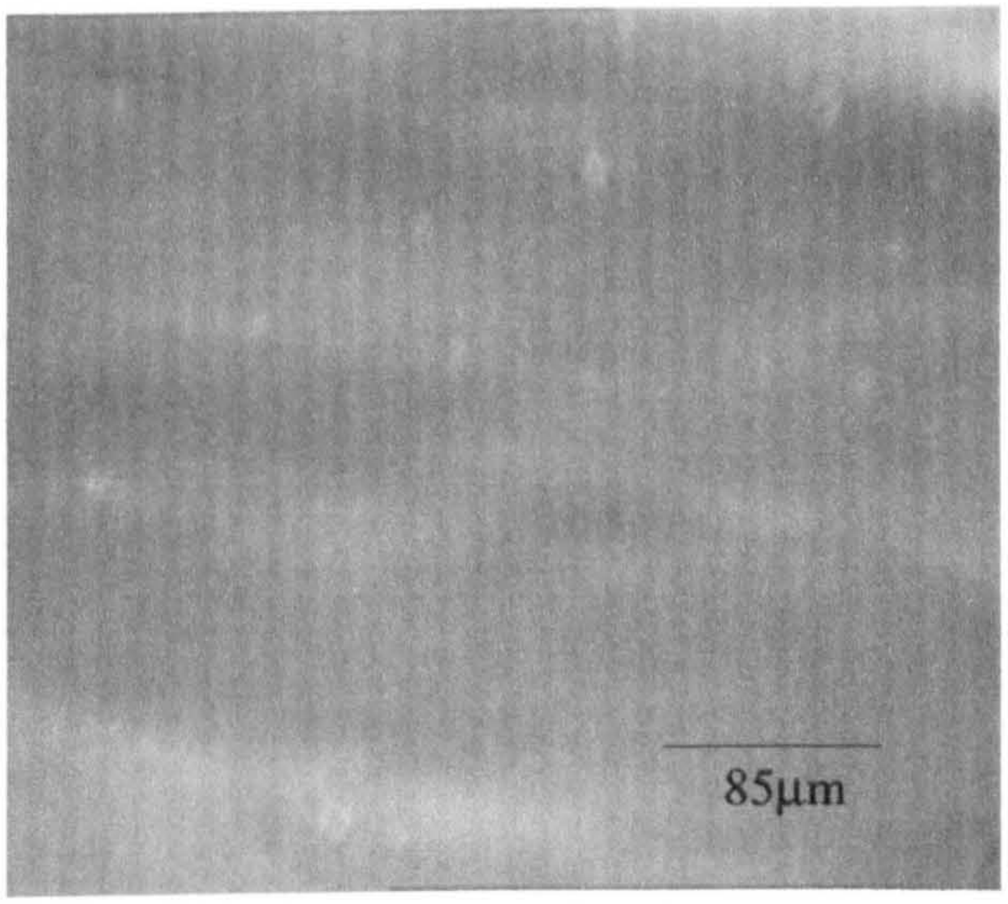

(b)

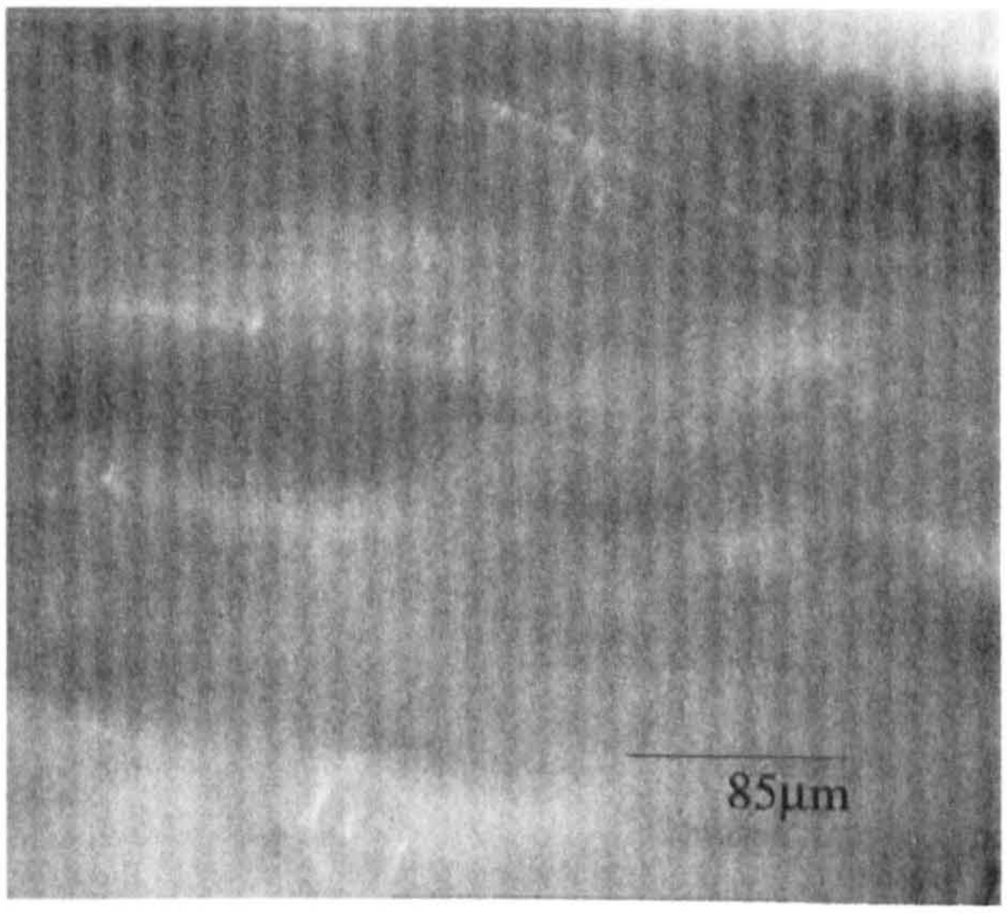

(c)

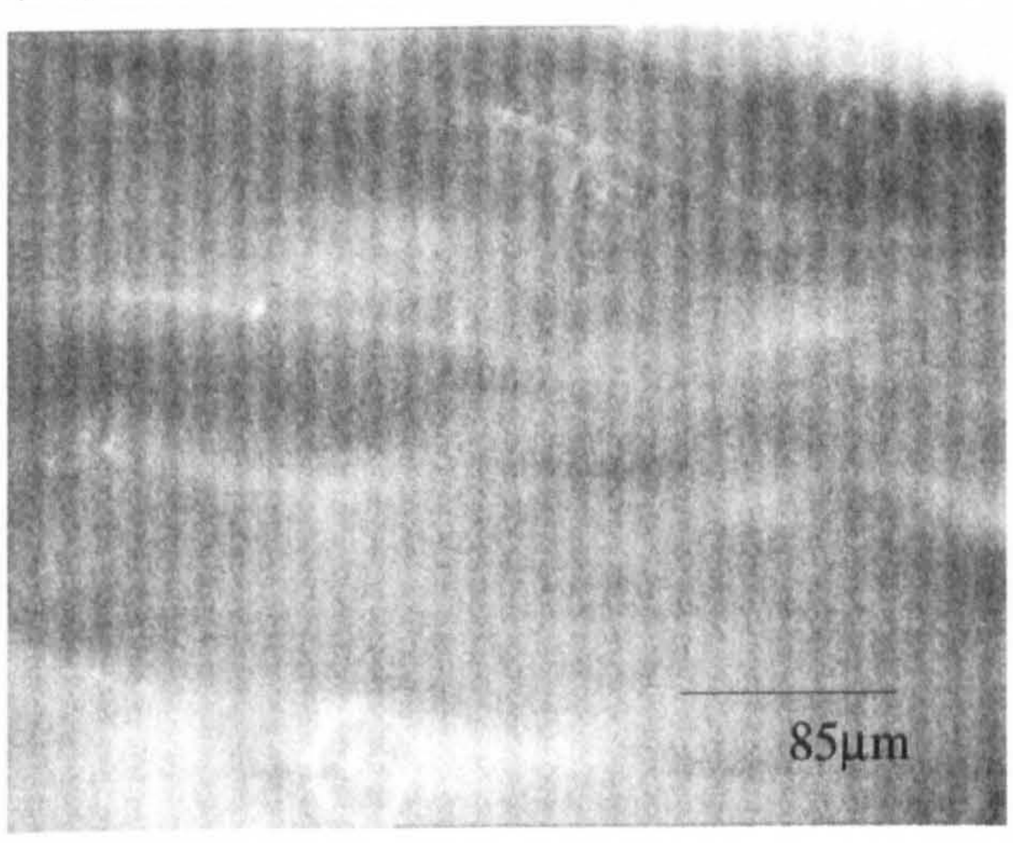

(d)

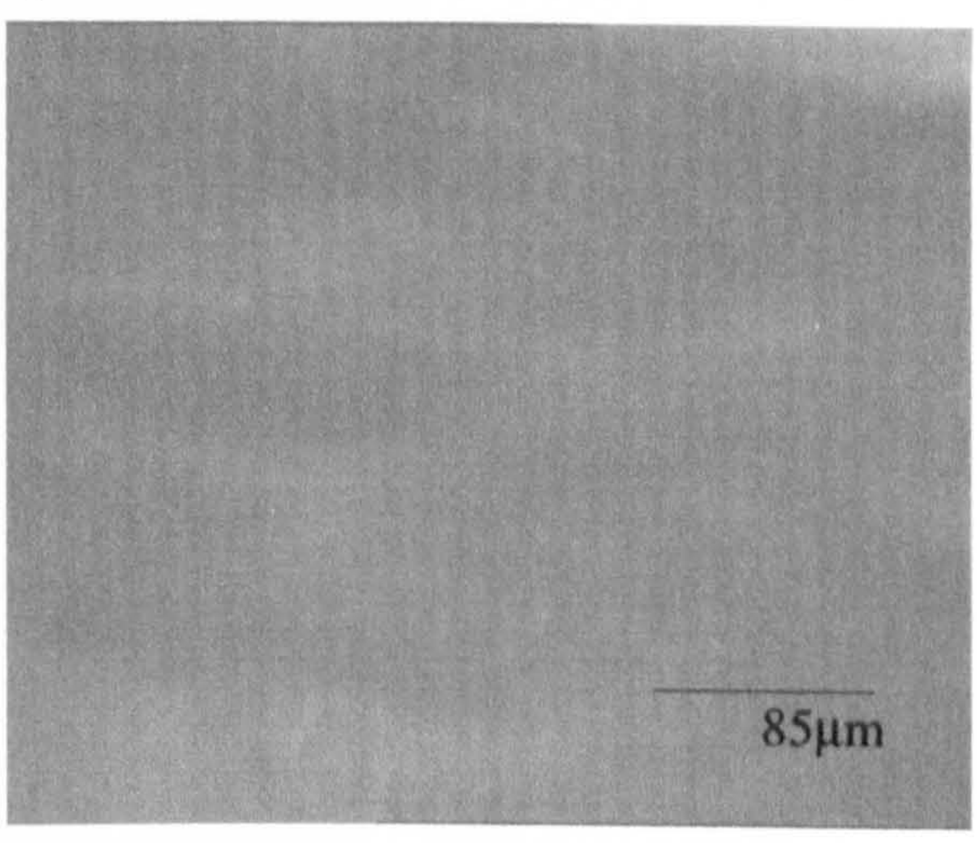

Fig 10.1 Droplet removal data as a function of MTMS ϕ ; a) 0.0(v/v) MTMS, b) 0.005(v/v) MTMS, c)0.01(v/v) MTMS, d) 0.05(v/v) MTMS, e) 0.1(v/v) MTMS, (f) 0.15(v/v), g) 0.2(v/v)

(a)

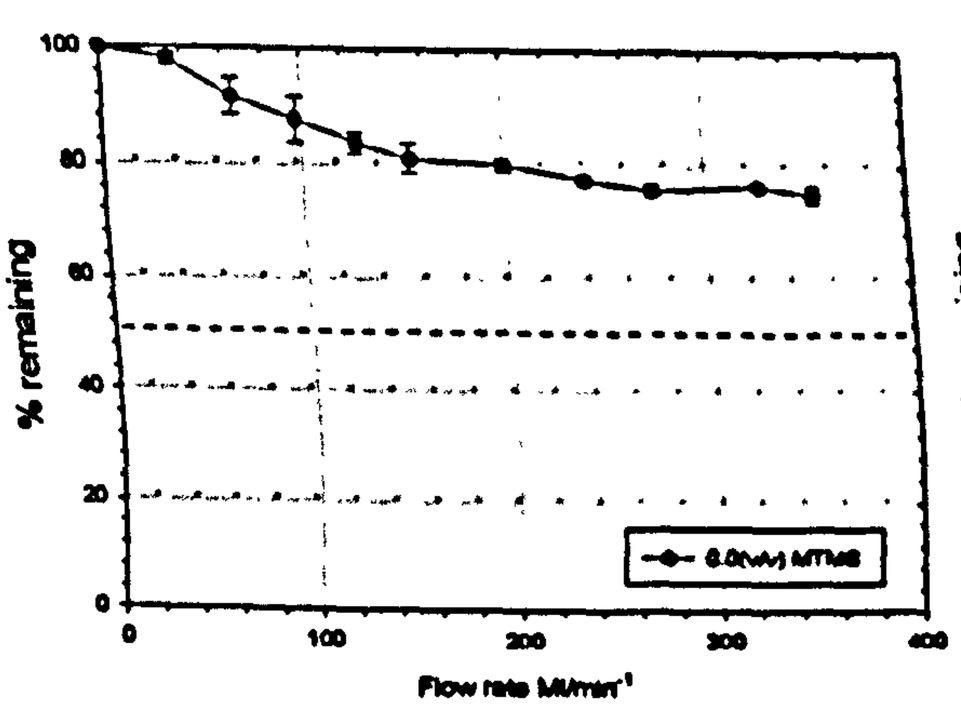

(b)

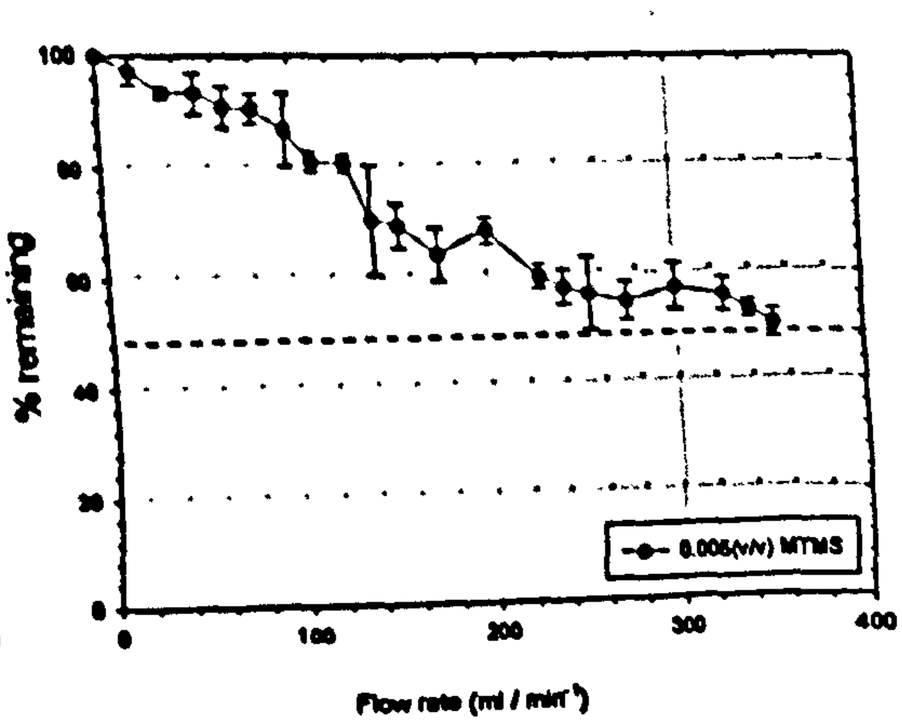

(c)

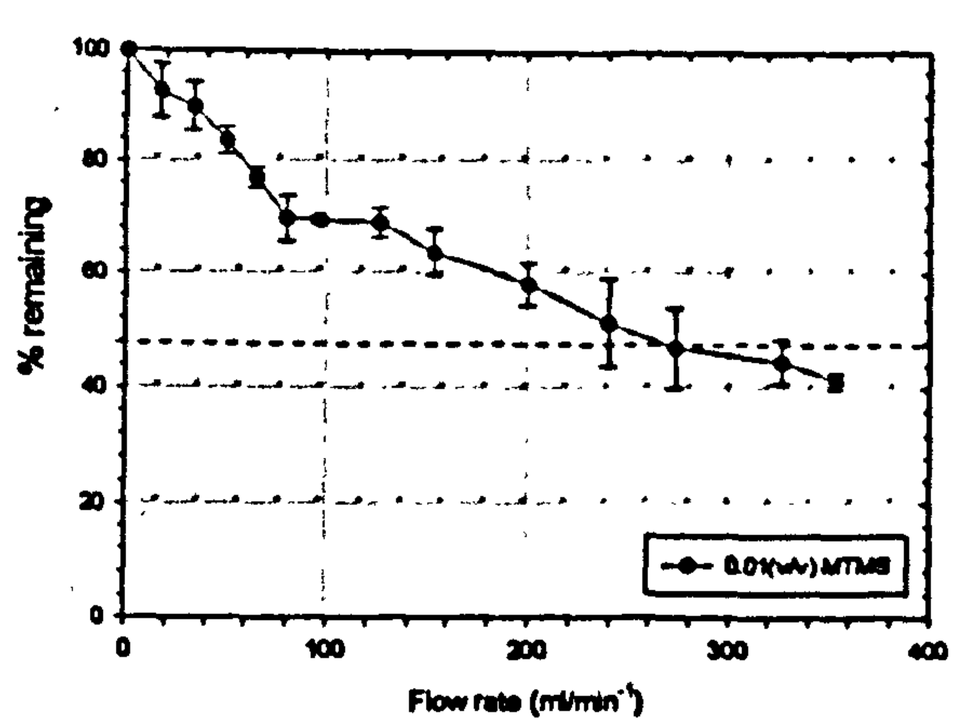

(d)

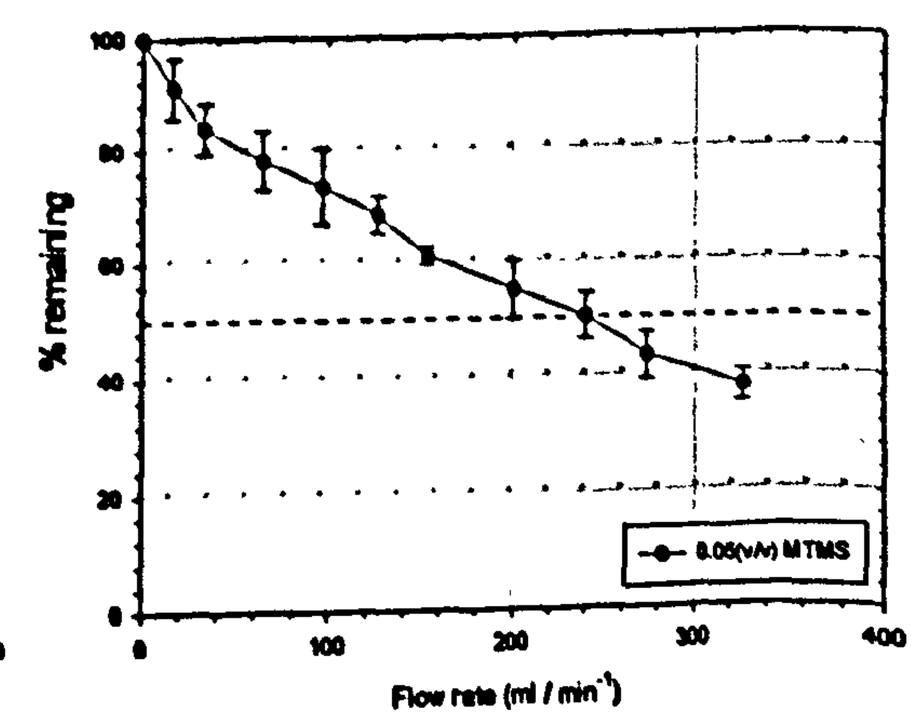

(e)

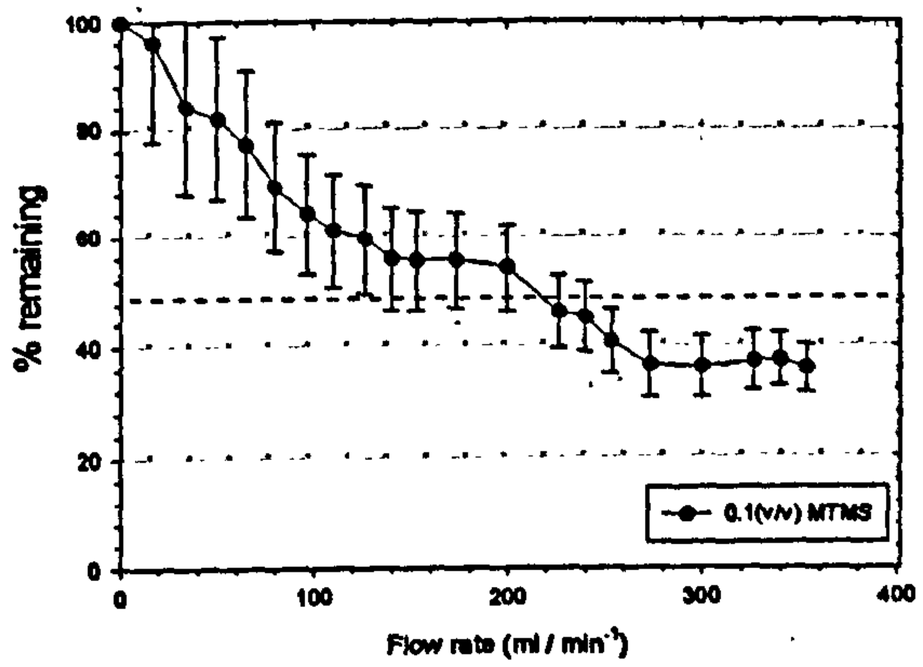
% remaining
Flow rate (ml / min-1)
0.1(v/v) MTMS

(f)

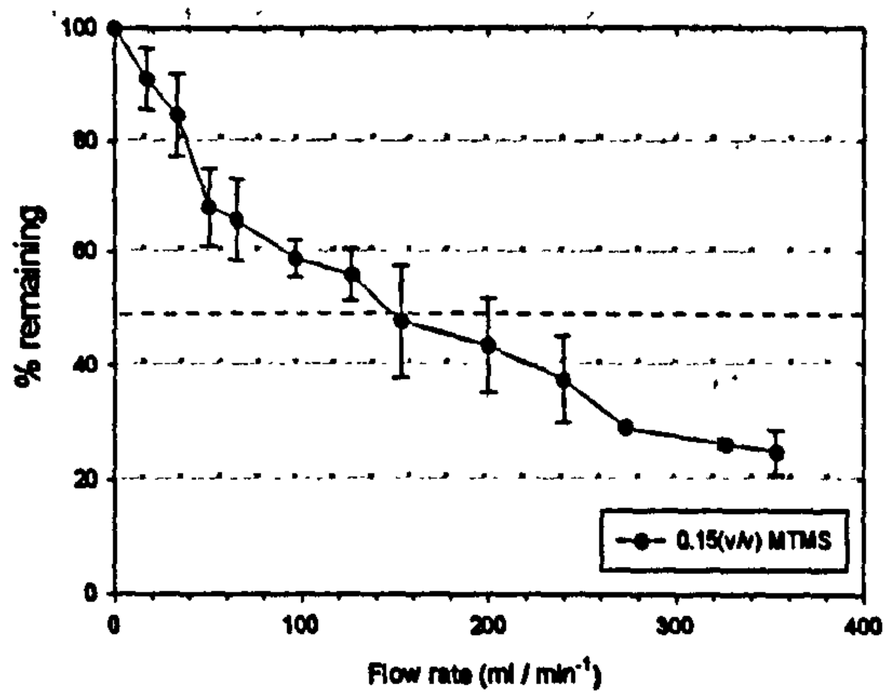
% remaining
Flow rate (ml / min-1)
0.15(v/v) MTMS

(g)

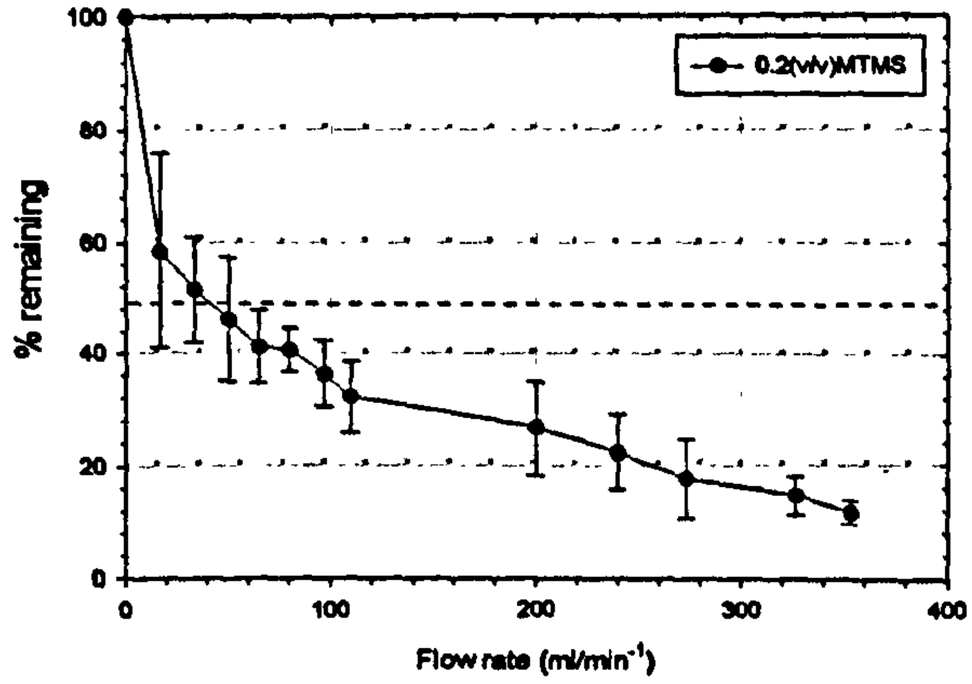
% remaining
Flow rate (ml/min-1)
0.2(v/v)MTMS

decrease in droplet surface negative ζ-potential. It can therefore be assumed that the difference in electrostatic charge between the two surfaces was not a dominant influence on the adhesion force strength in these systems. In addition, Sharma et al[1] noted that the gravity effects had a negligible influence on the hydrodynamic and adhesive force values for the detachment of particles > 10μm.

The detachment process was a relatively slow process for those systems containing <0.01(v/v) MTMS, and was shown by the low hydrodynamic force required to remove 50% particles from the mica substrate, F_{H50} >1.4x10^{-4}. This trend could be related to the wetting properties of the droplets in direct contact with the mica substrate observed during stagnation point deposition investigations, see chapter 9. It was interesting to note that the uncross-linked systems showed below 50% removal even at the highest shear rate. A "rolling" detachment mechanism was observed for these systems, while an uniformly shaped contact zone was maintained under the substrate surface, until a critical shear rate, γ_c, values was obtained. The F_{H50}, γ_c and the subsequent force of adhesion decreased with increasing MTMS ϕ. This trend corresponded to a simultaneous decrease in droplet diameter as the developing cross-linking density reduced the deformation and wetting properties of the PDMS droplets in contact with the collector surface. For those systems containing >0.1(v/v) MTMS, the detachment process was indicated as the front of the contact zone moved downstream. The droplet was then deformed while a water film was created downstream from the contact line. As the hydrodynamic force exerted on the droplets was increased, the aqueous film ruptured smoothly.

It is interesting to note that none of the systems investigated showed total droplet removal. In fact, the highest cross-linked systems investigated, >0.2(v/v) MTMS, which were predicted to show the lowest adhesive strength with the substrate, left over 10% of the droplets adhered to the surface after the highest shear rate. This behaviour implied that the adhesion force between the droplets and the mica surface was stronger than the highest applied shear stresses, >350ml min^{-1}.

The findings for cross-linked PDMS systems >0.1(v/v) MTMS were in agreement with Hubbe[2] who reported that the restraining torque was too small to be detected for deformable particles on a mica substrate in an aqueous solution. This was attributed to the presence of a thick electrostatic double layer which ensured the particles rested in a secondary minimum > 50-100 Å away from the substrate. At these distances the Born forces and atomic scale surface asperities of the substrate would not significantly influence the deposition and so the surface forces would be distributed almost symmetrically around the center of the contact region.

10.1.2 Colloidal removal as a function of electrolyte, NaCl

Further colloidal removal investigations were carried out in the presence of an aqueous NaCl solution wash at various concentrations between 10^{-5} mol dm^{-3} and $3x10^{-1}$mol dm^{-3}. An identical emulsion system to that described in chapter 9 was used during these investigations with a fixed 0.05(v/v) total monomer and 0.05 (v/v) MTMS. The removal data of cross-linked PDMS droplets from a mica surface was plotted as a function of NaCl concentration, see figure10.2 (a-c), and the removal images obtained shown in plates XXXI-XXXIII.

Plate XXXI $1x10^{-5}$ NaCl: (a) After 3hrs, (b) 100 ml/min^{-1}, (c) 200 ml/min^{-1}, (d) 350 ml/min^{-1}

(a)

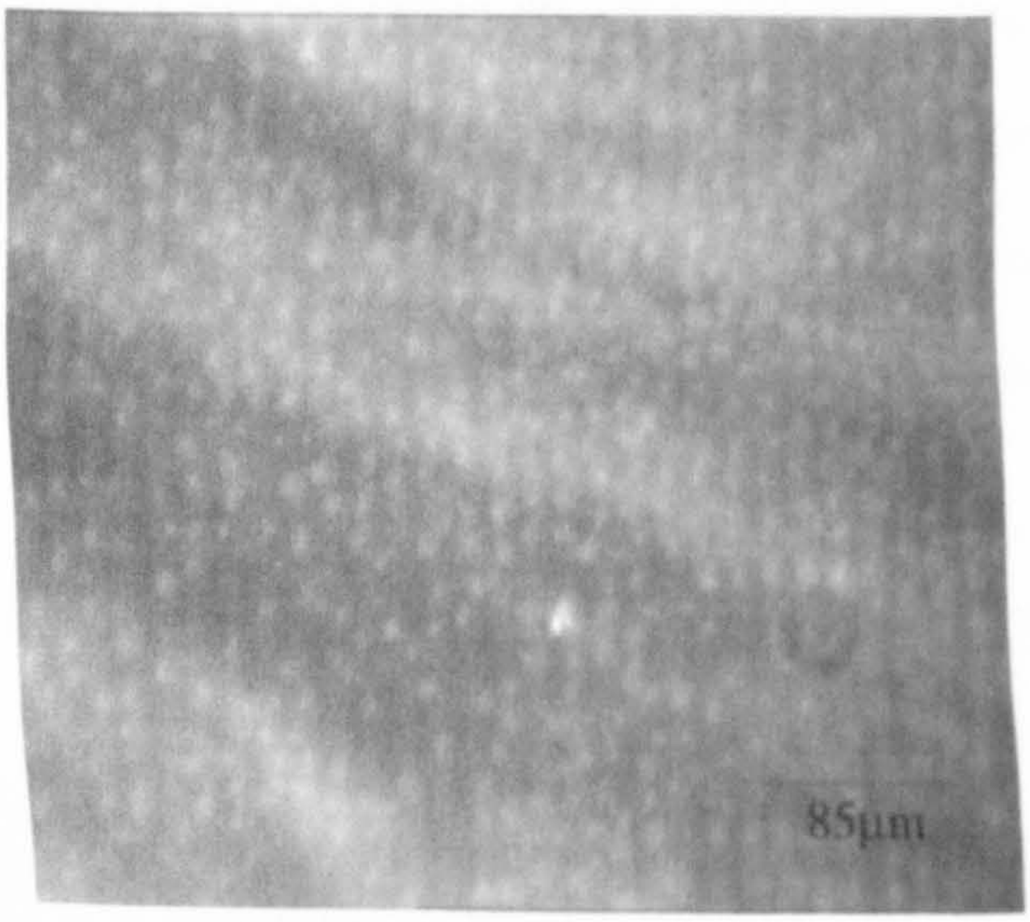

(b)

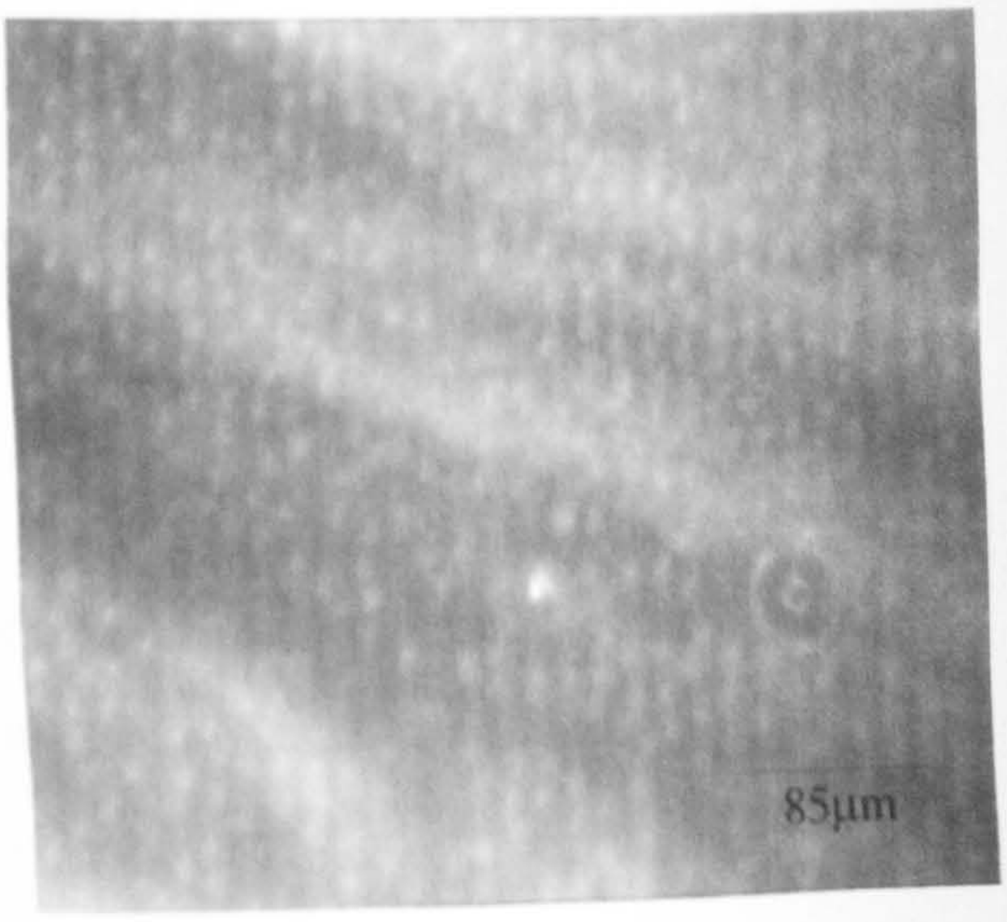

(c)

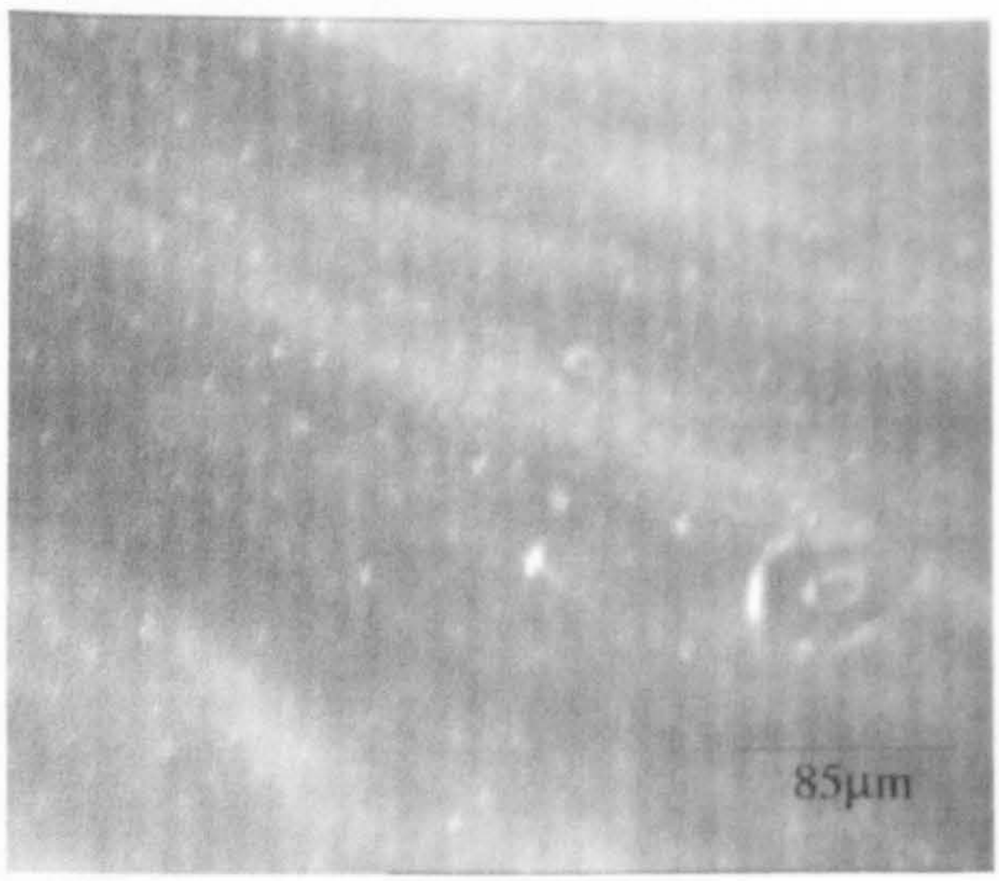

(d)

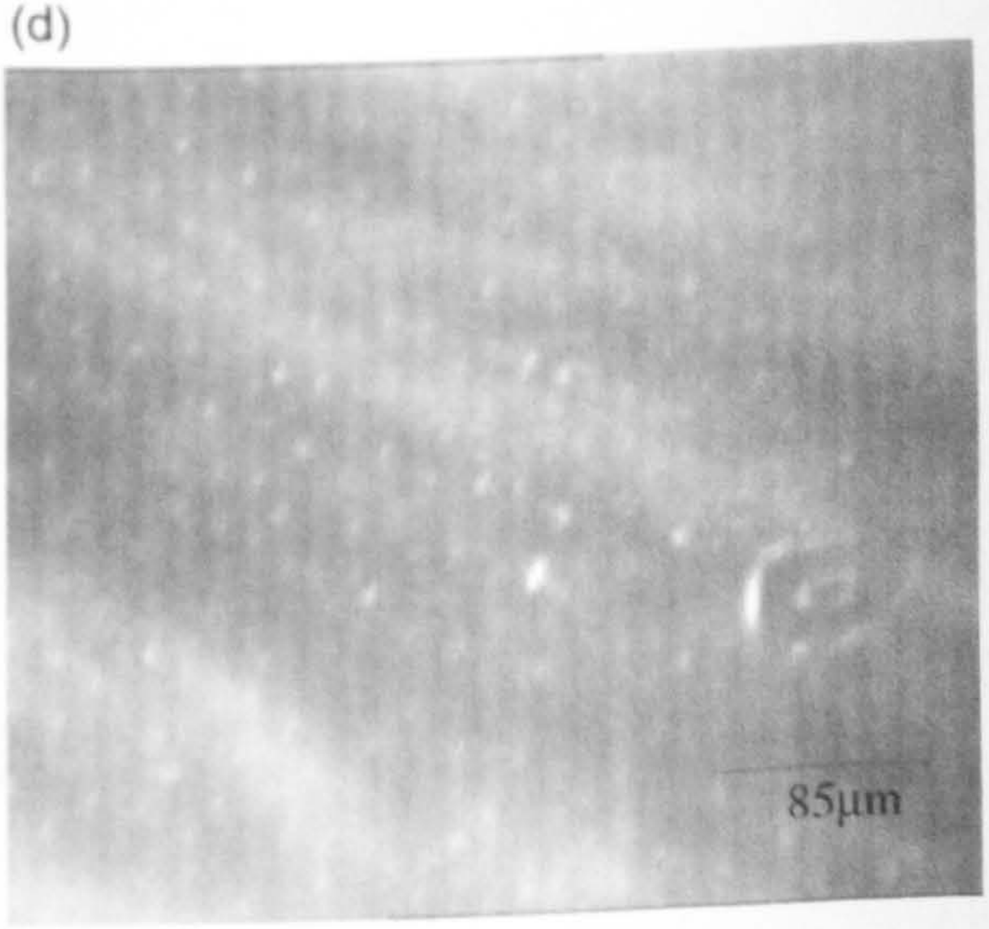

Plate XXXII $1x10^{-3}$ NaCl: (a)After 3hrs , (b) 100 ml/min^{-1}, (c) 200 ml/min^{-1},

(d) 350 ml/min^{-1}

(a)

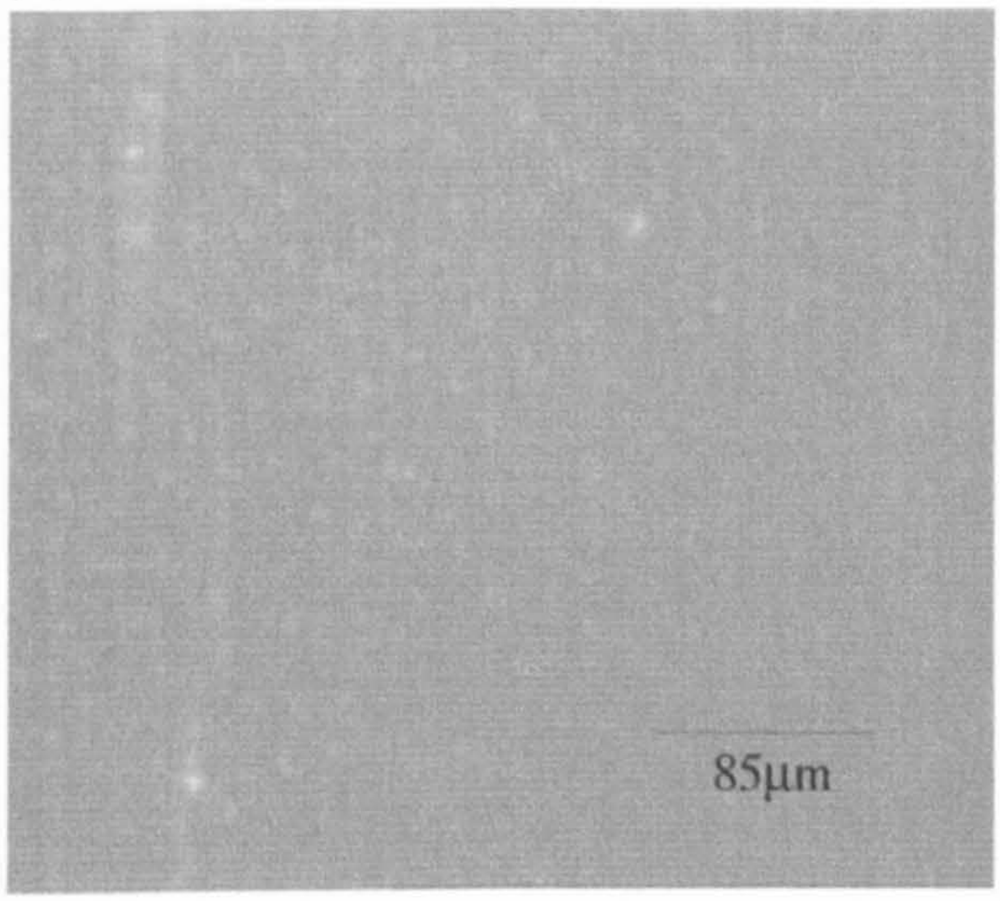

(b)

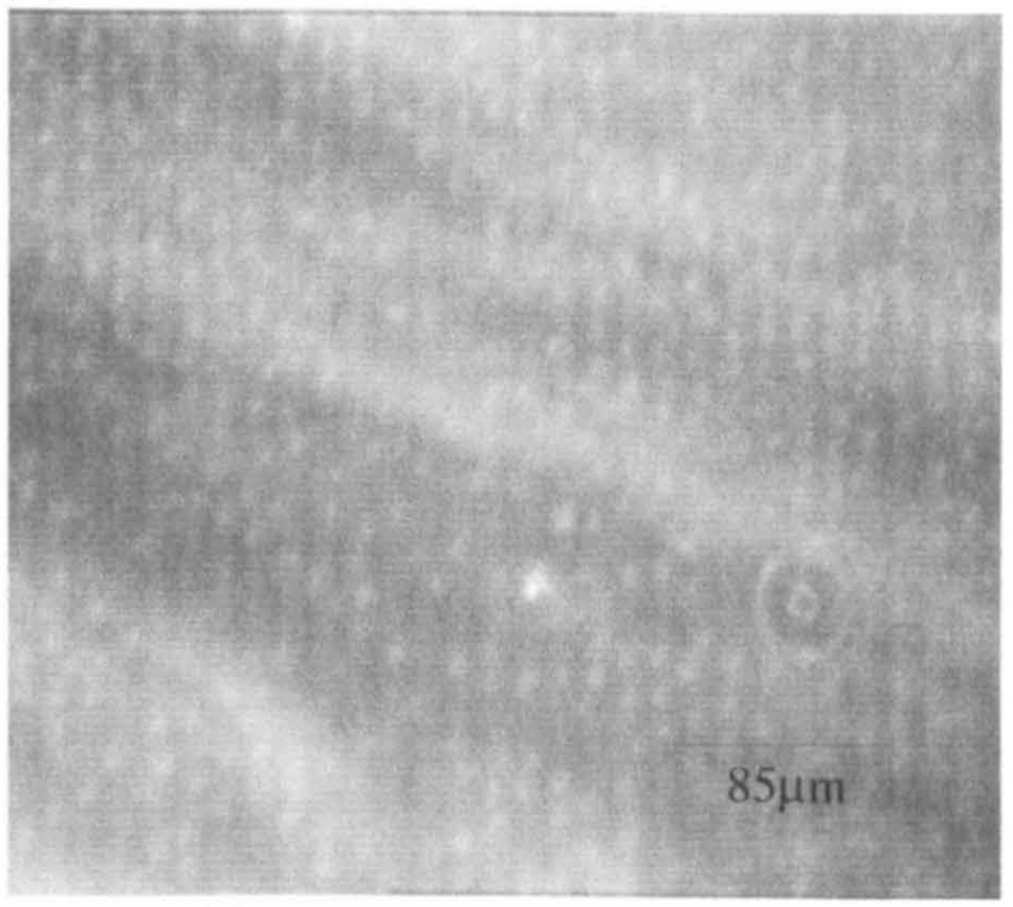

(c)

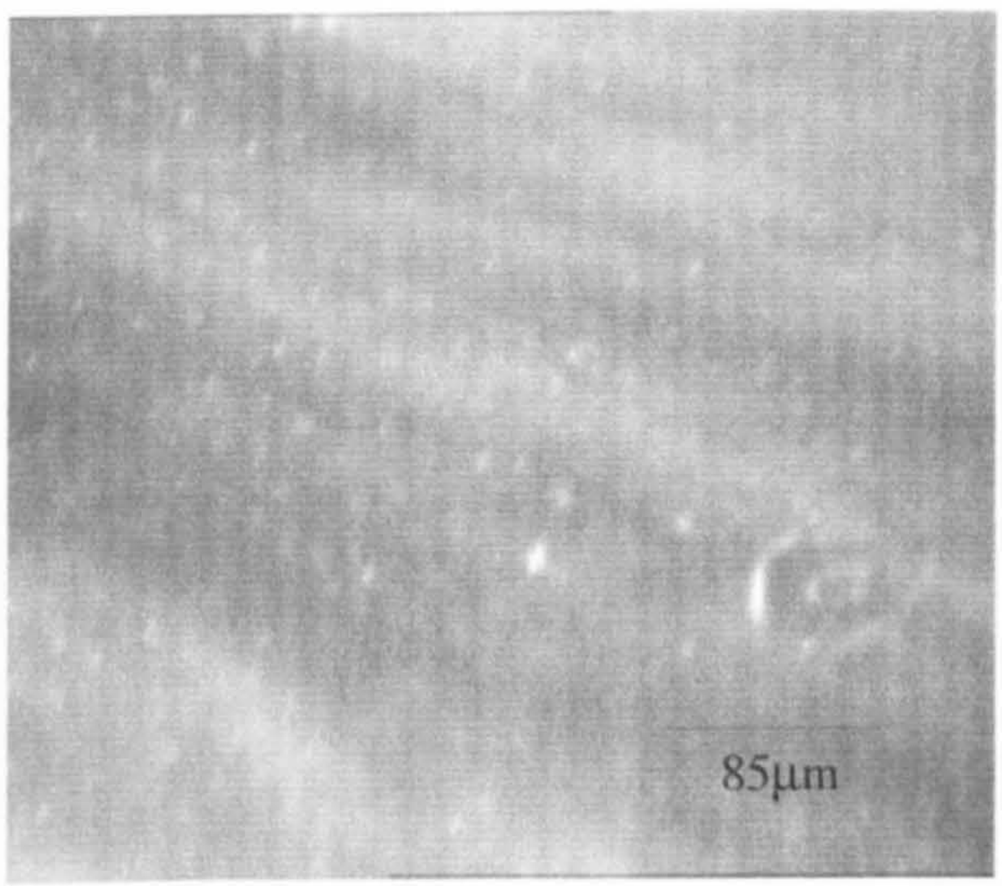

(d)

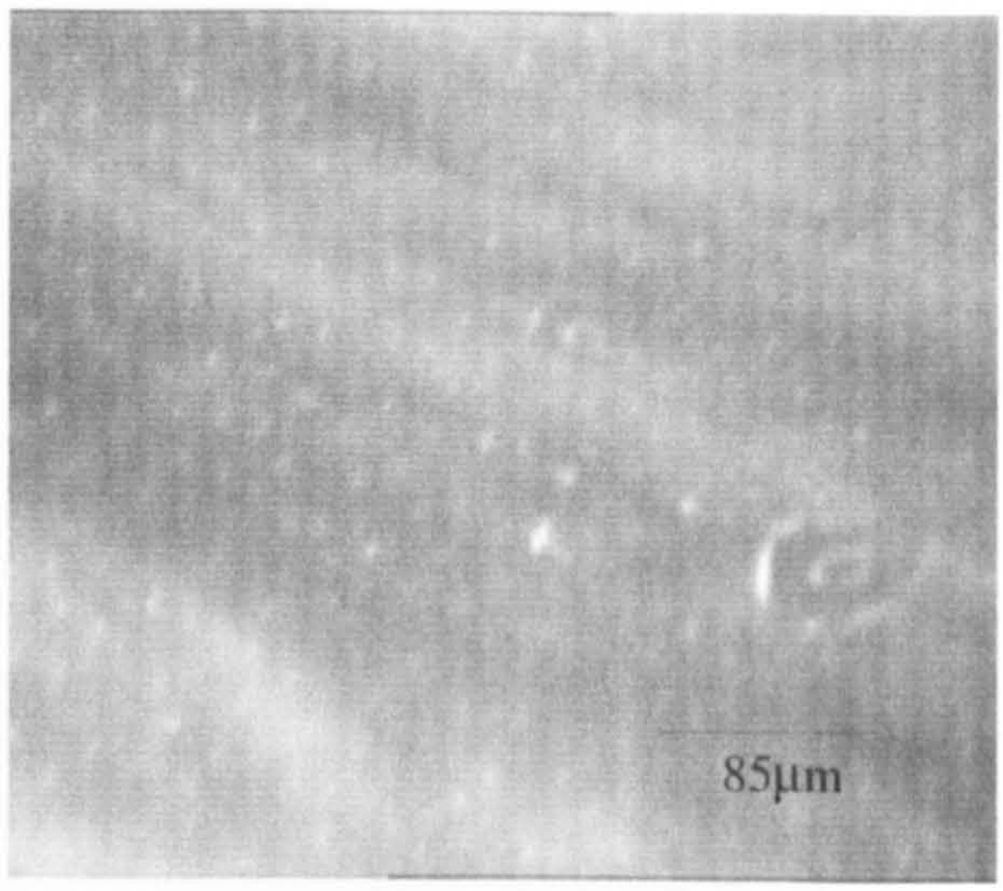

Plate XXXIII: $3x10^{-1}$ NaCl; (a) After 3hrs, (b) 100 ml/min^{-1}, (c) 200 ml/min^{-1}, (d) 350 ml/min^{-1}

(a)

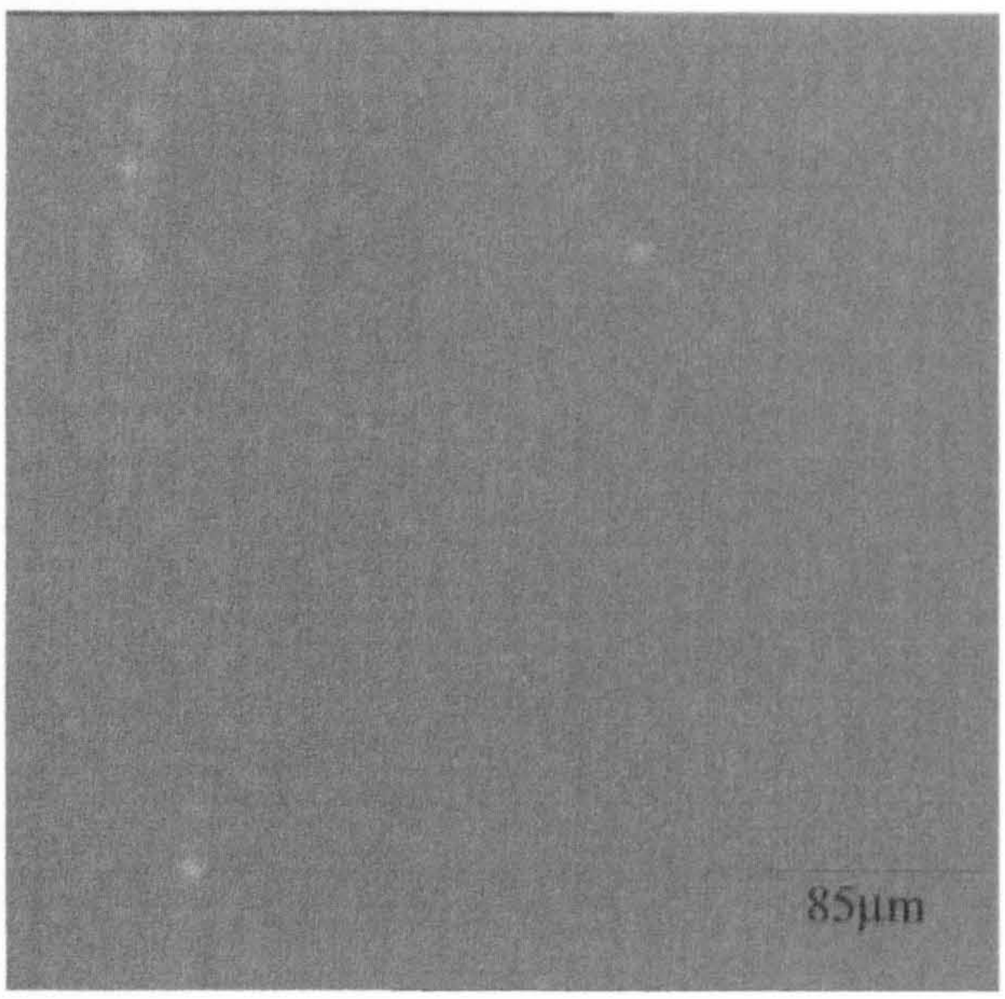

(b)

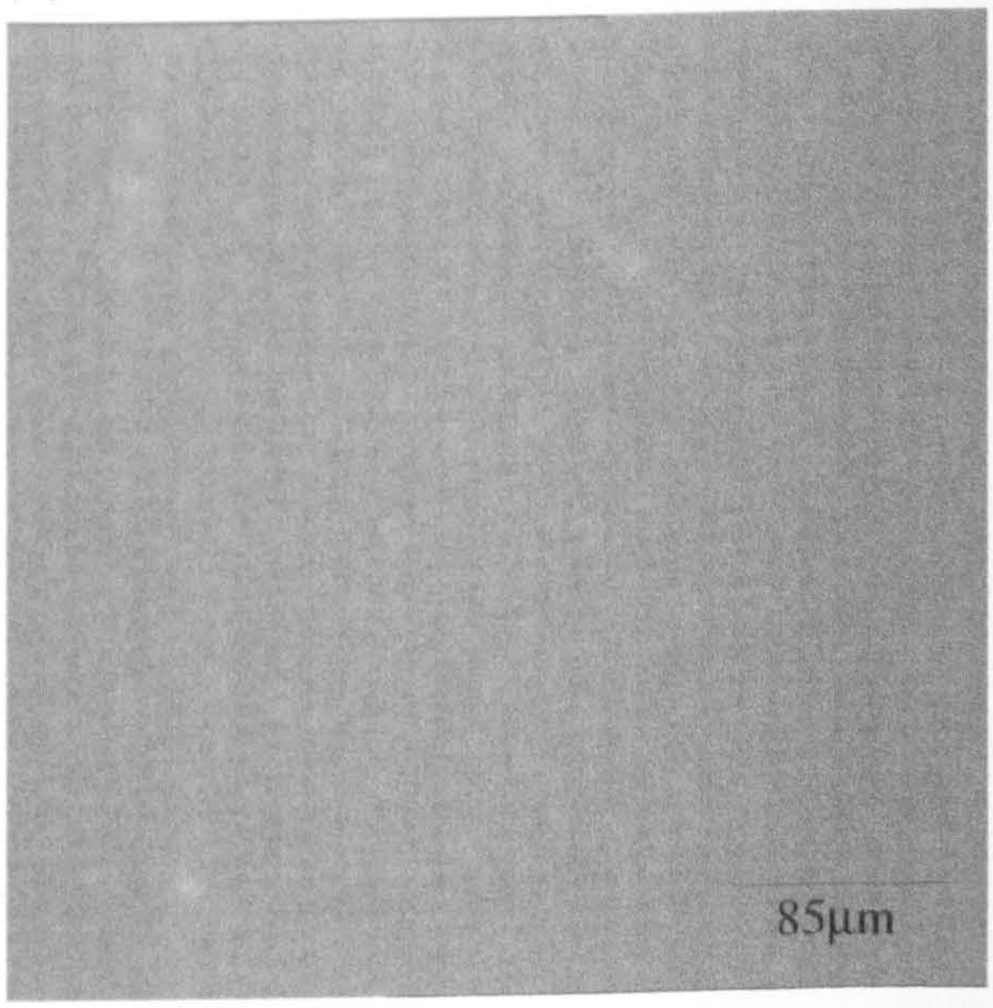

(c)

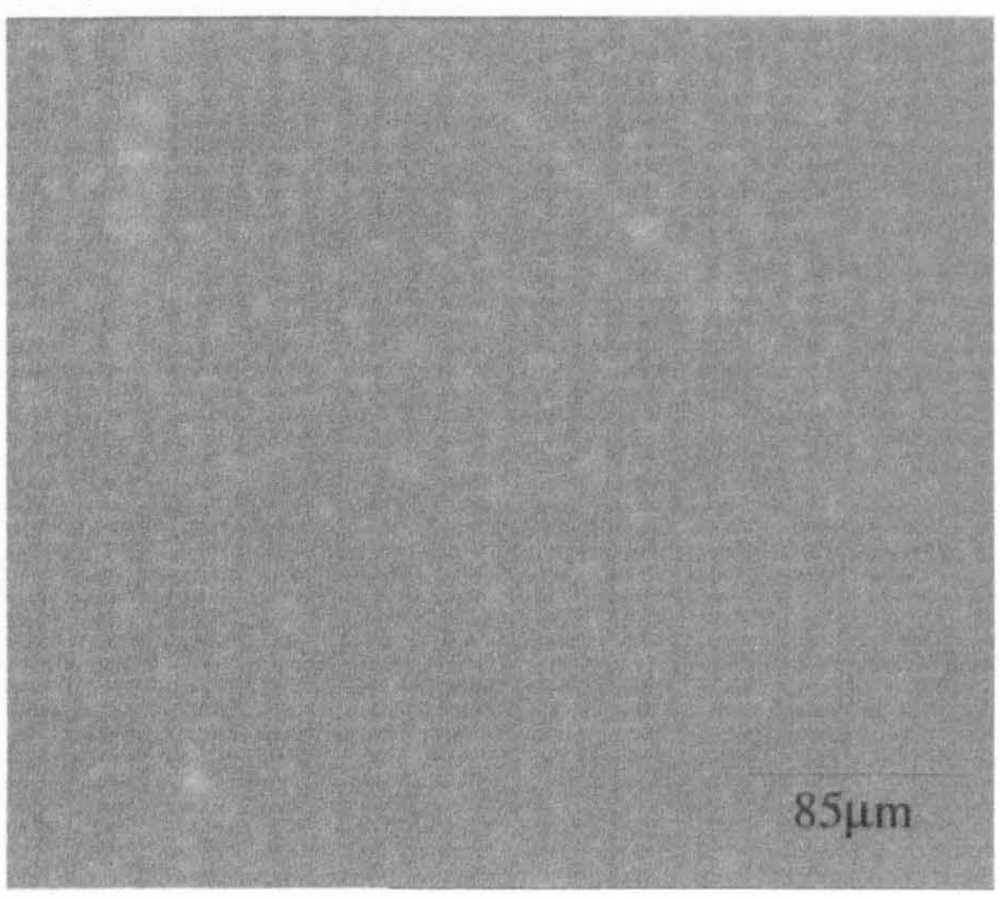

(d)

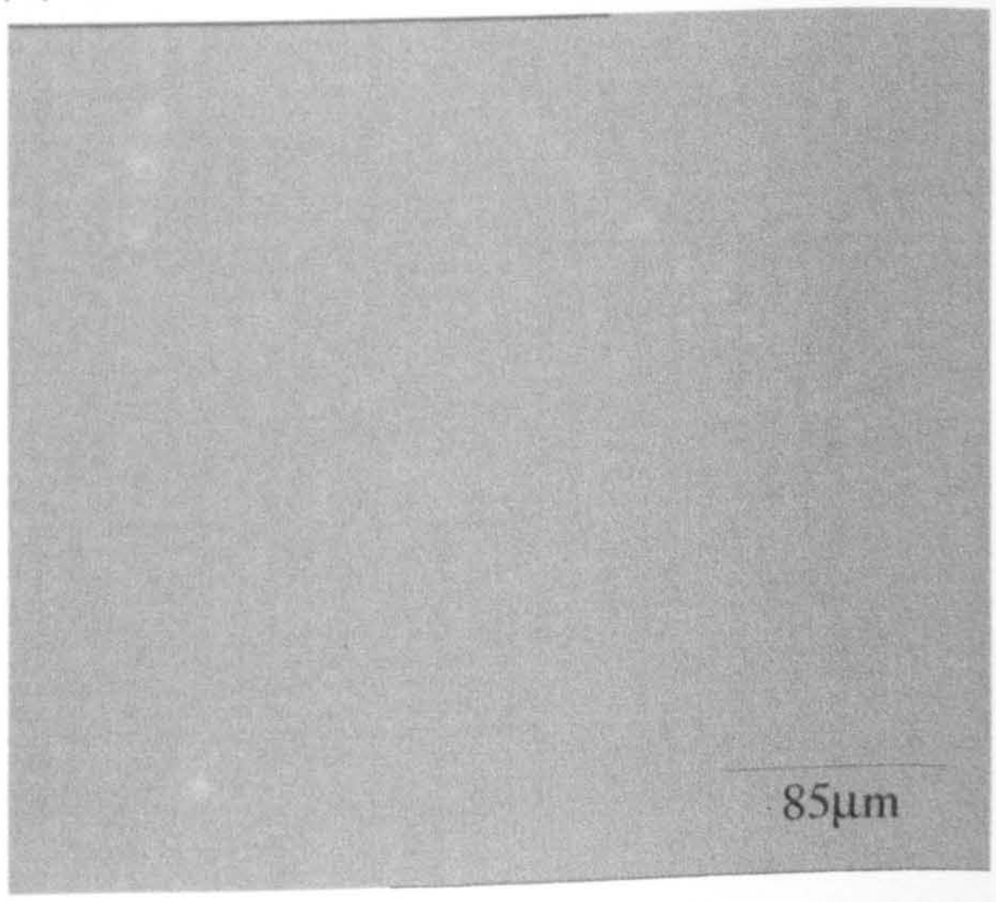

Fig 10.2: Droplet removal data as a function of electrolyte concentration, NaCl; (a) $1x10^{-5}$ mol dm^{-3}, (b)$1x10^{-3}$mol dm^{-3}, (c) $3x10^{-1}$mol dm^{-3}

a)

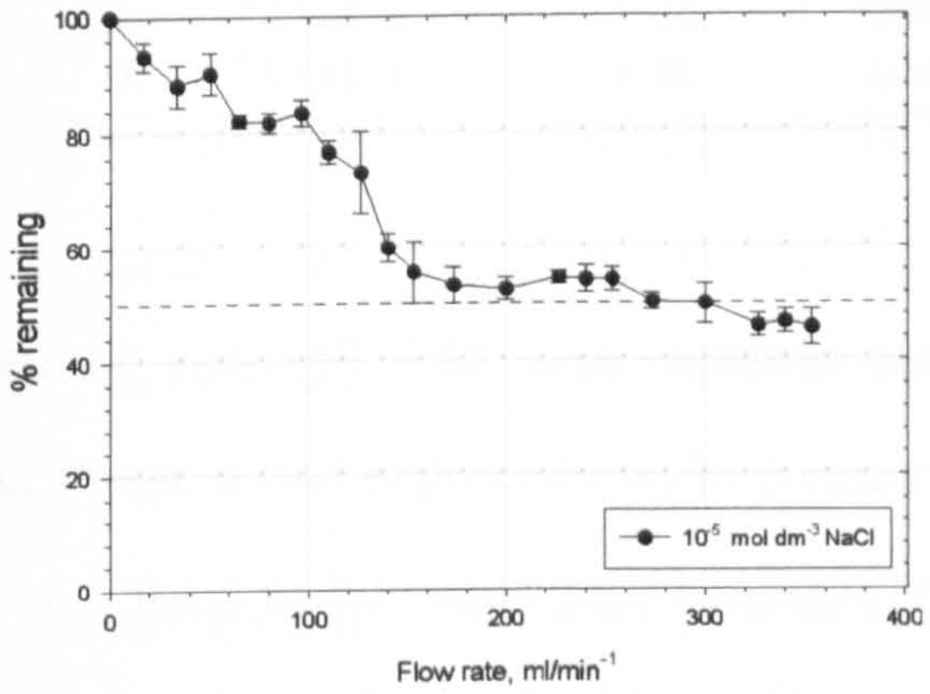

b)

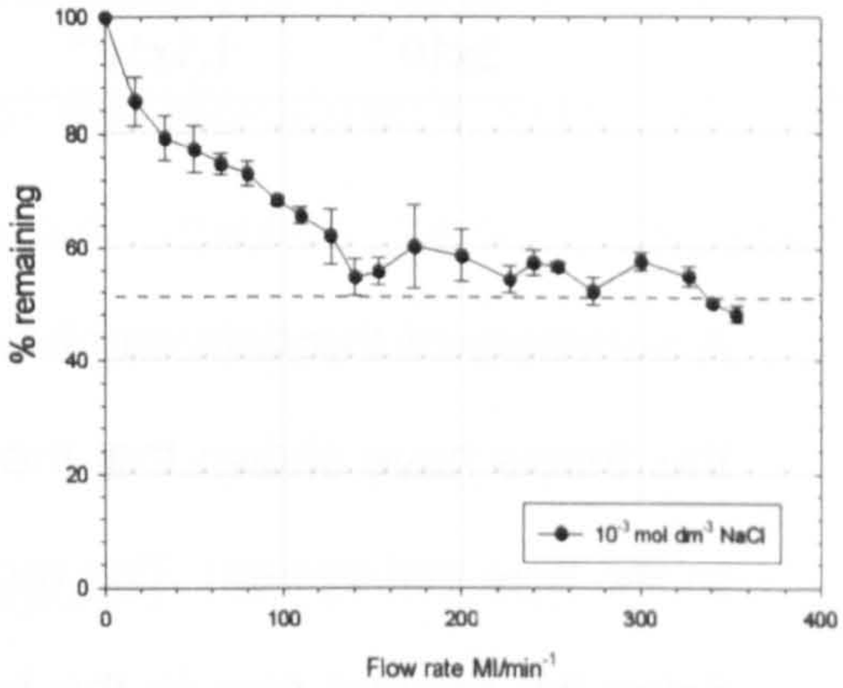

c)

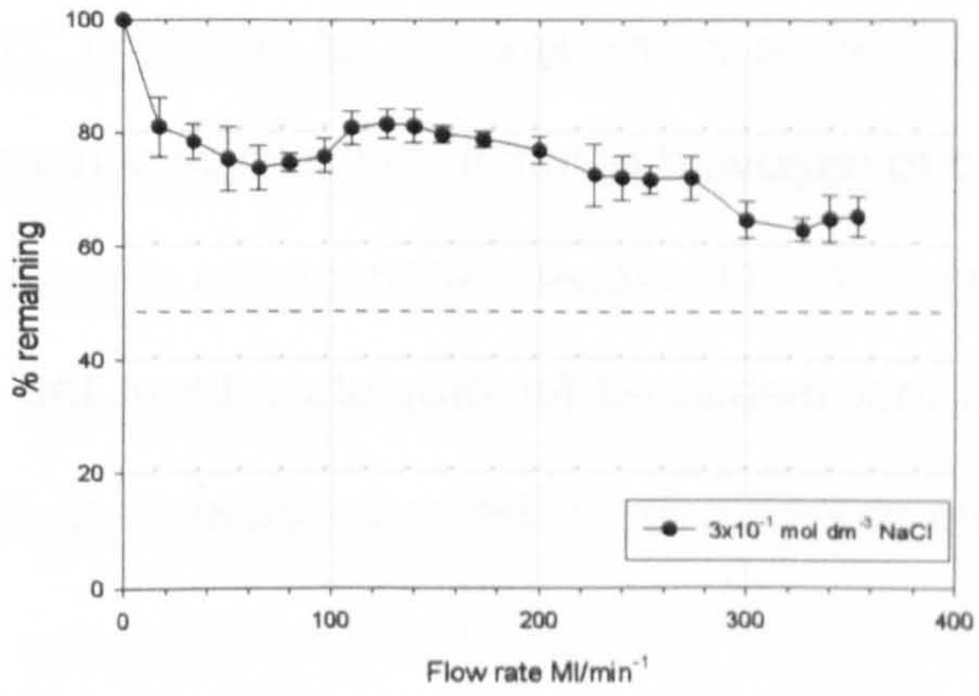

Table 10.2 F_{H50} removal data as a function of electrolyte concentration

[NaCl] (mol min^{-1})	F_{H50} (nN)	γ_0 (ml min^{-1})	% removed (F_{H50})	F_A (N)	ϕ_p (μm)
$1x10^{-5}$	$1.5x10^{-4}$	340	55.0	$8.9x10^{-9}$	8.5
$1x10^{-3}$	$1.4x10^{-3}$	350	50.1	$9.3x10^{-8}$	9.4
$3x10^{-1}$	$1.1x10^{-2}$	>353	38.4	$7.2x10^{-8}$	10.7

A summary of the data can be seen above in table 10.2. Previous discussions in this thesis have shown that the presence of an electrolyte had a significant effect in the flow cell system. The droplet diameter was observed to swell to over three times its' original size in the bulk solution, while the surface potential negativity was shown to decrease, see chapter 5. These effects correspond to a reduction in film stability as the droplets come into direct contact with the substrate surface and an increase in the strength of adhesion. Therefore the hydrodynamic force required to remove droplets from the mica surface increases in magnitude with the presence of the electrolyte. Although the average droplet contact diameter was 2-3 times that measured for droplets without the presence of electrolyte, there is very little change over all the investigations, +/- 2μm, see table 10.2.

Above 10^{-3} [NaCl], there is a dramatic decrease in the adhesive strength between the droplet and substrate. Although this behaviour is counterintuitive to the traditional DLVO theory, it can be rationalised as the presence of high electrolyte concentration only increases the negative potential of the droplets while the mica substrate remains fairly constant, see chapters 5 and 8. Therefore as the charge difference between the two surfaces increases the van der Waals attractive forces play a more dominant role and require a stronger shear force to be exerted for

droplet removal.

O'Neil et al[3] reported that a lower hydrodynamic force 0.01cm^3 s^{-1}, F_H 10^{-6} dyn was required to remove glass particles from a mica substrate using distilled water than when a NaCl flow solution was used. The length of deposition prior to removal was not noted to have any significant effect on the hydrodynamic force. Although no explanation was suggested for the increase in adhesion, the behaviour could not be rationalised in terms of the macroscopic DLVO theory alone.

10.1.3 Removal from Mica with [SDS] / Fl(aq) wash

The removal investigations were extended by the introduction of the same anionic surfactant, SDS, that was used during the deposition experiments described in chapter 9. A fixed PDMS emulsion system of 0.05(v/v) total monomer, 0.05(v/v) MTMS was used in the horizontal flow cell containing a mica substrate. A wash solution of SDS surfactants was introduced with concentrations above and below the cmc, 0.08mM-8.0mM. Removal data obtained from the investigations was plotted as a function of flow rate and displayed in figure 10.3(a-c) and summarised in table 10.3, while the removal images are shown in plates XXXIV-XXXVI.

The horizontal investigations showed that droplets became more easily detached from the hydrophobic surface with the increasing of SDS concentrations. This trend was in good agreement with the stagnation point deposition studies, see chapter 9, and with previous studies[4] that utilised hard, solid particles.

Plate XXXIV: O.O8mM SDS (a) After 3hrs, (b) 100 ml/min^{-1} (c) 200 ml/min^{-1} , (d) 350 ml/min^{-1}

(a)

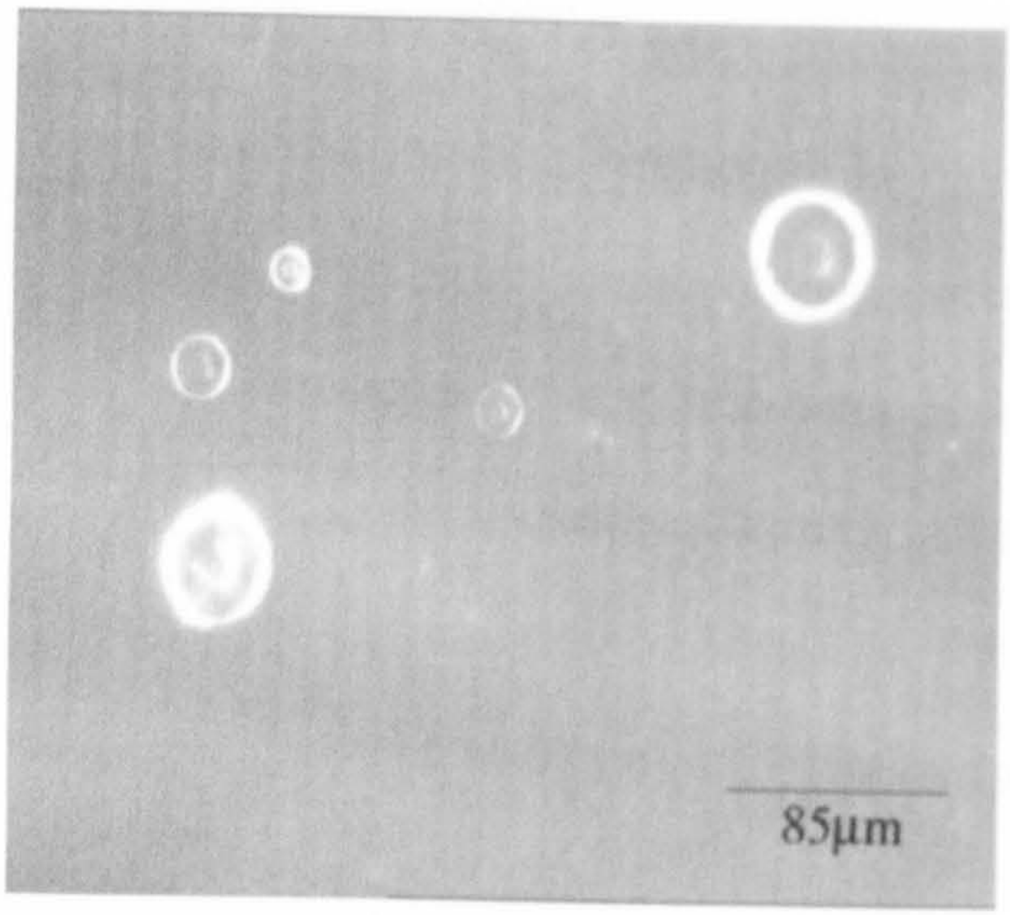

(b)

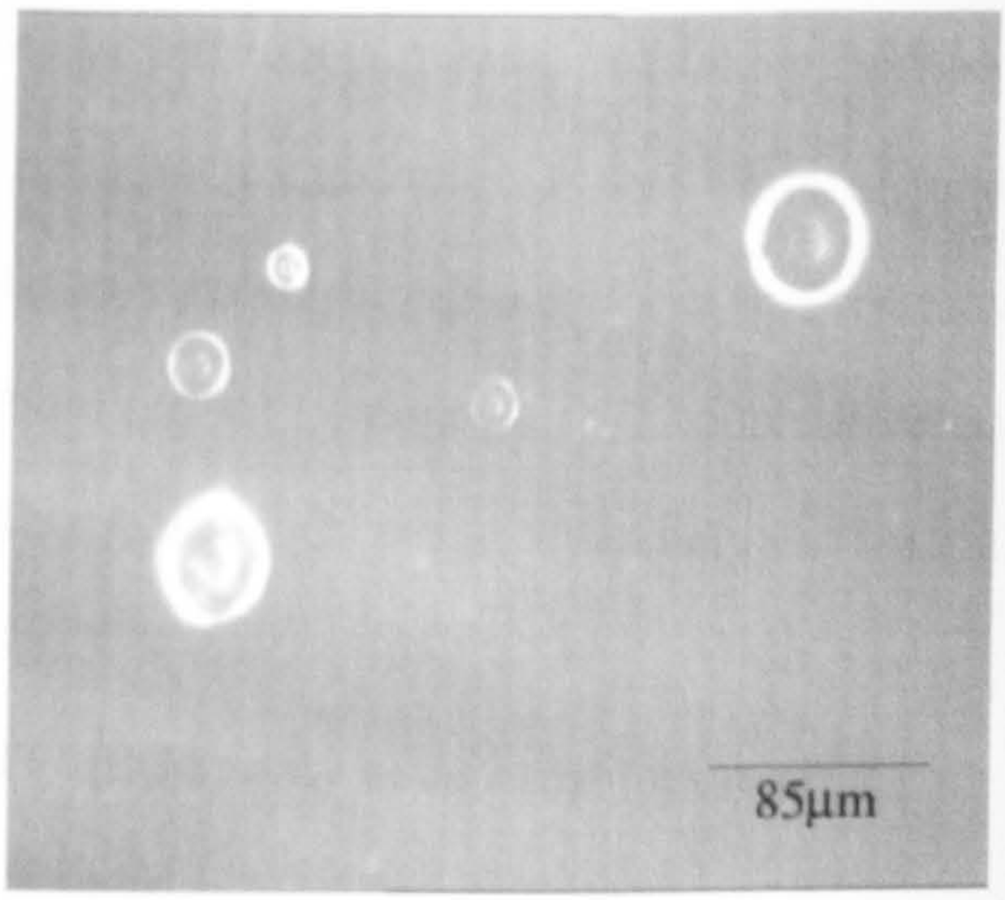

(c)

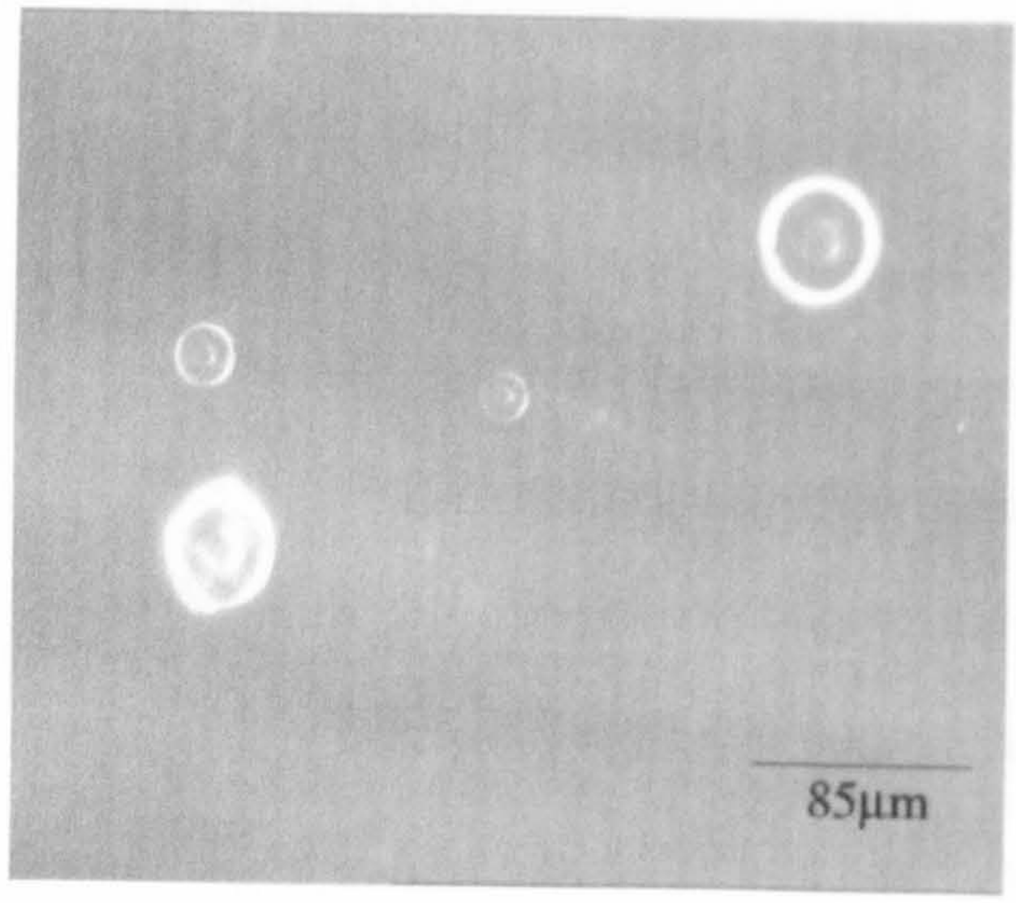

(d)

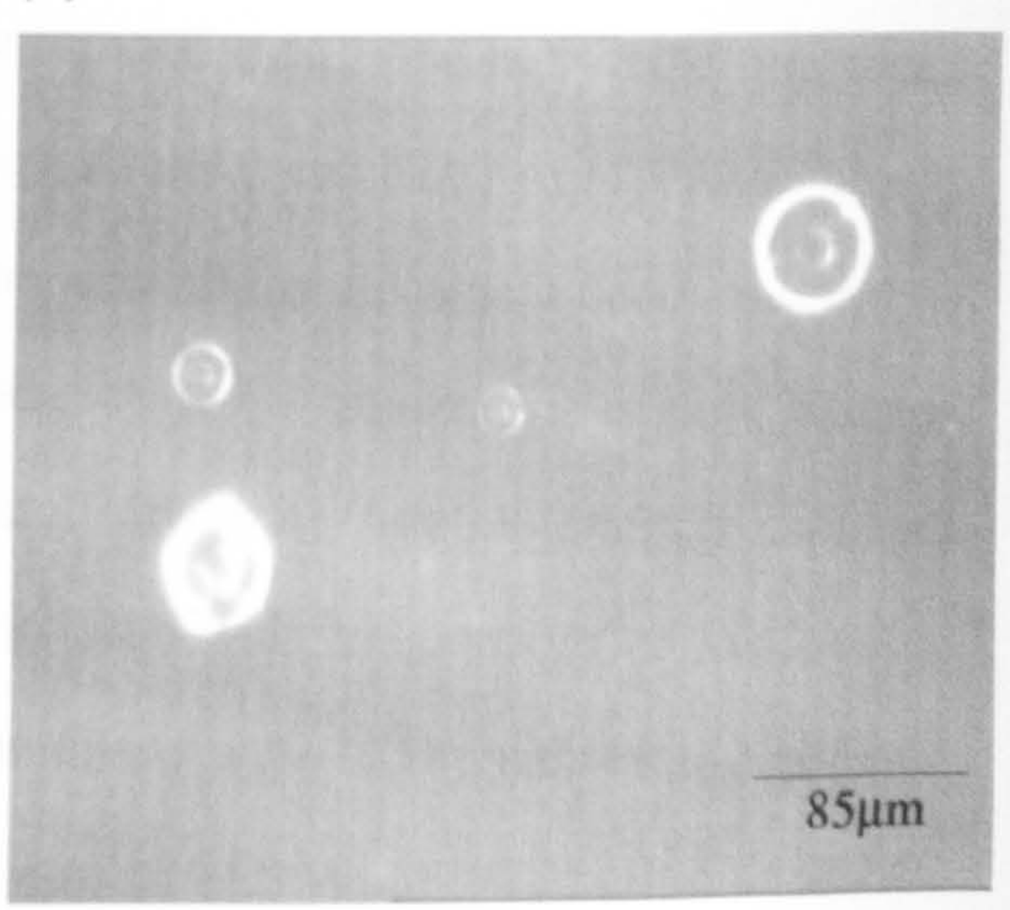

Plate XXXV: 0.8 mM SDS (a) After 3hrs (b) 100 ml/min^{-1} (c) 200 ml/min^{-1} (d) 350 ml/min^{-1}

(a)

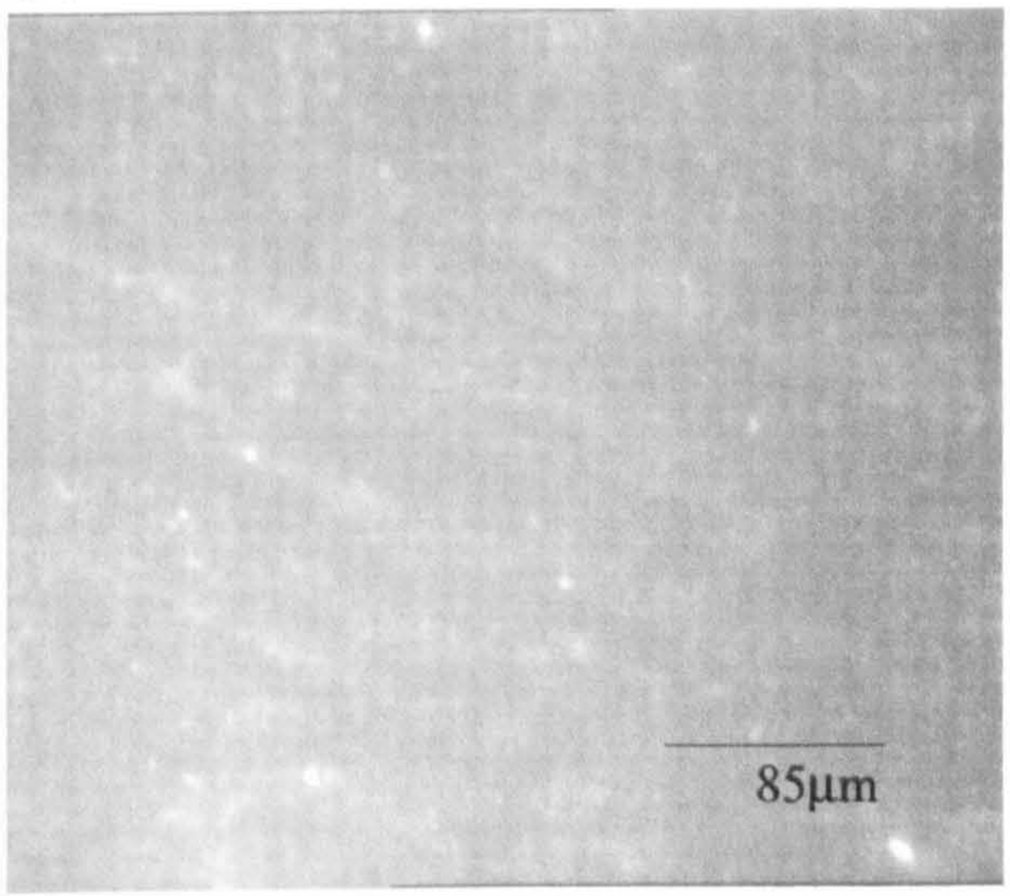

(b)

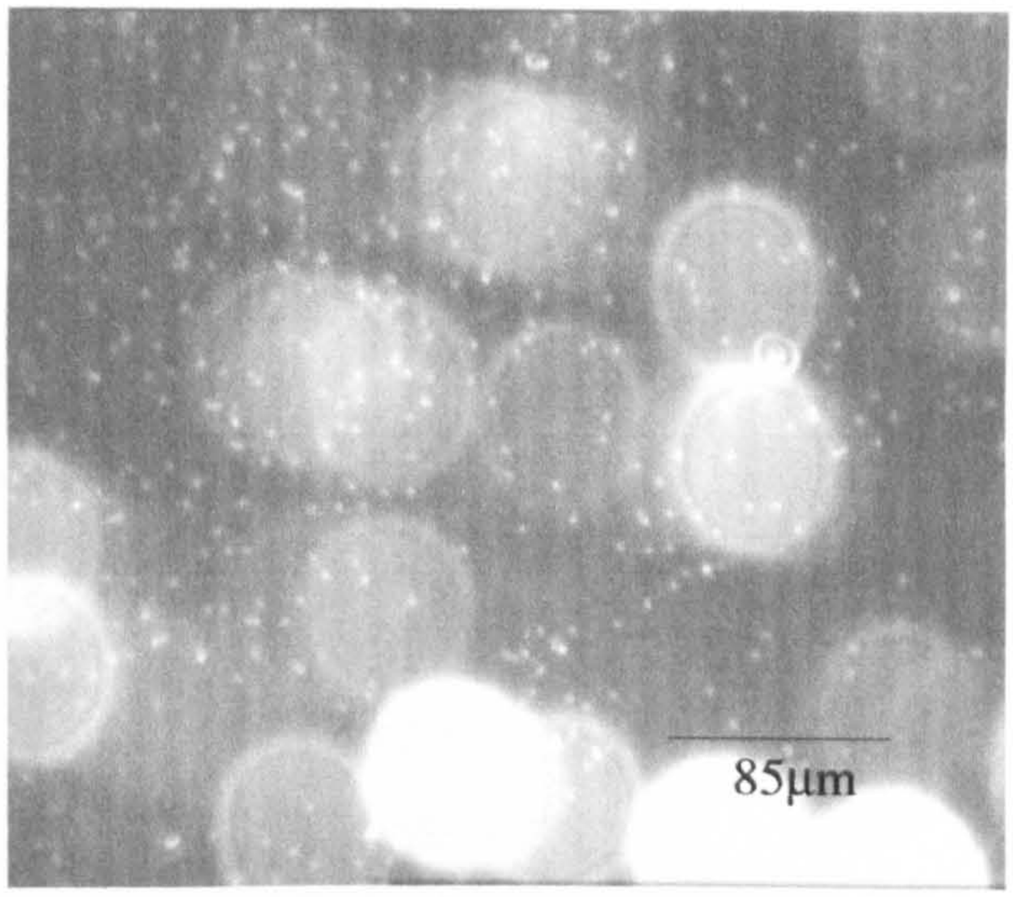

(c)

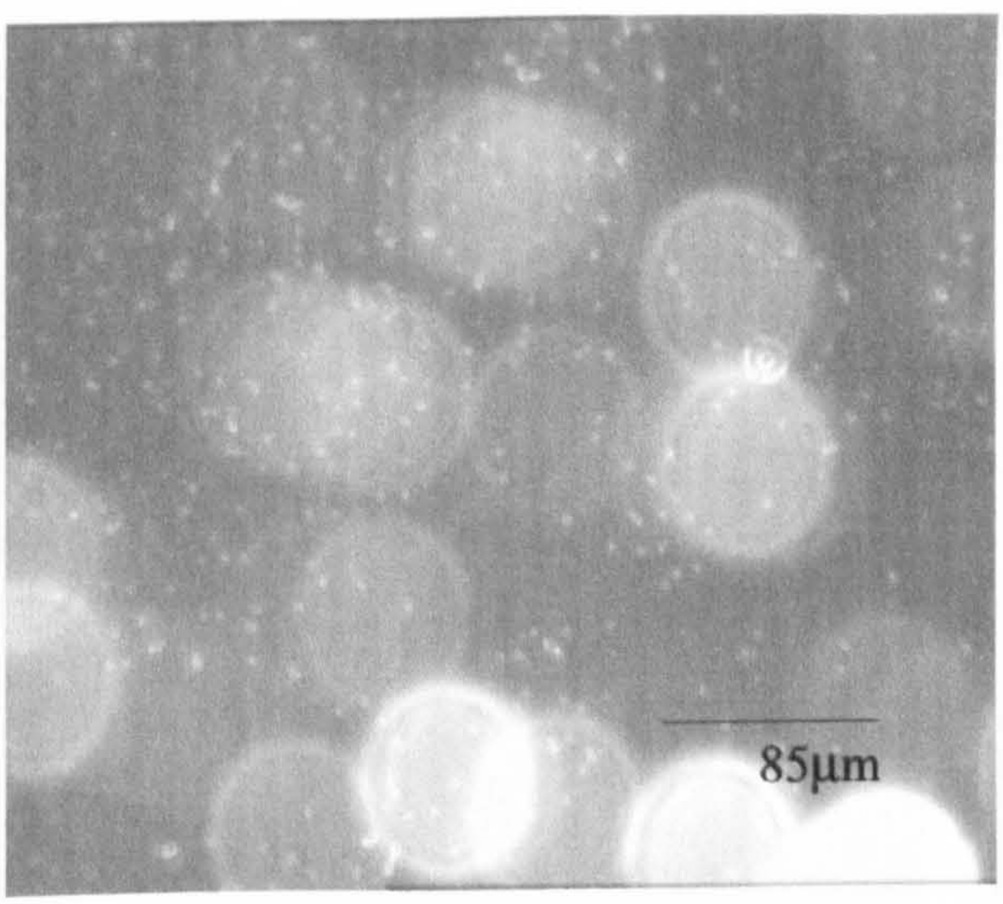

(d)

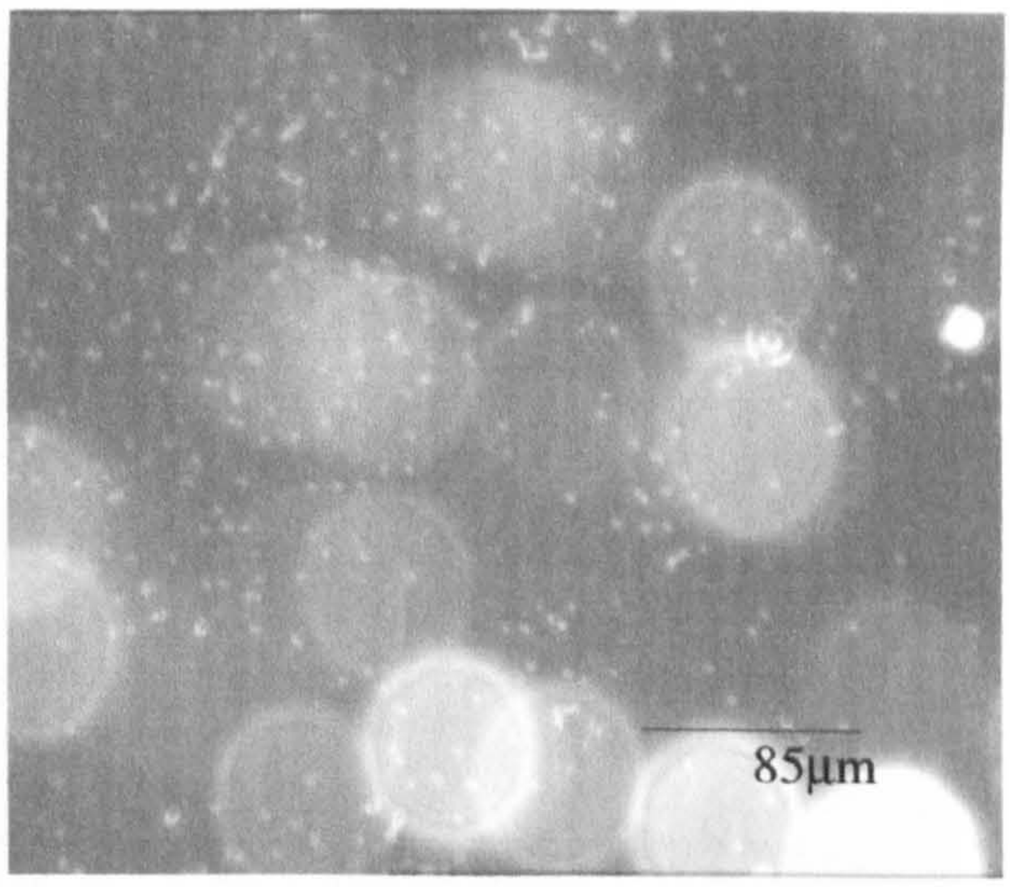

Plate XXXVI: 8.0mM SDS (a) After 3hrs, (b) 100 ml/min^{-1}, (c) 200 ml/min^{-1}, (d) 350 ml/min^{-1}

(a)

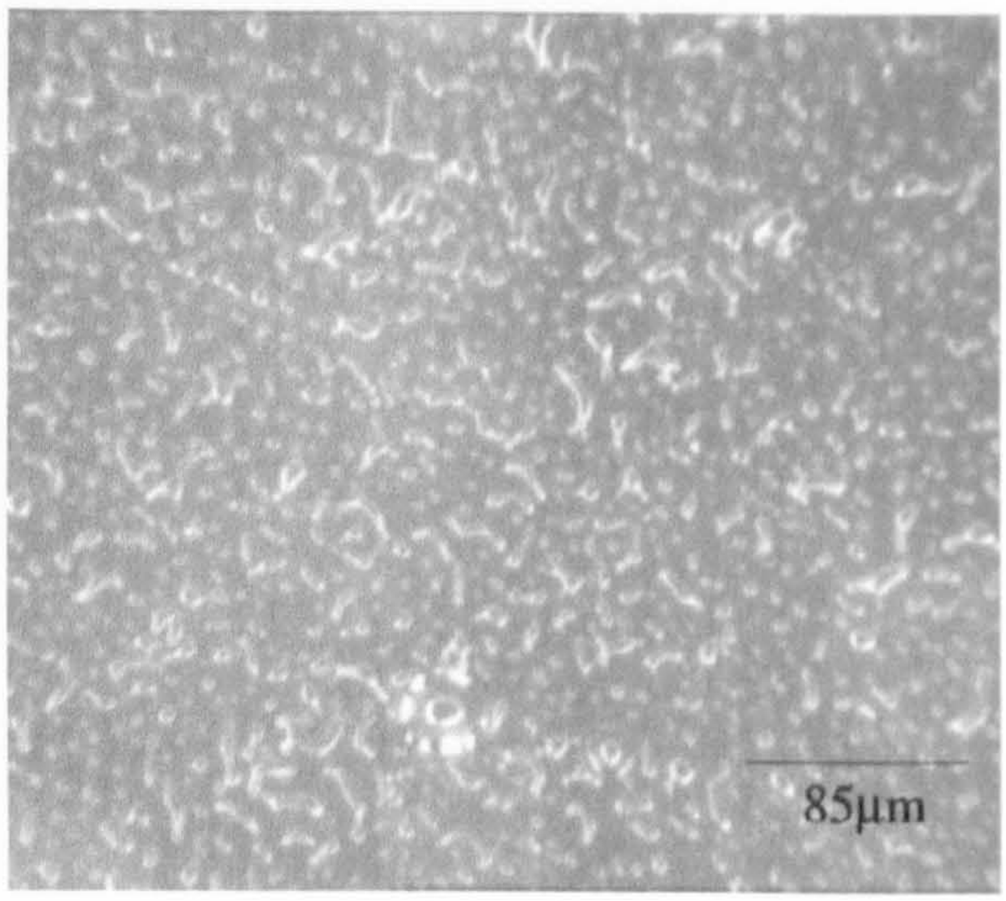

(b)

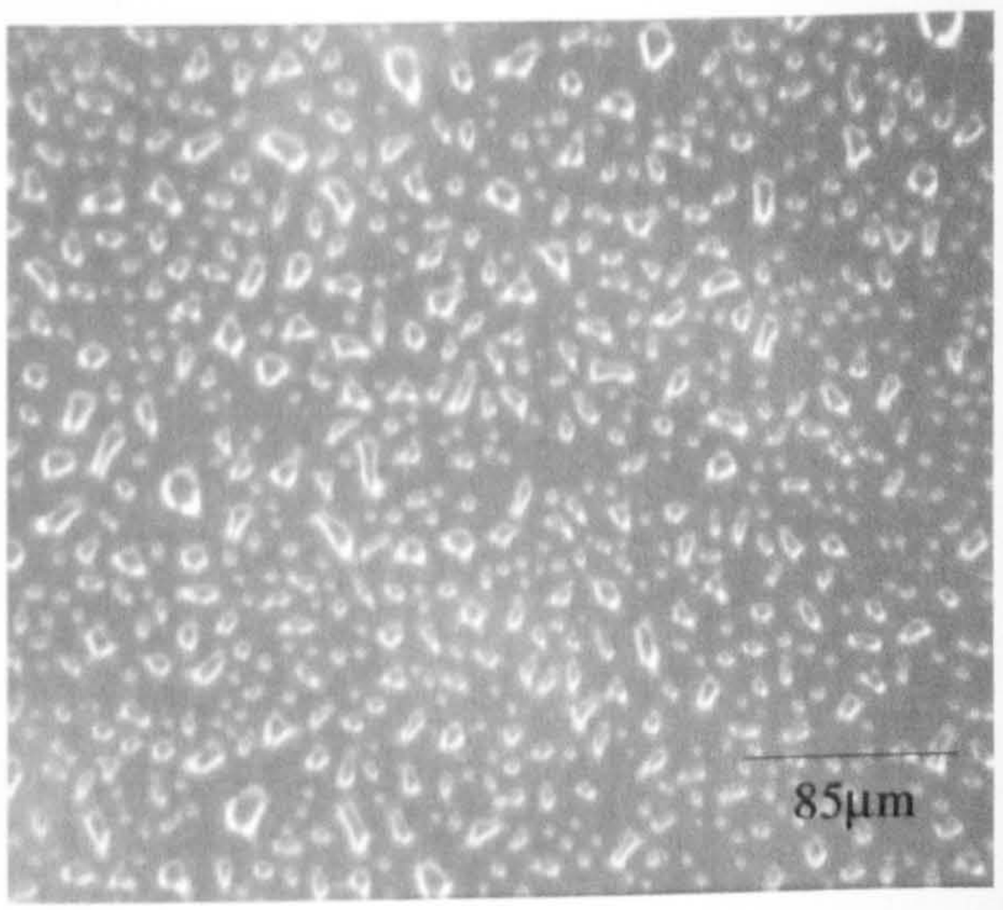

(c)

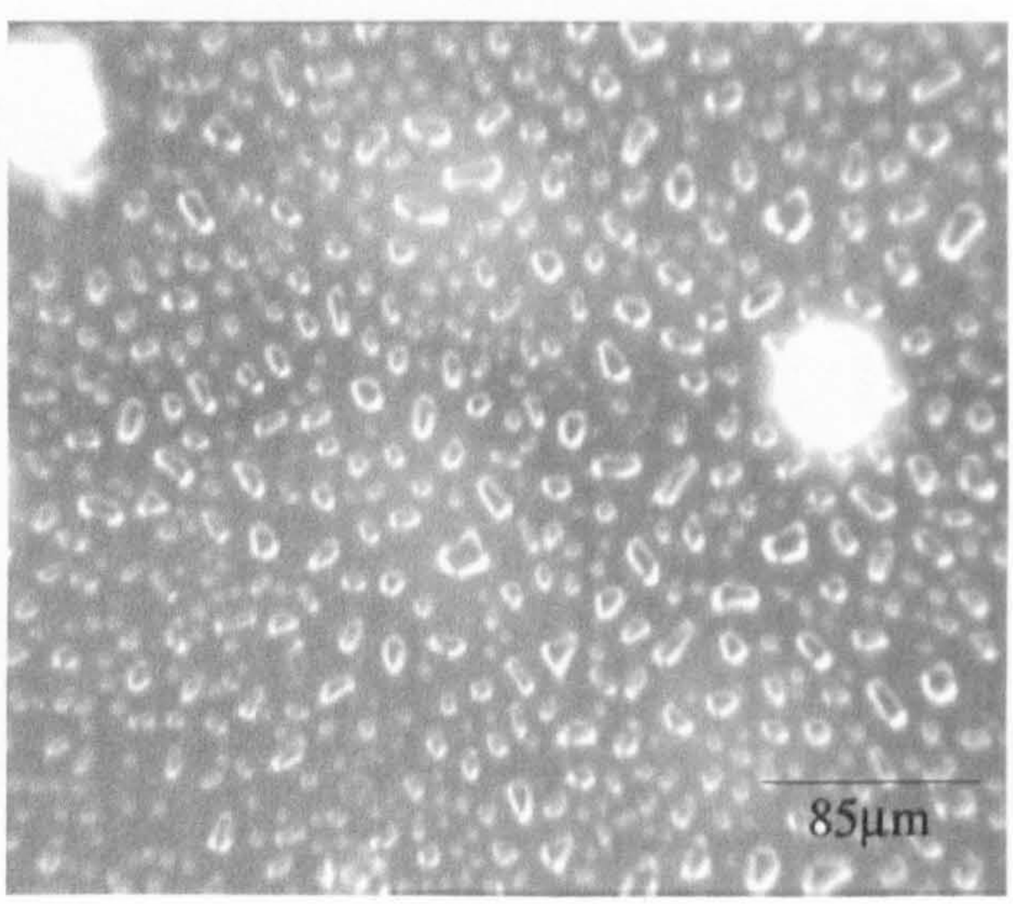

(d)

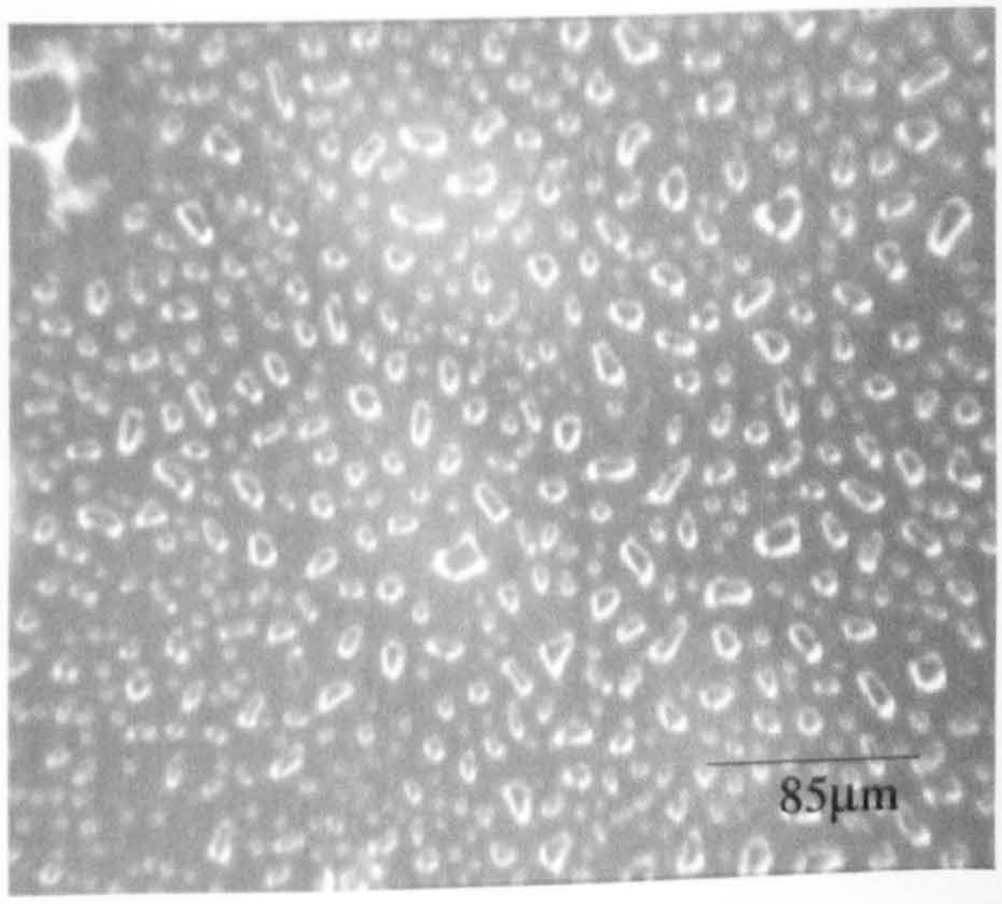

Those systems containing <0.08mM* SDS displayed the lowest droplet removal, < 30%, and the highest force of adhesion value, 3.2 N. The value was 1000 times higher than identical systems without the presence of surfactant or in the presence of electrolyte, $4.5x10^{-4}$ N and $4.1x10^{-3}$ N respectively. This behaviour could be related to the reduction in droplet surface tension which allowed the droplets to come into direct contact with the substrate, but the force of adhesion was enhanced by the close proximity of the surfactant molecules at the droplet surface and those already adsorbed at the mica surface, see figure 9.11. As the surfactant concentration was increased, droplets became more rigid in nature and the electrostatic repulsion between the negatively charged droplets became more significant. This leads to an overall reduction in the adhesive force and so the droplets become easier to remove. and easy to remove, see chapter 9. In addition, this resulted in an increase in the number of droplets removed from the substrate surface as their wetting properties reduce, while the inter-droplet and droplet-substrate separation distances simultaneously increased.

Table 10.3 F_{H50} removal data

[SDS] (mM)	F_{H50} (N)	γ_c (ml min^{-1})	% max. removed	F_{ad} (N)	ϕ_p (μm)
*0.08	*$1.5x10^{-2}$	*>353	*25.9	$8.9x10^{-8}$	10.2
0.80	*$1.4x10^{-2}$	*>350	*35.0	$8.9x10^{-8}$	9.0
8.00	$1.5x10^{-3}$	340	47.7	$9.3x10^{-9}$	4.9

Fig 10.3: Droplet removal data as a function of surfactant concentration;a) 0.08mM SDS, b) 0.8mM SDS, c) 8.0mM SDS

a)

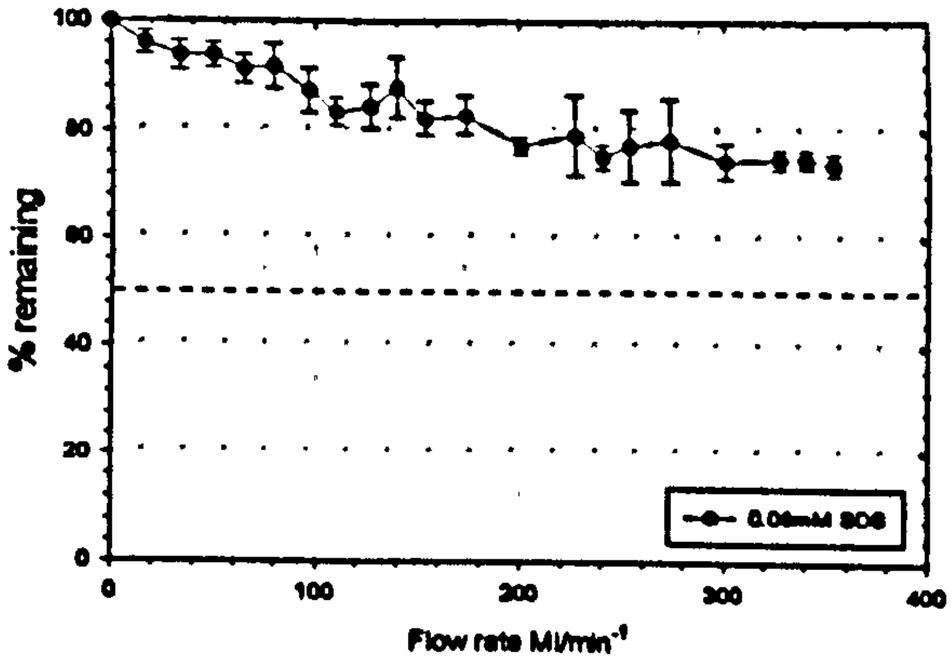

b)

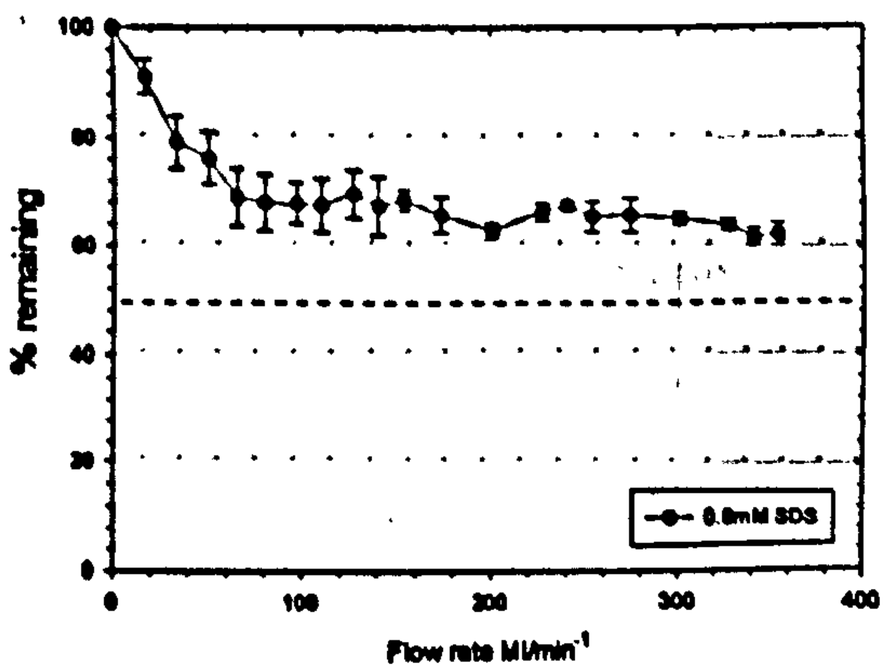

(c)

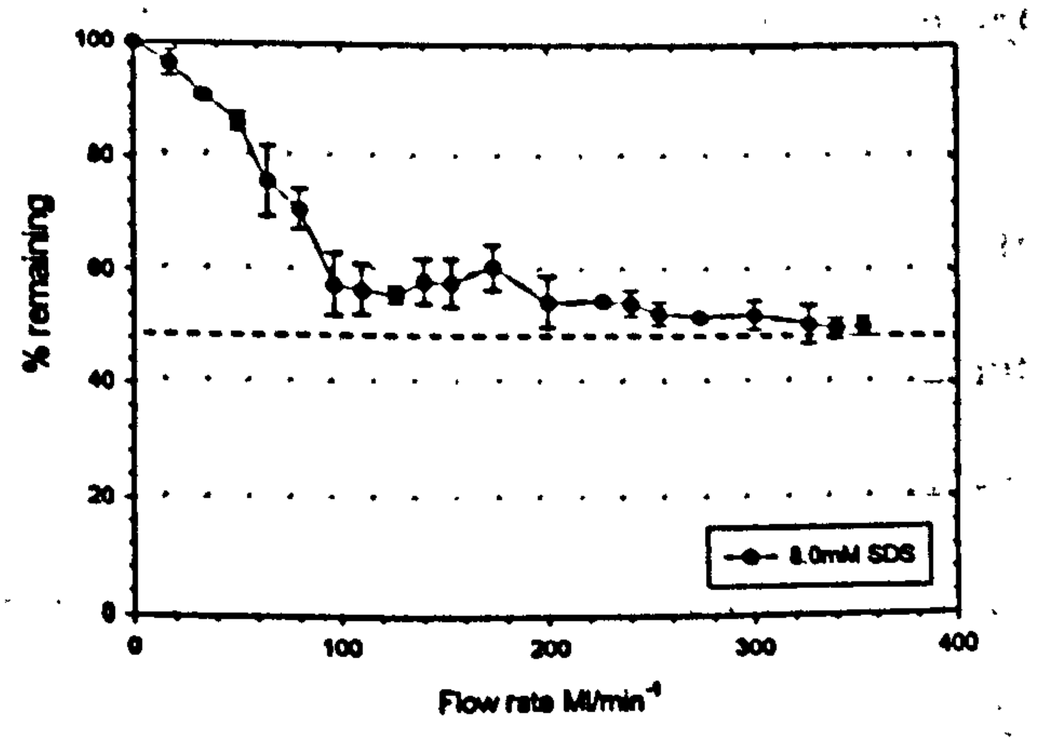

10.1.4 Colloidal removal as a function of substrate

The final development of the colloidal removal study involved the investigation of the influence of substrate surface asperities and chemical composition on the hydrodynamic force required to remove 50% of deposited cross-linked PDMS droplets. The substrates investigated included mica and glass chemically modified with acid, APTES, Repelcote and Lysine, see chapter 4. Identical horizontal flow cell parameters were used as described in section 10.1, using fixed emulsion of 0.05 (v/v) total monomer, 0.05(v/v) MTMS and an aqueous flow solution. The results obtained are shown in figure 10.4 (a-e) and plates XXXVII - XXXX,. The characterisation data discussed previously in chapter 5 and 8, including streaming potential, surface roughness and deposition studies etc. was used to understand the differences in the hydrodynamic force values between the substrates.

It has been suggested that the comparatively large critical hydrodynamic removal force observed for glass substrates was influenced by droplet contact deformation caused by height asperities present on the substrate surfaces. The short range Born forces then spread over the contact region and created a more symmetric distribution of forces over the droplet surface, which also created a stronger restraining torque on the droplet, irrespective of the contact area. However, Hubbe[2] determined the magnitude of the restraining torque and the lever arm was dependent on the contact radius rather than the height of the asperity. A study by Freitas et al[5] indicated that hydrophilic particles adsorbed onto hydrophobic surfaces display a van der Waals attraction in addition to the hydrophobic forces. The magnitude of these forces were found to be greater than that between two hydrophilic surfaces but not as great as two hydrophobic surfaces.

Plate XXXVII: Acid cleaned glass; (a)After 3hrs, (b)100 ml/min^{-1}, (c) 200 ml/min^{-1}, (d) 350 ml/min^{-1}

(a)

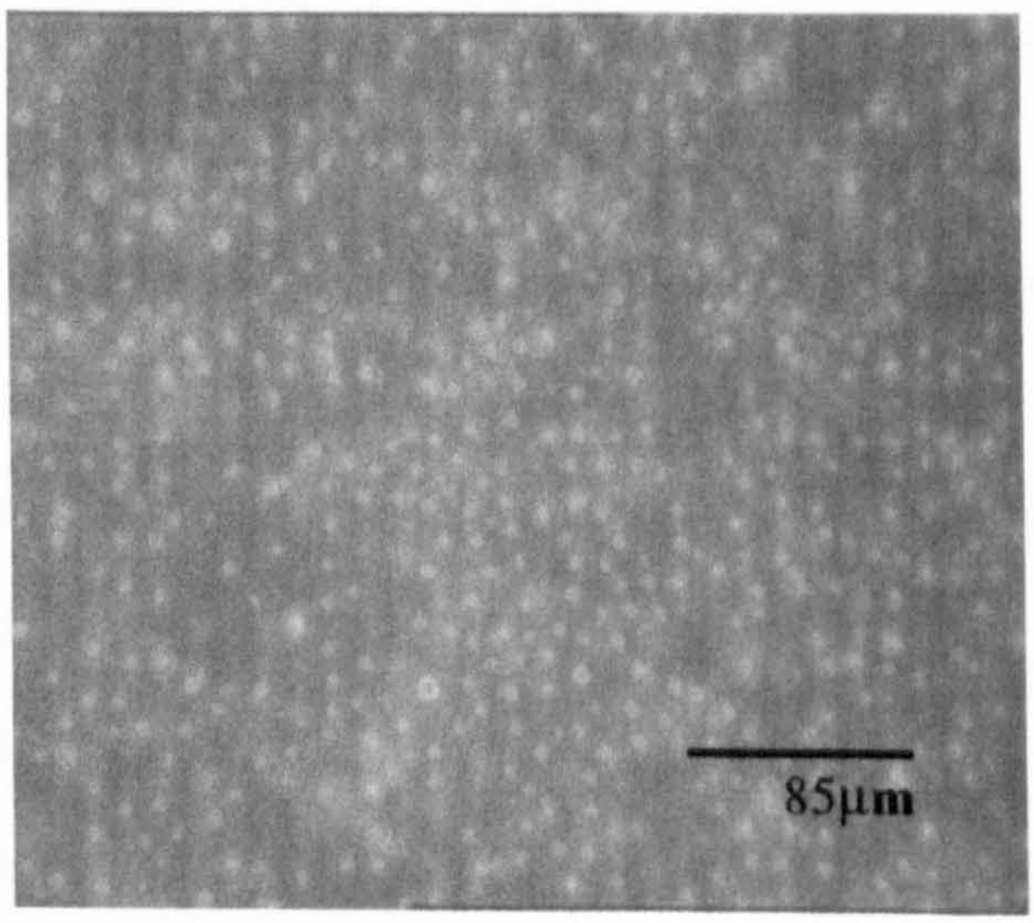

(b)

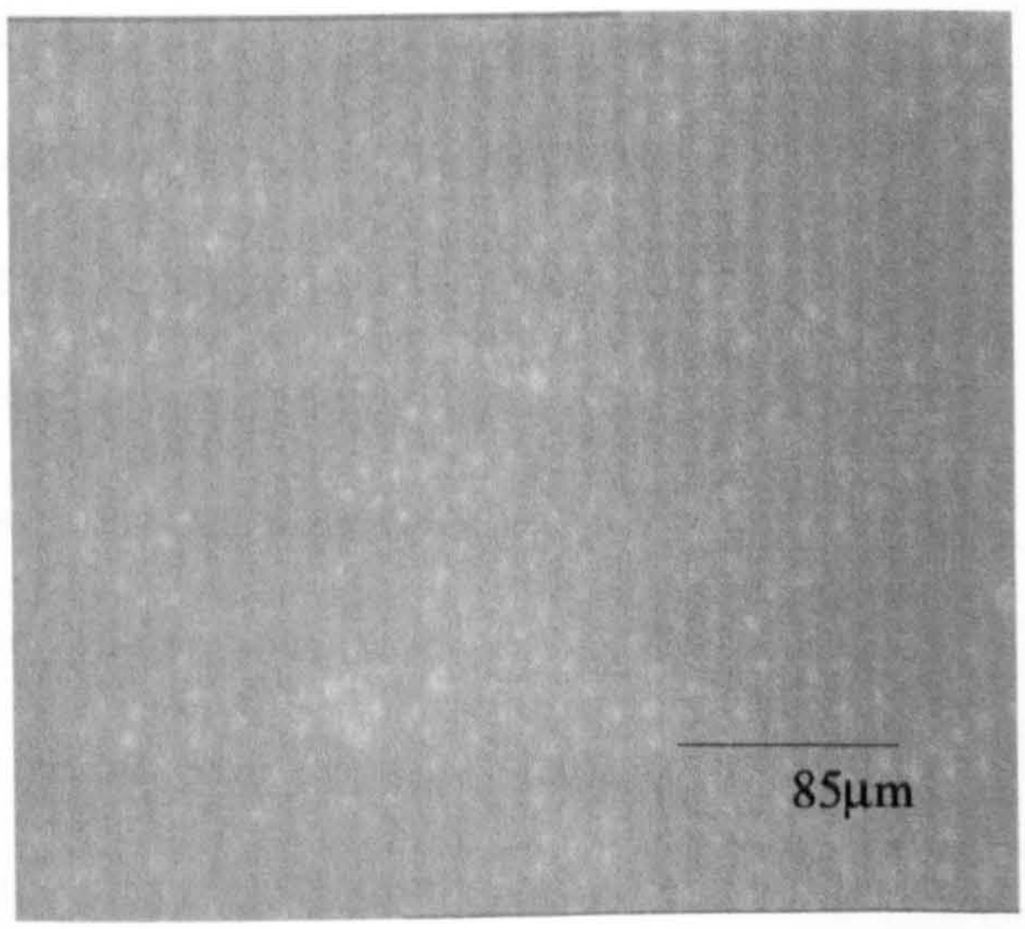

(c)

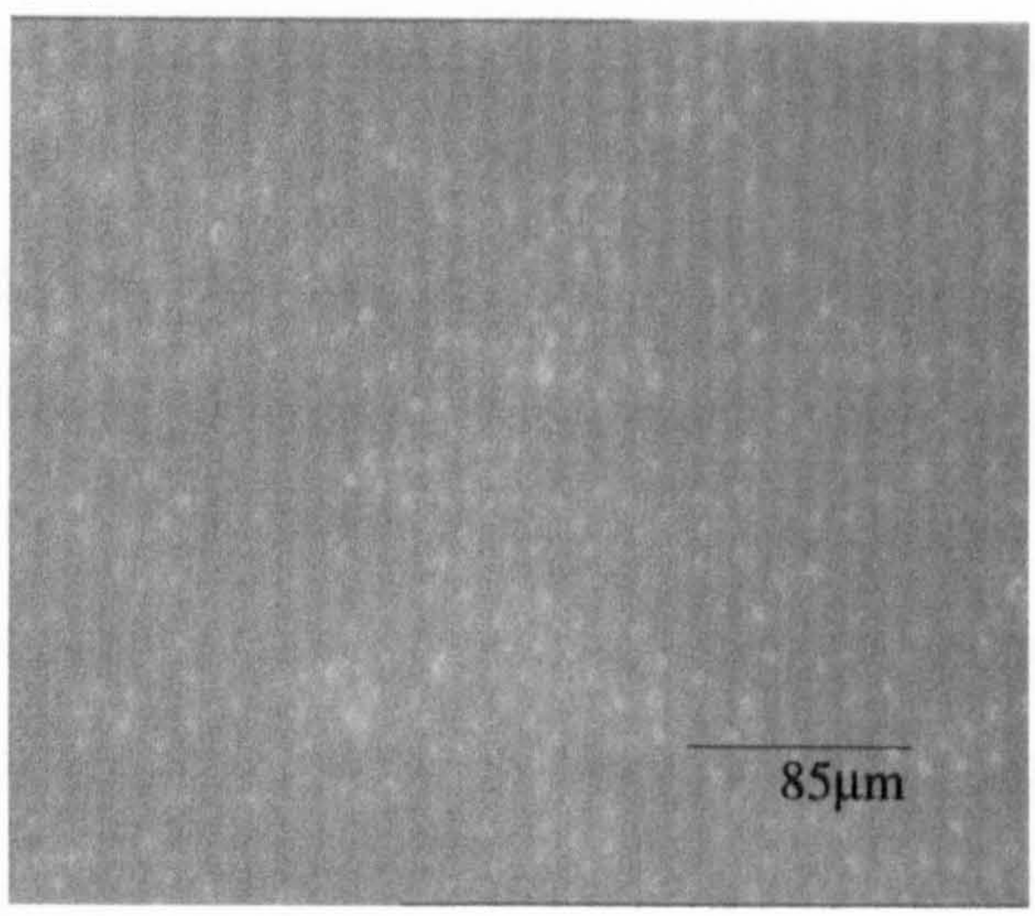

(d)

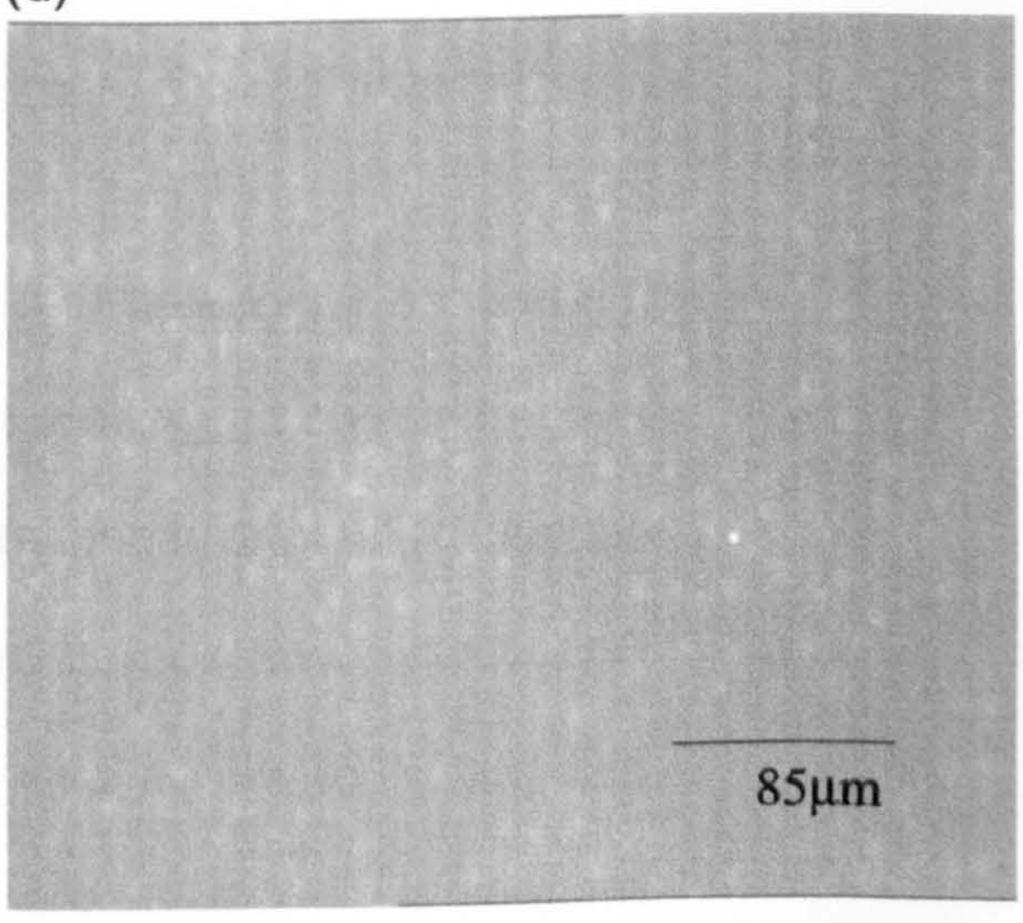

Plate XXXVIII APTES substrate; (a)After 3hrs (b)100 ml/min^{-1} (c)200 ml/min^{-1} (d) 350 ml/min^{-1}

(a)

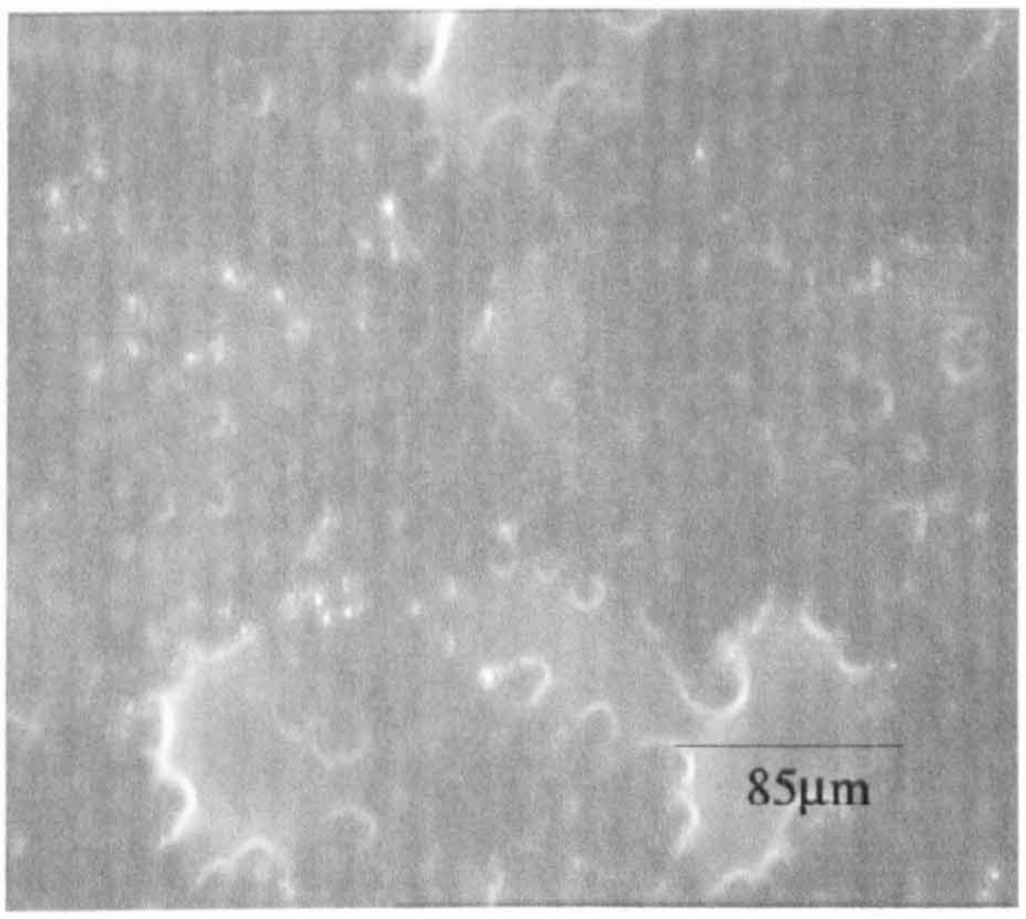

(b)

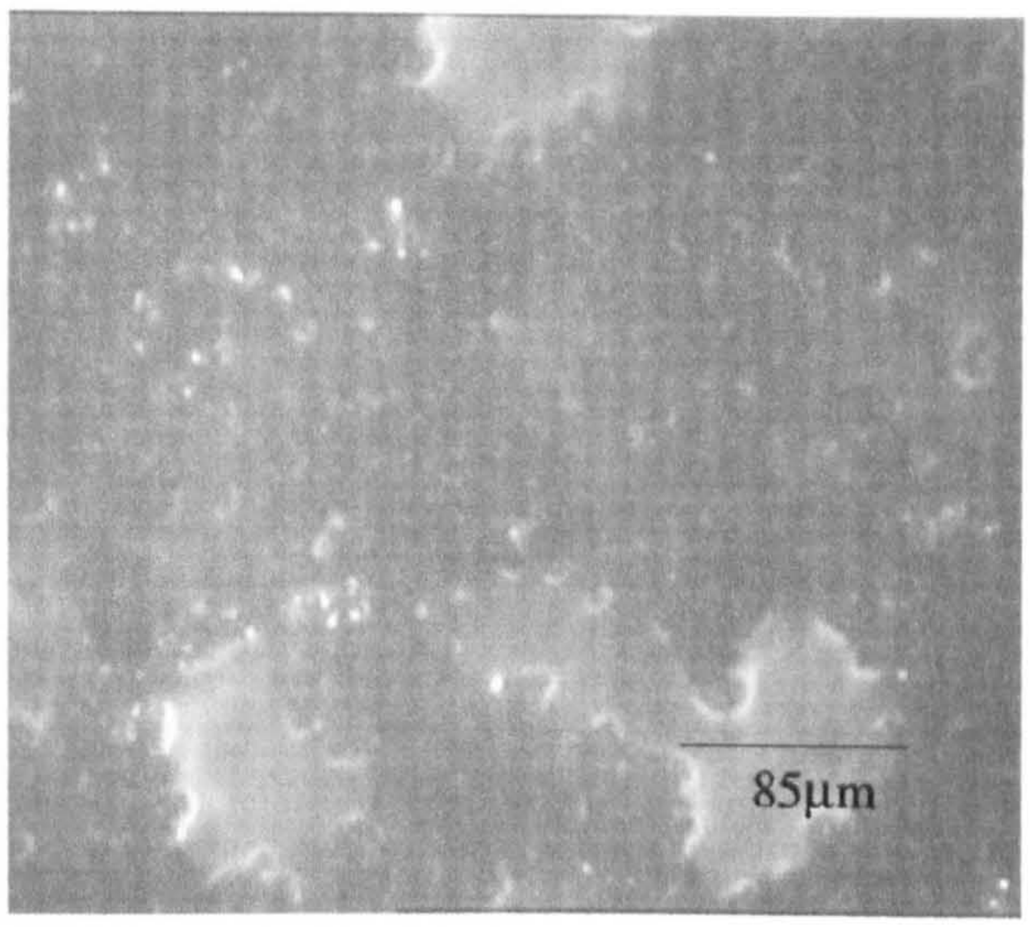

(c)

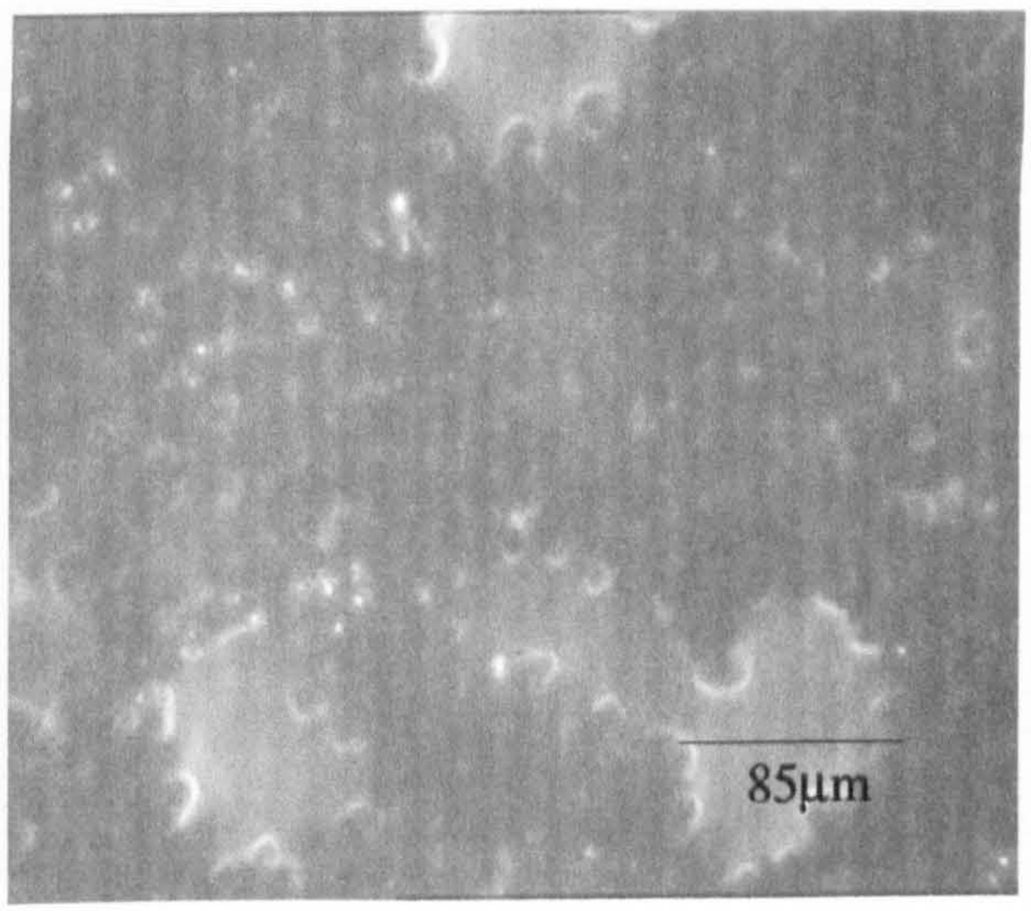

(d)

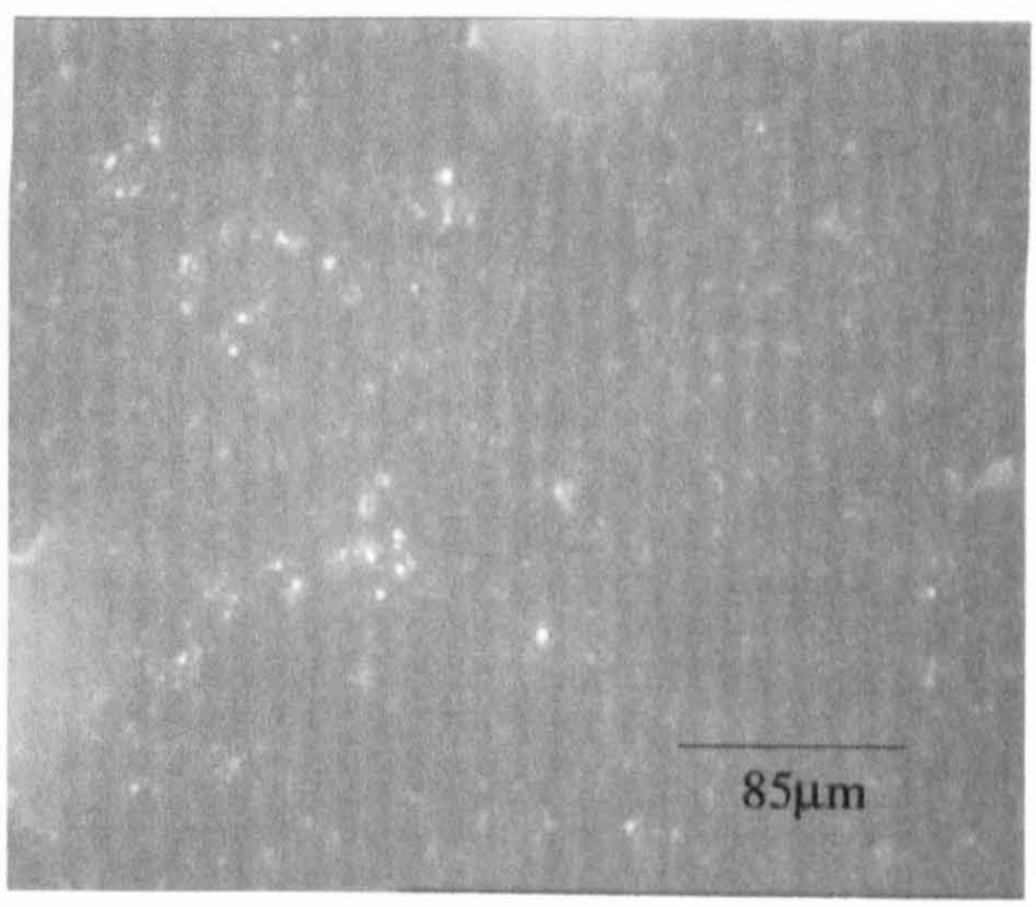

Plate XXXIX: Repelcote modified glass (a) After 3hrs, (b) 100 ml/min^{-1}, (c) 200 ml/min^{-1}, (d) 350 ml/min^{-}

(a)

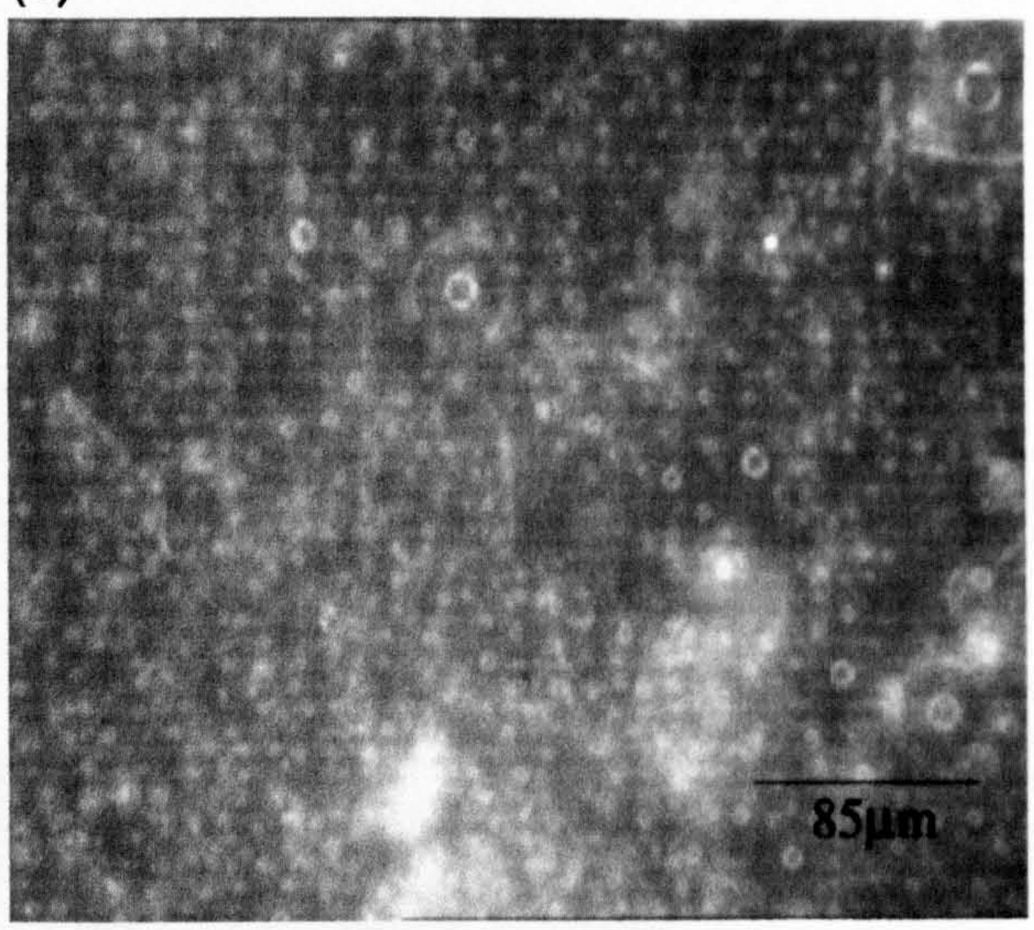

(b)

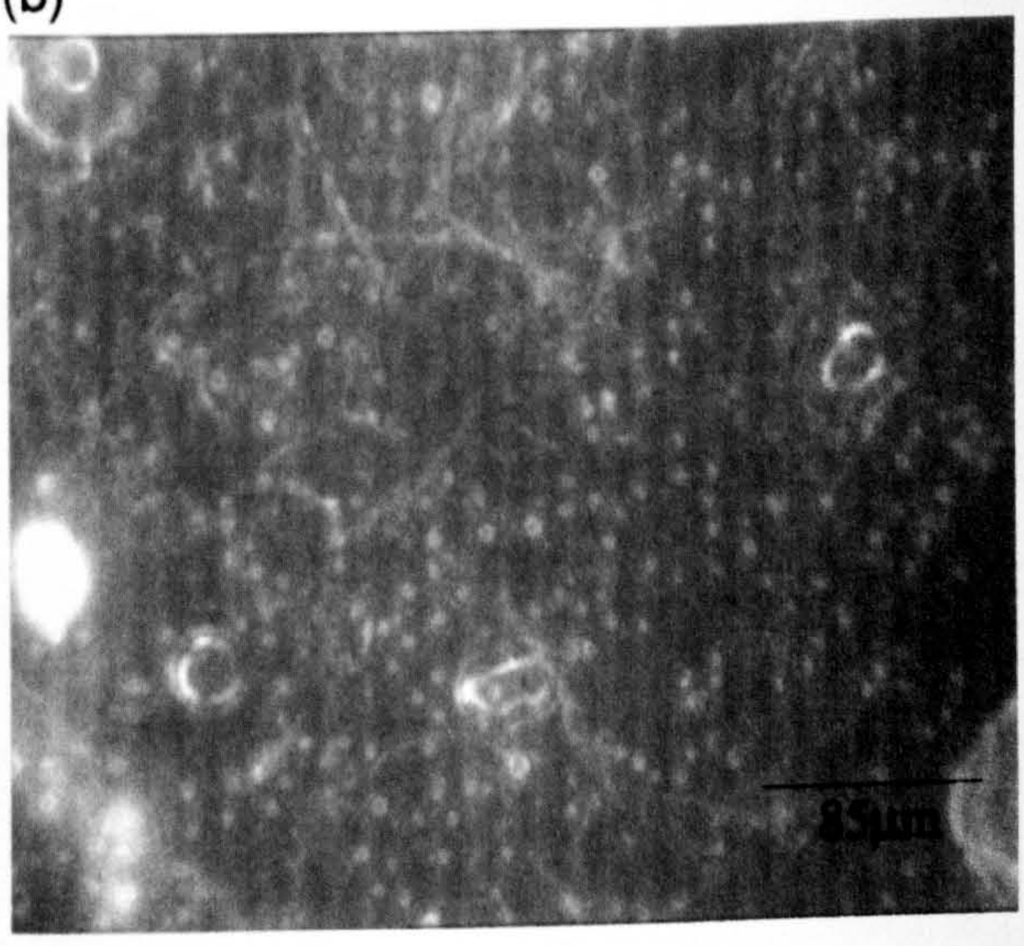

(c)

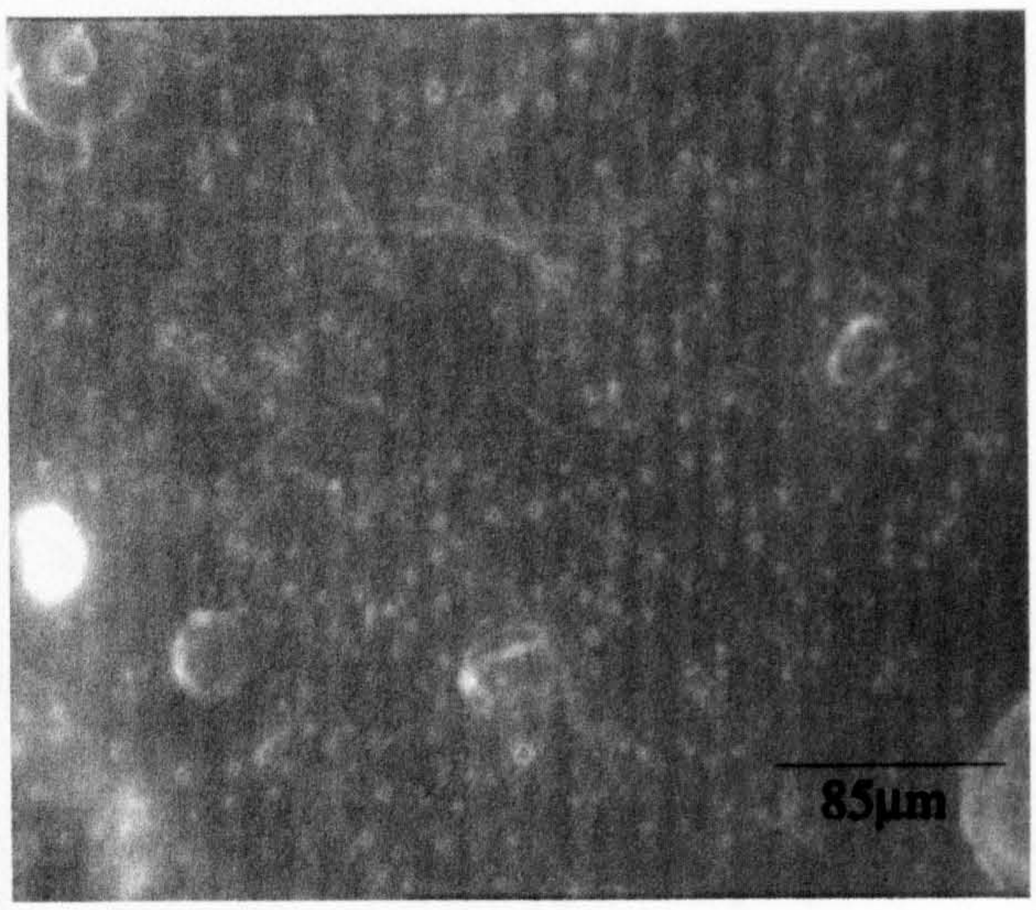

(d)

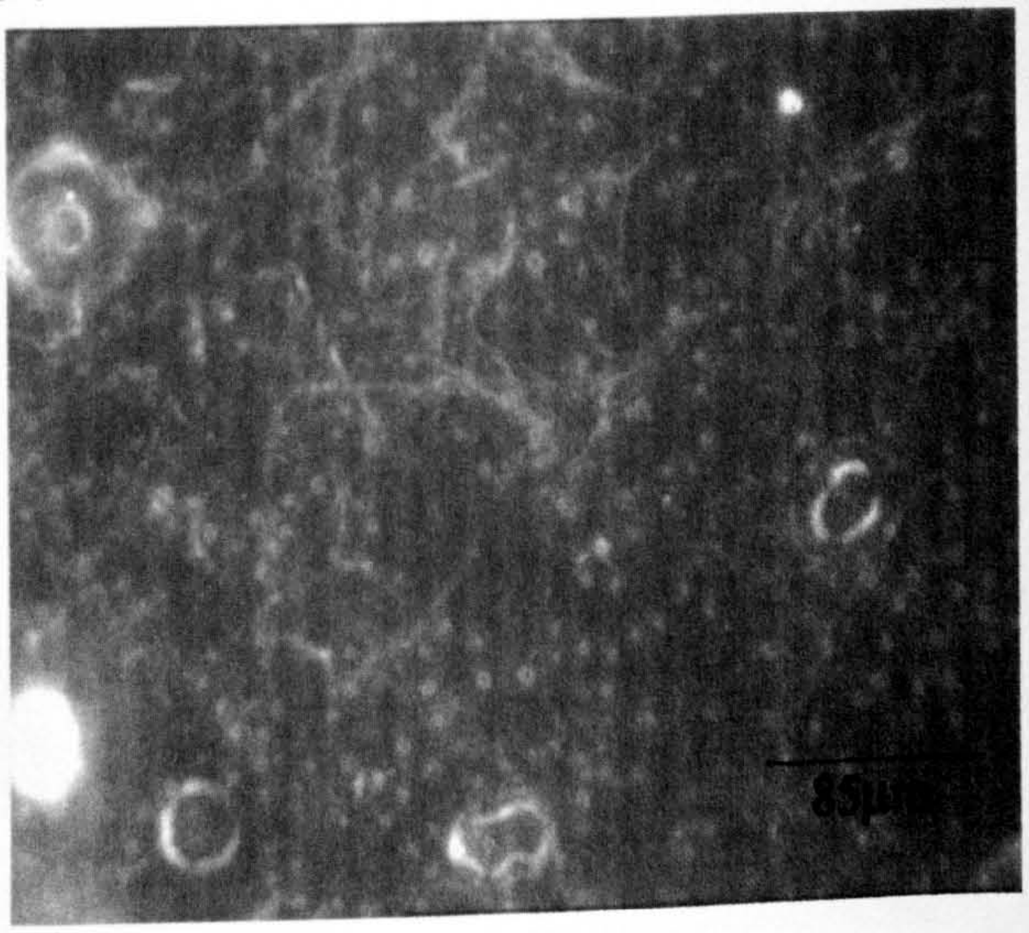

PLATE XXX: L-Lysine modified glass; (a) After 3hrs (b) 100 ml/min^{-1}
(c) 200 ml/min^{-1} , (d) 350 ml/min^{-1}

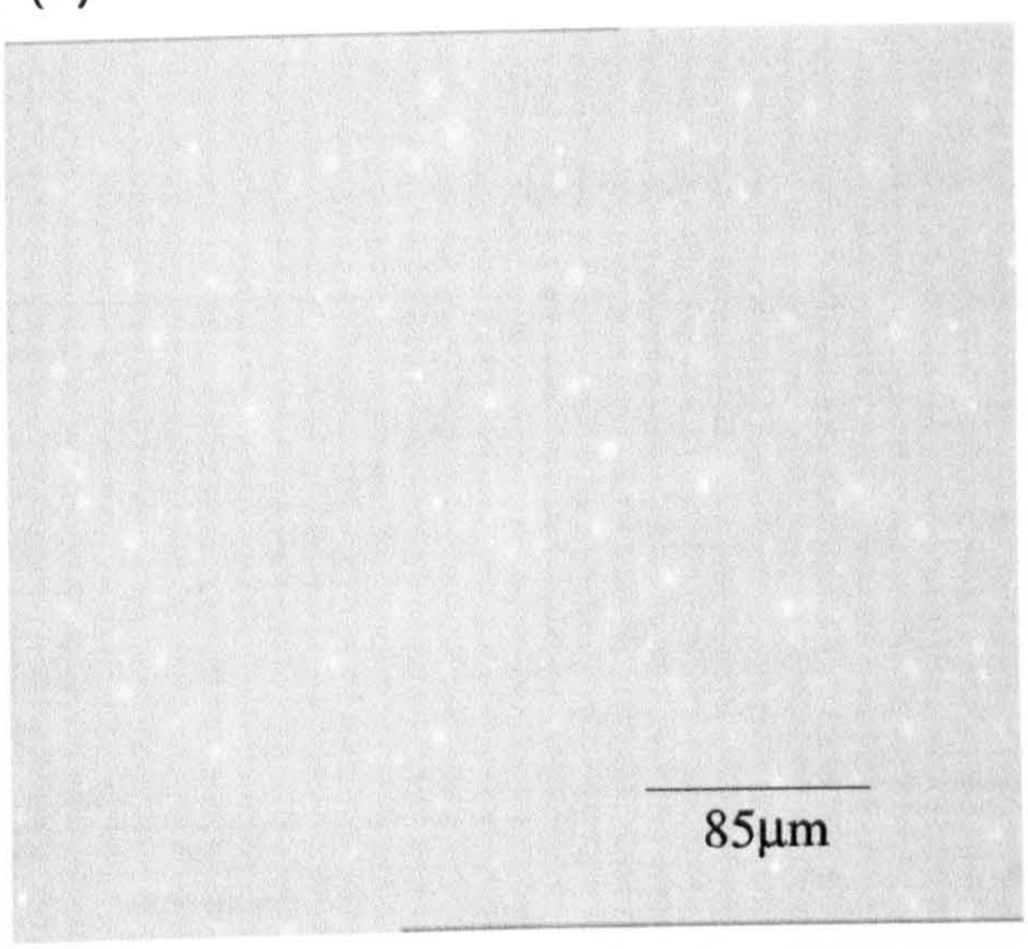

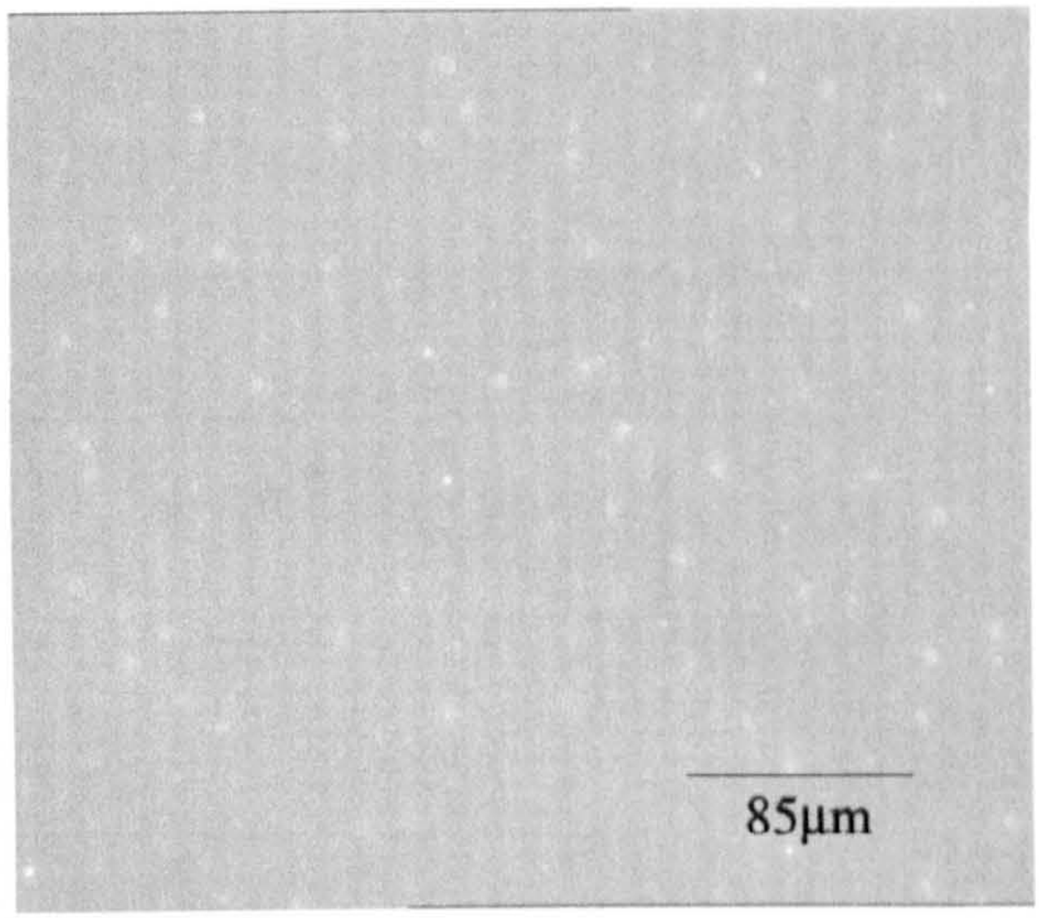

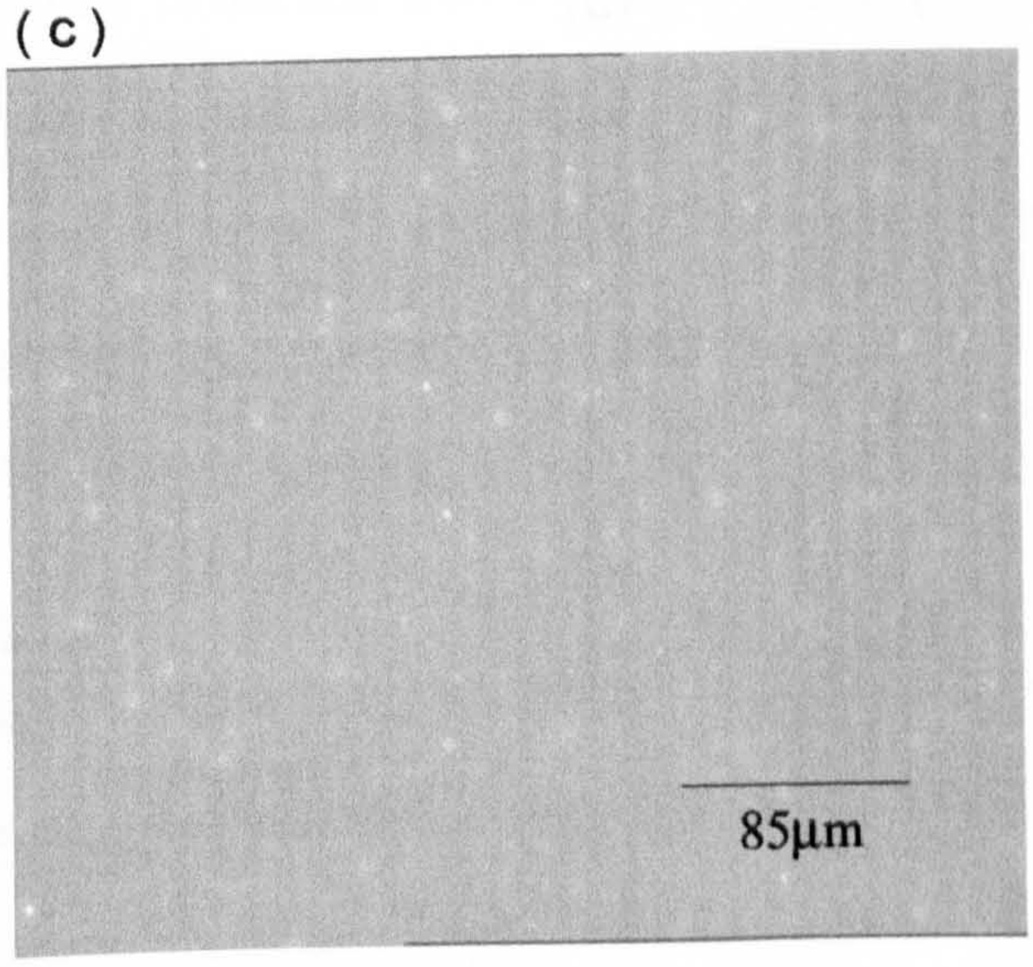

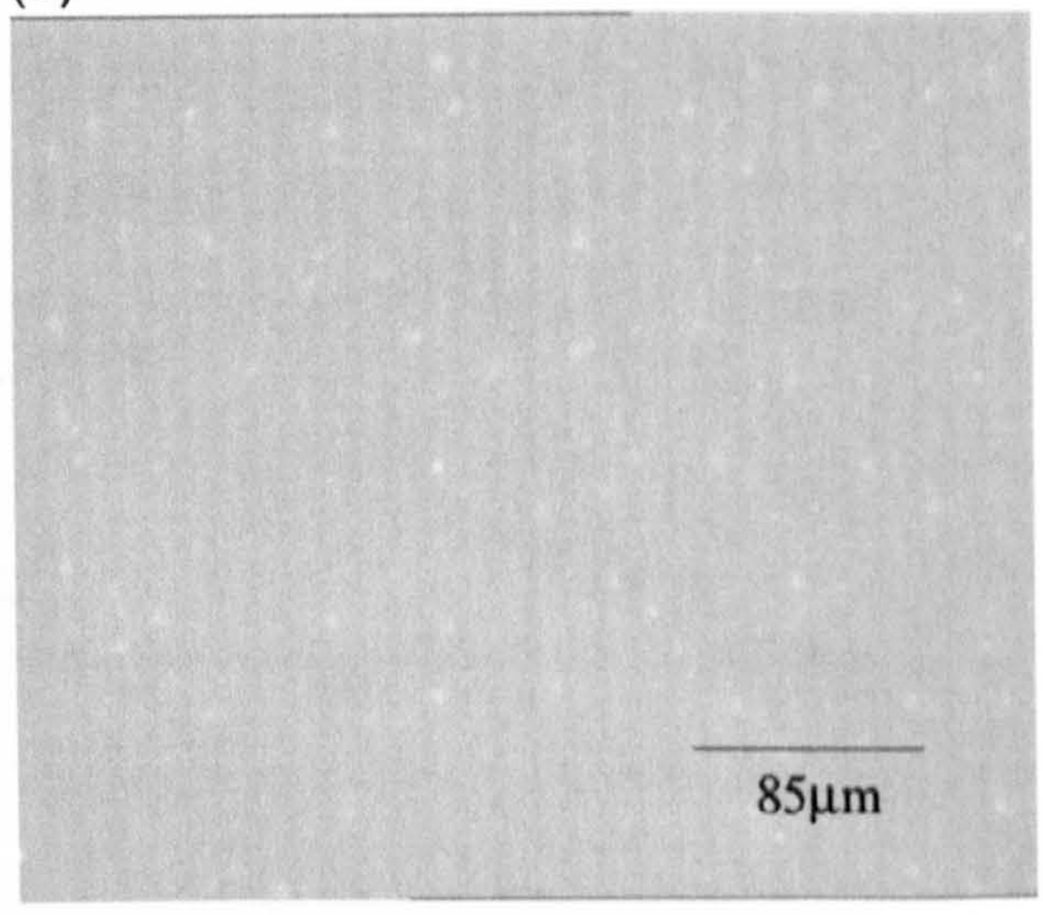

Fig 10.4 Droplet removal data as a function of substrate surface; a) APTES glass substrate, b) L-Lysine glass substrate, c) Acid cleaned glass substrate, d) Repelcote glass substrate,

a)

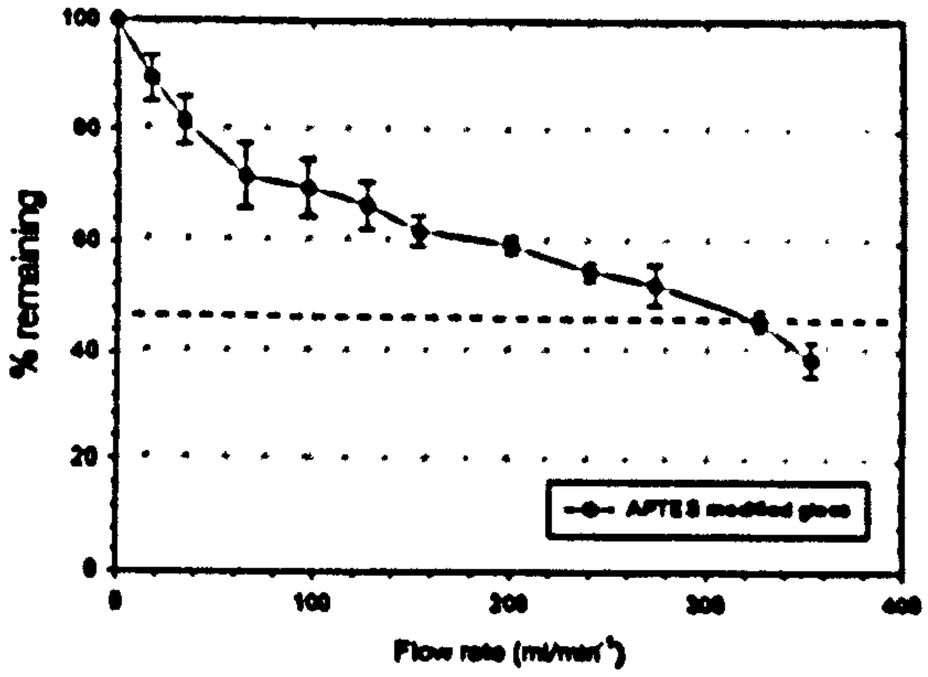

(b)

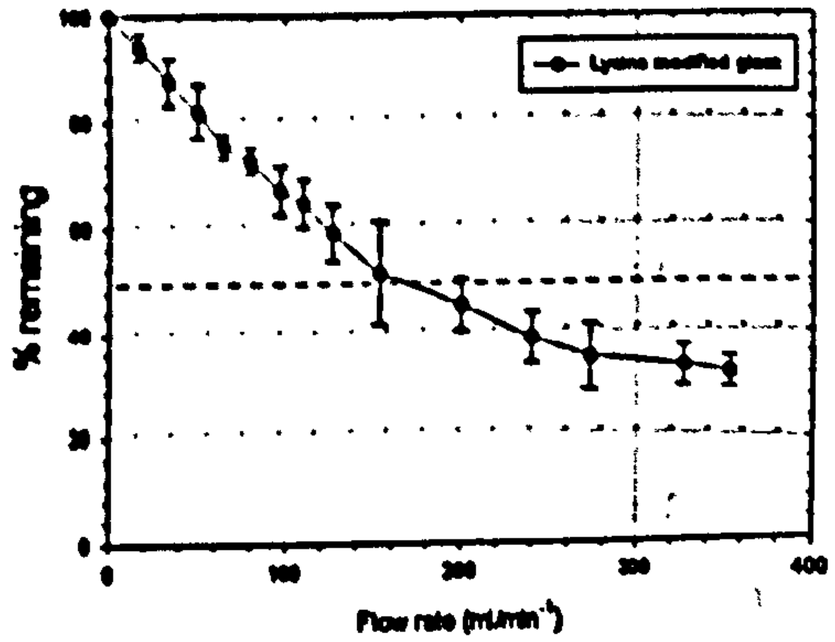

(c)

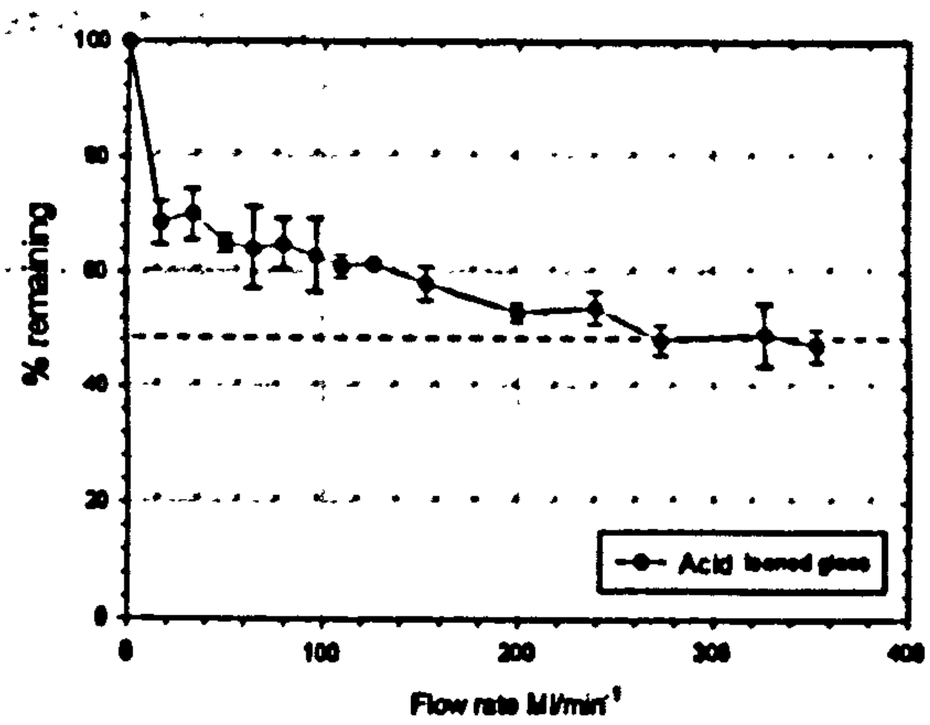

(d)

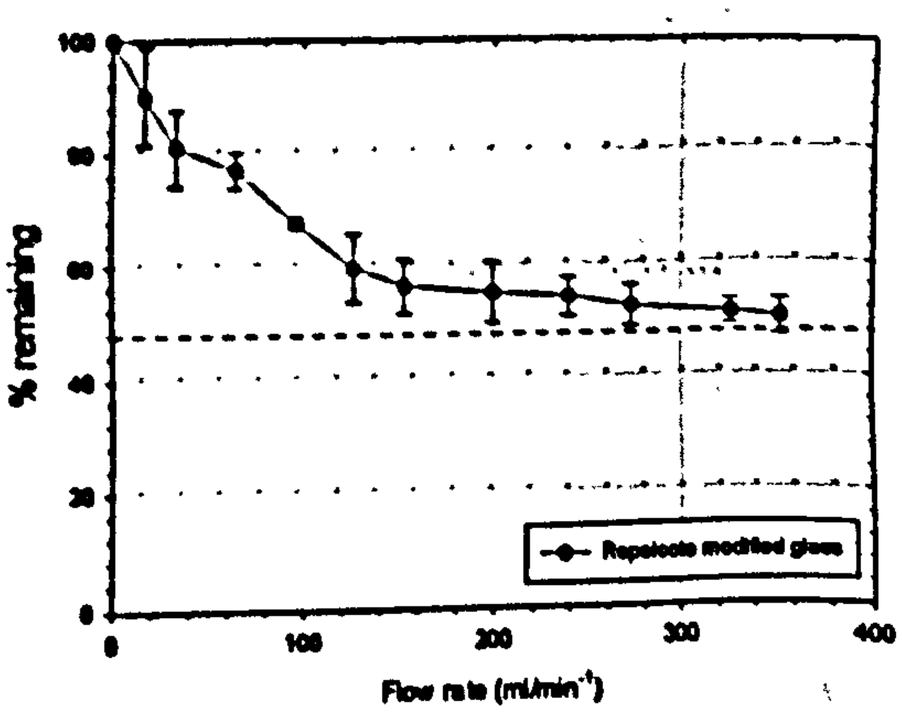

Although the exact origins of this force were unclear, it is possible that additional non-DLVO forces exist between the surfactant-like droplets and the hydrophobic slide used in this work.

The removal studies completed for the chemically modified substrates has allowed one to simultaneously investigate the influence of both these properties. In addition, it should be noted that as the droplet deforms to "fill" the contours of the substrate surface, it creates an "anchoring" stability, and it controls the level resistance to the applied removal force. Inter-droplet and droplet-substrate separation distances simultaneously increased.

It was observed that the mica substrate removal studies required the lowest hydrodynamic force to remove deposited droplets from the surface with respect to the substrates investigated. This could be attributed to the fact that mica has a similar surface asperity height to the droplet surface as both are almost molecularly smooth.

This surface feature allows the surface forces to be evenly distributed over the two surfaces and therefore allows the droplets to be more easily removed. The L-Lysine modified glass, used to model amino-acid interactions that occur with adhering droplet during deposition processes on hair, displayed a similarly low F_{H50} value to the mica surface.

The data obtained during the colloidal removal investigations is summarised in table 10.4

Table 10.4 : F_{H40} removal data

Sample	F_{H50} (nN)	γ_c (ml min^{-1})	% max. removed	F_A (N)	ϕ_p (μm)
Mica	2.9×10^{-3}	150	62.0	4.5×10^{-4}	4.0
Lysine modified glass	5.7×10^{-3}	126	70.6	3.6×10^{-8}	6.7
Acid cleaned glass	1.1×10^{-2}	260	55.4	7.2×10^{-8}	7.0
APTES modified glass	1.4×10^{-2}	326	60.3	8.6×10^{-8}	11.7
Repelcote modified glass	1.5×10^{-2}	353	51.2	9.3×10^{-8}	8.4

Although substrate had the lowest surface heterogeneity out of the glass substrates, 0.65nm, it also had a more negative surface potential than mica,- 0.4mV and -6.6mV respectively. The former property would have been expected to enhance the force of adhesion between the substrate and the PDMS droplets, it can therefore be observed that the electrostatic repulsive force created from surface charge differences is the dominant influence on droplet removal. This property is evident in the presence of a small droplet-substrate contact area.

The acid cleaned, the Repelcote modified and the APTES modified glass substrates have widely different surface charges -16.1mV, -18.7mV and 6.6mV respectively. This should alter the electrostatic repulsive and van der waals attractive forces present between the surfaces and influence the magnitude of force required for droplet removal. However they all required similar hydrodynamic forces to remove the adhered cross-linked PDMS droplets ~1.3×10^{-2} nN ,which was approximately 100 times stronger than those displayed by the mica substrate. In contrast to the mica and the L-lysine modified glass, the higher

average surface asperity present on these substrates is the more dominant influence on droplet interaction with the substrate surface. This is evident as the F_{H50} and γc values for the acid cleaned, the APTES modified and the Repelcote modified glass are observed to increase in the same order as the surface roughness, 1.6nm, 2.6nm and 2.7nm respectively.

Overall, it would appear that the hydrodynamic force of the removal of deformable droplets from substrates with an average surface asperity <1nm, and where droplet and substrate have similar surface textures, is dominated by coulombic differences between the two surfaces. However, if the substrate surface roughness was increased, >1nm, the critical F_{H50} value is influenced by the interaction of the droplet with the surface asperity.

10.6 References

1. Das.S.K., Sharma.M.M., Schecter.R.S., Particulate Science and Technology, 13, 227, (1995)

2. Hubbe, M.A., Colloids Surf. 12, 151 (1983)

3. O'Neil.M.E., Chemical Engineering Science, 23, 1293, 1968

4. Yamatmoto.T, Periasamy.R, Donovan.R.P, Ensor.D.S, Jomal of adhesion science and technology, 8, 543, 1994

5. Freitas.A, M.M.Sharma, 15, 2466,1999

Chapter 11: Conclusions and Further Work

11.1 Flow cell conclusions

The characterisation results presented in chapter 5 showed that the physical properties of cross-linked PDMS emulsion systems were able to be reproduced and manipulated as reported in previous studies[1,2]. Stable dialysed PDMS emulsions were able to be prepared from fixed total monomer, 0.05(v/v) DMDES, with low tri-functional monomer volume fraction, MTMS, < 0.1(v/v), to produce deformable cross-linked droplets visible under optical microscopy, > 2μm and with a polydispersity <10%. The ability to manipulate droplets' internal viscosity and charged surface chain end-groups and the ratio of tri-functional / di-functional linear, cyclic and cross-linked material has provided a more realistic model of the application of emulsions than presently used in the cosmetics industry. The behavioural study of a charged deformable body in contact with a rigid body has highlighted several deviations from classical hard sphere DLVO predictions. These include a large primary maxima against coagulation and coalescence both in the bulk solution and also after deposition onto a solid substrate. This behaviour is partially attributed to droplet deformation and the presence of a large attractive hydrophobic interaction.

The use of mica and glass substrates in this study proved it was possible to create flat, optically clear, rigid surfaces which could be used to manipulate the droplet-substrate interactions. This was successfully achieved through the modification of the substrates' surface chemical composition, surface potential and surface heterogeneity. The surface potential for the substrates was kept <30mV to ensure experimental conditions could be compared with theoretical pair potential curves. In addition, the average surface roughness was maintained <10Å to obey Wenzel's regime.

The stagnation point flow cell methods allowed real time deposition images to be obtained from flow regimes that were in good agreement with Brownian deposition regimes. The results presented in chapter 8 showed that it was possible to manipulate the deposition of deformable droplets by altering the experimental conditions. The experiments illustrated that the potential difference between the two approaching surfaces was the dominant influence on the droplet deposition kinetics. Further studies showed it was possible to manipulate the extent of droplet spread on a rigid substrate by lowering the MTMS volume fraction <0.01(v/v) and also introducing an electrolyte concentration above the CCC, > 10^{-3} mol dm^{-3}.

The main advantage of these studies has been the ability to observe the behaviour of charged deformable spheres in high surface coverage regimes, >50%, which has previously been unobtainable with hard sphere investigations[3-5]. It was interesting to note that no evidence of film formation was observed during any of the investigations, regardless of the extent of surface coverage.

The horizontal flow cell studies, discussed in chapter 10, provided a valid method of determining the manipulation of the adhesive strength between deformable cross-linked droplets and substrates under a variety of different experimental conditions. Although, the technique only provided a semi-quantitative indication of the interaction forces, the results proved to be in excellent agreement with the deposition data obtained from the Stagnation point flow cell studies. The design of the cell, together with the use of flow rates Re < 800 ensured a laminar flow was maintained throughout the investigations.

It was interesting to note that due to the spreading properties of the deformable droplets, the adhesive strength between the two surfaces was found to be independent of the

deposition time. This corresponded to relatively large hydrodynamic forces that were required to achieve any droplet removal compared with previously reported hard sphere studies[8,9].

The pair interaction potential curves calculated gave reasonable predictions with the deposition and removal experiments but could only be used as a estimate of the magnitude of the repulsive or attractive interactions. The theoretical calculations did not include any terms to account for substrate surface roughness, droplet deformation on approach to another body or the presence of fluctuating surface potential due to the mobility of the charged PDMS polymer chains.

It has been successfully shown that it was possible to control colloidal interaction with a rigid substrate by manipulating the volume fraction of tri-functional cross-linker. It was found that increasing the presence of MTMS from 0.0(v/v) to 0.1(v/v) reduced the deposition kinetics and the area occupied by each droplet as the internal cross-linked density decreased the deformability of the colloidal system. The presence of the cross-linker appeared to have a greater influence on the colloid-substrate interaction than the increasingly repulsive coulombic forces between the two surfaces. This trend was also observed during removal studies, where the lowest hydrodynamic forces observed throughout the entire project were required to remove PDMS droplets containing >0.01 (v/v) MTMS from a smooth surface.

The influence of electrolyte on the colloidal systems matched that predicted by DLVO pair potential calculations. Those deposition systems that contained NaCl concentrations above the CCC, $10^{-2} - 10^{-3}$ mol dm^{-3} showed some of the fastest deposition kinetics and largest contact areas between the droplets and the smooth substrates. This corresponded

to the predicted reduction in the EDL interactions between the surfaces, which allowed them to get to close proximity. In addition, the hydrodynamic forces required to remove the adhered droplets from the smooth substrate also increased as the electrolyte presence increased. However, the highest NaCl systems required removal forces of the same order of magnitude as that observed for cross-linked systems <0.01(v/v) ϕ without the presence of electrolyte.

The colloidal systems investigated which contained anionic surfactant SDS, showed the most remarkable deposition and removal behaviour within the entire investigation. As the surfactant concentration was increased, the average droplet size decreased and the surface potential partially adopted the surfactant charge as it was adsorbed at the interface. However, the observation of an ordered packing structure of the surfactant coated PDMS droplets on the smooth substrate provided evidence that the surfactant molecules were adsorbed onto the substrate surface. Fa et al[10] reported that the anionic surfactant formed "hemi-micellar"structures on the substrate surface which would correspond to the stable aqueous film present between the two surface and also the droplet linear packing arrangement for systems >0.8mM. It is interesting to note that the force required to remove the surfactant coated droplets from the smooth substrate appeared to be independent of the SDS concentration. However, the magnitude of the removal force was similar to that observed for those systems containing high electrolyte concentration or low MTMS ϕ, which would suggest that additional adhesion stability is provided by surfactant entanglement mechanisms.

The influence of substrate surface properties was investigated extensively in this study. The AFM measurements showed that all the substrate surface roughness were below 10μm, which ensured they were in Wenzel's regime and the depositing droplets

penetrated the gaps between each peak. This feature allowed the effect of slight changes in surface heterogeneity on droplet deposition behaviour to be observed more accurately. The influence of substrate surface heterogeneity could be rationalised in terms of the changes in lateral and normal interactions between deposited and approaching droplets. Overall, the spreading property of the deformable droplets on substrates, with similarly negative surface potentials, was dependent on the magnitude of substrate surface roughness. This property was observed to reduce the blocking effects exerted on approaching droplets by deposited droplets, while simultaneously increasing the substrate surface available for deposition. However, the increase in surface asperity height created a greater substrate surface area, creating a larger negative potential which in turn generated a stronger repulsive electrostatic force between the two surfaces

Those substrates with higher surface roughness, e.g Repelcote glass, acid cleaned glass and L-Lysine modified glass showed the least droplet spread but also the highest deposition number compared with the mica substrate. Therefore, it is possible to suggest that the magnitude of the surface roughness was a more dominant influence on deposition than the chemically generated surface charge. The exception to this hypothesis was the APTES modified glass. This substrate contained one of the roughest surface topographies investigated but displayed a deposition rate and a force of adhesion a magnitude greater than that observed for the mica substrate, while the deposition number was over three times larger.

Overall, it could be concluded that the deposition and removal profile of deformable droplet on a rigid substrate was a balance between surface charge and surface heterogeneity. The sign and magnitude of substrate surface potential was observed to dominate the long-range interactions between approaching droplets and the substrate by

increasing the rate of deposition. However, the surface topography controlled the short-range interactions by reducing the blocking effects exerted by deposited droplets on those still flowing in solution.

11.2 Further work

Development of the theory and equations used in both cells to better reflect more realistic models, applicable to the modern colloidal industry. The stagnation point deposition kinetics and the horizontal flow cell hydrodynamic forces equations are all based on a rigid sphere model which assumed both interacting surfaces were smooth, maintained a constant surface charge and a fixed droplet diameter. This systems has highlighted the fact the deformable droplet not only change their geometry on approach to the substrate as well as when the come into contact. In addition, the droplet surface charge fluctuates which also alters the interaction of the substrate with approaching droplets.

In addition the influence of substrate surface heterogeneity on droplet contact line pinning has been observed in these deposition and removal investigations as well as previously reported results[6,7] . However, it was not possible to include a surface roughness term in calculations. It would therefore be beneficial to develop a model that reflected the importance of surface asperities in colloidal-substrate interactions.

A further development of the colloidal interaction investigations would be to use lateral mode AFM, in aqueous solutions, to measure the adhesive force strength between the cross-linked droplets and the substrates. These profiles could then be compared against the hydrodynamic forces plots obtained from the flow cells and provide a more accurate

interpretation of the strength of adhesive forces present in these systems.

11.3 References

1Obey.T, Vincent.B., J.Coll.Int.Sci., 163, 454, 1994

2. Goller, Obey.T, Vincent.B, Colloids and Surfaces : A; Physicochemical & Engineering aspects, 123, 183, 1997

3. Van de Ven.T.G.M, Dabros.T, Colloidal Polymer Science, 201, 694, 1983

4. Dabros.T, van de Ven.T, Coll.Surf.A, Phys.Eng.Aspects, 75, 95, 1993

6.Das.K, Schechter.R, Sharma.M, J. Coll.Int.Sci, 164, 63, 1994

7. Soltani.M, Ahmadi.G, J.Adhesion Sci. Tech., 13, 325, 1999

8. Varennes.S, van de Ven.T, Physicochemical hydrodynamics, 10, 415, 1988

9. Yamamoto.T, Periasamy.R, Donovan, Ensor.D, J.Adhesion Sci.Tech., 8, 543, 1994

10.Fa.K, Paruchuri.V, Brown.S, Moudgil.B, Miller.J, Phys.Chem., Chem.Phys, 7, 678-684, 2005

Appendices

Additional work

A.1 Droplet-droplet interaction profiles

The theoretical pair potential was calculated for fixed 0.05(v/v) total monomer cross-linked PDMS droplets as a function of droplet surface potential with a fixed electrolyte 10^{-5} mol dm^{-3}. The height of the 1° maximum was predicted to decrease as the droplet surface zeta-potential decreased, with the lowest barrier at -10mV. This small barrier would imply that coalescence could occur in this system, due to the dominance of VDW forces over repulsive electrostatic interactions.

Figure A1.1 Potential energy profile as a function of droplet surface charge

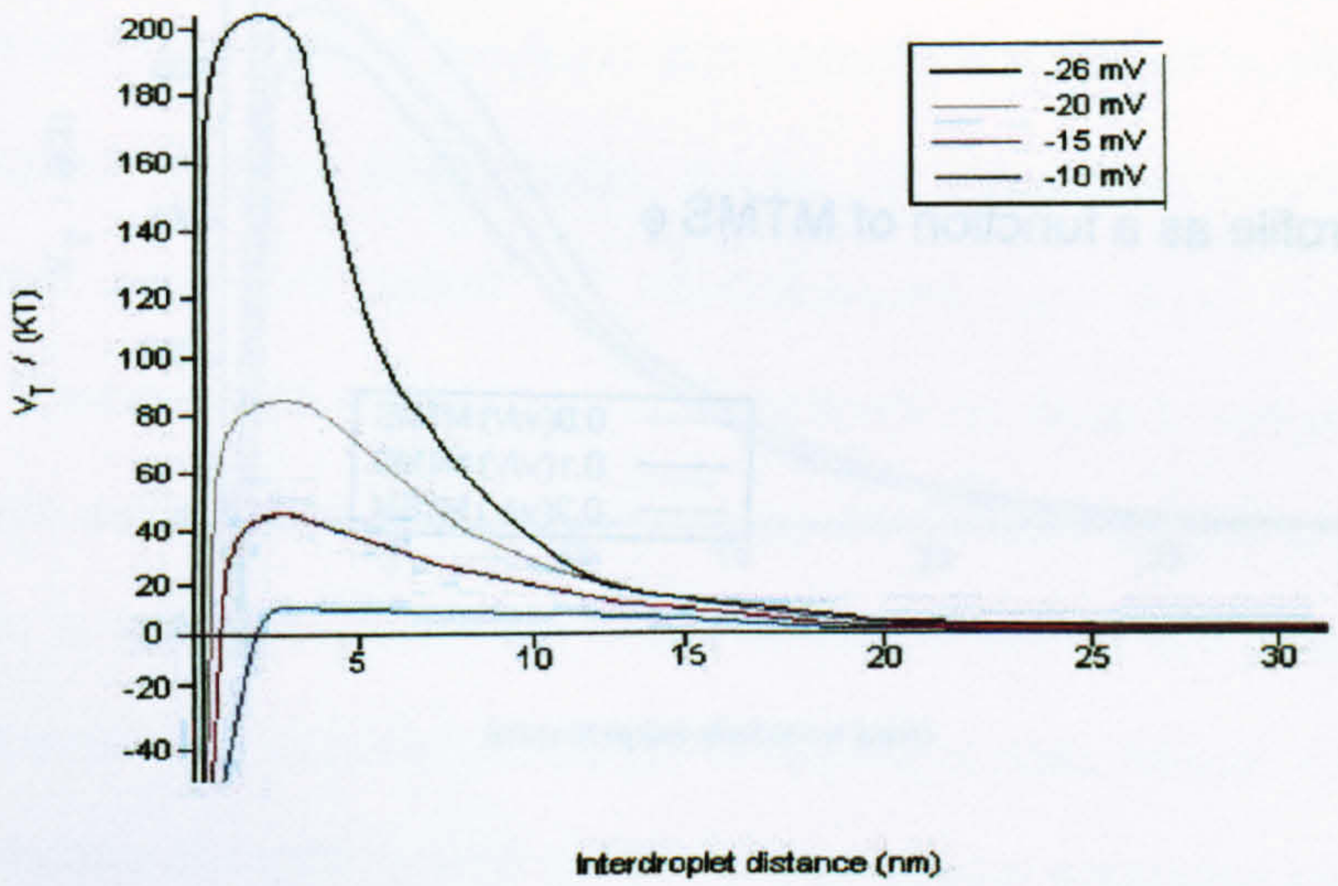

The pair potential calculations performed for the presence of electrolyte showed an overall decrease in 1° maximum and the highest energy barrier to droplet coalescence at close approach of the two PDMS droplets. This can be attributed to the screening effect of the electrolyte and subsequent EDL thickness decrease, $1/\kappa$. It could be predicted that above and below the CCC, there would be a large repulsive potential with respect to thermal energy.

Figure A1.2 Potential energy profile as a function of electrolyte concentration.

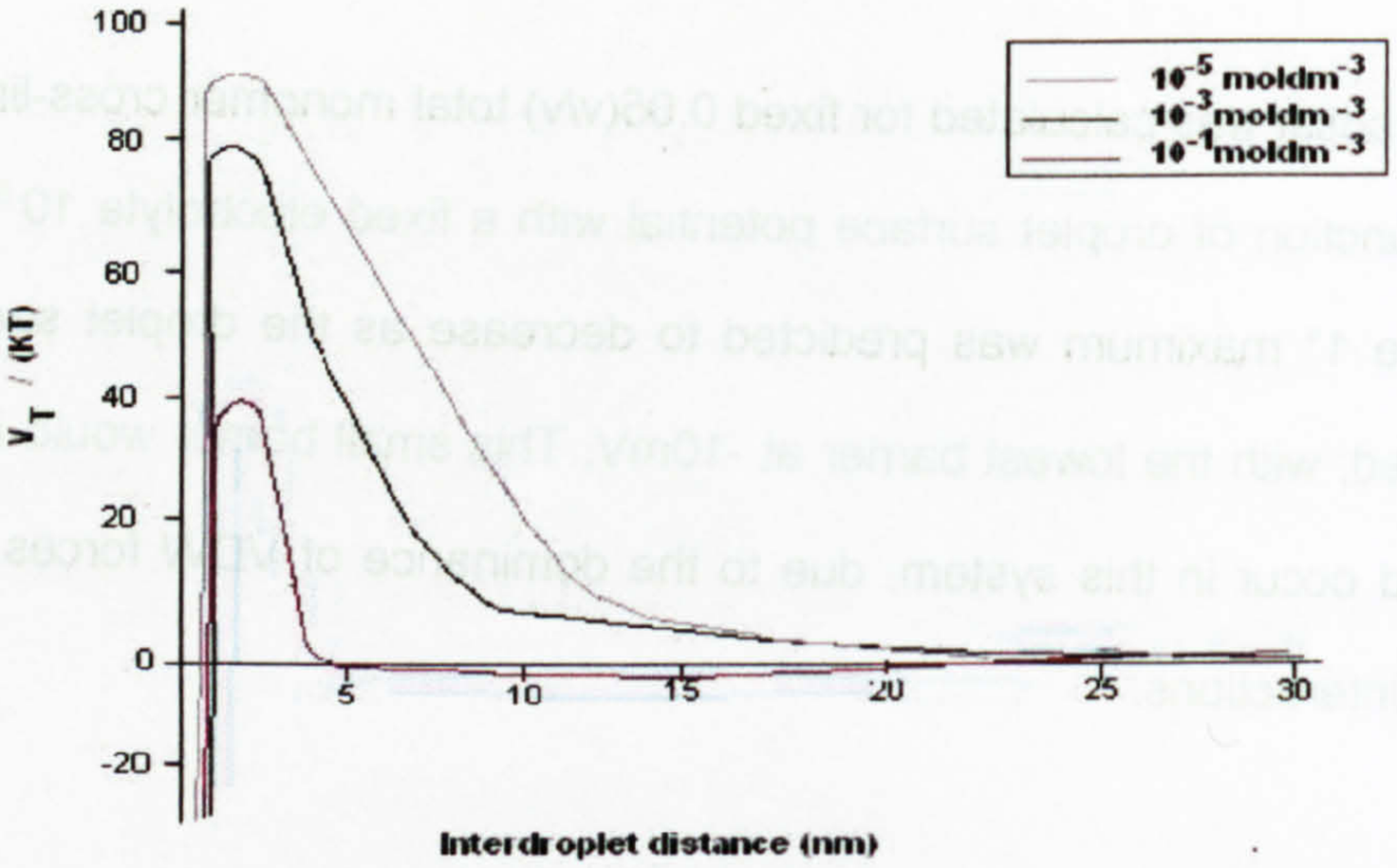

Figure A1.3 Potential energy profile as a function of MTMS ϕ

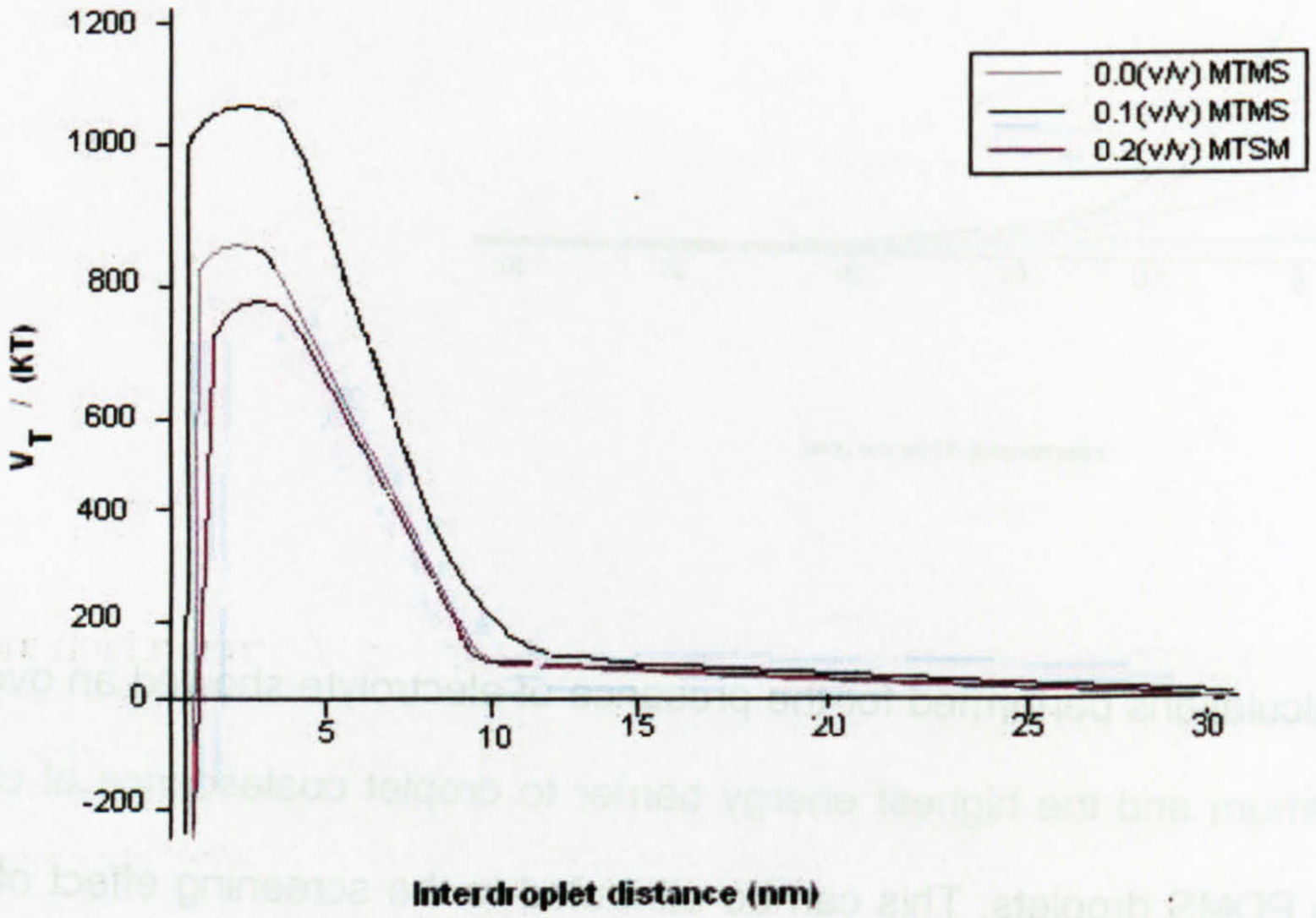

A potential energy profile was also calculated for the interaction between cross-linked PDMS droplet and a bare mica substrate, and shown in figure A1.4. It could be predicted that there was very little 1° maximum barrier height within the droplet diameter investigated. All the droplet parameters used showed a large energy barrier over a greater distance than previously calculated as a function of surface charge.

Fig A1.4 Potential energy profile as a function of cross-linked PDMS droplet radius.

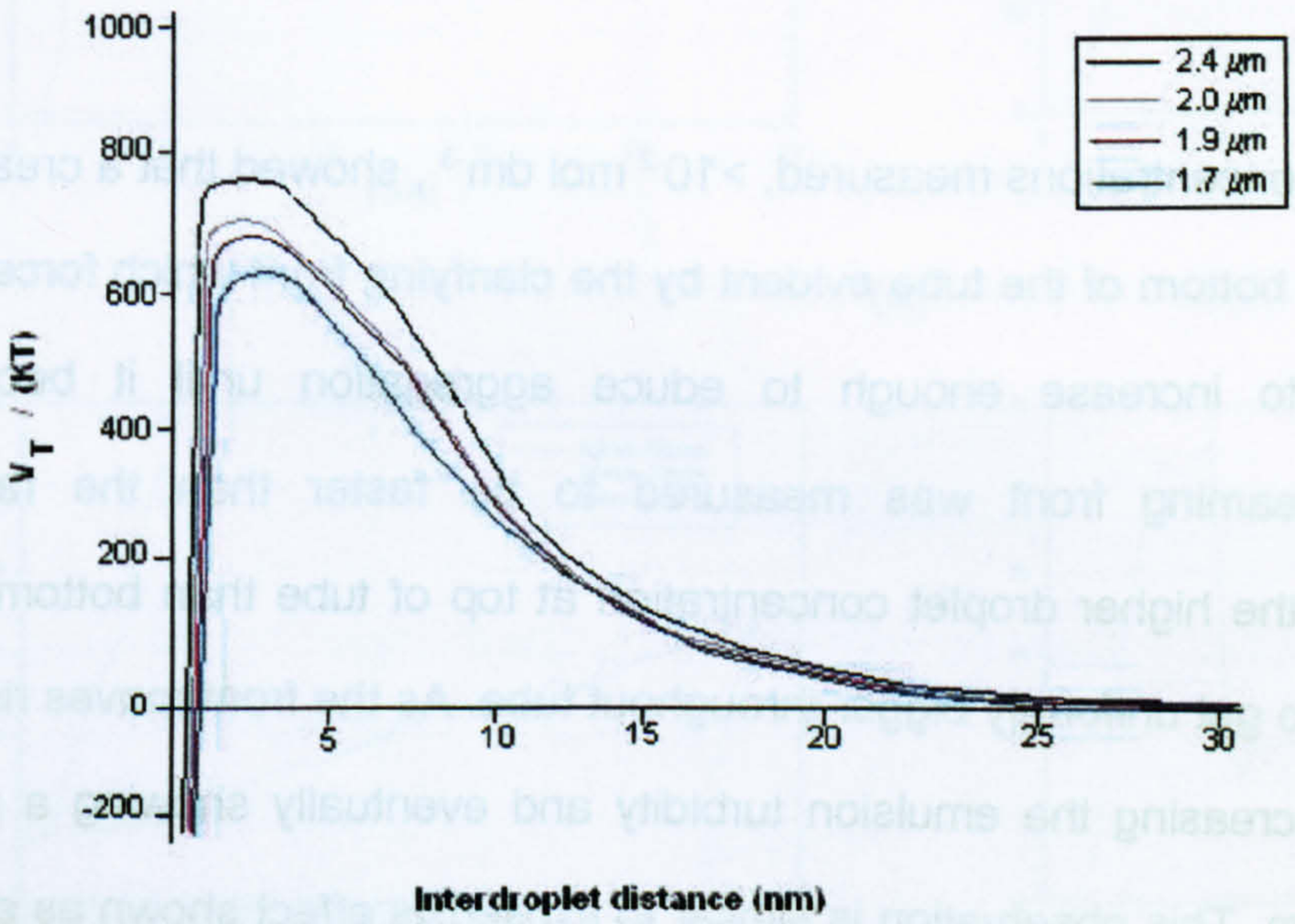

It must be noted that the above calculations do have several areas of error, which include surface potential fluctuations with varying droplet size and MTMS ϕ. The Hamaker value used in the calculations ignored any linear chain components in the PDMS oil phase and was therefore an underestimation for lower MTMS ϕ systems. In addition the presence of hydrophobic interactions were ignored

A.2 Phase stability study

The phase stability of dialysed PDMS emulsion systems, containing fixed 0.05(v/v) total monomer ϕ and fixed 0.05(v/v) MTMS ϕ was investigated in the presence of electrolyte using a Formulation Turbiscan Lab. The 40ml emulsion samples were scanned for changes in phase stability as a function of electrolyte concentration, in the range of 0 – 1 [M] NaCl. The transmission profiles, T(t), were plotted as a function of time at fixed scan heights and shown in figure A1(a-f).

The highest electrolyte concentrations measured, $>10^{-2}$ mol dm^{-3} , showed that a creaming front forms slowly at the bottom of the tube evident by the clarifying front which forces the particle concentration to increase enough to educe aggregation until it becomes homogeneous. The creaming front was measured to be faster than the rate of coalescence shown by the higher droplet concentration at top of tube than bottom, with the droplets observed to get uniformly bigger throughout tube. As the front moves rises to the top of the tube, decreasing the emulsion turbidity and eventually showing a partial clarification at the bottom. This observation is similar to synserisis effect shown as a foam drains water. As the electrolyte presence was lowered, $<10^{-3}$ M similar features occurred at slower rate. In general, at higher the salt concentrations, the creaming front occurs faster than coalescence, while lower concentrations of electrolyte, creaming still occurs but the rate decreases proportionally to decreasing salt concentration. None of the systems show distinctive phase boundaries. This could be as a result of poor refractive index difference between the dispersive and continuous phases. The additional peak observed at the top of the tube could relate to the meniscus between phases. This feature is quite unusual as the peak is observed at the same intensity in both the transmission and backscatter scans.

Fig A2.1 T(t) profiles at fixed scan heights, (a) no electrolyte, (b)10^{-1} moldm^{-3} NaCl, (c) 10^{-2} moldm^{-3} NaCl, (d) 10^{-3} moldm^{-3} NaCl, (e)10^{-4} moldm^{-3} NaCl, (f)10-5 moldm^{-3} NaCl

(a)

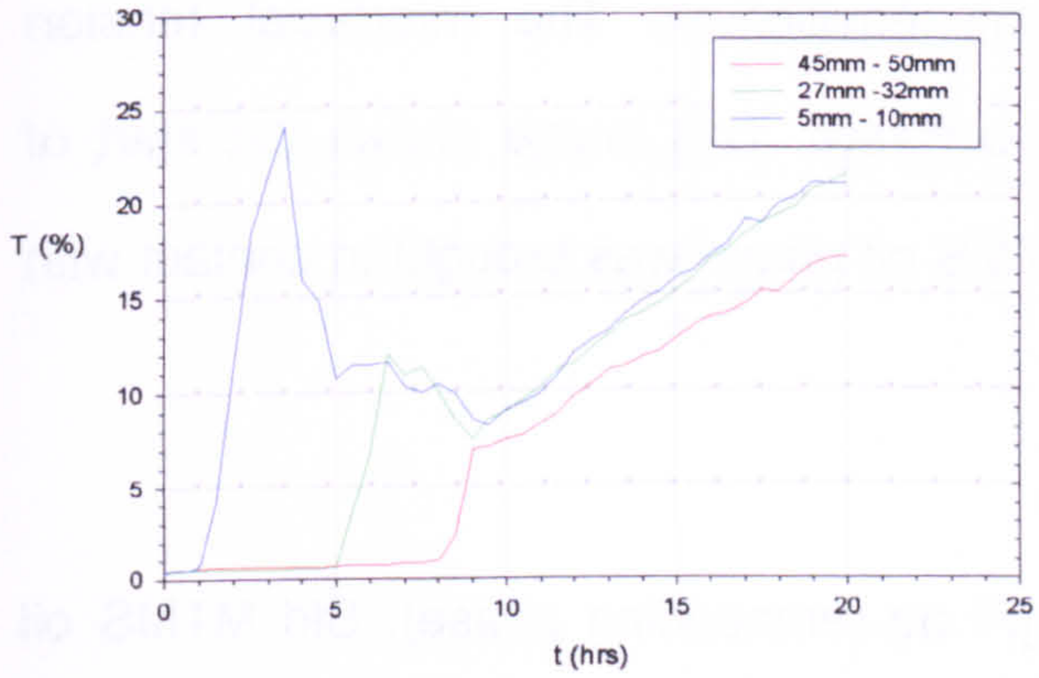

(b)

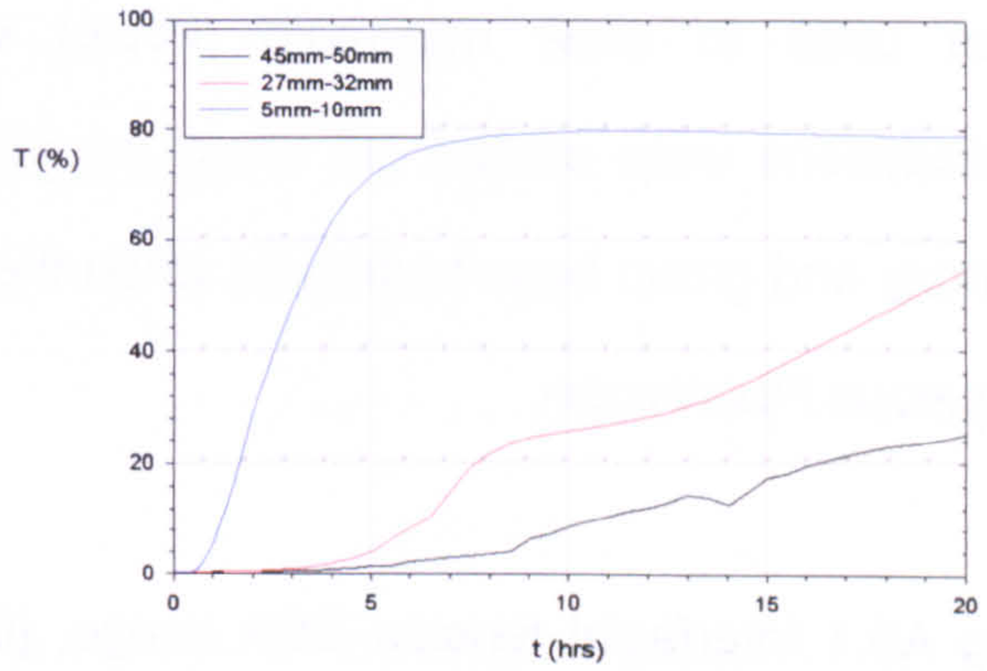

(c)

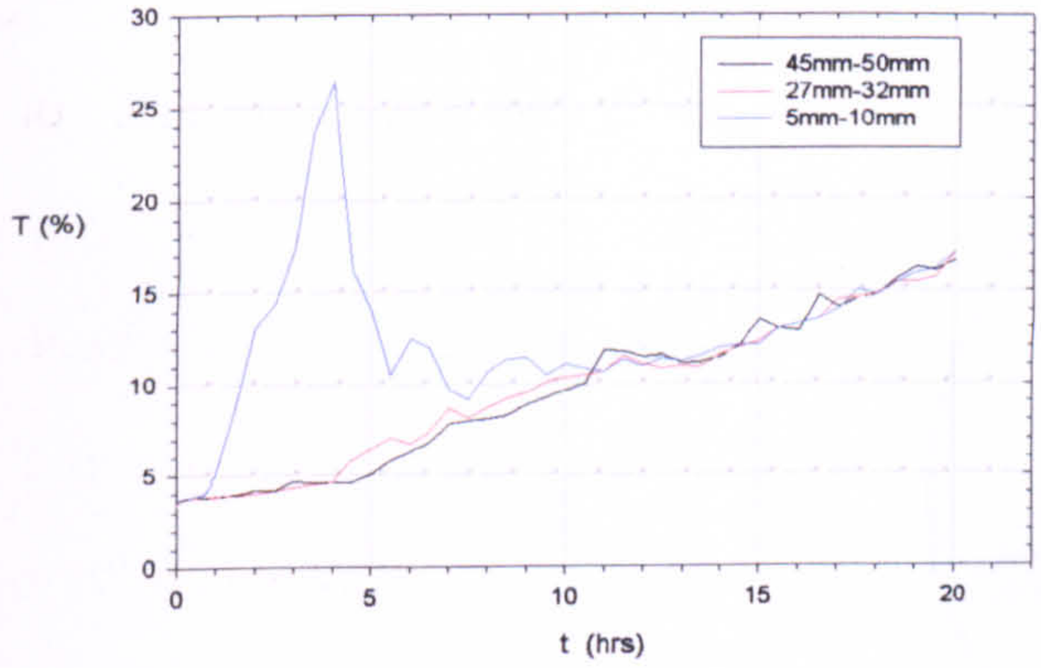

(d)

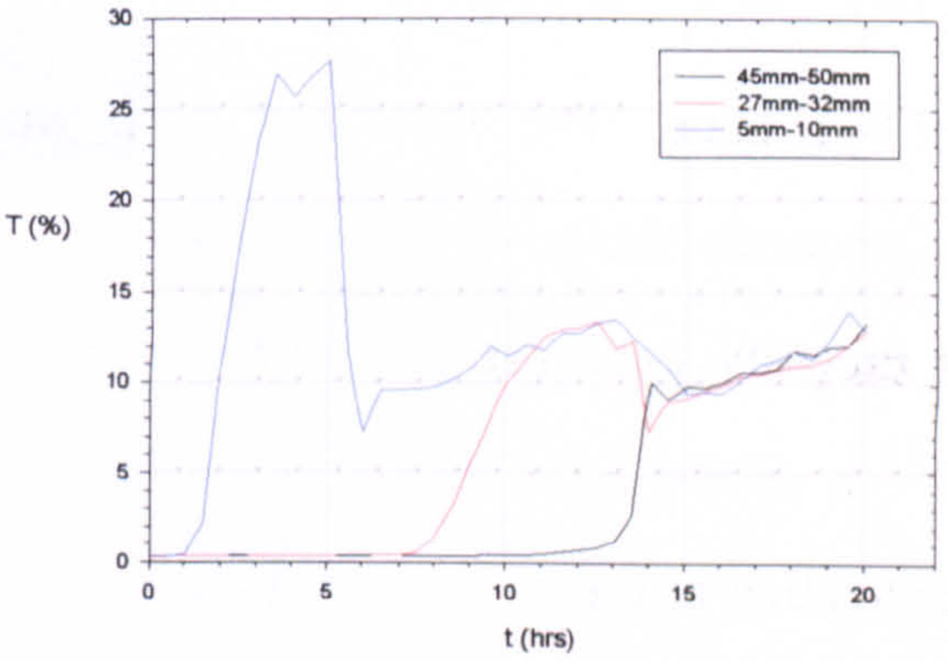

(e)

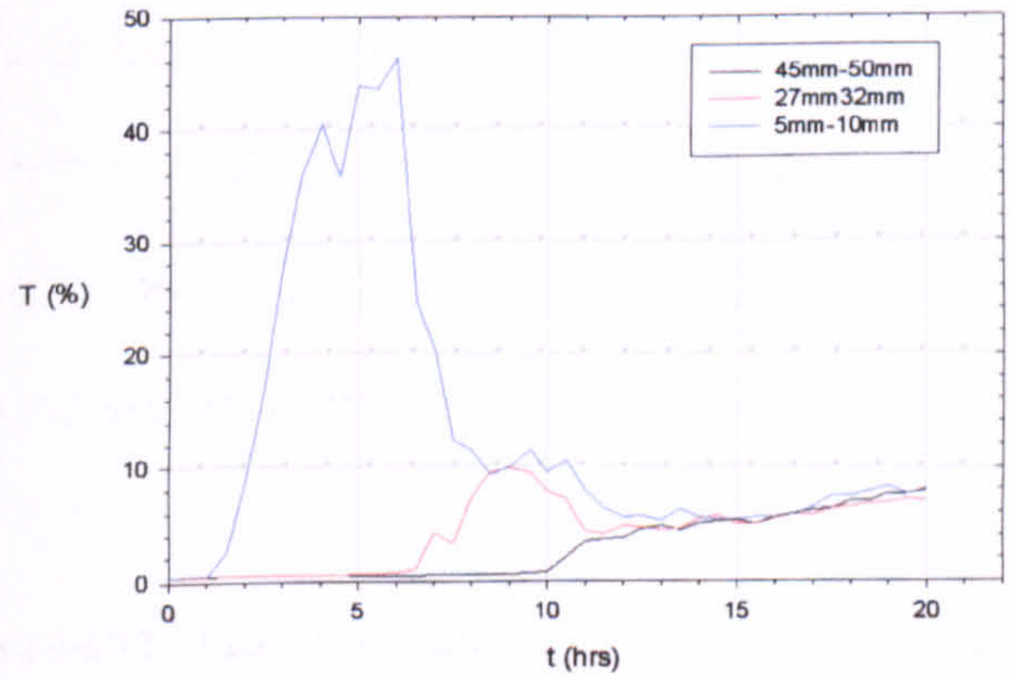

(f)

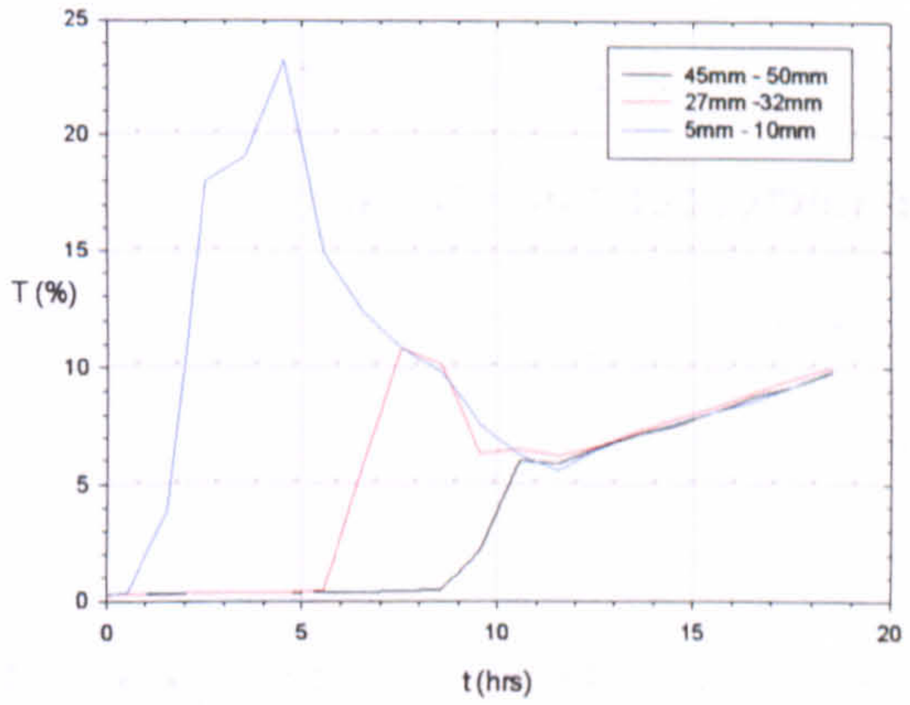

A.3 Influence of Fluorescein on O/W interfacial tension

The following images were taken by immersing a Std commercial MTMS oil 220 Mw, phase into aqueous Fluorescein of increasing concentration. A round quartz glass cuvette was used to allow maximum droplet volume equilibrium. The interfacial tension calculations were carried out using the inbuilt software. This image shows the start of ethoxy end group base hydrolysis when the MTMS oil phase was brought in contact with aqueous Fluorescein.

Fig A3.1 Interfacial tension DSA image, [0.01]Fl aq (embedding phase), Std MTMS oil (drop phase)

A.4 Substrate XPS spectra

The following XPS surface chemistry spectra were obtained from the same method described in chapter 4 and were compiled for comparison purposes.

Fig A4.1 Untreated glass surface

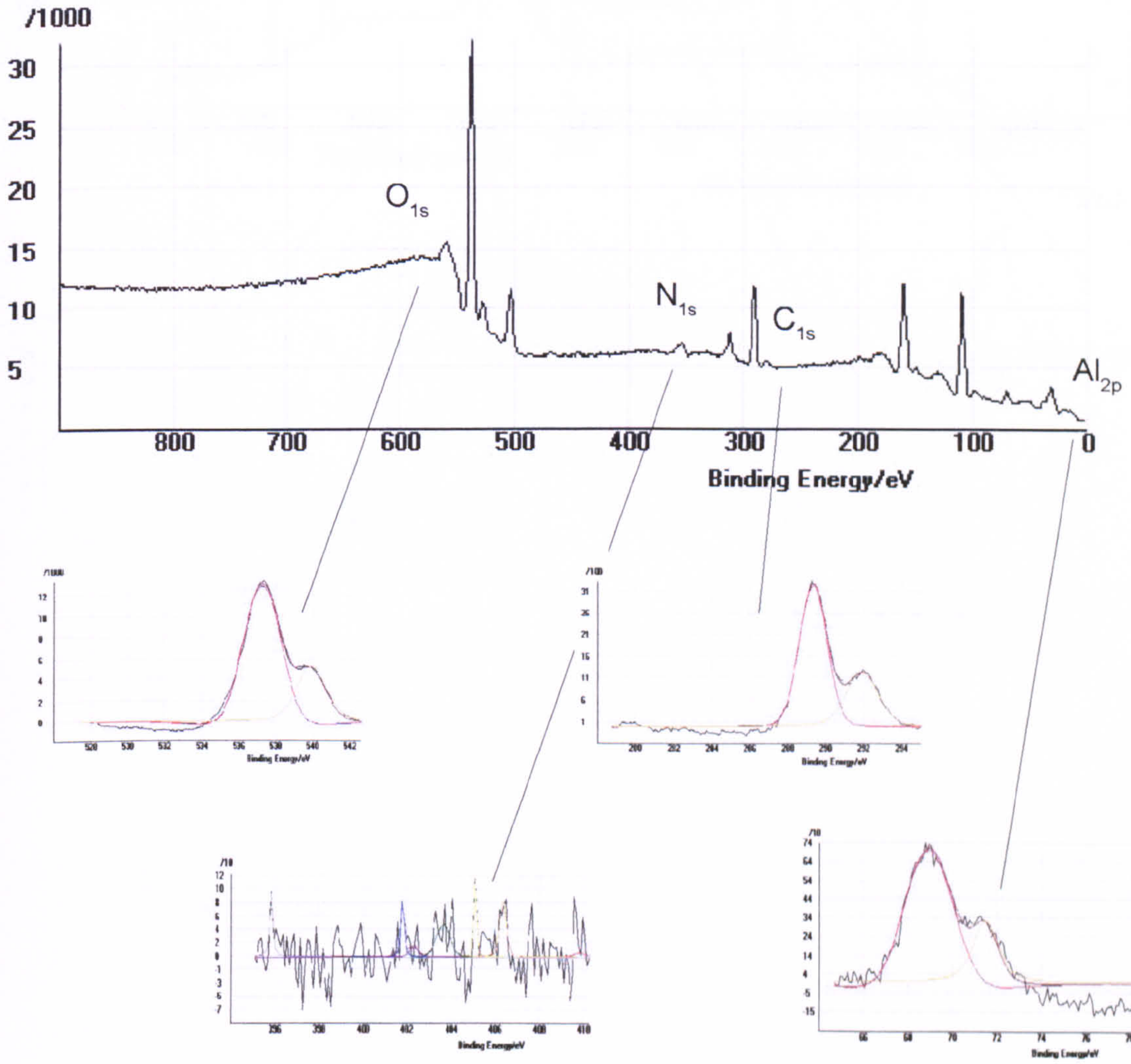

Fig A4.2 XPS spectra APTES modified glass substrate surface

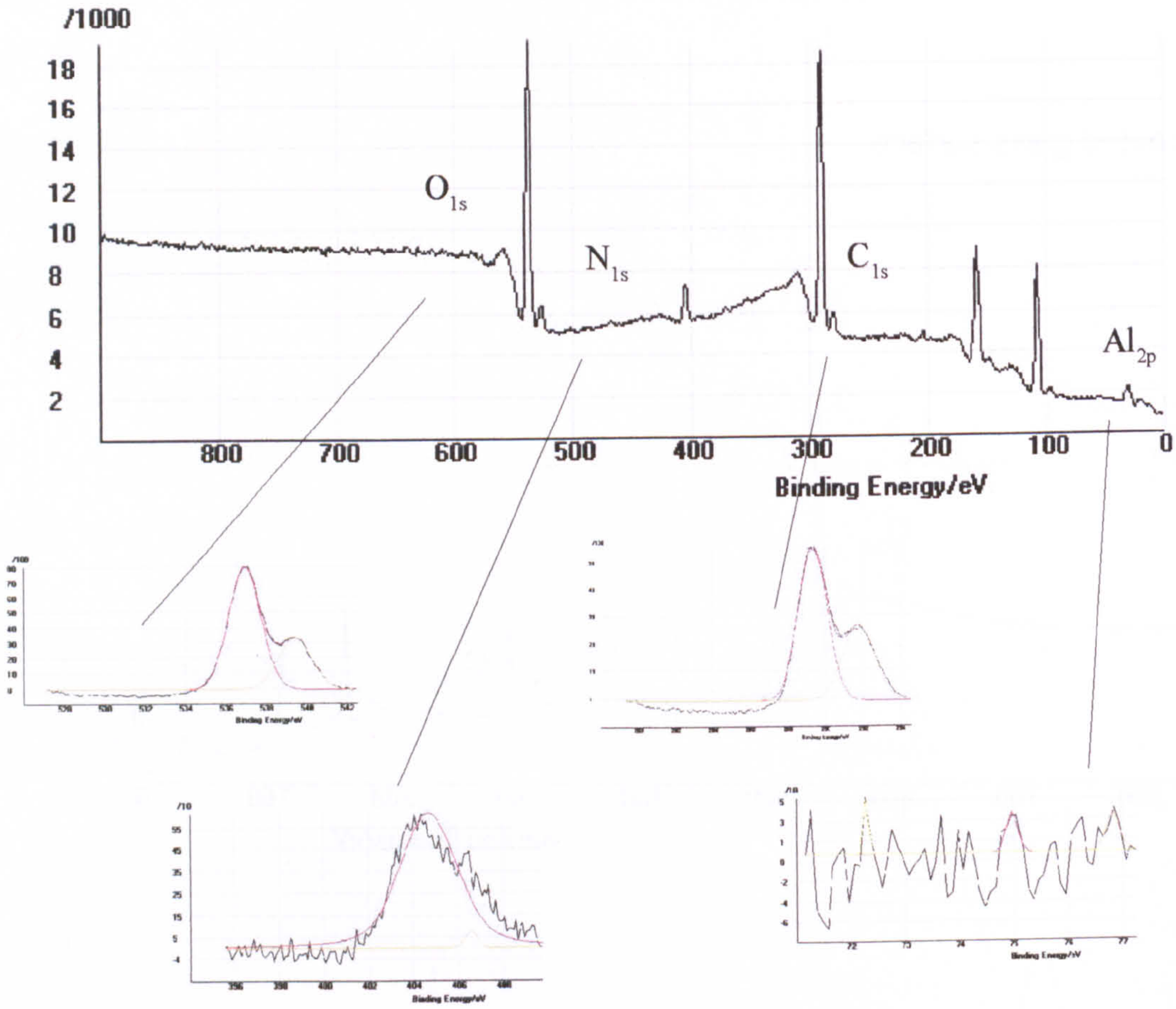

Fig A4.3 XPS spectra of Repelcote modified glass substrate surface

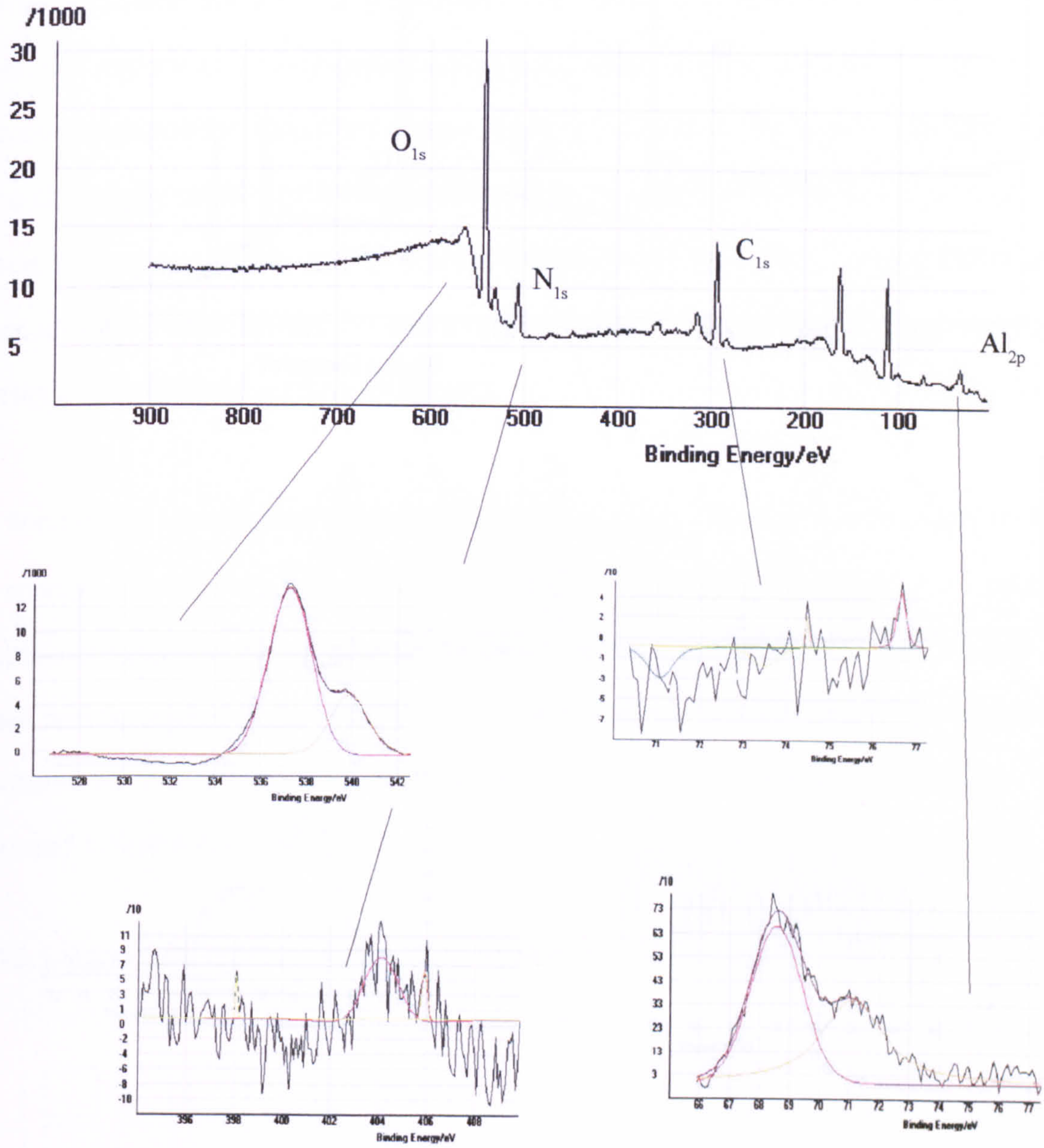

Fig A4.4 XPS spectra of L-Lysine modified glass substrate surface

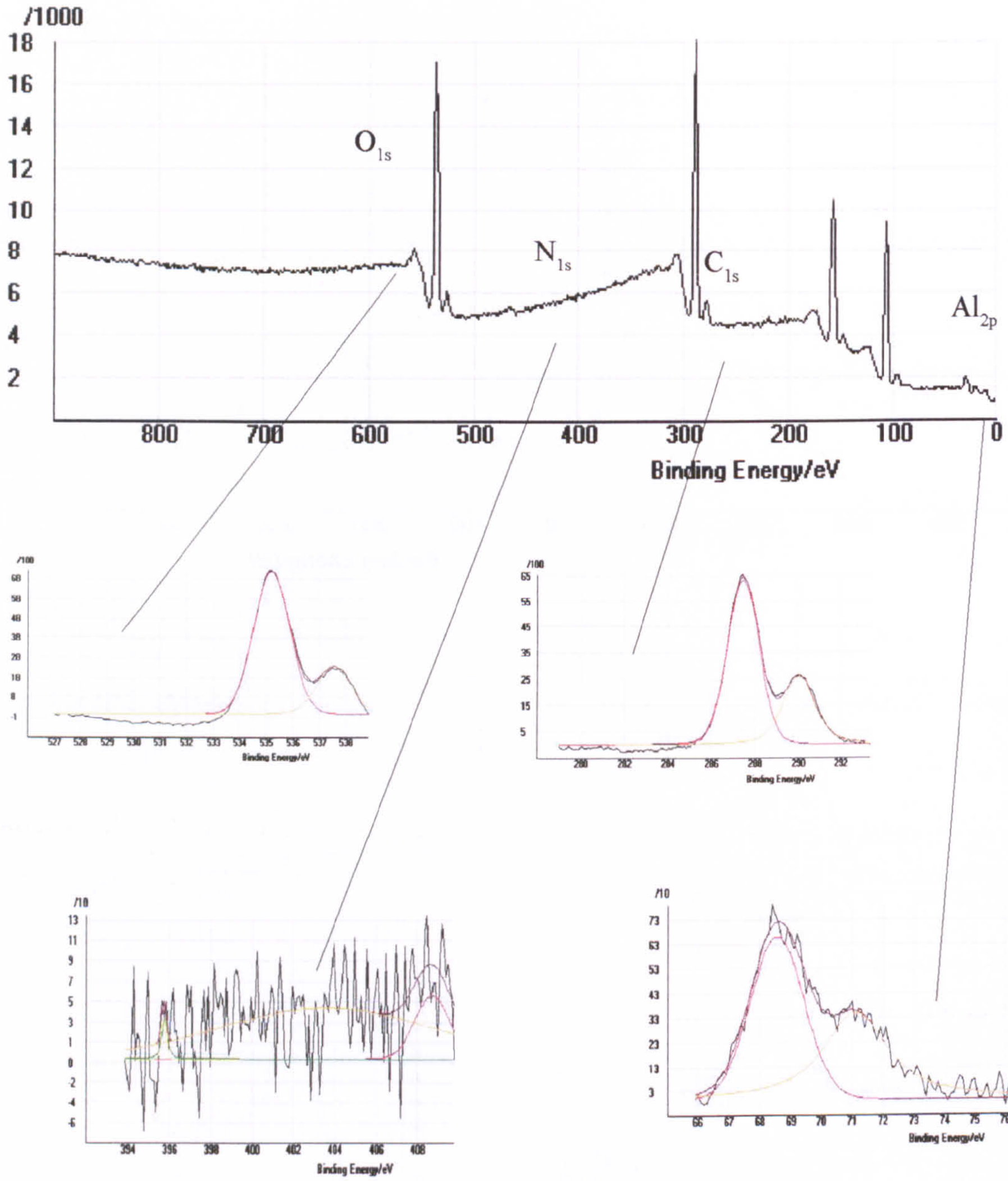

A.5 Uniform substrate surface heterogeneity

Stagnation point flow system experiments were conducted by Chen et al[1] to observe the colloidal deposition behaviour of polystyrene latex particles onto the silanised and unsilanised regions of a micro-patterned surface. These investigation was simultaneously compared to deposition data from untreated glass substrates. Those particles deposited on the chemically modified substrate appeared to form almost perfect arrays on the surface, while those on the untreated substrate deposited randomly. This behaviour was mainly attributed to the electrostatic and hydrodynamic interactions present using a fixed and regulated substrate surface roughness.

This finding was investigated by depositing a cross-linked PDMS emulsion systems, fixed total monomer 0.05(v/v) and fixed MTMS 0.05(v/v) ϕ on mica substrate with a second substrate of fixed uniform surface heterogeneity adhered to the surface. Gold coated square and hexagonal patterned TEM grids were adhered to the mica surface to provide an ordered surface homogeneity, see figure A5.1 (a-b). The deposition images are presented in figure A5.2, A5.3.

Fig A5.1 Schematic representation of (a) square grid, (b) hexagonal grid

(a)

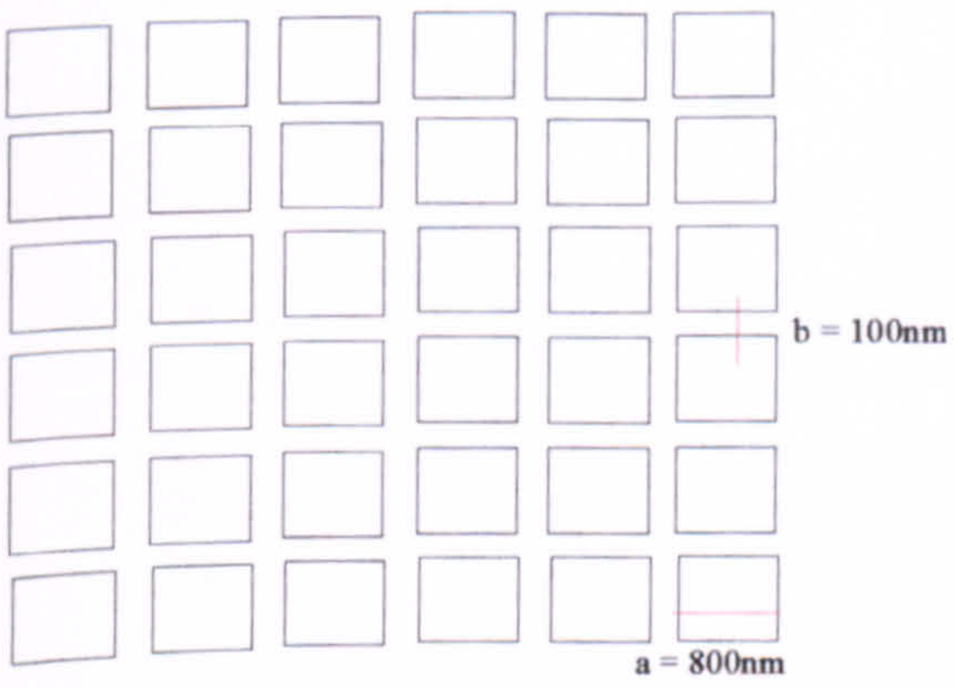

(b)

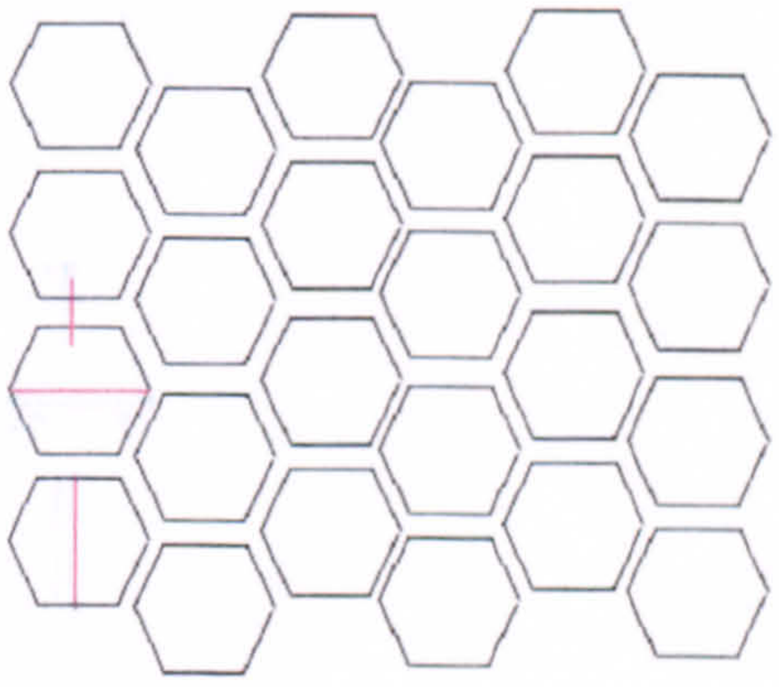

Fig A5.2 Square grid 0.05(v/v)MTMS (a)3mins, (b)60mins, (c)120mins, (d)180mins

(a)

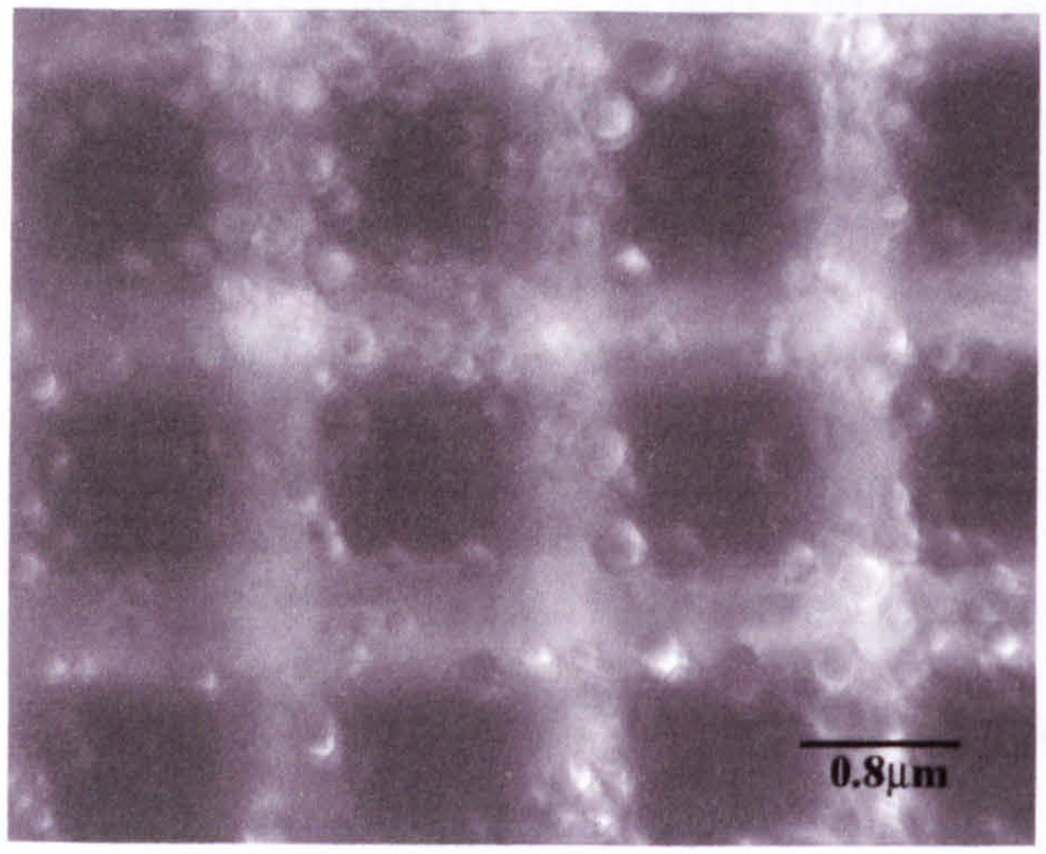

(b)

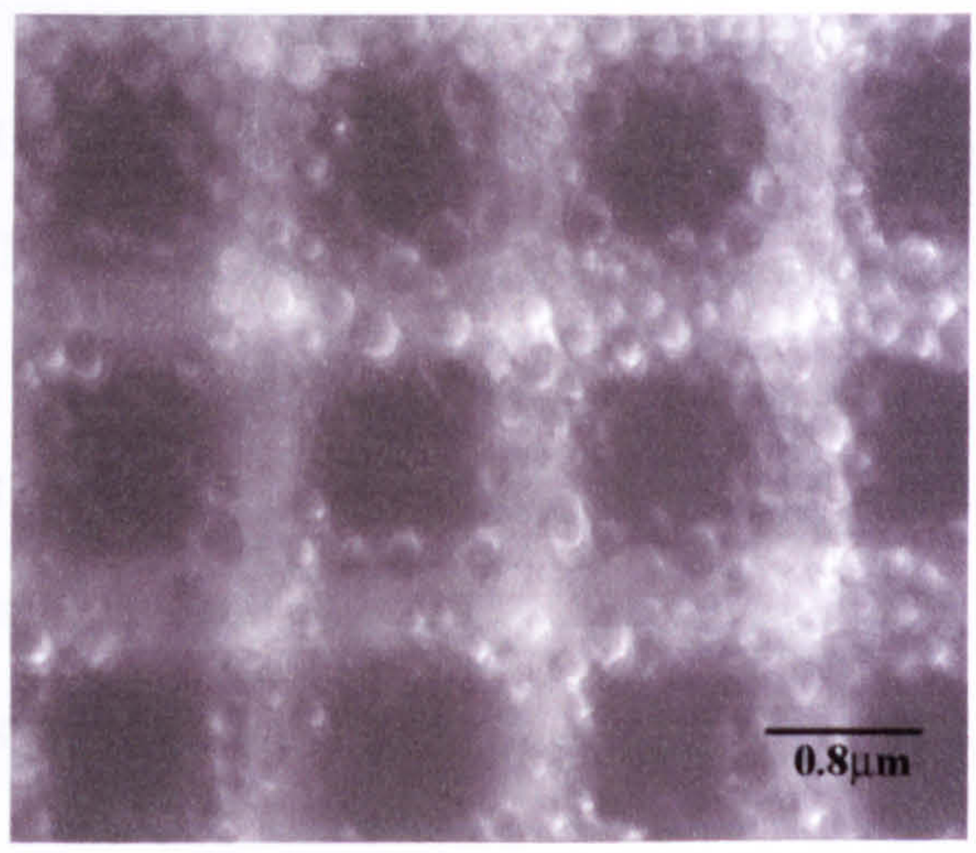

(c)

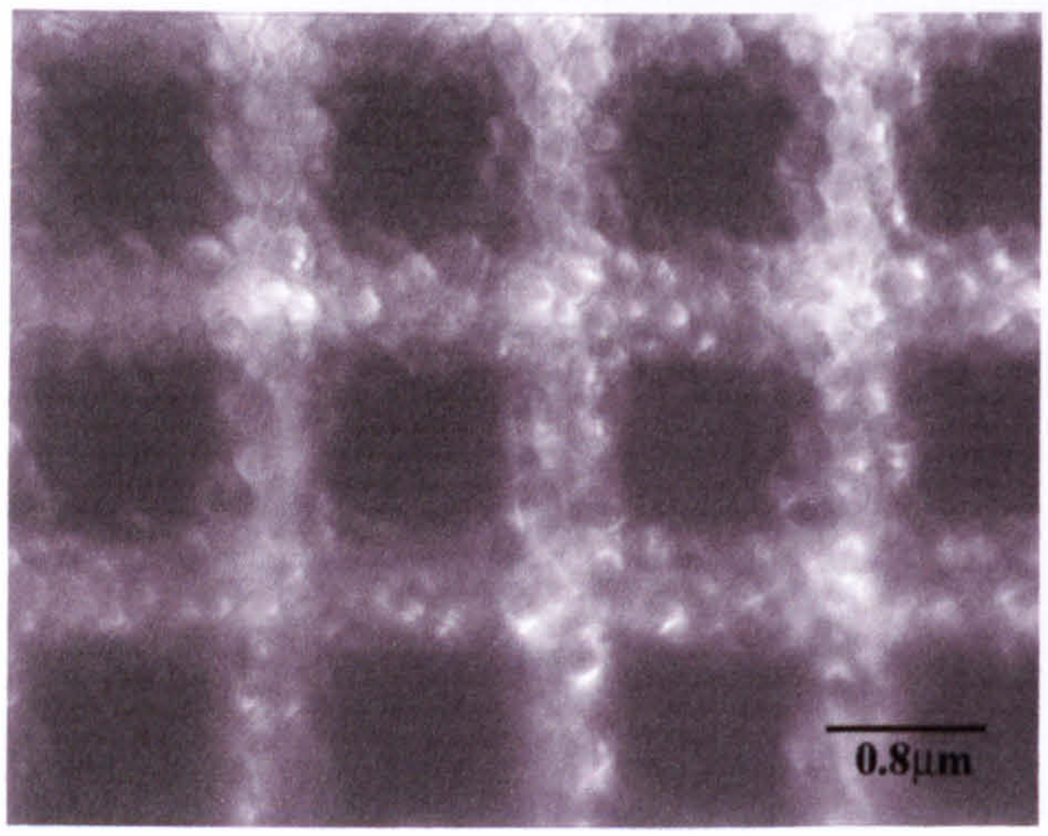

(d)

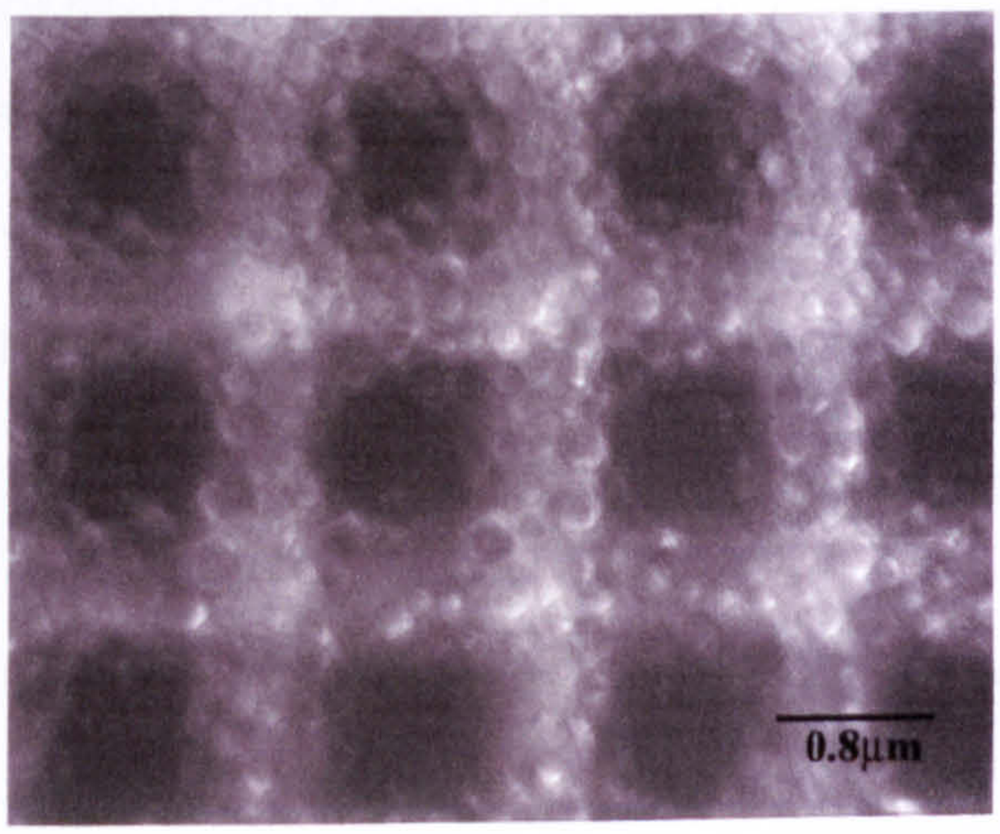

Fig A5.3 Hexagonal grid 0.05(v/v)MTMS (a)3mins, (b)60mins, (c)120mins, (d)180mins

(a)

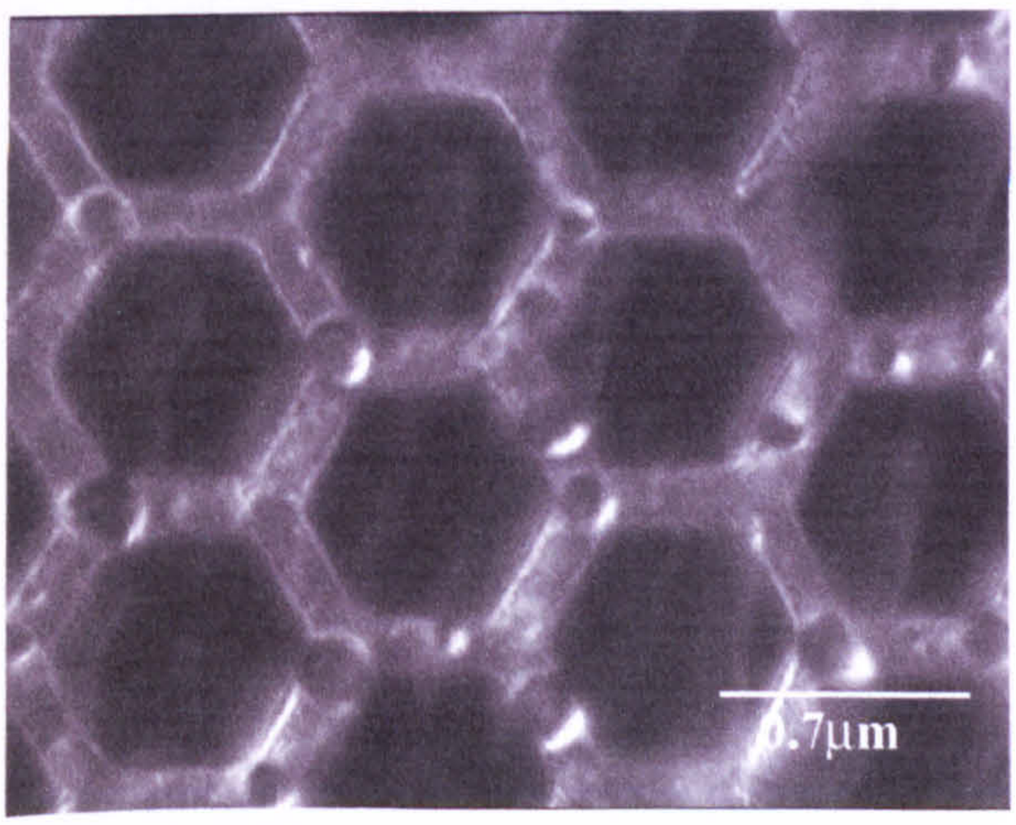

(b)

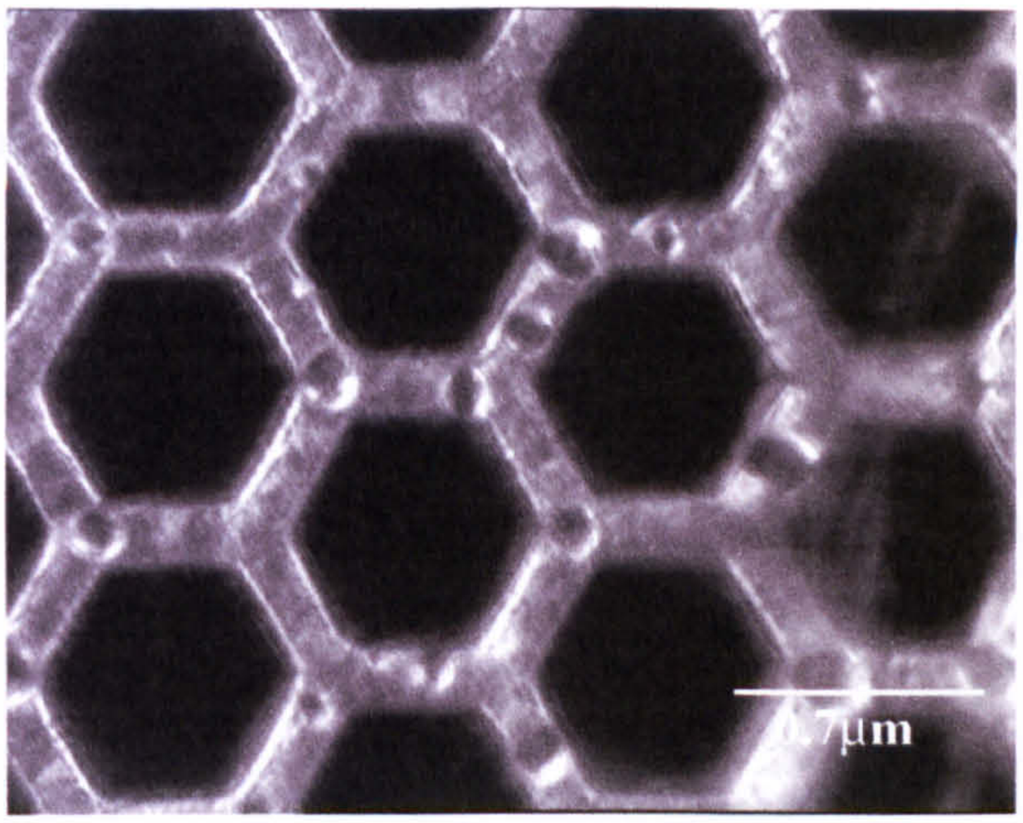

(c)

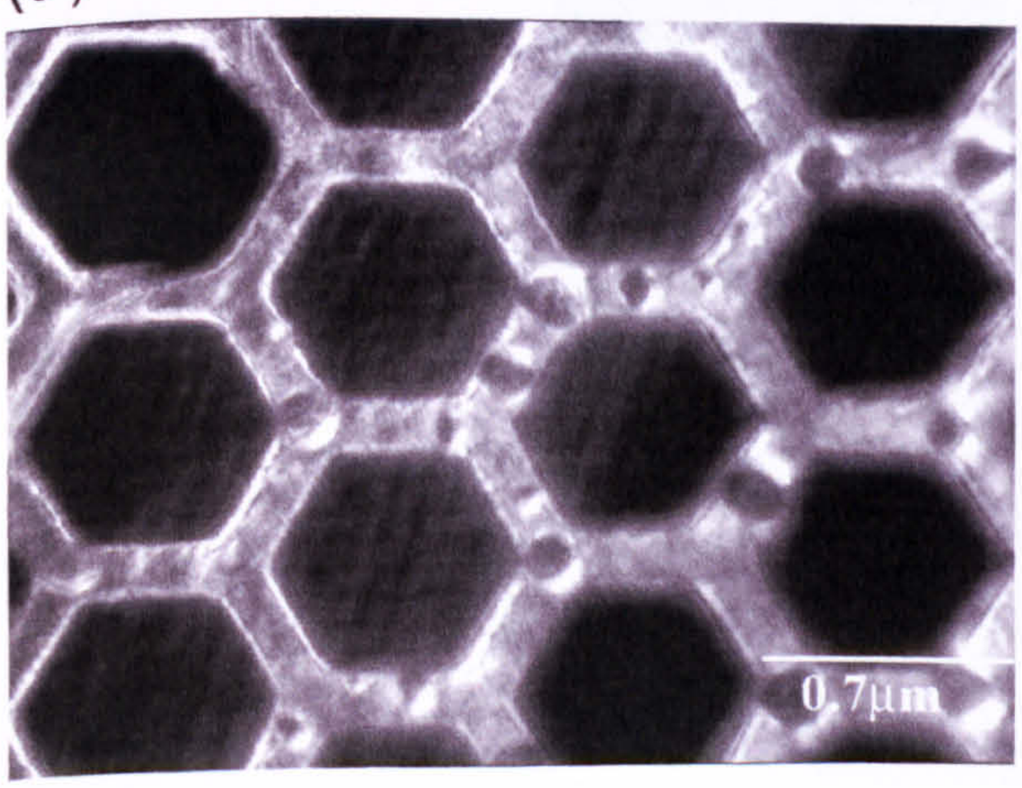

(d)

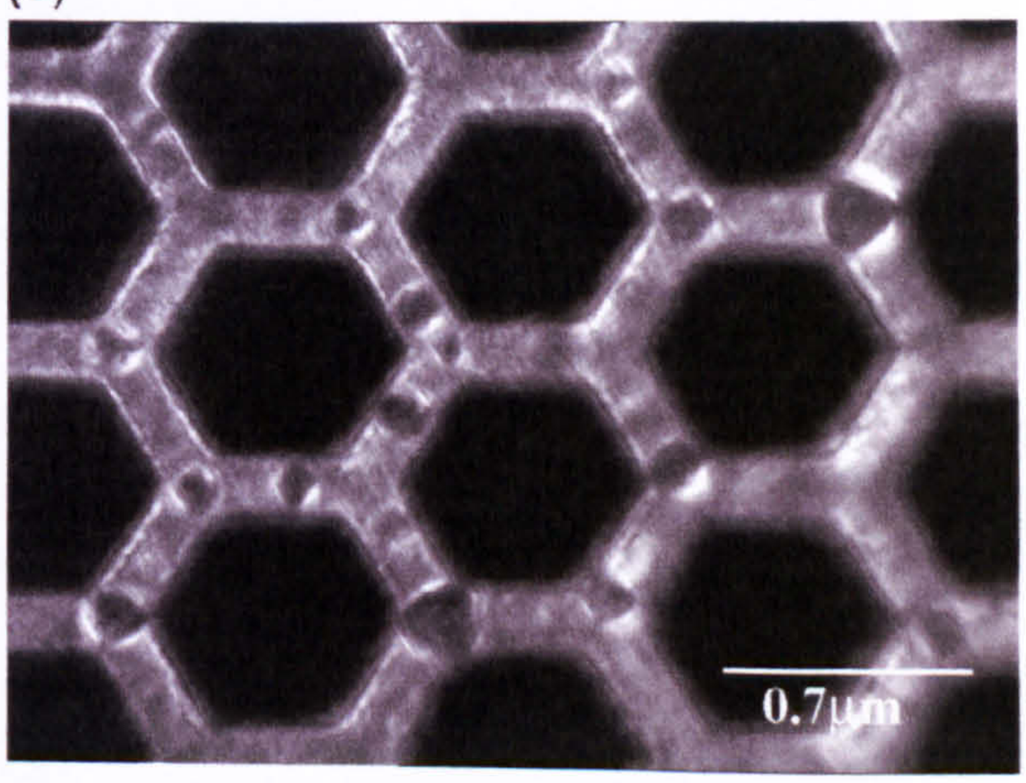

A.6 Deposition on Human epidermis

Deposition of cross-linked PDMS droplets, fixed 0.05(v/v) and fixed 0.05(v/v) MTMS was carried out on a sterile section of human epidermis. SEM was used to obtain a detailed understanding of the substrate topography, as shown in figure A7.1. The stagnation point deposition images obtained from the experimental procedure is also included, figure A7.2.

Figure A6.1 SEM image of human epidermis

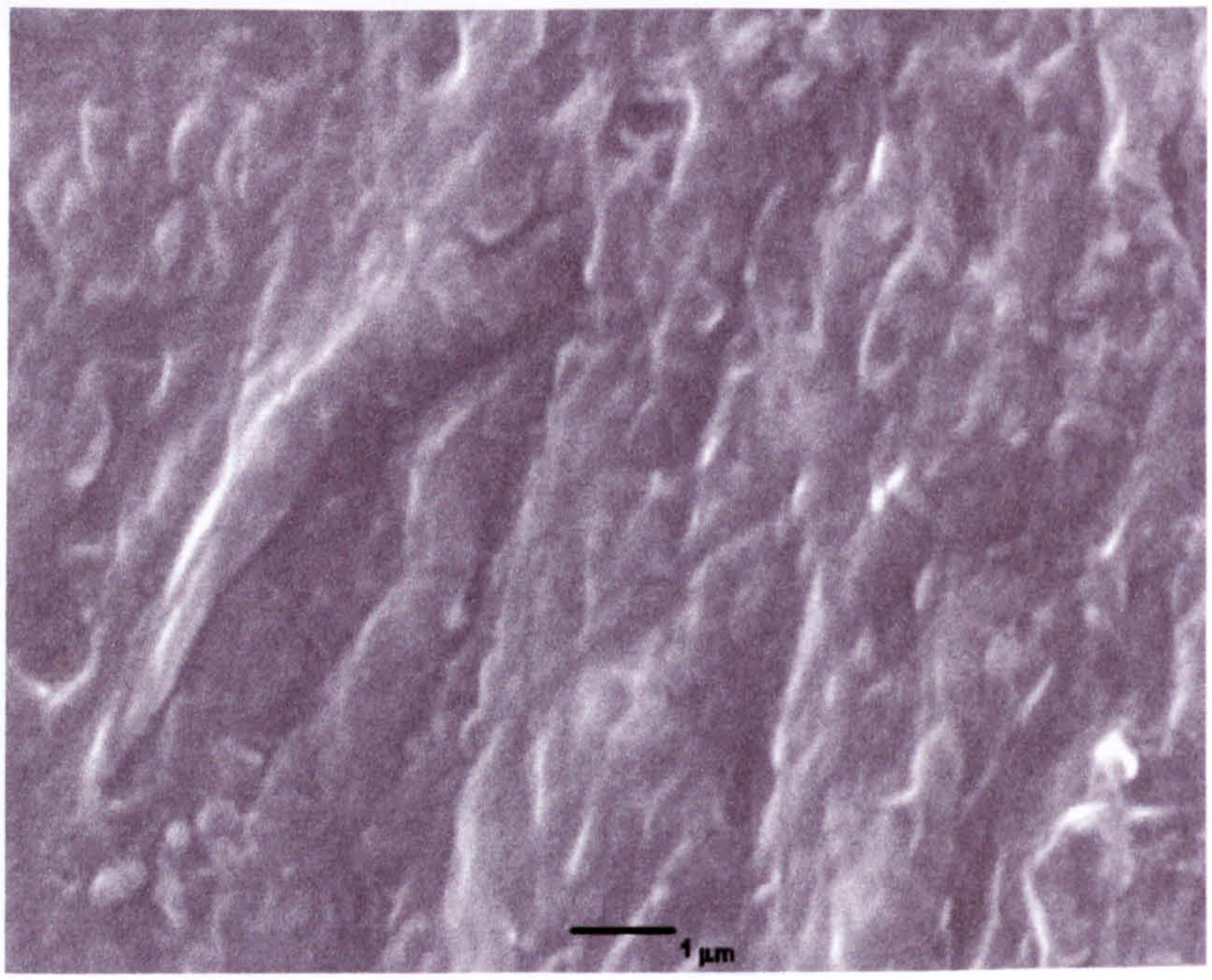

Figure A6.2 Deposition images on human epidermis, (a) initial deposition, (b) 60 mins, (c) 120 mins, (d) 180 mins

(a)

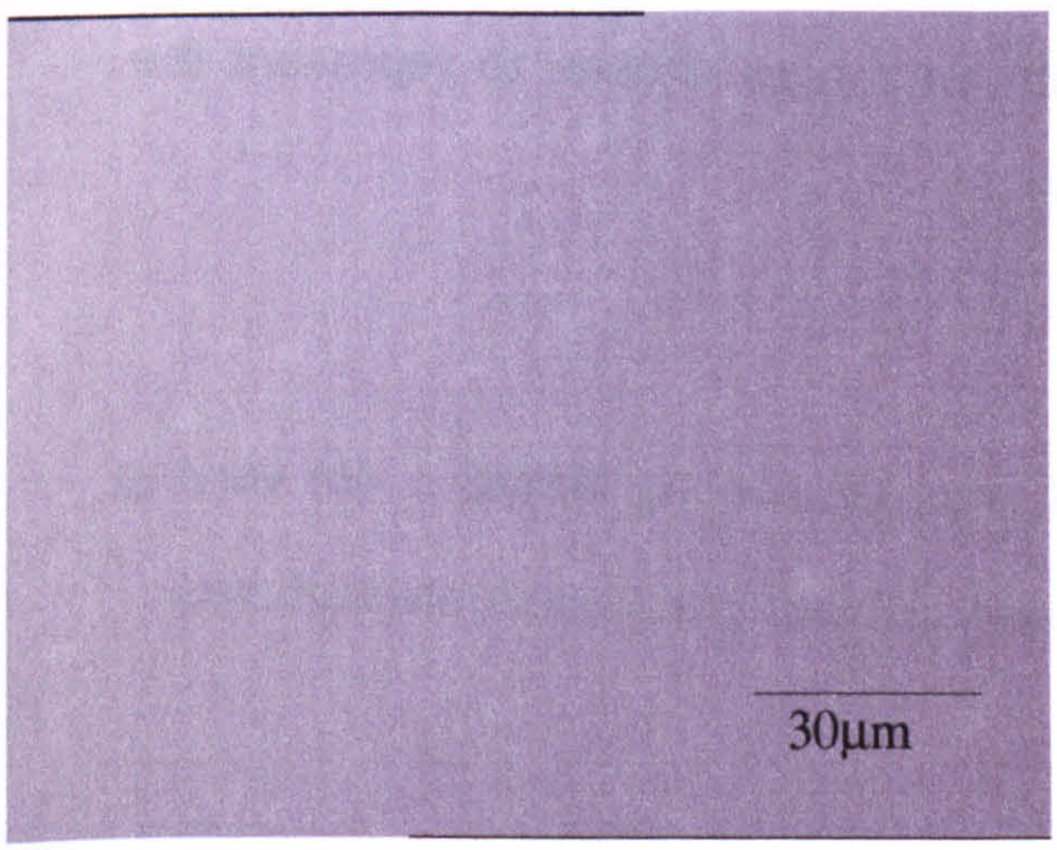

(b)

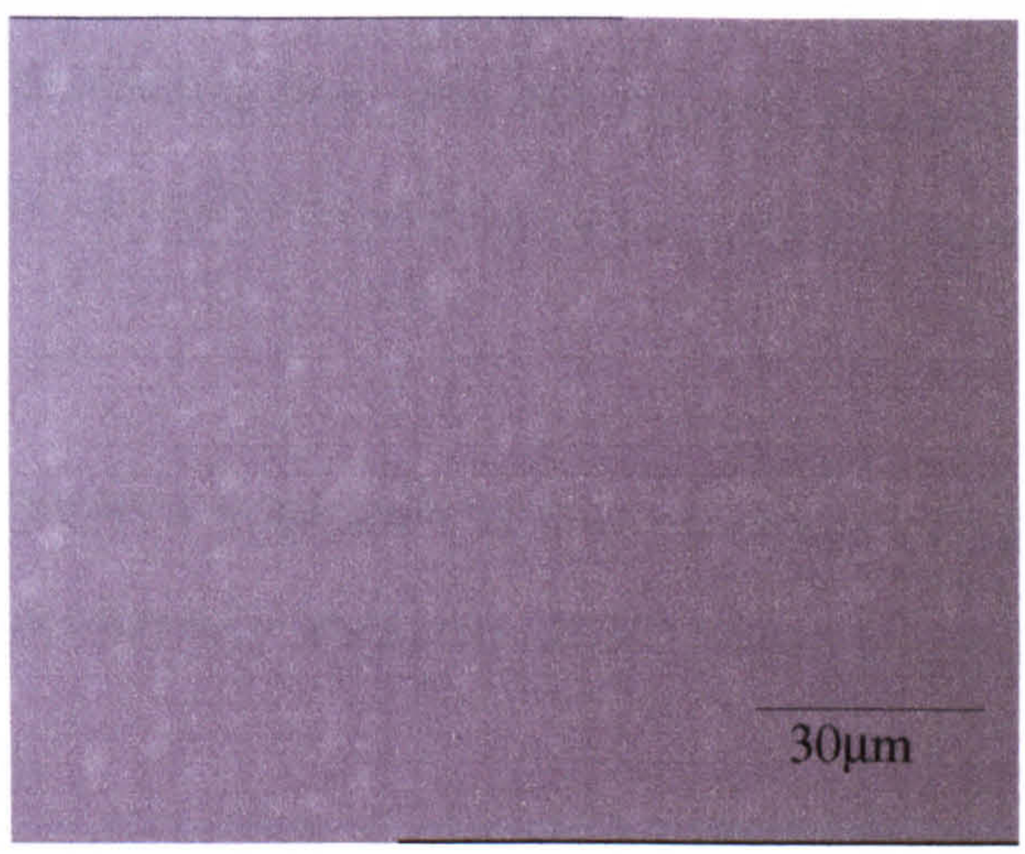

(c)

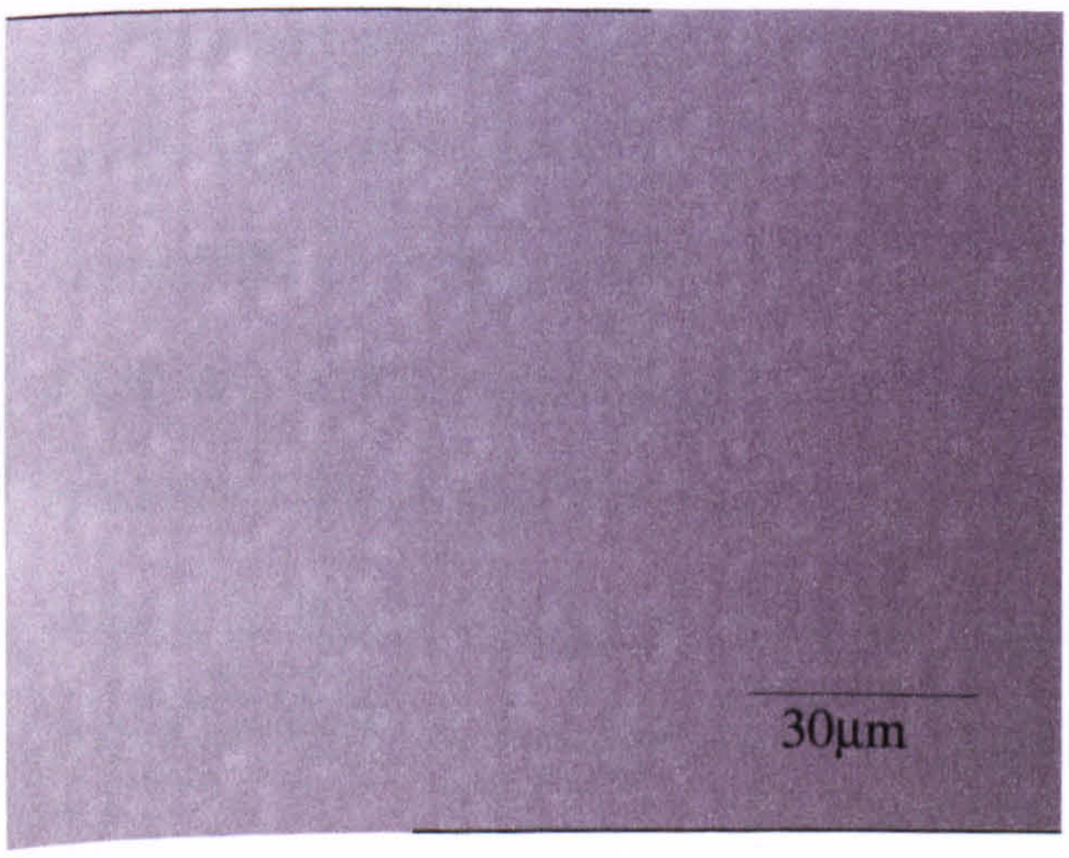

(d)

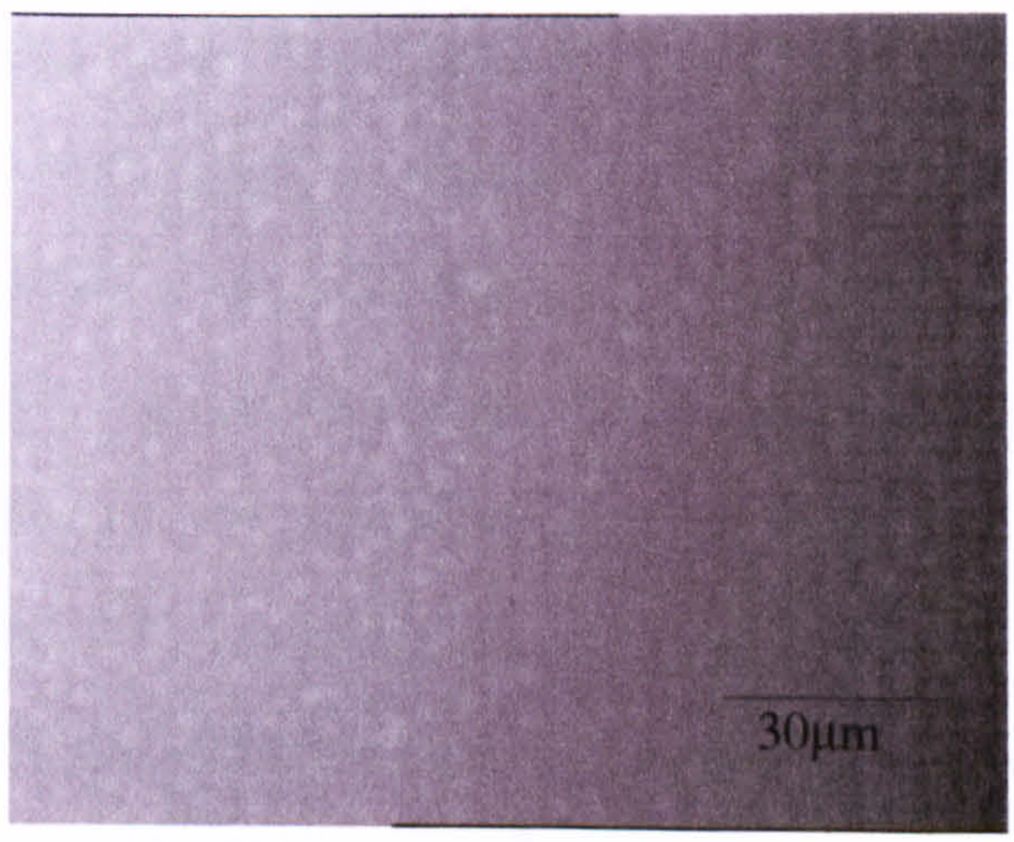

A.7 Stagnation point flow deposition rate profiles

The S and θ data obtained from deposition experiments was used in the first order rate equation to calculate the k_d values for each system investigated. A calculated line of best fit was made through the data and presented with error bars chosen to represent the distribution of the data obtained in the figures A7.1(a-d).

Fig A7.1 Deposition rate profiles as a function of time, (a) varying MTMS ϕ, (b) varying [NaCl], (c) varying [SDS], (d) glass substrate surfaces, (e) non-glass substrate surfaces.

(a)

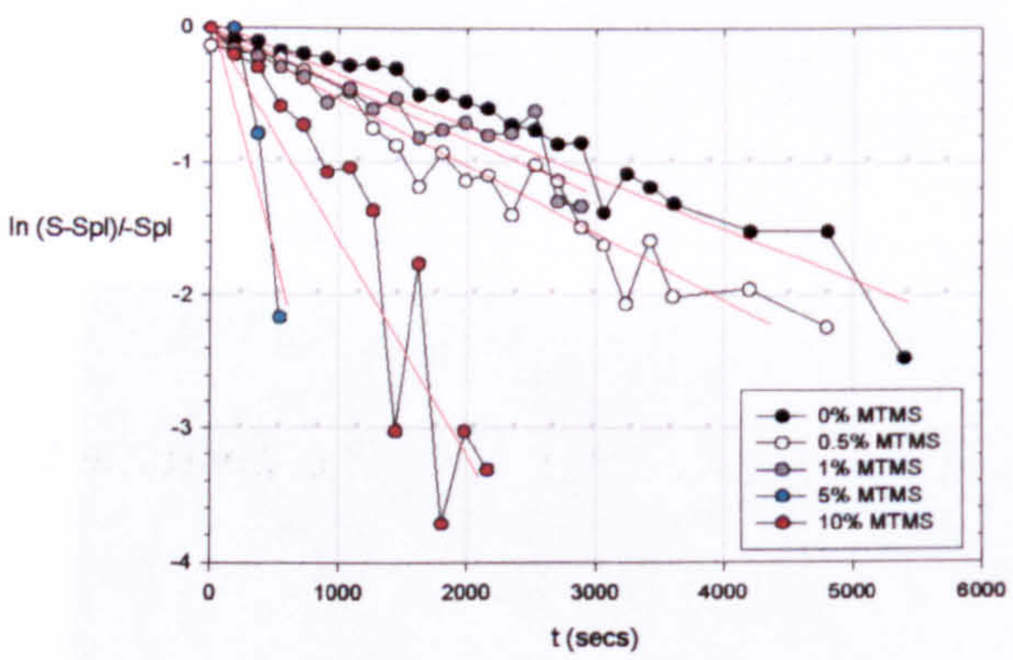

(b)

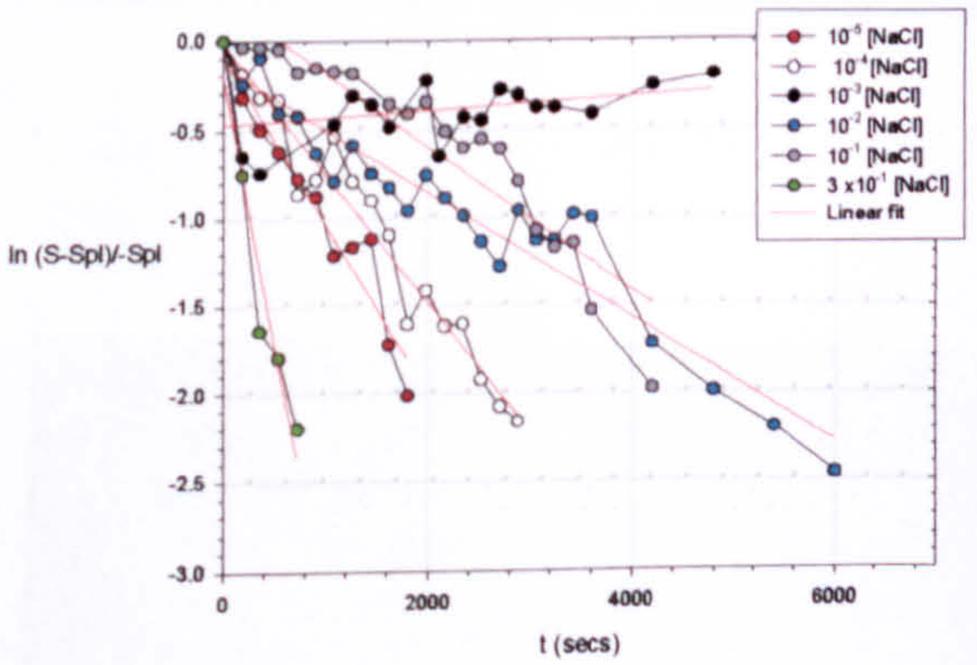

(c)

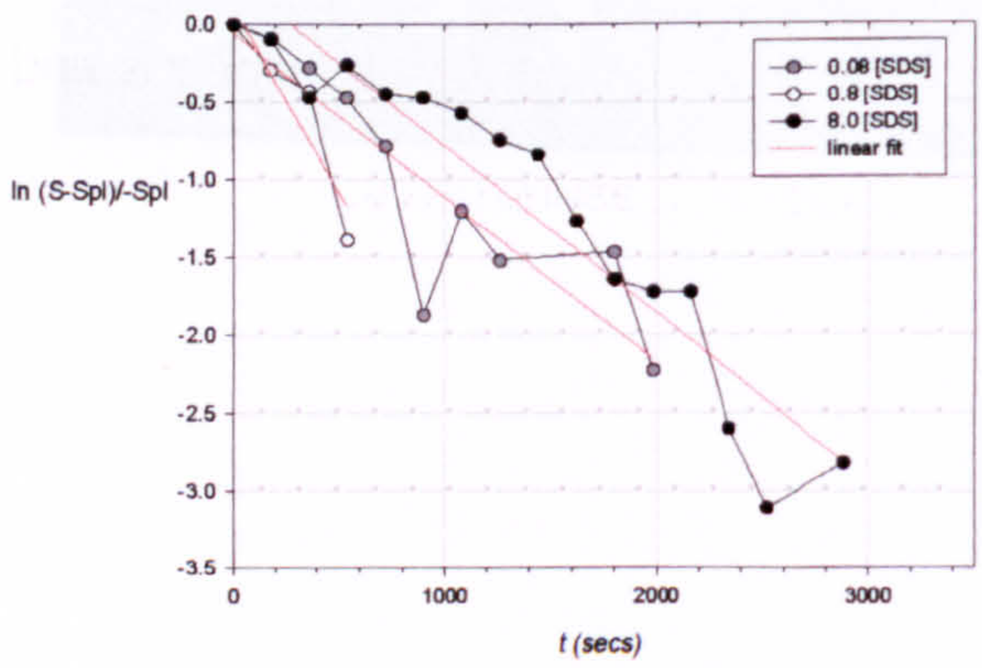

(d)

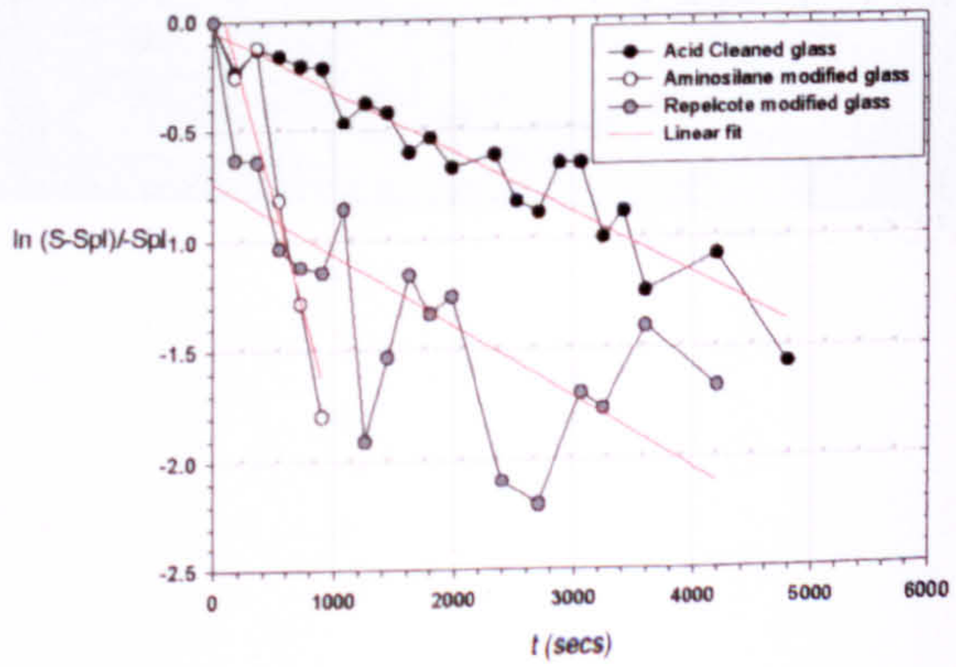

(e)

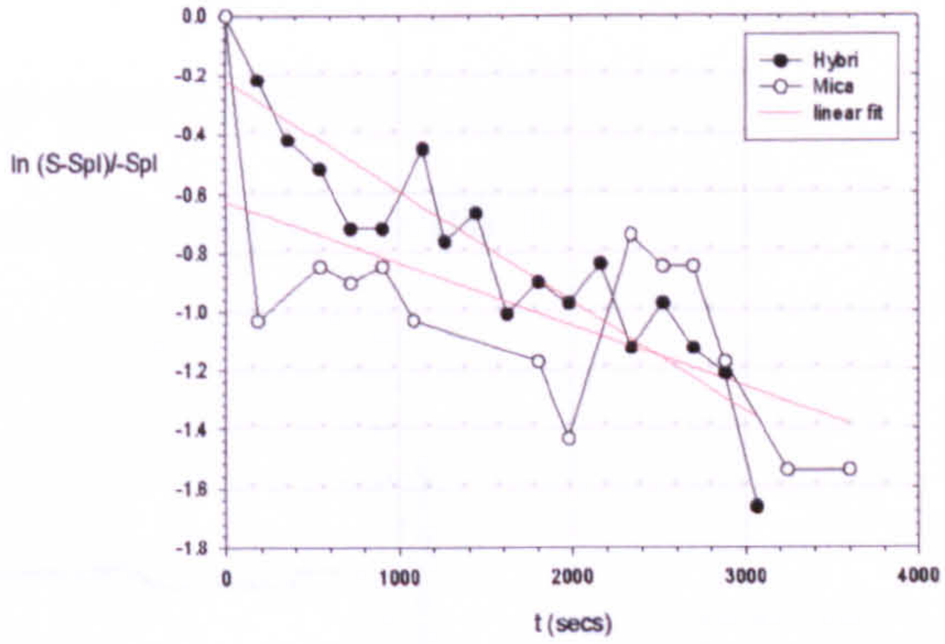

A.8 Deposition thickness; Reflectometry

A Reflectometer was used to measure the build up of PDMS droplets on a flat substrate under Brownian motion, at Unilevers' Port Sunlight research center, UK. The instrument comprised of a stagnation point flow cell in which a dialysed emulsion of fixed 0.05(v/v) total monomer, was introduced and a fixed wavelength laser was simultaneously measured the deposition thickness, (Ellipsometry). The resultant deposition profiles are shown in figure A4(a-c) as a function of time, with increasing tri-functional cross-linker present. However, due to the similarity between the refractive index of the continuous and discontinuous phases, it was not possible to obtain accurate measurements.

Fig A8.1 Deposition profiles as a function of time, (a) 0.05(v/v) MTMS, (b) 0.1(v/v) MTMS, (c) 0.2(v/v) MTMS

(a)

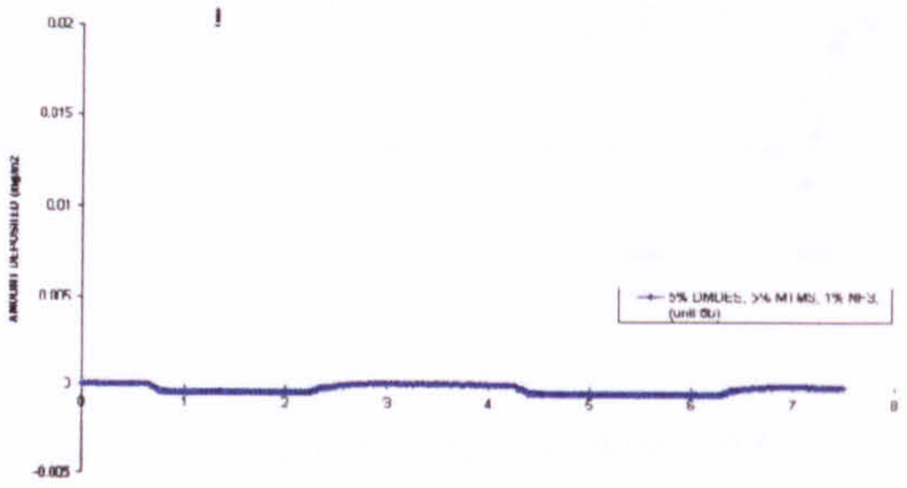

Time

(b)

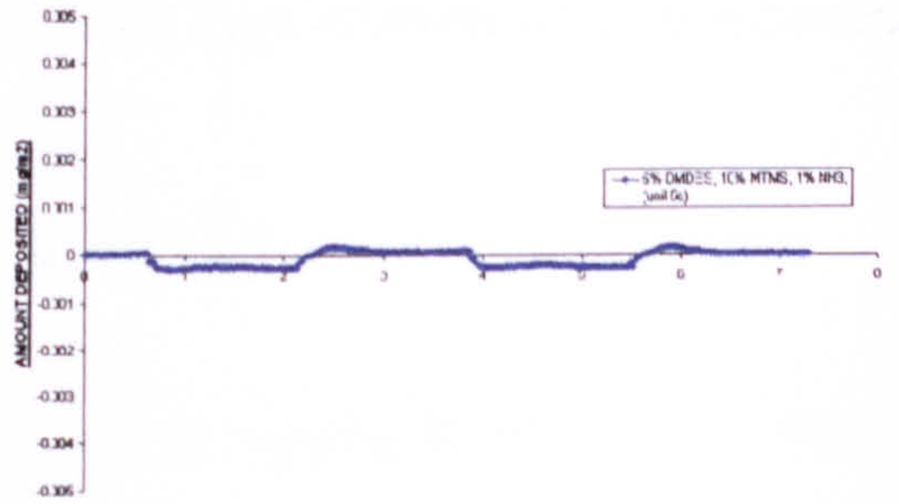

Time

(c)

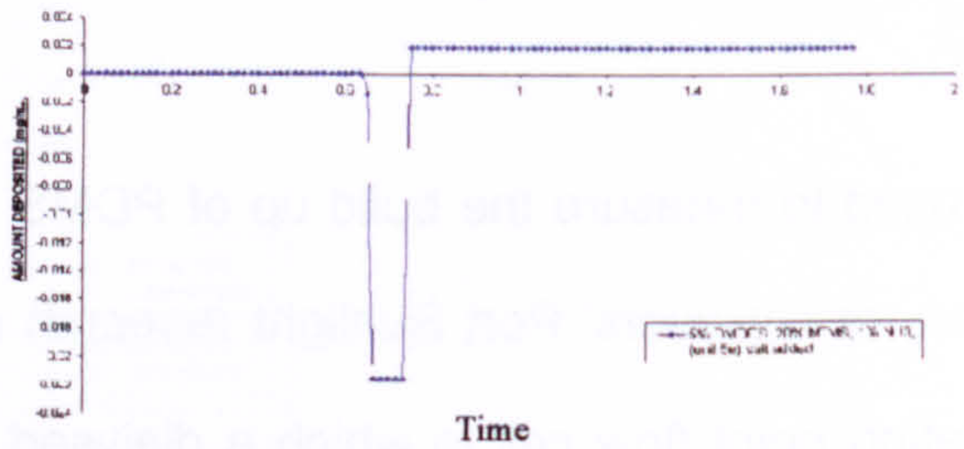

Time

A.9 Deposition under shear force; Diastrom

A Diastrom apparatus, Port Sunlight Research laboratories, was used to investigate forced deposition shear regimes using a series of PDMS emulsions, fixed total monomer 0.05 (v/v) ϕ, with a range of NaCl concentrations 10^{-5} mol dm^{-3} – $3x10^{-1}$ mol dm^{-3}. The influence

of electrolyte concentration salt on deposition was noted to reach an optimum deposition value at 0.3 mol dm^{-3} NaCl, fig A9.1. The deposition results obtained for fixed total monomer 0.05(v/v) ϕ droplets produced with a matrix of cross-linker concentrations to control viscosity and particle size. The results showed an increased deposition with increased inter-particle viscosity, A9.2.

Fig A9.1 Deposition under shear force as a function of (a) [NaCl], (b) MTMS ϕ